

## **Bedrock Hydrogeology**

### **Site investigation SFR**

Johan Öhman, Geosigma AB

Niclas Bockgård, Golder Associates AB

Sven Follin, SF GeoLogic AB

June 2012

#### **Svensk Kärnbränslehantering AB**

Swedish Nuclear Fuel  
and Waste Management Co

Box 250, SE-101 24 Stockholm  
Phone +46 8 459 84 00



ISSN 1402-3091

SKB R-11-03

ID 1265697

# **Bedrock Hydrogeology**

## **Site investigation SFR**

Johan Öhman, Geosigma AB

Niclas Bockgård, Golder Associates AB

Sven Follin, SF GeoLogic AB

June 2012

*Keywords:* Kravdatabas SFR-utbyggnad (N2X-276).

This report concerns a study which was conducted for SKB. The conclusions and viewpoints presented in the report are those of the authors. SKB may draw modified conclusions, based on additional literature sources and/or expert opinions.

A pdf version of this document can be downloaded from [www.skb.se](http://www.skb.se).

## **Preface**

The following people have contributed to Chapter 3 and Appendix C: Philip Curtis (Golder Associates AB) and Jesper Petersson (Vattenfall Power Consultant AB).

## Abstract

The Swedish Nuclear Fuel and Waste Management Company (SKB) has conducted site investigations for a planned extension of the existing final repository for short-lived radioactive waste (SFR). This report presents an integrated analysis and interpretation of the historic data from the existing SFR (1980–1986), as well as, from the recent investigations for the planned extension of SFR (2008–2009). The primary objective is to establish a conceptual hydrogeological model of the bedrock for safety assessment and design analyses.

Analyses and interpretations of all (old and new) hydraulic data are analysed with regard to the recently developed geological deformation zone model of the SFR model domain (Curtis et al. 2011). The methodology used by Curtis et al. (2011) has focussed on magnetic anomalies and deformation zone intercepts with ground surface greater than 300 m. In the hydrogeological modelling, however, it has been considered important to also explore the occurrence and characteristics of shallow horizontal to sub-horizontal structures (sheet joints) inside the SFR model domain. Such structures are of considerable importance for the hydrogeology in the uppermost c. 150 m of bedrock in SDM-Site Forsmark; hence the term Shallow Bedrock Aquifer was used to emphasise their hydraulic significance. In this study, the acronym SBA-structure is used for horizontal structures identified in the hydrogeological modelling.

In addition to the predominantly steeply dipping geological deformation zones, eight so-called SBA-structures are modelled deterministically in the hydrogeological model. The SBA-structures are envisaged as hydraulically heterogeneous and composed of clusters of minor gently dipping to horizontal fractures rather than extensive single features. A type of structures that is partly included in the definition of the SBA-structures is the Unresolved Possible Deformations Zone (Unresolved PDZ) intercepts identified by Curtis et al. (2011). The Unresolved PDZs represent borehole sections of deformation zone type characteristics that cannot be linked to surface lineaments and hence not included as deterministic deformation zones in the geological model.

Although the modelled SBA-structures can be fairly transmissive locally ( $T \approx 10^{-5} \text{ m}^2/\text{s}$ ), their spatial extension, or existence, beyond borehole coverage is uncertain. Notably, the historic hydraulic data vis-à-vis the recent data cover different parts of the SFR model domain and are also of different types and of markedly different quality. Therefore, it is difficult to clearly state whether the recently investigated area for a planned extension has identical or more or less similar hydraulic characteristics as the area hosting the existing SFR. Sheet joints of the same character as in SDM-Site are not expected to exist within the SFR model domain.

In conclusion, the flowing network of fractures outside the deformation zones is dominated by horizontal to sub-horizontal fractures. Some of the steeply dipping deformation zones are expected to have an essential role for the vertical hydraulic connection to the sea. However, the steeply dipping deformation zones are also judged to be hydraulically heterogeneous, discontinuous in character, and, in addition, possess a transmissivity trend with depth. Besides poorly interconnected (compartmentalised) rock mass volumes, the limited vertical hydraulic connection could be reinforced by hydraulic anisotropy in the overlying glacial and postglacial sediments.

Owing to the uncertainty regarding the spatial extent of the SBA-structures, three alternative approaches are discussed for groundwater flow modelling. Likewise, uncertainties also exist in the termination of the gently dipping deformation zone below SFR, ZFM871, as well as its contact with steeply dipping deformation zones. Therefore the importance of alternative extensions of ZFM871 should also be tested in the groundwater flow modelling.

# Sammanfattning

Svensk Kärnbränslehantering AB (SKB) har genomfört platsundersökningar för en planerad utbyggnad av den befintliga anläggningen för slutförvaring av kortlivat radioaktivt avfall, (SFR). Denna rapport redovisar en integrerad analys och tolkning av historiska data från det befintliga SFR (1980–1986) såväl som från den nyligen genomförda platsundersökningen för den planerade utbyggnaden av SFR (2008–2009). Det huvudsakliga målet är att utveckla en konceptuell hydrogeologisk modell av berggrunden för tillämpning säkerhets- och konstruktionsanalyser.

Analyser och tolkningar av samtliga hydrauliska data (gamla såväl som nya) har gjorts gentemot den senaste geologiska deformationszonsmodellen SFR v. 1.0 (Curtis et al. 2011). Metodiken som tillämpats av Curtis et al. (2011) har fokuserat på magnetiska anomalier samt de deformationszoner som skär markytan med spår längre än 300 m. I den hydrogeologiska modelleringen har det däremot visat sig nödvändigt att även undersöka förekomsten av subhorisontella strukturer (*Eng. sheet joints*) inom modellvolymen för SFR. Sådana strukturer har visat sig ha avsevärd hydrogeologisk betydelse inom de översta cirka 150 m av berggrunden i SDM-Site Forsmark. För att understryka deras hydrauliska betydelse i SDM-Site Forsmark myntades begreppet Shallow Bedrock Aquifer. I denna studie benämns därför de subhorisontella strukturer som har identifierats i den hydrogeologiska modelleringen med akronymen SBA-struktur.

Utöver de – företrädelsevis branta – geologiska deformationszonerna, så inkluderas även åtta deterministiskt modellerade så kallade SBA-strukturer i den hydrogeologiska modellen. SBA-strukturerna betraktas som hydrauliskt heterogena och kan liknas vid kluster med mindre, måttligt stupande, sprickor, snarare än vidsträckt, enhetliga strukturer. En typ av strukturer som delvis ingår i modelleringen av SBA-strukturer är de ”olösta potentiella deformationszonerna” (*Eng. Unresolved Possible Deformation Zone* eller *Unresolved PDZ*). De olösta PDZ representerar borrhålsintercept med deformationszonskaraktär som identifierats av Curis et al. (2010), men inte kunnat sammanlänkas med lineament i markytan, och därmed ej inkluderats som deformationszoner i den geologiska modellen.

Trots att de modellerade SBA-strukturerna lokalt kan vara relativt transmissiva ( $T \approx 10^{-5} \text{ m}^2/\text{s}$ ), så finns stora osäkerheter kring deras rumsliga utbredning, eller existens, utanför det område som täcks av borrhål. Anmärkningsvärt är att de två dataseten (dvs det historiska, respektive, det nyare) täcker olika delar av modellområden. De utgörs av olika sorters testmetoder och har dessutom en påtaglig skillnad i kvalitet. Det medför svårigheter i att avgöra huruvida det undersökta området för den planerade utbyggnaden av SFR har identiska, eller liknande hydrogeologiska egenskaper som det område där det befintliga SFR ligger. Den typ av ”högtransmissiva sheet joints” som påträffades i SDM-Site Forsmark bedöms inte finnas i modellområdet för SFR.

Sammanfattningsvis, så domineras det flödande spricksystemet av horisontella till subhorisontella sprickor. Därmed förväntas vissa branta zoner ha en nyckelroll för den vertikala förbindelsen till havet. De brantstående zonerna bedöms ha hydrauliskt heterogena och diskontinuerliga egenskaper, samt ha ett djupavtagande i transmissivitet. Utöver begränsad förbindelse mellan flödande spricksystem (*Eng. compartmentalised fracture network*), så kan den vertikala hydrauliska förbindelsen med havet ytterligare begränsas på grund av hydraulisk anisotropi i de ovanliggande glaciala och postglaciala sedimenten.

Med anledning av osäkerheten kring SBA-strukturernas utbredning diskuteras alternativa ansatser för hur dessa strukturer skall representeras i flödesmodellering. Likaså finns det osäkerheter kring termineringen av den flacka zonen under SFR, ZFM871, såväl som dess kontakt med branta zoner. Därför bör även alternativa utsträckningar av ZFM871 beaktas vid flödesmodellering.

# Contents

<b>1</b>	<b>Introduction</b>	9
1.1	Context	9
1.2	Scope and role of the hydrological model	9
1.3	Objectives and strategy	9
1.4	Setting	10
1.5	Scales and volumes	11
1.6	Model versions	12
1.7	This report	15
	1.7.1 Outline	15
	1.7.2 Nomenclature	15
	1.7.3 Data used	17
<b>2</b>	<b>Hydrogeological modelling</b>	21
2.1	Systems approach	21
2.2	Confirmatory testing	22
2.3	Primary concepts and assumptions	22
	2.3.1 Deterministic versus stochastic features	22
	2.3.2 Important hydrogeological features falling between deterministic and stochastic definitions	24
	2.3.3 Basic characteristics of single-hole tests	25
	2.3.4 Hydraulic Conductor Domain (HCD) model	27
	2.3.5 Hydraulic Rock mass Domain (HRD) model	28
	2.3.6 Hydraulic Soil Domain (HSD) model	29
<b>3</b>	<b>Geological conditions</b>	31
3.1	Regolith geology	31
3.2	Bedrock geology	32
	3.2.1 Rock domain model	33
	3.2.2 Deformation zone model	34
	3.2.3 Fracture domain model	36
3.3	Stress regime	36
<b>4</b>	<b>Evaluation of primary data</b>	39
4.1	Experiences from the existing SFR facility	40
	4.1.1 Tunnel construction experience	40
	4.1.2 Reported tunnel inflow	42
	4.1.3 Location of inflow and change with time	45
4.2	Open and Partly open fractures	48
	4.2.1 Fracture intensity	49
	4.2.2 Fracture characteristics of rock domains	50
4.3	Evaluation of single-hole hydraulic tests	52
	4.3.1 Single-hole transmissivity data from the existing SFR facility	52
	4.3.2 Single-hole transmissivity data from the SFR extension investigation	53
	4.3.3 Transient hydraulic evaluation from the SFR extension investigation	57
4.4	Evaluation of cross-hole (interference) tests	59
	4.4.1 Old interference data close to the existing SFR	60
	4.4.2 New interference data from the SFR extension investigation	61
4.5	Drawdown around SFR	67
	4.5.1 Excess groundwater head prior to SFR construction	67
	4.5.2 Long-term monitoring programme of head in tunnel boreholes	68
	4.5.3 Head in borehole sections from the SFR extension investigation	70
	4.5.4 Fresh-water head calculated in the PFL-f evaluation	72
4.6	Evaluation of hydrochemistry	73
	4.6.1 Water types	73
	4.6.2 Salinity and measured electrical conductivity	76

4.7	Sediment coverage and the hydraulic contact to the Sea	77
4.7.1	Hydraulic choking at fracture-sediment contacts	79
<b>5</b>	<b>Conceptual hydrogeological modelling</b>	<b>81</b>
5.1	Interpretation of hydraulic interferences	81
5.1.1	Conceptual interpretation	82
5.1.2	Hydraulic responses in deformation zones	83
5.2	Depth dependency in transmissivity	83
5.2.1	Depth domains for HRD parameterisation	83
5.2.2	Depth trends in transmissivity data	84
5.2.3	Analysis of HCD transmissivity with depth	85
5.2.4	Relation between HRD and HCD transmissivity with depth	87
5.3	Lateral contrasts in transmissivity data	88
5.3.1	Shallow Rock (0 to –60 m RHB 70)	88
5.3.2	Repository level (–60 m to –200 m RHB 70)	89
5.3.3	Lateral transmissivity contrasts in relation to deterministic structures	90
5.3.4	Conclusions	92
5.4	The role of deterministic structures on HRD connectivity	94
5.4.1	Connectivity between the HRD and the sea	95
5.4.2	Concepts in the connectivity analysis	96
5.4.3	Spatial inference for PFL data	97
5.5	Formulation of a conceptual model	99
5.6	Implementation alternatives	101
<b>6</b>	<b>Parameterisation of hydraulic domains</b>	<b>105</b>
6.1	Weighting use of old and new data	105
6.2	Hydraulic Conductor Domain (HCD) model	106
6.3	Hydraulic Rock mass Domain (HRD) model	108
6.4	Deterministic Shallow Bedrock Aquifer (SBA) structures	111
6.5	Hydraulic Soil Domain (HSD) model	112
<b>7</b>	<b>Discussion and conclusions</b>	<b>113</b>
7.1	Summary of the bedrock hydrogeological model	113
7.1.1	Hydraulic characteristics of Hydraulic Conductor Domains (HCD)	113
7.1.2	Hydraulic characteristics of the Hydraulic Rock mass Domains (HRD)	114
7.1.3	Hydrogeological characteristics of the SFR model volume	114
7.2	Hydrogeological key issues	114
7.3	Confidence and some remaining uncertainties	116
7.3.1	Data gaps	116
7.3.2	Old versus new data	117
7.3.3	Shallow Bedrock Aquifer (SBA)	117
7.3.4	Concluding remarks	117
<b>8</b>	<b>References</b>	<b>119</b>
<b>Appendix A</b>	Modelling strategy for Unresolved PDZs	123
<b>Appendix B</b>	Deterministic model of Shallow Bedrock Aquifer (SBA) features	141
<b>Appendix C</b>	Character of deformation zone sets	149
<b>Appendix D</b>	Analysis of hydraulic data from the construction of SFR	155
<b>Appendix E</b>	Analysis of hydraulic data from the SFR extension investigation	221
<b>Appendix F</b>	Monitored head and sea level fluctuation in the new data set	247
<b>Appendix G</b>	Updating the Hydro-DFN	255
<b>Appendix H</b>	Underlying data for Shallow Bedrock Aquifer structures	301

# 1 Introduction

## 1.1 Context

The first stage of a final repository for low and intermediate level radioactive operational waste (SFR) was constructed and taken into operation in 1987. During 2008, the Swedish Nuclear Fuel and Waste Management Company (SKB) initiated an investigation programme for SFR's future extension. This extension of SFR is necessitated by the pending decommissioning of the closed reactors Barsebäck, Studsvik, and Ågesta, the additional amounts of operational waste associated with the extended operating time of the remaining nuclear power plants, as well as the future decommissioning of running nuclear power plants Oskarshamn, Forsmark, and Ringhals (SKB 2008b). The overall purpose of the Site Investigation SFR extension is to develop a Site Descriptive Model (SDM) for the bedrock hosting SFR. The SDM is an integrated model for geology, hydrogeology and hydrogeochemistry.

This report provides a compilation and analysis of hydrogeological data that are relevant to form the basis for the SFR Site Descriptive Model (SDM-PSU). There are two main sources of hydrogeological data: 1) the early data obtained from the construction of the existing SFR, and 2) recent data from the SFR extension investigation programme. The work reported here was carried out in accordance with activity plan AP SFR-10-001. The controlling documents for performing this activity are listed in Table 1-1. Both the activity plan and the method descriptions are SKB's internal controlling documents.

**Table 1-1. Controlling documents for the performance of the activity reported here.**

<b>Activity plan</b>	<b>Number</b>	<b>Version</b>
Platsmodellering Hydrogeologi 1.0	AP SFR-10-001	1.0
<b>Method descriptions</b>	<b>Number</b>	<b>Version</b>
Hantering av data och modeller inom SFR – utbyggnad	SKB MD SDU-203	1.0
Hantering av primärdata vid platsundersökningar	SKB MD SDK-508	

## 1.2 Scope and role of the hydrological model

The purpose of the site characterisation is to provide means for an integrated evaluation of the suitability of the investigated site to host an extension of the SFR repository. As such, the development of a hydrogeological model is an important component of the site characterisation. The hydrogeological model is built from quality-assured hydrogeological data stored in SKB's data base Sicada, as well as models in the Geographical Information System (GIS) and Rock Visualisation System (RVS). The purpose of the hydrogeological model is to provide input for a site-adapted design and for safety assessment.

The role of the hydrogeological model is to describe the current status of the hydrologic cycle. It is not the task to address the future evolution of the site (e.g. land-lift, landscape dynamics, glaciation); such issues are addressed within the framework of the safety assessment.

## 1.3 Objectives and strategy

The primary objectives of the hydrogeological model are to provide a conceptual understanding of the site and to determine the hydraulic properties inside the SFR model domain (Section 1.5). Primary data are evaluated to formulate a conceptual model, suggest implementation alternatives, and to provide parameter values for a *groundwater flow model* for subsequent application in site-adapted design and safety assessment predictions. It is beyond the scope of the current study



to apply the model in numerical flow simulations for calibration and verification purposes; this is performed in a subsequent stage (Öhman et al. 2013). The focus of this study is to compile, analyse, and interpret the available hydrogeological data in context with the recently developed geological model SFR v. 1.0 (Curtis et al. 2011).

In addition to the new data gathered from the recent investigations at SFR, the hydrogeological description should also integrate – to the extent possible – hydrogeological information from the constructions of the Forsmark nuclear power plant and the existing SFR (Carlsson et al. 1986, Axelsson et al. 2002), as well as from the nearby site investigations for a deep repository for high level spent nuclear fuel (Follin et al. 2007b).

Four key issues have been specified for the SFR hydrogeological programme (SKB 2008b):

- 1) Hydraulic properties of deformation zones interpreted from low-magnetic lineaments.
- 2) Hydraulic properties of the bedrock between the deformation zones within SFR Regional model volume.
- 3) The extent and character of hydraulic connectivity within the model volume as well as the hydraulic connectivity to the surrounding bedrock.
- 4) Spatial extent and hydraulic properties of sheet joints and gently dipping deformation zones.

Other important issues in conceptual hydrogeological modelling have been raised by Follin et al. (2007a):

- 5) Is there a general observation that deformation zones are more conductive (i.e. higher intensity and transmissivity of flowing fractures) than the surrounding bedrock?
- 6) Is there any data support for dividing the bedrock between the deformation zones into different sub domains?
- 7) What is the statistical significance of a potential depth dependence in the fracture transmissivity?

## 1.4 Setting

The SFR repository is located in Forsmark in the northern part of Uppland, about a kilometre offshore from the Forsmark nuclear power plant and the candidate area for the deep disposal of spent nuclear fuel (Figure 1-1). The existing SFR disposal facilities are located in the bedrock approximately 60 m below the seabed of the Baltic Sea. The investigated SFR domain is part of the Forsmark Site Descriptive Model (See Section 1.5). The conceptual hydrogeologic modelling for the extension of SFR focuses on the defined SFR model volumes. The reader is referred to the Forsmark Site Descriptive Model (Follin 2008) for the full description of the hydrogeological setting outside the SFR sub-volume.

There are three differences between the SFR extension project and the Site Investigation project for disposal of spent nuclear fuel:

- The target depth for the SFR extension has not been finally decided, but it is expected to be located at *shallower depth* than the planned deep repository for spent nuclear fuel (the existing SFR storage facilities are located within a depth interval of –60 to –140 m RHB 70). This comparatively shallow target depth shifts the attention towards factors controlling shallow hydrogeology, e.g. topography, sediments and contact to the seafloor, stress-relief structures, land-lift, etc. It may be expected that deep regional flow and variable-density effects are of comparatively lesser importance, particularly with respect to the ongoing land-lift.
- The SFR Local model volume is delimited to a comparatively small area.
- The deep repository for spent nuclear fuel is targeted to the tectonic lens, which is believed to be a quite different hydro-structural environment to SFR, both near the surface and at depth.

## 1.5 Scales and volumes

Two different scales for the site descriptive modelling have been defined by the geoscientific execution programme (SKB 2008b): a local scale and a regional scale. The local scale covers the volume that is expected to host the SFR extension, while the regional scale covers a larger volume that places the description of the local volume in a larger context. The SFR model areas are related to the local model area used in the Forsmark Site Investigation in Figure 1-1. The SFR local model volume extends from elevation +100 m RHB 70 to –300 m RHB 70, while the regional model volume extends from +100 m RHB 70 to –1,100 m RHB 70. The coordinates defining the horizontal extent of the model volumes are provided in Table 1-2.

It should be emphasised that the distinct rectangular volumes (Figure 1-1 and Table 1-2 do not conform to hydrogeological boundaries, but primarily concern the development of the geological model. The geologic model (Curtis et al. 2011) defines three geologic units that provide a more appropriate context for conceptual hydrogeological modelling: 1) a Central block that is bounded by 2) a Southern boundary belt (Singö) and 3) a Northern boundary belt (ZFMNW0805A, or Zon 8; see Chapter 3). It is expected that the future extension of SFR will be located inside the Central block, at a depth that is fairly similar to the existing SFR.

**Table 1-2. Coordinates defining the model areas for SFR in metres. RT90 (RAK) system.**

Regional model volume		Local model volume	
Easting	Northing	Easting	Northing
1631920.0000	6701550.0000	1632550.0000	6701880.0000
1633111.7827	6702741.1671	1633059.2484	6702388.9854
1634207.5150	6701644.8685	1633667.2031	6701780.7165
1633015.7324	6700453.7014	1633157.9547	6701271.7311

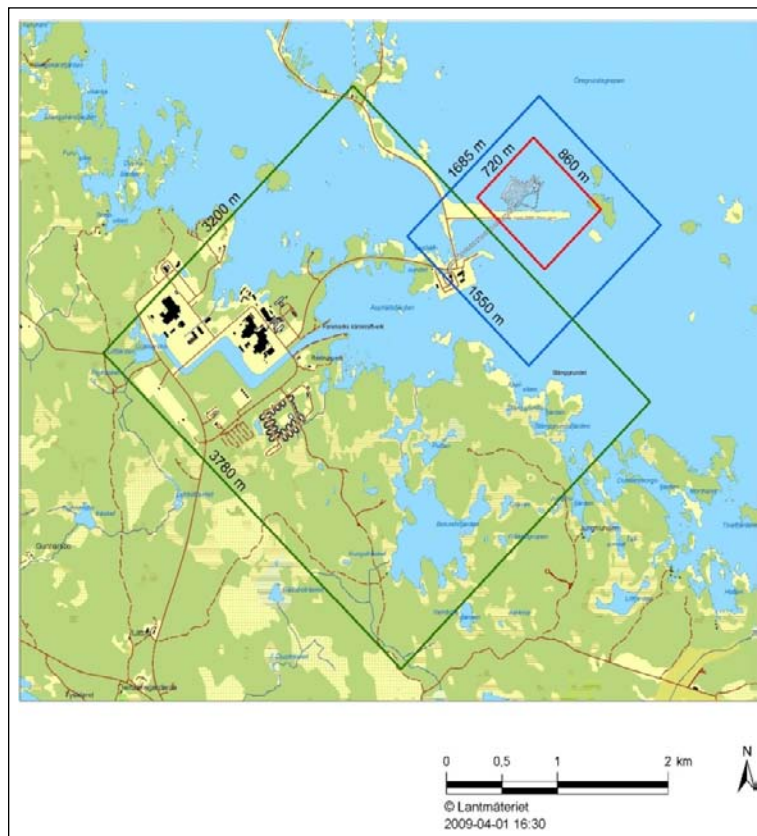


**Figure 1-1.** Regional (blue) and local (red) model areas for SFR model version 1.0 relative to the local model area used in the Forsmark site investigation, model stage 2.2 (green).

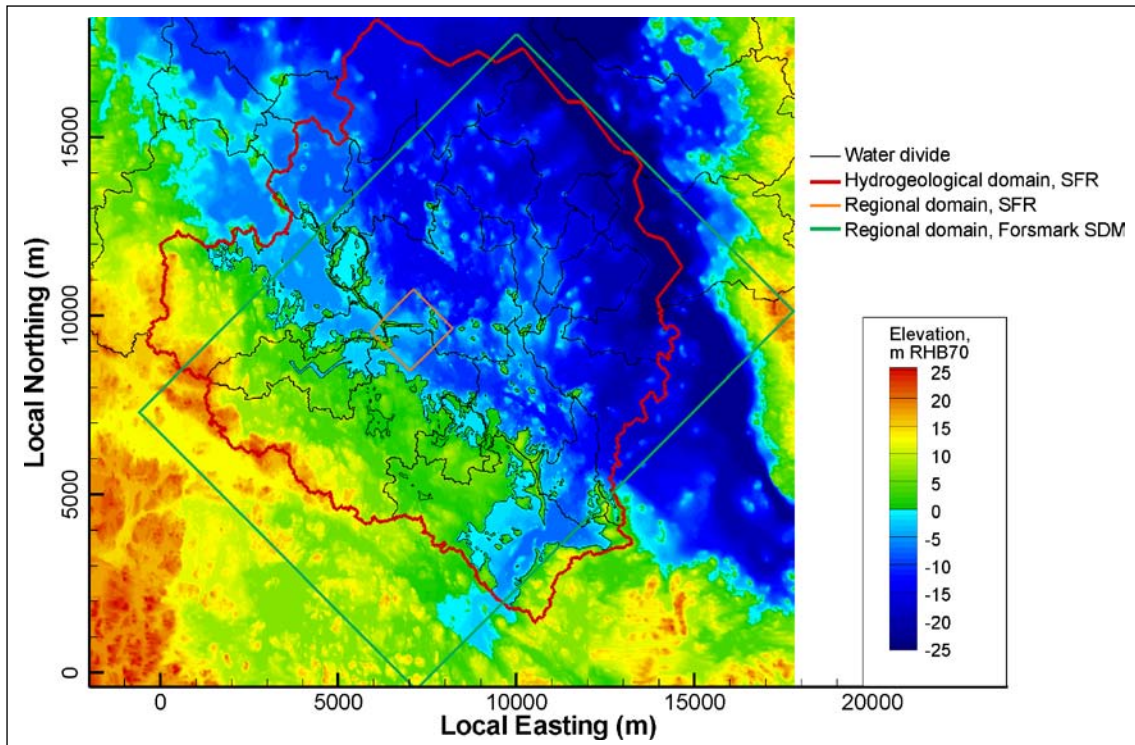


**Figure 1-2.** Hydrogeological model area SFR (red) defined by surface water divides. The Regional domain of the SFR structural model (orange) is a sub-volume of the Regional model domain used in the Forsmark site investigation, model stage 2.2 (green). Local origo set to Northing = 6692000, Easting = 1626000.

A hydrogeological model area was defined for groundwater flow and solute transport modelling with DarcyTools. The hydrogeological model area was defined from surface water divides that were interpreted from topographic data (Figure 1-2; see Öhman 2010 and Odén 2009). The parts of the model area that are currently below Sea have been chosen with respect to future topographical divides, as well as the deep Seafloor trench (the so-called Gräsörännan). The topographic data are available as a Digital Elevation Model (DEM) with a spatial resolution of 20 m scale in the horizontal plane. The hydrogeological model volume extends vertically from +100 m RHB 70 to -1,100 m RHB 70.

## 1.6 Model versions

### *Prior to the SFR extension investigation*

The early hydrogeological model of SFR, developed at the completion of the constructions included 6 steeply dipping zones: Singö, Zone 1, Zone 3, Zone 6, Zone 9, Zone 8, and the gently dipping Zone H2 (see Table 1-3 for reference to current nomenclature of zones) (Carlsson et al. 1985, 1986, 1987). The structural model was primarily based on the rock quality from an engineering viewpoint, increased frequency of Open (broken) fractures and also hydraulic parameters; this differs considerably from the current SKB methodology (Section 2.3.4). At this stage, Zone H2 was modelled with a minor extension; terminated by zones Zone 3, Zone 9, Zone 8, and Zone 6 (shaded region (A) in Figure 1-3). Within the same area, the upper c. 40 m bedrock was also modelled as a high-transmissive hydraulic unit, which represented stress-release structures (Zones H1 and H3; shaded region (A) in Figure 1-3). The shallow rock outside this area was modelled as one order of magnitude less transmissive (white region (B) in Figure 1-3), although it was recognised that this area had considerably less borehole coverage. Two different depth-trend models were considered. Carlsson et al. (1987) stated that "... since SFR is located in a tectonically complex environment the continuity of some zones is not always clear. This fact is one reason which may invite to alternative interpretations of the data."

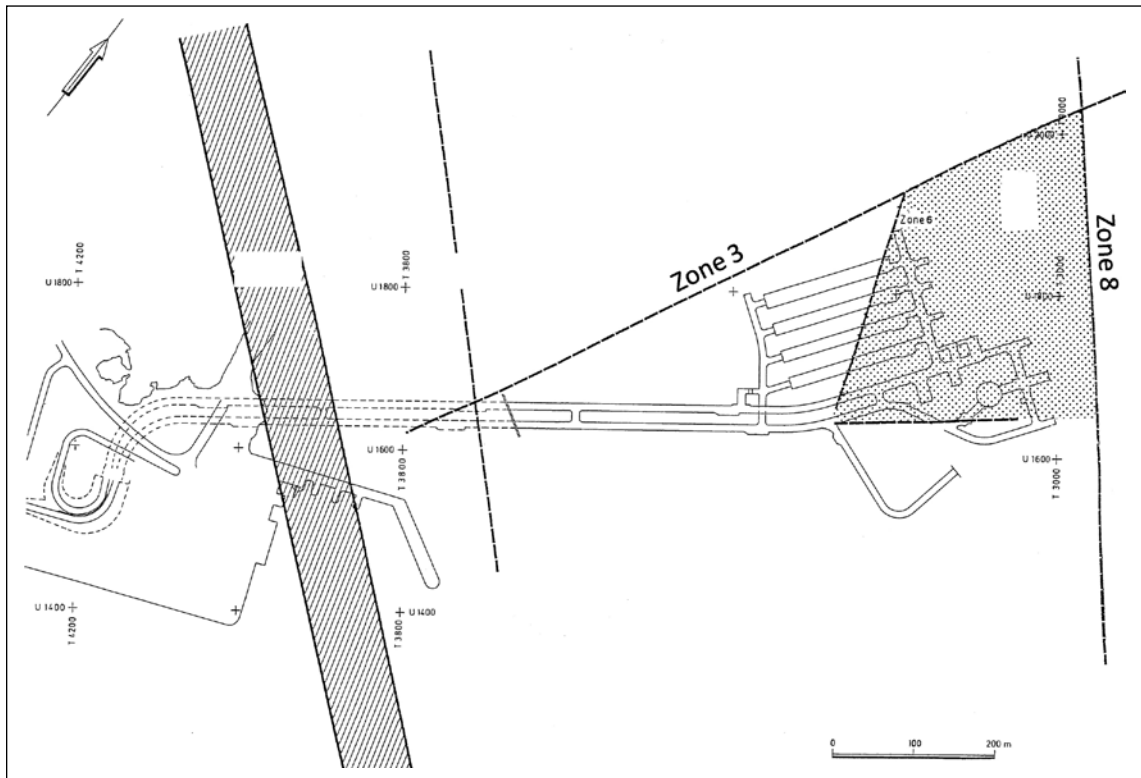


**Figure 1-3.** Hydraulic structures in the early SFR models, modified from Carlsson et al. (1987). The shaded region (A) represents the horizontal extensions of a high-transmissive hydraulic unit above SFR (Zones H1 and H3), as well as, the gently dipping ZFM871 (zone H2) below SFR.

At a later stage, a re-interpretation of interference tests lead to changes in the structural model (Axelsson and Mærsk Hansen 1997). Most notably, Zone H2 was extended in all directions beyond all its previously assumed terminations, even beyond the Singö zone (as well as outcropping to the Seafloor). From a hydraulic viewpoint, Zone 8 was interpreted as a less important zone. Horizontal structures were suggested as alternative interpretations for some data that had previously been interpreted as Zone 8.

Based on the updated structural model of Axelsson and Mærsk Hansen (1997), a hydrogeological model was calibrated versus measured tunnel inflow (including a grouting/skin resistance factor) (Holmén and Stigsson 2001) and used to predict future flow fields for the safety assessment of SFR. No conductivity depth trends were implemented. Effective conductivity values were assigned to zones, as well as, to the rock mass outside zones. A weakness of the inflow calibration of Holmén and Stigsson (2001) is that it renders non-unique solutions (i.e. inverse flow modelling where the number of unknown variables exceeds the number of constraints). Therefore, a probabilistic parameterisation of zones, as well as the rock mass outside zones, were established by Holmén (2005) (i.e. the ensemble of possible parameter combinations that reproduce measured inflow at SFR). Holmén (2005) also included test cases where the effective conductivity in the uppermost 25 m bedrock was increased by one order of magnitude (only applied to rock mass outside zones), as well as, introducing stochastic heterogeneity in rock mass between zones. The constraining power of the tunnel-inflow calibrations applied by Holmén (2005) suffers from the difficulty in differentiating the true, *non-disturbed* hydraulic properties of zones and rock mass from the combined effects of tunnel skin and grouting, as well as addressing the transient decline in tunnel inflow.

### **Model versions within the SFR extension investigation**

The SFR extension investigation has involved field investigations inside the SFR Regional model domain (Figure 1-1) as well as sequential model versions. The hydrogeological modelling has been

developed in three model versions, 0.1, 0.2 and 1.0, that successively incorporate data from the recent SFR field investigations and feedback from the other modelling disciplines. The work follows SKB's established methodology for modelling (Rhén et al. 2003, Follin et al. 2007a) and is described in Chapter 2.

Prior to these three model versions, the flow model developed by Holmén and Stigsson (2001) was numerically setup in DarcyTools v. 3.1; this numerical implementation is referred to as the SFR hydrogeological model v. 0.0 (Odén 2009). The purpose of version 0.0 was to reproduce the modelling results from the previous state-of-the-art SFR model using a different computer code (software) than Holmén and Stigsson (2001). The DarcyTools program package is comprehensively described in Svensson et al. (2010) and Svensson (2010).

Version 0.1 (Öhman and Follin 2010a) was a review of historic hydraulic data of SFR with respect to a preliminary version of the geological model SFR v.0.1 (Curtis et al. 2009). In other words, hydrogeological model v.0.1, was based on hydraulic data available prior to the initiation of the SFR extension investigation, the same hydraulic data as Holmén and Stigsson (2001), but used an updated model of the geological structures (Curtis et al. 2009). The associated flow modelling is reported in Öhman (2010).

For the v. 0.2 stage, it was originally planned that both geologic and hydrogeological models should be developed. According to SKB's established methodology (Rhén et al. 2003), the geological model has the essential role of classifying data into deterministic geologic structures or rock mass between deformation zones (see Chapter 2). However, at a later stage it was decided to omit the intermediate geological model version, and instead focus on the final Geologic model (v. 1.0). Consequently, a hydrogeological model v. 0.2 could not be developed according to the SKB methodology and instead, its focus was shifted to analyse the recent data outside possible deformation zones and to examine the Hydro-DFN concept.

This report (the final hydrogeological model v.1.0) presents a compilation and interpretation of all relevant data with respect to the final SFR geologic model v.1.0 (Curtis et al. 2010). This report also presents the hydraulic parameterisation of both zones and the rock mass between zones (Chapter 6). The Site Descriptive Model intended to provide the foundation for the long-term safety assessment and the detailed design for the extension of SFR.

The main differences between model versions 0.2 and 1.0 are that:

- 1) The final geological model is available, which provides means to analyse data with respect to deformation zone geometry. The final modelled deformation zone intercepts only reflect minor changes relative to the information available during the hydrogeological model v. 0.2 (i.e. Possible Deformation Zones (PDZ)s, as defined by the established geologic interpretation method Single Hole Interpretation (SHI); see Table 1-3). However, the geological model puts some borehole data in a completely different perspective. One example is the representativeness of the important borehole KFR27; see Section 1.7.3).
- 2) In total, 31 PDZs are not included in the geological model (i.e. borehole sections with deformation zone characteristics that have been identified in borehole interpretation, but not deterministically modelled). Some are highly transmissive ( $T > 10^{-5} \text{ m}^2/\text{s}$ ), which implies that they constitute a large heterogeneity and conceptual uncertainty in the hydrogeological model. This uncertainty can be reduced depending on the degree to which they can be constrained geometrically (see details in Appendix A).
- 3) Two additional boreholes are available, KFR106 and HFR106; these are located outside the Local SFR model domain, but inside the Regional domain. These boreholes provide essential information on cross-hole hydraulic interferences and the spatial inference between high transmissive features and deformation zones (Chapter 5).
- 4) Information on the orientation uncertainty in mapped fractures is available, which provides means to update the orientation model (Appendix G).

## 1.7 This report

### 1.7.1 Outline

This report presents the current understanding of the hydrogeological conditions of the bedrock at SFR and provides a summary of the bedrock hydrogeological model and the underlying data supporting its development. It constitutes the main reference on bedrock hydrogeology for the final site descriptive model, SDM-PSU, and is intended to summarise the hydraulic properties and hydrogeological conditions of the bedrock at the site and to give the information essential for demonstrating understanding. Chapter 2 in this report describes SKB's systems approach to groundwater flow and solute transport modelling in sparsely fractured crystalline bedrock as applied in the site descriptive modelling work (in essence, reproduced from Follin 2008). Chapter 3 provides a brief summary of the regolith geology and the bedrock geology at SFR. Chapter 4 provides an overview of the primary data and summarises the evaluation. Chapter 5, presents a more detailed analysis of observed trends in hydraulic data and suggests a conceptual model of the bedrock hydrogeology at SFR. Chapter 6 presents the suggested parameterisation of the different components of the hydrogeological model. Chapter 7 summarises the findings made and discusses confidence and remaining uncertainties.

### 1.7.2 Nomenclature

This report contains several terms and acronyms that are rarely used outside SKB work and makes several references to site-specific deformation zones. To facilitate the readability of the report these are listed in Table 1-3.

**Table 1-3. Terminology, acronyms and structures frequently referred to in the report.**

Central notations used in the hydrogeological modelling	
Shallow Bedrock Aquifer (SDM-Site Forsmark)	Conceptual representation of the upper c. 150 m of the bedrock in SDM-Site Forsmark, which hydraulically dominated by large-scale, sub-horizontal, transmissive structures.
Sheet joints (SDM-Site Forsmark)	Numerical model representation of the Shallow Bedrock Aquifer characteristics in SDM-Site Forsmark (Follin et al. 2007c). It is envisaged as three highly transmissive horizons (Figure 2-4).
SBA-structure (SFR SDM-PSU)	Network of interconnected, sub-horizontal, transmissive features ( $T > 10^{-6}$ m <sup>2</sup> /s) that is geometrically represented by a plane for deterministic modelling purposes. Inside the SFR Regional domain, eight structures are modelled in the upper 200 m bedrock (SBA1 to SBA8 in Figure 6-3). The term <i>SBA-structure</i> is used at SFR to emphasise that these structures are of lesser size and of less significant hydraulic nature as compared to the <i>sheet joints</i> modelled in SDM-Site Forsmark.
Unresolved PDZ	Borehole intervals geologically interpreted to have "deformation-zone like characteristics" are referred to as Possible Deformation Zones (PDZ). In the geological modelling, deterministic structures (ZFMxxx) are modelled by linking PDZs to surface lineaments. Remaining PDZs, which cannot be linked to lineaments, are referred to as "Unresolved PDZs"
Central block	The tectonic volume at the centre of the SFR Regional domain, enclosed by the Northern and Southern boundary belts (Figure 3-5). The Central block has considerably less evidence of transmissive SBA-structures. In the hydrogeological modelling, no distinct boundaries have been defined between the Central block and the rock mass affected by the bounding belts; the transition seems to be gradual.
Northern boundary belt	The geologic model (Curtis et al. 2011) defines a northern deformation zone belt acting as a geological boundary in the SFR model (ZFMNW0805A/B in Figure 3-5). The hydrogeological modelling refers to the Northern boundary belt as a <i>concept</i> ; in the rock mass <i>outside deformation zones</i> (HRD), the evidence of SBA-structures gradually increases towards the Northern boundary belt. In the hydrogeological modelling, the structural wedge between the Northern boundary belt and deformation zone ZFMNNW1034 is judged to be involved in the pattern of influenced rock mass. Consequently, data analyses make frequent references to "rock mass in the vicinity of the Northern boundary belt and ZFMNNW1034".
Southern boundary belt	The geologic model (Curtis et al. 2011) defines a southern geologic deformation zone belt in the SFR model (the Singö deformation zone, and splays, in Figure 3-5). It is judged likely that the Southern boundary belt also has a wider influence range on the rock mass outside deformation zones, although this cannot be confirmed in the hydrogeologic modelling due to lack of borehole support.

Acronym	Stands for	Explanation
COF	Connected Open Fractures	A network Open and Partly open fractures that connects to a hydraulic boundary (e.g. transmissive deformation zones, or the sea floor).
DEM	Digital Elevation Model	Topographic data of the Forsmark area, covering both land and seafloor with a spatial resolution of 20 m scale in the horizontal plane.
DFN	Discrete Fracture Network	In DFN modelling fractures, and fracture flow, are typically resolved as a network of planar geologic features.
ECPM	Equivalent Continuous Porous Medium	A hydrogeological modelling concept, where the hydraulic properties of conductive fracture network is approximated by that of a porous medium. ECPM does not resolve explicit fracture flow, and hence is useful in large scale simulations.
FWH	Fresh-water head [m]	Groundwater pressure measurement, expressed in terms of calculated free groundwater level of an assumed freshwater column, see Eq. (4-4).
GEHYCO	GEnerate HYdraulic COnductivity	A DarcyTools module used to translate a hydraulic DFN into an ECPM (Svensson et al. 2010).
HCD	Hydraulic Conductor Domain	Hydraulic unit representing deformation zones.
HFM	Hammarborrhål ForsMark	Percussion-drilled borehole, drilled during the SDM-Site Forsmark investigations.
HFR	Hammarborrhål SFR	Percussion-drilled borehole, only recent data from the investigations for the extension of SFR are included (2008 to 2009).
HMS	Hydro Monitoring System	Database storing measured groundwater level data. In a second step, quality assured data are transferred from HMS to SKB's primary data base Sicada.
HRD	Hydraulic Rock mass Domain	Hydraulic rock mass unit between deformation zones.
HSD	Hydraulic Soil Domain	Hydraulic unit representing Quarternary deposits.
HTHB	Hydraulisk Test HammarBorrhål	Hydraulic test method used in percussion boreholes, based on a combination of impeller flow logging and pump tests. Considerably lower resolution and higher detection limit than the method used in core boreholes (see PFL).
KFM	Kärnborrhål ForsMark	Core-drilled borehole, drilled during the SDM-Site Forsmark investigations.
KFR	Kärnborrhål SFR	Core-drilled borehole, drilled for the SFR investigations; a historic data set exists from the construction of the existing SFR (1982 to 1987), as well as, a recent data set drilled during the investigations for the extension of SFR (2008 to 2009).
NBT	Nedre ByggTunneln	A lower tunnel section in SFR.
PFL	Posiva Flow Logging method	Hydraulic test method used in core boreholes designed to detect <i>continuously flowing fractures</i> (see Section 4.3.2). Considerably higher resolution and lower detection limit than the method used in percussion-drilled boreholes (see HTHB).
PFL-f	Discrete inflow detected by the Posiva Flow Logging method	A Boremap feature coupled to a discrete borehole inflow and an evaluated apparent transmissivity (see Section 4.3.2).
PDZ	Possible Deformation Zone (defined in the SHI methodology)	A borehole section that has geologically been interpreted to have "deformation-zone like characteristics" (i.e. a possible deformation zone intercept). In the geological modelling, deterministic structures (ZFMxxx) are modelled by linking PDZs to surface lineaments. Remaining PDZs, which cannot be linked to lineaments, are referred to as "Unresolved PDZs".
PSS	Pipe String System device	Measurement device for short-term hydraulic injection testing of packed off borehole sections.
PWH	Point-water head [m]	Groundwater pressure measurement, expressed in terms of calculated free groundwater level for a reference-fluid column, see Eq. (4-4). Reference fluid densities are measured for each section.
RHB 70	z, elevation [m]	The national levelling system.
RVS	Rock Visualization System	Geology modelling tool.
SBA	Shallow Bedrock Aquifer	Conceptual representation of the upper c. 150 m part of the bedrock in SDM-Site Forsmark, hydraulically dominated by large-scale, sub-horizontal, transmissive structures.
SDM	Site-Descriptive Model	
SHI	Single Hole Interpretation	An established SKB method to identify borehole intervals with deformation zone characteristics, based on a selection of geological parameters.
SFR	SlutFörvaret för kortlivat Radioaktivt avfall	The existing final repository for short-lived radioactive waste.
SKB	Svensk Kärnbränslehantering AB	The Swedish Nuclear Fuel and Waste Management Company.
ZFM	Zone in the Forsmark SDM	Deterministically modelled deformation zone in the Geological model. Modelled by linking borehole intercepts with "deformation-zone like characteristics" to surface lineaments (see acronym PDZ).

Key deformation zones, modelled in RVS (Deterministic structures of the Geological model SFR v 1.0 shown in Figure 3-5)		Alternatively known as: (Structures in early SFR models shown in Figure 1-3)
ZFMWNW0001	Core of the bounding Southern deformation zone belt.	Singö deformation zone
ZFMNW0805A/B	Bounding Northern deformation zone belt.	Zone 8
ZFMNNW1034	Associated to high transmissivity and the Northern deformation zone belt.	Not modelled in previous SFR models
ZFM871	Gently dipping zone below SFR.	Zone H2
ZFMENE3115	Terminates ZFM871 to the southeast.	Not modelled in previous SFR models
ZFMNE0870	Low-transmissive zone parallel to access tunnel ByggTunnel (BT).	Zone 9
ZFMNNE0869	High-transmissive zone intersecting access tunnels.	Zone 3
ZFMNNW1209	Intersects the SFR disposal facilities.	Zone 6
ZFMWNW1035	At the northern rim of the Sothern Belt.	Zone 1

### 1.7.3 Data used

The data used in this report are summarised in Table 1-4. These are traceable trough, either the SKB GIS and Sicada data bases (specified data deliveries), or from the SKBdoc model data base (as indicated by footnotes). Borehole locations are showed in Figure 1-4.

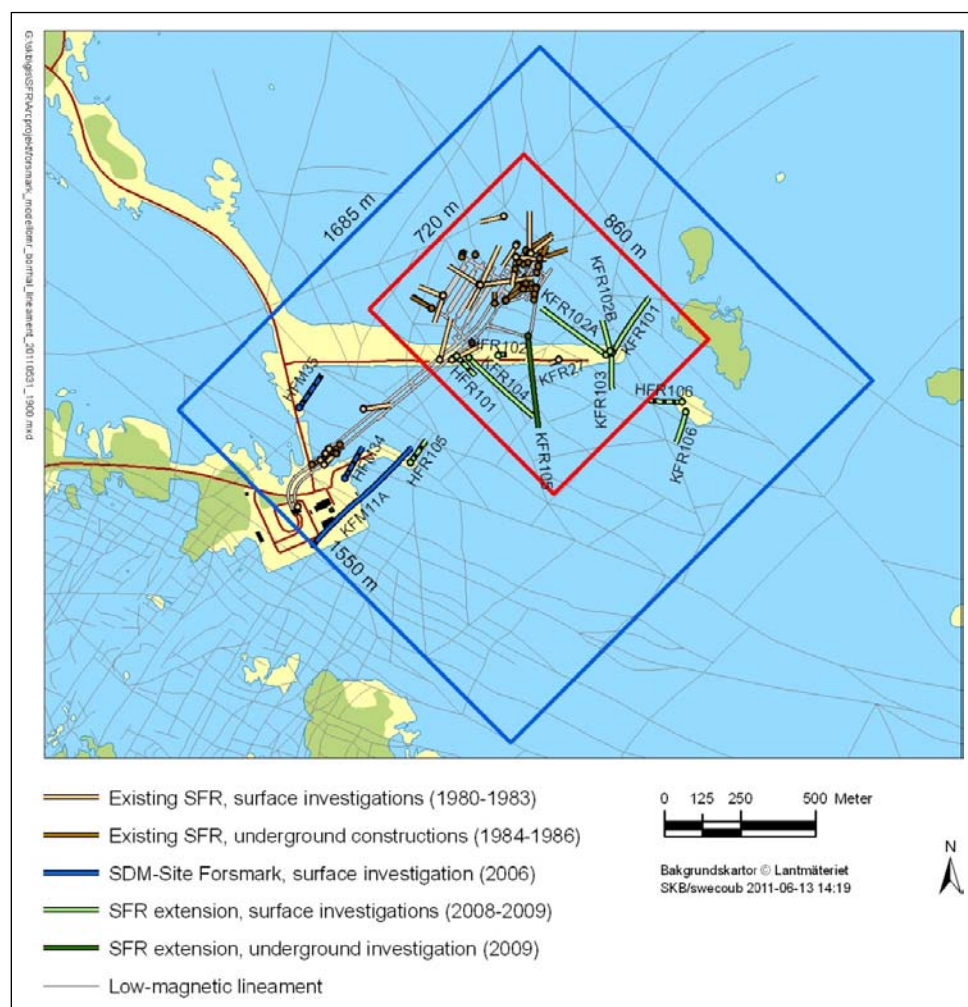


**Figure 1-4.** Boreholes drilled during different investigation phases: the existing SFR (brown), the nearby SDM-Site Forsmark (blue), and the planned SFR extension (green). Percussion boreholes (HFR and HFM) are dashed and core boreholes are shown as solid (KFR and KFM). Regional and local model areas of the SFR model version 1.0 are shown by blue and red rectangles, respectively.



**Table 1-4. Data used.**

Hydraulic data	Boreholes	Source
plu_pfl_diff_seq_flo.xls	KFR101–106, KFR27, KFM11A.	Sicada_2010_106
p_transmissivity.xls	KFR101–106, KFR27, KFM11A, HFR101, HFR105, HFR106, HFM33–35.	Sicada_2010_106
plu_pfl_inferr_anom.xls pfl_anom_crush_id.xls pfl_anom_fract_id.xls	KFR101–106, KFR27, KFM11A.	Sicada_2010_079
plu_impeller_anomaly.xls	HFR101, HFR105, HFR106, HFM33–35.	Sicada_2010_079
Old hydraulic data set <sup>1</sup>	Screened hydraulic data from the historic data set (obtained during the construction of SFR 1980–1986), see Öhman and Follin 2010a.	See footnote
Groundwater levels (HMS)	Measured groundwater levels in the HMS data base (quality-assured data in Sicada currently unavailable).	Sicada_2011_064
SFR tunnel inflow	Inflow measurements over different sections of the SFR disposal facilities/tunnels.	Sicada_11_076

**Hydraulic interferences**

SFR tunnel boreholes	Sicada_2011_029
KFR101–106, KFR27, HFR101, HFR106	Sicada_2011_029
HFM18, KFM03A	Table 6-4 (Gokall-Norman et al. 2004)
HFM16, HFM19, KFM02A	Table 6-25a (Gokall-Norman and Ludvigson 2005)
KFM04A, HFM10, HFM13, HFM19	Table 6-12 (Gokall-Norman et al. 2005a)
HFM01	Table 6-50 (Gokall-Norman et al. 2005b)
KFM02A, KFM03A	Table 6-10 (Gokall-Norman et al. 2006)
HFM14	Table 6-203 (Gokall-Norman and Ludvigson 2008b)
HFM33	Table 6-149 (Gokall-Norman and Ludvigson 2008a)
KFM02B	Table 5-8 (Lindquist et al. 2008)

**Geological data**

p_core_loss.xls p_fract_core.xls p_fract_percussion.xls p_fract_crush.xls p_fract_sealed_nw.xls p_rock_struct_feat.xls p_rock.xls p_rock_alter.xls p_rock_occur.xls	HFM33–35, HFR101, HFR105, KFM11A, KFR101–104, KFR27, KFR04, KFR08, KFR09, KFR13, KFR35, KFR36, KFR54, KFR55, KFR7A, KFR7C	Sicada_2009_101
	KFR105	Sicada_2009_127
	KFR106	Sicada_2010_007 Sicada_2010_035

**BIPS imagery**

92222_KFR101_KFR101_Geosigma_2_.bdt 96914_KFR102A_KFR102A_Geosigma_2_.bdt 93845_KFR102B_KFR102B_Geosigma_2_.bdt 93855_KFR103_KFR103_Geosigma_2_.bdt 94624_KFR104_KFR104_Geosigma1_.bdt 94644_KFR27_KFR27_Geosigma_2_.bdt KFR27_11-147m_20080709.bdt KFR27_140_500m_20081104.bdt KFR101_13-335m_20080710.BIP KFR102A_71-598m_20090114.BIP KFR102B_13-179m_20080910.BIP KFR103_13-199m_20080911.BIP KFR104_8-440m_20081014.BIP KFR27_11-147m_20080709.BIP KFR27_140_500m.BIP	KFR101–104, KFR27	Sicada_2009_110
--	-------------------	-----------------

97779_KFR105_No_BIPS2__.bdt 97780_KFR105_No_BIPS1__.bdt 97781_KFR105_Geosigma__.bdt KFR105_4-303m_20090616.BDT KFR105_4-303m_20090616.BIP	KFR105	Sicada_2009_127
98852_KFR106_No_BIPS_Geosigma__.bdt 98853_KFR106_Geosigma_KFR106__.bdt KFR106_9-297m_20090921.BIP	KFR106	Sicada_2010_007

#### Radar reflectors

radar_dir_antenna.xls	KFR101, KFR102A, KFR104, KFR105, KFR106, KFR27	Sicada_2010_094
-----------------------	---	-----------------

#### Geologic model files

Deformation zone model <sup>2</sup>	Three-dimensional geometry of deformation zones, as modelled in RVS (combined version of Regional and Local deformation zones).
Deformation zone intercepts <sup>3, 4</sup>	Tabulated deformation zone intercepts in boreholes
Possible stress-relief structure <sup>5</sup>	Borehole intercepts of possible stress-relief structure (referred to as SBA7), based on the original interpretation of Zone H1 and Zone H3, by Carlsson et al. (1985) (Appendix A).
Unresolved PDZ intercepts <sup>6</sup>	Tabulated intercepts of "possible deformation zones" in boreholes that were not included in the deterministic deformation zone model.

#### Geometric data

object_location.xls		Sicada_2011_029
Existing SFR tunnels and disposal facilities <sup>7</sup>	Laser-scanned geometry of the existing SFR (tunnels and disposal facilities in CAD STL format).	
861006_DZ_PFM_REG_v22_SJ.dt <sup>8</sup>	Geometric and hydraulic defined HCDs (SDM-Site Forsmark).	See footnote
081006_sheet_joints_v5.ifz <sup>9</sup>	Geometric and hydraulic defined sheet joints (SDM-Site Forsmark).	See footnote
SDEADM.UMEU_FM_HOJ_4528, SDEADM.UMEU_FM_HOJ_4529	Surface topography (DEM).	GIS_08_62
GIS_request09_26.mxd	Regolith depth model (RDM).	GIS_09_26

<sup>1</sup> SKBdoc 1233724 – Hydraulic data used for hydrogeological model v.0.1, Version 1.0, 2010-05-25.

<sup>2</sup> SKBdoc 1244246 – SFR\_DZ\_MASTER\_v1.0, Version 1.0, 2010-06-21.

<sup>3</sup> SKBdoc 1246851 – DZ\_by\_DZ\_after\_review\_100615, Version 1.0, 2010-08-19.

<sup>4</sup> SKBdoc 1246852 – BH\_by\_BH\_after\_review\_100615, Version 1.0, 2010-08-19.

<sup>5</sup> SKBdoc 1246853 – SFR\_DZ\_V1.0\_Possible\_stress\_relief\_structures, Version 1.0, 2010-08-19.

<sup>6</sup> SKBdoc 1246849 – SFR\_DZ\_V1.0\_PDZs\_not\_linked\_to\_DZs, Version 1.0, 2010-08-19.

<sup>7</sup> SKBdoc 1223130 – Befintligt skannat SFR i STL-format, Version 0.1, 2010-06-08. Please note that the final version of the CAD file is currently not available.

<sup>8</sup> SKBdoc 1287827 – Leverans av hydrogeologidata från SDM-Site Forsmark, Version 1.0, 2011-07-01.

<sup>9</sup> SKBdoc 1287827 – Leverans av hydrogeologidata från SDM-Site Forsmark, Version 1.0, 2011-07-01.

### Representativeness of KFR27

The borehole emplacement (Figure 1-4) reveals two regions of less data coverage: 1) the central model area (referred to as the Central block, Figure 3-5), which is considered likely for the SFR extension, and 2) the deep rock (below c. –300 m elevation). In perspective of these data gaps, KFR27 not only has a favourable position inside the Central block, but also covers the deep rock.

However, the decision on how to treat the KFR27 data is delicate, with implications in both the hydrogeologic interpretation (Chapter 5), as well as, in the DFN parameterisation (Appendix G). A few concerns exist regarding its data quality, as well as, to its representativeness of rock mass outside deformation zones. On the other hand, exclusion of borehole data reduces the data set,

which risks exposing the DFN calibration to the local heterogeneity of the boreholes retained. The concerns with KFR27 can be summarised as:

- 1) Sampling bias: the borehole is almost vertical (an average inclination of  $-86^\circ$ ), which effectively censors the sampling of vertical fractures to such an extent that they cannot be sufficiently compensated by Terzaghi-weighting.
- 2) Data quality and data gaps: its upper part (0 to 147.5 m) was drilled during the construction of the existing SFR. The core in this upper part is unavailable today. PFL-f data are only available below 99.3 m borehole length. The upper 99.3 m borehole length is only covered by sequential PFL data measured over 5 m sections, which cannot be coupled to Boremap fractures.
- 3) Deformation zone influence: in principle, the entire borehole KFR27 lies inside the modelled geometric bounds of a steeply dipping deformation zone (ZFMWNW0835; Figure 3-5), yet, there does exist two distinct *target intercepts* (notation by Curtis et al. 2011). Inside and in the vicinity of its lower intercept ( $-320$  to  $-464$  m RHB 70) a strong hydraulic signature of the zone can be observed in PFL-f data (Figure E-23), while above c. 300 m borehole length (c.  $-297$  m RHB 70) the hydraulic pattern does not differ notably from other borehole data, not even inside the upper intercept of ZFMWNW0835 ( $-105$  to  $-117$  m RHB 70). It is therefore unclear to which extent the borehole interval between the *target intercepts* is representative of rock mass outside deformation zones.

The decision on how to treat KFR27 is delicate. It was decided to include data from KFR27 as far as possible. However, it is judged that KFR27 cannot be used for intensity calculations of steep fracture sets or PFL-f data (see Appendix G).

## 2 Hydrogeological modelling

The hydrogeological modelling at SFR follows the principles and methodologies developed during the site investigation programmes for the disposal of spent nuclear fuel. Consequently, most of the content in Chapter 2 is reproduced, or modified from SDM-Site (Follin 2008).

### 2.1 Systems approach

In the established SKB methodology (Rhén et al. 2003), the hydrogeological system is conceptually divided into three hydraulic domains (Figure 2-1). These are:

- HSD (Hydraulic Soil Domain) represents the regolith (i.e. any loose material covering the bedrock, e.g. Quaternary deposits, artificial filling material, and weathered rock, see Section 3.1),
- HCD (Hydraulic Conductor Domain) represents deformation zones, and
- HRD (Hydraulic Rock mass Domain) represents the less fractured bedrock in between the deformation zones.

The division into hydraulic domains constitutes the basis for the conceptual modelling and the subsequent numerical modelling. The hydrogeological model consists of geometrical definitions and hydraulic parameterisation of these hydraulic domains. The HSD, HCD and HRD elements are based on the geological models of the regolith and the bedrock and the hydraulic investigations conducted in core and percussion drilled boreholes. That is, the geometries of the hydraulic domains are coherent with the geometries of the geological features, and their hydraulic properties reflect the anisotropy and spatial variability observed in the hydraulic investigations. Each of the three hydraulic domains can be split into subdomains, e.g. soil layers, individual zones, and fracture domains, respectively.

In addition to these three domains, the hydrogeological modelling of the Forsmark-Lens concluded that the shallow bedrock required an updated modelling strategy (Follin et al. 2007a); this upper part of the bedrock is referred to as Shallow Bedrock Aquifer (SBA; see Section 2.3.2). The SBA extends down to c. 100 to 150 m depth, i.e. potentially covering the depth interval for the extension of SFR, although it is not known if so-called SBA-structures exist inside the SFR model domain.

Besides the three hydraulic domains (Figure 2-1), a groundwater flow and solute transport model also consists of three additional elements:

- A solute transport model for the modelling of matrix diffusion.
- Initial conditions for groundwater flow and hydrochemistry.
- Boundary conditions for groundwater flow and hydrochemistry.

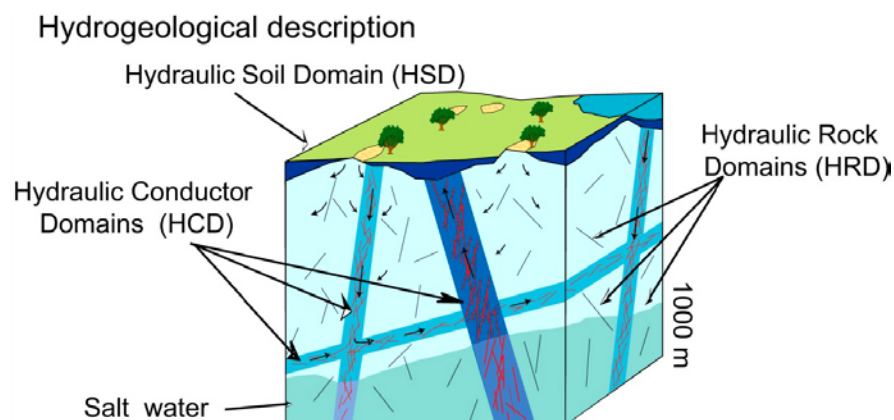


**Figure 2-1.** The hydraulic sub domains of a hydrogeological model; taken from Rhén et al. (2003).

## 2.2 Confirmatory testing

A system of confirmatory testing was developed during the site investigation programme for the disposal of spent nuclear fuel (e.g. Follin 2008). This confirmatory testing involves numerical calibration of the parameterised conceptual hydrogeological model, with respect to different data types (interference tests, groundwater levels, tunnel inflow, and hydrochemistry).

As stated in Section 1.3, the scope of this report is delimited to data review, conceptual modelling, and providing a Hydro-DFN parameterisation. The analyzed data are samples that describe the properties of a complex, unknown system with several different possible interpretations. The numerical calibration procedure is time consuming and does not inherently guarantee that the model representation is realistic. A major difference in confirmatory test data between SDM-Site Forsmark and SFR is that monitored pressures at SFR do not reflect natural groundwater levels, but instead a system disturbed by SFR inflow. Several uncertainties still remain concerning the transient development of tunnel inflow (Section 4.1.3).

Therefore, it was decided to report the numerical calibration phase and confirmatory testing separately (Öhman et al. 2013).

## 2.3 Primary concepts and assumptions

### 2.3.1 Deterministic versus stochastic features

With the exception of a few site-specific adaptations, the hydrogeological modelling of SFR follows the modelling concepts established during SKB's foregoing site investigation programmes (i.e. Follin 2008). A key concept is the characterisation of the more intensely fractured deformation zones and the less fractured bedrock in between. The methodology combines a deterministic geometrical representation of the HCD with a stochastic geometrical representation of the HRD using a discrete fracture network (DFN) approach, which relies on the tectonic continuum hypothesis (Figure 2-2).

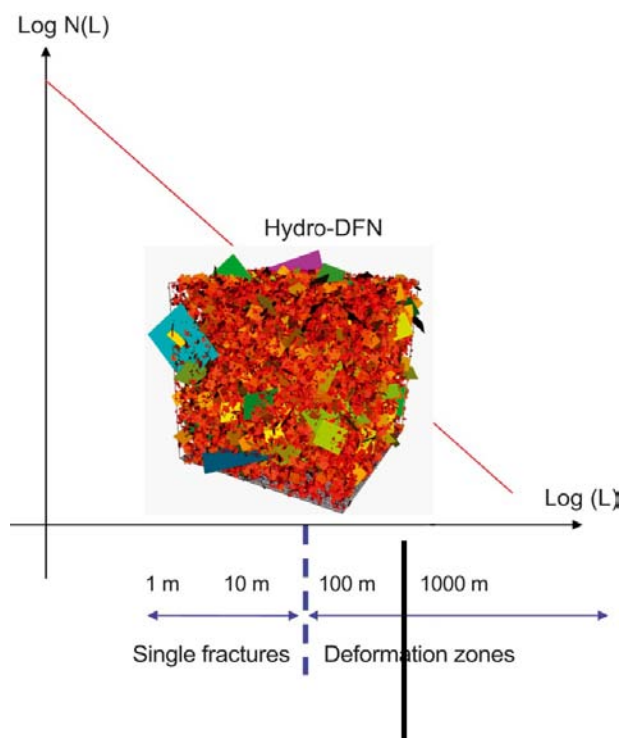


**Figure 2-2.** The tectonic continuum hypothesis assuming that the fracture size scaling can be approximated through the use of a single power-law density function. Features with trace lengths shorter than  $L = 300$  m are stochastically treated in the DFN concept. Unresolved PDZs must be stochastically represented (Figure 2-3 in Follin et al. 2007b).

The tectonic continuum hypothesis is a working hypothesis. It relies on the assumption that the size and intensity of fractures on multiple scales can be approximated through the use of a *single* power-law relationship. Fracture set orientation is assumed to follow the univariate Fisher distribution. Fractures are assumed to be Poissonian distributed in space. The Hydro-DFN is based on two types of borehole data:

- 1) *Potentially flowing features*: the fractures geologically interpreted as Open or Partly open are considered to be the parent population of the hydraulically connected fracture network.
- 2) Discrete flow measurements detected by the Posiva Flow Log method (so-called PFL-f features) are referred to as *continuously flowing features*; these are considered to reflect a sub-set of the hydraulically connected fracture network (i.e. the subset of connected fractures that are *detectable* with the PFL measurement device).

Additionally, there exist two types of structures (Unresolved PDZ and SBA-structures), which fall outside the definitions in Figure 2-2, but are highly significant in the hydrogeological model. These are briefly described in Section 2.3.2.

In the Forsmark SDM, the assumption of a tectonic continuum with a Euclidean scaling was tested in parallel with other variants (so-called geological DFN modelling, Fox et al. 2007). It was found that the spatial correlation of fractures is weak or absent beyond a few tens of metres or less, indicating that the spatial pattern of fracture clusters could be reasonably well approximated by a Poisson process and a Euclidean scaling. In effect, the primary concepts and assumptions of global fracture sets defined in the Forsmark SDM are the same as those used in the hydrogeological DFN modelling at SFR:

- Fisher distributed fracture orientations.
- Set-specific power-law size probability density functions.
- Poissonian fracture locations.

In SDM-Site Forsmark, two different methods were used to determine fracture size; the geological DFN modelling was primarily calibrated to *surface data* (outcrop data and lineament data) representing *all features*, whereas the hydrogeological DFN modelling focussed solely on the frequency of *borehole data* representing two different types (subsets) of features: (i) *potentially flowing features* (i.e. *Open and Partly open fractures*), and (ii) *continuously flowing features* detected by the Posiva Flow Log method (so-called *PFL-f data*)<sup>1</sup>.

The *potentially flowing features* constitute a fraction (subset) of *all features*; its envisaged relationship between the associated power-law size-scaling is illustrated in Figure 2-3. Figure 2-3 implies that completely Sealed fractures exist predominantly among the small features, whereas larger features, e.g. deformation zones, are generally heterogeneous with regard to aperture, i.e. at least Open over parts of their surface area.

Figure 2-3 also shows the conceived behaviour of the *continuously flowing fractures*. In the hydrogeological DFN modelling, the *PFL-f fractures* are imagined to be a subset of the latter category (i.e. the *detectable* subset owing to technical limitations in the measurement device).

---

<sup>1</sup> In the context of the Forsmark SDM, ‘*all features*’ means that no distinction was made between fractures with regard to fracture aperture. Hence, *Sealed* fractures were pooled with ‘*Partly open*’ and ‘*Open fractures*’ in the geological DFN modelling work. In contrast, the hydrogeological DFN modelling work focussed on the properties of the ‘*potentially flowing features*’, which implies that the analysed fractures must be at least Partly open. No distinction was made between Open and Partly open fractures; for the sake of simplicity they were all called *Open fractures*. In order for an *Open fracture* to be detected as a flowing feature with the PFL-f method it must be (i) connected to a positive hydraulic boundary (either directly or indirectly via a network of other flowing features) and (ii) have a sufficient transmissivity with regard to the measurement threshold of the test equipment used, cf. Section 2.3.3.

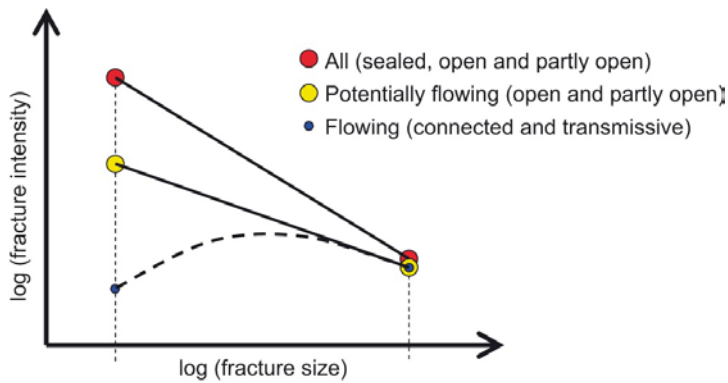


**Figure 2-3.** Cartoon showing the envisaged relationship between the probability density functions of all, the potentially flowing and the flowing fractures.

### 2.3.2 Important hydrogeological features falling between deterministic and stochastic definitions

All borehole intervals interpreted to have deformation zone characteristics, according to the Single Hole Interpretation methodology, are referred to as “Possible Deformation Zones” (PDZ). In the geological modelling, deterministic deformation zones (HCD) are defined by linking PDZs between boreholes and surface lineaments. The intervals that cannot be tied to surface lineaments remain unresolved in the geological modelling work and must be treated as stochastic features in the hydrogeological model. A strategy to simulate Unresolved PDZs is suggested in (Appendix A). There may be several reasons why some PDZs cannot be assigned a deterministic definition, for example related to data quality (see Appendix A). Two main cases are considered: 1) the surface lineament of the PDZ may be shorter than 300 m (Figure 2-2), and hence it is excluded from the deterministic model, or 2) the deformation zone is sub-horizontal and does not necessarily outcrop inside the SFR model domain. It should be noted that there exists a methodological discrepancy between the confidence in modelling steep and sub-horizontal zones; owing to geometrical issues, linking a sub-horizontal deformation zone borehole intercept to a potential outcrop is highly uncertain (i.e. a small uncertainty in zone orientation translates into a large uncertainty of the outcrop position).

The original SKB methodology (Rhén et al. 2003) (Section 2.1) was insufficient for characterising the upper c. 100 to 150 m bedrock in the Forsmark SDM (Follin et al. 2007a). Extraordinary well yields and rapid, large-scale hydraulic responses, lead to describing the upper bedrock in SDM-Site Forsmark as a Shallow Bedrock Aquifer (SBA). Detailed fracture flow data were unavailable in the upper 100 m due to borehole casing, as it was not considered necessary for the deep repository. To represent its characteristics in a numerical model, Follin et al. (2007a) introduced so-called deterministic *sheet joints* (Figure 2-4), which fall somewhere between the conceptual units HRD and HCD (cf. Figure 2-1). Sheet joints are large-scale, sub-horizontal, and highly conductive geologic structures (Follin et al. 2007c), and limited to the upper c. 100–150 m of the bedrock (i.e. similar depth interval as the existing SFR; Figure 2-4b). These sheet joints were assumed to undulate with topography and therefore, they were geometrically represented as three vertical offsets of the DEM. Based on interference-test data, the sheet joints in the Forsmark SDM were modelled to terminate against the Singö deformation zone (Figure 2-4a).

In spite of their anomalous hydrogeological character, sheet joints are not necessarily identifiable based on geological character (cf. deformation zone characteristics). They are not assumed to have formed solely from tectonic deformation; it is assumed that glacial loading/unloading, stress-relief and/or weathering processes are also involved. Owing to these circumstances, a key aspect in the SFR extension project has been to examine the potential existence of similar features north of the Singö deformation zone (Section 1.3). In fact, no evidence of sheet joints have been observed in the SFR data set, at least not of the same dignity as observed in SDM-Site Forsmark. On the other hand data analysis clearly demonstrates the hydraulic domination of horizontal to gently dipping fractures in the upper bedrock inside the SFR Regional domain. Therefore, so-called “SBA-structures”, have been deterministically modelled in the SFR Regional domain, based on hydrogeological interpretations (Section 6.4; details given in Appendixes B and H). An SBA-structure does not represent a single

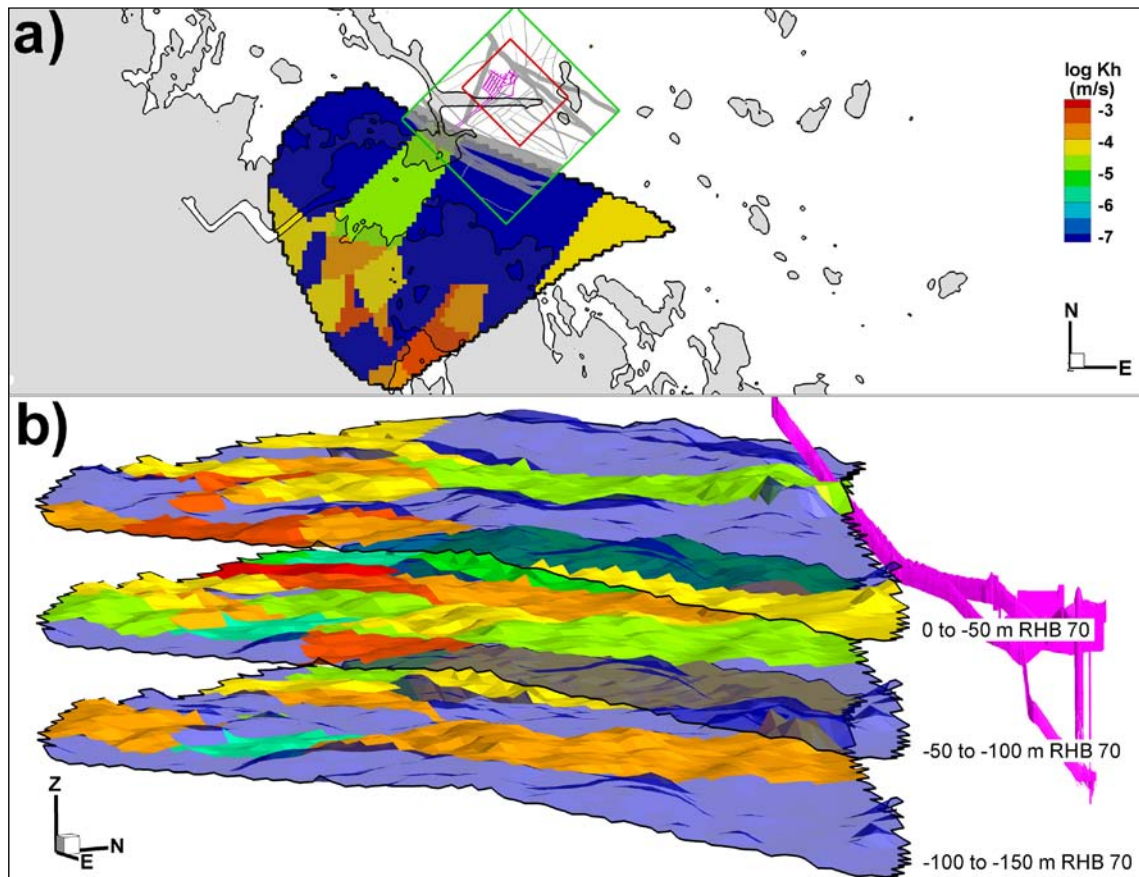


**Figure 2-4.** Sheet joints in the Forsmark SDM; a) top-view showing the horizontal extent of SBA-structures in relation to the SFR model domains (green = regional domain, red = local domain, pink = SFR) and b) side-view along the termination against Singö deformation zone. The conductivity value  $10^{-7}$  m/s is shown translucent. Vertical exaggeration factor = 10.

geological feature, but a hydraulically connected network of horizontal to gently dipping fractures; it is therefore envisaged as highly heterogeneous and not necessarily hydraulically connected over its entire modelled geometry. The term *SBA-structure* is introduced to relate to the previous experiences in the Forsmark area, but to highlight the fact that these structures are of considerably lesser dignity than the sheet joints modelled in SDM-Site Forsmark.

### 2.3.3 Basic characteristics of single-hole tests

The hydraulic parameterisation of the deformation zones and fracture domains is based on single-hole hydraulic tests. Essentially three different data sources are used in this study:

1. The old data set from the existing SFR (various short-term, double-packer hydraulic tests from the initial investigations and SFR construction, 1980 to 1986),
2. selected data from the nearby Site Investigation Forsmark (KFM11A, HFM34, and HFM35, in the vicinity of the Singö deformation zone), and
3. the new SFR data set (from the SFR extension investigation, 2008 to 2009).

It is not straightforward how these three data types should be combined; they reflect different entities (e.g. connectivity aspects in Figure 2-5), are of different quality, and cover different parts of the SFR model domain (Figure 1-4). Essential weaknesses of the old data are the deficiency of oriented fracture data, as well as, the confidence in data quality. The old data set is primarily used for conceptual understanding and as complementary data for the deformation zone parameterisation in the SFR near-field.



The more recent data sets (from Forsmark and the SFR extension investigations) include high-resolution difference flow-logging tests (PFL-f; see Section 4.3.2) in core-drilled boreholes and flow-logging pumping tests (HTHB) in percussion-drilled boreholes. The lower measurement limits of the PFL-f method are superior to that of the HTHB test method, but it cannot be used in the percussion-drilled boreholes for technical reasons.

The constituent parameters measured during the hydraulic tests are the flow rate,  $Q$ , and the pressure,  $p$ . Since these are dependent, the parameter studied is the specific capacity,  $Q/\Delta p$ , which has the same dimension as transmissivity,  $T$ . The measured specific capacity in fractured rock depends on several important aspects (cases A–F in Figure 2-5):

- $Q_{limit}$ ; the lower measurement limit of the test method.
- $T_{bh}$ ; the transmissivity of the tested fracture intersecting the borehole.  $T_{bh}$  can be affected during the drilling operations. For instance, the fracture can be clogged (positive skin) or stimulated (negative skin).
- $C$ ; the connectivity of the tested fracture to other fractures away from the borehole. Some fractures are isolated, or are a part of an isolated cluster of fractures. Others are well connected and a part of the overall hydrogeological system.
- $T/S$ ; the hydraulic diffusivity of the fracture system within the radius of influence.
- $t$ ; the duration of the hydraulic testing, i.e. the test time.
- $\Delta L$ ; the length of the test interval (test section).

The test duration,  $t$ , and the diffusivity,  $T/S$ , control the radius of influence of the test (its variability is indicated by dashed arrow in Figure 2-5). The measured  $Q/\Delta p$  declines if the radius of influence reaches the end of a compartmentalised network (cases A–C in Figure 2-5). Fractures connected to the global hydrogeological system (or a pseudo constant-head boundary, “CHB”; cases D–F in Figure 2-5) provide sustained flow, and are referred to as *continuously flowing fractures* detectable by the PFL device.

The PFL-f method uses a narrow test interval and a long test time. Thus, the resolution of the PFL-f method is sufficient to study the specific capacity of individual fractures and the method is used to evaluate the frequency of *continuously flowing fractures* (e.g. situations like cases D–F in Figure 2-5); however, isolated fractures/clusters or “hydraulic chokes” such as in cases A–C are

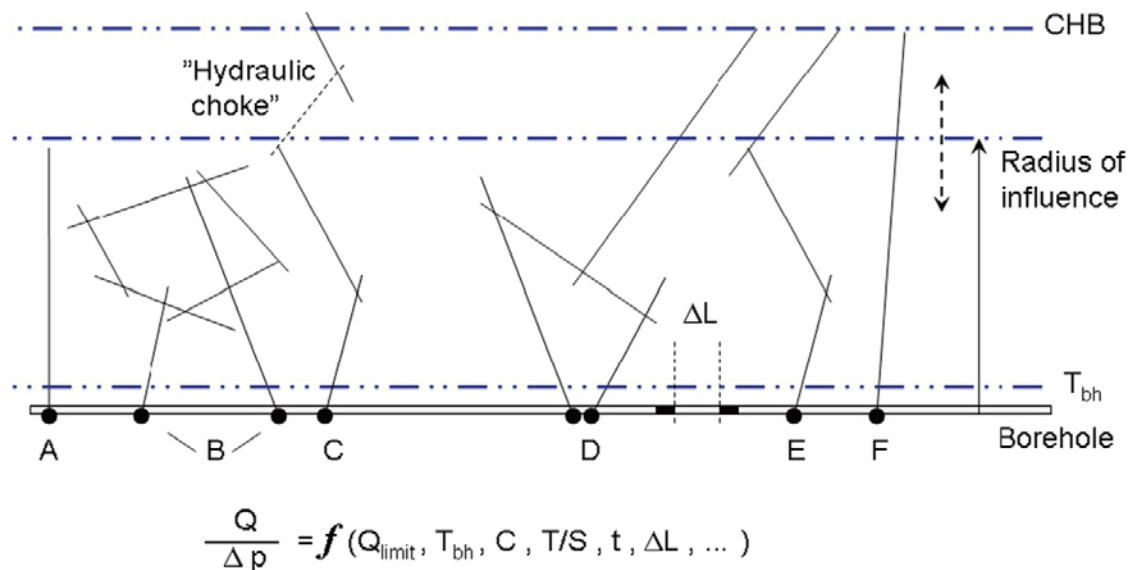


**Figure 2-5.** Cartoon showing a borehole with different cases of fracture connectivity; cases A–C represent compartmentalised fracture networks, while cases D–F represent connectivity to the global hydrogeological system (indicated by a constant head boundary “CHB”, suggesting a pseudo steady state flow regime at long test times). The cartoon is rotated 90° to improve the readability. (Figure 2-5 in Follin 2008.)

not detected in the PFL-f method. The term *apparent transmissivity* is used for PFL-f to emphasise that the measured specific capacity ( $Q/\Delta p$ ) does not necessarily reflect the transmissivity of the fracture specifically intersected by the borehole, but may instead be constrained by upstream hydraulic chokes.

In contrast, the double-packer data of the old data set have a wide test interval and a short duration and reflects the summed fracture transmissivity of *all* cases A–F. The detection limit in the old data set is generally  $5 \times 10^{-8} \text{ m}^2/\text{s}$  and most test intervals are 3 m. The lower threshold value of the PFL-f investigations at SFR ranges from  $10^{-10}$  to  $10^{-8} \text{ m}^2/\text{s}$  (Figure 5-5b).

### 2.3.4 Hydraulic Conductor Domain (HCD) model

The SFR deformation zone model is a sub-volume of the regional Forsmark structural model, and it is based on the conceptual geologic understanding gained from the Forsmark SDM (Stephens et al. 2007). Previous structural models of SFR (Carlsson et al. 1985, 1986) employed deformation zone definitions that differ considerably from the current SKB methodology; for example brittle zones were earlier based on hydrogeology and the frequency of Open fractures. The recent geologic SFR model v. 1.0 (Curtis et al. 2011) is based, to the extent possible, on the SHI borehole intercepts that also account for other characteristics, such as the frequency of Sealed fractures and hydrothermal rock alteration. However, all data required for SHI definitions were not available in the old boreholes. A number of boreholes of the old data set were re-interpreted, to define intercepts as close as possible SHI standard. Based on the information at hand, it was not considered meaningful to re-interpret all boreholes of the old data set. Two terms are used to distinguish the confidence level of intercepts, namely *Target borehole intercept* and *Geometrical borehole intercept* (Figure 2-6).

A *target intercept* is the geologically interpreted position of a deformation zone in an individual borehole (violet cylinders; Figure 2-6). In general, target intercepts conform to the geological SHI possible deformation zone intercepts but, in certain cases, adjustments have been made on the basis of other information outside the specific borehole.

A *geometrical intercept* is the modelled intercept between a zone and a borehole as they exist in the RVS model (pink shade; Figure 2-6). The geometrical intercepts were used to estimate modelled zone thickness, a method that differs somewhat from that used in the Forsmark site investigation (Stephens et al. 2007). The method used here has a tendency to provide a slightly more conservative estimate of the thickness of a zone.

The hydraulic parameterisation of deformation zones is fairly straightforward. All fracture data and transmissivity data between the upper and lower bounds of a deformation zone interval, as determined in the geological Single-Hole Interpretation (target borehole intercept), are integrated to form a single feature with a lumped in-plane transmissivity value for that interval. For simplicity, this in-plane transmissivity is *assumed* to be isotropic. Generally, little is known about its orthogonal effective hydraulic conductivity (i.e. controlling the flow across the structure). This approach implies that the hydraulic thickness is assumed to be equal to the geological. Multiple borehole intercepts of a given deformation zone provide insight into the in-plane heterogeneity in the effective transmissivity of the zone. The assumptions are illustrated in Figure 2-7 and Figure 2-8.

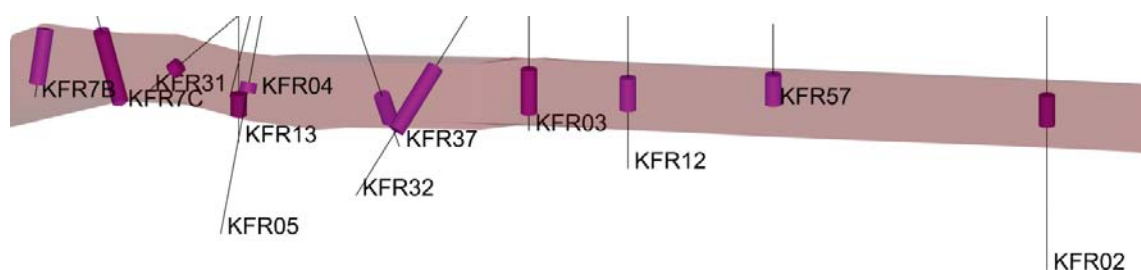


**Figure 2-6.** Side view of ZFM871 looking down dip to the south (modelled thickness of 20 m). Target intercepts in individual boreholes (violet cylinders) are equivalent of SHI PDZ sections. The modelled zone thickness in RVS (pink shade) is based on the maximum SHI thickness (KFR7C and KFR37). Geometrical intercepts are intersection of modelled zone thickness in RVS (pink shade).

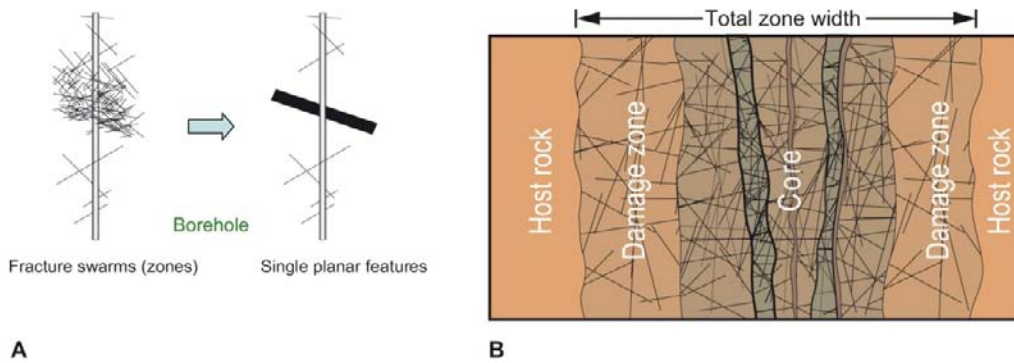


**Figure 2-7.** *A: The fracture data between the upper and lower bounds of a deformation zone interval are lumped together to form a single planar feature. In the same fashion, all hydraulic data in the interval are also lumped together in the hydrogeological modelling, to form a single in-plane transmissivity value. (Figure 2-3 in Follin et al. 2007b.). B: Cartoon of the typical fracturing associated with faults. The major deformation zones at SFR display various degrees of the fracturing shown in this illustration. (Modified after Figure 2-1 in Munier et al. 2003.)*

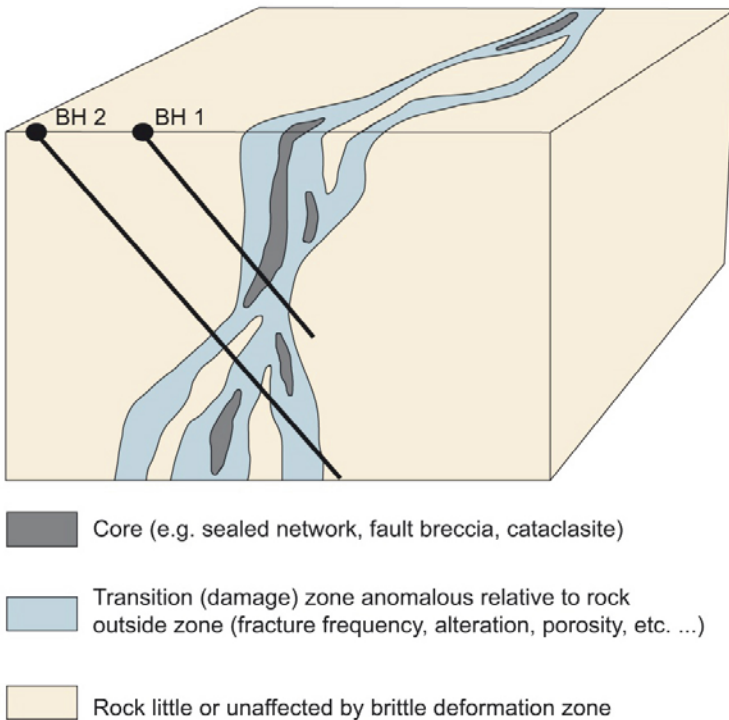


**Figure 2-8.** *Illustration of the typical fracturing associated with faults. The major deformation zones at SFR display various degrees of the fracturing shown in this illustration. The heterogeneity in the in-plane transmissivity of a given deformation zone was studied by means of single-hole tests at different locations in that zone. (Modified after Figure 5-1 in Stephens et al. 2007.)*

### 2.3.5 Hydraulic Rock mass Domain (HRD) model

The hydraulic description of the HRD between the deformation zones is focused on the flowing fracture frequency and the specific capacity,  $Q/\Delta p$  (or  $Q/s$ , where  $Q$  denotes flow rate and  $s$  denotes “drawdown”), of continuously flowing fractures. This means that the connected fracture network situations such as cases D–F in Figure 2-5 were regarded as more important for the hydrogeological DFN modelling and the groundwater flow modelling in the SDM than disconnected (compartmentalised) network situations such as cases A–C. The role of compartmentalised networks, if any, needs to be addressed in the safety assessment.

It is important to recollect what is actually measured with the PFL-f tests. For each PFL-f transmissivity value identified, the change in flux (inflow) and head (drawdown) after several days of pumping relative to conditions prior to pumping are calculated. The specific capacity,  $Q/\Delta p$ , has the same dimension as transmissivity,  $T$ , and a transmissivity value is interpreted for each PFL-f test conducted based on Thiem's equation and an assumed value of the radius of influence to borehole radius ratio ( $R_0/r_w$ ) = 500 (see equations in e.g. Hurmerinta and Väisäsvaara 2009). In reality, the radius of influence is expected to depend on fracture transmissivity (or more precisely, hydraulic diffusivity). The choice of 500 reflects that tests are performed over several days, and hence should represent an effective transmissivity of the fracture intersected, and possibly upstream parts of the network, but the choice of 500 is otherwise arbitrary.

Consequently, the interpreted transmissivity values should not be viewed as necessarily specific to the fracture intersected by the borehole. They are more indicative of the effective transmissivity over a larger scale (e.g. see discussion on upstream choking in Öhman and Follin 2010b). This remark influences the way the PFL-f data were used in the hydrogeological DFN modelling. Before carrying out the regional groundwater flow simulations, the hydrogeological DFN model must be calibrated. A preliminary version of the hydrogeological DFN model for SFR is reported in Öhman and Follin (2010b) and the final version is presented in Section 6.3 (see details in Appendix G).

The finest scale of heterogeneity in fracture transmissivity studied is the variability in transmissivity between fractures of different sizes. The heterogeneity in fracture transmissivity within individual fractures is not modelled due to lack of data to support this scale of modelling. That is, individual fractures were assumed to be homogeneous.

Furthermore, it is assumed that the groundwater flow and solute transport within the network of fractures can be represented by an equivalent continuous porous medium (ECPM) by upscaling to an appropriate grid size, see Figure 2-9. Since each ECPM model is based on a particular underlying stochastic realisation, the ECPM models are also stochastic.

### 2.3.6 Hydraulic Soil Domain (HSD) model

A detailed geometrical description of the near-surface system in the Forsmark area (including SFR) was developed as part of the Forsmark SDM (Hedenström and Sohlenius 2008, Hedenström et al. 2008). Effective hydraulic properties have been calibrated for the different regolith layers (i.e. Quaternary deposits, artificial filling material, and weathered rock) (Bosson et al. 2008). The sediments overlying SFR possibly control the hydraulic contact between the shallow bedrock and the sea. Data evaluation is therefore made with respect to sediment coverage, thickness and effective properties (Section 4.7).

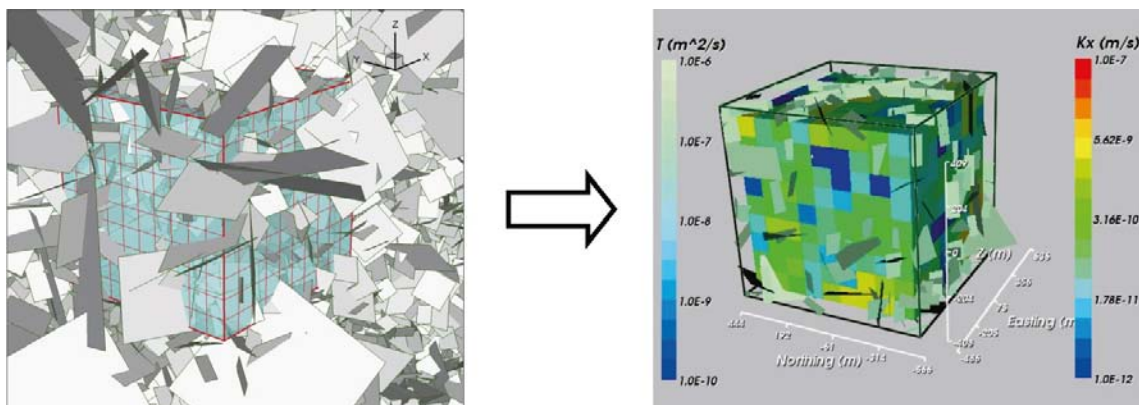


**Figure 2-9.** Illustration showing the upscaling approach from a DFN to an ECPM. (Figure 2-4 in Follin et al. 2007b.)

### 3 Geological conditions

Local deformation zone and rock domain sub-models have been developed within the SFR extension investigation. No specific GeoDFN model, Fracture domain model, or Regolith model was conducted as part of the SFR project.

#### 3.1 Regolith geology

The SFR Regional domain is mainly covered by Sea. The sediments, i.e. Hydraulic Soil Domain (HSD), potentially have an important role in controlling the hydraulic connection between the Sea and the underlying rock mass. The term “regolith” is used to include various types of loose material covering the solid bedrock, such as peat, weathered rock and artificial filling material, (e.g. the man-made SFR Pier). Most of the regolith in the Forsmark area was deposited during the Quaternary period and is therefore referred to as Quaternary deposits. Most of these Quaternary deposits were probably deposited during or after the latest deglaciation.

During the Forsmark Site Investigation programme, a conceptual model of the distribution of Quaternary deposits was developed, which covers the Forsmark inland as well as marine sediments above SFR (Hedenström et al. 2008). The conceptual model consists of nine layers (L1–L3, Z1–Z6; see Figure 3-1 and Table 3-1). Not all layers exist everywhere, and the spatially variable thickness was modelled with a horizontal spatial resolution of 20×20 m. The total thickness of the Quaternary deposits varies from less than a decimetre to a maximum of 42 m (Hedenström et al. 2008).

**Table 3-1. Names and definition of Quaternary deposits layers. (Modified from Hedenström et al. 2008.)**

Layer	Description and comments
L1	Layer consisting of different kinds of gyttja/mud/clay or peat. Is interpolated from input data, thickness will therefore vary.
L2	Layer consisting of sand and gravel. Is interpolated from input data, thickness will therefore vary.
L3	Layer consisting of different clay (glacial and postglacial). Is interpolated from input data, thickness will therefore vary.
Z1	Surface affected layer present all over the model, except where peat is found and under lakes with lenses. Thickness is 0.10 m on bedrock outcrops, 0.60 m elsewhere. If total regolith thickness is less than 0.60 m, Z1 will have the same thickness as the total, i.e. in those areas only Z1 will exist.
Z2	Surface layer consisting of peat. Zero thickness in the sea. Always followed by Z3.
Z3	Middle layer of sediments. Only found where surface layers are other than till, clay or peat.
Z4a	Middle layer consisting of postglacial clay. Always followed by Z4b.
Z4b	Middle layer of glacial clay.
Z5	Corresponds to a layer of till. No min or max range. The bottom of layer Z5 corresponds to the bedrock surface.
Z6	Upper part of the bedrock. Fractured rock. Constant thickness of 0.5 m. Calculated as an offset from Z5.

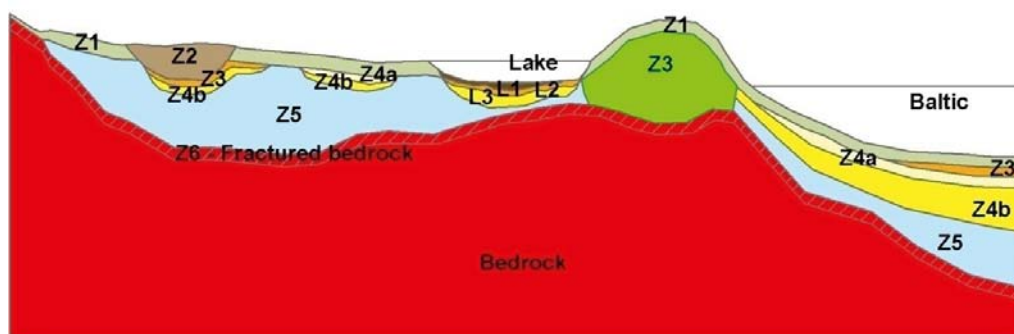


**Figure 3-1.** Conceptual model for the layering of Quaternary deposits. The different layers are described in Table 3-1.

Effective, anisotropic conductivity values have been calibrated for the different regolith layers by means of surface hydrological modelling of surface hydrologic data in the Forsmark inland (Bosson et al. 2008). Although this has not been explicitly confirmed, it is assumed that the calibrated effective parameters are also valid for offshore marine sediments at SFR. These are discussed in Section 4.7.

### 3.2 Bedrock geology

While the current project has increased the detailed knowledge concerning the geology in the SFR regional model area, no new data or interpretations have been forthcoming that affect the earlier established interpretation of the regional geological setting as described by Söderbäck (2008). The SFR area is situated within a high-strain belt that forms the north-easterly margin to the so-called Forsmark tectonic lens (SKB 2008a). The north-western part of this tectonic lens is the target area for hosting the potential repository for spent nuclear fuel. The rock volume that includes the SFR underground facility lies between two regional deformation zones of focused ductile and brittle strain, the Singö deformation zone (ZFMWNW0001) and zone ZFMNW0805A. The rock types, their grouping and temporal relationship in this lens are virtually identical to that of the rocks in the adjacent Forsmark tectonic lens, but they are generally affected by a higher degree of ductile strain and a well-defined WNW-ESE to NW-SE structural trend.

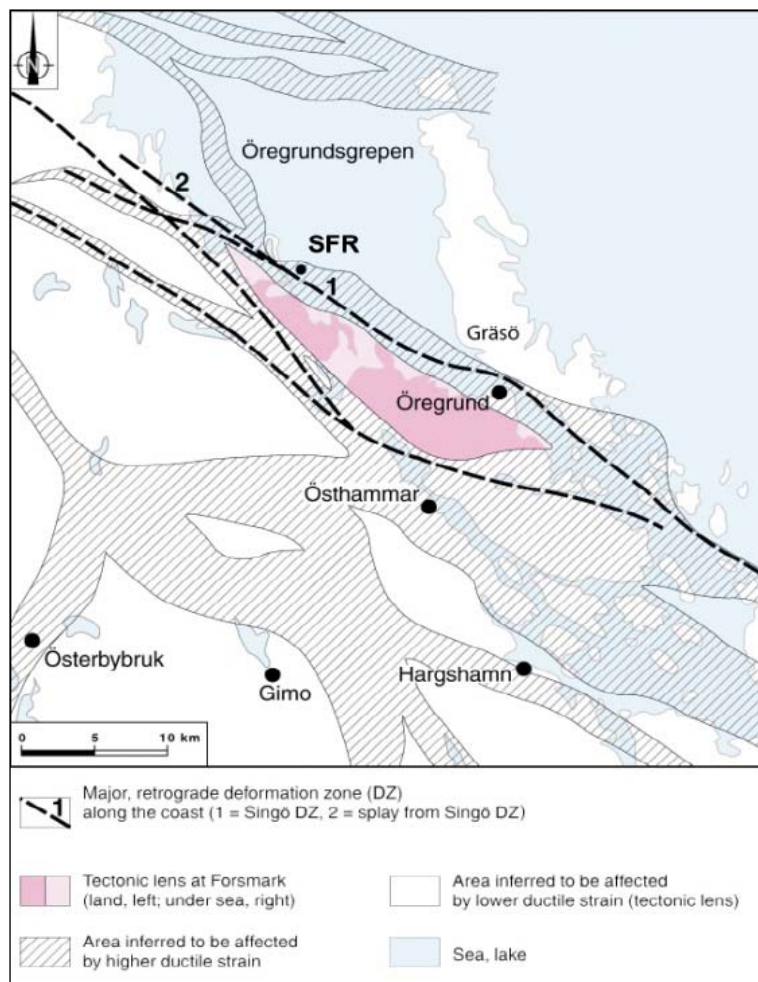


**Figure 3-2.** Map showing the structural framework in the Forsmark area with ductile high-strain belts that anastomose around tectonic lenses of lower ductile strain. The major retrograde deformation zones surrounding the Forsmark tectonic lens are also shown. Modified after Stephens et al. (2007).

### 3.2.1 Rock domain model

A model for the three-dimensional distribution of rock domains in the local SFR model volume was established by Curtis et al. (2011). The local SFR domain is divided into of four rock domains (Figure 3-3). The term rock domain is used here according to the general guidelines in Munier et al. (2003). More specifically, individual domains have been defined on the basis of an integration of the composition, grain-size, heterogeneity and character of ductile deformation in various rock units, as employed in the Forsmark site investigation (Stephens et al. 2007).

Rock domain RFR01 is a major fold structure dominated by pegmatitic granite and pegmatite (Figure 3-3). Another important constituent is fine- to finely medium-grained metagranodiorite (to granite), which is affected by amphibolites-facies metamorphism. The domain is characterized by a relatively high degree of homogeneity compared to RFR02. Other subordinate rock types occupy approximately only 10% of the mapped borehole length. The boundary between RFR01 and RFR02 is defined by inferred fold axes for the domain boundary mainly based on stretching lineation data from all boreholes included within RFR01 with a fold axis orientation of approximately  $090^{\circ}/70^{\circ}$ .

Rock domain RFR02 incorporates all subsurface geological data in the local SFR model volume that does not occur in RFR01. It is far more heterogeneous relative to RFR01. The dominant rock type is the fine- to finely medium-grained metagranodiorite (to granite), which is commonly indistinguishable from the felsic to intermediate metavolcanic rock. However, it needs to be emphasized that there is a considerable uncertainty in the exact estimate of the two rock types. The subordinate rock types are dominated by pegmatitic granite and pegmatite, younger granite, amphibolite and aplitic metagranite.

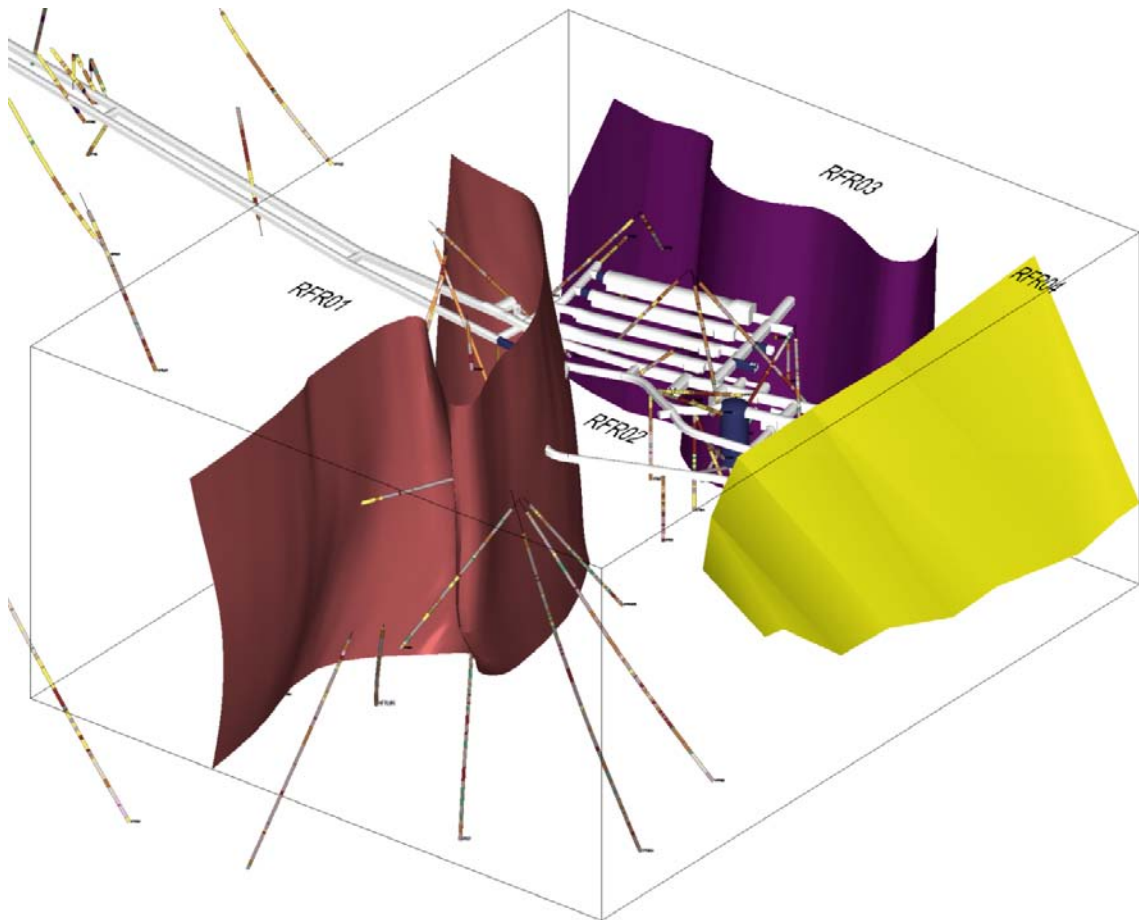


**Figure 3-3.** Three dimensional model view from east showing the boundaries between the four rock domains within the local SFR model volume relative to the borehole geology and the geometry of the SFR underground facility. The colour choice is only for legibility, where boundary RFR01–RFR02 is pinkish brown, RFR02–RFR03 violet and RFR03–RFR04 yellow.

There is little data to characterize RFR03. The low magnetic belt that forms the surface expression of RFR03 has been treated as a composite result of oxidation related to brittle structures and volumes dominated by pegmatitic granite and pegmatite. The character of the boundary between rock domains RFR02 and RFR03 (Figure 3-3) is unclear but, in a similar way to RFR01, it was modelled so as to define the core of a major fold structure, where the fold axes are parallel with the mineral stretching lineation. The geometrical extension towards the east and south-east of this domain remains uncertain in the absence of geological data.

Geological data from RFR04 are completely lacking and there are no other information available than the magnetic total field for the location and orientation of the boundary between RFR02 and RFR04. For this reason and in order to simplify future interaction between both the SFR local model and the rock domain model for Forsmark, it was decided to follow the contact between RFM021 and RFM033, as defined in the regional rock domain model stage 2.2 (Stephens et al. 2007). On the basis of the magnetic total field data, the boundary is tectonic, at least in its north-western part.

### 3.2.2 Deformation zone model

A deformation zone is a two-dimensional structure, along which there is a concentration of brittle, ductile, or combined brittle and ductile deformation. The boundaries of these structures are approximate. A conceptual model of the formation of deformation zones was developed during the Site Investigation Forsmark (Figure 3-4) (Stephens et al. 2007). In this model, four orientation sets of deformation zones were identified based on their geological character. Three of the deformation zone sets are steep to vertical: WNW to NW, N-S to NNW, and NNE to ENE, while the fourth set is gently dipping. This conceptual model, as well as the established methodologies, applies also to the SFR deformation zone modelling (Curtis et al. 2011). The character of different sets of SFR is summarised in Appendix C.

The deformation zone model is divided into a local and a regional model (Figure 3-5). The local model contains all modelled deformation zones with ground-surface trace lengths exceeding 300 m, while the regional model only contains zones with trace lengths exceeding 1,000 m. The combined regional and local model, containing all the modelled zones, is shown in Figure 3-5. There are altogether 40 deterministically modelled deformation zones. These are referred to as ZFMxxxx, where xxxx is an identification label which indicates the orientation of the zone (Figure 3-5). There are also 31 so-called “Unresolved Possible Deformation Zones” (PDZs), i.e. borehole intervals with deformation zone properties that have not been possible to link to a surface lineament. Based on the length of borehole intercepts, these have been judged to be smaller than the resolution level of the Geologic model v. 1.0, and hence they were not included in the deterministic model (details given in Appendix 12 in Curtis et al. 2011). Out of the 31 Unresolved PDZs, 17 are from old data set where fracture orientation is unavailable; hence no orientation analysis can be made. Among the 14 Unresolved PDZs in the new data set, the orientation could be evaluated for nine, based on fracture analysis. Results indicate that five are sub-horizontal and the other four are steeply dipping. Orientation estimation based on additional support from hydraulic data (PFL-f data) suggests that 10 out of 12 Unresolved PDZs are horizontal to gently dipping (see Table A-2 and Figure A-3).

A tectonic *Central block* is located between the dominant regional deformation zones ZFMWNW0001 and ZFMNW0805A (Figure 3-5). In the south, the Central block is bounded by a belt of WNW to NW-striking zones: ZFMWNW0001, ZFMWNW0813, ZFMWNW3259, ZFMNW0002 and, to some extent, ZFMWNW1035; this is referred to as the *Southern boundary belt* (Figure 3-5). In the north, the Central block is bounded by a secondary deformation belt (ZFMNW0805A and its splay ZFMNW0805B) with similar orientation and character as the Singö belt, but is much smaller (Figure 3-5); this is referred to as the *Northern boundary belt*. The terms *Central block* and its bounding *Northern* and *Southern boundary belts* are highly relevant in hydraulic data interpretations; they are therefore frequently used for reference in Chapters 4 and 5 (see Table 1-3). However, the hydrogeologic data analyses relate to conductive structures that act as positive flow boundaries and hence, the terms are used *in a wider sense*. Both the Northern boundary belt and the nearby ZFMNNW1034 are related to a large-scale, gradual influence on rock mass inside the model domain (Figure 3-5).



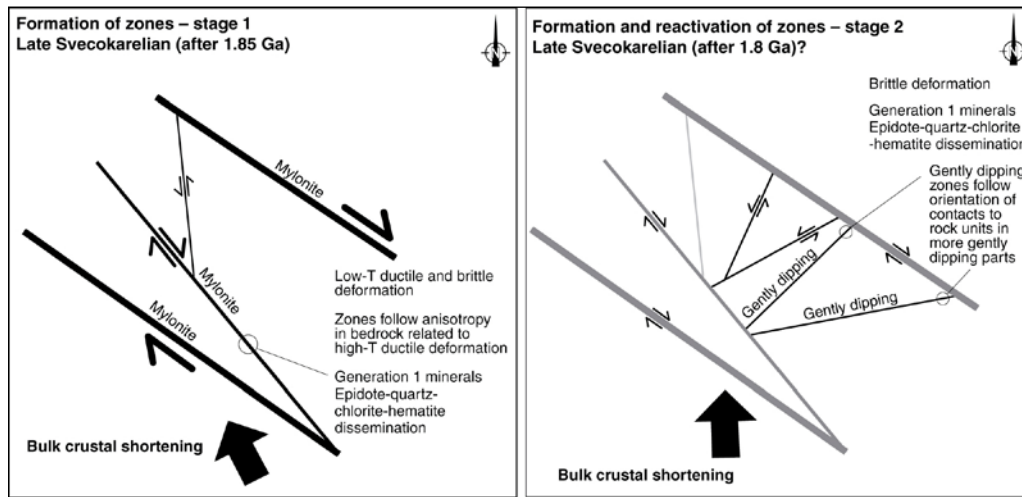


**Figure 3-4.** Two-dimensional cartoon illustrating the regional-scale geodynamics during the initial development of the master, steeply dipping WNW-ESE and NW-SE zones and the subordinate sets of brittle deformation zones in response to late stage Svecof Karelian tectonic activity. After SKB 2008a.

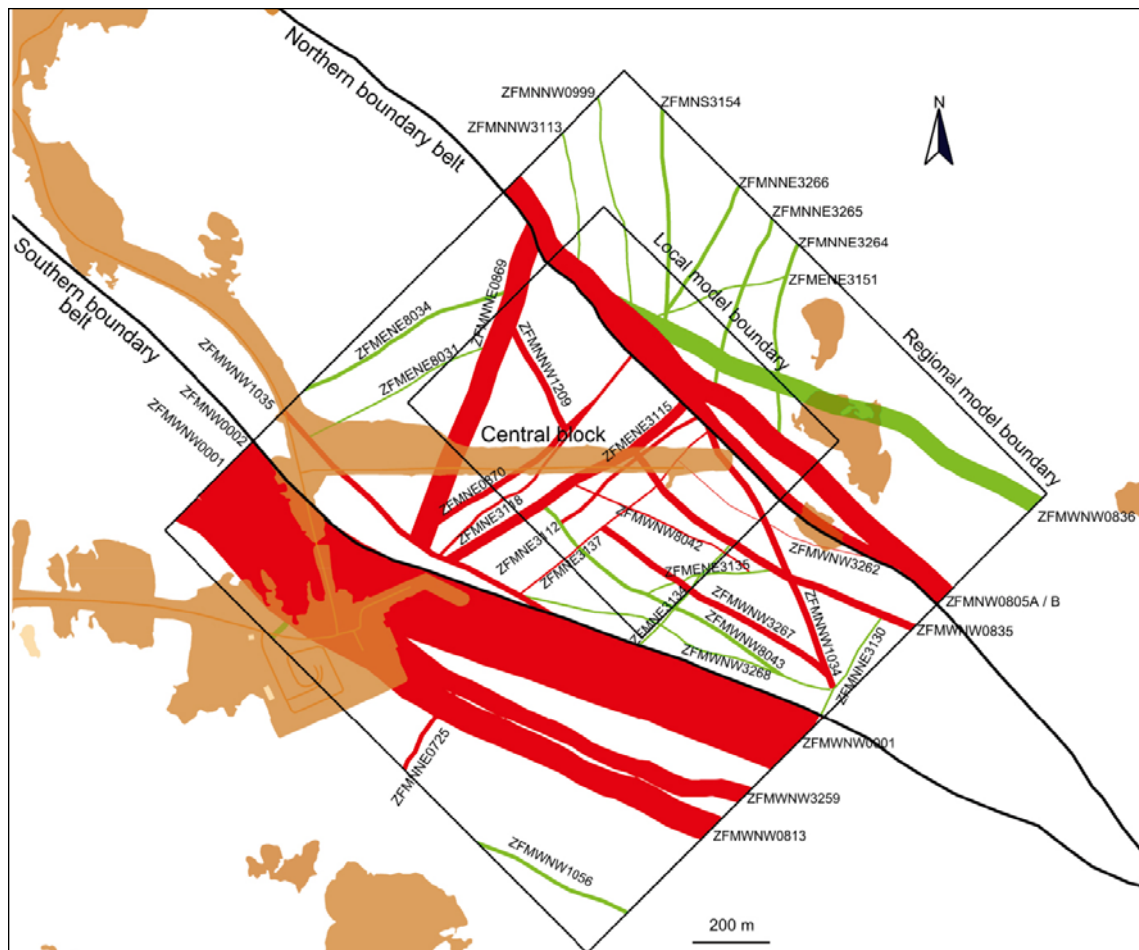


**Figure 3-5.** Intersection at the current ground surface of deformation zone traces of all sizes inside the regional model area i.e. a combined model version. The regional deformation zones ZFMWNW0001 and ZFMNW0805A, along with their major splays, form the Southern and Northern belt boundaries of the SFR tectonic Central block. Confidence in existence: high=red, medium=green.

There is a striking difference between the north-western and the south-eastern parts of the Central block; the NNW to NW deformation zones are abundant in the South-eastern part, but none of these are matched in SFR tunnel mapping. Perhaps the frequency of NNW to NW zones is related to the wedging between the two boundary belts in the South-eastern part. However, it may – at least in part – be an artefact related to data gaps and data quality. Uncertainty and the effects of magnetic disturbances on lineament interpretation are discussed in Appendix C.

None of the gently dipping deformation zones are modelled to outcrop inside the SFR Regional domain (i.e. including ZFM871, formerly referred to as Zone H2); they lack ground traces and are therefore not visible in Figure 3-5. They are instead shown in Appendix C. The only high confidence gently dipping deformation zone, ZFM871, is located just below SFR and is modelled to terminate against three steeply dipping deformation zones: ZFMNNE0869, ZFMNW0805A/B, and ZFMENE3115. The geologic modelling uncertainty to its terminations are discussed in Curtis et al. (2011, Appendix 11).

ZFM871 is interpreted to be a complex structure with a “stepped geometry” of hydraulic thickness varying from 2 to 20 m. It consists of groups of parallel, smaller hydraulically conductive structures that are separated by ordinarily fractured rock. The zone is associated with lenses of weathered and highly fractured rock, along with frequent clay-filled joints (Christiansson 1986).

### 3.2.3 Fracture domain model

No fracture domain model has been developed for the SFR model domain.

## 3.3 Stress regime

High stress levels have been found in the upper 35 m of the rock mass in Forsmark (about 30 MPa). Early overcoring measurements at SFR have lower magnitudes in the depth interval 40 to 140 m, possibly indicating lower stress levels east of the Singö deformation zone, at least in the shallow rock (Sjöberg et al. 2005). KFR27 has average magnitudes  $\sigma_1 \approx 17$  MPa,  $\sigma_2 \approx 9$  MPa,  $\sigma_3 \approx 2.5$  MPa ( $\sigma_3$  tends to be vertical). KFR51 and KFR52 indicate considerably lower magnitudes, but their representativeness is uncertain as the boreholes are sub-horizontal, drilled from the SFR tunnel. The major horizontal principal component has an orientation of  $145^\circ$  (SKB 2008a), but appears to be locally more parallel to ZFMWNW0001 at SFR, at least in KFR27 (Figure 3-6). The stress field is known to change in the vicinity of large zones. The minimum principal stress is vertical; tensile stresses have been found in Forsmark even at larger depths (c. –250 m RHB 70). The anisotropic ratio declines with depth, as stress magnitudes grow larger with overburden load.

In Forsmark, the stress anisotropy was found to correlate well with hydraulic anisotropy, both in deformation zones and the fracture network in HRD, such that the largest transmissivities are orientated orthogonal to the minimum principal stress (Glamheden et al. 2007, Follin 2008). The same correlations have been found in SFR, where the gently dipping ZFM871 (orthogonal to  $\sigma_3$ ) and steep WNW-striking deformation zones (orthogonal to  $\sigma_2$ ) are more transmissive (Öhman and Follin 2010a). The transmissivity correlation has been found to hold at the fracture scale; steep fractures are predominantly Sealed, while horizontal and gently dipping fractures are predominantly Open (Figure 4-9). The correlation is accentuated in PFL-f data: Gently dipping, and NW-striking fractures are considerably more transmissive than steep NE to EW-striking (Öhman and Follin 2010b) (see also Figure 4-15). Transmissivity also decreases with depth, which is partly explained by the increasing stress magnitudes with overburden weight.

The stress history of glacial loading/unloading cycles has created sheet joints in the shallow rock at Forsmark: extensive, highly transmissive, horizontal structures (Figure 3-7). The sheet joints have been observed down to c. 40 m depth and are described as heterogeneous, with channelized flow paths that have eroded through glaciofluvial sediment fill. Based on a large borehole data set the upper 100–150 m bedrock inside the Tectonic lens at Forsmark has been interpreted as a Shallow Bedrock Aquifer (SBA) with extraordinary high horizontal transmissivity (Figure 2-4). The current understanding is that the extreme SBA characteristics are confined to the Tectonic lens at Forsmark

(assumed to terminate at ZFMWNW0001; Figure 2-4). However, the SFR modelling domain has been exposed to the same glaciation cycles, and therefore the experiences from Forsmark indicate that the shallow bedrock at SFR is potentially also dominated by a horizontal flow pattern, even if less pronounced. Based on hydraulic connections, sub-horizontal stress-relief structures at an elevation of  $-25$  m RHB 70 were proposed in early structural models of SFR (e.g. Zone H1 and H3) (Carlsson et al. 1985).

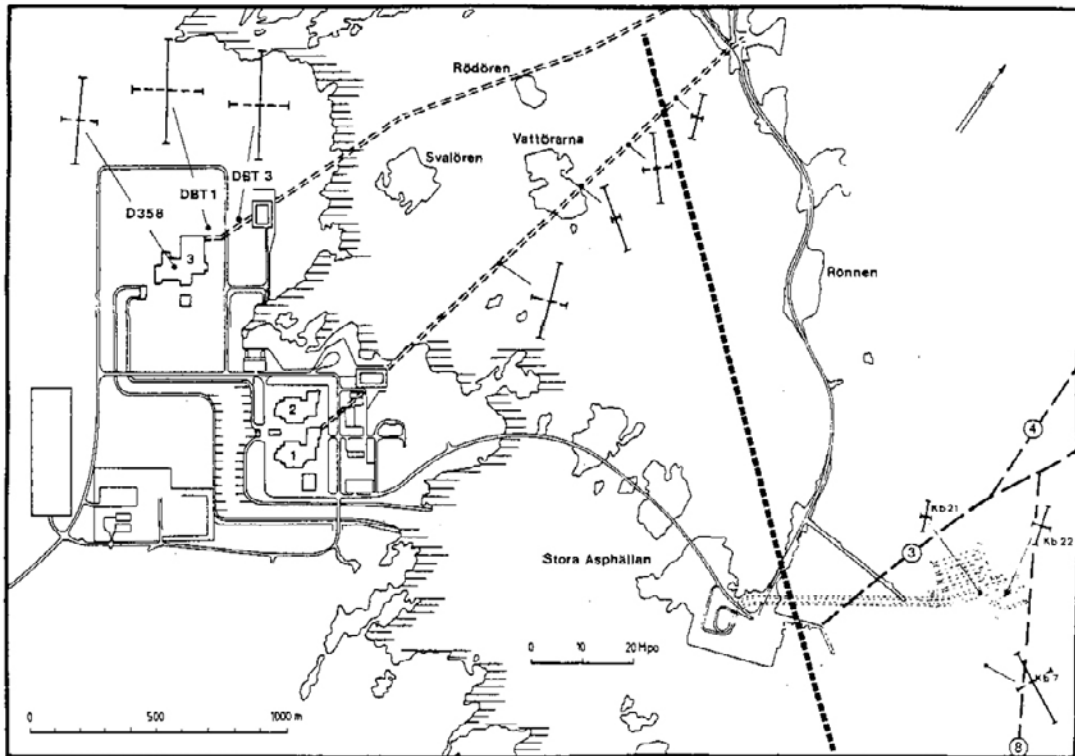


**Figure 3-6.** Stress measurements at SFR; KFR27 (denoted Kb7) is located in the middle of the Local model domain, KFR51 and KFR52 (denoted Kb21 and Kb22) located in the vicinity of the Silo. Taken from Carlsson et al. (1986).



**Figure 3-7.** The canal between the nuclear power reactors and the Baltic Sea exposing extensive undulating sheet joints. Taken from Carlsson och Christiansson (2007). Photograph by G Hansson.

## 4 Evaluation of primary data

Essentially three different data sources are used in this study (Figure 1-4):

1. The old data set from the existing SFR (from the initial investigations and SFR construction, 1980 to 1986),
2. data and the Site-Descriptive Model from the nearby Site Investigation Forsmark (2006), and
3. the new SFR data set (from the SFR extension investigation, 2008 to 2009)

It is not straightforward how these three data sources should be combined; they are of different quality and cover different parts of the model domain. Within the recent SFR extension project, only one borehole was drilled from the existing SFR (KFR105; Figure 1-4); the SFR facility is classified as a nuclear facility with safety regulations that restricts its accessibility (see details in Nilsson 2009).

Essential weaknesses of the old data set are the deficiency of oriented fracture data, as well as, the confidence in data quality. The benefit of the old data set is that it provides the additional information on the SFR near-field that is not covered by the new data set. The old data set is primarily used for conceptual understanding of the site and the parameterisation of deformation zones.

The SFR domain is a sub-unit of the Forsmark Regional model domain; therefore the conceptual understanding of the SFR hydrogeological system is intimately connected to the SDM-Site Forsmark (Follin 2008). The Forsmark boreholes KFM11A, HFM34, and HFM35 are relevant for SFR modelling; their location in the Southern boundary belt provides hydrogeological data useful for conceptual modelling and the parameterisation of deformation zones, but the data are not judged representative for the characterisation of HRD.

In contrast to the old data set, the data set provided by the SFR extension investigation programme follows the SKB quality standards and requirements in traceability. Additionally, this more recent data set provides oriented fracture data as well as oriented PFL-f data. These two data types form the basis for the established SKB methodology to describe the HRD by means of Hydro-DFN parameterisation. Thus, the recent data set is judged to be considerably more useful for the parameterisation of site-specific properties inside the SFR model volume.

The primary data types forming the basis of the hydrogeological modelling are:

- Experiences from the construction of SFR.
- Geologically mapped Open and Partly open fractures.
- Single-hole hydraulic test data (double packer data from the old data set, HTHB and PFL data from the new data set).
- Interference tests (intentional cross-hole tests, as well as monitored disturbances from ongoing investigation activities).
- Measured inflow to the existing SFR facility.
- Monitored point-water head field around the existing SFR facility.
- Hydrogeochemical data (electrical conductivity (EC) and classification of water types).
- The existing HSD model developed in the Site Investigation Forsmark project (describing the sediments above SFR that potentially constrains the contact to the sea).

These data types are described, cross-compared, and put into context of the final geological model of SFR v. 1.0, see Sections 4.1 through 4.7. Based on findings made, a conceptual model is developed in Chapter 5.

## 4.1 Experiences from the existing SFR facility

### 4.1.1 Tunnel construction experience

Tunnel construction experiences provide insight into characteristics of both deformation zones and the fracture system. Tunnels have been driven through the Singö deformation zone at SFR, but also for two cooling-water discharge tunnels from the Forsmark power plant (Carlsson and Christiansson 2007). Fracture traces in tunnel walls provide some additional information on fracture size, a property that cannot be directly assessed in boreholes. Trace data also provides the only source of fracture orientation in the older data set. Traces in SFR have been mapped as sketches (e.g. Figure 4-5), but are unavailable in a digital form. It is generally difficult to make the distinction between Open and Sealed fractures in trace data; traces are often found to be partly Sealed and partly Open. This makes it difficult to apply trace data in numerical modelling.

Today there are only fragmented areas of the tunnel left where fracture traces are still visible, as most tunnel walls were shotcreted for rock stability. Within the SFR extension project it was decided to re-map a part of the NBT tunnel (Nedre ByggTunneln) that exposed 482 traces. Due to installations, ventilation tubes, and other types of artificial cover, it was difficult to follow the complete trajectory of traces, as well as, making the distinction between Open and Sealed fractures (Berglund 2008).

#### ***Tunnel experience of horizontal structures and deformation zones***

Fracture traces and water bearing traces in SFR have been mapped by Christiansson and Bolvede (1987). Inflow has been described as “locally flowing” inside deformation zones, and as “moisture” or “dripping” outside zones. At the time of tunnel constructions, the existence of horizontal large-scale structures (so-called SBA-structures, Section 2.3.2; also referred to as sheet-joints) in the Forsmark inland was well-known from the earlier construction of the nuclear power plants (Carlsson 1979). No such structures were observed below the passage of the Singö deformation zone. The SFR tunnel constructions provide evidence of the *existence* of sub-horizontal structures, most of which are *not* of extraordinary hydraulic significance. Mapped structures of closely spaced, sub-horizontal parallel fractures (dip <15°; Figure 4-1), are *generally* neither associated to grouted tunnel sections, nor high inflows (Table 4-1). However, a few exceptions exist. Two of these horizontal structures are associated to grouting requirements (cf. Figure 4-3); one of these can in fact be correlated to a nearby transmissivity anomaly in KFR69 ( $T \approx 10^{-5} \text{ m}^2/\text{s}$ ; Figure D-57; Figure D-3; Section 4.3.1). Furthermore, the single largest noted inflow (150 L/min) was from a bolt hole drilled in the ceiling at chainage 1/600 (c. -50 m RHB 70; Figure 4-1, red arrow in Figure 4-2); it was suspected to origin from a horizontal structure that was *not* intersected by the tunnel (Christiansson and Bolvede 1987).

The first 600 m of the SFR tunnel (construction tunnel BT and operational tunnel DT), passes through shallow rock down to an elevation of c. -60 m RHB 70. This tunnel section is grouted (Figure 4-3) as it passes a sequence of deformation zones: the Southern boundary belt (ZFMWNW0001 with splays) followed by the junction of ZFMNNE0869 and ZFMNE0870 (Figure 4-2). The tunnel passage through Singö has been modelled in detail (Glamheden et al. 2007). Singö is clearly different from the two zones ZFMNNE0869 and ZFMNE0870 (Figure 4-3). Singö is described as a 15–35 m wide core zone, which is enclosed by wide transition zones. The core zone is described as a 2–12 m wide zone of crushed rock with a high degree of alteration and disintegration that is surrounded by partly clay-filled fractures. Water bearing fractures are NW-striking, but the inflow is relatively low owing to clayey infill.

The construction tunnel BT is intersected by ZFMNE0870 over more or less its entire extent. The lowest point of SFR (tunnel section 1NDB; Nedre DränageBassäng1) intersects ZFM871 (Zone H2). The four storage facilities 1BMA, 1BLA, 2BTF, and 1BTF are intersected by ZFMNNW1209 (Zone 6).

#### ***Grouting***

The analysis and interpretation of hydrogeological data must be made with respect to the grouting performed during tunnel construction. Records on grouted tunnel sections also provide information on the location of large tunnel inflows. The largest grouting efforts were made in the passages through Singö and the junction between ZFMNNE0869, ZFMWNW1035, and ZFMENE0870 (Figure 4-2). The core of Singö was also pre-grouted from ground surface (not shown in Figure 4-3).

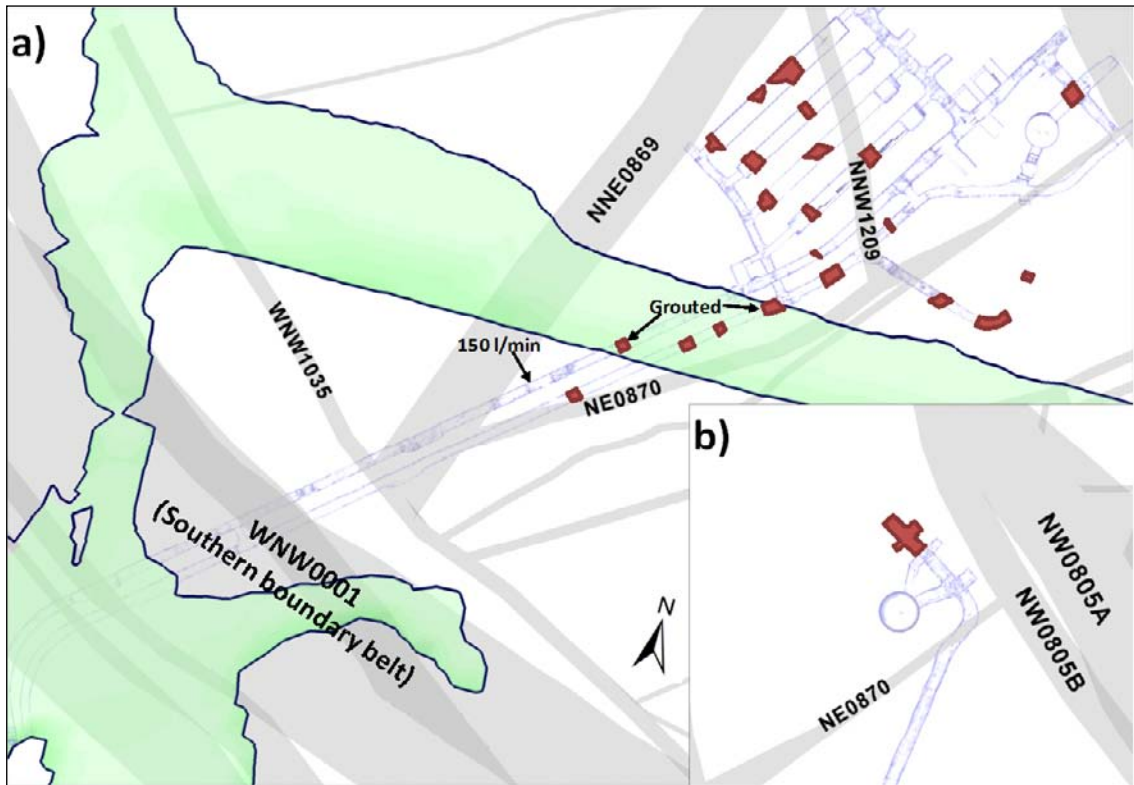


**Figure 4-1.** Structures of closely spaced, sub-horizontal parallel fractures (dip <math><15^\circ</math>) digitized from sketch 103 in Christiansson and Bolvede (1987). The in-fold, b) illustrates the lower level of the NDB tunnel that intersects ZFM871 (Zone H2). Only two of these structures required grouting (cf. Figure 4-3). Extrapolation between tunnel sections shown in Figure D-3.

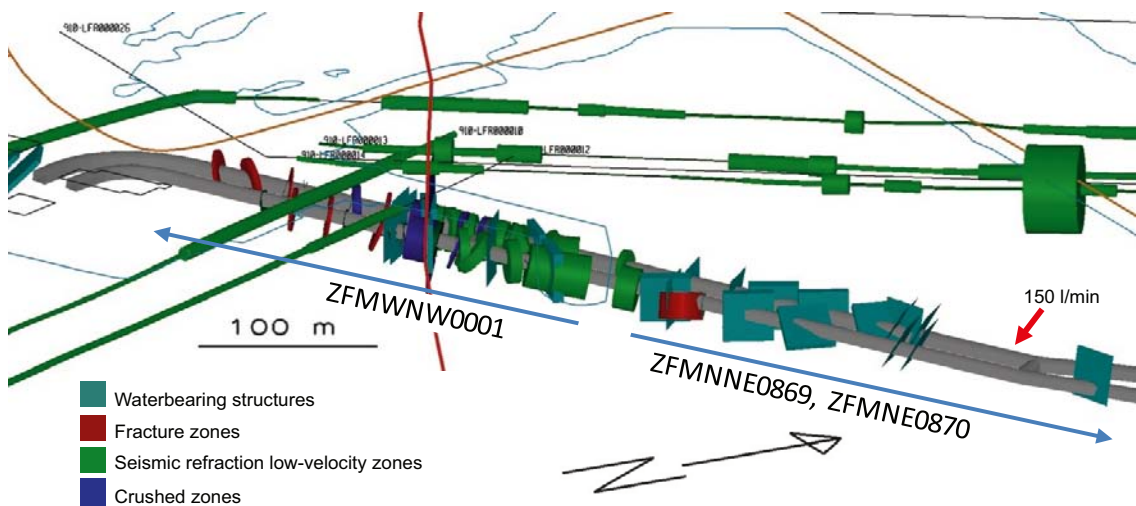


**Figure 4-2.** RVS model of the first c. 600 m of the SFR access tunnels BT and DT passing through Singö and a junction of ZFMNNE0869 and ZFMNE0870 (Zone 3 and Zone 9). Modified from Glamheden et al. (2007). Drilling a bolt in the ceiling at chainage 1/600 (red arrow) provided an inflow of 150 L/min.

The deepest tunnel sections, NBT/INDB (Nedre ByggTunneln/Nedre DränageBassäng1), penetrate the conductive, gently dipping deformation zone ZFM871 (Zone H2). The ZFM871 intersection was grouted by 20 tonnes of cement mixed with 60 m<sup>3</sup> of water (Figure 4-3), which corresponds to a grouted rock volume of 6,400 m<sup>3</sup> for an assumed rock porosity of 1% (Carlsson et al. 1986).

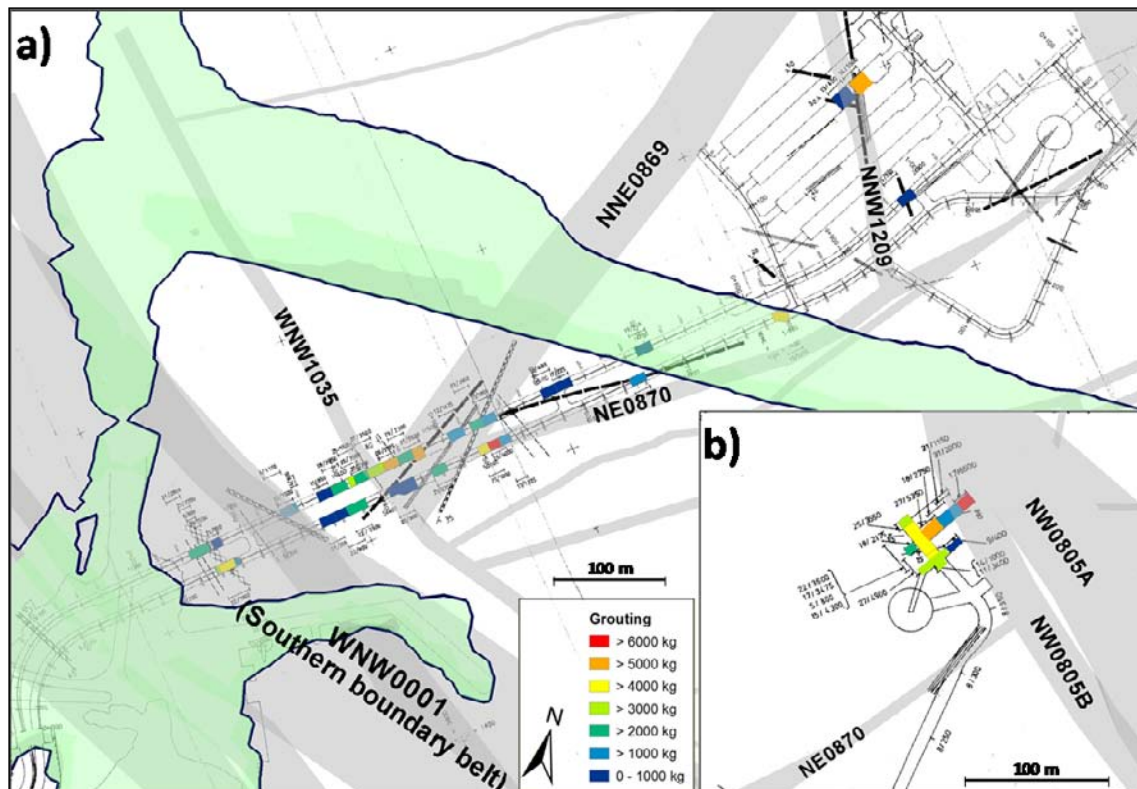


**Figure 4-3.** Grouted tunnel sections in the existing SFR. For readability, the original sketch 104 by Christiansson and Bolvede (1987) has been coloured by injected mass of cement and placed in the context of the ground traces of the deformation zones of the geological model SFR v. 1.0. The in-fold, b) illustrates the lower level SFR tunnels intersecting ZFM871 (Zone H2).

Two grouted sections are associated to horizontal structures (located underneath the Pier; cf. Figure 4-1). These required approximately 1 and 5 tonnes of cement, respectively. Ambient hydraulic borehole data indicate anomalous transmissivity at similar depths (see Section 4.3.1; Figure D-3). Based on analysis of transmissivity and drawdown data in KFR02, Axelsson et al. (2002) suggested that a conductive sub-horizontal structure may be located below the storage facilities and extend between zones ZFMENE0870 and ZFMENE0869 (i.e. located below the SFR tunnels, but above ZFM871). This provides key evidence for interpreting the spatial extension of so-called SBA-structures.

Vice-versa, non-grouted tunnel sections indicate less conductive rock. 1BLA is the only storage facility that required grouting. It was grouted by a mixing of 5.9 tonnes of cement and 15 m<sup>3</sup> of water, mainly related to ZFMNNW1209 (Zone 6). The other storage facilities, including the Silo, were not grouted at all. Note that tunnel section IB (InlastningsByggnad), which extends Northeast from the upper level of the Silo, was not grouted (Figure 4-3), in spite of being modelled as located inside ZFMNW0805B (Figure 4-12) in the geological model. There are several hydrogeological data reinforcing the notion that ZFMNW0805B is poorly interconnected (interference data, Appendix A, head data, Section 4.5, and hydrochemistry, Section 4.6).

#### 4.1.2 Reported tunnel inflow

##### **Mapped water bearing fractures**

Approximately 600 water bearing traces have been mapped in the ceiling of different tunnel sections of the existing SFR facility (Christiansson and Bolvede 1987). These are reported as 389 orientations that may represent packages or sequences of fractures and therefore fracture sets cannot be directly compared (i.e. in terms of intensity). There are also other factors to consider, including grouting, geometric sampling bias, and stress-redistribution. Four sets are distinguished NW, NE, and to a lesser extent Hz and EW (Figure 4-4). Horizontal traces are reported to have a maximum length of 10 m and sometimes appear interconnected. Steep traces are reported to have a maximum length of 10–15 m, and may appear in vertical structures extending over 100 m (related to ZFMENE0870).

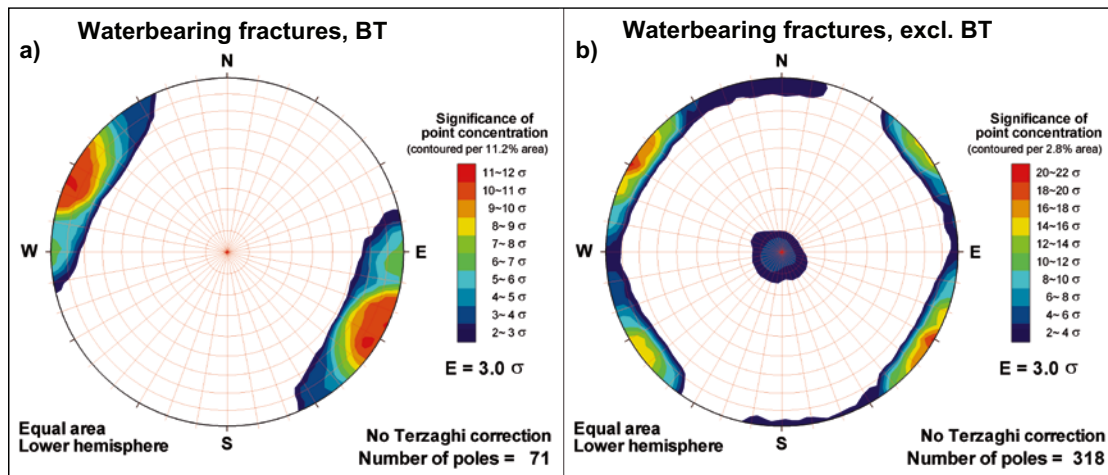


**Figure 4-4.** Mapped water bearing fracture orientations in the SFR tunnel ceiling; a) Access tunnel BT highly influenced of ZFMNE0870, while b) the other SFR tunnels reflect sets NE, NW, and to a lesser extent Hz and EW. Sets cannot be directly compared: some recorded orientations reflect packages or sequences of fractures (cf. Figure 4-9).

Large sections of access tunnel BT are intersected by ZFMNE0870, which explains its dominating inflow from NE-striking steep fractures (Figure 4-4a). Tunnel trace data have a strong geometrical sampling bias against horizontal fractures. Firstly, water bearing fractures could only be mapped in the ceiling, as the invert was not exposed and dripping water is difficult to detect in tunnel walls. Also, the access tunnels descend to c. -60 m RHB 70 during the first c. 600 m, a tunnel section that is grouted due to deformation zones (Figure 4-2). After this descend, the tunnel system is considerably less grouted, but is largely horizontal. Thus, the non-grouted mapped water bearing fractures have a strong sampling bias (with the exception of the Silo and its lower access tunnel NBT), which provides a biased picture of fracture flow. The Silo is non-grouted and has only minor geometric bias, and thus provides a unique insight into the fracture system, trace length and fracture orientation (Figure 4-5). It is dominated by steep NW and NE-striking traces (presumably Sealed) and subordinate horizontal traces. However, the Silo seems to be emplaced in atypically low-conductive rock (Figure 4-6), with low inflow (Section 4.1.3).

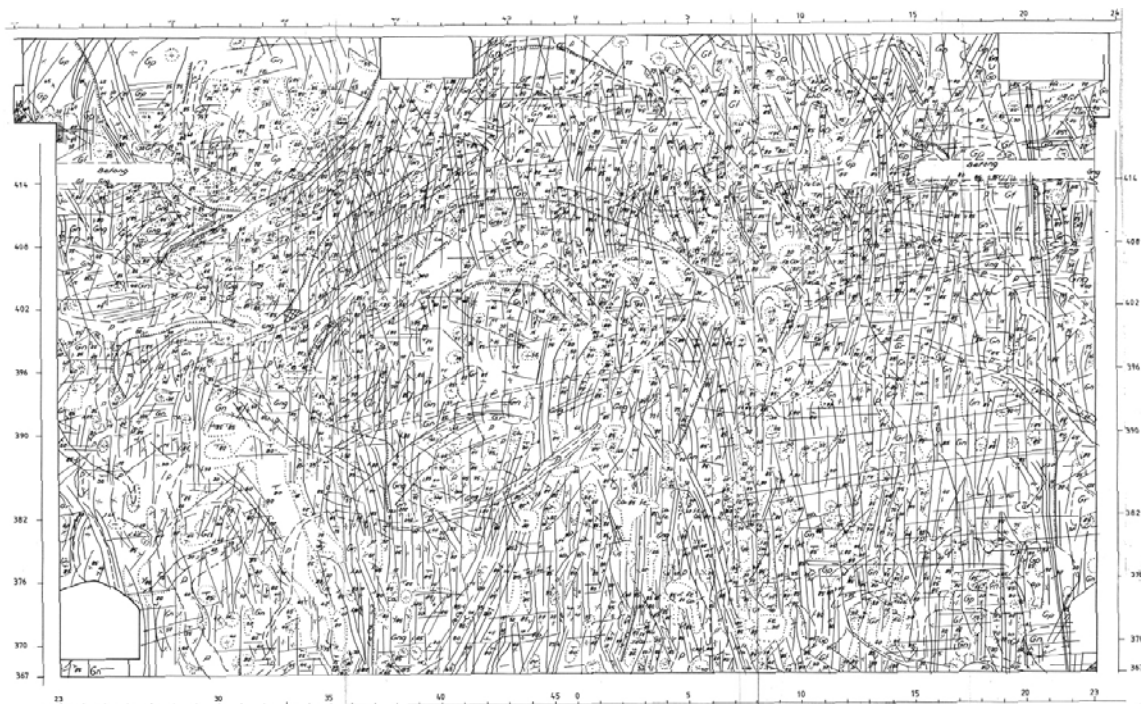


**Figure 4-5.** Mapped traces in the Silo. Sketch of the un-folded Silo from Christiansson and Bolvede (1987).



It is also questionable if mapped tunnel inflow is representative for the *in situ* rock mass. The tunnel construction affects the rock mass in the tunnel wall (e.g. stress re-distribution and blasting damage; see discussion in 4.1.3), which alters the flow pattern of fractures.

### Representativeness of the Silo characteristics

The Silo is often used as an example of the outstanding hydrogeological conditions at SFR. It provides evidence of surprisingly low-permeable, non-grouted rock, in spite of its location close to highly conductive deformation zones. The Silo has a vertical extent of 69 m (from –64 to –133 m RHB 70) and a diameter of 29 to 31 m. Relative to its designed layout, it was re-located 10 m in the horizontal direction to avoid contact with ZFMNE0870 (Zone 9) (Carlsson and Christiansson 2007). The Silo waste is encapsulated in a concrete construction which is protected by low-permeable bentonite barriers. Inflow from the cavern walls is collected by a drainage system that is covered by shotcrete; its design is not known in detail (Holmén and Stigsson 2001). There is also a drainage system collecting inflow from the ceiling. This relatively large underground cavity has an exposed area of c. 8,000 m<sup>2</sup> and is located close to two highly conductive deformation zones (10 m above ZFM871 and 60 m from ZFMWNW805B). The Silo was not grouted, but it nevertheless has a low inflow: originally 2 L/min, which has successively reduced to 0.5 L/min.

The uncertainty in design and functionality of the drainage system implies a concern on the reliability in measured inflow. The drainage system was installed to collect visible inflow; it cannot be expected to collect the diffuse inflow. There is also uncertainty in the internal resistance of the drainage system. Holmén and Stigsson (2001) estimated that without resistance from the drainage system, the Silo inflow would be 3 L/min.

Evaluation of hydraulic data suggests that the rock mass in the vicinity of the Silo is unusually low-conductive compared to the general SFR modelling volume (Figure 4-6). From a site characterisation viewpoint, it should be considered that the storage facilities were located in rock that is favourable from a hydraulic viewpoint, and therefore may exhibit characteristics that are not necessarily representative for the entire SFR modelling domain. In addition there exist general concerns to how representative tunnel inflow is of the natural flow system (see discussion in 4.1.3). On the other hand, boreholes are often intentionally targeted to characterise, or to verify the existence of, deformation zones (in both the old and the recent data sets). Such biased borehole coverage may render a contrasting, overly-pessimistic impression of the site, as the rock mass outside intercepts may be unrepresentative of the general model volume (i.e. the HRD characteristics may be subject to boundary effects, or so-called transition zones, of geological structures).

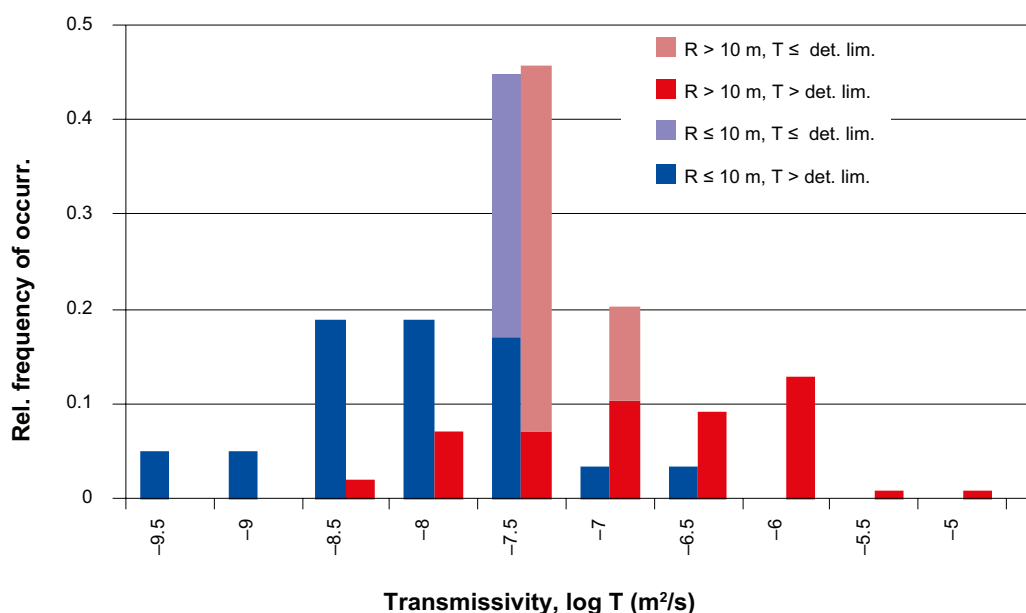


**Figure 4-6.** Comparison between transmissivity close to the Silo (58 values within 10 m radius of the Silo wall) and further away (192 values further than 10 m from the Silo). Only transmissivity data in HRD within the depth interval –60 to –140 m RHB 70 included.

### 4.1.3 Location of inflow and change with time

Measurements of the inflow to the SFR facility have been carried out regularly since January 1988 (Carlsson and Christiansson 2007). The earliest registered total inflow directly after the completion of excavations (1988) was about 720 L/min. Since then there has been a declining trend of inflow that has been relatively steady for the last 23 years (Figure 4-7); the total inflow has decreased to about 285 L/min (average for year 2010), which corresponds to a 60% decrease since the initial measurements. The declining inflow phenomenon is not unique to SFR, but is a general observation for underground facilities; for example similar observations have been made at the Stripa mine and the Äspö Hard Rock Laboratory (Jarsjö and Destouni 2000). Furthermore, a partial re-distribution in the inflow pattern was also observed, between the years 1998 and 1993, in early documentation of specific inflow locations (Axelsson et al. 2002).

The distribution of inflow to the tunnel system is shown in Table 4-1. About 20% comes from the rock caverns and other tunnels in the operational area (measuring point UB in Figure 4-8), whereas 80% comes from the access tunnels and the lower construction tunnel (measuring point NDB in Figure 4-8) (SKBdoc 1233642). Of the measured 160 L/min in the access tunnels, about 140 L/min is estimated to come from the ramp above the repository level (Carlsson and Christiansson 2007), including, the Singö zone (ZFMWNW0001). The inflow from the Singö zone has earlier been estimated to contribute with about 30 to 40% of the inflow to the ramp (Christiansson and Bolvede 1987). The inflow to the lower construction tunnel (NBT) is about 70 L/min or 25% of the total inflow. Assuming the same ratio between inflows that was applied by Carlsson and Christiansson (2007), the inflow from the sub-horizontal deformation zone ZFM871 (formerly known as Zone H2) in the lower end of the lower construction tunnel can be estimated to be about 54 L/min. The average groundwater inflow (2009) from tunnels below the crossing of the Singö zone is estimated to be about 5–6 L/min per 100 m tunnel. A comparison between the figures given in Christiansson and Bolvede (1987) and the recent data (and also the curves in Figure 4-7), shows that the proportions of inflow between the different parts of the facility appear to have been constant with time.

It should be noted that in addition to the drainage pumps discussed above (Table 4-1. Measured groundwater inflow to the SFR facility in 2010. The drainage from the operational area is collected in pump pit UB, the rest is collected in pump pit NDB in the lower construction tunnel.), there is also a pump pit in connection to the entrance gates to the SFR tunnel system at a elevation of about –12 m (RHB 70). This pump collects the drainage water and precipitation from the open uppermost part of the SFR ramp. The inflow collected at this pump is not included in the total inflow reported above, but it is a relatively small term. The average pumping rate has been estimated to about 20 L/min /Jakob Levén, personal communication/ or about 7% of the total inflow to the SFR facility. The inflow figures above are further not corrected for the contribution from the moisture transport with the in- and out-going ventilation air, which may be significant.

**Table 4-1. Measured groundwater inflow to the SFR facility in 2010. The drainage from the operational area is collected in pump pit UB, the rest is collected in pump pit NDB in the lower construction tunnel.**

Repository part	Inflow (L/min)	Estimated accuracy of measurement (L/min)	Fraction of total inflow (%)
BMA	4	± 1	< 2
1BLA	0	± 1	0
2BTF	7	± 1	< 3
1BTF	1	± 1	< 1
<b>Pump pit UB<sup>1</sup></b>	<b>49</b>	<b>± 1</b>	<b>~ 20</b>
Access tunnels	160	± 10	~ 60
Silo top	< 0.1	± 0.1	< 1
Silo walls and bottom	0.5	< ± 0.1	< 1
<b>Pump pit NDB<sup>2</sup></b>	<b>238</b>	<b>± 10</b>	<b>~ 80</b>

<sup>1</sup> Total inflow to pump pit UB shown by red area in Figure 4-8.

<sup>2</sup> Total inflow to pump pit NDB shown by white area in Figure 4-8.

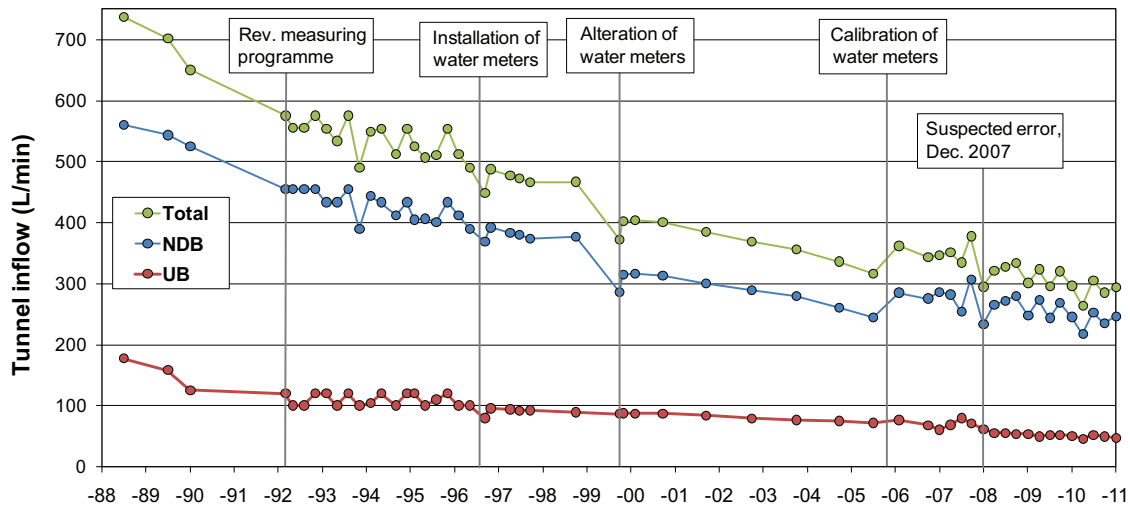


Figure 4-7. Inflow of groundwater to the SFR facility. Curves marked UB and NDB refer to drainage to the pump pits in the operational area and in the lower construction tunnel.

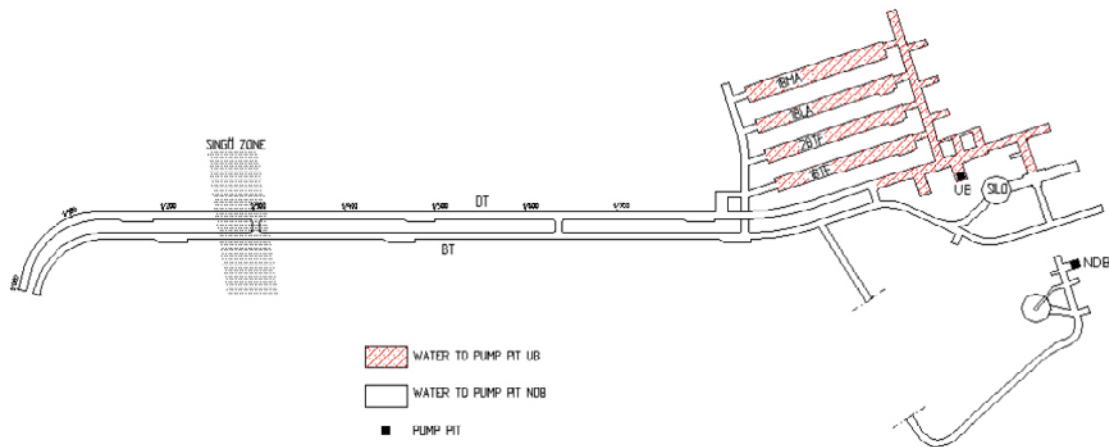


Figure 4-8. The locations of measuring points of groundwater inflow to the SFR underground facility (from Carlsson and Christiansson 2007).

There are two processes that may explain the declining trend of inflow with time. Firstly, there may be an ongoing transient drawdown around the facility, i.e. the flow around the facility has not yet reached steady-state. The observed decline in heads has generally been larger in the less conductive rock (in zone ZFMNE0870 and the rock mass east of it). This explanation agrees with the observations of an on-going relatively constant declining trend in heads in many boreholes around the facility (see Section 4.5). Secondly, the hydraulic properties of the surrounding bedrock may be changing with time. Three different causes to an increased flow resistance with time around rock caverns are discussed in the literature (Gustafson 2009): i) fractures close due to deformation of the rock mass; ii) development of two-phase flow in fractures; iii) clogging of fractures due to chemical precipitation and microbes. However, increased flow resistance close to the tunnel walls is expected to be accompanied by *increasing upstream groundwater pressures*. Consequently, in order to explain the coupled change in monitored head and tunnel inflow, the alteration in hydraulic properties must occur some distance away from the tunnel wall.

Such evidence of alteration is for example provided by borehole KFR7A, which is located at the junction between ZFM871 and ZFMNW0805A/B (section 4.5). High transmissivities were measured in 1985, in its two deeper sections ( $T \approx 10^{-5}$  and  $10^{-4}$  m<sup>2</sup>/s; Figure 4-12). Note that these transmissivities were evaluated from the pressure-build up after having released its shut-in pressure for approximately one day, and is therefore assumed not to include compartmentalised transmissivity.

Early interference tests indicate a good hydraulic connection between the deep section of KFR7A and those of KFR08 and KFR11 (inferred as connection between ZFM871 and ZFMNW0805A; Figure D-9 and Figure D-11). Recent data provide contradictory evidence; KFR7A has the largest observed decline in fresh-water head, which is clearly different from other monitored sections located inside ZFMNW0805A (KFR08 and KFR56, both in terms of magnitude and transient development; Figure 4-28). Analysis of water type composition reinforce the notion of poor hydraulic connectivity between KFR7A other monitored sections inside ZFMNW0805A (KFR08 and KFR56; Figure 4-32). In other words, scope calculations suggest that KFR7A reflects stagnant water, as otherwise its Littorina content would have been replaced by Local Baltic water type. This suggests that the hydraulic connectivity between ZFM871 and ZFMNW0805A, as well as, their internal hydraulic connectivity, has changed over time.

Five hypotheses are considered for the seemingly coupled ongoing transient decrease in inflow and surrounding heads:

- **Heterogeneity and isolated rock mass:** if the fracture system is low-transmissive, and/or highly compartmentalised, slow communicating parts of the rock mass may not yet have reached steady state (not even after 25 years). However, this would only explain a reduction in the fraction of inflow from low-conductive, isolated rock volumes, not to the inflow from the larger zones, and is therefore, in itself, considered insufficient for explaining the 60% reduction in Figure 4-7.
- **Unsaturated fracture flow:** Close to the tunnel wall, air may enter dewatered fractures. Even at some distance away from the tunnel walls, the decreasing groundwater pressure around an underground facility may cause dissolved gases to come out of solution (Jarsjö and Destouni 2000). Degassing may cause unsaturated fracture flow with a reduction on flow (i.e. at fracture scale, trapped air bubbles may form along conductive flow paths and partially block the flow). This phenomenon is coupled to declining head and does not necessarily occur close to the tunnel walls.
- **Particle clogging:** tunnel inflow may transport sediment particles from the seafloor into the fracture system, or cause existing fracture filling (sediments, gouge, clay, etc) to re-suspend and clog hydraulic paths. This phenomenon does not necessarily occur close to the tunnel walls.
- **Fracture sealing due to chemical precipitation and microbial growth:** Tunnel inflow cause disturbances to the natural groundwater conditions, which may cause mineral precipitation/dissolution, as well as, microbial growth on fracture walls (Laaksoharju et al. 2009). Sealing of fractures is known to decrease conductivity and cause re-distribution of flow paths, but primarily in the immediate vicinity of tunnel walls.
- **Hydro-mechanical fracture closure:** the transmissivity pattern is clearly related to the stress anisotropy (Figure 4-15). Hydraulic data measured before and after the Silo construction demonstrated a local conductivity reduction as the result of increasing stress in the walls of the Silo (Carlsson et al. 1986); this indicates that fracture transmissivity at SFR is sensitive to normal loading (i.e. has low fracture stiffness). The dewatering of conductive fractures during tunnel inflow implies increasing effective normal stress, causing fracture closure and decreasing fracture transmissivity, which in turn reduces tunnel inflow. The reduction in flow will slow down the propagation of the low-pressure front, appearing as a very slow, transient drawdown process. This phenomenon is coupled to declining head and does not necessarily occur close to the tunnel walls.

Scope-calculations of hydro-mechanical fracture closure are provided for the following example: the complete drainage of a horizontal fracture (i.e. head decline,  $\Delta H = H_0 - H_1 = -100$  m, at  $z = -100$  m RHB 70) results in a 67% increase in effective normal stress (i.e.  $(\sigma_v - \rho g(H_1 - z)) / (\sigma_v - \rho g(H_0 - z)) \approx 2.5$  MPa/1.5 MPa). In other words, owing to the low vertical stress (Section 3.3), the dewatering has a large *relative* effect on effective normal stress over horizontal fractures. Fractures closure with increasing normal stress increases the asperity contact area, which in turn gradually increases the fracture stiffness,  $k_n$ . However, at low stress levels, such as at the shallow depths of SFR, the fracture sensitivity to normal loading is known to be large. Scope calculations with Forsmark data,  $k_n = 160$  to 80 MPa/mm (SKB 2008a), render maximum fracture closure of 6 to 12  $\mu\text{m}$ . Scope calculations for sheet-joints,  $k_n = 10$  MPa/mm (Bono et al. 2010), render a maximum closure of 100  $\mu\text{m}$ .

These mechanical displacements are fairly small. Unfortunately, they cannot be directly related to transmissivity without making disputable simplifications of fracture geometry, such as parallel-plate representation, i.e. assumptions that are generally known to be inappropriate. For reference, in the so-called “cubic law”, a *hydraulic aperture* of 57  $\mu\text{m}$  between two planar parallel plates corresponds to a transmissivity of  $10^{-7} \text{ m}^2/\text{s}$ . However, it should be pointed out that the change in effective stress is extremely small in relation to historic stress changes (glacial loading), which may have crushed fracture wall asperities.

### ***In- and outflow of water transported by air***

Ventilation causes uncertainty in the reported inflow measurements. Evaporating inflow circumvents measurement, while condensing moisture leads to overestimations in reported inflow. Generally, it can be expected to be a net inflow of water by air to an underground facility during summer when the ingoing air is warm and relatively humid, and a net outflow can be expected during winter when the ingoing air is cold and dry. There are no measurements of the humidity of the air going in and out through the ventilation at the SFR facility /Jakob Levén, personal communication/. However, humidity measurements are a part of the meteorological measurements in Forsmark, and the constant total ventilation air flow through the facility is known to be  $32 \text{ m}^3/\text{s}$  /Jakob Levén, personal communication/. Limits of the net moisture flow transported by air may then be estimated. For these calculations, meteorological data from the one-year period October 2008–September 2009 was used. The estimated transport of water by in-going air varied from minimum about 4 L/min (occasionally during December–April) to maximum about 31 L/min (occasionally during July–August). The estimated mean inflow was about 13 L/min. The moisture content of the out-going air is unknown, but the flow is estimated to be at maximum about 33 L/min (20 °C, 100% RH). The range of the possible net flow can then be estimated to be from an outflow of about 30 L/min (winter, assuming maximum outflow) to an inflow of about 30 L/min (summer, assuming no outflow). This term is quite small but not insignificant in relation to the total inflow to the facility (Table 4-4).

## **4.2 Open and Partly open fractures**

Fracture data are geologically mapped as Open, Partly open, or Sealed. Open and Partly open fractures are assumed to form the backbone of the hydrogeological model. Open and Partly open fractures are regarded as *potentially flowing fractures*, whereas Sealed fractures are regarded to be impervious. More precisely, the flowing fracture system is conceptualised as the subset of Open and Partly open fractures that are globally connected to a positive hydraulic flow boundary (i.e. the Sea). The Open and Partly open fractures are combined into a single data set, which is simply referred to as “Open fractures”.

Fracture orientation data is unavailable in the old borehole data set. Fracture orientation data in *percussion boreholes* from the more recent investigations (Forsmark and SFR extension investigations) are judged unreliable for orientation analysis of Open fractures; this is related to the difficulty in distinguishing between the aperture of Open fractures and dark mineral infill of Sealed fractures in BIPS (Öhman and Follin 2010b). There is a clear difference in orientation patterns between Open and Sealed fractures in HRD; sub-horizontal fractures tend to be Open, while steep fractures are predominantly Sealed (Figure 4-9). There are several explanations for this, related to the anisotropic stress regime, fracture genesis, and age. Steeply to gently dipping fractures relate to tectonic regimes during the later part of the Svecokarelian orogeny (Stephens et al. 2007), whereas horizontal fractures in the shallow bedrock (down to c. –40 m RHB 70) are younger, formed by glacial loading/unloading (Carlsson and Christiansson 2007). The horizontal set stands out as the core of the more wide-spread gently dipping set, with extraordinary clustering and high transmissivity; it is possible that this pattern reflects stress-relief, primarily reactivating the horizontal component of pre-existing gently dipping fractures down at depths down to –200 m RHB 70 (Curtis et al. 2011). Further details on the fracture set definitions and the differentiation between the gently dipping and the horizontal set are provided in Öhman and Follin (2010b). The current stress regime ( $\sigma_1 = \sigma_H$  at a bearing of 145°, and  $\sigma_3 = \sigma_v$ ; see Section 3.3) tends to open horizontal fractures, and close steep NE-striking fractures. Over time, chemical weathering/precipitation processes may accentuate the hydraulic anisotropy of the fracture network.

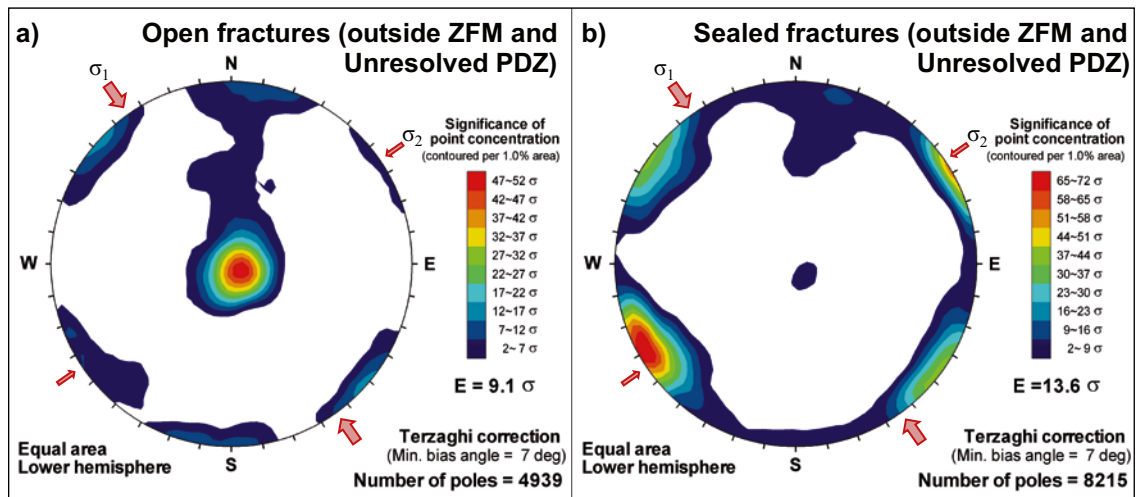


**Figure 4-9.** Kamb\*-contoured fracture orientation outside deformation zones, shown with respect to the stress-field; a) Open fractures and b) Sealed fractures. The horizontal principal stress orientations ( $\sigma_1$  and  $\sigma_2$ ) shown by red arrows (cf. Figure 4-15). Only data with uncertainty,  $\Omega$ , lower than  $15^\circ$  for Open fractures, and  $10^\circ$  for Sealed fractures, are included.

\*A Kamb contour is a visualised result of a statistical test on fracture orientation clustering significance and useful for the identification of fracture sets.

#### 4.2.1 Fracture intensity

The intensity of Open fractures inside HRD decreases somewhat with depth. The relation between set intensities is relatively constant. To reduce effects of data coverage gaps, the lateral analysis of Open fracture intensity is made for a selected depth interval. The depth interval ( $-60$  to  $-245$  m RHB 70) has best total borehole coverage of HRD and provides the best lateral representation. In this interval, the intensity of Open fracture in HRD was calculated for each set and for each borehole (Figure 4-10). The intensity was calculated as the sum of Terzaghi-weights divided by borehole length.

Different boreholes have different geometric sampling bias versus different sets and can therefore not be directly compared. Terzaghi weighting reduces these artefacts and provides more directly comparable fracture intensity estimates; however, it cannot fully eliminate the geometrical artefacts, particularly for fractures that are almost parallel to the borehole. This can be seen in two boreholes: the steep borehole KFR27 (average inclination of  $-86^\circ$ ), which has a strong sampling bias against steep fractures and the sub-horizontal KFR105 (average inclination of  $-10^\circ$ ), which has a strong bias against horizontal/gently dipping fractures (Figure 4-10).

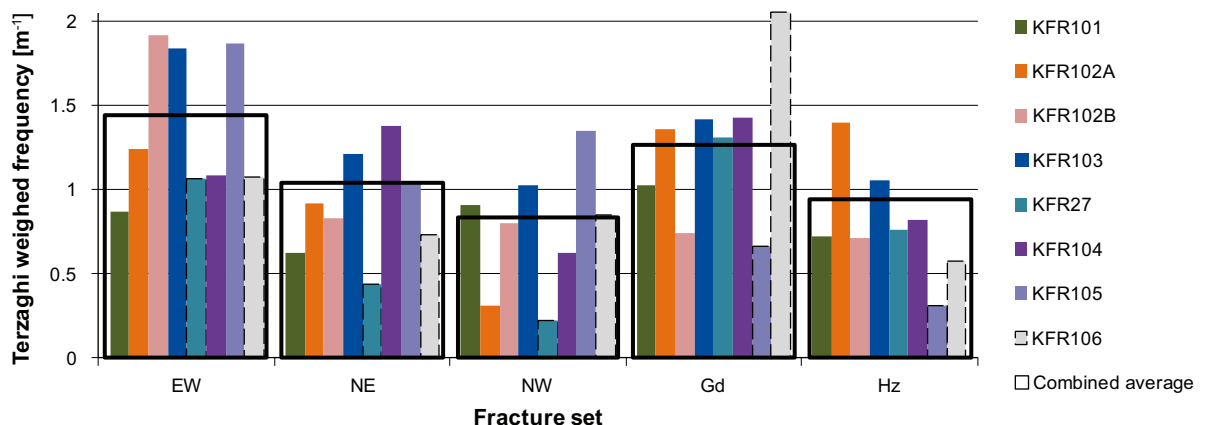


**Figure 4-10.** Set-wise Open fracture intensity at the Repository level ( $-60$  to  $-245$  m RHB 70). A combined average was calculated weighted by borehole length inside HRD. Excluded data shown by dashed lines: all data in KFR106, steep sets in KFR27, and gently dipping and horizontal sets in KFR105.

The borehole-to borehole variability in set intensity was related to a combined borehole-length weighted average (Figure 4-10), defined as the total Terzaghi-weight sum divided by total borehole length. Owing to sampling bias, the steep sets of KFR27 and the horizontal/gently dipping sets of KFR105 were excluded from this average. KFR106 was also excluded from the average; not primarily because of deviant characteristics, but because its location outside the SFR Local domain, close to the Northern boundary belt and ZFMNNW1034, which is judged unrepresentative for global parameterisation. KFR106 is not very different from other boreholes; its main deviant characteristic is its relation between horizontal and gently dipping fractures (Figure 4-10). Further details on fracture intensity calculation are provided in Appendix G.3.

The SFR model domain has high Open fracture intensity in HRD, relative to the observations made in SDM-Site Forsmark (Table 4-2). In SDM-Site Forsmark, a remarkable contrast was found between the intensively fractured uppermost 200 m (FFM02) and the sparsely fractured tectonic lens, below (FFM01). No such prominent contrast is observed at SFR; instead, the decline in Open fracture intensity with depth is small indeed (see also Öhman and Follin 2010b). It should be noted that FFM02 at SDM-Site Forsmark is mainly covered by borehole data below -100 m RHB70. Thus, for the uppermost part of the bedrock ( $z \geq -200$  m RHB70), the difference between the two sites may be smaller in reality, than that indicated by Table 4-2. In order to ensure consistency in the comparison between the two sites, the intensities are both Terzaghi-compensated with a maximum weight of 7 (or a minimum bias angle of  $8.2^\circ$ ). Note also that Partly open fractures are included as well. In the SDM-Site Forsmark, the horizontal set was defined as a rather dispersed set (Fisher  $\kappa = 8.2^\circ$ , alternatively,  $15.2^\circ$ ), which corresponds to both the gently dipping and horizontal sets SFR (see Öhman and Follin 2010b); hence the intensities of sets Hz and Gd at SFR were lumped together in this comparison. Furthermore, no steeply-dipping, NS-striking set has been defined at SFR; for comparative purposes it may be considered as part of the sets NE and NW at SFR.

#### 4.2.2 Fracture characteristics of rock domains

A central question is if the rock domain model motivates lateral subdivision of the rock mass into separate fracture domains. Observed contrasts should be interpreted cautiously, with respect to local heterogeneity, data gaps, sampling bias, and emplacement of boreholes. There is a clear risk of overestimating contrasts. RFR01 covers the central to Southwestern part of the SFR domain (KFR104 and parts of KFR105 and KFR27), which is associated with lower transmissivity. RFR02 covers the Eastern part (the Northern boundary belt), but also the northern part of the existing SFR, including its disposal facilities. In terms of frequency of different fracture types, the difference between RFR01 and RFR02 is judged to be minor (Table 4-3. Mean fracture frequency of mapped

**Table 4-2. Comparison of Open fracture intensity in HRD to SDM-Site Forsmark.**

Set	Upper bedrock, $z \geq -200$ m (RHB70)		Deeper bedrock, $z < -200$ m (RHB70)	
	SDM-Site Forsmark (FFM02)	SFR extension (all core data)	SDM-Site Forsmark (FFM01)	SFR extension (all core data)
NS	0.34	NA	0.07	NA
EW	0.16	1.58	0.09	1.07
NE	0.75	1.06	0.32	1.03
NW	0.34	0.84	0.11	0.67
HZ (+ Gd)	1.58	2.29	0.54	2.24
<b>Total</b>	<b>3.2</b>	<b>5.8</b>	<b>1.1</b>	<b>5.0</b>

**Table 4-3. Mean fracture frequency of mapped drill core outside deformation zones per rock domain. Modified from Table 4-9 in Curtis et al. (2011).**

	Open fractures ( $m^{-1}$ )	Partly open fractures ( $m^{-1}$ )	Crush equivalent ( $m^{-1}$ )	Total (Open + Partly open + crush equiv.)	Sealed fractures ( $m^{-1}$ )	Sealed network ( $m^{-1}$ )	Total (Sealed + Sealed network)
RFR01	3.32	0.24	0.01	3.57	5.75	7.43	13.18
RFR02	3.44	0.33	0.05	3.82	10.14	3.35	13.50

drill core outside deformation zones per rock domain. Modified from Table 4-9 in Curtis et al. (2011).). Note that the total intensities in Table 4-3. Mean fracture frequency of mapped drill core outside deformation zones per rock domain. Modified from Table 4-9 in Curtis et al. (2011). are different from those reported in Table 4-2. Comparison of Open fracture intensity in HRD to SDM-Site Forsmark. There are three reasons for this: 1) the values in Table 4-3. Mean fracture frequency of mapped drill core outside deformation zones per rock domain. Modified from Table 4-9 in Curtis et al. (2011). are only Terzaghi-compensated with a maximum weight of 3.8 (or a minimum bias angle of 15°), 2) borehole sections falling outside RFR01 and RFR02 are excluded in Table 4-3. Mean fracture frequency of mapped drill core outside deformation zones per rock domain. Modified from Table 4-9 in Curtis et al. (2011)., 3) the geometrically biased sets were excluded in Table 4-2. Comparison of Open fracture intensity in HRD to SDM-Site Forsmark (cf. “combined average” in Figure 4-10).

In terms of Open fracture orientation (Figure 4-11), the most striking differences are that horizontal set is more clustered in RFR02 and that set EW is virtually absent in RFR01. Set EW is not associated to large transmissivity values, and is expected to have minor importance in the hydrological model. The EW-striking fractures are found at shallow depth in the three boreholes originating from the tip of the pier: KFR102B, KFR103, and KFR101 (note that KFR101 is excluded as it is intercepted by ZFMNNW1034). These three boreholes basically origin from the same point, and therefore it may reflect local presence of set EW. Local EW dominance is also found in KFR102A at larger depth (-125 m RHB 70).

The horizontal set, on the other hand, is conceptualized as the hydraulic backbone. Possibly, the intensity of horizontal fractures weakens further away from the Northern boundary belt. However, one reason for the less dominance of set Hz in RFR01 could be that the sub-horizontal borehole KFR105 has a larger contribution of data (note its lower intensity of set Hz in Figure 4-10). The nearby KFR104 does not indicate particularly low intensity of Hz in the Repository depth interval (Figure 4-10).

In the light of heterogeneity, data gaps, and sampling bias, the differences in fracture frequency and orientation of Open fractures between RFR01 and RFR02 are considered significant for modelling. On the other hand, the Rock domain model boundary *partly* coincides with the transmissivity trends observed in the new data set (high transmissivity inside RFR02; Section 5.3), suggesting that PFL-f trends cannot be related to differences in fracture intensity or orientation. The existing SFR provides quite contradictory evidence; only minor inflow is measured in the disposal facilities located in RFR02 (Figure 3-3). Instead it was decided to use the geologic units *Southern* and *Northern boundary belts*, as well as, the *Central block* (Figure 3-4) as reference in the hydraulic data analysis (Chapter 5).

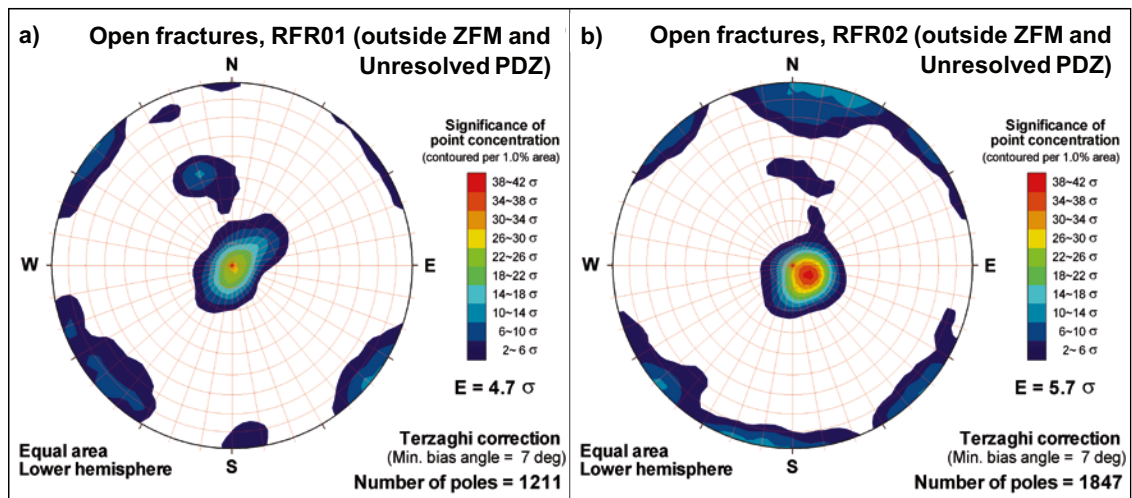


**Figure 4-11.** Orientation of Open fractures outside deterministic zones (ZFM) and Unresolved PDZ per Rock Domain; a) RFR01 and b) RFR02. Only cored boreholes inside the Local domain, visible in BIPS, and with  $\Omega < 10^\circ$ ; upper part of KFR27 with unavailable core excluded.



### 4.3 Evaluation of single-hole hydraulic tests

The hydraulic data from the old data set (existing prior to the initiation of the SFR extension investigation) and the recent data set (obtained during the SFR extension investigation) are reviewed in Appendices D and E, respectively.

#### 4.3.1 Single-hole transmissivity data from the existing SFR facility

The old data set from SFR is extensive. During the initial investigation phases prior to the construction of SFR, 1980 to 1983, surface boreholes were drilled from offshore platforms, ice-cover, and land. During the construction phase of SFR, 1984 to 1986, subsurface boreholes were drilled from underground constructions and access tunnels, to explore and verify locations of zones (primarily ZFMWNW0001, ZFM871 and ZFMNW0805A and B). Additionally, interference tests were performed to evaluate hydraulic properties of the structural model (Carlsson et al. 1986, Axelsson and Mærsk Hansen 1997) (see Section 4.4.1). Fracture orientation is unavailable in all boreholes of the old data set. Hydraulic data from the construction of SFR are available in 45 cored boreholes, described in Appendix D and Öhman and Follin (2010a). The hydraulic data are available as transmissivity measured over borehole sections sealed off by packers. In comparison to PFL-f data (Section 4.3.2), this type of double-packer data is expected to include compartmentalised fracture transmissivity as well as the risk of short-circuited flow between packers.

The single-hole transmissivity data available from the construction of SFR have been measured by four different methods: Falling head (FH), pressure build-up (BU), steady state injection (PH), and transient injection (TI). For technical reasons, the falling head and steady state injection methods were used in the early surface investigations, while underground boreholes were tested by the pressure build-up method (Figure 1-4). Altogether, there are 1,122 tested borehole sections, but the data are of varying quality; they have been evaluated with different test methods, at different test-scales, and under different test durations. Consequently, the data have different detection limits. However, most transmissivity data are measured over 3 m borehole sections and have a high detection limit, around  $5 \times 10^{-8}$  m<sup>2</sup>/s. Pressure Build-up tests and Transient injection tests have the longest durations (several hours) resulting in lower detection limits; unfortunately such data are relatively rare and have large variation in test scale. The falling-head and steady-state injection data had only test duration of a few minutes; they comprise a large sample size of consistent test scale (3 m sections). Falling-head data have an overall low confidence in relation to the other data types (Carlsson et al. 1987). In total, about 40% of the tested sections fall below detection limit. The hydraulic data set underwent a screening process, in which 179 overlapping data, erroneous data, and inconsistent data were excluded, described in Öhman and Follin (2010a).

Zones ZFMNW0805A and B are supported by high transmissivity data (Figure 4-12). ZFMNNE0869 has strong hydraulic support from tunnel intersection (Figure 4-2) and KFR09 and KFR36, but the hydraulic data in KFR10 seems more likely to suggest an extension of ZFM871 (as indicated by interference tests, Appendix D and hydrochemistry, Section 4.6). ZFMNE0870 has strong support from tunnel observations (Figure 4-4), but its hydraulic data are difficult to evaluate, as most borehole data come from sub-parallel intercepts of the zone. ZFMNNW1209 appears heterogeneous; hydraulically supported in KFR35 and from observed dripping/flowing partly clay-filled fractures in the ceiling of the storage caverns, but not in KFR33.

ZFM871 is well-supported by high transmissivity data east of ZFMNNW1209 (Zone 6), but there is little support west of this zone: a low-transmissive intercept in KFR02 and a single high-transmissive 3 m-section of KFR33 (Figure 4-12a). As mentioned earlier, it is speculated if possibly also KFR10 reflects an intercept of ZFM871. Note that four boreholes, KFR34, KFR35, KFR69, and KFR70, located west of ZFMNNW1209 and above ZFM871 (i.e. do not intersect; Figure 4-12b) indicate a transmissive depth-interval ( $T \approx 10^{-6}$  m<sup>2</sup>/s) just below the SFR tunnel that *is not related to ZFM871*. The transmissivity anomalies in KFR70 and KFR69 are located on either side of one of the grouted horizontal structures discussed in Section 4.1.1 (see Figure D-3).

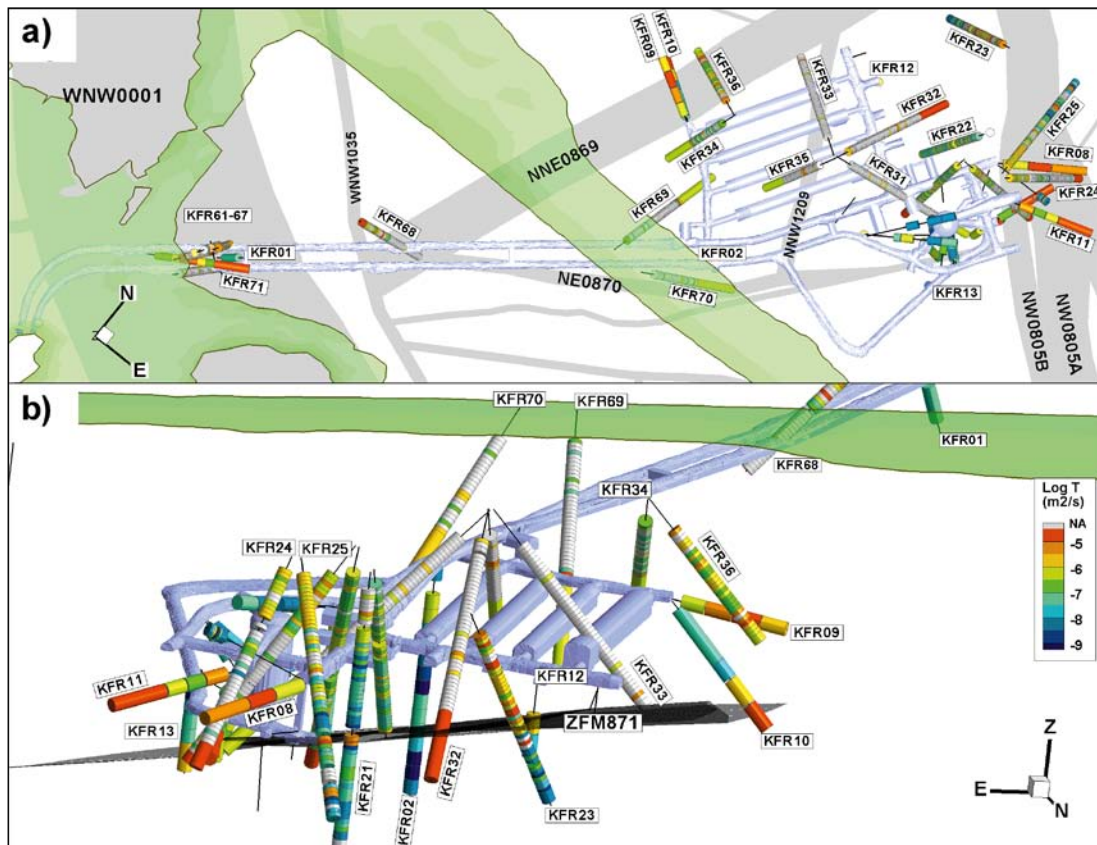


**Figure 4-12.** Screened single-hole hydraulic data from the existing SFR; a) top view with the traces of modelled deformation zones and b) side view towards south, along the dip of ZFM871. Note that ZFMNE0870 dips towards NW and intersects the construction tunnel (BT; ByggTunnel), more or less, over its entire extent.

#### 4.3.2 Single-hole transmissivity data from the SFR extension investigation

In essence, three types of transmissivity data are used from the new data set:

- 1) HTHB data, combined pump test and impeller flow logging performed in percussion boreholes,
- 2) sequential 5 m PFL data (in the upper 100 m of KFR27), and
- 3) PFL-f data.

Only a single 44 m scale injection test is available in HFR102 (Figure 4-17), as no impeller flow logging was performed. PFL-f data are unavailable in the upper part of KFR27 (above 99.3 m borehole length) and have lower confidence in the interval 99.3 to 148.5 m (due to unavailable core combined with a coarser 0.5 m resolution used in the interval 99.3 to 130 m borehole length; Figure E-23). Thus, the best available data in the upper 100 m of KFR27 is 5 m sequential PFL data (transmissivity defined at the 5 m scale). KFM11A only has PFL-f data south of the Singö deformation zone (i.e. outside the Local SFR domain).

Out of these three data types, the PFL-f data has the key role in describing the less fractured rock between deformation zones by means of a Hydro-DFN. A central assumption in this method is that the evaluated transmissivity for PFL-f records are assumed to reflect fracture transmissivity explicitly. The Posiva Flow Log (PFL) device (Figure 4-13) is developed to detect *continuously flowing features*, i.e. flow paths that are connected to a positive hydraulic boundary. Therefore, PFL-f measurements are based on several days of pumping, after which the flow regime is assumed to have reached radial steady-state. The risk of short-circuited fracture flow is small as the entire borehole is a line-sink (e.g. Figure 2-5). Problems may arise with the rubber disks if there exists large cavities in the borehole wall, or if the bypassing flow from below is too large (Figure 4-13). The advantage of the bypass pipe is that the PFL method avoids measuring cumulative flow, which makes the method less sensitive to large flows at the bottom of the hole.

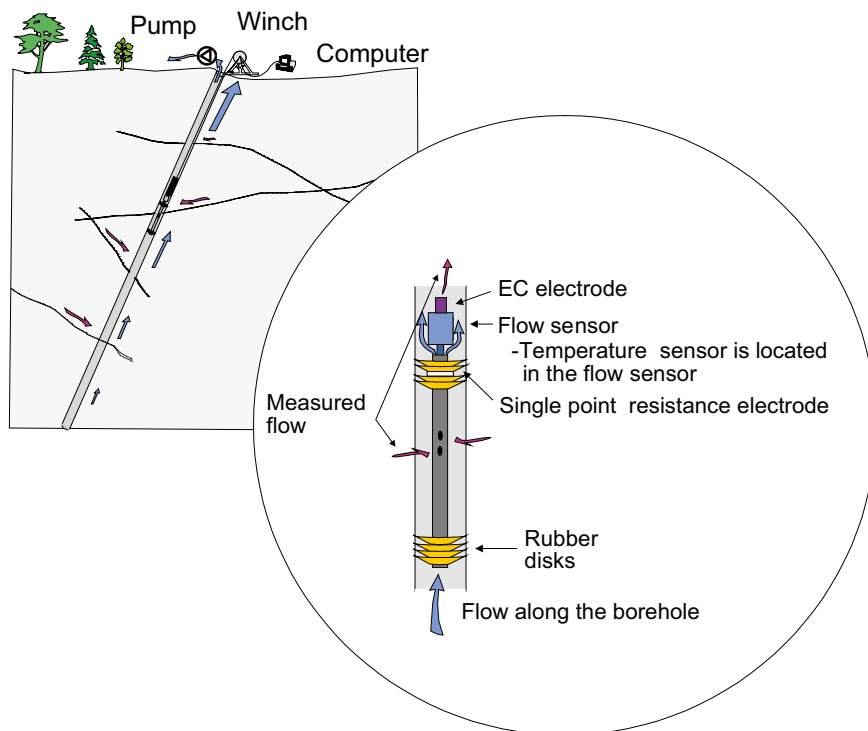


**Figure 4-13.** Illustration of the PFL device (from Hurmerinta and Väisäsvaara 2009).

After an initial overlapping/sequential PFL flow logging with 5 m sections under *natural flow conditions*, detected flow anomalies are re-examined with the PFL Difference Flow logging method under *pumped conditions*. In this Difference Flow logging method, flow is generally measured over a 1 m section, which is sequentially moved in steps of 0.1 m. Based on these measurements discrete inflows are identified (referred to as PFL-f data) and the *apparent* transmissivity is evaluated for each discrete feature (see details in e.g. Hurmerinta and Väisäsvaara 2009). Thus, the detected discrete inflows at 0.1 m resolution are assumed to reflect individual fractures, and evaluated *apparent* PFL-f transmissivities are then coupled to mapped geological fractures (Figure 4-14).

### **PFL-f coupling to Boremap**

The PFL-f data are linked to discrete Boremap features (Open fractures, Partly open fractures, and crush zones), as described in Öhman et al. (2010). The length measurements for PFL-f data,  $L_A$ , are synchronized to borehole reference marks, reducing the estimated uncertainty of  $L_A$  to  $\pm 0.2$  m (Hurmerinta and Väisäsvaara 2009). A discrete Boremap feature also has a certain extension along the borehole, depending on its  $\alpha$ -angle (and aperture), which is generally in the range 0.0 to 0.2 m. Boremap features with borehole cross-sectional area partly inside the geometric window of  $\pm 0.2$  m of a given PFL-f record are considered as possible candidates (Figure 4-14).

The linking is a desktop study, which involves a joint judgment of, primarily, three aspects:

- 1) Visual inspection of BIPS imagery of the borehole in the vicinity of each PFL-f record.
- 2) Geometric match between PFL-f record and nearby Boremap features.
- 3) Confidence in the geologic interpretation of Open and Partly open fractures.

As the result from Boremap linking, PFL-f data are attributed with orientation and can be divided into fracture sets (as described in Öhman and Follin 2010b). The anisotropy in PFL-f data appear well-correlated to the stress-field (Figure 4-15). The majority of PFL-f data, particularly the largest transmissivities ( $T > 10^{-6}$  m<sup>2</sup>/s) found above  $-200$  m RHB 70, are horizontal to gently dipping (Figure 4-15 and Figure 4-16). This depth interval is the same as the SBA-structures modelled in Forsmark SDM (Figure 2-4). The most transmissive features within this interval are horizontal Unresolved PDZs (cf. Figure 4-16c and d).

**KFR102A. Interpretation of PFL measurements and BOREMAP data**

**PFL-f No. 34**, Adjusted borehole length, LA = **188.4 m**,  $T \leq 2.6E-6 \text{ m}^2/\text{s}$ , PFL confidence = **CERTAIN**

Possible PFL-f features	Boremap data						BIPS Image	
	Adjusted secup (m)	Orientation (Strike/Dip)	Fract. interpret	Frac. interp. confidence	PFL-anom. confidence	Aperture (mm)	Corresponding Recorded secup in Boremap = <b>188.03 m</b>	Single hole interpretation = <b>RU3</b>
a <sup>1</sup>	188.28	181 / 2	Open	Probable	1	0.5		
b <sup>1</sup>	188.30	109 / 9	Crush zone			18		
c	188.34	38/18	Open	Possible	1	0.5		

**Comments:** Crush zone  
**Best choice:** b

Footnotes: 1) Closest, highest ranked open/partially open fracture, 2) This fracture can also be associated to an adjacent PFL-f No

**Figure 4-14.** Example of a PFL-f transmissivity record coupled to a Boremap feature (red arrows). The borehole length uncertainty  $\pm 0.2 \text{ m}$  is indicated by red lines. Three possible candidates are identified, and a crush zone (candidate b) is selected to be the Best Choice.

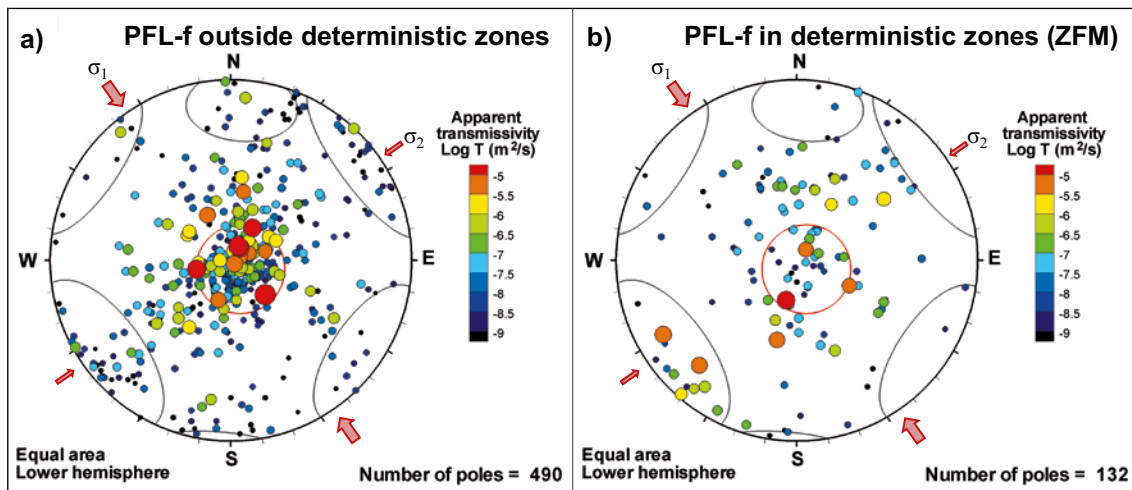


**Figure 4-15.** PFL-f orientation with respect to stress-field; a) outside deterministic deformation zones compared to b) inside deterministic deformation zones (ZFM). The horizontal principal stress orientations ( $\sigma_1$  and  $\sigma_2$ ) shown by red arrows (cf. Figure 4-9). Hard sectors representing fracture set clusters included for reference. The term “apparent transmissivity” is used to emphasise that measurements may be subject to upstream hydraulic chokes (Section 2.3.3).

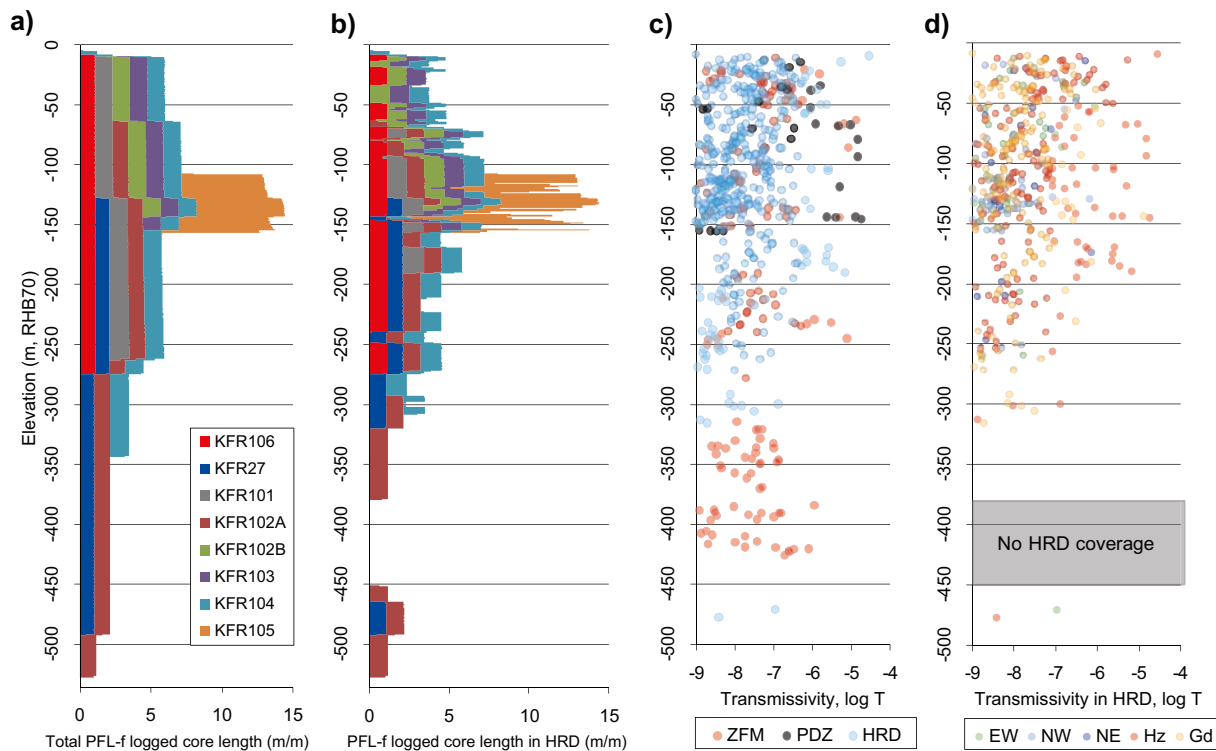


**Figure 4-16.** Borehole coverage and PFL-f transmissivity with depth; a) total PFL-logged core length binned by elevation, b) PFL-logged core length outside deterministic deformation zones (ZFM), c) transmissivity inside deterministic structures (ZFM), Unresolved PDZ, and outside deformation zones (PDZ), and d) transmissivity of stochastic features (HRD and Unresolved PDZ). Note that the sub-horizontal underground borehole KFR105 has a large contribution to PFL-f logged core length in the interval  $-105$  to  $-157$  m RHB70 (orange bars).

Below c.  $-200$  m RHB 70 (i.e. below the Shallow Bedrock Aquifer), the largest PFL-f transmissivity and frequency is found inside deterministic structures (Figure 4-16c). However, this notion must be taken with perspective to the HRD borehole coverage at depth (Figure 4-16b). In general, the orientation and transmissivity patterns in PFL-f data are very similar outside deterministic structures (HRD and Unresolved PDZs) and inside deterministic structures (ZFM; cf. Figure 4-15a and b). Most noteworthy is the large transmissivities associated to steep NW-striking features inside deterministic structures (Figure 4-15b); these are related to the Northern boundary belt and ZFMNNW1034. Note that no oriented data from the Southern boundary belt are included in Figure 4-15; PFL-f data in KFM11A are only available down to 475 m borehole length, south of Singö, and the HTHB data in HFR105, HFM34 and HFM35 are not oriented. Orientation estimates for HTHB data are highly uncertain (see Table E-2), but support the pattern in Figure 4-15b, with sub-horizontal and steep NW-striking high-transmissive features.

In general, the correlation between PFL-f data and the modelled deterministic structures is vague (See Appendix E; a few exceptions can be noted related to the Southern and Northern boundary belts, and ZFMNNW1034, as well as deep intercepts). However, a larger-scale, lateral pattern in PFL-f data seems to exist that is related to the Southern and Northern boundary belts (Figure 4-17). The largest transmissivities ( $T > 10^{-6}$  m<sup>2</sup>/s) are only found close to these geologic belts, and seem absent in the Central block – at least below  $-60$  m RHB 70. This pattern is analysed further in Section 5.3.

However, the data interpretation must account for borehole locations and their representativeness of the domain. Four of the cored boreholes origin from the same starting point at the tip of the Pier, KFR101, KFR102A, KFR102B, and KFR103; these boreholes are affected by the Northern boundary belt and ZFMNNW1034. Similarly, KFR106 and HFR106 drilled from the islet southeast of the Pier are also affected by the Northern boundary belt and ZFMNNW1034. The Central block, which is likely to host the SFR extension, has considerably less borehole coverage, particularly in terms of horizontal PFL-f data.

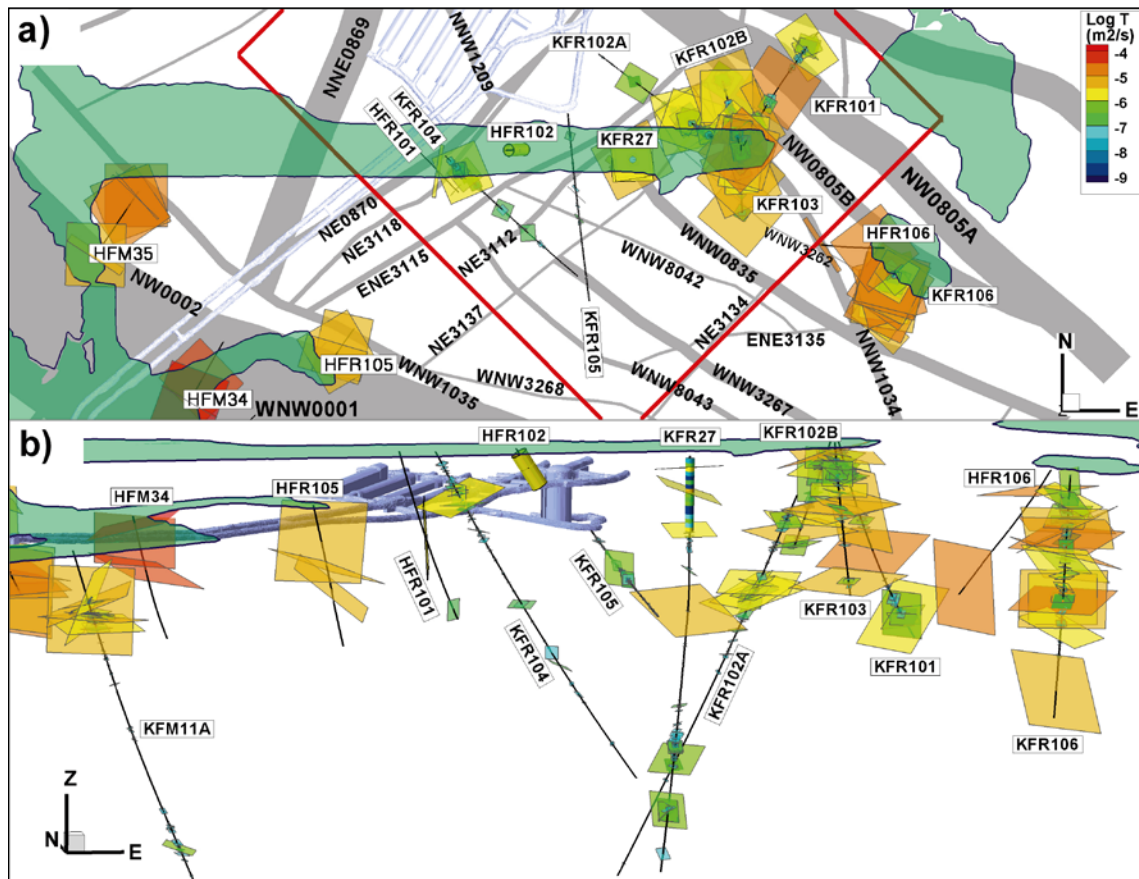


**Figure 4-17.** Transmissivity data from the SFR extension investigation; a) top-view and b) side-view towards north. Injection test in HFR102 and 5 m sequential PFL data in KFR27 shown as cylinders (details on 3 orientation estimates in the upper part of KFR27 given in Figure E-25). Oriented PFL-f (KFR-boreholes) and HTHB (HFR-boreholes, see Table E-2) data are shown as planes sized according to relationships estimated in Öhman and Follin (2010b). Note that estimated orientations for HTHB data are highly uncertain. SFR local model domain is shown by red lines.

The Central block is covered by KFR104, and with some deficiencies: KFR105, KFR27 and HFR101. KFR105 is sub-horizontal, entailing sampling bias versus the hydraulically important horizontal features (Figure E-17). Core is unavailable in the upper 148.5 m of KFR27 and the borehole is located more or less inside the deformation zone ZFMWNW0835 (Figure E-23). HFR101 has only two HTHB records and is not applicable for Hydro-DFN parameterisation.

### 4.3.3 Transient hydraulic evaluation from the SFR extension investigation

Transient data from borehole pumping allows the estimation of influence radii,  $r_{inf}$ , hydraulic flow boundaries and skin factors. In most cases the effective parameters have been evaluated at borehole scale (Table 4-4); it is assumed that they relate to the most conductive structures of the tested borehole (or borehole sections of KFR27 and HFR105). It should be emphasised that the evaluated influence radii are highly uncertain and should only be analysed indicatively. The results are commented and put into context of other data types in Table 4-4.

Most boreholes have negative skin, which implies stimulated fractures and overestimated transmissivity (i.e. conservative estimates). Only two boreholes, KFR102B and KFR103, have interpreted positive skin (clogged fractures), which implies the risk of underestimating transmissivity. Apparent negative hydraulic flow boundaries are interpreted to reflect either: 1) hydraulic contact to the existing SFR, or 2) compartmentalised of the fracture network, or 3) declining transmissivity with distance. Apparent positive hydraulic flow boundaries are assumed to reflect: 1) hydraulic contact to the sea, or 2) connection to one or several structures with higher transmissivity.

**Table 4-4. Transient evaluation of borehole pumping (influence radii are coloured to facilitate visual comparison: blue = shortest, red = longest).**

Borehole	Estimated $r_{int}$ (m)	Hydraulic boundary	Skin factor	Comment
HFR101	107	–	–7.6	PWH = –31 m in HFR101 (Figure 4-28), suggesting that the negative flow boundary reflects influence from SFR. Hydraulic interferences with KFR02, KFR104 and HFR105 observed at a maximum distance of 360 m (Figure 4-21)
HFR102	137	None	–1.5	Shallow test below the SFR Pier (–6 to –44 m RHB 70; $T \approx 10^{-6}$ m <sup>2</sup> /s) outside deformation zones. An influence radius of 137 m without flow boundary suggests horizontal flow. Modelled as SBA1.
HFR105 <sup>1)</sup>	145	+	0	Shallow pump test (21.1–38.0 m borehole length; $T \approx 10^{-6}$ m <sup>2</sup> /s) located inside the Singö deformation zone. The positive flow boundary may indicate channels inside Singö or connection to the Sea.
HFR105 <sup>2)</sup>	756	None	–7	Large influence radius without flow boundary effects. Highest HTHB located at c. 120 m borehole length ( $T \approx 10^{-5}$ m <sup>2</sup> /s) inside ZFMWNW1035. At least indirectly connected to KFR104, which has similar characteristics (Figure 4-21).
HFR106	244	–	n/a	Interpreted as linear flow dimension. Supported by channelled, remote connections to ZFM871 (c. 650 m; Figure 4-26). Possibly a horizontal channel in ZFMNNW1034?
KFR101	234	–	–6.4	KFR101 has a leaking casing ( $T \approx 10^{-5}$ m <sup>2</sup> /s) and hydraulic contact with the Northern boundary belt as well as SBA6. Its short influence radius and negative flow boundary suggests influence from SFR or hydraulic discontinuity in modelled structures.
KFR102A	1,100	None	–7.5	Large influence radius without flow boundary effects; assumed to reflect SBA6 or ZFMENE3115 (connected to ZFM871). Connection to ZFM871 is interpreted from interferences (Figure 4-24).
KFR102B	324	+	0.6	Interpreted as a leaky aquifer (contact to the Sea). KFR102B has EW-striking and horizontal PFL-f that are highly transmissive and is located parallel to ZFMNW0805B.
KFR103	359	+	7.2	KFR103 flow is dominated by leaking casing at shallow depth. The positive hydraulic boundary is assumed related to the leaking casing (at shallow depth).
KFR104	783	None	–4.9	Large influence radius without flow boundary effects; assumed to reflect ZFMENE3115 (connected to ZFM871).
KFR105	29	+	–3	KFR105 is dominated by steep NW-striking PFL-f with lower transmissivity. Possibly the positive boundary is a vertical connection to SBA1 or SBA6, which are located 50 m above, respectively, 65 m below. Interferences were observed at some 400 m distance (Figure 4-25 and Figure 4-22).
KFR106	108	–	–3.9	The short influence radius and negative flow boundary suggests influence from SFR or discontinuity in modelled structures. Only short interference distances observed from KFR106 (Figure 4-27).
KFR27 <sup>3)</sup>	199	+	–6.4	The upper 148.5 m of KFR27 intersects SBA1 and SBA2. The two upper monitored sections (above 109 m RHB 70) have PWH equal to –0.3 and –0.5 m, supporting contact to the sea. The upper part has more similarities to KFR102B, KFR103, and KFR105, while its deeper part is more similar to KFR102A and KFR104.
KFR27 <sup>4)</sup>	970	None	–7.8	Large influence radius without flow boundary effects; assumed to reflect SBA6 or ZFMENE3115 (connected to ZFM871). Connection to ZFM871 is interpreted from interferences (Figure 4-23).

<sup>1)</sup> Tested section (21.1–38.0 m).

<sup>2)</sup> Tested section (21.1–200.5 m).

<sup>3)</sup> Tested section (11.9–148.5 m).

<sup>4)</sup> Tested section (11.9–501.6 m).

Large influence radii,  $r_{inf} > 700$  m, without indications of hydraulic boundaries have been estimated for HFR105, KFR102A, KFR104, and KFR27. A common factor for these boreholes is that they also exhibit drawdown from SFR (Section 4.5), which is possibly related to direct or indirect contact with ZFMENE3115. ZFMENE3115 is expected to have hydraulic contact to SFR, as it is the steeply dipping deformation zone that terminates ZFM871 (Zone H2) to the southeast. KFR102A and KFR27 are possibly inter-connected via the horizontal hydraulic feature SBA6 (Appendix B).

It can be noted that the three boreholes, KFR101, KFR106, and HFR106, most intimately related to the *high transmissive* rock mass in the vicinity of the Northern boundary belt and ZFMNNW1034 (Figure 4-17), are all interpreted to have *apparent negative flow* boundaries. The high transmissivities yielded from the *continuous* PFL logging suggests that the boreholes are well-connected to the sea, but this cannot be inferred in the transient data. The apparent negative flow boundary is interpreted as discontinuity, or declining transmissivity at distance, in the most dominant hydraulic structures of the boreholes, possibly under influence from SFR. In other words, the continuity in the particularly high-transmissive rock mass around the Northern boundary belt and ZFMNNW1034 may have a limited spatial extension ( $r_{inf} \approx 100$  to 250 m).

#### 4.4 Evaluation of cross-hole (interference) tests

The experience from the SDM-Site Forsmark is that hydraulic interferences provided key evidence for the understanding and characterisation of the superficial bedrock (i.e. existence and character of sheet joints; Figure 2-4). Therefore, hydraulic interferences have been evaluated during the SFR extension investigations. It should be noted that these interferences occur below the Baltic Sea, which is an unusual situation for this type of analysis.

The flow pattern and drawdown around a pumped borehole in a heterogeneous fractured medium are highly dependent on the structure of the fracture system, as well as, on the connectivity to hydraulic boundaries (in this case the SFR facility and the Baltic Sea). However, an *apparent hydraulic diffusivity* may be estimated for the fracture network between a pumped borehole and an observation section. Diffusivity is a measure of the hydraulic communication in the bedrock, in terms of propagation rate of pressure changes between a disturbance and an observation point. For a confined, homogeneous, radial flow system, Streltsova (1988) defined the hydraulic diffusivity,  $\alpha$ , as:

$$\alpha = \frac{T}{S} = \frac{r_s^2}{4dt_L \left(1 + \frac{dt_L}{t_p}\right) \ln\left(1 + \frac{t_p}{dt_L}\right)}, \quad (4-1)$$

where T is transmissivity ( $\text{m}^2/\text{s}$ ), S is storativity (-),  $r_s$  is the 3D radial distance between the disturbance and the monitored borehole section (m),  $t_p$  is the duration of pumping (s), and  $dt_L$  is the measured response time (s). In other words, a highly transmissive, well-connected fracture system has a high diffusivity, while a highly compartmentalised fracture system, composed of poorly connected dead-end clusters, has a lower diffusivity.

A response is defined by a specified drawdown threshold,  $dp$  (m), which is normally set to  $dp = 0.01$  m (Follin 2008). Due to data noise levels at SFR (e.g. Figure 4-18 and see Appendix F), it was decided to use a higher drawdown criterion in the interpretation of interferences,  $dp = 0.1$  m (Walger et al. 2010). This methodological discrepancy must be accounted for when the SFR site is compared to the nearby SDM-Site Forsmark, which is discussed further in Section 5.1.



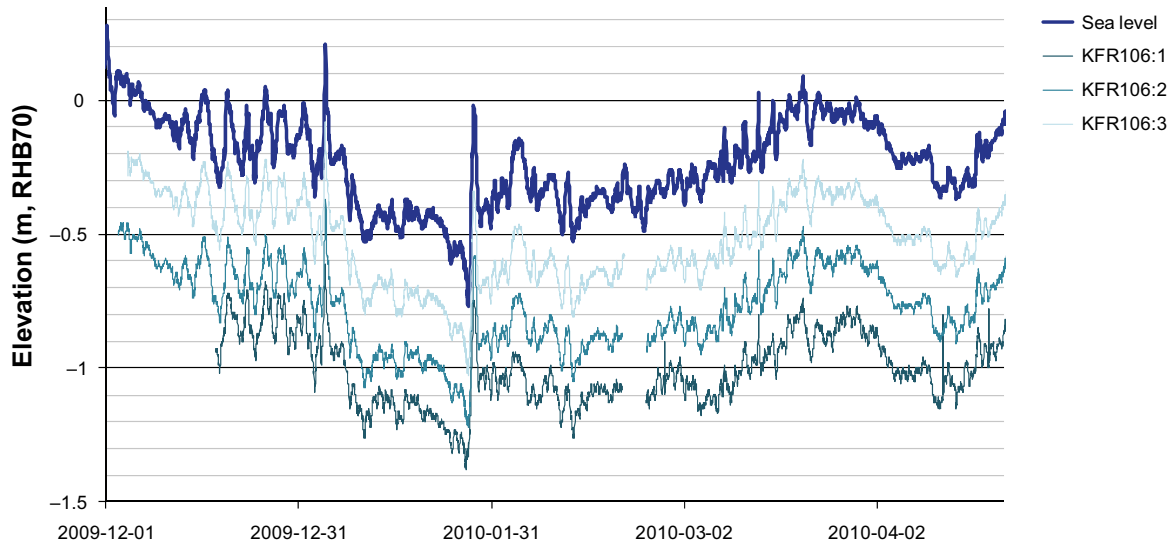


**Figure 4-18.** Example of correlation to sea-level fluctuations and PWH in monitored sections. Owing to data noise level, hydraulic responses were defined for a drawdown of 0.1 m.

Previous experience from the SDM-Site Forsmark investigations is that the upper bedrock is highly channelized. It may therefore be misleading to discuss hydraulic interferences in terms of apparent diffusivity, based on an inappropriate analogy to porous media with cylindrical flow regime. Instead, an alternative, more straight-forward measure of pressure propagation is evaluated, the so-called *response index 1* (Walger et al. 2010). This index is a simple ratio with the same units as diffusivity, but avoids the analogy to flow in a porous medium:

$$\text{response index 1} = \frac{r_s^2}{dt_L} \quad (4-2)$$

The strength of responses is also calculated in terms of a normalised drawdown (Walger et al. 2010)

$$\text{response index 2 new} = \frac{S_p}{Q_p} \ln \left( \frac{r_s}{r_0} \right) \quad (4-3)$$

where  $S_p$  is the maximal drawdown,  $Q_p$  is pumping rate at the end of the flow period, and  $r_0$  is a fictive borehole radius (set to 1 m). Note that the two indices are not necessarily related; for example: a rapidly propagating pulse (high index 1) may be weak (low index 2 new).

The responses in the old data set, underground interference tests performed during 1985 to 1987, only have qualitatively interpreted classifications: *direct response*, *indirect response* and *no response*.

#### 4.4.1 Old interference data close to the existing SFR

The old, underground interference tests, performed during 1985 to 1987, provide insight into the connectivity between zones surrounding the existing SFR facility. These interference tests were re-assessed by Axelsson and Mærsk Hansen (1997); their interpretation has been placed in context to the final geologic SFR model v. 1.0 (Table 4-5; see also Appendix D). The responses have only been used qualitatively; classed as *direct response*, *indirect response* and *no response*.

The general impression is that ZFM871 has a central role in the hydraulic connectivity around SFR; disturbances in ZFM871 are monitored in all steeply dipping deformation zones (ZFMNE0870, ZFMNW0805A,B, and ZFMNNE0869), and vice-versa, disturbances in steeply dipping deformation zones are generally monitored in ZFM871. There also exists evidence of lacking internal connectivity inside ZFM871 (i.e. monitored sections in ZFM871 not responding to an interference in ZFM871), as well as lacking or indirect responses between ZFM871 and surrounding steeply dipping zones (particularly ZFMNW0805A,B). ZFM871 is interpreted as conductive and heterogeneous.

**Table 4-5. Overview of cross-hole tests performed 1985 to 1987 (see Appendix D).**

Interference	Monitored sections					
	NE0870	NNE0869 <sup>2)</sup>	NW0805A, B	ZFM871 <sup>3)</sup>	PDZ <sup>4)</sup>	HRD
<b>NE0870<sup>1)</sup> (3 tests)</b>						
Direct response	9			5		12
No response	5			2		8
<b>NNE0869 (1 test)</b>						
Direct response		4		1		2
<b>NW0805A (1 test)</b>						
Direct response			2	1		
Indirect response	1		6	2		8
No response	4	6		5	1	21
<b>ZFM871 (5 tests)</b>						
Direct response	11	3	6	11	1	28
Indirect response	5	1	14	4		23
No response	6	10	7	8	2	51

<sup>1)</sup> Including one test below the Silo, at the rim of ZFMNE0870 (Zon 9).

<sup>2)</sup> KFR09\_DZ2 interpreted as part of ZFMNNE0869 (Zon 3).

<sup>3)</sup> KFR10\_DZ2 interpreted as extension of ZFM871 (Zon H2).

<sup>4)</sup> KFR20\_DZ1.

Most striking is the “unintentional interference test” in KFR80 (penetration of ZFM871 during grouting), which was interpreted to cause drawdown in KFR01, at 870 m distance. Also, ZFM871 is better connected to ZFMNW0805A than it is to ZFMNW0805B, which is quite surprising considering that ZFMNW0805A is located outside ZFMNW0805B (see Appendix D). Based on single-hole transmissivity, ZFMNW0805A is judged to be more transmissive than ZFMNW0805B. Note also that the SFR tunnel section IB intersects ZFMNW0805B, without need for grouting. The interference data, as well as single-hole transmissivity data, support the notion that KFR09\_DZ2 should be interpreted as a splay of ZFMNNE0869, and KFR10\_DZ2 as an extension of ZFM871.

#### 4.4.2 New interference data from the SFR extension investigation

##### Overview

Two planned interference tests were performed in the site investigation for the SFR extension; a pumping test in HFR101 and opening of the underground borehole KFR105. They were evaluated in terms of apparent hydraulic diffusivity, normalised drawdown, and boundary-condition interpretations for responding observation sections (Walger et al. 2010). The two response indices evaluated from the interference tests (“index 1” and “index 2 new”) are not particularly correlated (Figure 4-19). The premises for the planned interference tests were non-optimal as the two tested boreholes have quite low transmissivities, which limited the pumping flow rates (i.e. compare the magnitudes of evaluated index 1 between planned interference tests and drilling activities, respectively, in Figure 4-20).

In addition to the planned tests, interferences from borehole activities that cause hydraulic responses, like drilling and nitrogen flushing, were analysed and evaluated by Walger et al. (2010). The evaluation of *drilling responses* involved a qualitative classification of the responses at different drilling depths and a quantitative estimation of apparent hydraulic diffusivity between the drilled borehole and the observation section. For totally 86 observations from both the interference tests and drilling responses, the response index 1 range from 0.04 to 36 m<sup>2</sup>/s, with a geometric mean of 1.1 m<sup>2</sup>/s (Figure 4-20). The fastest observed responses relate to drilling responses (compare red and green hues in Figure 4-20). The response index 1 at SFR is about one order of magnitude lower than those observed at the SDM-Site Forsmark (details of the comparison given in Section 5.1).

The response index 1 is visualised for all clearly observed hydraulic interferences (drilling activities and planned interference tests) during the SFR site investigations (Figure 4-21 to Figure 4-27).

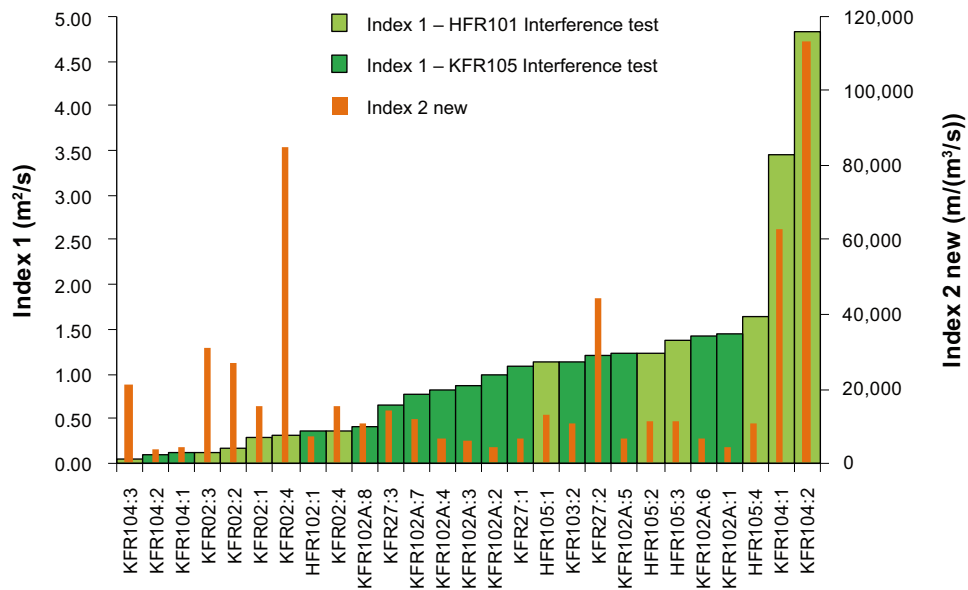


**Figure 4-19.** Evaluated response indices (propagation speed and response strength, respectively) for observation sections that responded to interference tests in HFR101 and KFR105. The two indices are explained in Section 4.4.

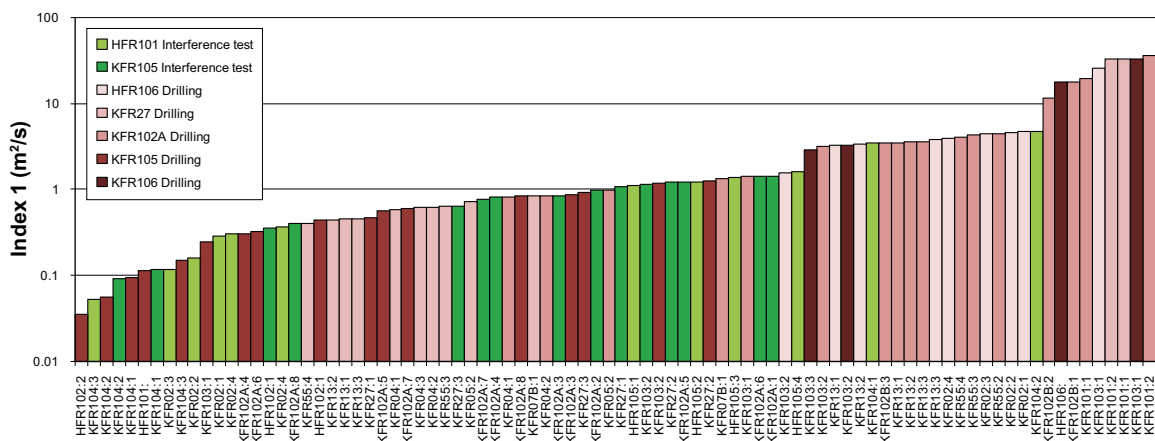


**Figure 4-20.** Response index 1 (normalised spherical distance with respect to response time) evaluated for interference tests and drilling responses at all observation sections that have been noted to respond. The response time was defined as the arrival time for a drawdown of 0.1 m (Walger et al. 2010).

### Visualisation and detailed analysis

The interference pumping test in HFR101 was performed by pumping the open borehole at a rate of about 10 L/min for three days. Groundwater pressure was monitored during the pumping period and the subsequent recovery period in all instrumented boreholes surrounding SFR, in total at 68 monitoring sections in 22 observation boreholes (Figure 4-21). Twenty of these are core-drilled (with a total of 62 monitoring sections) and two are percussion-drilled with totally 6 monitoring sections. HFR101 has a point-water head of  $-31$  m, indicating that (in spite of shallow casing at  $-4.65$  m RHB 70) its contact to the sea is poor relatively to its contact to SFR (ZFM871). The responses are found in monitored sections that also have notable drawdown related to the SFR inflow (Figure 4-29). The most rapid response (largest response index 1) is found in the two deepest sections of KFR104 (Figure 4-21). These sections of KFR104 also have large drawdown (PWH  $\approx -14$  m; Section 4.5.4), particularly at elevations close to the termination of ZFM871 (i.e. ZFM871 would intersect this monitored section, if ZFM871 does not terminate against ZFMENE3115).

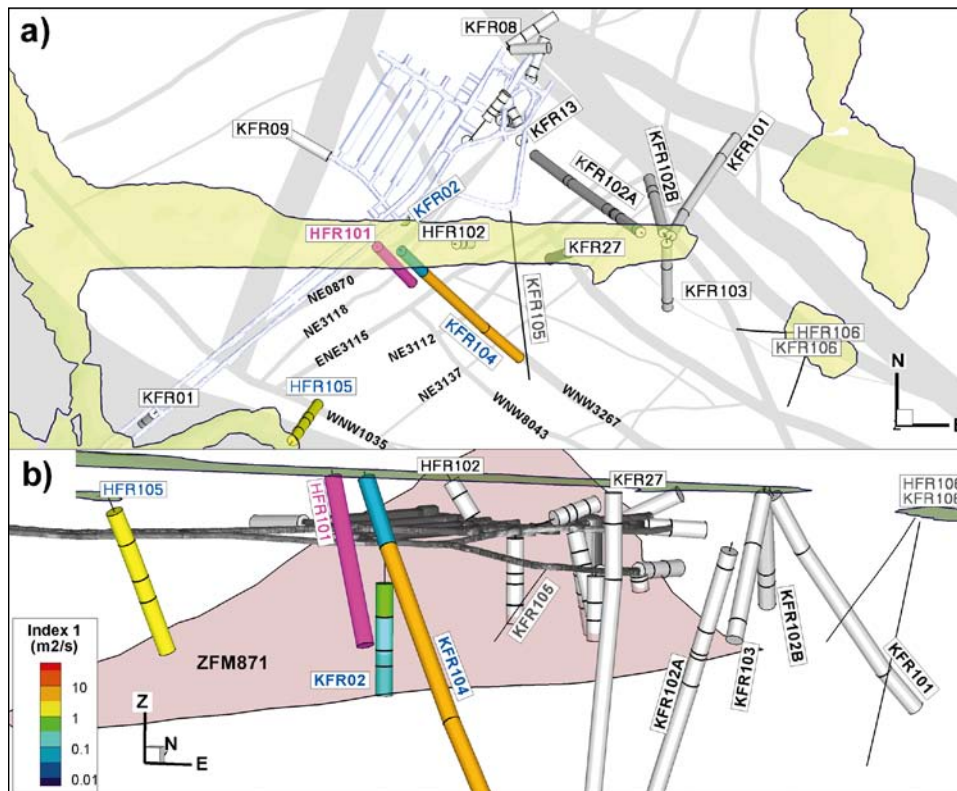


**Figure 4-21.** Hydraulic responses to the three-day long interference test conducted in HFR101 (purple) in April 2009; a) top view and b) side-view from the South. Clear test responses observed in 11 out of a total of 68 monitoring sections. Maximum observed radius of influence (spherical distance) was c. 360 m. The deformation zones are shown as surface traces.

The interference pumping test in the underground borehole KFR105 was performed by releasing the shut-in pressure in all its packed-off sections simultaneously for one day. The total flow rate from the borehole was about 11 L/min at the end of the flow period. Groundwater pressure was monitored at in total 76 monitoring sections in 24 observation boreholes (Figure 4-22). Twenty of these are core-drilled (with a total of 65 monitoring sections) and four are percussion-drilled with totally 11 monitoring sections. The evaluated response index 1 of this interference is higher towards the Northern boundary belt than it is inside the Central block (KFR104).

Pressure interferences were observed during drilling and the drilling activities in HFR102, KFR27, KFR102A, KFR105, HFR106, and KFR106. All available monitoring sections in the surroundings of SFR were analysed; the number of available sections grew with the progress of the investigation programme (Figure 4-26 to Figure 4-27). The interferences from drilling activities in KFR27 and KFR102A are very similar; responses are found both in ZFM871 and close to the Northern boundary belt (cf. Figure 4-23 and Figure 4-24). HFR106 and KFR106 are located outside the Local domain close to the Northern boundary belt and ZFMNNW1034. Both were drilled from an islet Southeast of the tip of the Pier and cause interferences at depth in KFR103 (Figure 4-26 and Figure 4-27). However, note that HFR106 also caused distant interferences (c. 650 m) in monitored sections inside ZFM871 (KFR02 and KFR13), which could not be clearly observed in KFR27 and KFR102A (Figure 4-26).

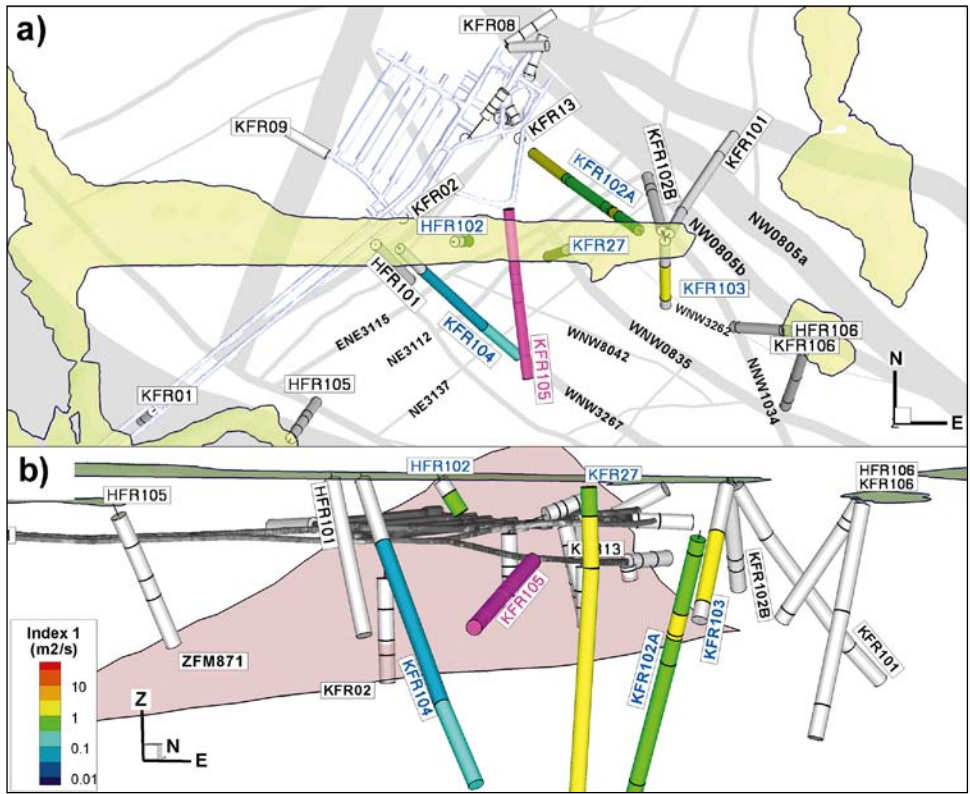


Figure 4-22. Hydraulic responses to the one-day long interference test in KFR105 (purple) March 2010; a) top view and b) side-view from the South. Clear responses observed in 15 of totally 76 monitored sections. Maximum observed radius of influence was c. 400 m.

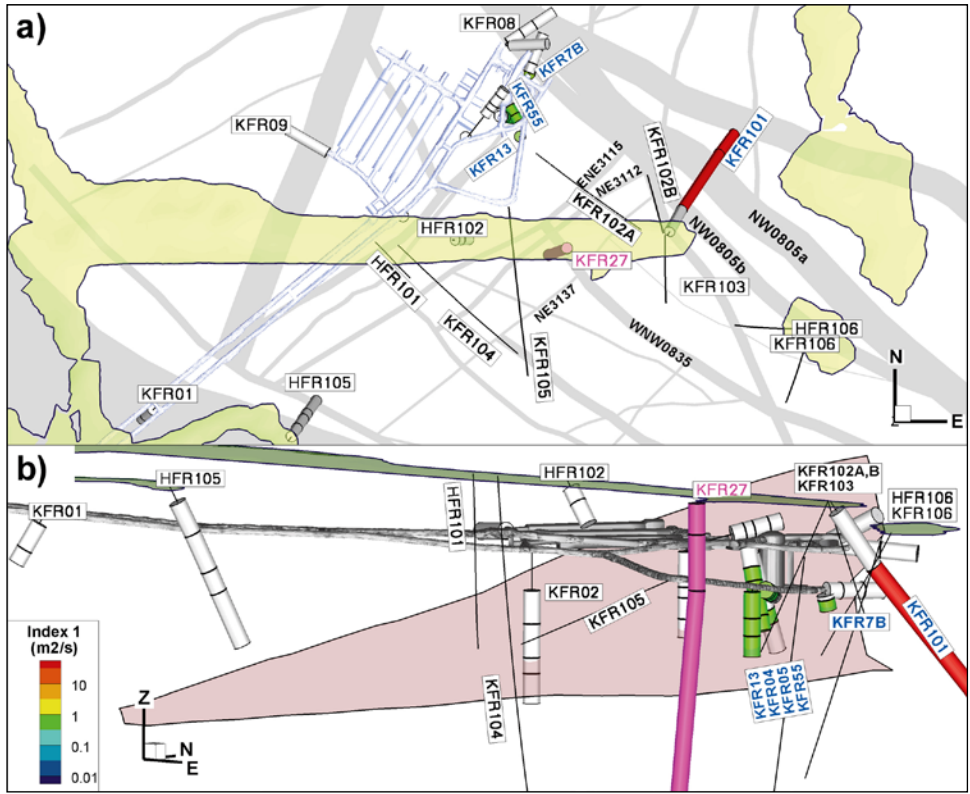
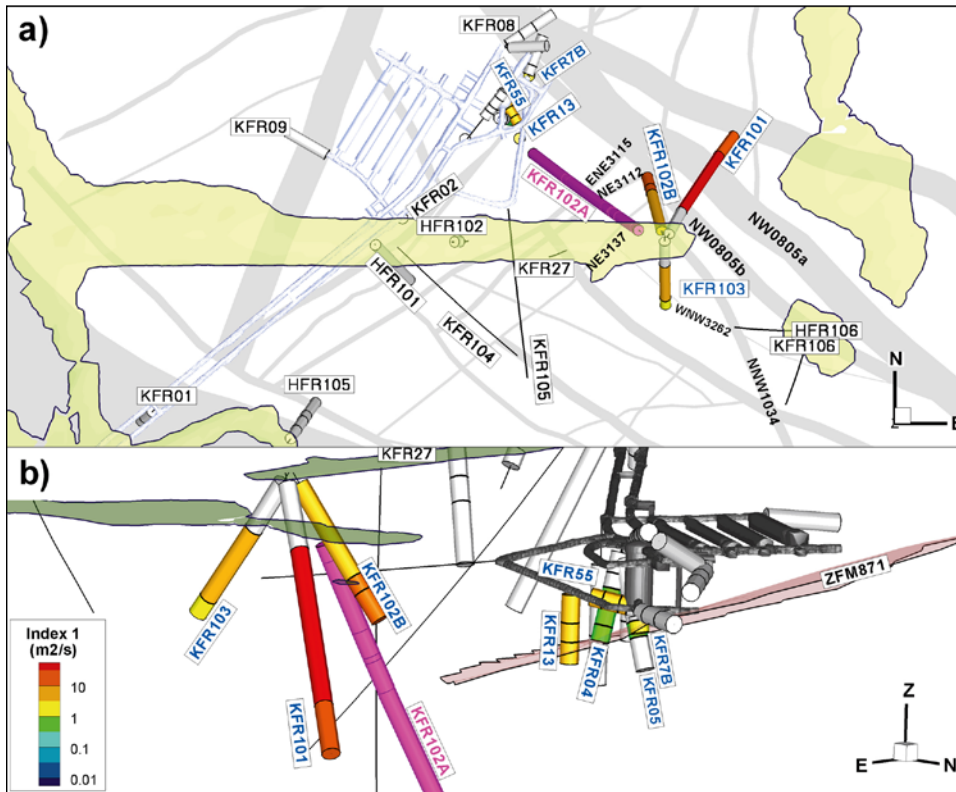
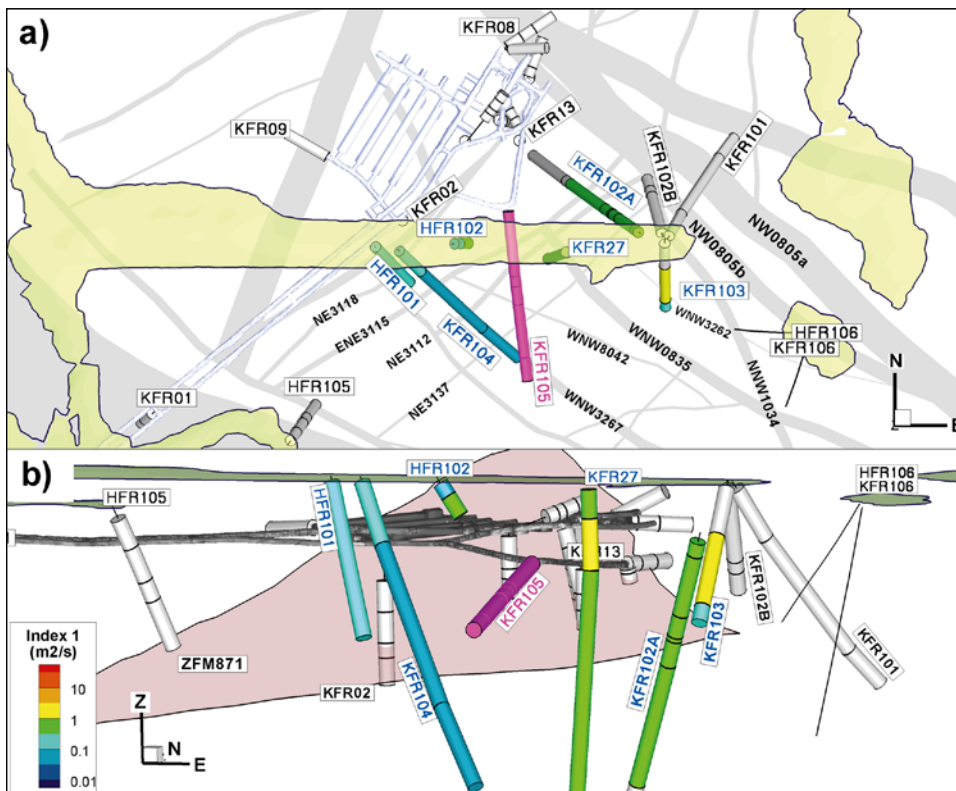


Figure 4-23. Hydraulic responses to the drilling (extension) of KFR27 (purple) in October 2008; a) top view and b) side-view from the Southeast. Clear responses observed in 12 out of a total of 48 monitoring sections. Maximum observed radius of influence (spherical distance) was c. 340 m.



**Figure 4-24.** Hydraulic responses to the drilling of KFR102A (purple) in November–December 2008; a) top view and b) side-view from the Northeast. Clear responses observed in 17 out of a total of 54 monitoring sections. Maximum observed radius of influence (spherical distance) was c. 290 m.



**Figure 4-25.** Hydraulic responses to the drilling of KFR105 (purple) in April–June 2009; a) top view and b) side-view from the Southeast. Clear responses observed in 14 out of a total of 69 monitoring sections. Maximum observed radius of influence (spherical distance) was c. 270 m.

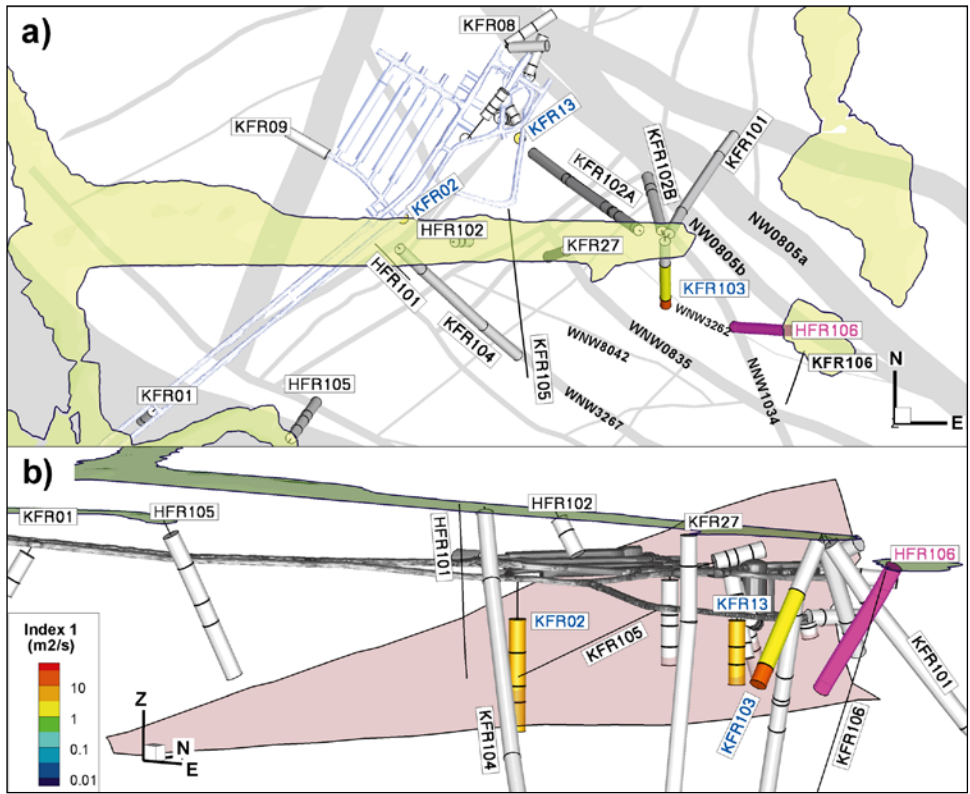


**Figure 4-26.** Hydraulic responses to the drilling of HFR106 (purple) in June–July 2009; a) top view and b) side-view from the Southeast. Clear responses observed in 9 out of a total of 69 monitoring sections. Maximum observed radius of influence was c. 650 m. Uncertain responses in KFR102A not shown.

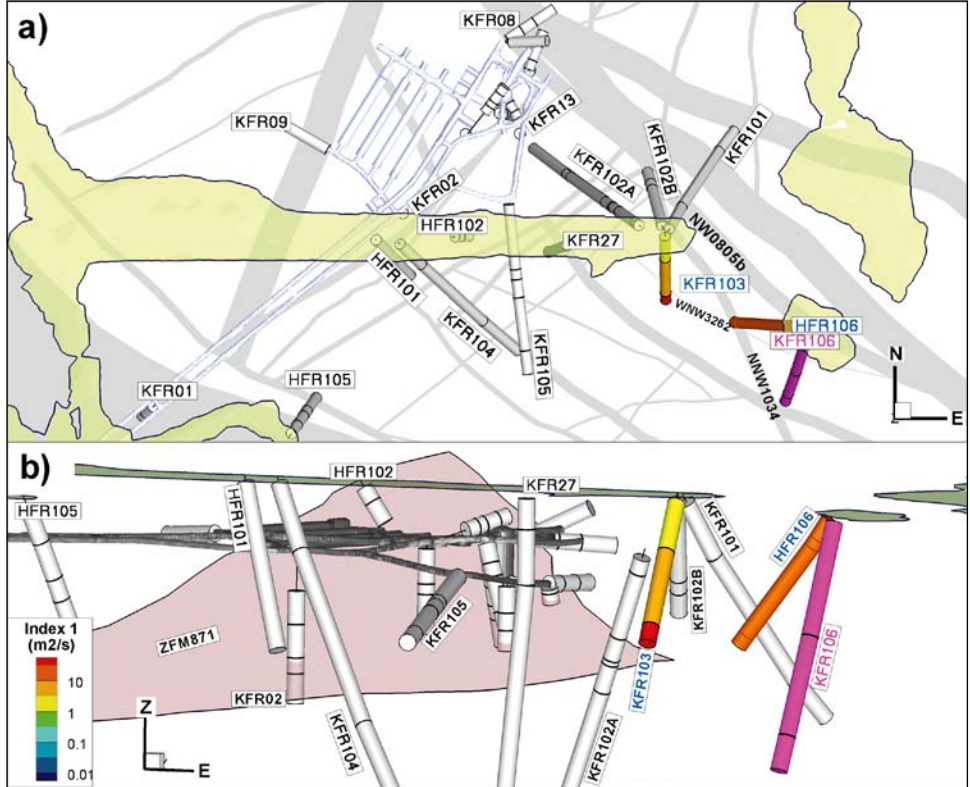


**Figure 4-27.** Hydraulic responses to the drilling of KFR106 (purple) in August–September 2009; a) top view and b) side-view from the South. Clear responses were observed in 5 out of a total of 76 monitoring sections. The maximum observed radius of influence c. 340 m.

## 4.5 Drawdown around SFR

Pressure data are available for SFR as either *fresh-water head* (FWH) or *point-water head* (PWH). The old, underground borehole data in SFR are reported as *FWH*, while the recent data from surface boreholes are reported as *PWH*. Owing to variations in density and temperature, neither of the two types is directly comparable to *hydraulic head* (or *environmental head*; i.e. the driving potential of vertical flow). The head concept for a borehole multi-packer system are explained in detail in Follin (2008). The measured entity is pressure,  $P$ , which is corrected for barometric changes. The pressure is converted into a head value,  $H_i$  (m) of type  $i$ , according to:

$$H_i = \frac{P}{g\rho_i} + z \quad (4-4)$$

where  $g$  is the gravitational acceleration constant,  $z$  is the elevation of monitoring interval, and  $\rho$  is the reference fluid density. This reference fluid density can be of two types,  $i$ ; if it reflects the actual fluid density of the borehole interval it is referred to as *point-water head*, otherwise fresh water is used as reference density, it is referred to as *fresh-water head*. The actual difference between fresh-water and environmental head is estimated to be at most 0.5 m in the SFR data (SKBdoc 1233647). Thus, a *fresh-water head* may well be slightly above the mean sea-level, as in the case of e.g. early reported measurements of KFR09 (Carlsson et al. 1987).

The natural groundwater levels and point-water heads in the Forsmark inland have been compiled by Johansson and Öhman (2008). In SDM-Site Forsmark, the possible hydraulic connection between SFR and the Forsmark inland was considered to be an important unresolved uncertainty. For instance, in the upper 130 m of KFM11A, the groundwater level is two meters below the datum (Follin 2008) (this borehole section is located south of the Singö deformation zone, c. 100 m from the SFR access tunnels).

The few indications of flow inside the SFR domain under natural conditions, i.e. prior to tunnel constructions, are discussed in Section 4.5.1. As of today, there hardly exists any undisturbed groundwater levels inside the SFR modelling domain; the entire head-field is more or less affected by the ongoing SFR inflow, since its construction in 1985. In fact, the drawdown around the SFR facility can be regarded as a large-scale long-term interference test (Section 4.5.2). At a given monitoring point, the measured drawdown can be interpreted as an indication of its hydraulic connection to SFR *relative* to its hydraulic connection to the Sea. In other words, a large drawdown observation far away from the SFR repository implies relatively poor connection to the overlying Sea, while a low drawdown close to SFR indicates poor connection to SFR. Drawdown is a dissipative process, implying that the dominant connection will mask subordinate connections.

### 4.5.1 Excess groundwater head prior to SFR construction

Five boreholes (KFR21–25) were drilled from a floating platform at sea during the early site investigations for SFR (1980–1981; i.e. previous to tunnel constructions). Falling-head tests and groundwater-head measurements were performed in these boreholes. Excess heads relative to the mean seawater level were reported for KFR21, KFR22, and KFR25 (Carlsson et al. 1986), varying between +0.11 meters and +0.75 meters (Table 4-6). It is stated that the excess heads were evaluated after due compensation to density differences between injected water and seawater. These excess heads were measured in highly transmissive intervals ( $10^{-6}$  to  $10^{-5}$  m<sup>2</sup>/s), which are located inside ZFM871 and ZFMNW0805A (Table 4-6). If these values are correct, it would correspond to an upward-directed gradient of c. 0.004 m/m (0.5 m/120 m) and thus, implying a large vertical hydraulic resistivity (i.e. with consideration to the low topographical regional gradient).

However, as of today, two aspects remain uncertain: 1) how the density compensation was made and 2) the extent to which the measured heads are affected by the preceding falling-head tests. According to Carlsson et al. (1987), the falling-head tests were performed by applying a 5 or 10 m excess head and monitoring its recovery during c. 5 minutes. According to theory, the proper evaluation of slug tests requires 90% recovery, which for a borehole section with transmissivity on the order  $10^{-6}$  m<sup>2</sup>/s would take on the order 1 hour. Therefore, Carlsson et al. (1987, p 55) concludes that the reported excess head is probably too high or possibly artefacts of the measurement and evaluation technique.



**Table 4-6. Excess head prior to the SFR construction. Modified from Carlsson et al. (1986).**

	Borehole section (m)	Reported head rel. to Baltic mean level (m)	Inside deformation zone (Geologic model SFR v. 1.0)
KFR21	115–118	+0.11	ZFM871
	118–121	+0.75	ZFM871
KFR22	148–151	+0.56	ZFM871
	148–157	+0.57	ZFM871
KFR25	139–142	+0.59	ZFMNW0805A <sup>1)</sup>
	142–145	+0.61	ZFMNW0805A <sup>1)</sup>

<sup>1)</sup> In the geologic model SFR v. 1.0, ZFM871 is terminated against ZFMNW0805B (Figure 3-5). The excess head is reported over the same elevation interval as the termination of ZFM871. In other words, if ZFM871 should extend beyond ZFMNW0805B, as interpreted in earlier structural models (e.g. Axelsson and Mærsk Hansen 1997), the KFR25 intercept may also relate to ZFM871 (see Appendix D).

Different hypotheses have been postulated and simulated for these excess heads (Carlsson et al. 1986, 1987, Holmén and Stigsson 2001). One hypothesis concerns shut-in pressures induced by the ongoing land lift (Holmén and Stigsson 2001); if the hydrogeological system is *slow* (storativity versus conductivity) relative to the uplifting of the rock mass (c. 5 mm/yr), the excess head may be the result of a transient process. The non-equilibrium between rock mass head and the sea can only be sustained if the vertical hydraulic contact to the sea is poor (e.g. constrained by sediments, hydraulic anisotropy). However, these five boreholes were drilled north of the Pier where sediment layers are thin and the material is coarse (cf. Figure 4-12 and Figure 4-34).

Another potential explanation relates to regional-scale flow via the Forsmark SBA-structures (Figure 2-4) entering a highly anisotropic, potentially confined hydrogeological system of SFR. If the SBA flow can cross the Singö deformation zone, at some point, the excess head may reflect topographically elevated parts of the Forsmark inland. This would require that Singö is not completely impermeable for orthogonal flow and that it is poorly connected to the Baltic (possibly plugged by glacial clay, Figure 4-34). This overpressure may propagate via the gently dipping ZFM871. A poor connectivity between ZFM871 and steeply dipping zones is indicated by differences in head and hydrochemistry between KFR08 and KFR07A, respectively, KFR09 and KFR10, Figure 4-28a and Figure 4-32b). See Table 4-5 for observed interference responses, as well as, lack of direct responses, between ZFM871 and steeply dipping zones.

#### 4.5.2 Long-term monitoring programme of head in tunnel boreholes

The long-term groundwater pressure evolution around the SFR facility is monitored in tunnel boreholes since the construction phase in 1985. In total, there are 39 sections in 12 boreholes being monitored and the results are reported on a yearly basis (e.g. SKBdoc 1233647). The observed general behaviour was a rapid drop in head during the construction period and the first time thereafter. The head quickly stabilised in the largest zones ZFMWNW0001 and ZFMNW0805A,B (the Singö zone and Zone 8). In the less conductive rock there has been a slow, relatively constant, declining trend in most borehole sections since 1987–1988. The head drop has been most pronounced in the vicinity of the Silo, associated to zones ZFMNE0870 (formerly known as Zone 9) and ZFM871 (formerly known as Zone H2; Figure 4-28b). In these boreholes the head decline was about –0.5 to –1 m/yr during year 2009. KFR7A has the highest drawdown as well as the largest decline during the monitoring period (–2 m/yr). KFR7A is located inside ZFMNW0805A,B, but clearly has different fresh-water head and transient development compared to other monitored sections inside the zone (KFR08 and KFR56; Figure 4-28). KFR7A also has a so-called *geometric intercept* with ZFM871; based on observations in head and electrical conductivity (Section 4.6.2) it is considered likely to represent a junction of the zones that is also affected by grouting. Note that the tunnel intersection of ZFM871 (NBT/NDB tunnel sections; Figure 4-3) was heavily grouted (67.5 m<sup>3</sup> cement). The head development in borehole sections that penetrate ZFM871 vary spatially; an increase in KFR02 (related to re-instrumentation in 2008), and different rates of decline in KFR03, KFR04, KFR05, KFR13, and KFR7B. This indicates that the zone is heterogeneous and hydraulically discontinuous. However, the trend is generally declining. Most notably, KFR09, located inside ZFMNNW0869 (Zon 3), only has a minor drawdown (FWH = –1.9 m), in spite of its location close to the non-grouted tunnel wall.

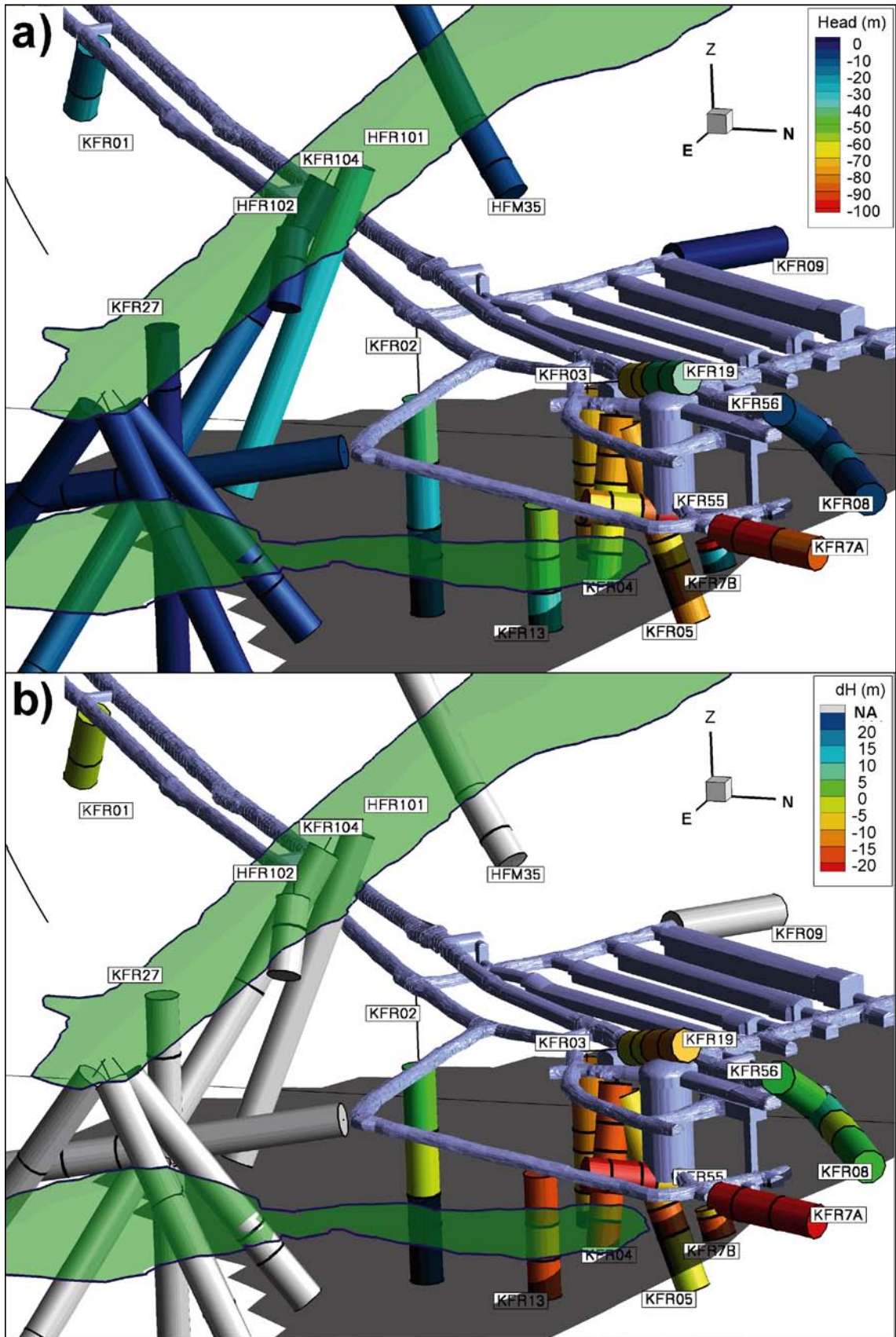


**Figure 4-28.** Head in SFR tunnel boreholes; a) 2010 and b) change in head between year 1988 and 2010. The reference year 1988 was chosen since it has been a relatively constant, declining trend in most borehole sections since then.

The head in a majority of the observation sections show a strong correlation with the sea-level fluctuations. A correlation with sea level and atmospheric pressure may be both due to pressure diffusion through the bedrock and an instantaneous mechanic effect due to surface-loading change. The ongoing transient development of head and inflow could indicate a slow system with constrained contact to the Sea (Figure 4-35), which would suggest that most observed correlations would be the result of mechanical loading. The correlation is highest inside deformation zones (including the sub-horizontal ZFM871), indicating connection to the Baltic Sea. The exception is the Singö zone (borehole KFR01:1) (SKBdoc 1233647). The measurements of the absolute groundwater pressure in this borehole section show a much lower correlation with Sea level and atmospheric pressure which indicate that the zone, or at least the hydraulic contact with this borehole section, is confined at the surface (and that the sensitivity to surface-loading variation is low (see Section 4.7.1). However, the other existing boreholes in the Singö zone (KFM11A, HFM 34, and HFM35) have stronger correlation with sea-level variation.

A seasonal variation in monitored head is an indication of connection to a groundwater system below land. Such seasonal variation has only been observed in borehole KFR02, which is the deepest and also located closest to land of the old SFR tunnel boreholes (disregarding KFR01 in the Singö zone; see Figure 4-29). Any deep flow paths between the mainland and KFR02 must pass the Southern boundary belt, and if so, any seasonal variation pattern is expected to vanish. KFR02 may be indirectly connected to the overlying Pier, via ZFM871 and ZFMENE0870. However, the Pier is constructed from blocky material (possibly including gravel and sand; Figure 4-34). It has an approximate width of 60 m in the North-South direction and its topography is a few meters above sea level. It is questionable if the Pier can be the source of seasonal variation at depths of KFR02; the brackish glacial water type in KFR02 indicates poor connection to the sea (Figure 4-32).

#### 4.5.3 Head in borehole sections from the SFR extension investigation

In general, the drawdown in monitored borehole sections is largest in the vicinity of SFR/ZFM871. As expected, the drawdown tends to decrease with distance away from SFR/ZFM871 (both laterally and vertically). For example, the drawdown is small in the remote boreholes HFR106 and KFR106 (–0.1 to –0.6 m, respectively). The lateral extension of drawdown appears to propagate further along the Northern and Southern boundary belts (Figure 4-29). Apart from the overall diffuse inflow to SFR, the two main discrete sinks are judged to be: 1) the intersection of the access tunnels BT and DT through the Southern boundary belt, and 2) the intersection of NDB/NBT and ZFM871. There is also a long diffuse line-sink along the intersection between tunnel BT and ZFMENE0870.

HFR101 and the mid section of KFR104 have the largest drawdown among the new boreholes (Figure 4-29). HFR101 has a point-water head of –31.0 m. This indicates that HFR101 is indirectly connected to SFR, via ZFMENE0870, ZFMENE3118, or the Unresolved PDZ HFR101\_DZ2. It also indicates poor connection to the sea, even at shallow depth (casing at –4.65 m RHB 70), possibly constrained by low-permeable sediments. The large drawdown in the two deepest sections of KFR104 clearly deviates from the general pattern. This suggests that the hydraulic connection to SFR (possibly via ZFMENE3115 or ZFM871) is relatively stronger than its connection to the sea (see analysis of high-resolved drawdown of PFL-f data in Section 4.5.4). The seemingly poor hydraulic connection between the deeper sections of KFR104 and the sea, could perhaps explain why relatively low PFL-f transmissivities have been evaluated in these sections.

ZFMWNW3267 can be interpreted to be heterogeneous (with poor internal connectivity) or to have low vertical conductivity at depth. It intersects both the deepest sections of KFR104 (KFR104:1) and KFR105 (KFR105:1), which have point-water heads of –13.8 m and –1.3 m, respectively. The elevation of its upper intercept in KFR104 is c. –308 m RHB 70 and c. –150 m RHB 70 in KFR105. The drilling and opening of KFR105 caused interferences in the KFR104:1 interpreted with low response index (Figure 4-22 and Figure 4-25).

The two mid-sections of HFR105 (HFR105:2 and HFR105:3) have point-water heads of –6.3 m. These two sections are intersected by ZFMWNW1035 and ZFMWNW0001, respectively, and contain HTHB transmissivities on the order  $10^{-5}$  m<sup>2</sup>/s (Appendix E). The deepest section of HFR105 has a point-water head of –10.9 m; no impeller-flow anomaly was found in this section. This is interpreted as general drawdown from tunnel BT, and that sections residing inside vertical zones are

better connected to the overlying Sea. The largest drawdown in KFM11A (−6.8 m) occurs over the section 690 to 710 m borehole length, at an approximate elevation of −600 m RHB 70. This section is interpreted as a junction between ZFMWNW0001, ZFMNW0002, and ZFMWNW1035, and corresponds to a local peak in transmissivity ( $T \approx 10^{-6} \text{ m}^2/\text{s}$ ). KFR102A also has low point-water head in its three deepest sections (−5.3 to −5.0 m in the elevation range −200 to −535 m RHB 70).

The general impression is that most borehole sections are strongly correlated to fluctuations in the Seawater level (see Appendix F). It is not clear to what extent this reflects hydraulic connectivity in relation to mechanical effects.

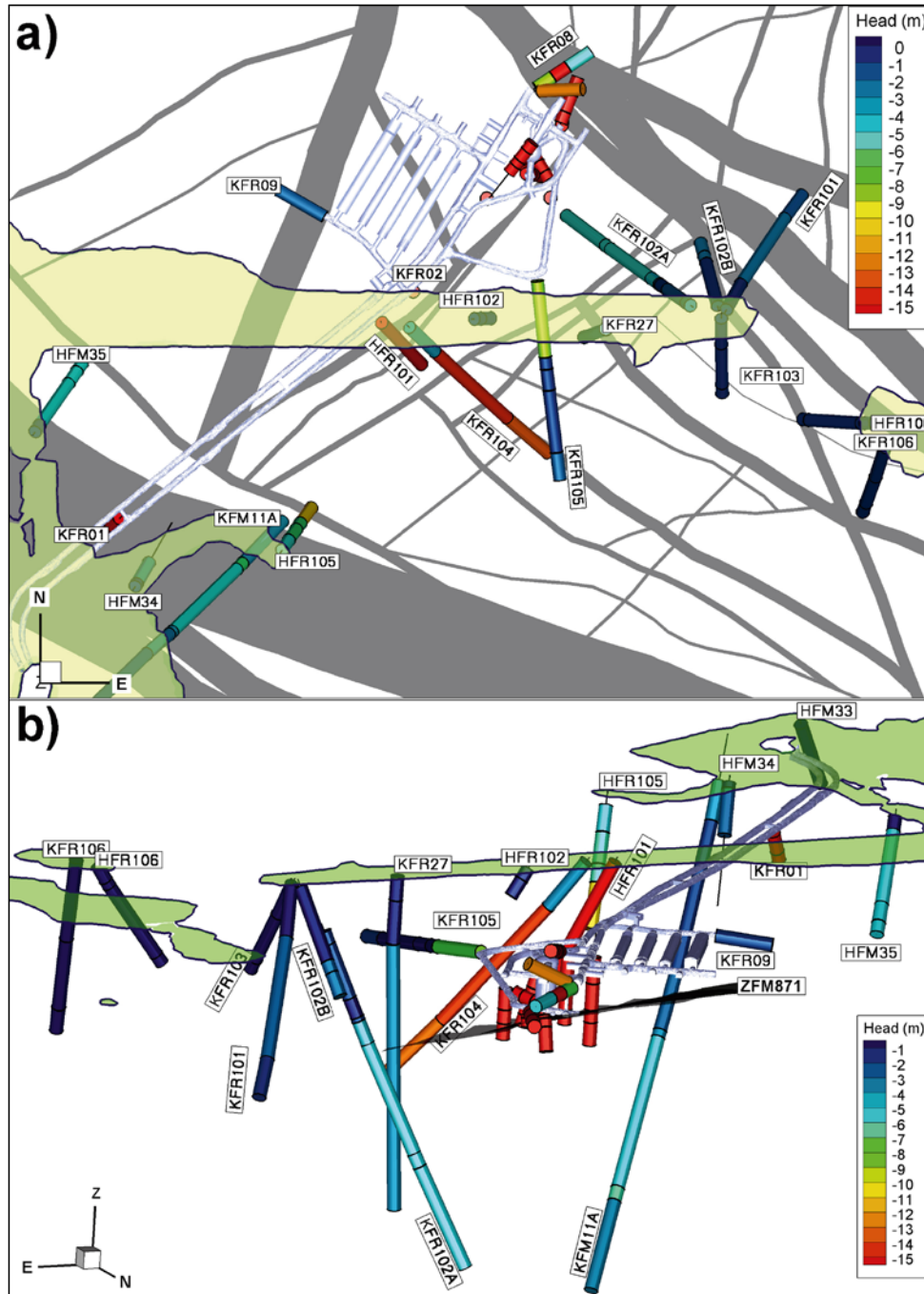


**Figure 4-29.** Measured point-water head in monitored sections 2010; a) top view and b) side view along the dip of ZFM871. The head in old data set is below −15 m and is resolved in Figure 4-28. The deepest section of HFM34 is not shown; its PWH cannot be measured, but is below −14 m.

#### 4.5.4 Fresh-water head calculated in the PFL-f evaluation

The calculation of apparent transmissivity of PFL-f features involves the calculation of undisturbed fresh-water head beyond the radius of influence (assumed to be the outer rim of the fracture; see equations in e.g. Hurmerinta and Väisäsvaara 2009). In general, the PFL-f fresh-water head is consistent with the PWH measured in sections, but it gives a more detailed picture of drawdown heterogeneity associated to PFL-f features. In particular, the minimum PFL fresh-water head is found at depths that are on par with the termination of ZFM871 against ZFMENE3115 (KFR27, KFR104, and KFR102A). Although none of these boreholes provide geological support for extending ZFM871 southeast of ZFMENE3115, these observations demonstrate that the hydraulic connection to ZFM871 continues beyond ZFMENE3115 (i.e. the horizontal connection to SFR exceeds the vertical hydraulic connection to the Sea; Figure 4-30).

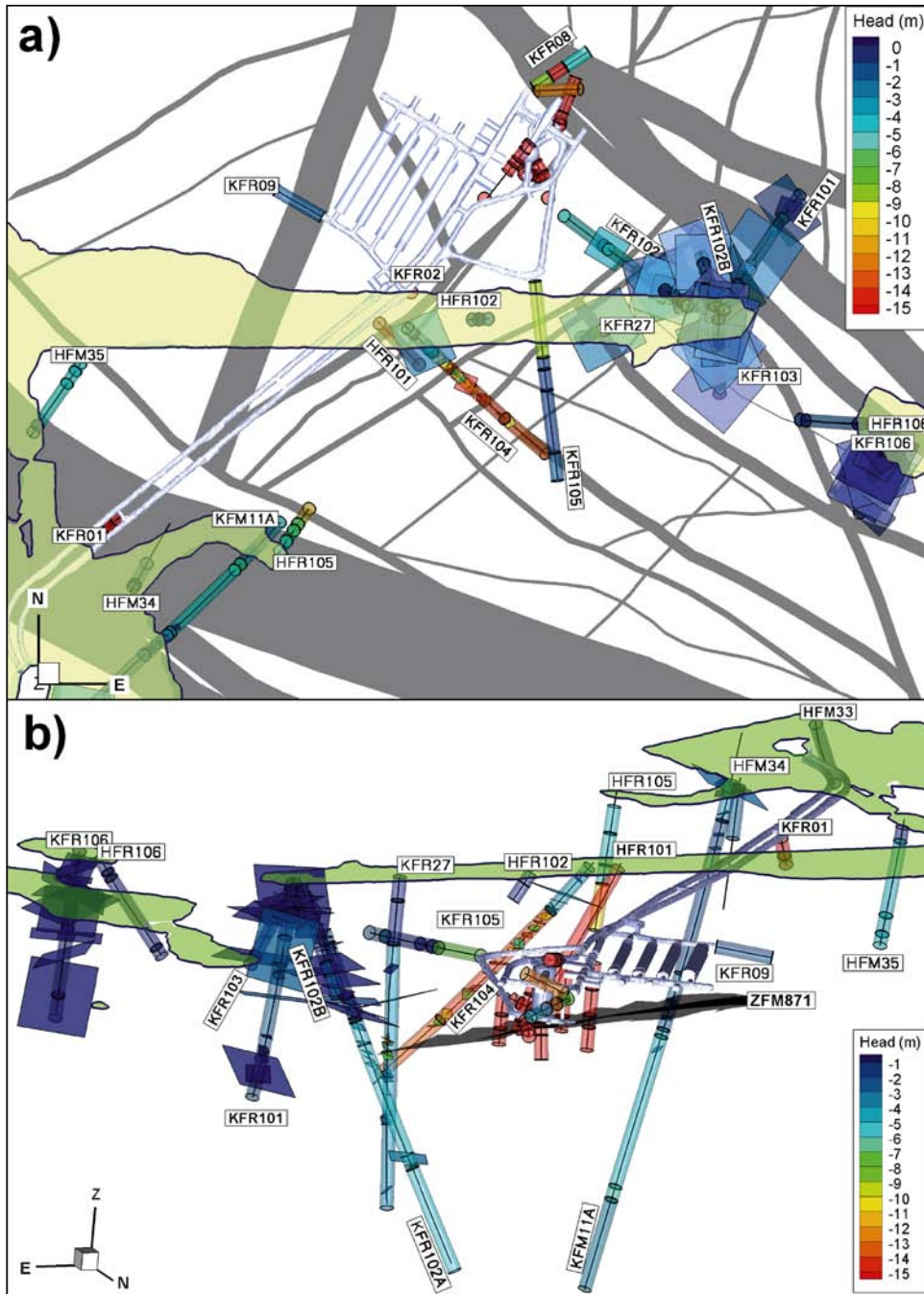


**Figure 4-30.** Evaluated fresh -water head in PFL-f data; a) top view and b) side view along the dip of ZFM871. Monitored sections head shown transparent. The head in old data set is below  $-15$  m and is resolved in Figure 4-28.

KFR27 has a borehole interval 250 to 280 m (–246 to –276 m RHB 70) with PFL-f features interpreted as low-transmissive with remarkably low fresh-water head (ranging from –15 to –7 m). It is suspected to be horizontally connected to ZFM871. The closest monitored sections in ZFM871 (KFR02:2 and KFR13:1) have fresh-water heads of –25 and –39 m, respectively. ZFM871 is modelled to terminate against ZFMENE3115, only 60 m away from KFR27, at an elevation range –218 to –238 m RHB 70. The packed-off monitored section KFR27:1 (110 to 501.64 m borehole length) has a point-water head of –3.0, suggesting that the connection to ZFM871 is subordinate to the total transmissivity of the section. The extended drilling of KFR27 caused not only interferences in ZFM871, but also outside the Northern boundary belt (Figure 4-23).

Similarly, KFR104 has an interval 145 to 320 m borehole length (elevation range –115 to –250 m RHB 70) with PFL fresh-water heads ranging from –15 to –6 m. ZFM871 terminates against ZFMENE3115 at an elevation interval –226 to –246 m RHB 70 approximately 80 to 100 m away (spherical distance). Shallow PFL features in KFR104 have low drawdown, indicating a better connection to the Sea.

The lowest PFL-f fresh-water head in KFR102A is –7.7 m. It was measured from the single PFL-f inside ZFMNE3118, located at 308 m borehole length (–277 m RHB 70), a steep, NE-striking, modestly transmissive feature, on the order  $10^{-8}$  m<sup>2</sup>/s. ZFM871 terminates against ZFMENE3115 at a spherical distance 69 m away from this PFL-f, at the elevation range –210 to –230 m RHB 70.

The two most transmissive PFLs in KFR101, associated to ZFMNW0805B and the horizontal feature SBA6 have particularly large drawdown (–2 and –1.8 m, respectively), with respect to distance from SFR and ambient head measurements. In KFR103 and KFR106, only positive or zero fresh-water heads are evaluated.

## 4.6 Evaluation of hydrochemistry

A strong correlation between hydrogeology and hydrochemistry was evident in the SDM-Site Forsmark (Follin 2008). Integration with hydrogeochemistry is useful for building the hydrogeological conceptual model, and also provides calibration targets in the later phase of numerical modelling. This chapter summarises the current hydrogeochemical understanding of the site (as of the hydrogeochemical model version 0.2 (Nilsson et al. 2010)) and the implications for the hydrogeological conceptual model.

The hydrochemical field investigations in the site investigation for the extension of SFR have resulted in data from a total of 12 borehole sections in four core-drilled boreholes and one percussion-drilled borehole. There are also data from additionally two open percussion-drilled boreholes. Furthermore, the data base contains data from two open percussion drilled boreholes in the Forsmark site investigation and from a total of 45 borehole sections in 18 older boreholes drilled from the SFR tunnels (Nilsson et al. 2010). Data on fracture-specific electrical conductivity (EC) from the PFL loggings have also been used to get a more complete picture of the salinity distribution.

### 4.6.1 Water types

The groundwater composition is brackish and three relatively conservative hydrochemical constituents (Cl, Mg, and  $\delta^{18}\text{O}$ ) were used to classify the sampled groundwaters into the different water types *Local Baltic*, *Littorina*, *Brackish glacial* and *Mixed transition* (Nilsson et al. 2010). There is no evidence of modern meteoric water, which may relate to the fact that the SFR volume is situated below the Baltic Sea. However, sheet joints in the Forsmark inland (Figure 2-4) potentially discharge large quantities of inland groundwater, which is expected to be a mixture of meteoric and Littorina water, into the Southern boundary belt; such a mixture cannot be confidently distinguished from the Baltic water type. The results indicate a large variation in origin of the groundwaters despite the relatively small variation in salinity.

The more than 20 years of monitoring of groundwater chemistry gives a unique possibility to study long-term trends in groundwater composition (Figure 4-32). The observed changes are generally slow but show a correlation with the structural geology. The largest changes have occurred in the major deformation zones while the groundwater composition has been more stable in the less transmissive bedrock.

The composition of current SFR inflow is highly dominated by the Local Baltic water type. The composition of historic inflow is not available, and hence it is not possible to fully evaluate the transient development. There exists no evidence of Local Baltic water type in the repository rock volume prior to the construction of the facility; the extent to which Baltic Sea origin existed before the construction of the facility is unclear. However, Baltic Seawater intrusion below an elevation of c. -50 m RHB 70 is assumed to be driven by the SFR drawdown; thus, *Local Baltic* type is interpreted as an indication of direct connection to the Sea. Historic water types, *Littorina* and *Brackish glacial*, have remained relatively isolated over thousands of years; they can be interpreted as, either relatively stagnant water volumes, or potentially slow, deep flow paths towards SFR that are poorly connected to the Sea. The *Mixed transition* type represents water of indistinctive origin and offers different interpretations. The mixing may be historic, owing to density driven or regional-scale flow, or it can be the result of recent convergent flow towards SFR, if its source flow paths are of different origin. The mixing reflects an *absence* of preservation and an *absence* of dominant Baltic intrusion; it may possibly indicate a fairly well-connected rock mass, with subordinate connectivity to the Sea.

The shallowest 11 measured sections (down to c. -100 m RHB 70) all are of the Local Baltic type; nine of these are measured inside the dominating deformation zones ZFMWNW0001, ZFMNNE0869, and ZFMNW0805A (Figure 4-31). This reinforces the interpretation of steeply dipping deformation zones acting as important vertical conductors between SFR and the overlying Sea.

Brackish glacial water type is found at depth in high-transmissive sections of the Northern and Southern boundary belts, below c. -250 m RHB 70 in KFM11A, KFR106, KFR104, and KFR101, as well as, in low-transmissive sections in a depth interval between ZFM871 and SFR (Figure 4-31). All samples from ZFMNE0870 are of Brackish glacial or Mixed transition type; suggesting that ZFMNE0870 is poorly connected to the sea, but potentially a conductor for deep flow paths. Please note that the sections of KFR02 with Brackish glacial water are located between ZFMNE0870 and

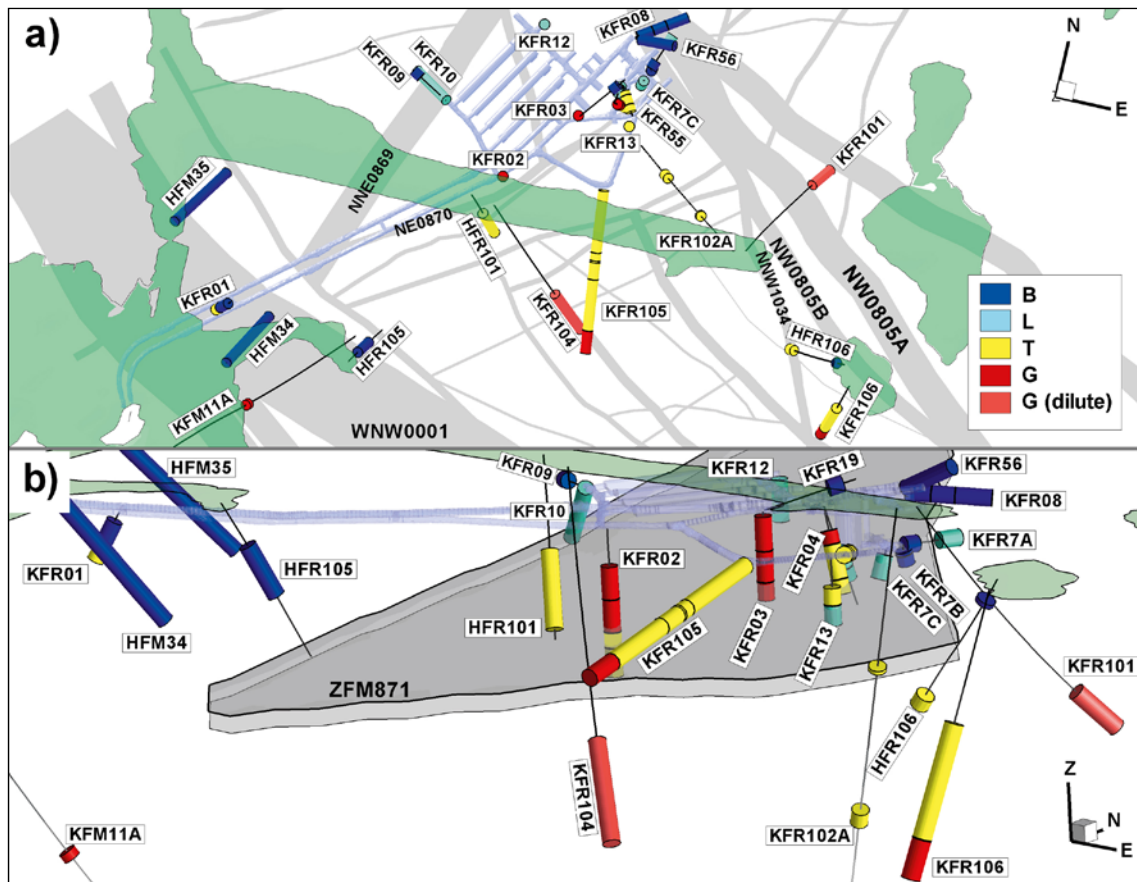


**Figure 4-31.** Present water types; a) top view and b) side view towards the Northwest. The stationary water types are Local Baltic (B; blue), Littorina (L; cyan), Brackish glacial (G; red), and Mixed transition (T; yellow). The sub-type “G (dilute)” is used to emphasise low salinity.

ZFMNE3118, although this is not clearly visible in (Figure 4-31 and Figure 4-32). The Brackish glacial water in the deepest sections of KFR101 and KFR104 is of a particular dilute type (i.e. low salinity; discussed further in Section 4.6.2).

The distribution of water types in zone ZFM871 (formerly known as Zone H2) is irregular (cf. the irregular head change with time in this zone, see section 4.5.2). Most samples from ZFM871 are of Littorina type, while others are changing towards a higher degree of mixing (Figure 4-32). Close to ZFMNW0805A, the water type in ZFM871 is changing from Littorina to Local Baltic type (i.e. KFR7B and the upper section of KFR7A Figure 4-32); this also indicates the role of ZFMNW0805A as a transport pathway for Seawater towards SFR. Close to ZFMNE0870, the water type in ZFM871 is changing from Brackish glacial and Littorina towards Mixed transition (i.e. KFR02, KFR03, and KFR04 Figure 4-32); suggesting that the central parts of ZFM871 are – to some extent – involved in the inflow to SFR, but with remote connection to the Sea.

The general picture from hydrogeochemistry interpretations is that the major flow paths from the Baltic Sea are vertical through ZFMWNW0001, ZFMNNE0869, and ZFMNW0805A (the Singö zone, Zone 3, and Zone 8) via horizontal features towards SFR. However, ZFM871 (H2) only seems to have channelized, local pathways between ZFMNW0805A and B and SFR, as considerable portions of older water (Littorina and Brackish glacial types) are still present in the zone and have not been flushed out. This can be explained by the general heterogeneous characteristics of ZFM871, as well as the grouting (Section 4.1).

Remnants of Brackish glacial and Littorina despite tunnel inflow during 25 years time suggest either poor connectivity to the sea or discrete compartments due to lack of connectivity. The undisturbed system would be expected to be stable with less saline Baltic water type above Littorina, provided that the Forsmark SBA do not discharge large quantities of inland groundwater across the Singö zone (see Section 4.5.1).

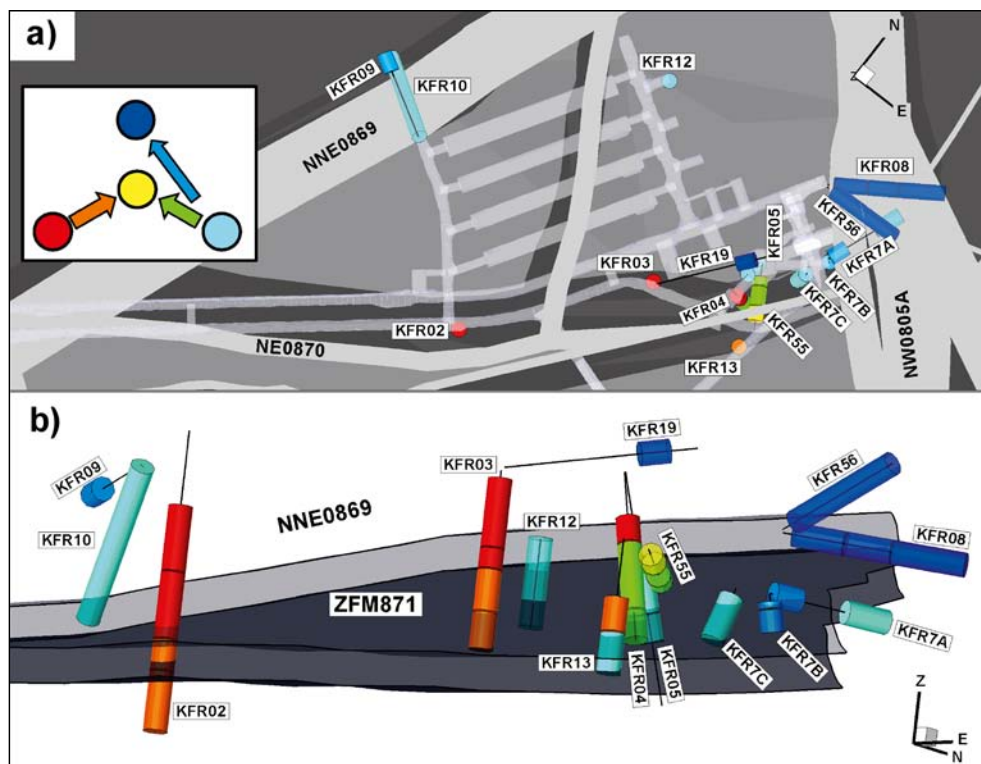


**Figure 4-32.** Change of water types between 1987 and 2006; a) top view and b) side view towards the Northwest. The stationary water types are Local Baltic (B; blue), Littorina (L; cyan), Brackish glacial (G; red), and Mixed transition (T; yellow). The transient changes are: Brackish glacial towards Mixed transition (G → T; orange), Littorina towards Mixed transition (L → T; green), and Littorina towards Baltic (L → B; light blue). Incomplete ongoing changes are not resolved. Sections with poor coverage of the chosen time interval are shown as translucent.



## 4.6.2 Salinity and measured electrical conductivity

During the entire observation period (1986–2010), the observed electrical conductivity at the SFR site is within the range 600–1,600 mS/m (Figure 4-33), which corresponds to a chloride concentration of 1,500–5,500 mg/L. The measured values should be related to the local Baltic Seawater which has a salinity of about 3,000 mg/L Cl, or an EC value of c. 890 mS/m. For example, with a few exceptions, most shallow data (elevation range c. 0 to –100 m RHB 70) have EC that are within the range 800 to 1,000 mS/m (Figure 4-33).

High salinity (1,100 to 1,300 mS/m) in borehole sections close to SFR is related to the sub-horizontal zone ZFM871 (H2) and its Littorina and Brackish glacial water components. Similar salinity is also found in sub-horizontal fractures at similar depth levels in KFR102A and KFR27 (as recorded by fracture-specific EC from PFL logging). The highest early recorded EC values (about 1,600 mS/m) were found in boreholes KFR7A and KFR10. The most drastic salinity changes observed over time is the decreasing salinity in these two boreholes. Note that KFR7A also has the largest decrease in head (Figure 4-28). KFR7A is located inside ZFMNW0805A and B (so-called *target intercepts*), but there exist indications that it is intercepted by ZFM871 (a so-called *geometric intercept*). KFR7A has both Littorina water type, drawdown, and EC that is more of ZFM871 characteristics; it is clearly different from other ZFMNW0805A,B intercepts in KFR08 and KFR56 (cf. Figure 4-33 and Figure 4-28). On the other hand, good hydraulic connections were established between KFR7A and KFR08 in interference tests (Appendix D). KFR10 has two deformation zone intercepts: ZFMNNE0869 (Zone 3) and a possible deformation zone KFR10\_DZ2 that is suspected to be an extension of ZFM871.

Less saline water has been found below more saline water in several boreholes (KFR02, KFR101, KFR102A, KFR104, KFR106, and KFR27; Figure 4-33). This is an unusual observation; owing to density potentials, salinity normally increases with depth in bedrock groundwater environments (Nilsson et al. 2010). According to Nilsson et al. (2010) this is a strong indication of the preservation of very isolated groundwater types in parts of the bedrock outside deformation zones (i.e. a slow transfer rate between flowing fractures/zones and stagnant water in low-permeable rock volumes). This reinforces the conceptual interpretation of the flowing fracture network being predominantly sub-horizontal with limited vertical connectivity.

Low EC values (c. 600 mS/m, corresponding to about 1,600 mg/L) are found in the lowest sections of KFR101 and KFR104 (elevation intervals c. –218 to –262 and –260 to –352 m RHB 70, respectively). The salinity of this diluted groundwater is significantly below the Baltic Sea and the chemical and isotope analyses reveal a significant glacial meltwater component. It is noteworthy that the water sample in KFR101, indicating a very isolated rock volume, was drawn from a borehole section inside zone ZFMNW0805A (Zone 8) and the fractures yielding the diluted water are highly transmissive ( $T > 10^{-6}$  m<sup>2</sup>/s). This borehole section has a point-water head of –1.6 m, with estimated PFL-f fresh-water heads of 0 m (Figure 4-29 and Figure 4-30), suggesting in spite of high transmissivity, and potential large-scale hydraulic connectivity, it is a peripheral source to SFR inflow. The deep section in KFR104 is subject to opposite conditions: exceptionally large drawdown, low PFL-f transmissivity, and slow communication (i.e. response to the KFR105 interference test).

There are no fracture-specific EC measurements in borehole KFR27. However, identified contrasts in logged EC along the borehole can be used to estimate the EC of the inflowing water,  $C_{in}$ , of a few specific PFL-f records, based on mass balance in the salinity above and below the anomaly as:

$$C_{in} = \frac{C(q_m + q_0) - C_0 q_0}{q_{in}} \quad (4-5)$$

where  $C$  and  $C_0$  is the EC above and below the anomaly, respectively, and  $q_{in}$  and  $q_0$  is the inflow from the anomaly and the flow in the borehole below the anomaly, respectively. Extremely low EC values are found at the bottom of KFR27 (shown as black feature at the lower end of the borehole in Figure 4-33). The measured EC value is 110 mS/m, which has been interpreted as contaminant tap water from the drilling activities (See Figure E-27, and further details in Appendix E and).

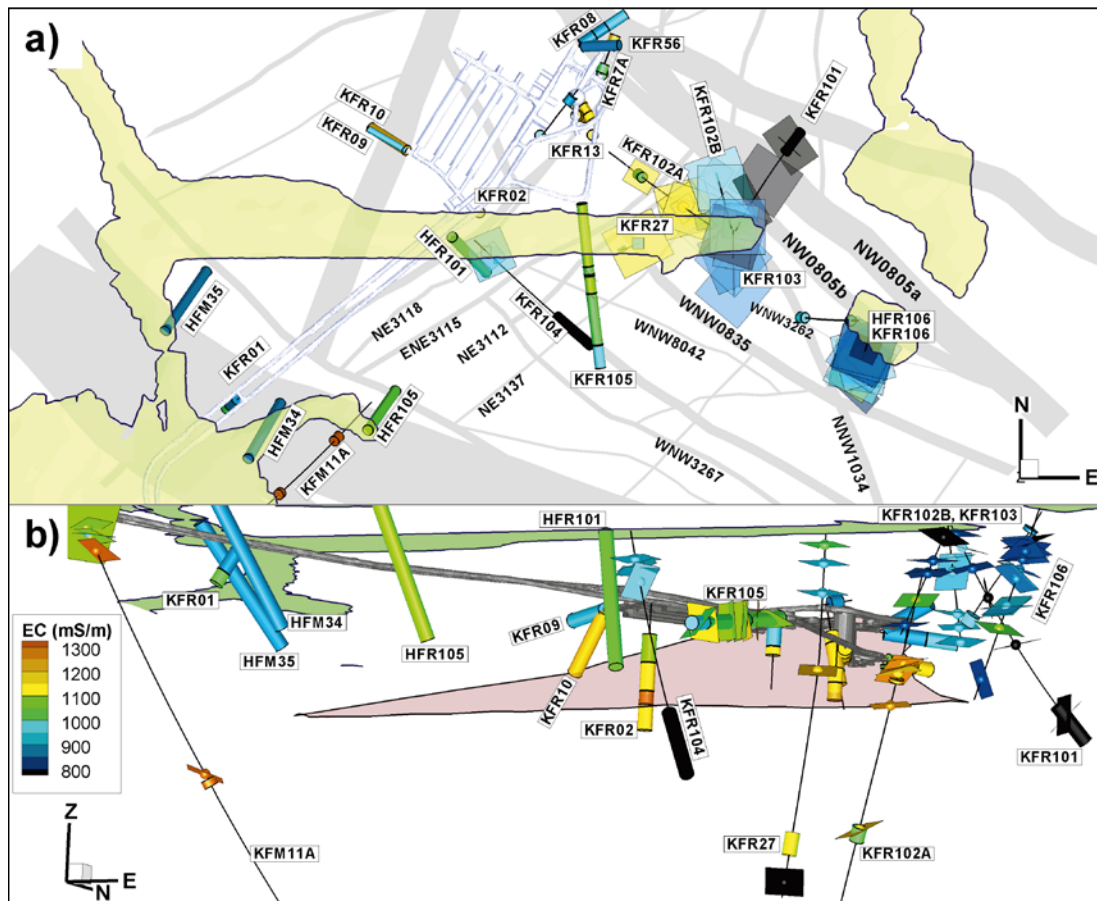


**Figure 4-33.** Electrical conductivity (EC) measurements; a top view and b) side view. EC from PFL flow logging shown as planes and EC from monitored borehole sections represented as cylinders. A deep PFL logged interval in KFR27 (409.6 to 435.6 m borehole length) is also represented by a cylinder. The deepest measured EC in KFR27 (black feature = 110 mS/m) is assumed to be contaminant tap water from drilling activities (Appendix E).

## 4.7 Sediment coverage and the hydraulic contact to the Sea

The SFR model domain is mainly covered by Sea. The sediments, e.g. Hydraulic Soil Domain (HSD), may have an important role in controlling the hydraulic connection between the Sea and the underlying rock mass. To the authors' knowledge, there exist no sediment conductivity measurements from SFR. Early documentation of the sediments above SFR (e.g. Carlsson et al. 1986) describes a domination of sandy till and fine material confined to topographical depressions (for example the Singö depression). Axelsson (1986) assigned the hydraulic conductivities  $10^{-8}$  to  $10^{-6}$  m/s to the till and  $10^{-10}$  to  $10^{-9}$  m/s to the clay/clayey till.

Within the SDM-Site Forsmark, a regolith model of Quaternary deposits have been developed, which covers the Forsmark inland as well as marine sediments above SFR (Hedenstöm et al. 2008). As described in Section 3.1, this regolith model is conceptually divided into layers, L1–L3, and, Z1–Z6, defined by a spatially variable thickness at a horizontal spatial resolution of  $20 \times 20$  m. Anisotropic effective conductivity values have been calibrated for the different regolith layers by means of surface hydrological modelling (Bosson et al. 2008). It should be noted that this calibration targeted surface hydrologic data in the Forsmark inland. It is assumed that the calibrated effective parameters are also valid for offshore marine sediments, although this has not been explicitly confirmed. It is possible that the hydraulic conductivity on land is somewhat enhanced due to frost-heaving, worm holes, tree roots, etc.

The overlying sediments potentially control the hydraulic contact between deformation zones and the Sea. The HSD control of the hydrogeological system is not permanent, as some sediment layers will eventually erode with the land-lift processes. Owing to wave erosion, the wave-breaking function of the pier, and the topographical depression of the Singö deformation zone, the sediment layers are considerably thicker on the south side of the pier, as compared to the northern side (Figure 4-34b). These sediments south of the pier also include glacial clay, Z4 ( $K = 1.5 \times 10^{-8}$  m/s; Figure 4-34d). The bottom sediment layer is till, Z5, which covers most of the Regional domain and has a calibrated vertical conductivity of  $7.5 \times 10^{-7}$  m/s. If the sediments form continuous layers, they may act as a choke at the contact between the fractured rock and the sea, at least for fracture transmissivities exceeding  $10^{-7}$  m<sup>2</sup>/s (see Section 4.7.1). Owing to potential head loss as flow changes medium, e.g. from a porous medium to a fractured medium, or vice versa, and the possibility that sediments clog fracture apertures, this choking effect could apply to even less transmissive fractures (see Section 4.7.1).

The contact to the Sea may be considerably better in areas with no, or partial, sediment coverage. The islet, from which KFR106 and HFR106 were drilled, has virtually no soil/sediment coverage (Figure 4-34b), and potentially provides an exceptionally good contact to the Sea for the zones ZFMWNW3262, ZFMNW0805B, and ZFMNNW1034. This could partly explain the extraordinary high transmissive PFL data found near the Northern boundary belt and ZFMNNW1034 (Figure 4-17;

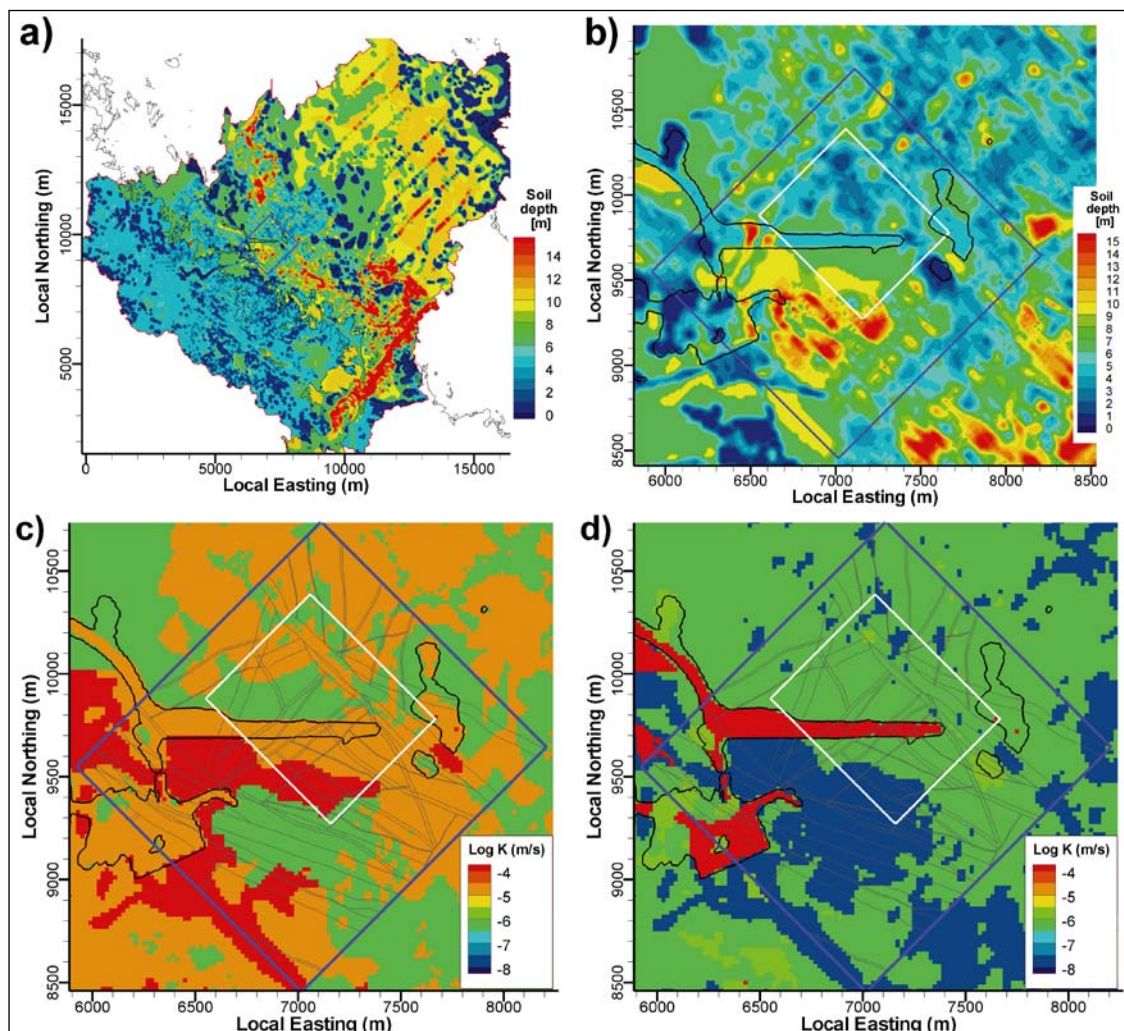


**Figure 4-34.** HSD model from Forsmark SDM; a) total regolith depth inside the Forsmark modelling domain, b) total regolith depth inside the SFR regional domain, c) vertical conductivity of the top layer, Z1, and d) vertical conductivity of sequential underlying layers, Z3 (conductive artificial fill), Z4 (low conductive glacial clay), Z5 (till), and Z6 (fractured bedrock). The purple square is the Regional SFR domain, the white rectangle is the Local SFR domain, and the faint lines are deformation zones from the geologic model.

see Section 5.3). The SFR pier itself is constructed from a coarse, permeable, blocky material, Z3, (Figure 4-34d) that also potentially allows good hydraulic contact to the underlying rock mass. However, a good hydraulic contact to the Sea requires that the porous gaps between blocks are not filled with finer material. It may be speculated if the space between blocks offers a sheltered environment for fine material to settle, or if the remains of sediment layers that existed prior to the construction of the pier are trapped between blocks. This is currently not known, but the pier is considered to potentially have a good hydraulic contact to the underlying rock. Most of the deformation zones that are covered by borehole data do have contact with the coarse material of the pier (Figure 4-34d).

It must be emphasised that the regolith model and its calibrated conductivity values is only a *model representation*, and does not fully resolve the local, detailed heterogeneity in HSD around SFR. In other words, local hydraulic connections may very well exist between the Sea and the underlying fracture network that cannot be resolved from the defined layer depths and effective conductivities of the 20×20 m<sup>2</sup> computational mesh.

#### 4.7.1 Hydraulic choking at fracture-sediment contacts

A hydraulic choking phenomenon occurs at the interface between a porous medium and a discrete fracture network. For example, this phenomenon acts at the interface between HRD and HSD, as well as, for example, between the fracture network and bentonite-filling in tunnels. This is caused by the head loss that occurs at the transition between channelized fracture flow and uniform porous medium flow, i.e. divergent or convergent flow field, depending on direction of flow. The significance of this phenomenon depends on geometric aspects as well as the ratio in hydraulic properties between the two media (i.e. fracture transmissivity and porous medium conductivity).

A schematic flow simulation of the contact between a single vertical fracture and overlying sediment is demonstrated in Figure 4-35. The purpose of this simulation is to demonstrate the general physical phenomenon, and not to address the site-specific complexity of the SFR fracture system; instead the set-up is highly idealized and simplified. A 1×1 m<sup>2</sup> vertical cross-section is simulated: the upper 0.9 m contains sediments with an isotropic vertical conductivity of 10<sup>-6</sup> m/s; while the lower 0.1 m consists of impermeable rock and a single fracture with a transmissivity of 10<sup>-6</sup> m<sup>2</sup>/s and an aperture of 1.0 mm (Figure 4-35). A vertical hydraulic gradient of -1.0 m/m is applied over the system; the upper sediment boundary is in contact with the sea and has a head of 0.0 m, while the lower end of the fracture (z = -1.0 m) has a head of -1.0 m. Based on symmetry, no-flow is assigned to the vertical sides (x = ± 0.5 m; i.e. assuming a frequency of 1 flowing fracture per meter). Flow is simulated in DarcyTools, using a highly refined mesh in the vicinity of the fracture (cell size < 0.1 mm). Owing to the fine discretisation, the fracture can be discretely represented by cells with a total width of 1.0 mm and with an isotropic conductivity of 10<sup>-3</sup> m/s (i.e. K = T/b = 10<sup>-6</sup> m<sup>2</sup>/s / 1.0 mm). The sediment is assigned an isotropic conductivity of 10<sup>-6</sup> m/s.

Consequently, there is a conductivity contrast of 3 orders of magnitude at the interface between the fracture and the sediment, which relates to the ratio in cross-sectional area of fracture flow relatively to porous medium flow. Note that real, large-scale applications in DarcyTools use equivalent continuous porous medium properties, typically defined at the 10 m scale, which effectively eliminates the *numerical representation* of conductivity contrast between the two media types. For example, had the system been discretised at the 1 m scale horizontally in DarcyTools, both the fracture network and the sediment would have been assigned the same effective conductivity.

Simulations show that flow is uniform in the upper part of the sediment (c. 0 ≤ Z < -0.7 m), with a hydraulic gradient of c. -0.23 m/0.7 m ≈ -0.3. In the lower 0.2 m of the sediments, the head drops from -0.23 m to -0.97 m, resulting in an average hydraulic gradient of c. -3.75 m. The simulated hydraulic gradient over the simulated fracture is -0.15 m/m. By conservation of mass (i.e. equal total vertical flow across any given horizontal cross-section), an *effective vertical conductivity* can be back-calculated for the sediment ( $K_{\text{eff}} = Q_{\text{tot}} / (dh/dz)$ ) to be 3.2×10<sup>-7</sup> m/s, which is a third of its parameterised value. Most of the head loss occurs close to the fracture sediment contact (Figure 4-35b); the calculated effective conductivity of the upper 0.7 m sediment is approximately equal to its true value, 10<sup>-6</sup> m/s, while it is only 9×10<sup>-8</sup> m/s in the lower 0.2 m of the sediment.

Various alternative geometric relations of fracture-sediment contact can be considered, as well as, different degrees of hydraulic contrast between the two media; the choking phenomenon is the largest for *sparsely fractured rock and highly transmissive fractures with small apertures*. The choking phenomenon is reduced if the sediment is anisotropic with high horizontal conductivity. On the other hand it can be large if the sediment enters the fracture aperture (i.e. combined effects of low conductivity and small cross-sectional area); this has a large effect on simulated flow, for example: if the upper 1 cm of the fracture is sediment-filled, and its aperture is 0.1 mm, the *effective vertical conductivity* of the sediment drops below  $10^{-8}$  m/s.

This type of high-resolved simulations is obviously unfeasible for real, large-scale applications. The local-scale results (e.g. Figure 4-35) are not readily transferable into a large-scale model. However, they demonstrate that, under certain circumstances, the sediments may choke the contact between the Sea and the underlying fracture network, even when sediment conductivity is on the same order as fracture transmissivity. In a real large-scale application, the choke phenomenon could perhaps be represented by a “skin-factor” at the interface between HRD and HSD.

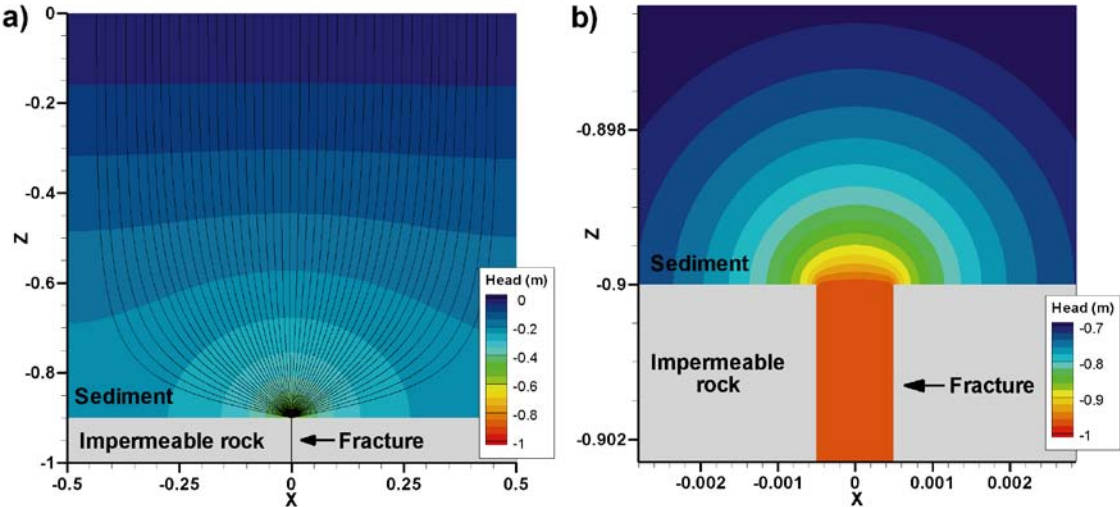


**Figure 4-35.** Schematic simulation of the hydraulic choke at the contact between a single fracture and overlying sediments; a) converging flow-field at the 1 m scale, shown by stream lines and b) large head loss in the vicinity of the fracture-sediment contact.

## 5 Conceptual hydrogeological modelling

The evaluation of primary data, presented in Chapter 4, provides notions and hypotheses about the hydrogeological system at SFR. These notions are pursued in this chapter with the aim to formulate a conceptual model. The suggested conceptual model is shown in Figure 5-14 and described in Section 5.5.

### 5.1 Interpretation of hydraulic interferences

Evaluation of hydraulic interferences had a key role in interpreting and describing the superficial bedrock of the nearby SDM-Site Forsmark (i.e. confirming the existence and character of so-called sheet joints; Figure 2-4). One of the key issues in the SFR extension project is to determine if similar structures also exist in the SFR model domain (Section 1.3). Both similarities and differences between the two sites have been demonstrated in the evaluation of primary data (Chapter 4). A common trait is that the highest transmissivities in the shallow rock mass outside deformation zones are horizontal or gently dipping. A difference is that the measured transmissivities in the SFR area are at least two orders of magnitude smaller (see Table I-1 in Follin et al. 2007c).

A drawback of single-hole data is that it provides little insight into the spatial continuity of the tested transmissive features. Thus, it tells little about the large-scale hydraulic communication inside the model domain. For example, it cannot be resolved if a given PFL-f record (with particular emphasis to high-transmissive, horizontal PFL data) is only hydraulically connected to the nearest HCD, or if it is part of a larger system of interconnected horizontal structures (so-called SBA-structures). Insight to this matter can be gained by an analysis of interferences put in context to the observations made in SDM-Site Forsmark.

However, in such a comparison a few differences between the two data sets should be noted:

- The SFR interferences occur below the Baltic Sea, close to an open underground facility, which is an unusual situation for this type of analysis. It is not fully clear how the combined effects of sea-level fluctuations and SFR drawdown affect the interpretation of responses.
- In SDM-Site Forsmark, cross-hole responses were not discussed in terms of apparent diffusivity, Eq. (4-1), but instead by the so-called “*response index 1*”, Eq. (4-2). This response index is calculated as  $r_s^2/dt_L$ , where  $r_s$  is the 3D radial distance between the pumped section and the monitoring interval, and  $dt_L$  is the measured response time (s). The index is a straight-forward, direct measure of pressure propagation that circumvents analogies to porous medium flow and assumed flow dimension of Streltsova (1988).
- The response index 1 is dependent on the drawdown criterion being used,  $dp$  (m). In SDM-Site Forsmark the response time ( $dt_L$ ) is defined for a drawdown in a monitoring interval of  $dp = 0.01$  m, while the noisiness induced from sea-level fluctuations at SFR necessitated a larger response-time criterion,  $dp = 0.1$  m (Figure 4-18, Appendix F). Obviously, a 0.01 m drawdown occurs before a 0.1 m drawdown, and therefore – owing to methodological differences – the response times in SFR relate to a somewhat later stage of response. The effect of the methodological differences depends on the shape of the drawdown curve and therefore *cannot be generalized*. However, previous experience from Forsmark indicate that the criterion  $dp = 0.1$  m provides slower index 1 by *a factor 2 to 14*, compared to if the criterion  $dp = 0.01$  m is used (Lindquist et al. 2008).
- Differences in sample size; 260 responses from SDM-Site Forsmark are compared to the 86 documented responses in SFR. Thus there exists a large population of non-responding sections in both Forsmark and SFR that are not included in the comparison. In other words the comparison addresses the upper tail of distributions, and the probability of finding the most rapid responses in this upper tail increases with larger data set.

Without accounting for the methodological difference in drawdown criteria,  $dp$ , the response index 1 is, on average, a factor 46 higher in Forsmark (percentile-to-percentile matched; Figure 5-1a).

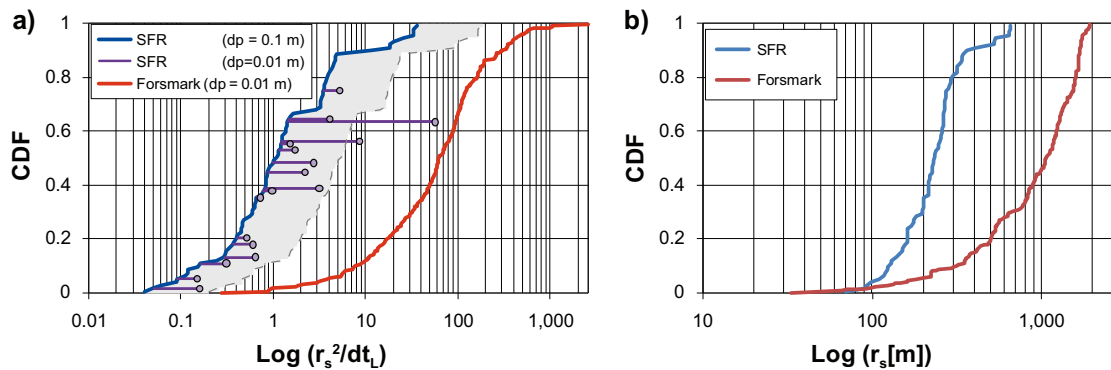


**Figure 5-1.** Comparison of hydraulic interferences between the SFR and Forsmark sites: a) cumulative distribution of the so-called “response index 1” and b) cumulative distribution of response distance,  $r_s$ . The data noise level at SFR necessitates a higher response criterion,  $dp = 0.1$  m, which is higher than that used in Forsmark,  $dp = 0.01$  m. The criterion used in SFR reflects a later stage of the response, providing lower values of index 1 (purple lines = 17 responses at SFR evaluated with both criteria, grey-shaded area = assumed conservative estimate of methodological differences). Regardless of methodological differences, the SFR responses are about an order of magnitude slower.

To enable a comparison, 17 responses in SFR were evaluated by both criteria,  $dp = 0.1$  m and  $dp = 0.01$  m (purple lines in Figure 5-1a). The extent to which this is caused by different drawdown criteria is unclear (methodological uncertainty illustrated by grey shade in Figure 5-1a, which is taken as a constant compensation factor of 5). However, it would seem that the SFR responses are about one order of magnitude less rapid than those in SDM-Site Forsmark. The evidence of responses also exists for greater distance in Forsmark (Figure 5-1b).

### 5.1.1 Conceptual interpretation

Pressure pulses follow the paths of least resistance; therefore observed interferences can be taken as evidence of hydraulic connectivity, but the absence of observed responses, or low evaluated diffusivity, does not necessarily prove poor hydraulic connectivity. The apparent hydraulic diffusivity between a source/sink and an observation section in a heterogenous system is strongly correlated to the flow connectivity, i.e. the continuity of high transmissivity paths, or in other words the effective transmissivity (Knudby and Carrera 2006). It neither provides detailed information on the transmissivity distribution along the flow path, nor on the actual (physical) storativity within the system. However, the low observed hydraulic diffusivities at SFR imply one or both of two possible situations: (i) the structure connecting source/sink and observation section has limited connectivity, and (ii) the structure is crossed by other structures that divert the main pressure pulse towards a hydraulic boundary (the Baltic Sea or the SFR facility).

The planned interference tests in the Central block (HFR101 and KFR105) had slower responses than many of the drilling activities close to the Northern boundary belt and ZFMNNW1034 (Figure 4-20). The interference test in KFR105 had faster responses towards north, while the pump test in HFR101 caused disturbances towards south, with monitored sections that – similarly to HFR101 – exhibit drawdown. The drilling activities associated to the Northern boundary belt and ZFMNNW1034 (KFR27, KFR102A, HFR106, and KFR106) have the fastest responses parallel to and across the Northern boundary belt, but none caused responses in the Central block. Also the furthest responses are observed parallel to the Northern boundary belt (Figure 4-26).

Slow responses are normally interpreted as indicating a choked, compartmentalised system, with large fracture porosity in relation to transmissivity and/or poor large-scale connectivity. Many boreholes in the vicinity of the Northern boundary belt and ZFMNNW1034 are dominated by sub-horizontal PFL-f that are relatively transmissive (see section 4.3.2). The PFL logging involves several days of pumping and therefore these sections are assumed well-connected to the Baltic Sea hydraulic boundary. Potentially, connections to the sea could act as an apparent storativity term,  $S$ , which could dampen and delay a pressure pulse (i.e. the evaluated propagation speed is related to  $T/S$ , Eq. (4-1)).

The estimated apparent hydraulic diffusivities are considered to be representative for the interconnecting structures between the pumping borehole section and the observation section. However, the transmissivity and storativity estimated from the transient test evaluation generally represents an average value for a large volume of rock within the influence volume of the test. The transmissivity estimated from sections with good hydraulic connectivity should be more representative of the actual hydraulic connection (Walger et al. 2010). That is, the division of the diffusivity into  $T$  and  $S$  is valid only for the sections with the highest diffusivities. In this case only three hydraulic connections between boreholes are assessed to fulfil this criterion: the connection between HFR101 and the two deepest sections in KFR104 as well as the connection between KFR105 and KFR27:2.

### 5.1.2 Hydraulic responses in deformation zones

Only three of the observed hydraulic interferences were judged possible to relate to modelled deformation zones. The first of these was interpreted as interference via deformation zone ZFMENE3115. A relatively weak response was observed in section KFR102A:1–2 at the interference test in borehole KFR105 (Walger et al. 2010). The dominating flow anomalies in the observation sections are considered to be related to the deformation zone ZFMENE3115. However, the zone intercept in borehole KFR105 only contains low PFL-f transmissivities. The response index 1 for interferences associated to ZFMENE3115 is about  $1 \text{ m}^2/\text{s}$ . This corresponds to the median value in (Figure 4-20). Note that no responses were identified in KFR102A:1–2 during the drilling of KFR105 (cf. Figure 4-22 and Figure 4-25). During the KFR105 interference test, only slow responses were observed in two sections of the nearby KFR104 (response index c.  $0.1 \text{ m}^2/\text{s}$ ), in spite of the fact that the two boreholes have four mutual deformation zone intercepts: ZFMENE3115, ZFMNE3112, ZFMWNW3267 and ZFMNE3137 (Figure 4-22), none of which convey a rapid response.

Another zone-related interference was interpreted to be related to deformation zone ZFMWNW3262. A strong response was observed in observation section KFR103:1 during the drilling of HFR106. The highest PFL-f transmissivities in the observation section are concentrated to this deformation zone. However, the hydraulic contact with borehole HFR106 must be indirect since deformation zone ZFMWNW3262 does not intersect the borehole. The response index 1 of the hydraulic connection between the boreholes was estimated to about  $25 \text{ m}^2/\text{s}$  from the time lag analysis. This is one of the most rapid responses (Figure 4-20).

The response index 1 in HFR106 from the drilling of KFR106 was about  $30 \text{ m}^2/\text{s}$ . Both boreholes have deep intercepts of ZFMWNW1034 (between  $-127$  and  $-248 \text{ m RHB } 70$ ), which is interpreted as a highly transmissive zone (a depth-adjusted transmissivity,  $T_0$ , on the order  $10^{-4} \text{ m}^2/\text{s}$ ; see Figure 5-2).

The hydraulic responses are also interpreted in the alternative context of the so-called SBA-structures (Appendix B).

## 5.2 Depth dependency in transmissivity

### 5.2.1 Depth domains for HRD parameterisation

Previous model versions (Öhman and Follin 2010a, b), identified a contrast in transmissivity with depth, which seems to occur at c.  $-60 \text{ m RHB } 70$ . Based on that, three depth domains were suggested to represent the depth trend in fracture transmissivity:

- The Shallow domain (0 to  $-60 \text{ m RHB } 70$ ),
- the Repository domain ( $-60$  to  $-245 \text{ m RHB } 70$ ) and
- the Deep domain (below  $-245 \text{ m RHB } 70$ ).

The boundary between the Repository and the Deep domains is not clear-cut, but was chosen with respect to data sample size and the preliminary geologic modelling of ZFM871. In the final geologic model, ZFM871 is terminated at ZFMENE3115 and thus, does not provide a geologic boundary for separation between the two depth domains. Furthermore, a steeply dipping deformation zone,



ZFMWNW0835, is modelled in the very vicinity KFR27, suggesting that its hydraulic data are potentially affected by the zone – more or less over its entire extent. In effect, this considerably reduces the sample size of HRD data at depth (cf. Figure 4-16a and b) and motivates changing the definition of the Deep depth domain. The elevation –200 m RHB 70 was selected to achieve representative borehole coverage for analysis of lateral variation (Section 5.3).

## 5.2.2 Depth trends in transmissivity data

Transmissivity is generally known to decrease with depth (e.g. Gustafson 2009). Different depth-trend models of early SFR models are compiled and presented in Öhman and Follin (2010a). The transmissivity in the shallow bedrock is expected to be enhanced by stress release from the glacial rebound; this effect is expected to gradually diminish with depth and thus resulting in a transmissivity depth trend. At greater depths, the transmissivity depth-trend is explained by several factors, including increasing stress from overburden load, decreasing fracture intensity, and lower connectivity (see relation between Open fracture intensity and PFL-f data with depth, discussed in Öhman and Follin 2010b). For example, PFL-f data are assumed to reflect *continuously flowing* features that are part of the globally connected fracture network. Thus, deep fracture networks have longer flow paths to the Seafloor implying a lower probability of global connectivity combined with a higher degree of hydraulic choking. During PFL-logging, the applied drawdown also declines with depth due to the cumulative fracture inflow along the borehole. Furthermore, the surroundings of SFR are subject to drawdown due to tunnel inflow, which may result in small gradients between the pumped borehole and the surrounding rock (in fact, a few PFL-f in KFR27 had flow *out of the borehole*, even under pumped conditions; these occur at the same depth level as an extrapolation of ZFM871; Figure E-28). However, this is accounted for in the transmissivity evaluation, but it implies that the physical detection limit may deteriorate somewhat at depth. Quite contradictory, the *practical* detection limit actually improves with depth as it is controlled by the frequency and magnitude of fracture inflow.

To put the hydraulic data from the recent SFR investigations in context of previous experience, the PFL-f transmissivity data are compared against corresponding tabulated values for fracture domains of SDM-Site Forsmark, FFM01 and FFM02 (Table 10-25 in Follin et al. 2007b). Differences are highlighted by colouring pair-wise comparisons (Table 5-1; the lower value shown in blue and the higher in red). Notably, the SFR data set has higher PFL-f frequency (cf. Open fracture intensity comparison in Table 4-2. Comparison of Open fracture intensity in HRD to SDM-Site Forsmark.). However, this comparison should be cautiously interpreted; there are substantial differences in borehole coverage between the two data sets. FFM02 in SDM-Site Forsmark represents borehole data below –100 m RHB70; the highly transmissive bedrock above –100 m was mainly covered by percussion borehole data and separately modelled as three sheet joints (Figure 2-4). Thus, for the uppermost bedrock in FFM02 is considerably more transmissive, than indicated by Table 5-1. The SFR data set has considerably less borehole coverage at depth, below –200 m elevation.

**Table 5-1. PFL-f data comparison between SFR<sup>1)</sup> and SDM-Site Forsmark (outside deterministic deformation zones, ZFM).**

Depth interval	PFL Log T (m <sup>2</sup> /s)			Average frequency
	Min	Average	Max	P <sub>10</sub> , PFL-f
SFR ( 0 to –200 m)	–10.23	–7.84	–4.55	0.338
FFM02 (–100 to –200 m)	–9.61	–8.02	–5.14	0.221
SFR (–200 to –400 m)	–9.08	–8.14	–6.52	0.109
FFM01 (–200 to –400 m)	–9.57	–8.51	–6.74	0.028
SFR (below –400 m)	–8.42	–7.87	–6.96	0.026
FFM01 (below –400 m)	–9.21	–8.19	–7.05	0.040

<sup>1)</sup> SFR data from boreholes inside the Local model domain, KFR101, KFR102A, KFR102B, KFR103, KFR104, KFR105, and KFR27. All data outside deterministic deformation zones are included, even data interpreted as Unresolved PDZs and SBA-structures.

### 5.2.3 Analysis of HCD transmissivity with depth

The SFR structural model (Curtis et al. 2011) is a subdomain of the Site Investigation Forsmark model (Stephens et al. 2007). Unless evidence should prove otherwise, it is reasonable to expect that the local hydrogeological system of SFR is similar to its surrounding settings (with the exception of the particular characteristics inside the Forsmark lens). In the Forsmark SDM, a depth trend model was defined based on 116 intercepts representing 57 different zones (Follin 2008). Based on observations in maximum HCD transmissivity with depth, an exponential model was formulated for the depth dependency in HCD transmissivity (Follin et al. 2007b):

$$T(z) = T_0 10^{-z/k} \quad (5-1)$$

where  $T(z)$  is transmissivity at elevation  $z$  (RHB 70),  $T_0$  is the expected transmissivity at zero elevation, and  $k$ , set to 232.5 m, is the depth interval over which transmissivity decreases one order of magnitude. The value of  $T_0 = T(0)$  can be calculated by inserting a measured value  $T(z')$  at its reference elevation  $z'$ .

$$T_0 = T(z') 10^{-z'/k} \quad (5-2)$$

The HCD transmissivity at reference elevation 0 m RHB 70,  $T_0$ , is calculated for each intercept. A mean  $T_{eff}(0)$  is calculated for a deformation zone set, or for a single zone in case there exists several intercepts of the same zone, as the geometric mean of the intercepts. These calculations require that  $k$  is known. Therefore, it was first examined if it is reasonable to use  $k = 232.5$  m for the SFR data set.

A couple of factors complicate a site-specific depth trend analysis for the SFR data set:

- The within HCD heterogeneity requires a large sample size, i.e. a large number of borehole intercepts, to obtain confidence in a depth trend model. In the Forsmark SDM, transmissivity could vary more than two orders of magnitude laterally within the same deformation zone (Follin 2008). Similar heterogeneities are observed in the SFR data set.
- The new and old SFR hydraulic data sets cannot be readily combined, as they are based on different test methodologies with different confidence and quality. Uncertainty in treatment of the old data set is discussed in Öhman and Follin (2010a). In the new SFR data set, there are 31 HCD intercepts and 14 Unresolved PDZ intercepts, and the corresponding sample sizes in the old data set are 53 and 9, respectively (supported by hydraulic data). Most intercepts are concentrated to the shallow bedrock.
- A number of intercepts, mainly ZFMWNW0001, only has partial borehole coverage and/or hydraulic data of the true deformation zone thickness, leaving uncertainty on how representative the intercept is for the full width of the zone. Incomplete intercepts must be judged if they should be: retained, rejected, or perhaps extrapolated to the full zone thickness.
- The amount of borehole data declines with depth. Scarce data at depth implies uncertainty at the lower end in the model extrapolation. Also, if the sample size declines with depth, a depth trend fitted to maximum transmissivity may be artificially exaggerated, as smaller sample size reduces the probability of finding large values. This phenomenon relates to the fact that hydraulic data often highly skewed towards low values, i.e. following log-normal, or power-law distributions.
- Below an elevation of -300 m RBH70, there are only seven HCD intercepts available (Figure 5-2). Four of these intercepts reflect a complex junction of the Southern boundary belt in KFM11A (Figure 5-2a). This junction is not likely to be representative for the general population of deformation zones.
- Non-perpendicular borehole intercepts artificially exaggerates HCD transmissivity. Considerably longer intercepts than the true thickness implies an overestimation when HCD transmissivity is calculated as the sum of measured transmissivities inside. One such example, ZFMENE3115 in KFR102A is discussed below.

To compare the SFR data to the Forsmark SDM depth-dependency model, Eq. (5-1), the data were divided into sub-groups: The Southern boundary belt (Figure 5-2a), old hydraulic data outside the Southern boundary belt (Figure 5-2b), and new hydraulic data outside the Southern boundary belt (Figure 5-2c).

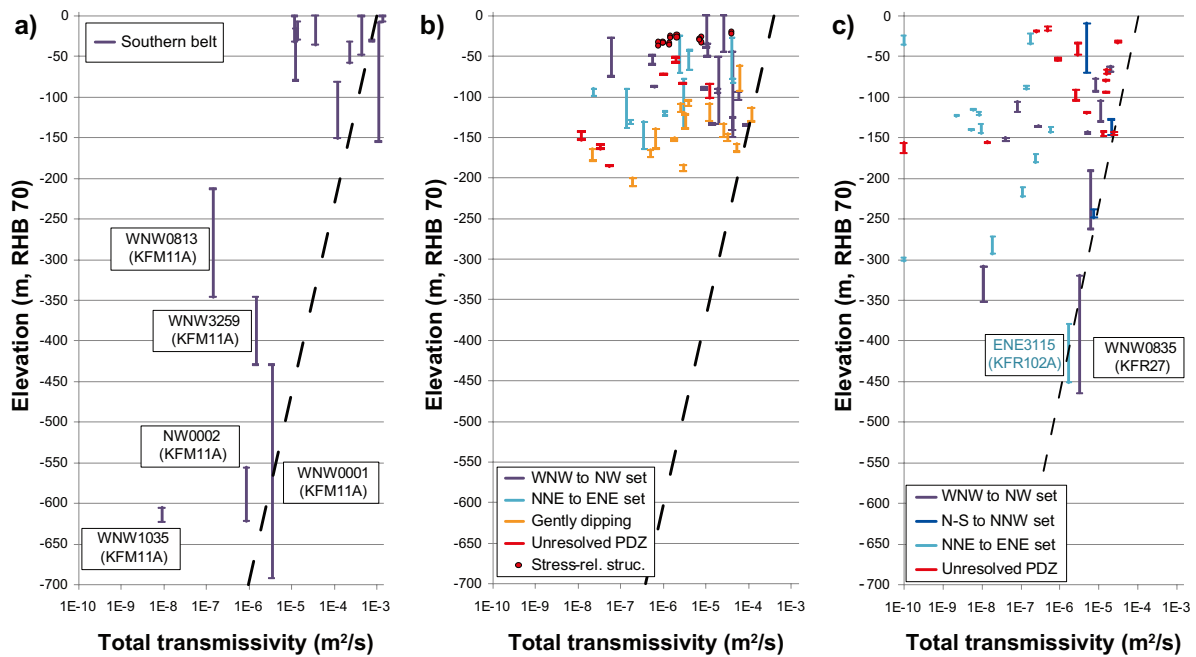


**Figure 5-2.** Summed transmissivity inside HCD intercepts with elevation; a) Southern boundary belt intercepts, b) old SFR data, and c) recent SFR data. The depth trend model from SDM-Site Forsmark,  $k = 232.5$  m, Eq. (5-2), have been fitted to the maximum values of each data set. Transmissivity below detection limit is shown as  $10^{-10}$  m<sup>2</sup>/s.

The Southern boundary belt intercepts (Figure 5-2a) are covered by recent data from Site Investigation Forsmark, HFM34, HFM35, and KFM11A, as well as older data from the construction of SFR, KFR61, KFR62, KFR64, KFR65, KFR67, KFR68, and KFR71. For Singö, ZFMWNW0001, only one complete intercept exists. This corresponds to the lower part of the 579 m long PDZ KMF11A\_DZ1, which is complex and overlapped by other splays of the Southern boundary belt. The shallow intercepts of the Southern boundary belt are incomplete (penetrates only part of the modelled zone thickness). Nevertheless, shallow intercept transmissivities are extremely large for the Southern boundary belt ( $T_{\text{HCD}} > 10^{-4}$  m<sup>2</sup>/s). Potentially, these shallow values reflect sheet joints of the type that was found in SDM-Site Forsmark (Figure 2-4). This type of extremely large transmissivity values at shallow depth does not exist outside the Southern boundary belt (Figure 5-2b, c).

Outside the Southern boundary belt, the largest transmissivities of the old data set (Figure 5-2b) are found in the Northern boundary belt, ZFMNNE0869 (Zone 3), ZFM871 (Zone H2), and shallow possible stress-relief structures. The NNE to ENE set consists of two very different zones: the 60 m wide, highly transmissive ZFMNNE0869 (formerly Zone 3;  $T_{\text{HCD}} \approx 10^{-5}$  m<sup>2</sup>/s) and the 16 m wide ZFMNE0870 (formerly Zone 9;  $T_{\text{HCD}} \approx 10^{-7}$  m<sup>2</sup>/s). ZFMNNE0869 is uncharacteristic for the NNE to ENE set, in terms of width, transmissivity and orientation. The largest transmissivity of ZFMNE0870 comes from an uncertain *geometrical* intercept (RVS modelling) in KFR70. Unusually large transmissivities are found in KFR70, and these are closely located to the transmissive HFR101\_DZ2 (Appendix A). The gently dipping ZFM871 (Zone H2) may possibly have a stronger depth trend than the steeply dipping zones, as previously observed in the model v.0.1 (Öhman and Follin 2010a) (Figure 5-2b). The vertical span of the old data set, 0 to –200 m RHB 70, is insufficient for determining depth dependency.

The data from the SFR extension investigation has a somewhat larger vertical span (Figure 5-2c). The NNE to ENE set has lower transmissivity than other types of intercepts. They are on the same order as ZFMNE0870 in the old data set. The largest transmissivities are found in the Northern boundary belt and ambient deformation zones: ZFMNNW1034, ZFMWNW3262, and Unresolved PDZs. The two deepest intercepts are possible outliers in the depth trend analysis, ZFMWNW0835 and ZFMENE3115. These deep intercepts are considerably more transmissive – and *excessively long* in relation to shallower intercepts. The deep intercept of ZFMWNW0835 comes from the parallel borehole KFR27 (Figure E-23), covering three PDZs of the geological Single Hole Interpretation.

This intercept is a factor 12 longer and 40 times more transmissive, than its shallower intercept. The deep intercept of ZFMENE3115 in KFR102A is 81 m long, with  $T_{\text{HCD}} \approx 10^{-6} \text{ m}^2/\text{s}$  (Figure E-5; extending from  $-379$  to  $-451$  m RHB 70), while its shallow intercepts in KFR104 and KFR105 (at c.  $-120$  m RHB 70) are 5 to 7 m long with  $T_{\text{HCD}} \leq 10^{-8} \text{ m}^2/\text{s}$ . A hypothesis during the development of the Geological model v.1.0 was that the deep intercept in KFR102A represented more than one zone, although that was rejected during revisions. This deep intercept is more than a factor 11 longer, and 200 times more transmissive, than its shallower intercepts. Both deep intercepts contain vuggy granite, which is quite rare in the SFR data. It cannot be concluded if these two zones grow with depth, or if it is an artefact of non-perpendicular intercepts or the uncertainty in the geologic linking between PDZ and lineament data; an uncertainty that may be expected to grow with depth.

### 5.2.4 Relation between HRD and HCD transmissivity with depth

Hydraulic analysis with depth must consider variations in sample size (i.e. available borehole length; Figure 5-3). The maximum borehole coverage is found within the depth interval,  $-100$  to  $-150$  m RHB 70, with c. 13 m of PFL-f logged core length per vertical meter (Figure 5-3b; the sub-horizontal KFR105 contributing the most). Below  $-300$  m RHB 70, the average coverage of HRD is 1.0 meters core per vertical meter. In the range  $-380$  to  $-450$  m RHB 70 there is no HRD coverage at all, as both KFR27 and KFR102A intercepts deformation zones (ZFMWNW0835 and ZFMENE3115, respectively; Figure 5-2c). The PFL-f data from different boreholes are here treated as a homogenous population; thus, there is a risk that gaps in borehole coverage with depth – in combination with local heterogeneity and lateral trends – may be erroneously interpreted as depth trend.

With the exception of the deep intercept of ZFMENE3115 (Figure 5-2c), the NNE to ENE set has low transmissivity and follows the same pattern as maximum PFL-f data in HRD (Figure 5-3). The most transmissive PFL-f in HRD are horizontal, or dip less than  $40^\circ$ . The PFL-f in HRD seem to have a stronger depth dependency (grey line representing  $k = 140$  m, which is the same as was fitted to the old data set in the Hydrogeological model v.0.1 (Öhman and Follin 2010a). Intercepts associated to the Northern boundary belt, ZFMNNW1034, Unresolved PDZs, and SBA-structures (see Appendix B), exhibit less depth dependency and are more than an order of magnitude more transmissive (Figure 5-3).

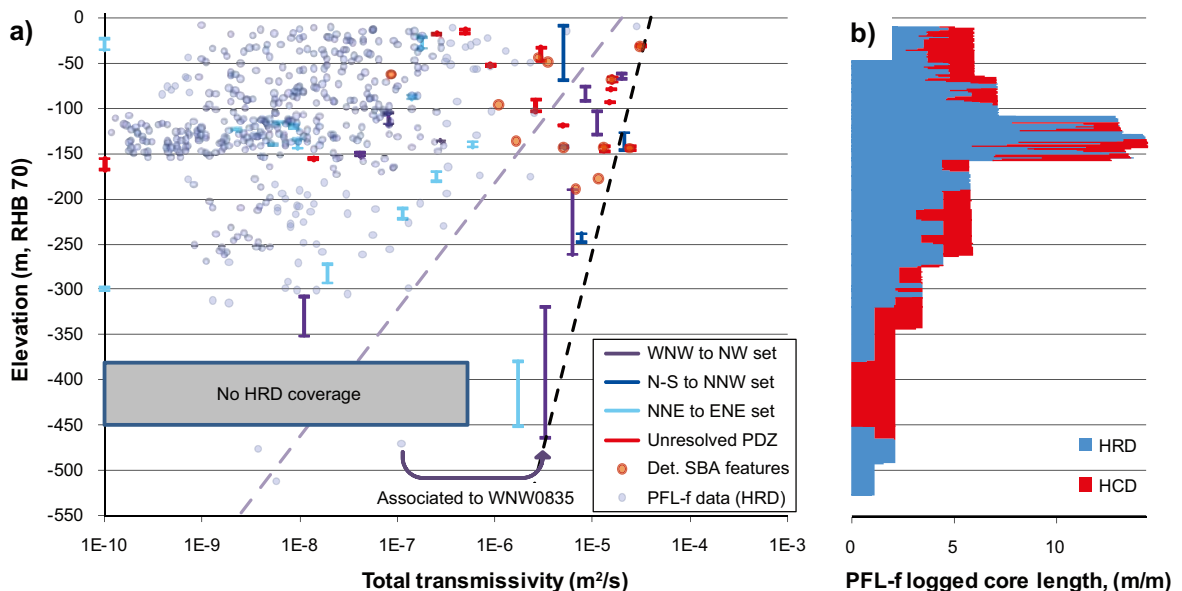


**Figure 5-3.** Transmissivity of various geologic features with elevation; a) PFL-f data in HRD compared to HCDs, deterministic SBA-structures, and Unresolved PDZs, b) borehole coverage with elevation. The depth trend model from Forsmark,  $k = 232.5$  m, Eq. (5-2), is shown with a black line, and the HRD depth trend model from Öhman and Follin (2010a) is shown with a grey line. The Silo and the four rock caverns (black silhouette) included for vertical reference.

This could suggest a conceptual model where the Northern boundary belt (as well as ZFMNNW1034) forms a hydraulic flow boundary, vertically connected to the overlying Sea. Horizontal stochastic fractures, SBA-structures, and Unresolved PDZs form a horizontal connection between the Northern boundary belt and the interior HRD, and possibly also for the NNE to ENE set. The declining frequency and transmissivity of PFL-f data in HRD at depth (Figure 5-3) could suggest a deteriorating horizontal connectivity to the Northern boundary belt. This notion is pursued in the analysis of lateral transmissivity contrasts (Section 5.3).

### 5.3 Lateral contrasts in transmissivity data

The transmissivity data (Figure 4-17) suggests a contrast between rock mass at the centre of the Central block and the rock mass located closer to the Northern boundary belt and ZFMNNW1034 (Figure 3-5). In this section, the lateral trends of PFL-f transmissivity in HRD are analysed separately for the Shallow Bedrock (0 to –60 m RHB 70; Section 5.3.1) and the Repository level (–60 to –200 m RHB 70; Section 5.3.2). The subdivision of depth intervals is necessary due to: a) relevance for the emplacement for the extension of SFR, b) support from observations in data, and c) gaps in data coverage. The depth for the SFR extension has not been decided, but the elevation interval of the existing SFR was taken as guidance (i.e. –60 to –140 m RHB 70). If the depth intervals are inappropriately chosen, data gaps in borehole coverage, in combination with the transmissivity depth trend, may mask lateral variability and/or provide misleading results. Lateral contrasts cannot be interpreted for the deeper rock (below –200 m RBH70) owing to data scarcity. At these depths (below –200 m RHB 70), the PFL-f data seem to be more directly controlled by deformation zones.

Boreholes KFR105, KFR104, HFR101, and HFR102 are located central in the Central block (Figure 3-5); these are marked by darker colours in Figure 5-4. Boreholes HFR106, KFR106, KFR103, and KFR102B are located closer to the Northern boundary belt and ZFMNNW1034 (Figure 3-5); these are marked by paler colours in Figure 5-4. In the Shallow rock there exist no hydraulic data in KFR102A and in KFR27 there only exists PFL data tested over 5 m sections; these boreholes are regarded to have an intermediate location “between the Central block and the Northern boundary belt and ZFMNNW1034”. There are also no shallow data in the underground borehole KFR105; note that its sub-horizontal orientation entails sampling bias against the transmissive horizontal fracture system.

#### 5.3.1 Shallow Rock (0 to –60 m RHB 70)

In the superficial rock outside zones, the largest transmissivities ( $T > 10^{-5} \text{ m}^2/\text{s}$ ) are found in the vicinity of the Northern boundary belt and ZFMNNW1034 (i.e. the bin –4.5 in Figure 5-4 includes only HFR106 and KFR103). However, at shallow depths, all boreholes, irrespectively of location,

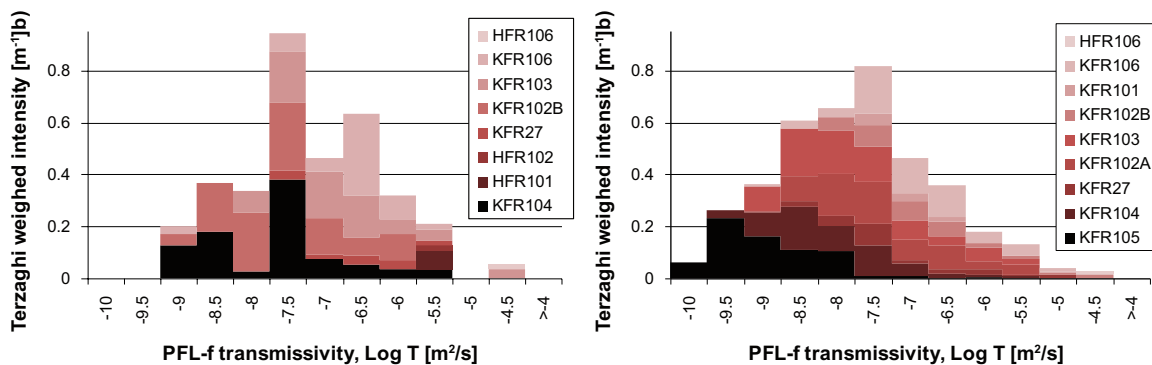


**Figure 5-4.** Stacked histograms of transmissivity distribution outside deterministically modelled deformation zones; a) Shallow rock (0 to –60 m RHB 70) and b) at Repository level (–60 to –200 m RHB 70). Boreholes are ordered and coloured by distance from the Northern boundary belt and ZFMNNW1034; pale colour indicate location closer to the Northern boundary belt, while dark colour represents a central location in the Central block.

have transmissivities exceeding  $10^{-6}$  m<sup>2</sup>/s (i.e. all boreholes are represented in the logarithmic bin  $-5.5$  or higher; Figure 5-4). Note that various different data types have been used in this comparison: a single 44 m injection test in HFR102, 5 m sequential PFL data in KFR27, HTHB data from HFR101 and HFR106, and PFL-f data in cored boreholes. Note also that HFR101 has no HTHB above  $-60$  m RHB70 (detection limit on the order  $10^{-7}$  m<sup>2</sup>/s).

To summarise, although the highest transmissivities ( $T > 10^{-5}$  m<sup>2</sup>/s) are only found close to the Northern boundary belt and ZFMNNW1034 in the Shallow bedrock, its lateral contrast is judged to be small. A class of relatively high transmissivities ( $T > 10^{-6}$  m<sup>2</sup>/s) is found in all boreholes, without spatial interference. This may imply the existence of stress-relief structures (sheet joints) with large horizontal extent formed by glacial loading/unloading processes. Another explanation is that the shallow fracture network may be connected to the Seafloor (i.e. a positive hydraulic boundary); if the hydraulic boundary is close, the flow paths are short and less subject to hydraulic chokes. It is unclear to what extent the sediments choke the connectivity between the seafloor and the underlying shallow bedrock.

The South-western part of the domain is poorly covered by hydraulic data, but it may be suspected that similarly transmissive features exist in the vicinity of Singö and ZFMWNW1035. Below the Shallow rock, the lateral transmissivity contrast is stronger (cf. Figure 5-4a and b). The underlying Repository level ( $-60$  m to  $-200$  m RHB 70) is expected to cover the extension of SFR. It was therefore decided to pursue the analysis of lateral transmissivity contrasts at the Repository level in more detail (Sections 5.3.2 and 5.3.3).

### 5.3.2 Repository level ( $-60$ m to $-200$ m RHB 70)

Based on the appearance of Figure 5-4b, the boreholes are divided into two groups. Group 1 consists of boreholes with a central location in the Central block: KFR104, KFR105 and HFR101. Group 2 consists of boreholes located closer to the Northern boundary belt and ZFMNNW1034: KFR101, KFR102A, KFR102B, KFR103, KFR106, and HFR106. The steep borehole KFR27 is judged to have “intermediate location and characteristics” (and involves several uncertainty aspects) and hence is not included in either data set. It should be emphasised that this analysis includes all transmissivity data outside deterministically modelled deformation zones (i.e. including HRD, Unresolved PDZs, and a particular subset of high-transmissive horizontal to gently dipping fractures, which a later stage will be defined as deterministic SBA-structures in, see Appendix B).

In this comparison it must be considered that Group 1 has less borehole coverage than Group 2; the total borehole length in the Group 1 is 612 m, while it is 782 m in Group 2. For the aspect of sub-horizontal SBA-structures, orientation sampling bias and vertical borehole coverage must also be considered. Most borehole length in Group 1 (within the elevation interval  $-60$  to  $-200$  m) comes from the sub-horizontal borehole KFR105, which only has a vertical coverage of 49 m (from  $-107$  to  $-156$  m RHB 70). In terms of vertical coverage, the difference between the two data sets is even larger: 316 and 687 m, respectively. As discussed above, the exceptionally low practical detection limit in KFR105 is partly the result of abundance of high-transmissive features, but also entails a methodological difference.

Transmissivities exceeding  $10^{-8}$  m<sup>2</sup>/s are considerably more frequent in Group 2 (Figure 5-5a). Note that Group 2 has higher practical detection limit than KFR104 and KFR105 (Figure 5-5b), and thus its transmissivity below  $10^{-8}$  m<sup>2</sup>/s is largely censored. Only non-censored borehole intervals are included in intensity calculations; hence the underlying borehole length varies between transmissivity bins (Figure 5-5). For example, the intensity for Group 2 is undefined below c.  $10^{-9}$  m<sup>2</sup>/s, as the total non-censored length is equal to zero. On the other hand, the low practical detection limits in KFR104 and KFR105 are partly the result of absent highly transmissive features. However, KFR105 is a subsurface borehole, and consequently its PFL-logging set-up and evaluation differ from the standard methodology for surface boreholes (Väisäsvaara 2009). The largest transmissivities ( $T > 10^{-5}$  m<sup>2</sup>/s) are found inside Unresolved PDZs in KFR101, KFR103, and KFR106 (see Appendix A).

Percussion HTHB data have considerably higher detection limit. It was nevertheless considered useful for including data in the upper tail of the transmissivity distributions. The HTHB detection limit in HFR106 is reported to be  $2 \times 10^{-6}$  m<sup>2</sup>/s, and consequently, it was only included in intensity calculations for logarithmic transmissivity bins larger than  $-6$  (Figure 5-5). Similarly, the detection limit in HFR101 has been reported to be on the order  $10^{-7}$  m<sup>2</sup>/s.

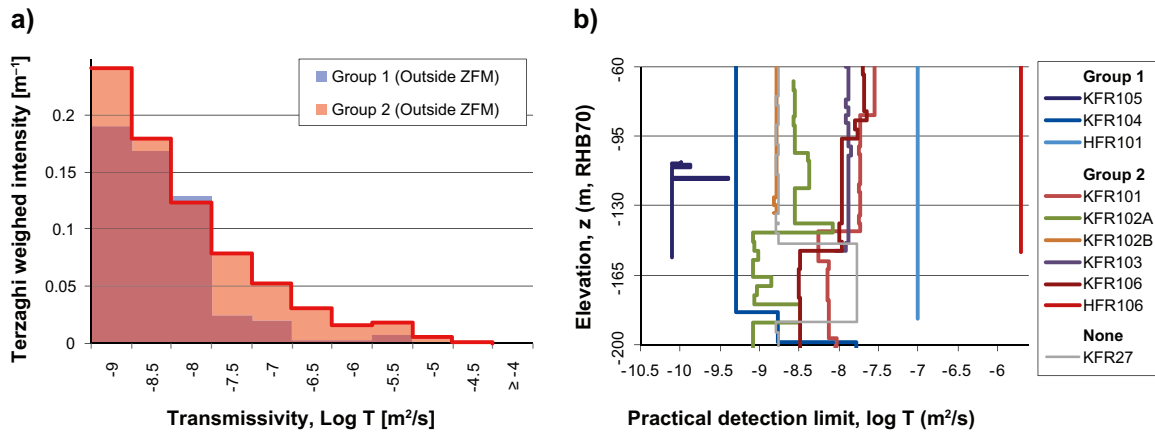


Figure 5-5. Transmissivity distribution outside deterministically modelled deformation zones (ZFM) in the depth interval  $-60$  to  $-200$  m RHB 70; a) comparison between Groups 1 and 2, and b) practical detection limit.

### 5.3.3 Lateral transmissivity contrasts in relation to deterministic structures

The contrasts between the two borehole groups were also put in context to the difference between deterministically modelled structures (HCD) and rock mass in outside (HRD, Unresolved PDZ, and SBA). These contrasts were compared as stereographical projected PFL-f orientation (Figure 5-6), as well as, histograms of PFL-f and HTHB transmissivity distributions (Figure 5-7).

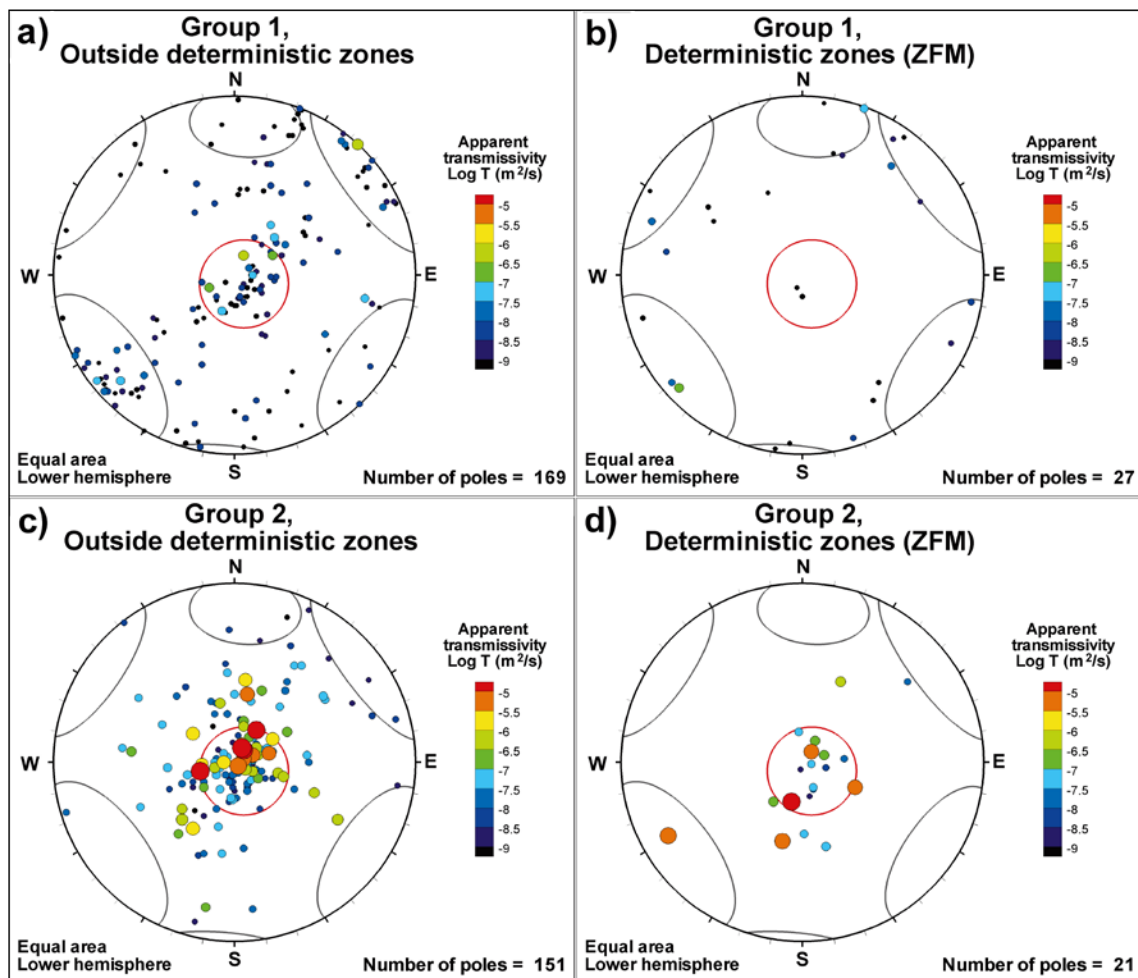
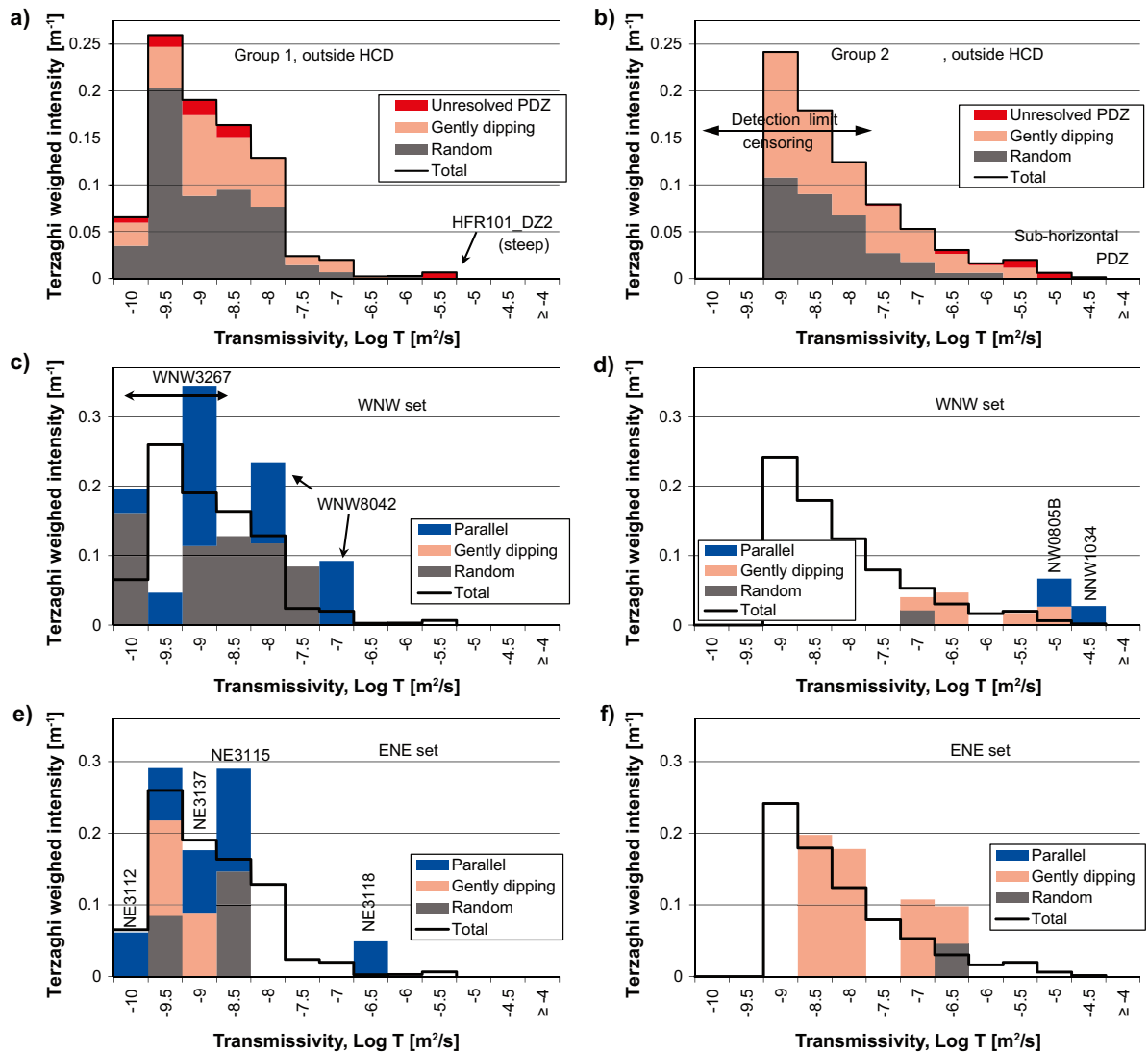


Figure 5-6. Comparison of PFL-f orientation at the Repository level ( $-60$  to  $-200$  m RHB 70) between Group 1 (KFR104 and KFR105) and Group 2 (KFR101, KFR102A, KFR102B, KFR103, and KFR106). Percussion boreholes, as well as, KFR27 are excluded. Poles are coloured and scaled by apparent transmissivity (cf. Figure 4-15).



**Figure 5-7.** Transmissivity comparison between Groups 1 and 2 (left and right column, respectively) made in terms of stacked histograms of Terzaghi-weighted intensity. Data outside deformation zones (a and b) are compared to data inside WNW-striking deformation zones (c and d), and ENE-striking deformation zones (e and f). Only data in the elevation range  $-60$  to  $-200$  m RHB 70 included.

The PFL-f data inside zones are classified into three groups: “Parallel” (if the dihedral angle between the PFL-f feature and the zone is less than  $45^\circ$ ), “Gently dipping” (dip  $< 30^\circ$ ), and “Random” (dip  $\geq 30^\circ$ , and striking more than  $45^\circ$  away from the zone). Obviously, the class “Parallel” cannot be defined for the rockmass outside deformation zones, but instead the class “Unresolved PDZ” (which are PDZs not included in the deterministic model) is demonstrated separately. The *a priori* expectation is that the pattern in transmissivity data should exhibit different characteristics inside deformation zones (in terms of orientation and/or transmissivity values). Particular emphasis is paid to the upper tail of distributions (logarithmic transmissivity bins larger than  $-5$ ).

Based on the orientation patterns (Figure 5-6), the difference between the borehole groups is clearly more pronounced than that inside/outside deterministic structures. Note that the estimated orientations of HTHB data reinforce the steep WNW-striking component of deterministic structures in both Northern and Southern boundary belts, but these are *not included* in (Figure 5-6), as their orientation estimates are highly uncertain.

### Observations made

Outside deformation zones, the upper tail of PFL-f transmissivity (e.g. transmissivities exceeding  $10^{-7}$   $m^2/s$ ) is predominantly gently dipping in Group 2. Such features are comparatively rare in Group 1 (cf. Figure 5-7a and b). The PFL-f in Group 1 are steeper and have lower transmissivity



(generally below  $10^{-8}$  m<sup>2</sup>/s). Thus, it is quite possible that low-transmissive, steeply dipping PFL-f exist also in Group 2, although being censored by the practical detection limit (as indicated in Figure 5-7a; see also Figure 5-5b).

In Group 2, the high-transmissive, sub-horizontal to gently dipping PFL-f are also abundant inside deformation zones – WNW- as well as ENE-striking (Figure 5-7c and e). However, the WNW-striking zones have a stronger hydraulic signature, reinforced by a few, high-transmissive PFL-f that are parallel to the zones (ZFMNNW1034 and ZFMNW0805B). Such parallel PFL-f are also found at depth in ZFMNW0805A and ZFMWNW0835, but below –200 m and –350 m RHB 70, respectively; however no data below –200 m are included in Figure 5-7d. On the contrary, no parallel PFLs are found in ZFMWNW3262 (Figure 5-7d), or in the ENE-striking deformation zones (Figure 5-7e). For Group 2, the data inside ENE zones does not stand out as different from the data outside deformation zones; however, only 24 out of 846 m borehole length is interpreted as inside ENE zones. A plausible interpretation is that a true ENE-zone hydraulic signature indeed exists in Group 2, but it is masked by pervasive high-transmissive, sub-horizontal to gently dipping PFL-f.

The Group 1 data set provides quite different characteristics; the high-transmissive, sub-horizontal to gently dipping PFL-f are virtually absent inside the deformation zones (Figure 5-7d and f). Note that the absence of sub-horizontal PFL-f within this data set is partly caused by sampling bias. Nevertheless, KFR105 (10° inclination) does have a vertical coverage of 49 m, and the sub-horizontal PFL-f mapped therein are low-transmissive (typically on the order  $10^{-9}$  m<sup>2</sup>/s). Instead, the PFL-f inside deformation zones of Group 1 are predominantly of the “parallel” type (Figure 5-7d and f). Again, many of these parallel PFL-f have relatively low transmissivity, which in many cases would have fallen below the practical detection limits of Group 2 (Figure 5-5b).

### 5.3.4 Conclusions

In spite of various data limitations, involving differences in sample size, spatial coverage, detection limits, and geometric sampling bias, a lateral hydraulic contrast has been identified at the Repository level. This contrast is related to high-transmissive sub-horizontal features (e.g. Figure 2-4) that seem related to the Northern boundary belt and ZFMNNW1034. These features seem to override the hydraulic signature of the less conductive ENE-striking deformation zones. Similarly, it is plausible that *some* – but *not* all – shallow dipping PFL-f inside the WNW-striking zones are not the characteristics of the zone, but instead part of a self-sustained SBA system (see alternative deterministic modelling of so-called SBA-structures in Appendix B).

Three deformation zones in Group 2 are exceptionally transmissive: ZFMNNW1034, ZFMNW0805A, and ZFMWNW3262. The PFL-f in ZFMNNW1034 and ZFMNW0805B (also ZFMNW0805A, although not presented here) are parallel to the deterministic structure. The fact that high-transmissive, sub-horizontal PFL-f outside zones seem related to the Northern boundary belt and ZFMNNW1034, with decreasing frequency and transmissivity with depth and towards the Central block, suggests that the Northern boundary belt, together with ZFMNNW1034, acts as an important positive flow boundary to the hydrogeological system at SFR.

In contrast, the PFL-f inside ZFMWNW3262 intercepts are distinctly of SBA-type (KFR103 and KFR106; Appendix E). In fact, this very distinctive pattern of narrow borehole intercepts with horizontal PFL-f and transmissivities on the order  $10^{-5}$  m<sup>2</sup>/s has a striking resemblance to the *Unresolved PDZs* in the same boreholes (Figure E-11 and Figure E-20). In the Hydro-DFN methodology, transmissivity is assumed to be correlated to size (e.g. Öhman and Follin 2010b). Thus, the highly transmissive, sub-horizontal PFL-f put into context of the modelled geometry of ZFMWNW3262, a 2 m wide steep structure (Figure 5-8), suggests three alternative hypotheses:

- 1) ZFMWNW3262 is *highly anisotropic*, channelized horizontally (Figure 5-8a).
- 2) The detected sub-horizontal pattern is an artefact of sampling bias, the *true* hydraulic backbone of ZFMWNW3262 may well be steep WNW-striking, but remains *undetected* owing to intercepting borehole orientations.
- 3) Similar to the general characteristics of the WNW- to NW-set outside the Northern and Southern boundary belts, ZFMWNW3262 has low, or fragmented, transmissivity; the detected PFL-f does not reflect the zone, but invasive SBA-structures (Figure 5-8b).

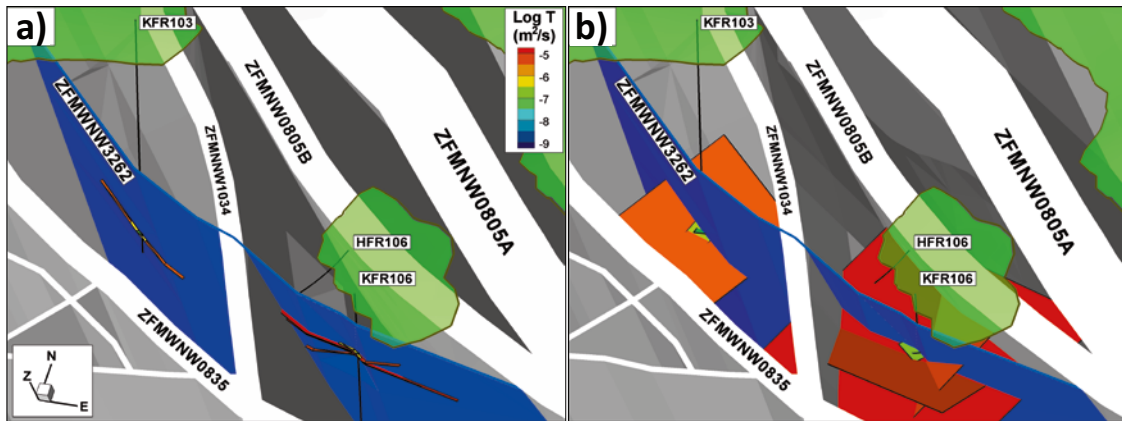


**Figure 5-8.** PFL-f data inside ZFMWNW3262 (blue structure) inside intercepts from KFR103 and KFR106; alternatively shown as: a) square planes sized according to empirical relationship by Öhman and Follin (2010b), or b) sub-horizontal channels inside the structure.

These key characteristics raise concerns to the conceptual interpretation of data, leading to:

- Critically addressing the hydraulic role of geologically modelled zones (Section 5.4).
- Formulation of a conceptual model (Section 5.5).
- Alternative implementation strategies in numerical modelling (Section 5.6).
- A model alternative with deterministic SBA-structures (Section 6.4 and Appendix B).

### HRD

The hydrogeological interpretation of the available data set conforms into conceptual model where Unresolved PDZs and SBA-structures are defined and modelled separately. The suggested modelling for Unresolved PDZs and SBA-structures provides spatial control of the most transmissive subset of hydraulic data (Appendixes A and B, respectively). The remaining stochastically handled data set, HRD, is thus defined as the rock mass outside: 1) deformation zones (HCD), 2) Unresolved PDZs, and 3) deterministic SBA-structures. This remaining HRD data set exhibits considerably less lateral contrast between the borehole groups 1 and 2 (Figure 5-9 and Figure 5-10). It should be noted that some data types are not included in the Hydro-DFN model (details in Appendix G); the excluded data are percussion data, HFR101 and HFR106, as well as, core data in KFR106 and parts of KFR27.

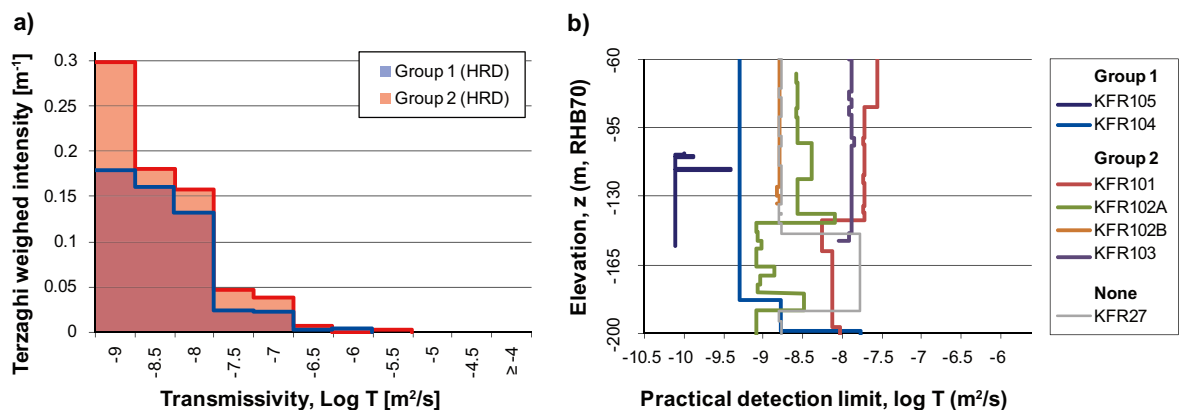


**Figure 5-9.** Repository-level HRD transmissivity distribution ( $-60$  to  $-200$  m RHB 70) after defining Unresolved PDZs and SBA-structures; a) comparison between Groups 1 and 2, and b) practical detection limit. Separate handling of data in Unresolved PDZs and SBA-structures reduces the contrast between the groups (cf. Figure 5-5). KFR106 is not included.

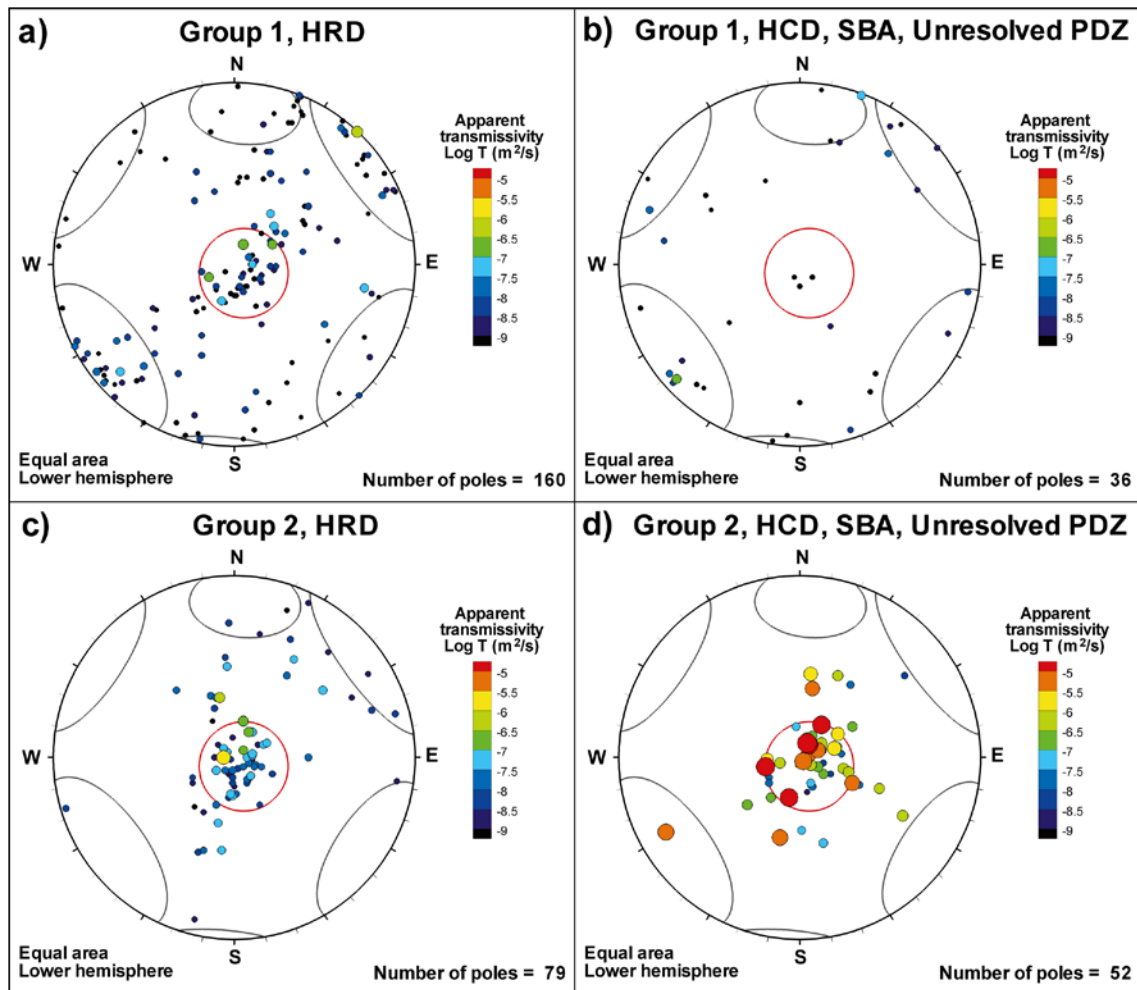


**Figure 5-10.** Repository-level PFL-f data pattern ( $-60$  to  $-200$  m RHB 70) after defining Unresolved PDZs and SBA-structures (cf. Figure 5-6). Comparison is made between Group 1 (KFR104 and KFR105) and Group 2 (KFR101, KFR102A, KFR102B, KFR103, and KFR106). Percussion boreholes, as well as, KFR27 and KFR106 are excluded. Poles are coloured and scaled by apparent transmissivity.

## 5.4 The role of deterministic structures on HRD connectivity

Deterministically modelled structures have a fundamental role in the hydrogeological model, not only in the numerical implementation of the regional-scale flow model, but also a conceptual role in describing the hydraulic connectivity in the rock mass outside deformation zones (HRD). The HRD is described as a stochastic network of connected Open fractures, *flowing fractures*, by means of DFN modelling. The Hydro-DFN parameterisation is assessed from borehole data. Fracture size is a crucial parameter for the connectivity that cannot be directly assessed from borehole data.

In the established SKB methodology, the size distributions of the Open fractures are calibrated in the DFN model by means of a *connectivity analysis* (Follin et al. 2005). In this approach, an *a priori* assumption is that deterministic structures of the geological model have the essential role of flow boundaries. This assumption is disputable; in several cases the internal continuity of zones is unclear, as discussed in early SFR models (Section 1.6), in the recent geological model (Appendix C), as well as, interference test interpretations (Section 4.4.2). Deformation zones are strictly defined on geological merits (Section 2.3.4); potentially forming large-scale, transmissive flow paths, but this is not necessarily always the case. Thus, the term *Hydraulic Conductor Domain* (HCD) may in some sense be misleading. A general notion in the analysis of PFL-f data was that the correlation between PFL-f anomalies and deterministic structures is not clear-cut (Section 5.3; Appendix E). Therefore, the relationship between PFL transmissivity and deterministic structures is discussed in Sections 5.4.1 and 5.4.3. The model representation of Unresolved PDZs and are SBA-structures also expected to have an essential role in the connectivity analysis. These are discussed in Appendixes A, B and, G, respectively.

### 5.4.1 Connectivity between the HRD and the sea

Hydraulic boundaries form the framework of a hydrogeological model. These define source terms and the driving potential at the outer borders of the model. PFL data are assumed to reflect *continuously flowing features* that are globally connected to a positive flow boundary, which strictly speaking implies an infinite source of water. The SFR domain is largely located below the sea and therefore the overlying sea is assumed to be the positive flow boundary for PFL-f data. In practise, PFL-f data are based on at least three days of pumping, which results in a *pseudo steady state*. This implies that, in certain aspects, highly conductive structures may also act as pseudo boundaries, at least for the detection of lesser transmissive features.

The predominantly horizontal pattern of PFL-f data inside HRD (Figure 4-15a) suggests that the limiting factor for PFL-f data is the vertical connectivity to the sea. This suggests two possible configurations of the *flowing fracture network* in HRD:

- 1) The hydraulic connectivity between a fragmented horizontal fracture network and the overlying sea is dictated by large vertical conductive structures (i.e. deterministic ZFM structures; Figure 5-11a).
- 2) The data reflects autonomous large-scale horizontal structures (Figure 5-11b; based on findings from the Forsmark Site Investigation; Figure 2-4). The large horizontal extension may be remotely connected to the Sea, or sufficient to sustain 3 days of pumping. Anyhow, large horizontal extent implies that the connectivity to the sea is less critical.

In the first case, conductive deformation zones are considered as hydraulic boundaries for fracture network connectivity, in the second case they are assumed to be of relatively lesser importance.

Thus, the deficit of steep, high-transmissive PFL-f data outside zones suggests that deformation zones may have a key role in the vertical connection to the Sea. Therefore the patterns in PFL-f data are analysed with respect to three-dimensional geometry of ambient deformation zones (Section 5.4.3). If zones indeed are important vertical conductors, the prior expectation is that the PFL-f transmissivity and intensity should be high inside, or in the vicinity of, deformation zone intercepts. However, this expectation cannot be observed in data, at least not above an elevation of –200 m RHB 70 and if no distinction is made to the type of deformation zones (see Figure 4-16). Data are scarce below –200 m RHB 70, but at these depths the PFL appear more correlated to deformation zones (Figure 5-3). It should also be emphasized that deformation zones should not be regarded as a uniform collective; some zone intercepts do exhibit distinctive hydraulic signatures.

Consideration of within-plane channelling and 3-D geometry may provide an explanation to a seemingly poor PFL correlation with deformation zone intercepts. The flow inside zones may be highly channelized into narrow flow paths that are unlikely to be found in a borehole intercept (Figure 5-11a). On the other hand, PFL-f detected *outside* the actual intercept may represent large, less channelled, horizontal fractures that are well-connected to the paths inside the zone. Thus, strongly channelled flow paths within the zone may induce a very diffuse spatial correlation to PFL data, particularly if the distance between the borehole and the zone is smaller than the typical fracture size.

In the SFR data set, the distance between boreholes and deformation zones is generally small (Figure 5-13), and the PFL-f data are dominated by horizontal features. This causes ambiguity to if the sub-horizontal fractures depend on steeply dipping deformation zones for vertical connection to the sea, or if they form a large-scale autonomous inter-connected backbone (cf. Figure 5-11a and b). In this aspect, it should be emphasized that different deformation sets exhibit varying hydraulic characteristics. The Southern and Northern boundary belts, as well as the nearby ZFMNNW1034, exhibit *distinct hydraulic signatures*, with high-transmissive PFL-f inside intercepts, parallel to the zone (Appendix E); these are interpreted as important vertical conductors. Structures inside the Central block are generally more inconclusive (Figure 5-11a or b).

Some insight into the heterogeneity of zones can be gained from KFR27 (Figure E-23; also discussed in Section 5.2.3). Its deep intercept of ZFMWNW0835 covers 146 m borehole length, while most of its total depth-adjusted transmissivity reflects three steep PFL-f, which are located inside a 2 m interval at c. –424 m RHB 70. This implies that the zone is highly channelized and that the chance of finding the channelized network with a borehole is normally slim.

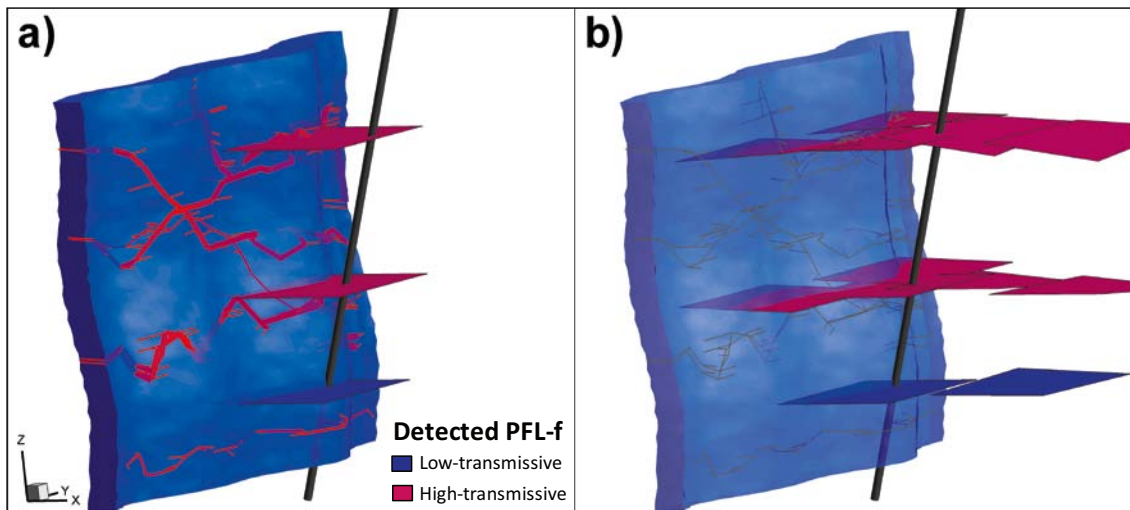


**Figure 5-11.** Conceptual figure demonstrating alternative explanations for a hypothetical case where high-transmissive PFL-f are detected outside a deformation zone intercept; a) internal channelling inside zones masks the connectivity pattern between PFL-f data and the zone, b) the data reflects an autonomously connected horizontal fracture system, which is independent of subordinate transmissivity inside zones (cf. Figure 5-8). Red represents flowing features and blue represents non-flowing features.

#### 5.4.2 Concepts in the connectivity analysis

The key assumptions in the *connectivity analysis* are that: 1) observed intensity differences between Open fractures and PFL-f data reflects the connectivity of the flowing fracture network, and 2) this connectivity can be reproduced by finding the underlying size distribution of the parent population, i.e. Open fractures, or *potentially flowing fractures*. In this approach, any fracture that is directly or indirectly connected to a positive flow boundary is considered to be part of the globally connected flowing fracture network (i.e. a potential PFL-f). Two flow boundary types are considered possible: 1) the overlying sea (possibly limited by sediments), and 2) large-scale deterministic structures. In other words, the deterministic structures are assumed to be well-connected to the sea and highly transmissive – relative to PFL-f detected in the HRD.

In the connectivity analysis, multiple DFN realisations are generated to explore how the connectivity of the fracture system responds to various input size distributions. In the first step, Open fractures, or *potentially flowing fractures*, are generated with various input size distributions. In the second step, the non-connected Open fractures are removed, leaving a network of connected fractures, or *flowing fractures*. The fraction of remaining *flowing fractures* that *exceeds the detection limit of the PFL-logging device* is assumed to be equivalent with PFL-f data. Thus, on a trial-and-error basis, the input size distribution is varied until the ratio between *potentially flowing fractures* and *connected flowing fractures* match the observations in data (i.e. the intensity ratio between Open fractures and PFL-f data).

A preliminary size calibration for Open fractures was demonstrated in v. 0.2 (Öhman and Follin 2010b). The geological model was unavailable during the 0.2 modelling stage, and therefore a simplified setup was used in the connectivity analysis. A cuboid domain was used in this simplified setup (Figure 5-12), with vertical sides separated 100 m taken as positive flow boundaries for simulated borehole exploration. The 100 m side length was intended to represent a general separation distance between steeply dipping deformation zones. A conclusion of the v. 0.2 stage was that the connectivity analysis should be improved by introducing the true orientation of boreholes and deterministic structures, as well as spatially variable PFL-f detection limits. Data evaluation in context of the final geologic model (Chapter 4 and Sections 5.2 and 5.3) suggest that not only steep deterministic structures are candidate flow boundaries for large-scale connectivity, but potentially also horizontal SBA-structures (Section 6.4). Therefore, the spatial relation between PFL data and deterministic structures are examined Section 5.4.3.

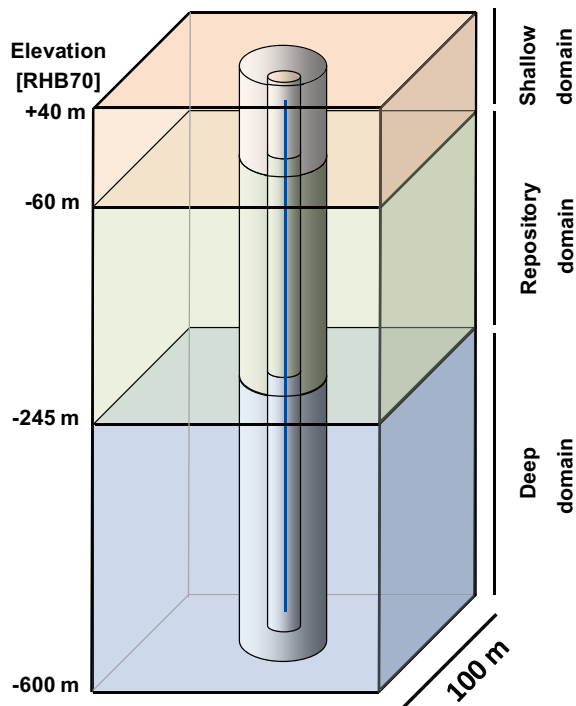


**Figure 5-12.** DFN connectivity analysis setup during the 0.2 modelling stage, divided into three depth domains. Computational demand was reduced by use of fracture generation volumes (cylinders), which includes small fractures only in the vicinity of the sampling scan-line (blue).

### 5.4.3 Spatial inference for PFL data

The pattern of PFL transmissivity over 5 m test sections is evaluated with distance to the nearest deformation-zone boundary (Figure 5-13; as modelled in RVS). The reason for analysing interval transmissivities instead of PFL-f data is that low-transmissive borehole intervals can be included (represented by detection limit, if it falls below). 146 of the totally 532 test sections (or 27%) are located partly inside the HCD target intercepts (sample size shown as pink line in Figure 5-13; the first bin from the left indicates data partly inside target intercepts). 91 test sections (or 17%) are located less than 2 m outside the geometric boundary of the nearest HCD (Figure 5-13; second bin from the left covering data with spherical distance less than 2 m). The maximum distance from a PFL-logged borehole section to the nearest geometrical boundary of a deterministic structure is c. 42 m, and the median distance is c. 11 m (the distances are larger if the central plane is used as reference for structures). If these deterministic structures truly function as hydraulic flow boundaries for HRD connectivity, the assumed c. 50 m radial distance in version 0.2 (Figure 5-12) underrepresented the closeness to vertical conductors.

The proportions of the transmissivity distribution in each distance interval are shown by colours in Figure 5-13. To reduce depth dependency, an alternative figure is shown (Figure 5-13b), with depth-adjusted  $T_0$ , for  $k = 232.5$  m, Eq. (5-2). The proportion of high-transmissive PFL data is somewhat higher inside the target intercepts (first bin from the left in Figure 5-13a and b) than it is outside the intercepts. However, there exists no clear correlation with distance away from the nearest zone, suggesting that: 1) not all transmissivity patterns are correlated to deterministic structures, and 2) some structures may have a minor role in the HRD connectivity.

An alternative analysis was made (Figure 5-14), in which the transmissivity is only related to the minimum distance from a few selected features. These are the features suspected to be particularly important for large-scale connectivity in HRD: 1) the Northern boundary belt and ZFMNNW1034, 2) the deterministic SBA-structures (SBA1 to SBA6; see Section 6.4), 3) the sea ( $z = 0$  m RHB 70), and 4) the two deep target intercepts of ZFMWNW0835 and ZFMENE3115 (shown in Figure 5-2). A vague trend in the transmissivity proportions can be observed, starting at c. 25 m distance away from the selected features (including more than half of the PFL population outside the selected features).

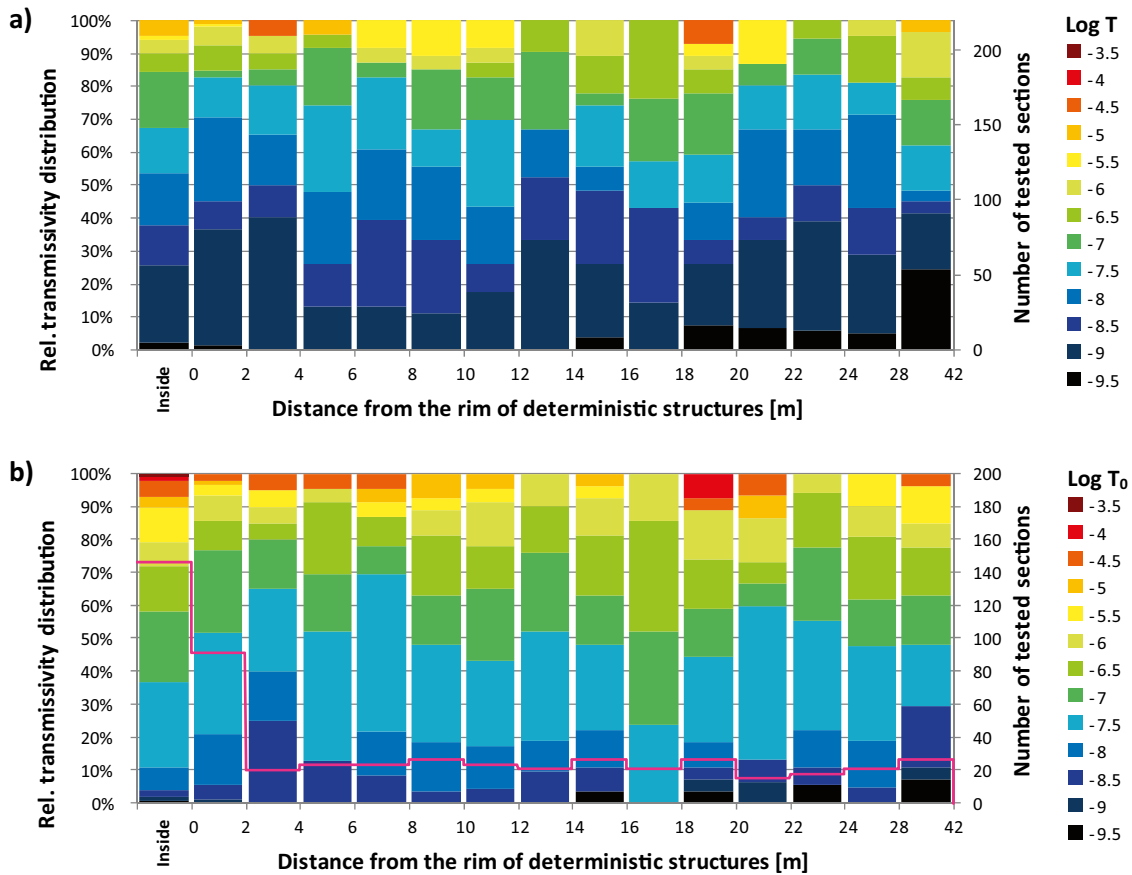


**Figure 5-13.** Relative distributions of 5 m sequential PFL data with spherical distance to the nearest deterministic structure; a) transmissivity measured over 5 m test sections, and b) depth-adjusted transmissivity,  $T_0$ , for  $k = 232.5$  m, Eq. (5-2). The number of tested sections in binned intervals is shown by pink line.

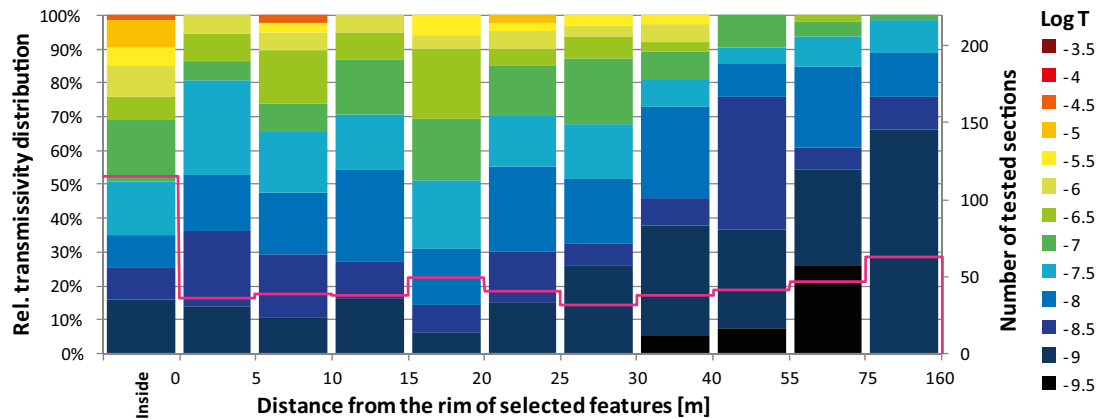


**Figure 5-14.** Relative distributions of 5 m sequential PFL data with spherical distance to selected features of potential significance for hydraulic connectivity. Number of tested sections in binned intervals is shown by pink line.

This indicates that deformation zones have different roles in the large-scale hydrogeological system. Some zones may be interpreted as fragmented, or discontinuous, with only a minor part of their geologically modelled area being hydraulically active (see suggested implementation alternatives in Table 5-2). On the other hand, it is still unclear to what extent this trend reflects an *actual fracture-scale properties*, relative to, an *apparent scaling effect* (i.e. reflecting effective properties related to flow path length; see discussions on the role of PFL data subject to hydraulic chokes in Öhman

and Follin (2010b)). In other words, measurements inside the Central block reflect longer flow paths to the positive hydraulic boundaries and are therefore more subject to bottlenecks in upstream connectivity of the flowing fracture network.

## 5.5 Formulation of a conceptual model

Five fracture sets of Open fractures have been defined within the Local model domain. These sets have similar intensities (approximately  $1 \text{ m}^2/\text{m}^3$ ). Open fractures exhibit local heterogeneity, but spatial trends in Open fractures inside the local model domain are not judged significant in relation to gaps in borehole coverage (Figure 4-10). The intensity of Open fractures decreases somewhat with depth, and the set-wise intensity varies somewhat between boreholes, although this may well be an artefact of local heterogeneity and gaps in borehole coverage. The core borehole data outside the Local model domain, KFM11A and KFR106 are not judged to be representative of the general Regional model domain, as they are influenced of the Southern and Northern boundary belts, respectively.

Anisotropy and trends are more comparatively more distinctive in PFL-f data, in terms of set-wise intensity and transmissivity, depth dependence, and lateral trends. PFL-f data are predominantly horizontal and gently dipping with accentuated transmissivity close to the Northern boundary belt and ZFMNNW1034. The Central block has lower PFL-f transmissivity, although it is difficult to state its significance due to its poorer data coverage. The correlation between transmissivity and deterministic deformation zones is irregular: The NE to ENE deformation set has weak hydraulic support, while the Northern boundary belt and ambient zones correlate well to hydraulic patterns. Owing to data gaps caused by the emplacement of boreholes, there is no clear evidence that the Southern boundary belt has a similar role in the hydrogeological system of SFR, although it is considered to be a realistic hypothesis.

The bedrock hydrogeology of the SFR volume is sketched in the following points (Figure 5-15):

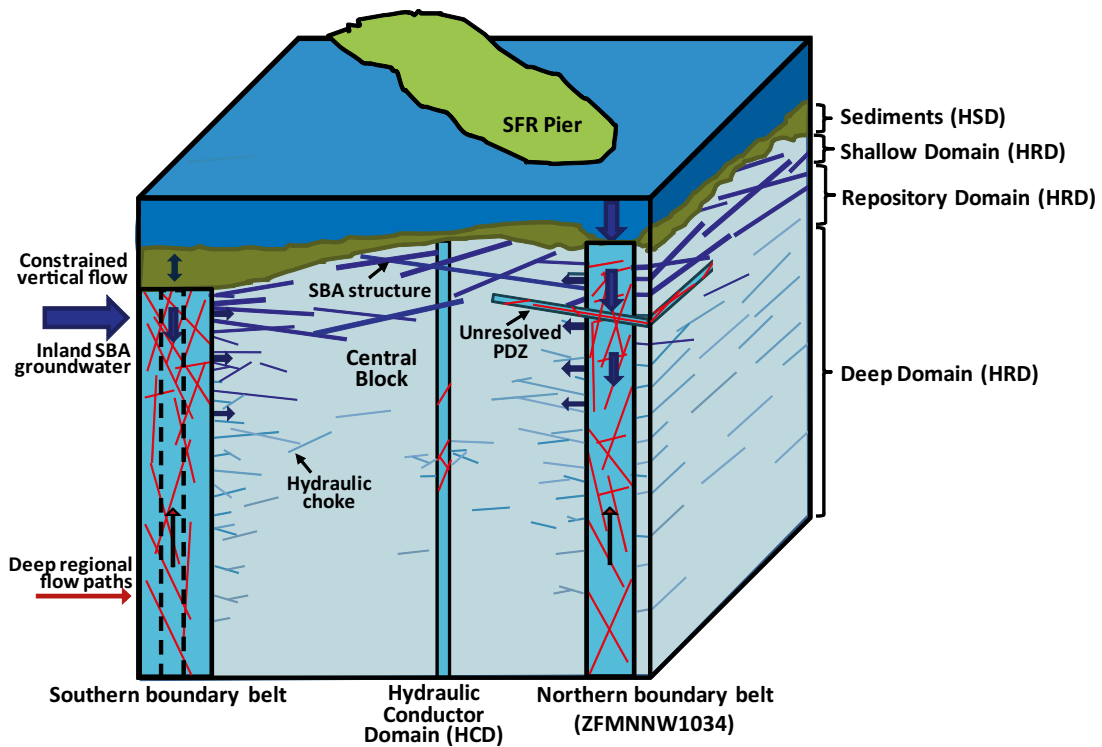


**Figure 5-15.** Conceptual model of hydraulic units, the connected flowing fracture network, and flow paths towards the Central block (e.g. driven by SFR inflow or borehole pumping). The Southern and Northern boundary belts as well as ZFMNNW1034 form vertical connectivity to the sea and act as positive hydraulic boundaries for the underlying sub-horizontal fracture network. Flow from the bounding belts towards the Central block is successively being constrained by connectivity and hydraulic chokes.



### **Steeply dipping deformation zones (HCD)**

- The inflow into the SFR facility is dominated by water originating from the Baltic Sea. The Southern and Northern boundary belts, and probably also ZFMNNW1034, act as important vertical flow paths for seawater towards SFR. This is shown by the transient development in water composition towards the Local Baltic water type (Section 4.6). ZFMNNE0869 and ZFMNE0870 are related to inflow in the access tunnels BT and DT; ZFMNNE0869 has Baltic water type (and possibly Littorina, although it may be related to ZFM871), while ZFMNE0870 has a scattered pattern.
- The hydraulic connection of the deformation zones to the sea is supported by strong correlation with sea water level in most monitored borehole sections (Section 4.5). However, for borehole sections that do not exhibit Baltic water type, this correlation may be a mechanical effect due to the surface-loading changes rather than hydraulic pressure diffusion through the bedrock.
- High PFL-f transmissivity (inside and outside zones) is intimately related to the Northern boundary belt (ZFMNW0805A,B; but also ZFMNNW1034; Figure 4-17), supporting its role as an important vertical conductor. There is poor PFL-f data coverage around the Southern boundary belt, but it is plausible that the Southern boundary belt has an equivalent role.
- Inside the Central block, deformation zones (ENE to NNE set and WNW to NW sets) are interpreted as generally less transmissive and more heterogeneous ( $T_0$  in the range  $10^{-8}$  to  $10^{-6}$  m<sup>2</sup>/s), potentially with local high-transmissive channels (Sections 5.2 and 5.4).

### **Gently dipping deformation zone ZFM871**

- ZFM871 (formerly known as H2) is currently not a significant pathway for seawater inflow to the SFR facility, as considerable portions of Littorina type water are still present in the zone and have not been flushed out (Section 4.6.1). This raises a question concerning the connectivity between ZFM871 and steeply dipping zones ZFMNNE0869 and ZFMNE0870. Possible explanations are channelling as well as the grouting at the intersection of NDB/NBT (Figure 4-3).
- The large drawdown of ZFM871 (Section 4.5.2) and its potential virgin excess head (Section 4.5.1) suggest that its hydraulic connection to the sea is relatively weak, or at least that its contact via steeply dipping zones is heterogeneous (Table 4-5).
- The transient decrease in head is large in ZFM871 (Section 4.5.2). This suggests that the decrease in groundwater inflow to the lower construction tunnel with time (Section 4.1.3) may be due to a transient drawdown in the zone, possibly suggesting that the storage of Littorina water type is being emptied.
- The spatial extension of ZFM871 is uncertain. Indications of moderate hydraulic connections to ZFM871 are found southeast of its termination against ZFMENE3115 (Section 4.5.4). Hydrochemistry suggests extension beyond ZFMNNE0869 as well as ZFMNW0805B.

### **Shallow Bedrock Aquifer (SBA)**

- The uppermost c. 60 m of the bedrock has higher transmissivity; all boreholes have transmissivity in the interval  $10^{-6}$  to  $10^{-5}$  m<sup>2</sup>/s without clear lateral contrasts (uncertain due to gaps in borehole coverage; Section 5.3.1). This could relate to low vertical stress, larger fracture transmissivity, and short flow paths to the Sea (supported by negligible drawdown in monitored sections and PFL-f data).
- Lateral transmissivity contrasts are identified in the depth interval c. 60 to c. 200 m, with sub-horizontal high-transmissive PFL-f in the vicinity of the Northern boundary belt and ZFMNNW1034 (Figure 4-16), implying that the structures provide a crucial hydraulic connection to the sea (the positive flow boundary). No evidence of these features is found inside the Central block (KFR104, KFR105, HFR101, as well as, experience from the existing SFR). The steep structures judged to constitute the main connections to the sea are: ZFMNW0805A,B and ZFMNNW1034 (Section 5.3). Presumably, ZFMWNW1035 has a similar role in the Southern boundary belt.

- The hydraulic responses at SFR are slower compared to observations in the shallow bedrock in SDM-Site Forsmark (Section 4.4.2). This is interpreted as an indication of lacking continuity in the SBA system of the Central block, whereas closer to the Northern boundary belt, the pressure propagation is possibly dampened by connection to the sea via steeply dipping deformation zones (Section 5.1.1).
- A deterministic alternative for modelling SBA-structures is presented (described in Appendix B). The spatial extension of these features is highly uncertain; their potential extension towards Singö deformation zone is *plausible*, but cannot be deduced from data owing to gaps in borehole coverage.

### **Unresolved PDZs**

- 31 borehole intervals with deformation zone characteristics were not included in the deterministic model (Curtis et al. 2011). These are of varying hydrogeological significance and confidence. Similar to the general pattern, the most transmissive Unresolved PDZs tend to be sub-horizontal and located close to the Northern boundary belt and ZFMNNW1034 (Appendix A).

### **Hydraulically isolated rock volumes**

- There is evidence of hydraulically isolated rock volumes as shown by significant remaining glacial melt-water and Littorina components (Section 4.6.2). The isolation of the borehole section inside zone ZFMNW0805A associated with the glacial water type in KFR101 is further supported by a low drawdown from the SFR facility (Section 4.5.4).
- The declining tunnel inflow combined with declining heads over the last 25 years has been interpreted as an ongoing transient drawdown of the less conductive rock mass, suggesting that part of the hydrogeological system is very slow (large storativity relative to transmissivity), as well as limited contact to the sea (Section 4.5.2).
- Highly uncertain excess head (relative to the mean sea level) were reported from early investigations prior to the SFR construction (Section 4.5.1). A hypothesis was suggested by Holmén and Stigsson (2001): an excess head can reflect a transient flow field induced by the ongoing land lift, if the hydrogeological system is comparatively slower (i.e. large storativity relative to transmissivity).
- Low diffusivity in the Central block interpreted from observed interferences (i.e. supporting the indications of a slow hydrogeological system; Section 5.1).

## **5.6 Implementation alternatives**

This chapter has discussed vertical and lateral trends in PFL-f data. These trends in PFL-f transmissivity are not clearly related to fracture network characteristics, as the corresponding trends in Open fracture intensity are considerably weaker (see Section 4.2.1 and Öhman and Follin 2010b). Instead, this suggests that the observed PFL-f data trends reflect *global connectivity to the sea* (see discussion on hydraulic choking in Section 5.4.1 and Öhman and Follin 2010b). There also exists uncertainty to how deformation zones that lack distinctive hydraulic signatures should be interpreted in the context of vertical hydraulic connectivity to the sea (i.e. their role in the connectivity analysis; Figure 5-11). The connectivity to the sea may also partly be controlled by sediment coverage and the vertical hydraulic conductivity of sediments (Section 4.7). The lateral contrast in PFL-f data mainly consists of a population of sub-horizontal, high-transmissive features that are not found in the Central block at the Repository level (boreholes KFR104, KFR105, and HFR101). Nor do the experiences from the existing SFR facility indicate frequent occurrence of such features inside the Central block (only two horizontal structures required grouting; Figure 4-3). Some, *but not all*, of these sub-horizontal, high-transmissive features are found inside Unresolved PDZs (Appendix A), or included in the so-called SBA-structures (Table B-1). Gaps in borehole coverage cause uncertainty to the *significance* of this lateral contrast. Here, the word significance is not used in the strict statistical sense, but instead with respect to judged confidence/relevance in a modelling context. Owing to these circumstances, *alternative model setups* are considered for propagation to the safety assessment for the SFR extension.

Transmissivity depth dependency is judged to be significant; the phenomenon is frequently reported in hydraulic investigations, including SDM-Site Forsmark, as well as, the early SFR models. It is recommended that the depth dependency is modelled by dividing the domain into depth intervals Shallow rock, Repository level, and Deep rock (Section 5.2.1). A reasonable boundary between Shallow rock and Repository level is judged to be –60 m RHB 70 (based on transmissivity contrast, but also from a pragmatic aspect, as the depth level of the SFR extension is expected to be below –60 m RHB 70). The boundary between the Repository level and Deep rock is less clear-cut, at c. –200 to –250 m RHB 70; it should be decided from a practical perspective considering the deteriorating sample size with depth (Figure 5-3), in relation to the importance of a well-founded characterisation of the Deep rock.

The main decision concerns the *significance* of lateral transmissivity contrasts with respect to data at hand. This dilemma could be resolved by a verification borehole in the Central block. If the contrasts should be judged significant, a second dilemma arises concerning how it should be geometrically represented and numerically implemented in a flow model. In the vicinity of the Southern boundary belt, there is essentially no hydraulic data coverage outside deformation zones (Figure E-1, Figure D-14 and Figure D-15). Thus, should it be assumed that the high-transmissive features found in the vicinity of Northern boundary belt/ZFMNNW1034 exist also close to the Southern boundary belt? If so, which method should be used? From the perspective of connectivity to the sea, it should be noted that the sediment coverage is thicker and less conductive above the Southern boundary belt (Section 4.7).

One possibility to tackle the uncertainty in spatial extension of SBA-structures could be breaking the defined structures into their individual intercepts (Table B-1) and adding them to the population of stochastic features. As pointed out earlier, a drawback of the standard stochastic representation is that it becomes unrealistic for high-transmissive features (large square planes with homogeneous hydraulic properties). Furthermore, some of the individual intercepts do not represent single fractures but intervals with deformation zone like properties (Appendix H); cf. the geological definition of PDZs. Another difficulty is therefore the estimation of a proper size distribution for this type of data.

Another possibility, which circumvents the dilemma of size distribution, yet allows flexibility in modelling spatial extension of SBA-structures, could be the pragmatic method used in SDM-Site Forsmark. The sheet joints in SDM-Site Forsmark were assumed to be ubiquitous (i.e. wide extending) planes that undulate with topography, but with isolated internal conductive pathways (i.e. nearest-neighbour interpolated transmissivity between boreholes, which requires dense conditional data; Figure 2-4). For application to the SFR data set, there is a clear risk that the few conditioning boreholes at hand may cause the selection of interpolation method to have large effects on the safety assessments. Perhaps, conditional random-component kriging is a more realistic alternative. Another drawback is that beforehand, it is difficult to judge which simplified SBA geometry is optimal for performance assessments (i.e. what separation distance between vertical displaced topography planes is the most realistic to use). To resolve the horizontal structures in a continuum grid (i.e. DarcyTools modelling), the vertical separation distance between planes must be at least twice the vertical cell size. It has currently been suggested that the cell size should be 16 m inside the Regional SFR domain and 2 m in the vicinity of tunnels.

To summarise, hydrogeological conditions to host the SFR extension seems to be better at the centre of the Central block, below 60 m depth. Note however, that hydraulic connections to ZFM871 Southeast of ZFMENE3115 are indicated in PFL-f FWH of KFR104 and KFR27. Gaps in borehole coverage render uncertainty in interpretations. The hypothesized conceptual model could gain much confidence from one (or several) well-placed verification borehole(s). The conceptual uncertainty can be evaluated by a comparison of different test cases. Three alternatives are considered in Table 5-2. The selected method for representing the most transmissive features (stochastic or large-scale structures) is expected to have a key role in the connectivity analysis. The complete evaluation of these modelling alternatives involves analysis of multiple stochastic realisations and is time-consuming.

**Table 5-2. Considered strategies for numerical implementation of the conceptual model.**

- 
- 1) **Classic approach:** The original methodology by Rhén et al. (2003) is pursued. In a first step, the lateral transmissivity contrasts are considered insignificant with respect to uncertainties. All borehole data are combined to formulate a global DFN model. In the connectivity analysis, *all deformation zones* are assumed to be positive flow boundaries. Both Unresolved PDZs and individual SBA intercepts (Table B-1) are included in the population of *stochastic features*, assumed to follow a Poissonian spatial distribution. This may result in an overly connected fracture network and overrate the hydraulic continuity of zones, as there exist indications of zones of minor hydraulic significance.
- In this strategy it may be difficult to formulate a realistic method to estimate sizes of transmissive sub-horizontal features (as the upper tail of the size distribution primarily consists of steeply dipping deformation zones). In a second step, lateral contrasts can be implemented by sub-dividing the model volume into sub-domains. However, it is not clear exactly where the boundaries between fracture generation volumes should be drawn, but possibly with guidance from geology and the rock domain model.
- 
- 2) **Designed connectivity analysis related to deterministic zones:** This alternative is a connectivity-analysis adaptation intended to honour: 1) the lateral contrasts and 2) deformation zone heterogeneity and geometry. The purpose is to honour the concept of connectivity analysis and avoid defining highly uncertain fracture generation sub-volumes.
- In the connectivity analysis, all deformation zones are assumed to be *potential vertical connectors* with variable connectivity (or capability to connect stochastic features) depending on its parent hydraulic properties. This method allows flexibility in model set-up, such that any deformation zone has a specified probability (or capability) to act as a flow boundary for stochastic fractures depending on its interpreted *hydraulic signature*. The connectivity analysis is performed in a hierarchical manner, such that high-transmissive stochastic features must be connected to the sea by *at least* equally transmissive zones (i.e. a non-conductive zone has no role in the connectivity analysis). The SBA-structures can either be implemented as deterministic flow boundaries, or they can be broken down into individual intercepts (Table B-1) and included in the population of stochastic features.
- The drawback of this method is that it makes complex assumptions that are subject to conceptual idealisation, which is less transparent and difficult to verify by data.
- 
- 3) **Deterministic spatial inference:** This is a deterministic alternative for implementing the notion of lateral contrasts. Unresolved PDZs are stochastically modelled with spatial inference to the structural wedge between the Northern boundary belt and ZFMNW1034. To compensate gaps in borehole coverage, Unresolved PDZs are also modelled with inference to the Southern boundary belt. SBA-structures are modelled deterministically; the distinction between SBA-structures and Unresolved PDZs is unclear, and therefore their potential existence near the Southern boundary belt is partly covered by Unresolved PDZs. KFR106 is not judged representative for the Central block, and therefore not included in the DFN parameterisation.
- This alternative potentially risks underestimating the existence of Unresolved PDZs, SBA-structures, and high-transmissive stochastic fractures in uncharted areas. However, it can be argued that this risk is subordinate to other model uncertainties (e.g., unrealistic stochastic model representation of high-transmissive fractures, as large homogeneous planes).
-

## 6 Parameterisation of hydraulic domains

### 6.1 Weighting use of old and new data

Fracture network compartmentalisation may be of significance for the dispersion of solute transport. The level of compartmentalisation in fracture transmissivity can be evaluated from comparing injection test data (e.g. PSS data, which includes compartmentalized transmissivity) to PFL-f data (continuously flowing fractures). The PSS is a 20 min injection packer test performed over 5 m borehole sections, according to current SKB standards. However, no complementary PSS measurements were performed during the SFR extension investigation, and thus there exists no possibility to evaluate the level of compartmentalisation.

The Forsmark Site Investigation facilitated a cross-comparison between PFL-f data and PSS data performed in the same boreholes (Figure 6-1). The correlation between PSS data and summed PFL-f transmissivity over the PSS test interval was found to be good above  $10^{-8}$  m<sup>2</sup>/s. Below this value the PSS data reflect choked (compartmentalized fracture networks). In SFR the typical detection limit for 3 m packer data is  $5 \times 10^{-8}$  m<sup>2</sup>/s, suggesting that if the same relationship holds for the SFR bedrock minor compartmentalized transmissivity is measured. This could indicate that, possibly, the discrepancy between the old data and the new data is within the error bounds of one order of magnitude. In this comparison it should be emphasized that the old SFR data set is not of comparative standard to PSS data currently used by SKB.

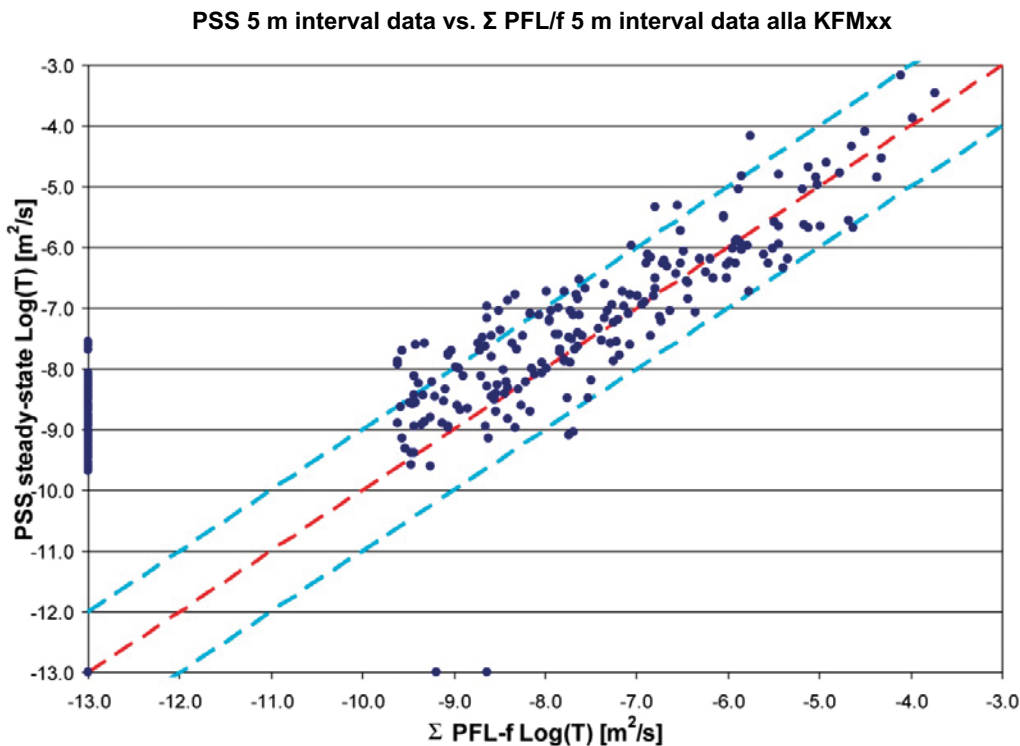


**Figure 6-1.** Transmissivity data cross-plot of borehole sections measured with both PFL-f and PSS methods in Forsmark. The red line indicates unit slope and the blue lines a deviation of  $\pm 1$  order of magnitude. PSS data without PFL-f records above detection limit are plotted to the left at an arbitrary low value on the abscissa. Reproduced from Figure 4-18 in Follin et al. (2007b).

## 6.2 Hydraulic Conductor Domain (HCD) model

The distribution of depth-adjusted HCD intercept transmissivity,  $T_0$ , is summarised in Figure 6-2. Details are given in Appendixes D and E. These evaluated data are compared to transmissivity parameterisation in SDM-Site Forsmark (Figure 6-2; boxes) and the previous state-of-the-art SFR model (Holmén and Stigsson 2001) (Figure 6-2; circles). The Forsmark SDM has depth dependency and hence the values were taken from the depth interval 0 to –100 m RHB 70. The Holmén and Stigsson (2001) model have no deformation zone depth dependency. According to Eq. (5-1), transmissivity at the disposal facility level is about 0.4 logarithmic units below the ground-surface transmissivity,  $T_0$ . The largest transmissivities are found in ZFM871 and in the Southern and Northern boundary belts. The NNE to ENE set has the lowest transmissivities, although ZFMNNE0869 (Zon 3) is clearly atypical of the set.

The Southern boundary belt is a complex conjunction of deformation and the subdivision into ZFMWNW0001 and its splays is – to some extent – artificial (Curtis et al. 2011). The Southern boundary belt has a wide range of intercept transmissivity (Figure 6-2c); including 5 deep intercepts in KFM11A, two intercepts at c. –100 m RHB 70 in HFM35 and HFR105, and 7 shallow intercepts from the old data set. The shallow intercepts may – to some extent – include SBA-structure transmissivity.

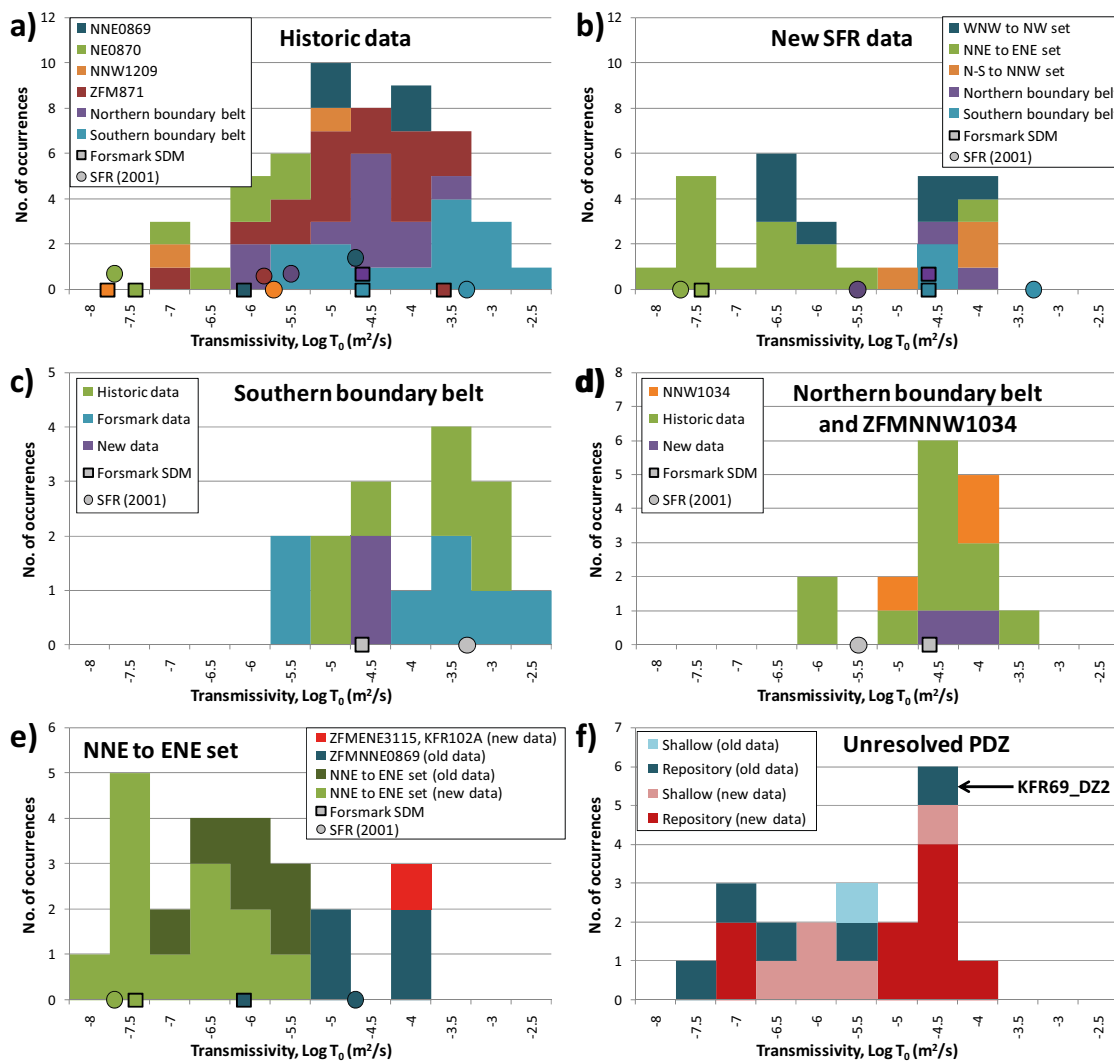


**Figure 6-2.** Depth-adjusted HCD intercept transmissivity,  $T_0$ ; a) old data set (including KFM11A, HFM34, and HFM35); b) new data set, c) Southern boundary belt, d) Northern boundary belt and ZFMNNW1034, e) NNE to ENE set, and f) Unresolved PDZs. Previously used model values shown along the x-axis: the Forsmark SDM for the depth range 0 to –100 m RHB 70 (boxes) and Holmén and Stigsson (2001) (circles).

The Forsmark SDM values corresponds to the lower tail of the  $T_0$  distribution, including the new HFR105 intercepts (Figure 6-2c; purple), while the Holmén and Stigsson (2001) value corresponds to the upper mode of the  $T_0$  distribution.

The Northern boundary belt together with ZFMNNW1034 has a more homogeneous pattern (Figure 6-2d); both the old data (green) and the new data (purple), agree well with the Forsmark SDM model values. PFL-f data inside ZFMNW0805A and B, as well as ZFMNNW1034 (orange; Figure 6-2d), are parallel to the deformation zone and have similar magnitudes of  $T_0$ ; from a hydraulic perspective ZFMNNW1034 has similar characteristics to the Northern boundary belt. In summary, the new data exhibit a bimodal appearance (Figure 6-2b) that is clearly related to spatial location of intercepts; the low transmissivities ( $T_0 \leq 10^{-6}$  m<sup>2</sup>/s) are located at the centre of the Central block, while the large transmissivities ( $T_0 > 10^{-6}$  m<sup>2</sup>/s) are found inside or closer to the Northern boundary belt. The pattern is very similar to observations in HRD (Section 5.3). The two exceptions to this trend are the deep intercepts of ZFMENE3115 and ZFMWNW0835 (discussed in Section 5.2).

The old data provide higher intercept transmissivity (cf Figure 6-2a and b); this may be a consequence of data quality and the geometric uncertainty in the geological model. For example, in SDM-Site Forsmark ZFMNNE0869 (Zon 3) was modelled as 10 m wide with  $T_0 = 8 \times 10^{-7}$  m<sup>2</sup>/s (Figure 6-2e), while in the SFR geologic model v. 1.0, it has a 60 m width and its 4 intercepts range from  $T_0 = 3 \times 10^{-6}$  to  $4 \times 10^{-5}$  m<sup>2</sup>/s. The four intercepts have a logarithmic geometric mean of  $-4.6$ , which agrees very well with Holmén and Stigsson (2001). The deep intercept of ZFMENE3115 in KFR102A is clearly atypical of the NNE to ENE set (Figure 6-2e).

Among the Unresolved PDZs, the largest  $T_0$  are found in the new data set (Figure 6-2f). These are located in the vicinity of ZFMNNW1034 (see Appendix A). In the old data set, there are only 3 intercepts with transmissivity exceeding  $10^{-7}$  m<sup>2</sup>/s; KFR31\_DZ1 located 14 m below SBA7, KFR20\_DZ1, located 9 m west of ZFMNE0870, and KFR69\_DZ2 (see Appendix A). KFR69\_DZ2 is alternatively modelled as SBA8 (see Appendix H.8).

The depth-trend determined for SDM-Site Forsmark is applied to calculate HCD parameterisation,  $T_{eff}(0)$ , according to the established SKB methodology (Table 6-1).

**Table 6-1. Deformation-zone parameterisation inside the SFR Regional model domain.**

Deformation zone	log Teff(z=0) (m <sup>2</sup> /s) <sup>1)</sup>	No. data <sup>2)</sup>	Basis for determining $T_{eff}(z=0)$
ZFM871	-4.8	14	Average of KFR02, KFR03, KFR04, KFR12, KFR13, KFR21, KFR22, KFR23, KFR31, KFR32, KFR33, KFR37, KFR7B, KFR7C.
ZFMA1	-4.8	None	Taken from SDM-Site Forsmark.
ZFMB10	-4.8	None	Assumed similar to ZFMA1.
ZFMENE3115	-6.5	3	Average of KFR102A, KFR104, KFR105.
ZFMENE3135	-6.7	None	Pooled average of the NNE to ENE set (only new data).
ZFMENE3151	-6.7	None	Pooled average of the NNE to ENE set (only new data).
ZFMENE8031	-6.7	None	Pooled average of the NNE to ENE set (only new data).
ZFMENE8034	-6.7	None	Pooled average of the NNE to ENE set (only new data).
ZFMNE0870	-6.2	7	Average of HFR101, KFR02, KFR03, KFR04, KFR53, KFR55, KFR70. Transmissivity exaggerated by unfavourable borehole orientation.
ZFMNE3112	-6.6	4	Average of KFR102A, KFR102B, KFR104, KFR105.
ZFMNE3118	-6.2	2	Average of HFR101 and KFR104.
ZFMNE3134	-6.7	None	Pooled average of the NNE to ENE set (only based on new data).
ZFMNE3137	-7.3	4	Average of KFR102A, KFR102B, KFR104, KFR105.
ZFMNNE0725	-4.0	None	Taken from SDM-Site Forsmark.
ZFMNNE0869	-4.6	4	Average of KFR09, KFR10, KFR36, KFR68.
ZFMNNE2308	-6.1	None	Taken from SDM-Site Forsmark.
ZFMNNE3130	-6.7	None	Pooled average of the NNE to ENE set (only new data).
ZFMNNE3264	-6.7	None	Pooled average of the NNE to ENE set (only new data).
ZFMNNE3265	-6.7	None	Pooled average of the NNE to ENE set (only new data).
ZFMNNE3266	-6.7	None	Pooled average of the NNE to ENE set (only new data).

Deformation zone	log Teff(z=0) (m <sup>2</sup> /s) <sup>1)</sup>	No. data <sup>2)</sup>	Basis for determining T <sub>eff</sub> (z=0)
ZFMNNW0999	-7.8	Rejected	Rejected overlapping intercept. Value taken from pooled average of NNW group in SDM-Site Forsmark.
ZFMNNW1034	-4.4	3	Average of HFR106, KFR101, KFR106.
ZFMNNW1209	-5.9	2	Average of KFR33, KFR35. Interpreted as highly heterogeneous.
ZFMNNW3113	-7.8	None	Taken from SDM-Site Forsmark, pooled average of NNW group.
ZFMNS3154	-4.4	None	Assumed similar to ZFMNNW1034, based on location and orientation.
ZFMNW0002	-3.6	1	Single intercept KFM11A.
ZFMNW0805A	-4.3	7	Average of KFR08, KFR11, KFR24, KFR25, KFR56, KFR7A, KFR101.
ZFMNW0805B	-4.7	7	Average of KFR08, KFR11, KFR24, KFR25, KFR38, KFR7A, KFR101.
ZFMWNW0001	-3.8	9	Average of KFR61, KFR62, KFR64, KFR65, KFR67, KFR71, HFM34, HFR105, KFM11A.
ZFMWNW0813	-5.7	1	Single intercept KFM11A.
ZFMWNW0835	-5.2	2	Taken as average of the 2 intercepts in KFR27.
ZFMWNW0836	-7.1	Rejected	Two rejected intercepts. Value taken from SDM-Site Forsmark.
ZFMWNW1035	-4.0	4	Average of KFR68, HFM35, HFR105, KFM11A.
ZFMWNW1056	-7.1	None	Taken from SDM-Site Forsmark.
ZFMWNW3259	-4.2	1	Single intercept KFM11A.
ZFMWNW3262	-4.6	2	Average of KFR103 and KFR106.
ZFMWNW3267	-6.7	2	Average of KFR104 and KFR105.
ZFMWNW3268	-5.8	None	Pooled average of the WNW to NW set (only new data).
ZFMWNW8042	-6.0	1	Single intercept KFR105. Supported by sub-parallel PFL-f data.
ZFMWNW8043	-6.5	None	Pooled average of the WNW to NW set (only new data).

1) Initial deformation-zone parameterisation. Ground-surface transmissivity, T<sub>0</sub>, based on geometric mean of available intercepts (details in Table D-2 and Table E-1). Pooled deformation zone-set statistics, or values from SDM-Site Forsmark, are applied to zones without data support.

2) Number of intercepts with hydraulic data for the HCD. Hydraulic data at junctions between deformation zones may be unrepresentative for subordinate zones.

### 6.3 Hydraulic Rock mass Domain (HRD) model

The Open fracture system is described by means of a Hydro-DFN. The Hydro-DFN provides a stochastic model representation of the flowing fracture network outside: 1) deterministic deformation zones (ZFM), 2) Unresolved PDZs, and 3) SBA-structures. It is largely based on the principles described in the preliminary v. 0.2 Hydro-DFN (Öhman and Follin 2010b). However, during the v.0.2 modelling stage the geologic model v. 1.0 was unavailable, which necessitated a number of assumptions and simplifications in the model setup. Also, nine methodological issues of the preliminary Hydro-DFN were raised in Table 5-1 in Öhman and Follin (2010b). Since the v. 0.2 modelling stage, the understanding of the hydrogeologic system at SFR has also progressed (Chapters 4 and 5), primarily due to data analysis in context of the final geological model, as well as, the inclusion of additional data (KFR106 and HFR106).

The implementation of methodological issues, as well as, necessary conceptual updates of the v. 1.0 model are summarized in Table G-1. In summary, the four most significant changes are:

- Introducing SBA-structures as an alternative deterministic representation for sub-horizontal, high-transmissivity data (Appendix B; this depletes a subset of high-transmissive data from stochastic representation).
- Suggesting spatial inference to constrain the Unresolved PDZs to the Southern boundary belt, as well as to the structural wedge between the Northern boundary belt and ZFMNNW1034 (Appendix A).
- Honouring the geometry between boreholes and deterministic structures in the connectivity analysis (Figure G-15 and Figure G-16).
- Accounting for practical limitations of the PFL device (variable detection limit and spatial resolution) in the simulated borehole exploration (Appendix G.1.8).
- Adjusting the boundary between the Repository and Deep domains (Appendix G.3).



## **Orientation**

The Hydro-DFN is defined by a global orientation model and the intensity, size, and transmissivity of the different fracture sets. Five fracture sets are defined: steeply dipping EW-, NW, and NE-striking, as well as, gently dipping, and horizontal (see details in Öhman and Follin 2010b). Fracture set orientation is parameterised by a mean pole and the spread around the mean pole. The dispersion around the mean pole is assumed to follow the univariate Fisher distribution, defined by the concentration parameter,  $\kappa$ . The measurement error in fracture orientation data is estimated by a maximum dihedral angle,  $\Omega$ , a parameter that was unavailable during model version 0.2. Fracture-set orientations were re-calculated by excluding data with large uncertainty. In the SFR data set, the measurement errors are generally small for fractures visible in BIPS, and hence the improvement is of minor character (Appendix G.2).

## **Depth domains**

Transmissivity depth trends have been identified in Section 5.2, as well as, in previous model versions (Öhman and Follin 2010a, b). This depth trend is numerically represented by dividing the rock mass into three depth domains. The subdivision of rock mass by depth is a pragmatic method to differentiate the hydraulic properties of the rock mass expected to host the SFR extension, from the shallow, high-transmissive rock mass above, as well as, the low-transmissive deep rock mass, underneath. In this differentiation, it must also be ensured that the different depth domains have sufficient data support (see details in Appendix G.3).

Thus, the division into depth domains must balance three different aspects: 1) relevance for the emplacement for the SFR extension, 2) data support (i.e. observed vertical contrasts in transmissivity, as well as, intensity of Open fractures and PFL-f), and 3) borehole coverage with depth (with particular consideration to data gaps and decoupling influence from lateral trends). The exact depth of the planned SFR extension has not yet been finally decided, but with guidance from the existing SFR, the following depth domains are suggested to represent the depth trend in fracture transmissivity:

- Shallow domain (0 to –60 m RHB 70),
- repository domain (–60 to –200 m RHB 70) and
- deep domain (below –200 m RHB 70).

The boundary between the Repository and Deep domains may be re-considered once the depth of the SFR extension has been decided. Furthermore, the relative significance of these two domains (i.e. the need to support the Deep domain by more data, contra the drawback of reducing the data support from the Repository domain) should be resolved in the Safety Assessment.

## **Lateral rock mass representation**

Data analysis indicates a large-scale hydrogeological pattern related to the geological concepts Central block, the Southern and Northern boundary belts, as well as, ZFMNNW1034 (Section 5.3). The rock mass is low-transmissive (and/or compartmentalised) at the centre of the Central block, but the transmissivity (and/or connectivity) gradually increases closer to the boundary belts. The pattern is not clearly observed in Open fracture intensity (Figure 4-10). The combination of borehole coverage gaps, sampling bias, and variable detection limits complicates assessing the confidence of the conceptual model. Without complementary PSS data (Section 6.1) it is unclear if this trend reflects *actual fracture-scale properties*, or an *apparent scaling effect* (i.e. reflecting effective properties related to flow path length; see discussions on the role of PFL data subject to hydraulic chokes in Öhman and Follin (2010b)). In the light of borehole emplacement and gaps in borehole coverage, it was therefore decided *not* to define lateral subdivided fracture domains. However, it should be emphasized that the dominant subset of high-transmissive data are spatially constrained according to the conceptual model by means of: 1) deterministic deformation zones (ZFM), 2) SBA-structures, and 3) Unresolved PDZs (see Figure G-1).

## **Fracture size and transmissivity**

Fracture size cannot be directly inferred from borehole data and is therefore the most uncertain parameter in the Hydro-DFN. Open fractures are assumed to be power-law distributed, defined

by a size scaling exponent,  $k_r$ , which is bounded by the interval,  $r_0 = 0.038$  m to  $r_{max} = 169$  m. In the preliminary Hydro-DFN v. 0.2, two alternative methods were used to define  $k_r$  (referred to as Connectivity analysis and Tectonic continuum (Öhman and Follin 2010b); see Appendix G.4.1). These alternative models are considered as bounds to the uncertainty in estimated size distributions; both methods were applied in the Hydro-DFN v. 1.0. The difference between these two methods concerns the modelled size of steeply dipping fracture sets. In the Connectivity analysis, steeply dipping sets are modelled small (i.e. high  $k_r$ ) related to their low transmissivity values (Figure G-17). In the Tectonic continuum approach, they are modelled large (i.e.  $k_r$  on par with sets Gd and Hz), inferred from surface lineaments (Figure G-18). Hence, the two approaches are considered to provide realistic bounds for size uncertainty.

Transmissivity,  $T$ , is assumed to be directly correlated to fracture radius,  $r$ , with a factor,  $a$ , and an exponent,  $b$  (e.g. in Follin et al. 2005):

$$T(r) = a r^b \quad (6-1)$$

The two parameters,  $a$  and  $b$ , are fitted by the criterion that simulated borehole exploration for multiple realizations of connected open fractures must reproduce the PFL-f data, per set and per depth domain. The final parameter setup of Hydro-DFN v. 1.0 is provided in Table 6-2.

**Table 6-2. Hydro-DFN model parameterisation for alternative size models.**

					Connectivity analysis			Tectonic continuum		
Set intensity <sup>2)</sup>		Orientation <sup>3)</sup>			Size	(T = a r <sup>b</sup> )		Size	(T = a r <sup>b</sup> )	
Set	P <sub>32</sub>	Tr	PI	Fisher κ	k <sub>r</sub>	a	b	k <sub>r</sub>	a	b
<b>Shallow domain</b> (z > -60 m RHB70)										
EW	2.32	4.8	13.9	10.1	3.2 <sup>4)</sup>	2.1E-8	1.3	2.694	1.6E-9	1.25
NW	0.99	233.8	7.2	13.7	3.2 <sup>4)</sup>	5.3E-8	1.3	2.626	3.3E-9	1.2
NE	1.31	125.4	1.8	13.7	3.45	1.8E-8	1.0	2.778	1.2E-9	1.0
Gd	1.79	339.1	87	7.2	2.79	2.1E-8	1.09	2.79	2.1E-8	1.09
Hz	0.96	127.5	83.7	41.9	2.6	9.8E-8	1.32	2.60	9.8E-8	1.32
<b>Repository domain</b> <sup>1)</sup> (-60 ≥ z > -200 m RHB70)										
EW	1.44	4.8	13.9	10.1	3.1 <sup>4)</sup>	2.1E-9	1.1	2.63	7.9E-11	1.4
NW	0.81	233.8	7.2	13.7	3.0 <sup>4)</sup>	1.1E-8	1.1	2.596	1.3E-9	1.1
NE	1.00	125.4	1.8	13.7	3.3 <sup>4)</sup>	2.2E-9	1.3	2.752	8.6E-11	1.35
Gd	1.21	339.1	87	7.2	2.72	4.0E-9	0.8	2.72	4.0E-9	0.8
Hz	0.95	127.5	83.7	41.9	2.55	8.5E-10	1.35	2.55	8.5E-10	1.35
<b>Deep domain</b> <sup>1)</sup> (-200 ≥ z > -1,100 m RHB70)										
EW	1.06	4.8	13.9	10.1	3.2 <sup>4)</sup>	3.6E-9	1.6	2.585	7.1E-13	2.5
NW	0.67	233.8	7.2	13.7	3.15 <sup>4)</sup>	4.7E-9	1.13	2.597	1.5E-10	1.31
NE	1.03	125.4	1.8	13.7	3.2 <sup>4)</sup>	1.9E-9	1.0	2.75	1.6E-10	1.25
Gd	1.49	339.1	87	7.2	2.7	2.7E-10	1.6	2.7	1.4E-10	1.7
Hz	0.75	127.5	83.7	41.9	2.75	1.9E-9	1.15	2.75	1.3E-9	1.25

<sup>1)</sup> Based on data characteristics and borehole coverage the boundary between the Repository and Deep domains is changed to -200 m elevation. In the v. 0.2 model the boundary was set to -245 m elevation, based on the preliminary geometrical modelling of ZFM871 (SFR geologic model v.0.1).

<sup>2)</sup> The intensity of open fractures reflects the size interval  $r_0$  to  $r_{max}$ . The smallest modelled deterministic zones are on the order 300 m (SFR geologic model v.1.0), corresponding to a radius of 169 m. Stochastic open fractures are therefore assumed to have a maximum radius of  $r_{max} = 169$  m. The smallest fracture modelled are set equal to borehole radius,  $r_0 = 0.038$  m.

<sup>3)</sup> Global orientation model used for all three depth domains. The same orientation model is used in both the Connectivity analysis and in the Tectonic continuum approach.

<sup>4)</sup> Adjusted  $k_r$ , relative to the preliminary Hydro-DFN v. 0.2 (Öhman and Follin 2010b).

## 6.4 Deterministic Shallow Bedrock Aquifer (SBA) structures

In the original established SKB methodology (Rhén et al. 2003), the hydrogeological system inside the bedrock is divided into deterministic deformation zones (HCD) and the less fractured rock between (HRD; Figure 2-1). Experiences from the Forsmark Site investigation (Follin et al. 2007a) lead to an updated strategy, introducing *sheet joints*: an additional type of deterministic discrete hydraulic features in the superficial bedrock. To emphasize hydraulic significance of these sheet joints, the superficial bedrock was referred to as a Shallow Bedrock Aquifer (SBA; Figure 2-4). Analysis of hydrogeological data (Chapters 4 and 5) indicate that SBA-structures *also exist in the SFR model domain*, even if they are of *lesser dignity* comparatively to those found above the Forsmark lens (Figure 5-1). The persistence of these SBA-structures seems related to the Northern boundary belt and ZFMNNW1034. Without additional data the existence of such features in the vicinity of the Southern boundary belt (i.e. north of Singö) is not fully clear, but it is judged to be plausible.

The heterogeneity of the flowing fracture network outside deterministic structures are normally modelled *stochastically* in a Hydro-DFN framework, in which transmissive features are represented as square planes with homogeneous properties and size correlated to transmissivity. The realism in such a stochastic approach deteriorates for high-transmissive features (e.g.  $T > 10^{-5} \text{ m}^2/\text{s}$ ), as it has a severe impact on model heterogeneity, failing to honour conditional data. Thus, an alternative modelling approach is to introduce a number of deterministic large-scale structures to represent the transmissive sub-horizontal fracture network. The details of the development and the parameterisation of the deterministic SBA model are given in Appendix B.

There are four of key differences between the SBA modelled at SFR and those modelled in Forsmark:

- *Visual confirmation*: the existence of SBA-structures in the SDM-Site Forsmark model has been confirmed, during the construction of the nuclear power plants and in the canal to the Baltic Sea (Figure 3-7). Horizontal fracture structures were observed during construction of SFR, but most are *hydraulically insignificant* (Figure 4-1). Only two of these observed horizontal structures required grouting, and one of them is possibly related to a nearby transmissivity anomaly at similar depth (tentatively modelled as SBA8, Figure D-3). Another reported anomalous inflow potentially relates to a horizontal structure, but it could not be visually confirmed Figure 4-2).
- *Dignity*: the suggested deterministic SBA-structures at SFR are considerably smaller in terms of size, and of less extraordinary hydraulic nature, transmissivity and hydraulic interferences (cf. Figure 2-4 and Figure 6-3).
- *Data support and geometrical representation*: The Forsmark SBA are primarily based on extraordinary yield, rapid large-scale responses, and uniform groundwater levels, observed in a large number of percussion boreholes; the Forsmark data motivates representing: a) *SBA geometry* as vertical offsets of topography, and b) its *conductive channels* numerically interpolated between boreholes. The modelled SBA at SFR have more *detailed* support (PFL-f and supported by various data *at exact intercepts*; see Appendix B and H), but less support from *areal borehole coverage* and *diffusivity*. The SBA-structures at SFR were modelled in a RVS-frame work, based on informed judgement of borehole intercepts and termination against steeply dipping zones.
- *Significance in the safety assessments*: The exact details of the SBA-structures are of comparably lesser importance in the Forsmark SDM, as the repository has a greater target depth (c. –500 m RHB 70). In contrast, the existing SFR facility is within the depth interval of possible SBA-structures (c. –60 to –140 m RHB 70). Thus, the high uncertainty in the deterministic spatial extent of SBA-structures (owing to insufficient borehole coverage) has comparatively larger implications in the confidence of the safety assessments. On the other hand, the potential SBA-structures at SFR are of comparably *lesser dignity*, as stated above.

Based on interpretations of various sources of hydrogeological data, six structures are defined and referred to as SBA1 to SBA6 (Figure 6-3). A seventh structure, referred to as SBA7 (Figure 6-3), was defined as a possible sub-horizontal stress-relief structure by Curtis et al. (2011), based on the original interpretation of Zones H1 and H3, by Carlsson et al. (1985) (Appendix H). Note how the existing SFR storage facilities are enclosed by steeply dipping zones, SBA7 (above) and the gently dipping ZFM871 (underneath). Sub-horizontal structures have been mapped at several locations of the SFR facility (Figure 4-1), which are *generally* not related to high inflows. However, one of these structures is related to 5 tonnes of grouting, as well as, local supporting borehole data ( $T > 10^{-5} \text{ m}^2/\text{s}$ ; Figure D-3).

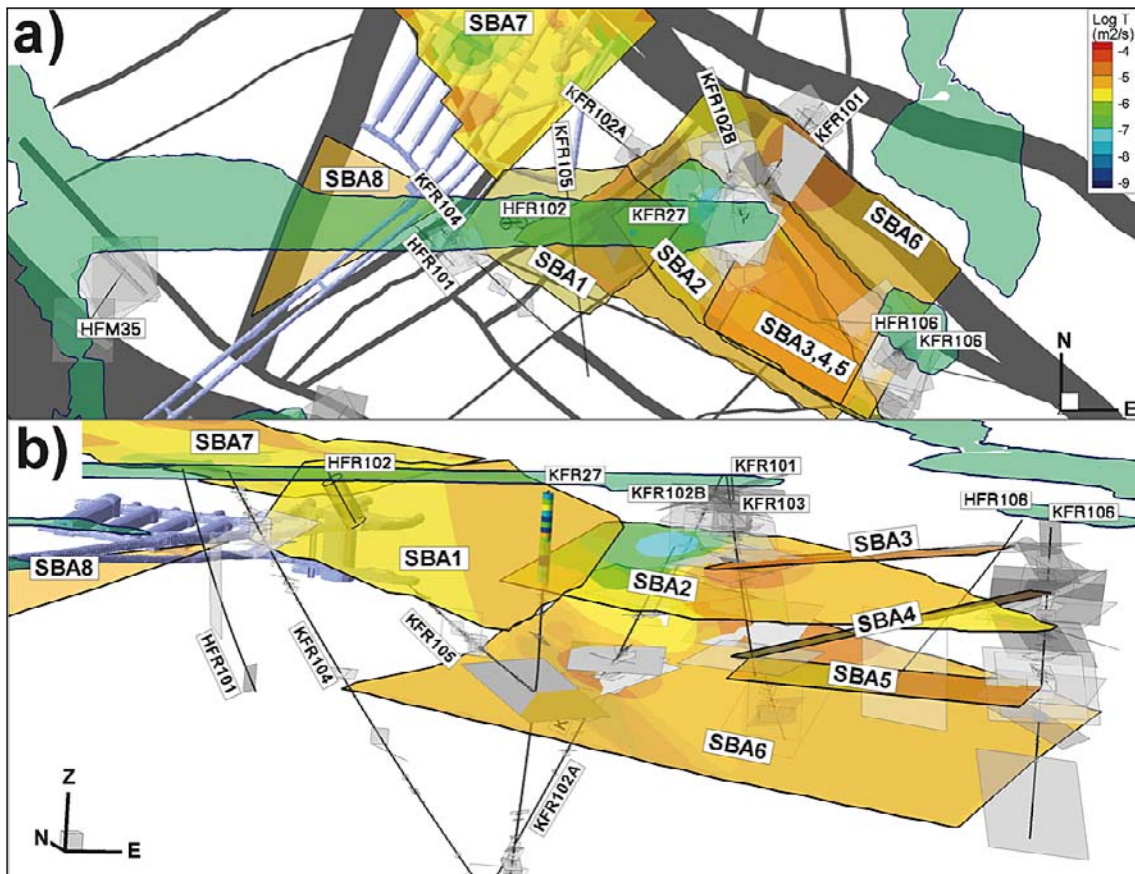


**Figure 6-3.** Deterministically modelled Shallow Bedrock Aquifer (SBA) structures; a) top view and b) side view from southwest. The structures are coloured by transmissivity interpolated from the transmissivity of the borehole intercepts.

It is tentatively modelled as SBA8, although its modelled geometry is judged to be highly uncertain (Appendix H).

It should be pointed out that in reality each feature is believed to represent a network of connected sub-horizontal fractures rather than a single fracture and that the extensions of the features outside the borehole intercepts are unknown. Note also that these structures are not expected to form perfect horizontal planes, but to bend and undulate, possibly related to topography. Also, the deterministically modelled structures are probably only a sub-set of the total number of horizontal hydraulic conductors in the model area, as only features intercepted by boreholes are detected. It is quite possible that the modelled structures, or other similar, should also occupy the southern part of the SFR model domain (cf. Figure 2-4), but information about the existence of SBA-structures is unavailable due to the lack of boreholes.

## 6.5 Hydraulic Soil Domain (HSD) model

No updated HSD model is currently available. However, there is ongoing work within the SFR extension project to develop an updated DEM, Regolith model, and HSD model, which will be available for safety assessments.

## 7 Discussion and conclusions

### 7.1 Summary of the bedrock hydrogeological model

The investigated bedrock volume is situated within a high-strain belt at the margin of the Forsmark tectonic lens described in SDM-Site Forsmark (SKB 2008a). The rock types are identical to those inside the lens, but they are generally affected by a higher degree of ductile strain. Unlike the lens, the investigation area is submerged, i.e. located below the sea (Figure 1-1), which would result in very low natural hydraulic gradients in the bedrock. However, due to the existing SFR facility, which was taken into operation in 1987, strong hydraulic gradients towards the depressurised tunnel system have developed (the deepest parts of the SFR facility reach approximately –140 m RHB70). It should also be noted that the groundwater flow pattern around the re-saturated SFR is expected to change significantly in future, due to ongoing land lift and shore-displacement (e.g. Holmén and Stigsson 2001). The investigated bedrock is overlain by sediments consisting of till and to some extent also low-conductive clay. These sediments may limit the hydraulic contact between the Baltic Sea and the bedrock.

The bedrock hydrogeology within the SFR regional model volume has been investigated with single-hole tests (PFL and HTHB) and interference (cross-hole) tests. There is also a relatively large amount of older hydraulic data from boreholes made during the construction of the existing SFR facility. Various types of observations in the tunnels of the SFR have also been used for the modelling. In SKB's systems approach to hydrogeological modelling, the large deformation zones that are deterministically modelled based on geological merits are named Hydraulic Conductor Domains (HCD) and the less fractured rock mass volumes between the HCD are named Hydraulic Rock mass Domains (HRD).

The main findings in the work reported here are: 1) at depths similar to the existing SFR facility groundwater flow is dominated by sub-horizontal features, at least in the vicinity of the Northern boundary belt and ZFMNNW1034, and 2) inside the Central block there is generally a weak transmissivity contrast between the fractures contained in the deformation zones and the fractures in the rock mass volumes outside the deformation zones.

#### 7.1.1 Hydraulic characteristics of Hydraulic Conductor Domains (HCD)

The following characteristics are interpreted for the deterministically modelled deformation zones:

- The division of the deterministically modelled deformation zones into four orientation sets is the basis for the hydrogeological modelling of HCDs. There are three sets of steeply dipping zones (WNW to NW, N-S to NNW, and NNE to ENE) and one set of gently dipping zones. In total, there are 37 steeply dipping zones and three gently dipping zones inside the SFR Regional model domain.
- Hydraulic data are scarce at depth and do not lend themselves to the determination of depth trend. The depth-trend model derived for SDM-Site Forsmark is suggested, which implies a contrast of about 150 times in HCD transmissivity in the upper 500 m of bedrock.
- The largest transmissivities are found in the steeply dipping zones forming the Southern and Northern boundary belts and ZFMNNW1034 (striking WNW to NW), as well as in the gently dipping zone ZFM871 and ZFMNNE0869, lying between the boundary belts.
- In contrast, the steeply dipping zones in the Central block (striking WNW to NW and NNE to ENE) are judged to be fairly low-transmissive ( $10^{-8}$  to  $10^{-6}$  m<sup>2</sup>/s). A few high-transmissive intercepts are found at depth, indicating considerable heterogeneity (channelling) within zones.
- In addition to the geologically modelled deformation zones, seven shallow sub-horizontal structures (referred to as SBA1 to SBA7) are modelled deterministically. The SBA-structures are hydraulically significant, but their existence is more evident close to the Northern boundary belt, than it is in the vicinity of the Southern boundary belt.

### 7.1.2 Hydraulic characteristics of the Hydraulic Rock mass Domains (HRD)

The following characteristics are interpreted for the fracture bedrock between deterministically modelled deformation zones:

- Flowing discrete features that are not deterministically modelled (fractures and Unresolved PDZs) are grouped in five orientation sets; three steeply dipping sets that strike EW, NW, and NE, one gently dipping set, and one horizontal set. Each set is assigned geometrical and hydraulic properties based on the underlying statistics (Appendix G).
- The horizontal and gently dipping flowing features dominate hydraulically, both in terms of frequency and transmissivity.
- Both frequency and transmissivity of all flowing features show a strong decline with depth. The discrete fracture network model for conductive fractures is split into three fracture domains with regard to depth (Section 6.3; Appendix G).
- No lateral trend in transmissivity can be inferred in the Shallow or the Deep domains. In the Repository domain, PFL-f transmissivity is low in the Central block and gradually increases towards the Northern boundary belt and ZFMNNW1034. It is unclear if this trend relates to *actual fracture-scale properties*, or an *apparent scaling effect* (i.e. related to hydraulic choking and the flow path length to the nearest positive flow boundary). Moreover, due to modelling uncertainties in this hydraulic pattern, no lateral subdivision of fracture domains is therefore applied in the Hydro-DFN (Section 6.3).
- There is generally a weak transmissivity contrast between the HRD and the HCDs inside the Central block. SBA-structures, Unresolved PDZs, and stochastic features dominate hydraulically above –200 m RHB 70, whereas flowing features are predominantly found inside the steeply dipping, deterministically modelled deformation zones at greater depths.

### 7.1.3 Hydrogeological characteristics of the SFR model volume

The key components of the conceptual hydrogeological model of the SFR bedrock volume are summarised in Figure 5-15. The flow at repository depth of the existing and the planned extension of the SFR facility is dominated by flow in horizontal to gently dipping features, at least in the vicinity of the Northern boundary belt and ZFMNNW1034. The most transmissive features are associated to Unresolved PDZs or Shallow Bedrock Aquifer (SBA) structures. The network of sub-horizontal structures is interpreted as connected to the steeply dipping deformation zones that form the Southern and Northern boundary belt. These act as important vertical conductors between the Baltic Sea and the existing SFR facility. However, the hydraulic contact to the sea is probably restricted by spatially variable sediment coverage, possibly with less coverage above the Northern boundary belt and ZFMNNW1034 (Figure 4-34). The hydraulic impact of the boundary zones gradually decreases with distance and limited connectivity in the discrete structures inside the Central block is envisaged. Significant remnant glacial melt water components inside the Northern boundary belt provide evidence of hydraulically isolated rock volumes.

## 7.2 Hydrogeological key issues

The main issues raised for the overall hydrogeological modelling of the SFR extension project are numbered 1–7 in Section 1.3. Some, but not all, of these issues have been addressed at this conceptual modelling stage:

- 1) **Hydraulic properties of HCDs:** The transmissivity of deformation zone intercepts have been evaluated (Appendixes D and E; also shown in Figure 6-2). It is suggested that deformation zones without borehole intercepts are parameterised based on set of belonging, as was done in SDM-Site Forsmark. The deformation zones of the Northern and Southern boundary belts (Figure 3-5) are highly transmissive and interpreted to control the hydraulic connectivity of the bedrock to the sea. Deformation zones inside the Central block (ENE to NNE set and WNW to NW sets) are interpreted as highly heterogeneous; considerably less transmissive ( $T_0$  in the range  $10^{-8}$  to  $10^{-6}$  m<sup>2</sup>/s), but with local high transmissivity channels (Sections 5.2 and 5.4). The contact between ZFM871 and the steeply dipping zones ZFMNNE0869 and ZFMNW0805A/B appears to be heterogeneous. There are several indications that ZFMNW0805B is heterogeneous and discontinuous: 1)

less transmissive in the vicinity of the existing SFR, 2) only indirect in responses with ZFM871, and 3) evidence of relic water type.

- 2) **Hydraulic properties of HRD:** The PFL-f data are clearly anisotropic, dominated by horizontal, gently dipping, and to a lesser extent, steep NW-striking fractures (Figure 4-15). The hydraulic anisotropy seems intimately related to the prevailing stress-regime. A conceptual model has been suggested to explain observations in lateral transmissivity contrasts (Figure 5-15). The flowing fracture network outside deterministic deformation zones (ZFM), Unresolved PDZs, and SBA-structures is described by means of a Hydro-DFN. The base case parameterisation is provided in Table 6-2, depending on size models of the steeply dipping fracture sets. An alternative parameterisation, in which KFR106 is included in the underlying data, is provided in Table G-7.

- 3) **Hydraulic connectivity within the model volume and to the surrounding rock mass:** Unfortunately, the degree of compartmentalization cannot be evaluated by a comparison between PFL-f and PSS data, as the latter data type is unavailable. Long-term decline in tunnel inflow and monitored heads of the less conductive rock in the vicinity of ZFMNE0870 (formerly known as Zone 9) suggests that the SFR inflow has not yet reached steady state (Sections 4.1.3 and 4.5.2). Cross-hole interferences indicate that pressure propagation is about one order of magnitude slower than that in Forsmark (Section 5.1). Hydrochemistry and reversed salinity profiles suggest existence of isolated rock mass or poor vertical connectivity (Section 4.6). Reported excess head values prior to tunnel constructions are highly uncertain (Section 4.5.1), but may also indicate a slow hydrogeological system, poorly vertically connected to the sea. Potentially, the connectivity to the sea in the Central block is constrained by overlying sediments.

Below –60 m RHB 70 there is less evidence of SBA-structures (high-transmissive, sub-horizontal PFL-f data) in the Central block (KFR104, KFR105, HFR101, as well as, experience from the existing SFR facility). Relatively large drawdown observed southeast of the termination of ZFM871 (KFR104 and KFR27; Section 4.5.4) suggests hydraulic connectivity to SFR. Absence of, or only minor, drawdown in the upper c. 50 m bedrock suggests that in the Shallow rock the hydraulic connection to the sea exceeds the connection to SFR.

- 4) **Spatial extent and hydraulic properties of sheet joints and gently dipping deformation zones:** Based on indications from various data types, six deterministic sub-horizontal structures have been suggested (referred to as SBA1 to SBA6; Appendix B). The earlier modelled stress-relief structures, Zones H1 and H3, were combined by (Curtis et al. 2011) (referred to as SBA7; Appendix D). Due to gaps in borehole coverage their spatial extension towards southwest is uncertain, although possibly a similar structure has been identified in tunnel mapping (referred to as SBA8; Figure D-3). The largest transmissivities are on the order  $10^{-5}$  m<sup>2</sup>/s, which is considerably less compared to the shallow rock above the Forsmark lens.

It is recommended that alternative extensions of ZFM871 are explored in the Safety Assessment. In the geologic model SFR v. 1.0, ZFM871 is terminated against three steeply dipping deformation zones: ZFMNNE0869, ZFMNW0805A/B, and ZFMENE3115 (Figure 3-5). The modelling uncertainties in these decisions are discussed in Curtis et al. (2011, Appendix 11). Hydrochemical classification of water types (Section 4.6) suggests extension beyond ZFMNNE0869 (KFR10) as well as ZFMNW0805B (KFR7A). The transient drawdown development in KFR7A (Section 4.5.2) and the high transmissivity in the possible deformation zone KFR10\_DZ2 (Figure 4-12) reinforce this suspicion. Observed drawdown also suggests that the *hydraulic connection* of ZFM871 extends c. 60 to 100 m southeast of its modelled termination against ZFMENE3115 (boreholes KFR104, KFR102A, and KFR27; Section 4.5.4). However, none of these boreholes provide geological evidence for the continuation of ZFM871 beyond its modelled geometry (i.e. does not exhibit deformation-zone characteristics associated to ZFM871). However, hydrogeological connection does not imply continuation of the geological structure.

Furthermore, two gently dipping structures are modelled at depth by Curtis et al. (2011) (Appendix C); these are not covered by borehole data and probably have minor significance for the SFR extension, owing to their deep location.

- 5) **Hydraulic difference between deformation zones and the surrounding bedrock:** The deterministic ZFM structures do not comprise a uniform population and cannot be compared against

the HRD, as such. With exceptions of ZFM871, ZFMNNE0869, ZFMNNW1034, the Southern and Northern boundary belts, the general impression is that in the upper c. 200 m, deterministic structures do not differ significantly from the rock mass outside zones. This notion should be considered in context to the geologic modelling uncertainties in continuity and extent of zones inside the Central block (Appendix C; Figure C-1) and underlines the necessity of alternative conceptual interpretations. It should also be emphasized that the geological modelling is strictly based on geological criteria (e.g. involving Sealed fracture frequency); thus, a geologically defined zone is not automatically conductive, *per se*. Data coverage deteriorates with depth, but it appears that the hydraulic signature of zones is larger below c. 200 m depth (Figure 4-16). Highly transmissive Unresolved PDZs have been identified in the vicinity of the Northern boundary belt and ZFMNNW1034.

- 6) **Support for dividing the bedrock between the deformation zones into different sub domains:** Indications of possible lateral trends have been observed between the Central block and the Southern and Northern boundary belts (and ZFMNNW1034). The differences are minor in terms of Open fracture patterns and intensity, but considerable in terms of PFL-f transmissivity (with lower transmissivity in the Central block). It is difficult to state the significance of these observations in relation to artefacts of data gaps, sampling bias, local heterogeneity, and borehole location with respect to deformation zones. Hence alternative methods are suggested in Section 5.6.
- 7) **Depth trend:** Based on visual inspection, a depth trend is judged to exist both in HRD and HCD transmissivity data, (Section 5.2). This is difficult to prove by statistical tests, owing to non-uniform data coverage. In spite of data gaps, the shallow rock, i.e. the upper 60 m, seems to be more transmissive in general. This upper 60 m was found to be statistically more transmissive in the old hydraulic data set (Öhman and Follin 2010a). Below c. 200 m depth, the borehole coverage outside deformation zones is relatively scarce, but transmissivity appears to be lower and the intensity in PFL-f data is considerably lower. In lack of contradictory evidence, it is assumed reasonable to use the depth-dependency model of the SDM-Site Forsmark also for the SFR domain, Eq. (5-1).

## 7.3 Confidence and some remaining uncertainties

### 7.3.1 Data gaps

As no complementary PSS measurements have been performed within the SFR extension investigation, the hydrogeological analysis heavily relies on PFL-f data, which are representative of the *flowing fracture system* (and subject to hydraulic choking). Complementary PSS data are useful for the evaluation of compartmentalised fracture transmissivity, if it needs to be addressed. The old data set consists of short-term hydraulic packer data and hence includes compartmentalised transmissivity, but it covers a different part of the domain and is of a poorer quality.

No interference tests have been specifically targeted to the interpreted SBA intercepts and Unresolved PDZs. Transient evaluation of a few selected packed-off pump tests targeting SBA intercepts and Unresolved PDZs may potentially shed some insight to their lateral extension.

The hypothesised absence of SBA-structures below –60 m RHB 70 in the Central block is motivated by HFR101, KFR104, and KFR105, as well as the general experience from the existing SFR (with one notable exception, shown in Figure D-3). It should be noted that KFR105 is a sub-horizontal borehole with limited vertical coverage of a sub-horizontal SBA system. It is difficult to use hydraulic data from KFR27, as it is effectively modelled inside or along the boundary of a steeply dipping deformation zone. Thus, a well-placed verification borehole in the Central block could potentially reinforce the hypothesised absence of SBA-structures, and in effect avoid propagating overly pessimistic model alternatives to the safety analysis.



### 7.3.2 Old versus new data

Essentially three different data sources are used in this study:

1. The old data set from the existing SFR (various short-term, double-packer hydraulic tests from the initial investigations and SFR construction, 1980 to 1986),
2. selected data from the Site Investigation Forsmark (KFM11A, HFM34, and HFM35, in the vicinity of the Singö deformation zone), and
3. the new SFR data set (from the SFR extension investigation, 2008 to 2009).

It is not straightforward how these three data types should be combined; they reflect different entities (e.g. connectivity aspects in Figure 2-5), are of different quality, and cover different parts of the SFR model domain (Figure 1-4). Essential weaknesses of the old data are the deficiency of oriented fracture data, as well as, the confidence in data quality. There also exists uncertainty in the geological modelling of deformation zone intercepts in the old data set (Appendix D), which propagates into an uncertainty in the assignment of hydraulic data. The old data set seem to result in higher transmissivity values of deformation zones (e.g. Figure 6-2e). The old data set is primarily used for conceptual understanding and as complementary data for the deformation zone parameterisation in the SFR near-field. Similarly, HFR105, KFM11A, HFR34, and HFM35 are also only used for the parameterisation of deformation zones; not because of poor quality, but owing to their location in the vicinity of the Singö deformation zone.

The established SKB methodology is to describe the HRD by means of a Hydro-DFN derived from a connectivity analysis of PFL-f data. Therefore only core-drilled boreholes are used in the Hydro-DFN for SFR.

### 7.3.3 Shallow Bedrock Aquifer (SBA)

The PFL-f data in boreholes located close to the Northern boundary belt and ZFMNNW1034 indicate that SBA-structures do exist north of the Singö deformation zone, even if these seem to be of considerably less dignity in relation to those modelled in SDM-Site Forsmark. The SBA-structures are interpreted to have an important role in the hydraulic connectivity of the rock mass, at least in the vicinity of the Northern boundary belt and ZFMNNW1034. The spatial extension of SBA-structures is uncertain, but borehole data (HFR101, KFR104 and KFR105) and SFR tunnel experiences suggest that these are of minor hydraulic significance in the Central block, below -60 m RHB 70. As pointed out earlier, KFR105 is sub-horizontal and thus, has a poor vertical coverage of SBA-structures. The old data set provides little guidance for interpretation of SBA-structures; most are short term measurements (a few minutes) and have no oriented fracture data. Several sub-horizontal structures are mapped in the SFR tunnel, but *generally* not related to significant inflow; only two required grouting (Figure 4-1) and one of these is supported by borehole data (tentatively referred to as SBA8;  $T > 10^{-5} \text{ m}^2/\text{s}$ ; Figure D-3).

### 7.3.4 Concluding remarks

A conceptual hydrogeological model for SFR has been proposed, along with model alternatives (Table 5 1). This report provides hydraulic parameterisation of deformation zones (HCD), deterministic SBA-structures, as well as a modelling strategy for Unresolved PDZs. The flowing fracture network outside the aforementioned structures is stochastically represented by means of a Hydro-DFN model. Alternative parameterisation setups may be considered during the stage of safety assessment.

The numerical implementation of the hydrogeological model in the computational software DarcyTools will be performed in a subsequent stage, which addresses issues such as flow model calibration and confirmatory (numerical) testing /Öhman et al. 2013/. As a Base case for confirmatory testing, the following parameterisation is suggested:

- 1) Deterministic deformation zones are parameterised according to Table 6-1, based on the depth-trend model derived for SDM-Site Forsmark.
- 2) Unresolved PDZs are modelled stochastically, spatially related to the Southern boundary belt, as well as, the structural wedge between the Northern boundary belt and ZFMNNW1034, according to the strategy described in Appendix A.

- 3) SBA-structures, SBA1-7, are modelled deterministically as described in Appendix B. SBA8 is not included due to its low confidence (Appendix H).
- 4) The remaining fracture network of connected open fractures, HRD, is modelled stochastically by means of a Hydro-DFN (Table 6-2). The size model based on the Connectivity analysis approach is suggested. The Hydro-DFN is based on data falling outside: 1) deterministic structures, 2) Unresolved PDZs, and 3) SBA-structures. KFR106 is judged unrepresentative of the Local SFR domain and is therefore not included. The details of the Hydro-DFN parameterisation are given in Appendix G.

## 8 References

SKB's (Svensk Kärnbränslehantering AB) publications can be found at [www.skb.se/publications](http://www.skb.se/publications).  
References to SKB's unpublished documents are listed separately at the end of the reference list.  
Unpublished documents will be submitted upon request to [document@skb.se](mailto:document@skb.se)

**Andersson J, Ström A, Svemar C, Almén K-E, Ericsson L-O, 2000.** What requirements does the KBS-3 repository make on the host rock? Geoscientific suitability indicators and criteria for siting and site evaluation. SKB TR-00-12, Svensk Kärnbränslehantering AB.

**Axelsson C-L, 1986.** Modeling of groundwater flow with salt-water interference at the final repository for reactor waste (SFR). SSI P 311.85.

**Axelsson C-L, Mærsk Hansen L, 1997.** Update of structural models at SFR nuclear waste repository, Forsmark, Sweden. SKB R-98-05, Svensk Kärnbränslehantering AB.

**Axelsson C-L, Ekstav A, Lindblad Pässe A, 2002.** SFR – Utvärdering av hydrogeologi. SKB R-02-14, Svensk Kärnbränslehantering AB. (In Swedish.)

**Berglund J, 2008.** Site investigation SFR. Geological mapping and laser scanning of the lower construction tunnel. SKB P-09-74, Svensk Kärnbränslehantering AB.

**Bono N, Fredriksson A, Mærsk Hansen L, 2010.** Sättningsanalys Forsmarks kärnkraftsverk – Aggregat 1. SKB P-10-48, Svensk Kärnbränslehantering AB. (In Swedish.)

**Bosson E, Gustafsson L-G, Sassner M, 2008.** Numerical modelling of surface hydrology and near-surface hydrogeology at Forsmark. Site descriptive modelling, SDM-Site Forsmark. SKB R-08-09, Svensk Kärnbränslehantering AB.

**Carlsson A, 1979.** Characteristic features of a superficial rock mass in Southern central Sweden: horizontal and sub-horizontal fractures and filling material. PhD thesis. Uppsala University, Sweden. (Striae 11).

**Carlsson A, Christiansson R, 2007.** Construction experiences from underground works at Forsmark. Compilation report. SKB R-07-10, Svensk Kärnbränslehantering AB.

**Carlsson L, Carlsten S, Sigurdsson T, Winberg A, 1985.** Hydraulic modelling of the final repository for reactor waste (SFR). Compilation and conceptualization of available geological and hydrogeological data. Edition 1. SKB SFR 85-06, Svensk Kärnbränslehantering AB.

**Carlsson L, Winberg A, Arnefors J, 1986.** Hydraulic modelling of the final repository for reactor waste (SFR). Compilation and conceptualization of available geological and hydrogeological data. SKB SFR 86-03, Svensk Kärnbränslehantering AB.

**Carlsson L, Winberg A, Grundfelt B, 1987.** Hydraulic modelling of the final repository for reactor waste (SFR). Evaluation of the groundwater flow situation at SFR. SKB SFR 86-07, Svensk Kärnbränslehantering AB.

**Christiansson R, 1986.** Geologisk beskrivning av zoner kring slutförvaret. SKB SFR 86-02, Svensk Kärnbränslehantering AB. (In Swedish.)

**Christiansson R, Bolvede P, 1987.** Byggnadsgeologisk uppföljning. Slutrapport. SKB SFR 87-03, Svensk Kärnbränslehantering AB. (In Swedish.)

**Curtis P, Petersson J, Triumf C-A, Isaksson H, 2009.** Site investigation SFR. Deformation zone modelling. Model version 0.1. SKB P-09-48, Svensk Kärnbränslehantering AB. (In Swedish.)

**Curtis P, Markström I, Petersson J, Triumf C-A, Isaksson H, Matsson H, 2011.** Site investigation SFR. Bedrock geology. Model version 1.0. SKB R-10-49, Svensk Kärnbränslehantering AB.

**Follin S, 2008.** Bedrock hydrogeology Forsmark. Site descriptive modelling, SDM-Site Forsmark. SKB R-08-95, Svensk Kärnbränslehantering AB.

- Follin S, Stigsson M, Svensson U, 2005.** Regional hydrogeological simulations for Forsmark – numerical modelling using DarcyTools. Preliminary site description. Forsmark area – version 1.2. SKB R-05-60, Svensk Kärnbränslehantering AB.
- Follin S, Johansson P-O, Levén J, Hartley L, Holton D, McCarthy R, Roberts D, 2007a.** Updated strategy and test of new concepts for groundwater flow modelling in Forsmark in preparation of site descriptive modelling stage 2.2. SKB R-07-20, Svensk Kärnbränslehantering AB.
- Follin S, Levén J, Hartley L, Jackson P, Joyce S, Roberts D, Swift B, 2007b.** Hydrogeological characterisation and modelling of deformation zones and fracture domains, Forsmark modelling stage 2.2. SKB R-07-48, Svensk Kärnbränslehantering AB.
- Follin S, Johansson P-O, Hartley L, Jackson P, Roberts D, Marsic N, 2007c.** Conceptual model development and numerical modelling using CONNECTFLOW, Forsmark modelling stage 2.2. SKB R-07-49, Svensk Kärnbränslehantering AB.
- Fox A, La Pointe P, Hermanson J, Öhman J, 2007.** Statistical geological discrete fracture network model. Forsmark modelling stage 2.2. SKB R-07-46, Svensk Kärnbränslehantering AB.
- Glamheden R, Maersk Hansen L, Fredriksson A, Bergkvist L, Markström I, Elfström M, 2007.** Mechanical modelling of the Singö deformation zone. Site descriptive modelling Forsmark stage 2.1. SKB R-07-06, Svensk Kärnbränslehantering AB.
- Gokall-Norman K, Ludvigson J-E, 2005.** Forsmark site investigation. Hydraulic interference tests. Boreholes HFM16, HFM19 and KFM02A. SKB P-05-78, Svensk Kärnbränslehantering AB.
- Gokall-Norman K, Ludvigson J-E, 2008a.** Forsmark site investigation. Large-scale interference test with borehole HFM14 used as pumping borehole, 2007. SKB P-07-228, Svensk Kärnbränslehantering AB.
- Gokall-Norman K, Ludvigson J-E, 2008b.** Hydraulic interference test with borehole HFM33 used as pumping borehole, November of 2007. SKB P-07-229, Svensk Kärnbränslehantering AB.
- Gokall-Norman K, Svensson T, Ludvigson J-E, Jönsson S, 2004.** Forsmark site investigation. Hydraulic interference test. Boreholes HFM18 and KFM03A. SKB P-04-307, Svensk Kärnbränslehantering AB.
- Gokall-Norman K, Ludvigson J-E, Jönsson S, 2005a.** Forsmark site investigation. Hydraulic interference test. Boreholes KFM04A, HFM10, HFM13, HFM19 and HFM252. SKB P-05-186, Svensk Kärnbränslehantering AB.
- Gokall-Norman K, Ludvigson J-E, Jönsson S, 2005b.** Forsmark site investigation. Hydraulic interference test in borehole HFM01. SKB P-05-236, Svensk Kärnbränslehantering AB.
- Gokall-Norman K, Ludvigson J-E, Jönsson S, 2006.** Forsmark site investigation. Hydraulic interference test. Boreholes KFM02A and KFM03A. SKB P-06-09, Svensk Kärnbränslehantering AB.
- Gustafson G, 2009.** Hydrogeologi för bergbyggare. Stockholm: Formas. (In Swedish.)
- Hedenström A, Sohlenius G, 2008.** Description of the regolith at Forsmark. Site descriptive modelling, SDM-Site Forsmark. SKB R-08-04, Svensk Kärnbränslehantering AB.
- Hedenström A, Sohlenius G, Strömngren M, Brydsten L, Nyman H, 2008.** Depth and stratigraphy of regolith at Forsmark. Site descriptive modelling, SDM-Site Forsmark. SKB R-08-07, Svensk Kärnbränslehantering AB.
- Holmén J G, 2005.** SFR-1. Inverse modelling of inflow to tunnels and propagation of estimated uncertainties to predictive stages. SKB R-05-74, Svensk Kärnbränslehantering AB.
- Holmén J G, Stigsson M, 2001.** Modelling of future hydrogeological conditions at SFR. SKB R-01-02, Svensk Kärnbränslehantering AB.
- Hurmerinta E, Väisäsvaara J, 2009.** Site investigation SFR. Difference flow logging in boreholes KFR104 and KFR27 (extension). SKB P-09-20, Svensk Kärnbränslehantering AB.
- Jarsjö J, Destouni G, 2000.** Degassing of deep groundwater in fractured rock around boreholes and drifts. Water Resources Research 36, 2477–2492.

- Johansson P-O, Öhman J, 2008.** Presentation of meteorological, hydrological and hydrogeological monitoring data from Forsmark. Site descriptive modelling, SDM-Site Forsmark. SKB R-08-10, Svensk Kärnbränslehantering AB.
- Juhlin C, Zhang F, 2010.** Site investigation SFR. Reprocessing of reflection seismic profiles 5b and 8, Forsmark, Sweden. SKB P-10-50, Svensk Kärnbränslehantering AB.
- Knudby C, Carrera J, 2006.** On the use of apparent hydraulic diffusivity as indicator of connectivity. *Journal of Hydrology* 329, 377–389.
- Laaksoharju M, Gimeno M, Auqué L F, Gómez J B, Acero P, Pedersen K, 2009.** Hydrogeochemical and microbiological effects on fractures in the Excavation Damaged Zone (EDZ). SKB R-09-05, Svensk Kärnbränslehantering AB.
- Lindquist A, Hjerne C, Nordqvist R, Byegård J, Walger E, Ludvigson J-E, Wass E, 2008.** Forsmark site investigation. Confirmatory hydraulic interference test and tracer test at drill site 2. SKB P-08-13, Svensk Kärnbränslehantering AB.
- Munier R, Stenberg L, Stanfors R, Milnes A, Hermanson J, Triumf C-A, 2003.** Geological Site Descriptive Model. A strategy for the model development during site investigations. SKB R-03-07, Svensk Kärnbränslehantering AB.
- Nilsson G, 2009.** Site investigation SFR. Drilling of the cored borehole KFR105. SKB P-09-41, Svensk Kärnbränslehantering AB.
- Nilsson G, Ullberg A, 2009a.** Site investigation SFR. Drilling of the traditional borehole KFR27. SKB P-09-12, Svensk Kärnbränslehantering AB.
- Nilsson G, Ullberg A, 2009b.** Site investigation SFR, Drilling of the telescopic borehole KFR102A. SKB P-09-19, Svensk Kärnbränslehantering AB.
- Nilsson A-C, Tullborg E-L, Smellie J, 2010.** Preliminary hydrogeochemical site description SFR (version 0.2). SKB R-10-38, Svensk Kärnbränslehantering AB.
- Odén M, 2009.** Site investigation SFR. Hydrogeological modelling at SFR using DarcyTools. Site description SFR version 0.0. SKB P-08-94, Svensk Kärnbränslehantering AB.
- Rhén I, Follin S, Hermanson J, 2003.** Hydrogeological Site Descriptive Model – a strategy for its development during Site Investigations. SKB R-03-08, Svensk Kärnbränslehantering AB.
- Sjöberg J, Lindfors U, Perman F, Ask D, 2005.** Evaluation of the state of stress at the Forsmark site. Preliminary site investigation. Forsmark area – version 1.2. SKB R-05-35, Svensk Kärnbränslehantering AB.
- SKB, 2008a.** Site description of Forsmark at completion of the site investigation phase. SDM-Site Forsmark. SKB TR-08-05, Svensk Kärnbränslehantering AB.
- SKB, 2008b.** Geovetenskapligt undersökningsprogram för utbyggnad av SFR. SKB R-08-67, Svensk Kärnbränslehantering AB. (In Swedish.)
- Stephens M B, Fox A, La Pointe P, Simeonov A, Isaksson H, Hermanson J, Öhman J, 2007.** Geology Forsmark. Site descriptive modelling, Forsmark stage 2.2. SKB R-07-45, Svensk Kärnbränslehantering AB.
- Stephens M B, Simeonov A, Isaksson H, 2008.** Bedrock geology Forsmark. Modelling stage 2.3. Implications for and validation of the deterministic geological models based on complementary data. SKB R-08-64, Svensk Kärnbränslehantering AB.
- Stigsson M, 2007.** Analysis of uncertainty and changes in orientation of fractures coupled to PFL anomalies. Forsmark site investigation. SKB P-07-178, Svensk Kärnbränslehantering AB.
- Streltsova T D, 1988.** Well testing in heterogeneous formations. New York: Wiley.
- Svensson U, 2010.** DarcyTools version 3.4. Verification, validation and demonstration. SKB R-10-71, Svensk Kärnbränslehantering AB.
- Svensson U, Kuylenstierna H-O, Ferry M, 2010.** DarcyTools version 3.4 – Concepts, methods and equations. SKB R-07-38, Svensk Kärnbränslehantering AB.

**Söderbäck B (ed), 2008.** Geological evolution, palaeoclimate and historical development of the Forsmark and Laxemar-Simpevarp areas. Site descriptive modelling, SDM-Site. SKB R-08-19, Svensk Kärnbränslehantering AB.

**Väisäsvaara J, 2009.** Site investigation SFR. Difference flow logging in borehole KFR105. SKB P-09-09, Svensk Kärnbränslehantering AB.

**Walger E, Ludvigson J-E, Gentschein B, 2010.** Site investigation SFR. Evaluation of selected interference tests and pressure responses during drilling at SFR. SKB P-10-43, Svensk Kärnbränslehantering AB.

**Öhman J, 2010.** Site investigation SFR. Hydrogeologic modelling of SFR v 0.1. Influence of the ridge on the flow fields for different target volumes. SKB R-09-43, Svensk Kärnbränslehantering AB.

**Öhman J, Follin S, 2010a.** Site investigation SFR. Hydrogeological modelling of SFR. Data review and parameterisation of model version 0.1. SKB P-09-49, Svensk Kärnbränslehantering AB.

**Öhman J, Follin S, 2010b.** Site investigation SFR. Hydrogeological modelling of SFR. Model version 0.2. SKB R-10-03, Svensk Kärnbränslehantering AB.

**Öhman J, Follin S, Odén M, 2013.** Site investigation SFR. Bedrock hydrogeology – Groundwater flow modelling. SKB R-11-10, Svensk Kärnbränslehantering AB.

**Öhman J, Sträng M, Moverare J, 2010.** Site investigation SFR. PFL-f linking to Boremap data KFR101, KFR102A, KFR102B, KFR103, KFR104, KFR105, KFR106 and KFR27. SKB P-10-01, Svensk Kärnbränslehantering AB.

#### Unpublished documents

SKBdoc id, version	Title	Issuer, year
1233642 ver 1.0	SFR Kontrollprogram. Bergkontroll. Bergkontrollgruppens årsrapport 2009. Huvudrapport.	Vattenfall Power Consultant, 2010
1233647 ver 1.0	SFR – Registrering av grundvattentryck under 2009	Geosigma, 2010

## Modelling strategy for Unresolved PDZs

This section suggests a modelling strategy for borehole intervals defined as Possible Deformation Zones (PDZs) in the Single Hole Interpretation (SHI) that are not included in the deterministic model. These are borehole intervals with deformation zone characteristics that could neither be geologically matched to intercepts in surrounding boreholes, nor to lineaments exceeding the resolution of the geological model. This type of structures is therefore referred to as *Unresolved PDZs*. The information available for this type of structures is partially deterministic (its borehole intercept, as well as, *absence* of nearby borehole intercepts and lineaments exceeding the resolution of the geological model). However, the deterministic, geometrical information is incomplete and therefore includes uncertainties. These are addressed by including *stochastic* components.

Unresolved PDZs are the residue from the geological modelling, and therefore comprise a non-uniform data population. Firstly, the SHI interpretation of these PDZs has varying confidence (e.g. many have a low to medium confidence in existence). Secondly, they are interpreted to be of highly variable hydraulic significance in the hydrogeological modelling (i.e. interpreted hydraulic properties, as well as, depending on their location relative to the planned extension of SFR). Thirdly, the historic data set<sup>2</sup> is of considerably lower quality (which causes low confidence in existence, as well as, in hydraulic properties); the lack of orientation data complicates numerical modelling.

A subset of Unresolved PDZs identified as exceptionally transmissive (exceeding  $10^{-5}$  m<sup>2</sup>/s) is identified as primarily horizontal to gently dipping (see Section A.1). In contrast, the deterministically modelled structures (ZFM) are primarily steep, and hence the tectonic continuum hypothesis offers little guidance for the size estimation of gently dipping structures. The combination of high transmissivity and uncertain size causes a key model uncertainty in the hydrogeological modelling and implies that the decision on *how* to implement these features in the model may influence predicted model heterogeneity. The numerical representation of these structures is simplified as square planes with homogeneous hydraulic properties. It should be pointed out that this simplification is not very realistic for this type of structures (relatively large in size, combined with a high-transmissivity).

The objectives of this appendix are to:

- 1) Present a hypothesis for spatial inference of the Unresolved PDZs (formed out of the necessity to fill in borehole coverage gaps, rather than well-underpinned by evidence in data), and,
- 2) based on this hypothesis (as well as numerical simplifications), apply a numerical calibration procedure to examine the potential in using existing borehole data to constrain the size distribution of Unresolved PDZs (i.e. a probabilistic size estimation).

Gaps in borehole coverage cause a key uncertainty to the hydraulic parameterisation in the southern part of the SFR model domain (i.e. orange rectangle in Figure A-1). Therefore particular emphasis is paid to cover this area in the modelling of Unresolved PDZs, by means of geometrical inference to geological structures. Only the features considered to be most significant for the hydrogeological modelling are addressed in this study. The features excluded from this study have low confidence, transmissivity, and/or lack spatial inference (see Section A.1); they do not stand out as anomalous relative to HRD are therefore considered to be subordinate to the DFN model (Appendix G).

### A.1 Presentation of data

Altogether 31 Unresolved PDZs have been identified by Curtis et al. (2011). These are of considerably variable characteristics, confidence in existence, and judged significance in the hydrogeological model (indicated by coloured geometries in Figure A-1). There are distinct differences between the 17 PDZs in the old data set in the vicinity of SFR and the 14 PDZs in the new data set (Figure A-1). To some extent this difference relates to borehole coverage, data quality, available data support.

<sup>2</sup> The terms “old” and “historic” are exchangeable and refer to the data acquired during the construction of SFR, while the terms “new” or “recent” refer to data acquired during the Forsmark and SFR extension site investigations (Figure 1-4, main report).

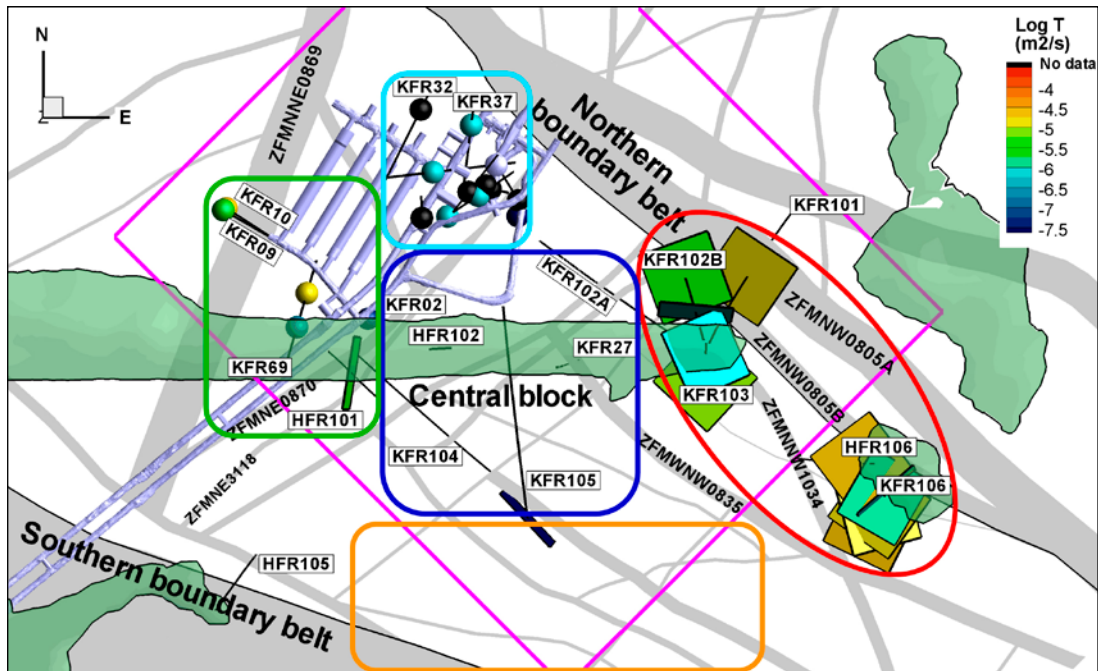


**Figure A-1.** Unresolved PDZs compared to ground intercepts of deterministic structures (grey). Features lacking modelled orientation are shown as spheres (old borehole data, close to SFR), while oriented features are shown as planes (new borehole data, southeast of SFR). Coloured geometries refer to subareas of different confidence/relevance/hydraulic interpretation. The red oval indicates features judged as most hydraulically significant for the SFR extension. The blue rectangle indicates absence of hydraulically significant features. The orange rectangle emphasises lack of borehole coverage.

There are several reasons to primarily focus the attention to the Unresolved PDZs of the new data set (red oval in Figure A-1). Note that four Unresolved PDZs of the new data set are *alternatively* included in the definitions of deterministic SBA-structures (Section A.1.1).

The Unresolved PDZs in the historic and the recent data sets are presented in Sections A.1.1 and A.1.2, respectively. In summary, the following apply to the Unresolved PDZs in the **historic** data set:

- Many have a low SHI confidence in existence (Table A-1).
- Many have poor, or no hydraulic data (black spheres indicate lacking hydraulic data; Figure A-1).
- Many are located close to the tunnel wall, or Silo, of the existing SFR, without geologic evidence, or hydraulic indication (high inflow) of tunnel interception (light-blue rectangle in Figure A-1), which suggests that they are minor structures with minor hydraulic significance for the existing SFR.
- The lack of interpreted orientation and true thickness complicates modelling.
- A few exceptions with high confidence and high transmissivity values (green rectangle in Figure A-1) have been assigned deterministic interpretations.

The following apply to the Unresolved PDZs in the **recent** data set.

- Generally high SHI confidence in existence (except percussion boreholes HFR101 and HFR106).
- Distinct hydraulic signature compared to surrounding rock; high PFL-f transmissivity, predominantly sub-horizontal to gently dipping (red oval in Figure A-1). Exceptions with respect to location, orientation, and/or transmissivity are indicated in Figure A-2.
- Owing to borehole locations with respect to the planned SFR extension, they are comparatively more important for the safety analysis.

Some Unresolved PDZs of the new data set lack a geologically interpreted orientation (Table A-2). Hence, orientation interpretations were complemented by orientation estimations from PFL-f data (Figure A-3; these indicate good agreement to the geologically estimated orientations Table A-2).



### A.1.1 Unresolved PDZs in the historic data set

The 17 Unresolved PDZs in the historic data set lack modelled orientation and in many cases supporting hydraulic data are unavailable, have incomplete coverage, or unfavourable packer spacing (Table A-1, details provided in Appendix D). As an example, the hydraulic support for KFR32\_DZ1 cannot be differentiated from ZFM871 (Figure D-37). To some extent these PDZs may be an artefact of the poor data quality, which propagates into geometric uncertainty in the geological modelling (i.e. applied deformation zone terminations). A few PDZs, with high confidence and supported by high transmissivity data, are possible extensions of, or splays to, the modelled deterministic structures. KFR10\_DZ2 is associated to a potential extension of ZFM871 and KFR09\_DZ2 is considered to be a possible splay of ZFMNNE0869. Another example is KFR69\_DZ2, which is located immediately South and below the SFR disposal facility and has been linked to grouted horizontal structures in tunnel DT (modelled as SBA8; see Appendix D, Figure D-3).

Some moderate-confidence PDZs are located at shallow depths (e.g. KFR31\_DZ1, KFR37\_DZ1, and KFR69\_DZ1). Although the supporting hydraulic data are on the order  $10^{-6}$  m<sup>2</sup>/s, they are not inferred as anomalously transmissive in context of other data at similar depths and the general quality in the historic data set. Several PDZs lack hydraulic data, but are inferred to have minor hydraulic significance due to their location in the vicinity of the Silo (Figure A-1), which is an area that is reported to have minor tunnel inflow (Christiansson and Bolvede 1987).

Many of the Unresolved PDZs are located close to ZFMNE0870, in particular close to the Silo. The low Silo inflow (see Section 4.1) would suggest that these PDZs are of minor hydraulic importance. Thus, attempts to honour the spatial pattern of PDZs in a stochastic DFN framework are likely to result in overestimated Silo inflow. With respect to data uncertainty and the lack of hydraulic support it appears unlikely that the PDZs from the old data set should belong to the same population as the new data set. Therefore, it is suggested that the PDZs from the old data set are not used in the DFN modelling.

**Table A-1. Seventeen Unresolved PDZs in the old borehole data set.**

PDZ	SHI <sup>1)</sup> conf.	Borehole interval (m)		Hydraulic data			Suggested interpretation	
		From	To	No. <sup>2)</sup> data	$\Sigma L$ <sup>3)</sup> $\Delta L$	Log T (m <sup>2</sup> /s)	(Geometrical reference)	Hydraulic support
KFR02_DZ2	1	99.2	100.2	1	10	-7.3	Possibly connects ZFM871	Weak
KFR03_DZ1	2	6	12	1	6.5	-6.0	Possible splay of NE0870? (NBT)	Possible <sup>4)</sup>
KFR04_DZ1	1	0	3	0	-	-	On boundary of NE0870 (Silo)	-
KFR09_DZ2	3	69	74.3	1	3.3	-5.6	Connection to NNE0869 (East of NNE0869)	Assumed splay
KFR10_DZ2	3	95.7	107.3	1	1.7	-4.5	Related to ZFM871 (East of NNE0869)	Assumed extension
KFR13_DZ1	3	20	30	2	2	-7.9	Likely connects to NE3118 (Below NBT)	Low T
KFR13_DZ2	2	36	41	1	2	-7.5	Likely connects to NE3118 (Below NBT)	Low T
KFR19_DZ1	2	38.5	49.3	0	-	-	Meeting point of long fractures (Silo)	No data
KFR20_DZ1	1	48.5	52	1	4	-6.0	NNE-striking steep fractures (Silo)	Moderate
KFR31_DZ1	2	82.1	91.7	4	1.2	-6.1	NW-striking steep fractures (Shallow depth)	Moderate
KFR32_DZ1	3	155.7	159	2	16.7	(-3.9)	Data mainly covers ZFM871 (Just above ZFM871)	Weak
KFR37_DZ1	2	36.6	45.6	4	1.3	-6.0	ZFMNW0805b (Shallow depth)	Strong
KFR51_DZ1	1	9.8	11.2	0	-	-	NNE-striking steep fractures	No data
KFR52_DZ1	2	19.9	22.4	0	-	-	(Silo)	No data
KFR55_DZ1	2	0	3.3	0	-	-	NBT	No data
KFR69_DZ1	2	52.4	79	10	1.1	-6.6	(Shallow depth)	Moderate
KFR69_DZ2	3	121.6	146.1	5	3.3	-4.9	Grouted HZ-structures (Below SFR)	Strong

<sup>1)</sup> SHI confidence level: 1 = low, 2 = medium, 3 = high.

<sup>2)</sup> Number of packer intervals used to calculate intercept transmissivity.

<sup>3)</sup> Excess hydro data coverage factor, expressed as the sum of hydraulic test data sections,  $\Sigma L$ , divided by the PDZ borehole interval,  $\Delta L$ . A value close to 1.0 indicates that the PDZ is well resolved by hydraulic data test sections.

<sup>4)</sup> Mapped waterbearing fractures (Christiansson and Bolvede 1987).

### A.1.2 Unresolved PDZs in the recent data set

In comparison, the Unresolved PDZs of the recent data set have very distinct hydraulic signature, characterized by a single, or a few, high-transmissive PFL-f records on the order  $10^{-5}$  m<sup>2</sup>/s. The PFL-f data are predominantly horizontal to gently dipping (Figure A-3) and with orientations very similar to geologically modelled PDZ orientation (see Table A-2). These PDZs are found down to c. 160 m depth (Figure A-2) and seem laterally concentrated to the wedge between the Northern boundary belt and ZFMNNW1034 (red oval in Figure A-1). Three exceptions can be identified: HFR101\_DZ2, KFR105\_DZ5 and KFR101\_DZ4; these are considered to be of lesser confidence/significance in the hydrogeological model, and are discussed below.

HFR101\_DZ2 (101 to 115 m borehole length) is a low confidence PDZ located in the Central block, rather close to the SFR tunnel DT, inside a wedge between ZFMNE0870 and ZFMNE3118 (Figure A-1). It correlates to a transmissivity of  $2.6 \times 10^{-6}$  m<sup>2</sup>/s (as measured at 107.3 to 108 m borehole length by the HTHB method; Table 1-3). There is no detectable transmissivity inside the ZFMNE0870 intercept. The mapped Open fractures in this borehole section are sub-parallel: steeply dipping and NS-striking. Although the confidence in orientation estimation is low (poor BIPS image), the estimated orientation is ( $9^\circ/86^\circ$ ). Inside the same wedge between ZFMNE0870 and ZFMNE3118, at approximately 50 m horizontal distance, identical transmissivity is found at the same level in KFR70. Outside this wedge, 60 to 70 m away on either side of the wedge, considerably lower transmissivities are found in KFR104 and KFR02 at the same level. It is unclear if this PDZ should be included in the Unresolved PDZs modelling or deterministically related to either of the NE-striking zones. Inspection of the old data set suggests that PDZs are frequently observed in along ZFMNE0870 (Figure A-1). It was decided to exclude it from the Unresolved PDZs modelling, due to its low confidence in existence, as well as, deviates from the general pattern related of other Unresolved PDZs, i.e. the possible inference to the structural wedge (Figure A-4), which is the primary focus of this analysis.

KFR105\_DZ5 also has a central location in the Central block (Figure A-1), between ZFMWNW3267 and ZFMWNW8043 and has a steep WNW-striking orientation of ( $319^\circ/88^\circ$ ). The PFL-f data have similar orientations, but a low total transmissivity of  $1.4 \times 10^{-8}$  m<sup>2</sup>/s, and thus have minor hydraulic significance. This PDZ is clearly deviant, both in terms of transmissivity, orientation, and location. It would seem appropriate to associate this PDZ deterministically as a splay to ZFMWNW3267, and to exclude it from the Unresolved PDZs modelling.

KFR101\_DZ4 has geologically been interpreted as a splay between ZFMNW0805A and ZFMNW0805B. It has no PFL-f data above detection limit (reported to be  $7.4 \times 10^{-9}$  m<sup>2</sup>/s). It is considered to have negligible hydraulic relevance and was therefore excluded from the Unresolved PDZs modelling.

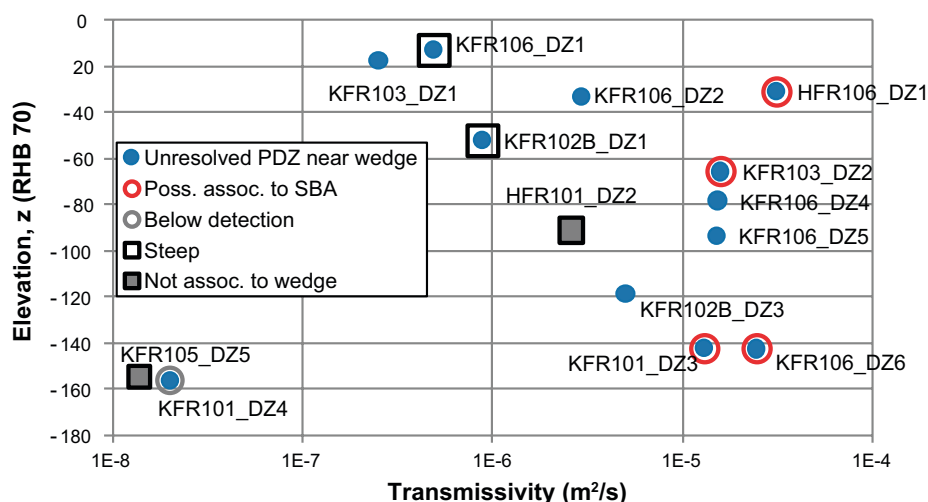


**Figure A-2.** Unresolved PDZ transmissivity with elevation (only recent data). Most PDZs are horizontal to gently dipping (12 blue dots) and located close to a structural wedge between the Northern boundary belt and ZFMNNW1034 (Figure A-4). PDZs alternatively associated to deterministic SBA shown with red circles. Steeply dipping PDZs are indicated by squares and PDZs located far from the wedge are shown in grey.

**Table A-2. Unresolved PDZs in the new data set.**

	Borehole length (m)		Elevation (m, RHB 70)		SHI conf. <sup>4)</sup>	Orientation (Strike/Dip)		Dominant PFL-f	
	From	To	From	To		Geologic	PFL-f <sup>5)</sup>	Log T	Set
<b>DZs included in the stochastic modelling</b>									
KFR102B_DZ1	67	70	-51.9	-54.3	3	(098/81)	(95/79)	-6.1	EW
KFR102B_DZ3	149.5	150.5	-118.4	-119.2	2	(229/08)	(160/4)	-5.3	Hz
KFR103_DZ1	24.5	26.5	-17.5	-19.1	3	-	(336/29)	-6.6	Gd
KFR103_DZ2 <sup>3)</sup>	84	91	-65.6	-71.2	3	(343/12)	(223/2)	-5	Hz
KFR106_DZ1	15	20	-13.1	-17.8	3	(216/90)	(49/83)	-6.3	NE
KFR106_DZ2	36.5	52	-33.2	-47.8	2	-	(30/23)	-5.8	Hz
KFR106_DZ4	84.5	86	-78.3	-79.7	3	(181/14)	(125/7)	-4.8	Hz
KFR106_DZ5	100.5	101	-93.3	-93.7	3	(012/12)	(344/16)	-4.8	Hz
KFR106_DZ6 <sup>3)</sup>	153	157	-142.4	-146.1	3	(098/19)	(116/7)	-4.7	Hz
HFR106_DZ1 <sup>3)</sup>	38	40	-30.9	-32.6	1	-	(233/7) <sup>1)</sup>	-4.5 <sup>2)</sup>	Hz
KFR101_DZ3 <sup>3)</sup>	179	186	-142.0	-147.5	3	-	(124/18)	-4.9	Hz
<b>DZs excluded from the stochastic modelling</b>									
KFR101_DZ4	197	213	-156.0	-168.2	2	(120/90)	-	<-8	-
KFR105_DZ5	293.6	304	-154.7	-156.2	2	(319/88)	(317/85)	-8.3	NW
HFR101_DZ2	101	115	-90.9	-103.6	1	-	(9/86) <sup>1)</sup>	-5.6 <sup>2)</sup>	-

<sup>1)</sup> Orientation has low confidence, estimated from BIPS inspection of percussion borehole.

<sup>2)</sup> HTHB data.

<sup>3)</sup> Alternatively, part of deterministic SBA-structures .

<sup>4)</sup> SHI confidence level: 1= low, 2 = medium, 3 = high.

<sup>5)</sup> Orientation estimated from PFL-f data (Figure A-3).

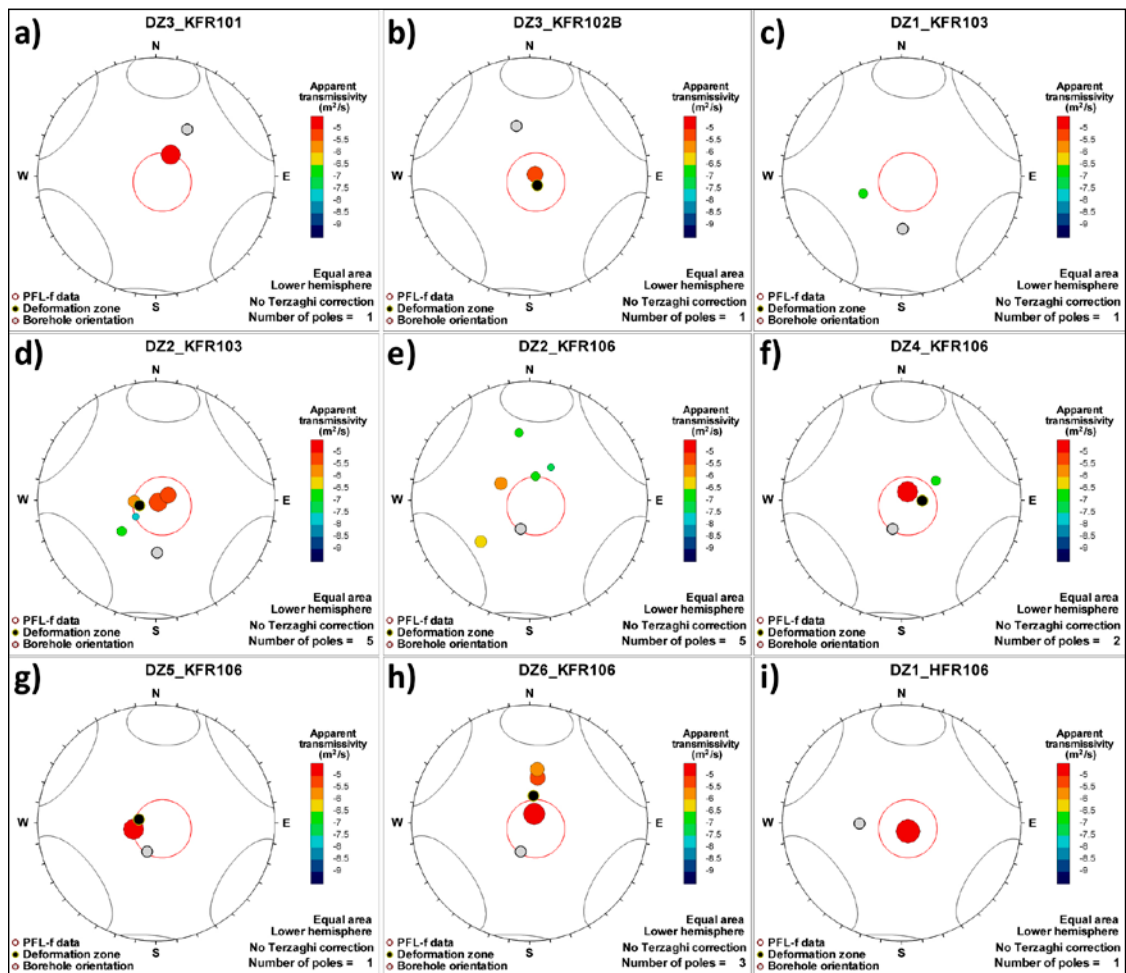


**Figure A-3.** PFL-f in sub-horizontal, Unresolved PDZ, located near the wedge between ZFMNNW1034 and the Northern boundary belt.

## A.2 Hypothesis on spatial inference

The most basic approach would be to assume a poissonian spatial distribution of the Unresolved PDZs (i.e. uniformly distributed in space). Such an approach is expected to exaggerate model heterogeneity (or performance uncertainty). However, model heterogeneity can potentially be reduced by formulating a hypothesis to constrain the spatial pattern by geometrical/geological inference. Therefore, the possibility to infer a spatial pattern of PDZs coupled to deterministic structures (Figure A-1) is considered. This inference must be made cautiously, as Figure A-1 entails a biased picture, caused by *borehole coverage*, *borehole orientations*, and *variable data quality*. Conditional simulation imposes a risk of being non-conservative, as it may underestimate the potential existence of PDZs in rock volumes that are poorly covered by borehole data (e.g. the southern part, indicated by orange rectangle in Figure A-1).

Nevertheless, a hypothesis is put forward, where the hydraulically most significant Unresolved PDZs (red oval in Figure A-1) are associated to the wedge between the Northern boundary belt and ZFMNNW1034 (Figure A-4). The data at hand are not enough to provide solid evidence for this inference. However, consideration to the rock-mechanical conditions around the wedge provides conceptual support. During deformations in the surrounding bedrock, tensional stress tends to concentrate in thin rock blocks with small acute angles (e.g. the wedge); this makes them more prone to breakage. The freedom of movement is also higher close to large ambient deformation zones (i.e. the Northern boundary belt). Owing to the high horizontal in situ stress, an increased fracturing can, in turn, reduce the normal stresses over fractures, particularly in presence of gently dipping structures. In the South-eastern part of the SFR Regional domain, the extension of ZFMNNW1034 forms a wedge against the Southern boundary belt, potentially with similar rock-mechanical conditions for hydraulically significant horizontal to gently dipping features. Therefore, the Southern boundary belt (i.e. numerically represented by ZFMWNW1035) is assumed to have a similar role, although it cannot be explicitly inferred from data. The structures used in numerical simulations are shown as brown surfaces in (Figure A-4; exclusion of the Northern boundary belt close to SFR is motivated below).

Conditional simulation does not only honour the *existence of PDZs*, where they are found in boreholes, but also their *non-existence* at locations where they are known to be absent (i.e. borehole locations or ground surface intersections). For example, KFR102A, KFR104 and KFR105 (and possibly KFR27) have no Unresolved PDZs judged to be of significance for the hydrogeological model (blue rectangle in Figure A-1). Also, the Silo and its surrounding tunnels of the existing SFR provide evidence that, although several PDZs are present (light-blue rectangle in Figure A-1), they must be of lesser hydraulic significance. Note the lack of Unresolved PDZs close to the tunnel intersection of ZFMNW0805B, suggesting a different character of the Northern boundary belt close to SFR.

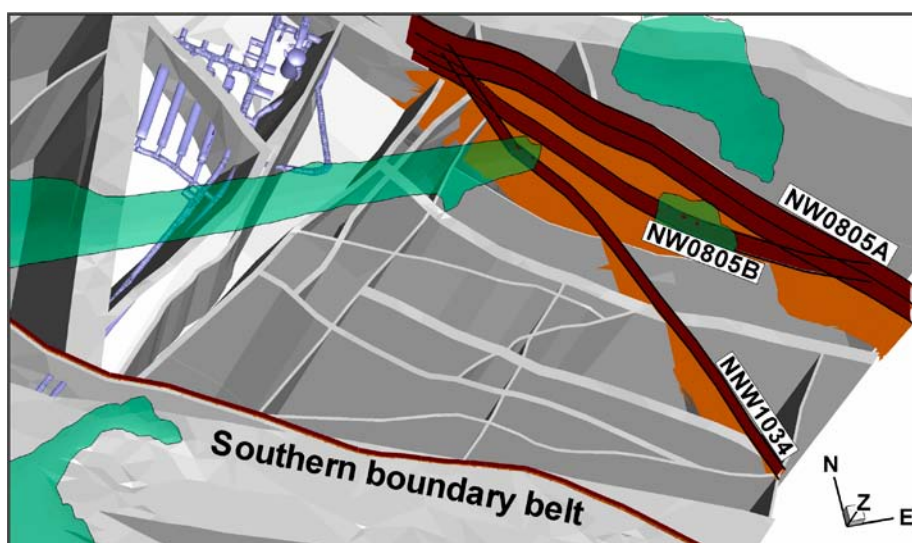


**Figure A-4.** Structures assumed related to existence of high-transmissive Unresolved PDZs. The hydraulically most significant features (red oval in Figure A-1) are located close to or inside the wedge between the Northern boundary belt (ZFMNW0805A and B) and ZFMNNW1034. The Southern boundary belt is expected to have a similar role. Stochastic generated PDZs are conditioned to be in direct contact to brown surfaces.

Hence, the existence of PDZs is not assumed to be directly linked to the Northern boundary belt, but instead to the wedge it forms with ZFMNNW1034 (Figure A-4). This wedge has been identified as an important vertical connection between the overlying sea (positive hydraulic boundary) and the predominantly sub-horizontal to gently dipping flowing fracture network (Chapter 5, main report).

Numerical simulation is useful to account for complex 3D geometrical conditions and to compensate for geometrical bias factors. Hence, it is explored if a few simple criteria are sufficient for providing a reasonable realistic spatial inference for the Unresolved PDZs, and a numerical calibration procedure is set up to test if the hypothesis allows a probabilistic estimation of the underlying size distribution for the Unresolved PDZs. The selected features are presented in Table A-2. Note that three PDZs were excluded from this analysis. The reason for this is that they have been interpreted to be of lesser hydraulic significance (Table A-2).

The Unresolved PDZs are generated as stochastic planar features (with homogeneous transmissivity) that are conditioned by their borehole intercept. The stochastic components are assumed to be: 1) size (specified by square side-length), 2) the exact location in 3D space, 3) the exact orientation. The orientation of the Unresolved PDZs was based on estimations from PFL-f data (Table A-2).

Three criteria are defined to retain generated features:

- 1) Honour the location and orientation at its conditional borehole intercept (Table A-2), and
- 2) be in direct contact with the hypothesised structural wedge (Figure A-4), and
- 3) most importantly – honour the geologically interpreted *absence* of PDZs in surrounding boreholes (Figure A-5), the existing SFR, and ground-surface intercepts exceeding 300 m (Section A.3.2).

A probabilistic approach is then taken to test a range of possible sizes (side lengths were varied from 1 to 300 m) and to evaluate the fractions of fulfilled criteria (1 to 3, above) as a function of size. Features lacking contact to the wedge (criterion 2) are classified as “*too small*”, features dishonouring data on absence of PDZs (criterion 3) are classified as “*too large*”, while features that fulfil all criteria are classified as “*OK*” (see Figure A-8, Figure A-9, Figure A-10).

Criterion 2 is motivated by the high-transmissivities measured after several days of pumping. The wedge has been interpreted as an important vertical connector between the overlying sea (positive hydraulic boundary) and the sub-horizontal to gently dipping flowing fracture network (Öhman et al. 2013).

Concerning criterion 3, uncertainty exists to which borehole data are valid information for conditioning absence of PDZs. For example, can a junction between a deterministic structure (ZFM) and the so-called Unresolved PDZ be distinguished in the SHI methodology? Or, put in other words, can a borehole interval covering a deterministic structure (ZFM) be considered as evidence for absence of Unresolved PDZs? A similar question concerns the data quality of percussion boreholes (as well as the upper 147.5 m of KFR27 with unavailable core); are data lacking support from core valid as evidence for the absence of Unresolved PDZ?

Hence, three Cases for *conditioning the absence of PDZs* are compared:

- 1) All boreholes in their entire extent – except casing and the particular borehole, where the PDZ was originally identified – are used for conditioning. In other words, an intercept with a so-called Unresolved PDZs *are assumed to be identifiable* in borehole sections identified as deterministic structures (ZFM or SHI PDZ; see example in Figure A-5b).
- 2) Only borehole intervals defined as outside PDZ in the SHI are used for conditioning. In other words, potential junctions with so-called Unresolved PDZs *are assumed to be concealed* inside borehole sections identified as deterministic structures (ZFM or SHI PDZ; visualised as orange cylinders in Figure A-5).
- 3) Only intervals defined as outside PDZ in the original SHI in **cored boreholes** are used to condition absence of PDZs. In other words, this is the same as case 2), but percussion boreholes (as well as upper part of KFR27) are excluded from conditioning, due to poorer data quality (see example in Figure A-5c).

### A.2.1 Identifying borehole intervals with geometrically possible cross-hole intercepts

In order to provide a preliminary estimate of the significance of how conditional data are used (Cases 1 to 3), a test was made with 10,000 realizations of each PDZ having a side length of 500 m. Note that 500 m is not considered to be a realistic size; the intention of using excessive size is to evaluate the potential of intersections inside borehole intervals classified as ZFM or SHI PDZ (Table A-3).

**Table A-3. Probabilistic estimation of potential cross-hole intersections. Probability is indicated by number of intersections (red = high, blue = low).**

Intersection	KFR101_DZ3	KFR102B_DZ1	KFR102B_DZ3	KFR103_DZ1	KFR103_DZ2	KFR106_DZ1	KFR106_DZ2	KFR106_DZ4	KFR106_DZ5	KFR106_DZ6	HFR106_DZ1
Casing <sup>1)</sup> of KFR101									62		
Casing <sup>1)</sup> of KFR102A				10,000	1,488			131	1,969		1,590
Casing <sup>1)</sup> of KFR102B									138		
Casing <sup>1)</sup> of KFR103									140		
Casing <sup>1)</sup> of KFR106					13						
Casing <sup>1)</sup> of KFR27									105		
KFR101_DZ3 <sup>2)</sup>	x									150	
KFR101_DZ4 <sup>2)</sup>										190	
KFR102B_DZ1 <sup>2)</sup>		x						65	121		92
KFR102B_DZ3 <sup>2)</sup>			x							19	13
KFR103_DZ1 <sup>2)</sup>				x					44		10
KFR103_DZ2 <sup>2)</sup>					x			301	362		429
KFR105_DZ5 <sup>2)</sup>			22					1		18	
KFR106_DZ1 <sup>2)</sup>					209	x					1,008
KFR106_DZ2 <sup>2)</sup>					563		x				562
KFR106_DZ4 <sup>2)</sup>			17	106	74			x			
KFR106_DZ5 <sup>2)</sup>			20	48	40				x		
KFR106_DZ6 <sup>2)</sup>				17						x	
Missing core in KFR27 <sup>3)</sup>			4,230		6,074			460	540	131	1,530
ZFMENE3115 <sup>4)</sup> in KFR104			50		102						
ZFMENE3115 <sup>4)</sup> in KFR105		160	71		56						4
ZFMNE3112 <sup>4)</sup> in KFR102B										91	54
ZFMNE3112 <sup>4)</sup> in KFR104	59		60								
ZFMNE3112 <sup>4)</sup> in KFR105			58								18
ZFMNE3118 <sup>4)</sup> in KFR104					84						
ZFMNE3137 in KFR102A <sup>5)</sup>		1,257	994							454	30
SBA 6 in KFR102A <sup>2)</sup>	3,312	807									
ZFMNE3137 <sup>4)</sup> in KFR102B					290			10		47	114
ZFMNE3137 <sup>4)</sup> in KFR104	6										
ZFMNE3137 <sup>4)</sup> in KFR105			53							4	1
ZFMNNW1034 <sup>2)</sup> in KFR101		9,621		9,193	2,964			1,322	1,631		2,258
ZFMNNW1034 <sup>2)</sup> in KFR106	130										
ZFMNNW0805B <sup>2)</sup> in KFR101				25	1,460			903	721	154	604
ZFMWNNW0835 <sup>2)</sup> in KFR27		511	1,244					52		1	157
ZFMWNNW3262 <sup>2)</sup> in KFR103										823	
ZFMWNNW3262 <sup>2)</sup> in KFR106				267	236						
ZFMWNNW3267 <sup>4)</sup> in KFR104	75										
ZFMWNNW3267 <sup>4)</sup> in KFR105			64					5		34	
ZFMWNNW8042 <sup>4)</sup> in KFR105			28					1			9

<sup>1)</sup> Borehole sections inside casing provide no evidence for absence of PDZs.

<sup>2)</sup> Unlikely to provide evidence for absence of PDZs (hydraulic signature potentially masked).

<sup>3)</sup> The quality in upper part of KFR27 with unavailable core assumed equivalent to percussion boreholes.

<sup>4)</sup> Low probability of intersection.

<sup>5)</sup> Borehole section used as evidence for absence of PDZs.

For example, the upper part of KFR27 may provide bounds for the extension of KFR102B\_DZ3 and KFR103\_DZ2, depending on how its data quality is judged (Cases 1 to 3). Some borehole sections (e.g. casing, other Unresolved PDZ intervals, ZFMNW0805B, ZFMWNW0835, ZFMNNW1034, and SBA6) have frequent PDZ intercepts; in these intervals it is unlikely that a “Unresolved PDZ” could have been resolved in geologic/hydrogeologic interpretation and hence it is considered valid to exclude these borehole sections discriminating PDZ extension in Case 2. On the other hand, in most of the low-transmissive borehole sections (where the hydraulic signature of an Unresolved PDZ is expected to be identifiable), the probability of intersection was considered negligible (shown by grey colour in Table A-3). One exception is ZFMNE3137 in KFR102A; it was decided retain this borehole section for bounding the size estimate of KFR102B\_DZ2 and KFR102B\_DZ3 (based on hydraulic signature).

### A.3 Set-up of conditional simulations

Unresolved PDZs are generated as square planes with a side-length randomly ranging from 1 m to 300 m (uniform distribution). A random component  $\pm 10^\circ$  (uniform distribution) was added to both the strike and dip of the estimated orientations from PFL-f data (Table A-2; Figure A-3). In order to reduce numerical artefacts of the simplistic geometrical representation, the planes are generated with an arbitrary orientation around its pole (i.e. its normal to the fracture plane). The location of features is only partly conditioned at its borehole intercept (i.e. the borehole length specified in Table A-2). However, the intercept is allowed occur anywhere within its fracture plane and therefore the exact location in 3D space includes a stochastic component.

As an example, the suggested numerical procedure is demonstrated for KFR103\_DZ2 (Figure A-5). First, 10,000 stochastic realizations were generated for KFR103\_DZ2, where the spatial extension of features is bounded according to Case 1 (all borehole intervals except casing constrain the spatial extension; Figure A-5b). Another 10,000 realizations are generated for Case 3 (Figure A-5c), where only borehole sections with core support and defined as outside deterministic structures (ZFM or PDZs in SHI) constrain the spatial extension of stochastic features (i.e. shown by blue cylinders). Note how intersections are allowed in the casing of KFR102A (grey cylinder Figure A-5). As the result, Case 1 indicates a lower probability of features exceeding a side-length of c. 250 m, while this upper bound is less evident in Case 3 (Figure A-6).

Likewise, the approach to estimate the optimal size for all stochastic PDZs are investigated (Figure A-7, Figure A-8, Figure A-9, and Figure A-10).

The three different cases of *conditioning absence data of Unresolved PDZs* are compared for each of the 11 Unresolved PDZs (10,000,000 realisations for each PDZ). Features lacking contact to the wedge (failing criterion 2) are classified as “*too small*”, features dishonouring data on absence of PDZs (failing criterion 3) are classified as “*too large*”, while features that fulfil all criteria are classified as “*OK*” (see Figure A-7). Small features (side-lengths shorter than c. 25 m to 50 m) are typically rejected as they do not reach between the borehole intercept and the wedge (dark red). The fraction of realisations fulfilling all three criteria tends to dominate for side-lengths typically in the range 50 m to 150 m (green-shaded area). Larger features (side-lengths longer than c. 150 m) tend to be more frequently rejected due to intersections with neighbouring boreholes (blue area). As can be expected, the fraction of rejections of large features (blue shade) decreases with exclusion of borehole intervals that condition the absence of PDZs (compare the three cases in Figure A-7).

The optimal PDZ size (i.e. the size range with dominating fraction of retained realisations; green shade) varies from borehole to borehole (see Figure A-8, Figure A-9, Figure A-10). For example, the fraction of retained realisations of KFR103\_DZ1 and KFR103\_DZ2 *does not dominate for any size*; either realisations lack contact to the wedge, or they intersect borehole intervals that indicate absence of PDZs. This possibly suggests that the hypothesised inference to the wedge is less suitable for these two PDZs (it can be noted that KFR103\_DZ2 is alternatively modelled as SBA1/SBA2). On the other hand, few realisations of KFR106\_DZ1 and KFR106\_DZ6 are rejected due to intersection in neighbouring boreholes (particularly if HFR106 is excluded from conditioning absence of PDZs; Figure A-10).

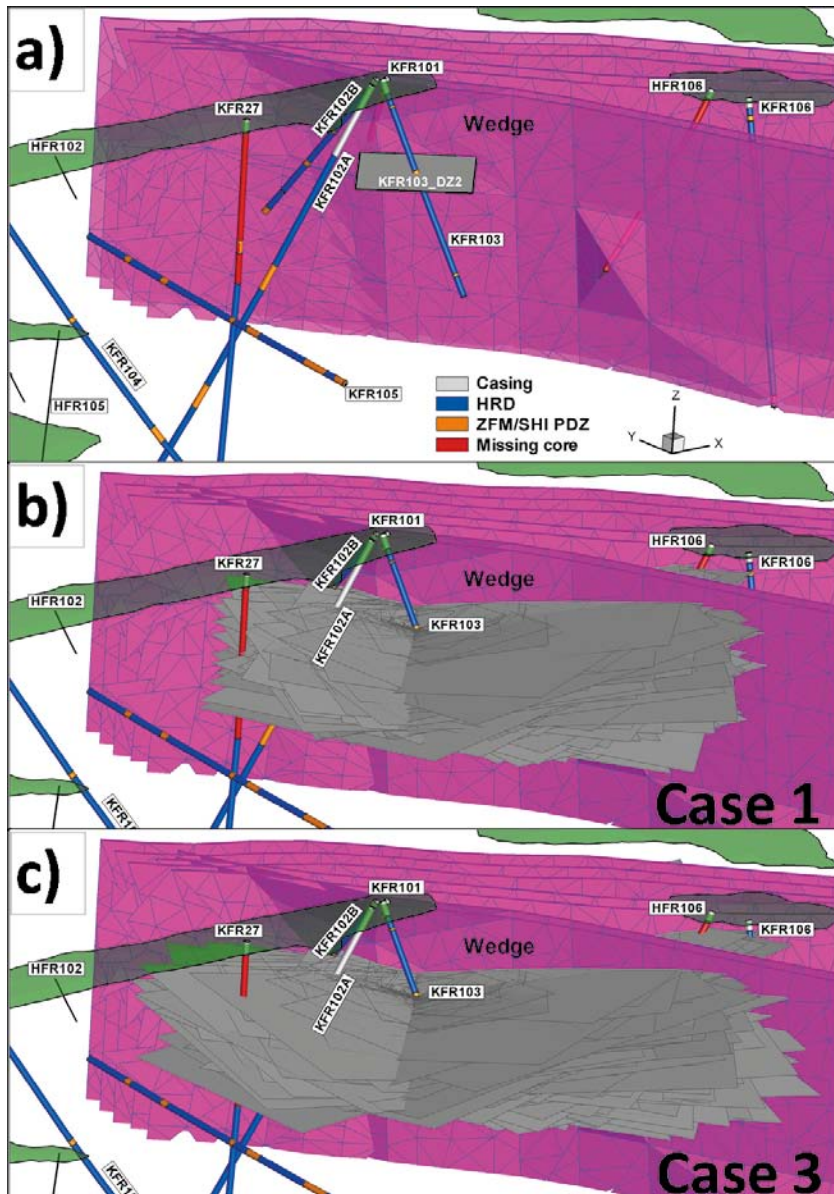


**Figure A-5.** Demonstration of a few realisations of KFR103\_DZ2 for different cases of conditioning spatial extension; a) interpreted intercept, b) Case 1, and c) Case 3. Grey cylinders indicate casing, red cylinders indicate unavailable core (HFR106 and upper part of KFR27), orange cylinders indicate intervals of deformation zone characteristics (ZFM or SHI PDZs), while blue cylinders represent intervals defined as outside SHI PDZs.

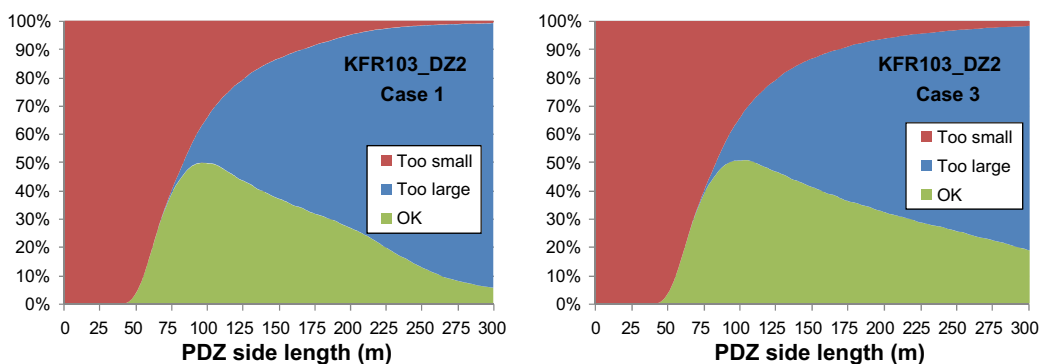


**Figure A-6.** For the example of KFR103\_DZ2, Case 1 (PDZ absence conditioned by all borehole sections outside casing; Figure A-5b), suggests that it is unlikely that the feature exceeds a side-length of c. 250 m, while this is not supported in Case 3 (where borehole intervals lacking core and/or has been classified as ZFM/DZ in SHI are excluded from conditioning; Figure A-5c).



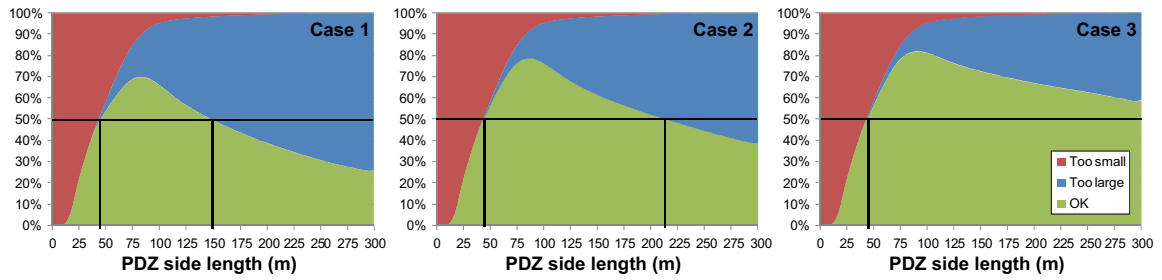


**Figure A-7.** Fraction of realisations fulfilling the conditional criteria as a function of size, and depending on conditional data for absence of PDZs; case 1) including all borehole intervals (i.e. outside casing), case 2) excluding all borehole intervals identified as PDZ in SHI, and case 3) additionally excluding all data without core. “Too small” = lacks contact to the wedge, “too large” = intersects a nearby borehole, and “OK” = fraction of realisations satisfying all criteria

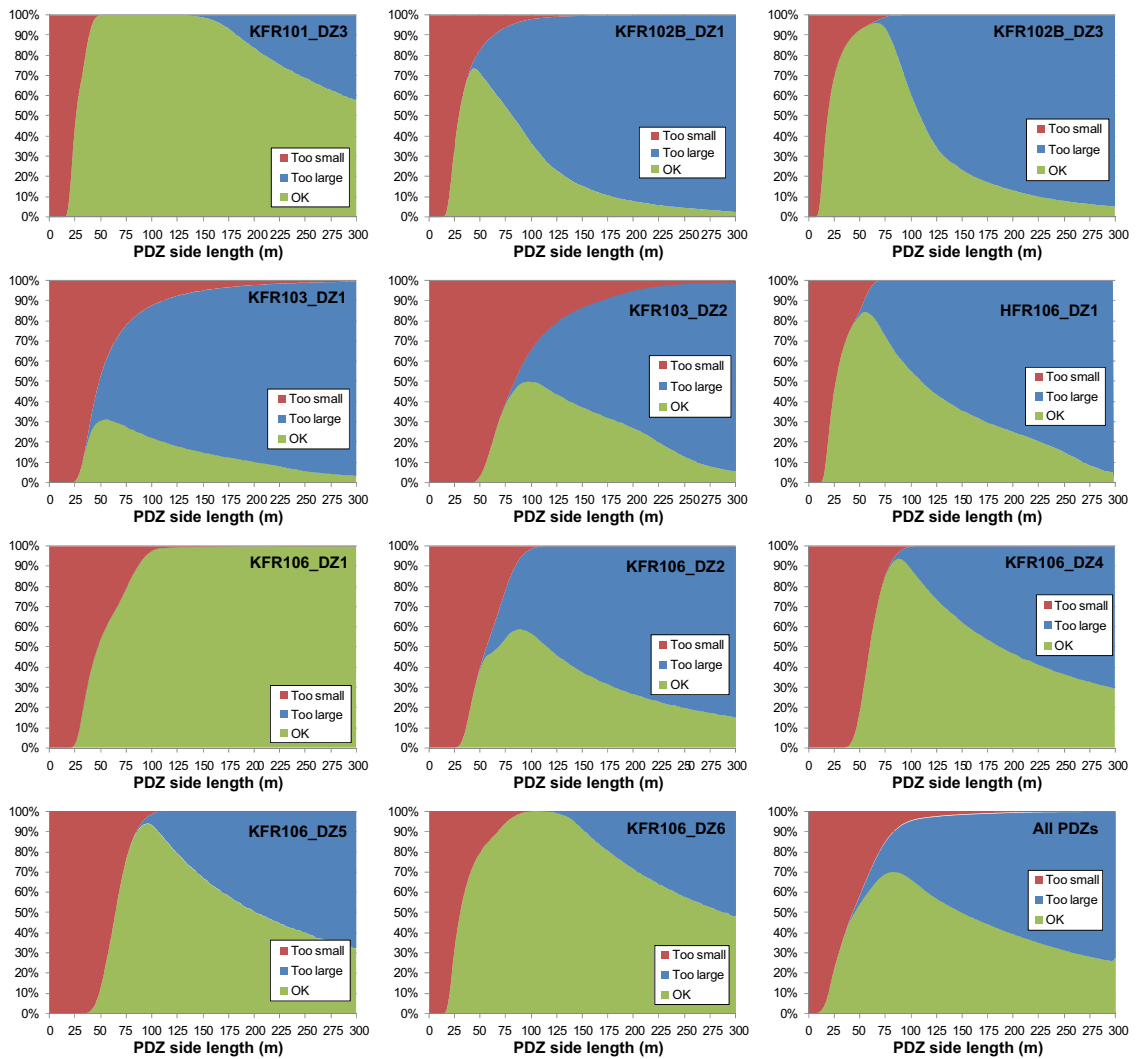


**Figure A-8.** Conditioning case 1: all boreholes in their entire extent – except casing and the particular borehole, where the PDZ was originally identified –condition absence of PDZs. Too small = lacks contact to the wedge, too large = intersects a nearby borehole, and OK = fraction of realisations satisfying all criteria.

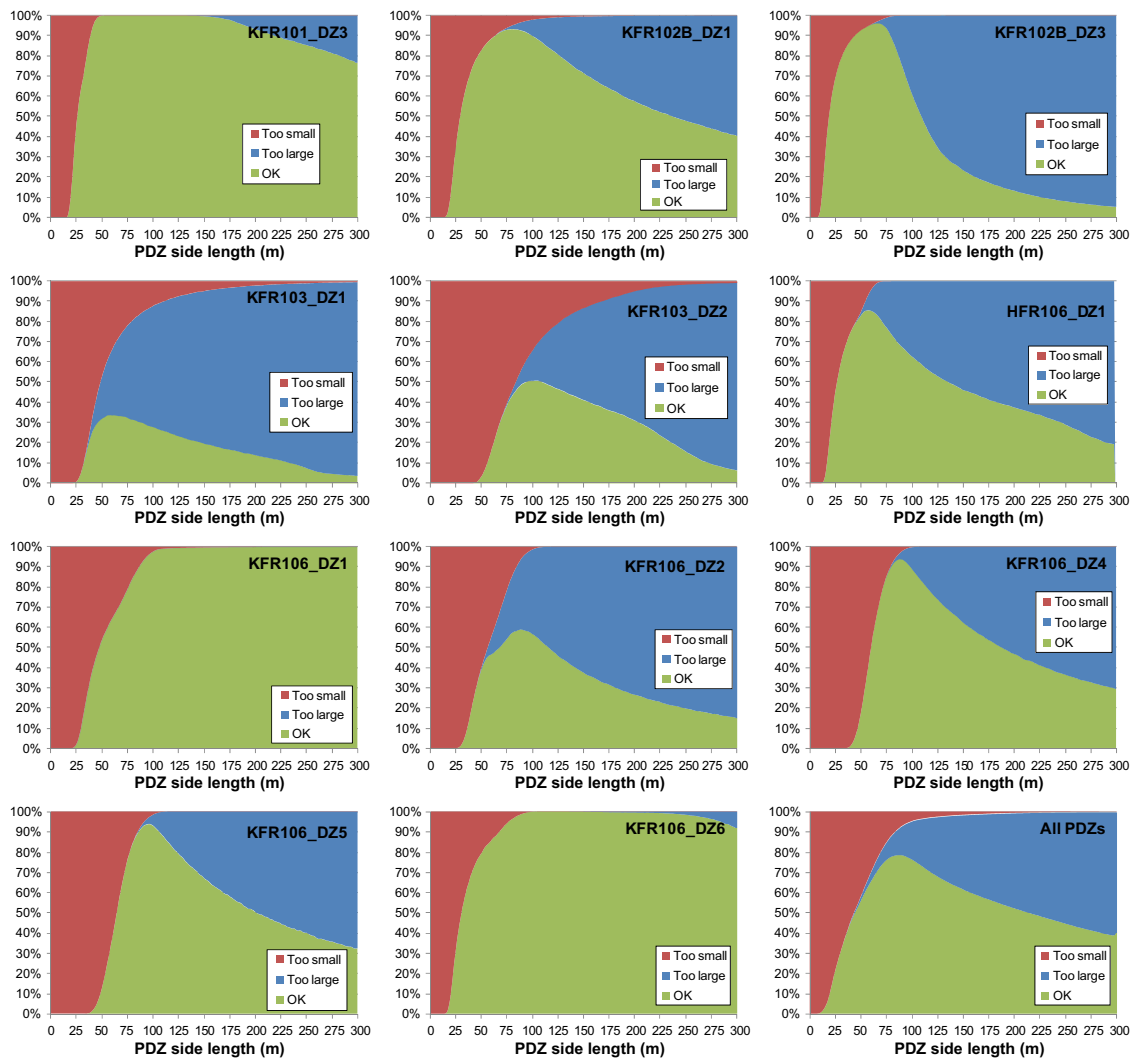


**Figure A-9.** Conditioning case 2: only borehole intervals defined as outside PDZ in the original SHI condition absence of PDZs. Too small = lacks contact to the wedge, too large = intersects a nearby borehole, and OK = fraction of realisations satisfying all criteria.

### A.3.1 Preliminary regional-scale demonstration for 11 Unresolved PDZs

After the probabilistic size estimation at known intercepts close to the structural wedge, a recipe must be formulated to cover the spatial distribution of Unresolved PDZs on the regional scale. At the regional scale generation, the Southern boundary belt is therefore assumed to have an equivalent role (hydraulic and geological boundary) in controlling the existence of PDZs. In other words, stochastic features are required to be in contact to either the structural wedge or the Southern boundary belt (Figure A-11). Two preliminary full-scale realisations are demonstrated including all 11 Unresolved PDZs (in spite of the fact that four are alternatively included in the deterministic so-called SBA-structures).

The generation procedure can be described as follows. Stochastic features are randomly generated within a generation volume with an elevation interval from 0 to  $-200$  m (cf. Figure A-2) and within a lateral extent exceeding the SFR regional model volume by at least 300 m. Only features in contact with the wedge or the Southern boundary belt are retained (Figure A-11). The size distribution for each PDZ is taken from the probabilistic estimation on individual basis, i.e. the size distributions are equivalent to the green-shaded areas shown in Figure A-8 (case 1). Each PDZ is randomly generated until a *retained* feature (i.e. in contact with wedge or the Southern boundary belt) is intercepted by an arbitrary borehole (shown in Figure A-11). In other words, until its expectation value has been reached. This intersected feature does not honour the conditional data (intersection in correct borehole and at the exact location). Therefore, the intersected feature is removed and replaced by a random feature from the conditioned realisation (e.g. Figure A-12a and c). Thus, the end result is a random realisation with the correct expectation value, and where intercepts are conditioned to the exact boreholes location (Figure A-12b and d).

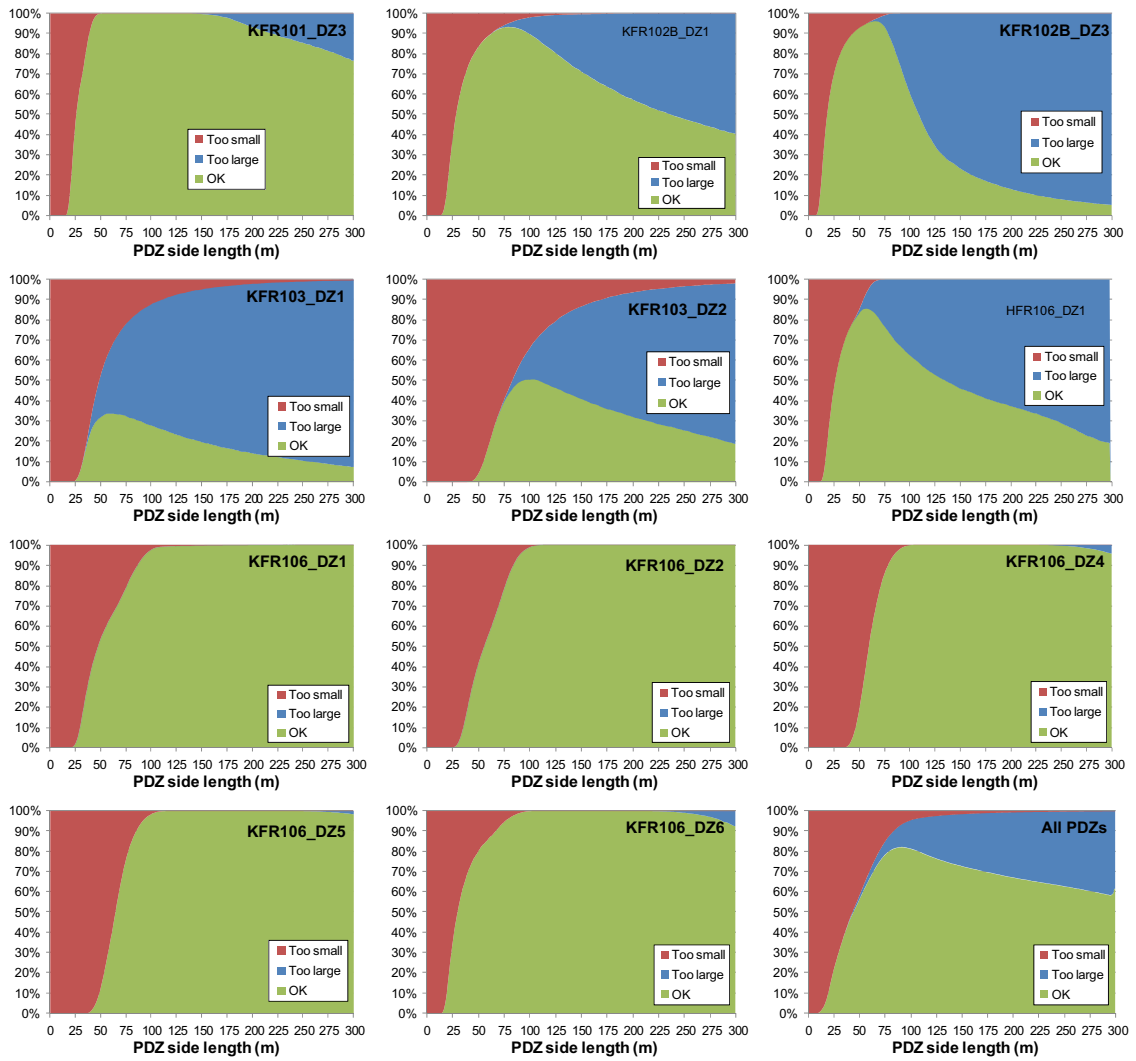


**Figure A-10.** Conditioning case 3: only core data used, intervals defined as outside PDZ in the original SHI condition absence of PDZs. Too small = lacks contact to the wedge, too large = intersects a nearby borehole, and OK = fraction of realisations satisfying all criteria.

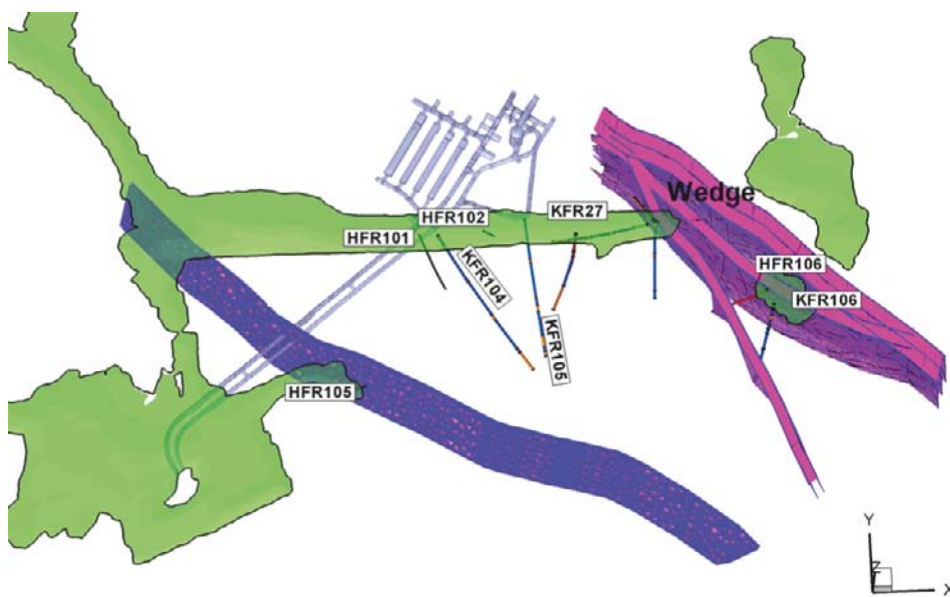


**Figure A-11.** Demonstration of stochastic realisations. Geological structures used as conditional contact boundaries for generated stochastic features are shown in purple.

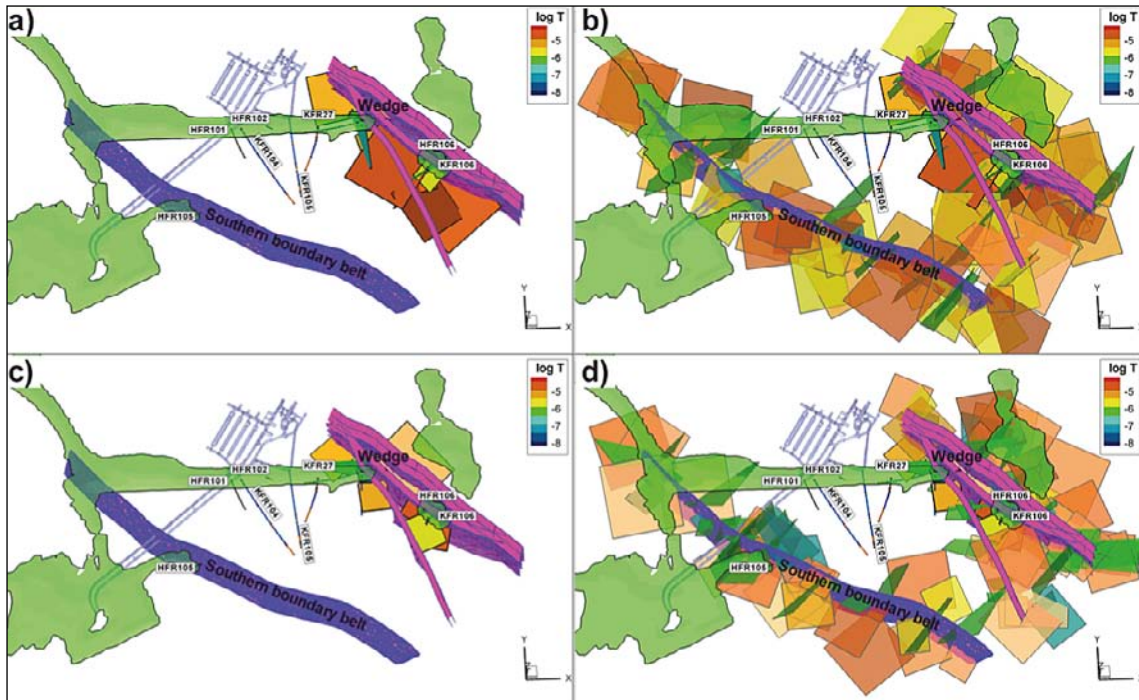


**Figure A-12.** Demonstration of two stochastic realisations of retained features; a, c) features conditioned by borehole intercepts, and b), d) merged with stochastic features that are **not** intercepted by boreholes.

In effect, the network Unresolved PDZs forms a fringe around the Central block (i.e. the target area for the SFR extension) that is hydraulically connected to the Southern boundary belt and the structural wedge. The impression is that the pattern to some extent is artificial, formed by existing borehole locations, data gaps, and the postulated hypothesis for inference. Nevertheless, it provides potential guidance to the expectation in the southern corner of the SFR model domain, which particularly suffers from data gaps (obviously depending on the validity in the postulated assumption for geologic inference).

The simulations presented in Figure A-12 are only intended as a preliminary demonstration, as two issues have not yet been addressed:

- 1) Four PDZs are alternatively associated to the so-called SBA-structures (Table A-2); these can alternatively be included in deterministically modelled SBA-structures (see Appendix B, Figure A-15).
- 2) There exists several ground-surface intercepts of steeply dipping structures. It could be argued that if such intercepts indeed exists, any trace length exceeding the resolution level of the geologic model should have been included as deterministic structures (ZFM). Hence, the possibility to use ground surface intersection to constrain the size of stochastic features is examined in Section A.3.2.

### A.3.2 Ground-intercept conditioning for steeply dipping structures

Ground-surface intercepts of gently dipping structures are difficult to identify in geological modelling, and therefore large uncertainties exist concerning outcropping (even if potential outcropping of gently dipping structures should exceed the resolution level set for the geological model). Hence, conditional trace length thresholds cannot be motivated for stochastic gently dipping structures.

However, two of the Unresolved PDZs are identified as steeply dipping (KFR102B\_DZ1 and KFR106\_DZ1; Table A-2). Based on expected terminations against deterministic structures (Northern boundary belt), geological interpretation have estimated a spatial extension of c. 150 to 200 m. It can be argued that it is unrealistic to generate such features without taking the geological model resolution into account; should these PDZ have ground surface intercepts exceeding 300 m, they could

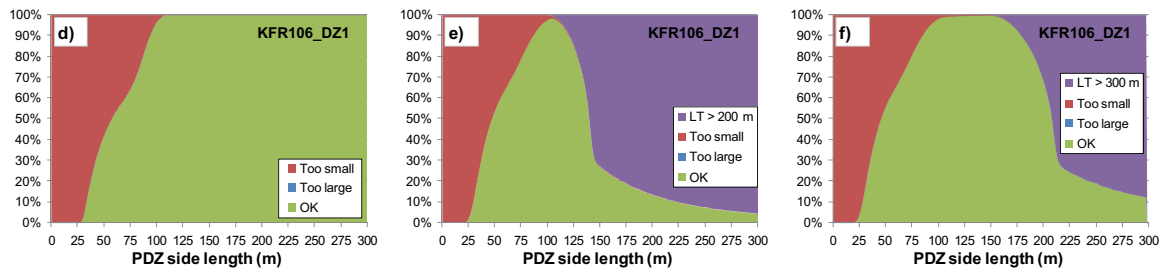


**Figure A-13.** KFR102B\_DZ1 and KFR106\_DZ1 constrained by ground intercepts: a) and c) only using borehole data (case 1), b) and e) rejecting realisations with trace length,  $L_T > 200$  m, c) and f) rejecting realisations with trace length,  $L_T > 300$  m.

have been identified as lineaments in the geological modelling (depending on data quality). Hence, additional constraints in ground-surface intercepts can be applied to improve their probabilistic size estimation. The size-distribution estimation was therefore re-processed for the two steeply dipping Unresolved PDZs (rejections due to long trace lengths,  $L_T$ , shown with purple shade in Figure A-13). Two trace-length thresholds are compared 200 m and 300 m, respectively; however, note that the 200 m truncation limit is only included for reference. Only the 300 m threshold is conceptually justified by the resolution of the geological model. The additional criterion from ground-surface intersection is particularly important for KFR106\_DZ1, as it is not geometrically constrained by surrounding boreholes (Figure A-13d).

Results indicate that the ground-surface intersection constrain has little impact on KFR102B\_DZ1 (as it is already well-constrained by surrounding boreholes; cf. Figure A-13a, b, and c). In comparison, the ground surface criterion is far more important for the shallow located KFR106\_DZ1 (cf. Figure A-13d, e, and f). Results indicate that few features with a side length longer than 200 m satisfies the 300 m threshold (Figure A-13f), which agrees well with the geologically estimated length (c. 150 m to 200 m).

#### A.4 Summary and conclusions

The existence of Unresolved PDZs causes uncertainty in the hydraulic modelling (particularly with consideration to the location of boreholes with respect to the planned SFR extension and gaps in borehole coverage; Figure A-1). The Unresolved PDZ data set is inhomogeneous in terms of confidence in existence, hydraulic significance, and data quality. Only a handful (11 out of totally 31) has been identified as particularly important for the hydrogeological modelling at SFR and selected for numerical model implementation. Note that 4 of these 11 Unresolved PDZs are alternatively included in deterministic SBA-structures (Table A-2).

A hypothesis has been suggested where the existence of 11 Unresolved PDZs is related to a structural wedge (between the Northern boundary belt and ZFMNNW1034; Figure A-4), as well as, along the Southern boundary belt. Based on this hypothesis, a numerical calibration procedure has been undertaken to provide probabilistic size estimates (e.g. Figure A-5), as well as, a reasonable representation at the regional scale. Three Cases were compared to examine the role of conditional absence of PDZs in the probabilistic estimation of size distributions. The Unresolved PDZs are numerically represented as square planes with homogeneous hydraulic properties, although this is known to be an unrealistic overrepresentation of this type of large, high-transmissive structures. In the light of this, it was decided to propagate Case 1 (which provides the most constrained estimated size estimations) to the DFN modelling (Appendix G).

In summary, results indicate that the information on absence of PDZ intercepts in surrounding boreholes can partly constrain the range of possible size (i.e. depending on: 1) the validity in the postulated hypothesis and 2) the data quality in surrounding boreholes).

Given the constraining power of surrounding borehole coverage and ground-surface intercepts, the PDZs should be represented with a side-length of c. 50 to 175 m. In other words, it is unlikely that the structures can be much larger without intersecting surrounding boreholes. Shorter structures tend

to lack direct contact with the wedge and are hence less likely to yield high-transmissive continuous flow. The estimated size distributions of Case 1 combined with constraints in trace length of ground-surface intercepts are summarized in Figure A-14 (i.e. the fraction of retained realisations as a function of size, corresponding to the green area in Figure A-8 combined with Figure A-13c and f). Note that these size distributions only reflect the probability of bounds for size; it does not infer the type of size distribution, e.g. power-law scaling.

The postulated hypothesis, with geometrical inference to the Northern and Southern boundary belts, forms a hydraulically connected fringe of Unresolved PDZs around the Central block (i.e. the target area for the SFR extension Figure A-15b). Thus, in regional-scale modelling, the Unresolved PDZs (as well as deterministic SBA-structures) have a key role in connecting the flowing fracture network inside the Central block to the Northern and Southern boundary belts. In the regional-scale implementation, 4 Unresolved PDZs are modelled as part of the SBA-structures (Figure A-15a), while the stochastic representation of Unresolved PDZs is only based on the remaining 7 (Figure A-15b, i.e. features that are not part of the SBA-structures). The regional-scale generation sequence is described in Section A.3.1. The 7 Unresolved PDZs are generated separately, retaining only features in contact with defined boundaries (Figure A-11). The generation is stopped when a retained feature is intersected by an arbitrary borehole. The feature with arbitrary intersection is removed and replaced by a random realisation of the conditional intersection. The end result is regional-scale coverage with the correct expectation value and conditional intercepts.

This model concept relies on the realism of the postulated hypothesis for geological inference, which is not well-underpinned by data. The lack of hydraulically significant features of this type in the vicinity of the Silo is a clear exception to the hypothesis and the reason for this is not fully clear. Although the historic data is of lower quality, it provides a considerably higher density in borehole coverage close to the Silo. In combination with tunnel information this location provides a considerably better deterministic hydraulic determination. One possible explanation could be that the deterministically modelled ZFM871 (just below SFR) and SBA7 (just above SFR) are both part of the pattern studied in this approach (i.e. the difference in interpretations and definitions may partly relate to the fact that different data types cover different parts of the domain).

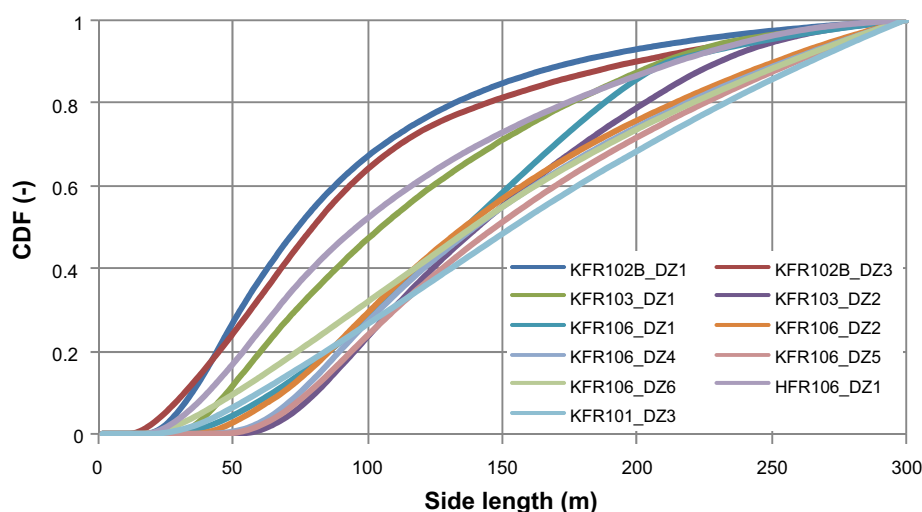


**Figure A-14.** Optimised size distributions based on conditional data from boreholes (case 1) as well as ground surface intercepts. Used for generating stochastic features (corresponding to green-shaded areas in Figure A-8).

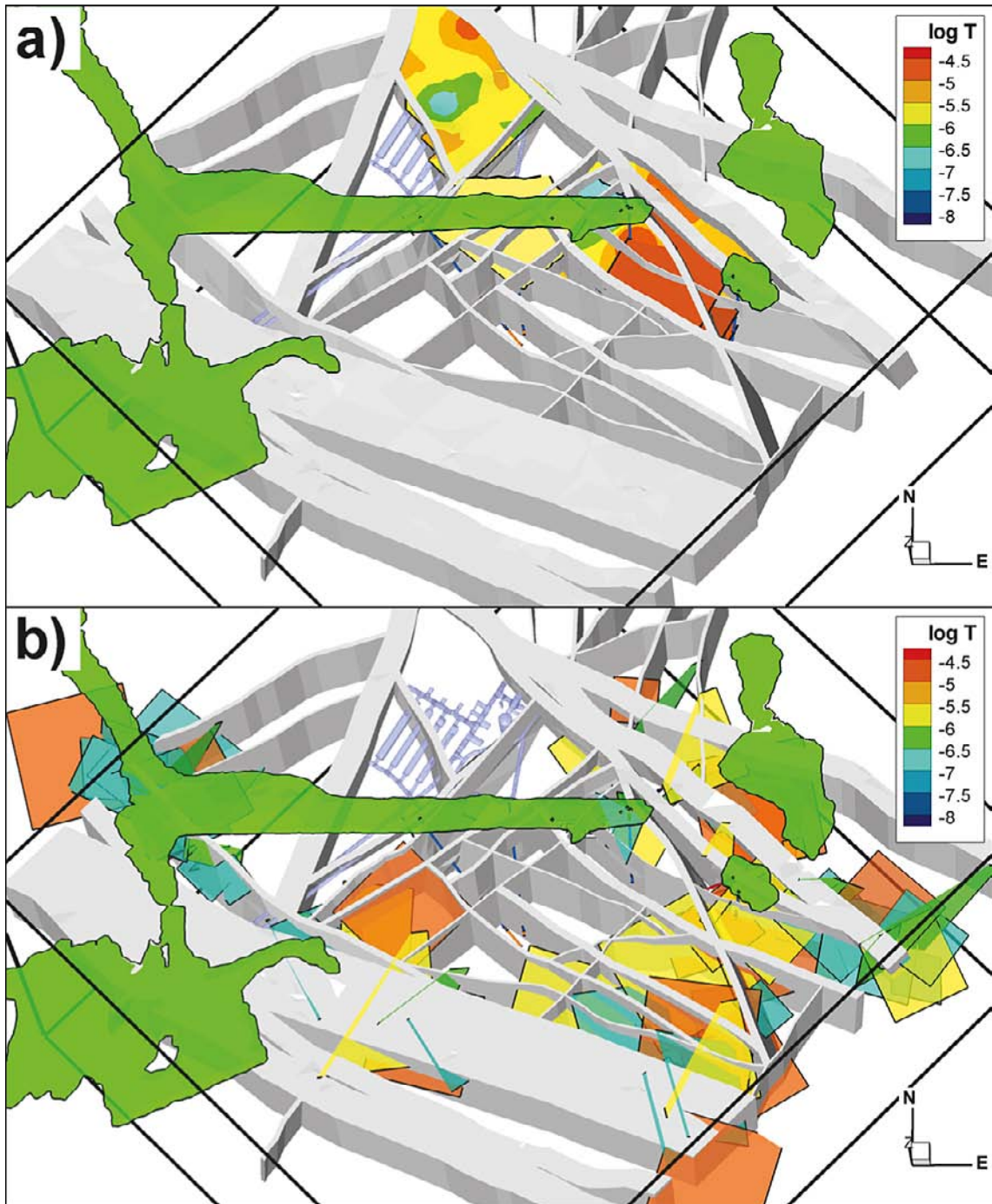


**Figure A-15.** Overview of the interpreted spatial pattern of the most hydraulic significant structures; a) deterministically modelled SBA-structures (including 4 Unresolved PDZ intercepts) and b) stochastic representation of the remaining Unresolved PDZs (based on the 7 conditional intercepts).

## Deterministic model of Shallow Bedrock Aquifer (SBA) features

### Conceptual model

The established modelling methodology divides the bedrock into two hydraulic units: 1) deterministic deformation zones (HCD) and 2) stochastic fractures outside zones (HRD; Figure 2-1; main report). A conclusion from the hydrogeological-data interpretation is that the upper c. 200 m of the bedrock is hydraulically dominated by a system of high-transmissive, connected, sub-horizontal fractures. An alternative supplement to the established methodology is therefore to introduce a deterministic interpretation of the most prominent responses in the superficial bedrock. This additional model component is referred to as SBA-structures (details of the underlying data support are presented in Appendix H). The purpose of modelling these data separately is to honour deterministic data and to avoid an overly pessimistic representation in the stochastic model component (i.e. to exclude high-transmissive features, which are not perceived as uniformly distributed, from the Hydro-DFN model). The motive for dividing the model into HCD, Unresolved PDZs, SBA-structures, and HRD is described in Chapter 5.3 (main report) and the statistics of their final distinction is presented in Appendix G.

The SBA-structure modelling was based on informed judgement of cross-hole hydraulic interferences (see Section 4.4.2) coupled to borehole intercepts with anomalous PFL-f transmissivity (or HTHB data in percussion drilled boreholes). The selected PFL-f data were sub-horizontal and, with one exception, high-transmissive ( $T \approx 10^{-6} \text{ m}^2/\text{s}$ ). The selection of borehole intercepts was supported by hydraulic head data, meaning that boreholes intersecting the same feature show similar drawdown. In several cases the location and orientation of the intercepts are supported by oriented radar reflectors and other geophysical data (Table B-1). The features were terminated against modelled deformation zones and/or borehole intercepts lacking hydraulic responses. The details in the underlying data in borehole intercepts and the modelling philosophies are presented in Appendix H. As the result, six SBA-structures, SBA1 to SBA6, are defined based on data from the recent field investigations (shown in Figure 6-3; main report). A seventh structure, referred to as SBA7 (See Appendix D), has been defined by Curtis et al. (2011), based on the original interpretation of zones H1 and H3 by Carlsson et al. (1985). Finally, an eighth structure, referred to as SBA8, is extrapolated between tunnel mapping and a nearby transmissivity anomaly (Figure D-3); this extrapolation is considerably more uncertain, as it less underpinned by hydrogeological data.

It should be pointed out that in reality each SBA-structure is envisaged as a network of connected sub-horizontal fractures, rather than a single fracture, and that the extension outside borehole coverage is highly uncertain. Also, the deterministically modelled features are probably only a sub-set of the total number of horizontal hydraulic conductors in the model area, since only features intercepted by boreholes are possible to observe. Different strategies to compensate for this are suggested in Section 5.6, main report.

**Table B-1. Summary of modelled borehole intercepts for deterministic Shallow Bedrock Aquifer (SBA) structures.**

Feature	Borehole	Intercept (length m)	Supporting data (in addition to interferences and PWH)
SBA1	KFR27	55	5m PFL, radar reflector, geophysics
SBA1	HFR102	eoh <sup>1)</sup>	Interference only
SBA2	KFR27	98	5 m PFL, geophysics
SBA2	KFR102A	72	PFL-f (concealed behind installed steel pipe)
SBA2	KFR103	86	PFL-f, Unresolved PDZ
SBA3	KFR103	86	PFL-f, Unresolved PDZ
SBA3	HFR106	39	HTHB, radar reflector, Unresolved PDZ
SBA4	KFR103	182	PFL-f (alternative to ZFMWNW3262)
SBA4	KFR106	71	PFL-f, radar reflector, (alternative to ZFMWNW3262)
SBA5	KFR103	182	PFL-f (alternative to ZFMWNW3262)
SBA5	KFR106	155	PFL-f, radar reflector, Unresolved PDZ
SBA6	KFR27	193	PFL-f, radar reflector
SBA6	KFR101	181	PFL-f, radar reflector, Unresolved PDZ
SBA6	KFR102A	206	PFL-f, radar reflector
SBA6	KFR102B	172	PFL-f (rim of ZFMENE3112)

<sup>1)</sup> eoh = end of borehole.



## Parameterisation

Hydraulic data for parameterisation of the deterministically modelled SBA-structures were available as orientated PFL-f transmissivities from core-drilled boreholes and HTHB flow anomalies from percussion-drilled boreholes intersecting the features. At least two boreholes intersect each feature. For each modelled borehole intercept (Table B-1), sub-horizontal PFL-f flow anomalies (and HTHB flow anomalies in percussion-drilled boreholes) that were clustered around the intercept were assumed to belong to the feature. The total transmissivity was then calculated as the sum (Table B-2) of the selected flow anomalies for each borehole intercept (Table B-3). Next, the distribution of transmissivity was interpolated for each feature using inverse-distance weighted interpolation. The resulting transmissivity distributions are shown in Figure B-1 to Figure B-4.

**Table B-2. Summed transmissivity at borehole intercept for the deterministically modelled structures SBA1 to SBA6 (SBA7 intercepts presented in Table D-2). Empty cells indicate absence of intercepts.**

Feature	Transmissivity (m <sup>2</sup> /s)							
	HFR102	HFR106	KFR101	KFR102A	KFR102B	KFR103	KFR106	KFR27
SBA1	2.8·10 <sup>-6</sup>							3.5·10 <sup>-6</sup>
SBA2				8.6·10 <sup>-8</sup>		1.6·10 <sup>-5</sup>		1.1·10 <sup>-6</sup>
SBA3		3.1·10 <sup>-5</sup>				1.6·10 <sup>-5</sup>		
SBA4						5.1·10 <sup>-6</sup>	2.4·10 <sup>-5</sup>	
SBA5						5.1·10 <sup>-6</sup>	2.4·10 <sup>-5</sup>	
SBA6			1.3·10 <sup>-5</sup>	1.1·10 <sup>-5</sup>	1.7·10 <sup>-6</sup>			6.8·10 <sup>-6</sup>

**Table B-3. Flow anomalies from PFL (core drilled b.h.) and HTHB (percussion-drilled b.h.) flow logging used for parameterisation of parameterise the deterministically modelled Shallow Bedrock Aquifer (SBA) features.**

SBA feature	Borehole	PFL-f ID	Borehole length (m)	Elevation (m RHB 70)	Orientation <sup>1)</sup>		Transmissivity (m <sup>2</sup> /s)	PFL head <sup>2)</sup> (m)	Head borehole section <sup>3)</sup> (m)
					Strike	Dip			
SBA1	HFR102	–	55.04	–44.1	–	–	2.8E–06	–	–0.8
SBA1	KFR27	– <sup>4)</sup>	50.17	–48.1	322	13	1.8E–06	–	–0.5
SBA1	KFR27	– <sup>4)</sup>	54.74	–51.1	14	31	1.8E–06	–	–0.5
SBA2	KFR102A	KFR102A_001	72.00	–63.1	–	–	8.6E–08	–	–1.4
SBA2	KFR103	KFR103_031	84.58	–66.1	357	15	1.2E–06	–0.20	–0.5
SBA2	KFR103	KFR103_032	85.67	–67.0	223	2	9.5E–06	–0.20	–0.5
SBA2	KFR103	KFR103_033	86.61	–67.7	157	9	4.7E–06	–0.10	–0.5
SBA2	KFR103	KFR103_034	89.15	–69.8	318	32	3.3E–07	–0.10	–0.5
SBA2	KFR103	KFR103_035	89.69	–70.2	321	18	2.8E–08	–	–0.5
SBA2	KFR103	KFR103_036	91.83	–71.9	327	16	1.5E–08	–	–0.5
SBA2	KFR27	– <sup>4)</sup>	98.5	–96.1	84	9	1.1E–06	–	–0.5
SBA3	HFR106	HFR106_001	39	–31.9	233	7	3.1E–05	–	–0.2
SBA3	KFR103	KFR103_031	84.58	–66.1	357	15	1.2E–06	–0.20	–0.5
SBA3	KFR103	KFR103_032	85.67	–67.0	223	2	9.5E–06	–0.20	–0.5
SBA3	KFR103	KFR103_033	86.61	–67.7	157	9	4.7E–06	–0.10	–0.5
SBA3	KFR103	KFR103_034	89.15	–69.8	318	32	3.3E–07	–0.10	–0.5
SBA3	KFR103	KFR103_035	89.69	–70.2	321	18	2.8E–08	–	–0.5
SBA3	KFR103	KFR103_036	91.83	–71.9	327	16	1.5E–08	–	–0.5
SBA4	KFR103	KFR103_041	180.69	–143.1	268	33	6.8E–08	–	–0.6
SBA4	KFR103	KFR103_042	181.23	–143.5	120	11	2.1E–07	–	–0.6
SBA4	KFR103	KFR103_043	181.89	–144.0	130	6	4.8E–06	0.30	–0.6
SBA4	KFR106	KFR106_015	67.22	–62.1	307	22	2.2E–07	–	–0.3
SBA4	KFR106	KFR106_016	68.24	–63.0	286	19	1.3E–05	–	–0.3
SBA4	KFR106	KFR106_017	69.38	–64.1	255	40	1.0E–07	–	–0.3
SBA4	KFR106	KFR106_018	71.5	–66.1	284	37	6.3E–06	–	–0.3
SBA4	KFR106	KFR106_019	73.02	–67.5	206	26	4.6E–06	0.20	–0.3
SBA5	KFR103	KFR103_041	180.69	–143.1	268	33	6.8E–08	–	–0.6
SBA5	KFR103	KFR103_042	181.23	–143.5	120	11	2.1E–07	–	–0.6
SBA5	KFR103	KFR103_043	181.89	–144.0	130	6	4.8E–06	0.30	–0.6
SBA5	KFR106	KFR106_047	154.36	–143.7	98	38	2.3E–06	–	–0.6
SBA5	KFR106	KFR106_048	154.58	–143.9	100	32	4.0E–06	–	–0.6
SBA5	KFR106	KFR106_049	156.08	–145.3	116	7	1.8E–05	0.80	–0.6
SBA6	KFR101	KFR101_026	180.95	–143.6	124	18	1.3E–05	–1.80	–2.5
SBA6	KFR102A	KFR102A_034	188.3	–169.0	109	9	2.6E–06	–1.10	–0.9
SBA6	KFR102A	KFR102A_035	188.77	–169.5	345	9	5.4E–07	–	–0.9
SBA6	KFR102A	KFR102A_036	190.35	–170.9	196	23	6.0E–07	–1.10	–0.9
SBA6	KFR102A	KFR102A_037	192.01	–172.4	205	30	2.3E–08	–	–0.9
SBA6	KFR102A	KFR102A_039	196.32	–176.3	208	16	5.9E–09	–	–0.9
SBA6	KFR102A	KFR102A_040	196.89	–176.8	246	14	3.0E–08	–	–0.9

SBA feature	Borehole	PFL-f ID	Borehole length (m)	Elevation (m RHB 70)	Orientation <sup>1)</sup>		Transmissivity (m <sup>2</sup> /s)	PFL head <sup>2)</sup> (m)	Head borehole section <sup>3)</sup> (m)
					Strike	Dip			
SBA6	KFR102A	KFR102A_041	197.45	-177.3	125	40	3.1E-08	-	-0.9
SBA6	KFR102A	KFR102A_042	200.81	-180.4	147	20	2.2E-06	-1.00	-0.9
SBA6	KFR102A	KFR102A_043	201.52	-181.0	146	12	7.0E-07	-	-0.9
SBA6	KFR102A	KFR102A_044	202.01	-181.5	201	39	4.1E-07	-	-0.9
SBA6	KFR102A	KFR102A_045	202.38	-181.8	205	9	3.5E-07	-	-0.9
SBA6	KFR102A	KFR102A_046	203.32	-182.7	163	18	4.8E-08	-	-0.9
SBA6	KFR102A	KFR102A_047	204.5	-183.8	195	20	5.3E-07	-	-0.9
SBA6	KFR102A	KFR102A_048	205.89	-185.0	166	16	3.4E-06	-0.60	-0.9
SBA6	KFR102B	KFR102B_086	171.95	-136.4	214	6	8.7E-07	-0.80	-2.5
SBA6	KFR102B	KFR102B_087	172.6	-136.9	216	13	2.0E-07	-	-2.5
SBA6	KFR102B	KFR102B_088	173.15	-137.3	161	10	2.3E-07	-	-2.5
SBA6	KFR102B	KFR102B_089	173.57	-137.7	115	41	3.6E-07	-	-2.5
SBA6	KFR27	KFR27_013	192.51	-189.6	63	23	6.8E-06	-1.80	-3.0
SBA6	KFR27	KFR27_014	193.01	-190.1	33	19	1.0E-08	-	-3.0

<sup>1)</sup> Orientation of associated fracture. <sup>2)</sup> Calculated freshwater head for PFL-f. <sup>3)</sup> Monitored point water head for the borehole section containing the flow anomaly. <sup>4)</sup> No detailed flow logging, flow anomaly evaluated from 5-m measurement.

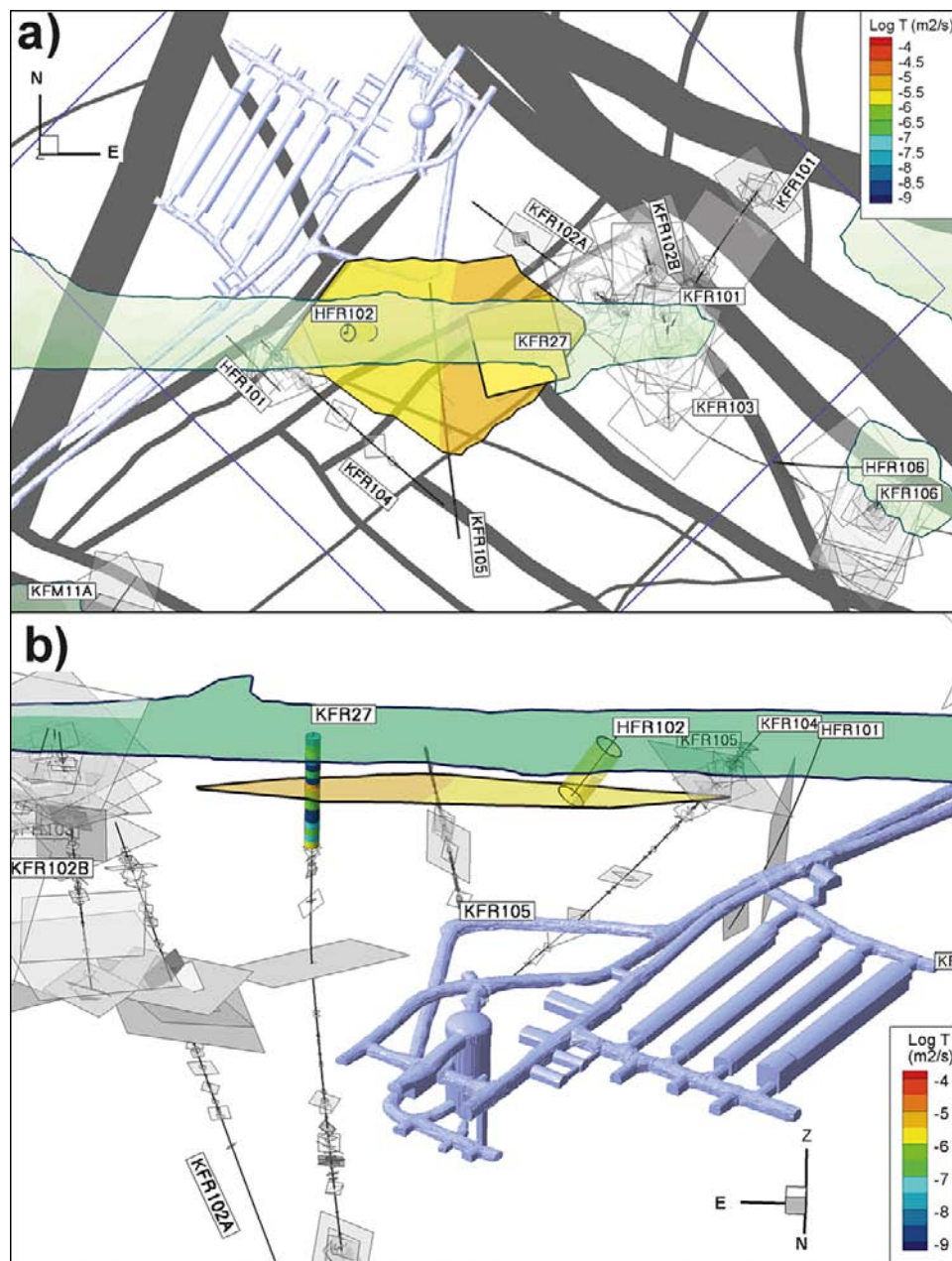


**Figure B-1.** Deterministically modelled Shallow Bedrock Aquifer (SBA) feature SBA1. The feature is coloured by transmissivity interpolated from the transmissivity of the borehole intercepts. The flow anomalies in the boreholes used for the parameterisation are also coloured by transmissivity; a) top view and b) perspective view from north.

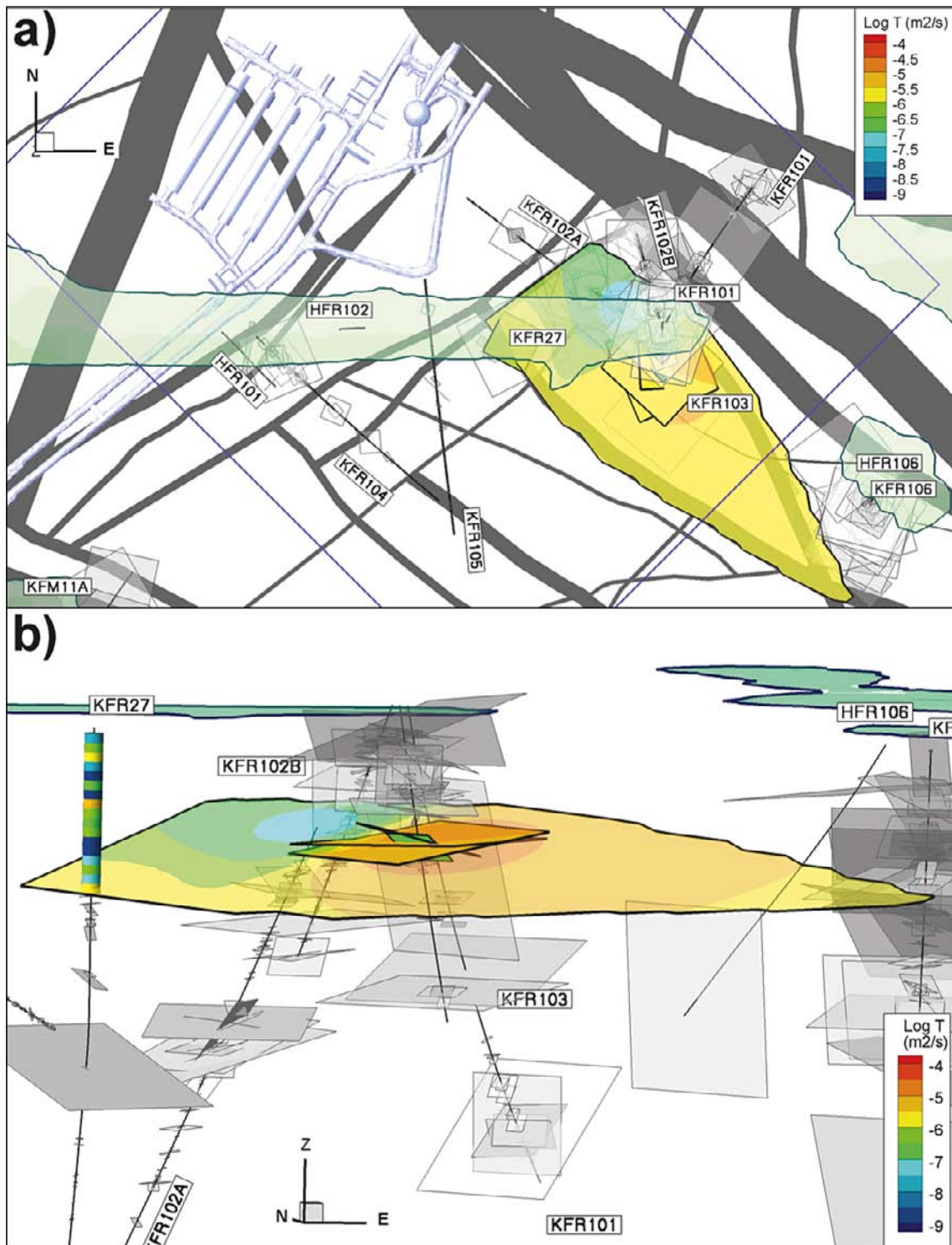


**Figure B-2.** Deterministically modelled Shallow Bedrock Aquifer (SBA) feature SBA2. The feature is coloured by transmissivity interpolated from the transmissivity of the borehole intercepts. The flow anomalies in the boreholes used for the parameterisation are also coloured by transmissivity; a) top view and b) perspective view from southwest.

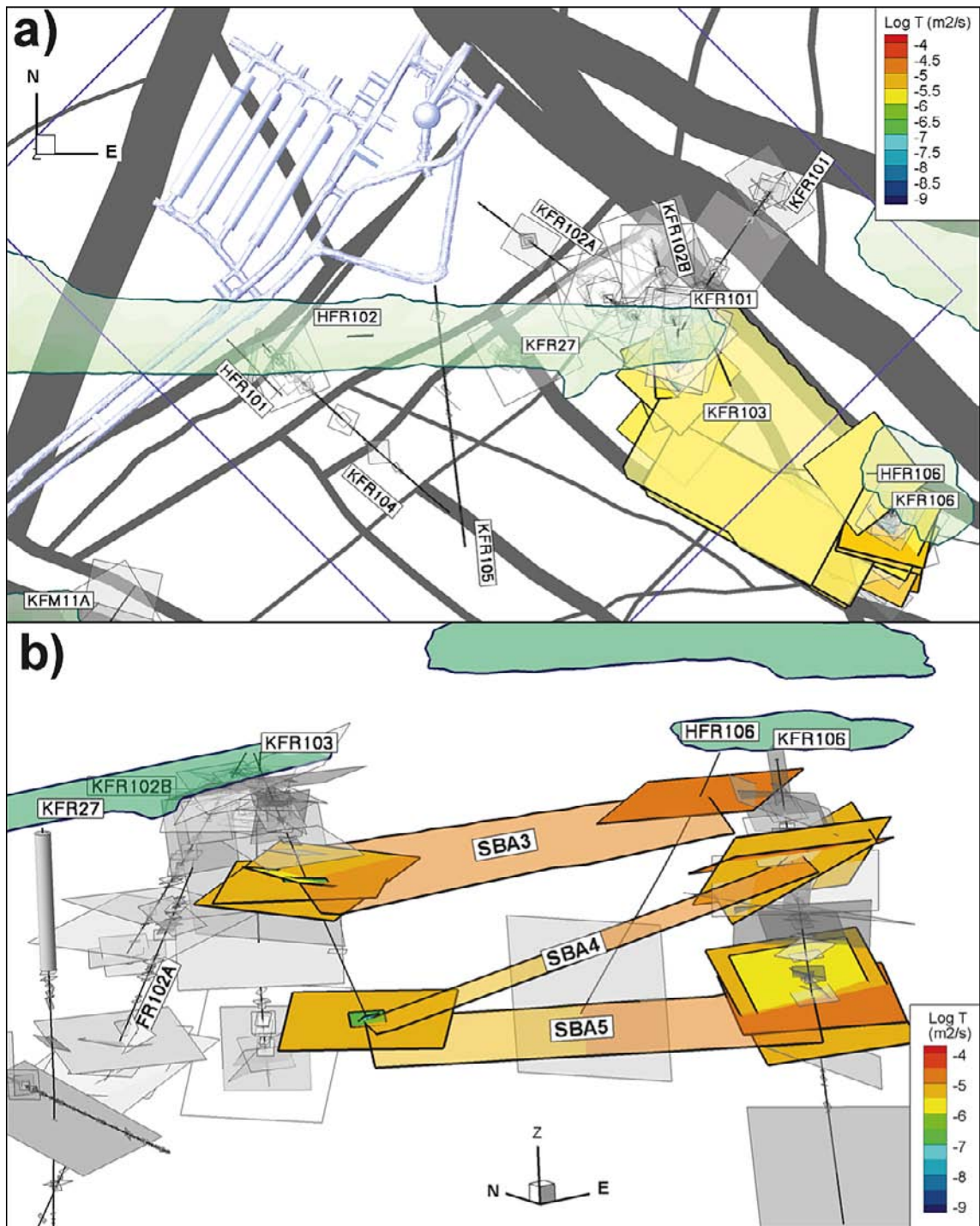


**Figure B-3.** Deterministically modelled Shallow Bedrock Aquifer (SBA) features SBA3, SBA4, and SBA5. The features are coloured by transmissivity interpolated from the transmissivity of the borehole intercepts. The flow anomalies in the boreholes used for the parameterisation are also coloured by transmissivity; a) top view and b) perspective view from southwest.

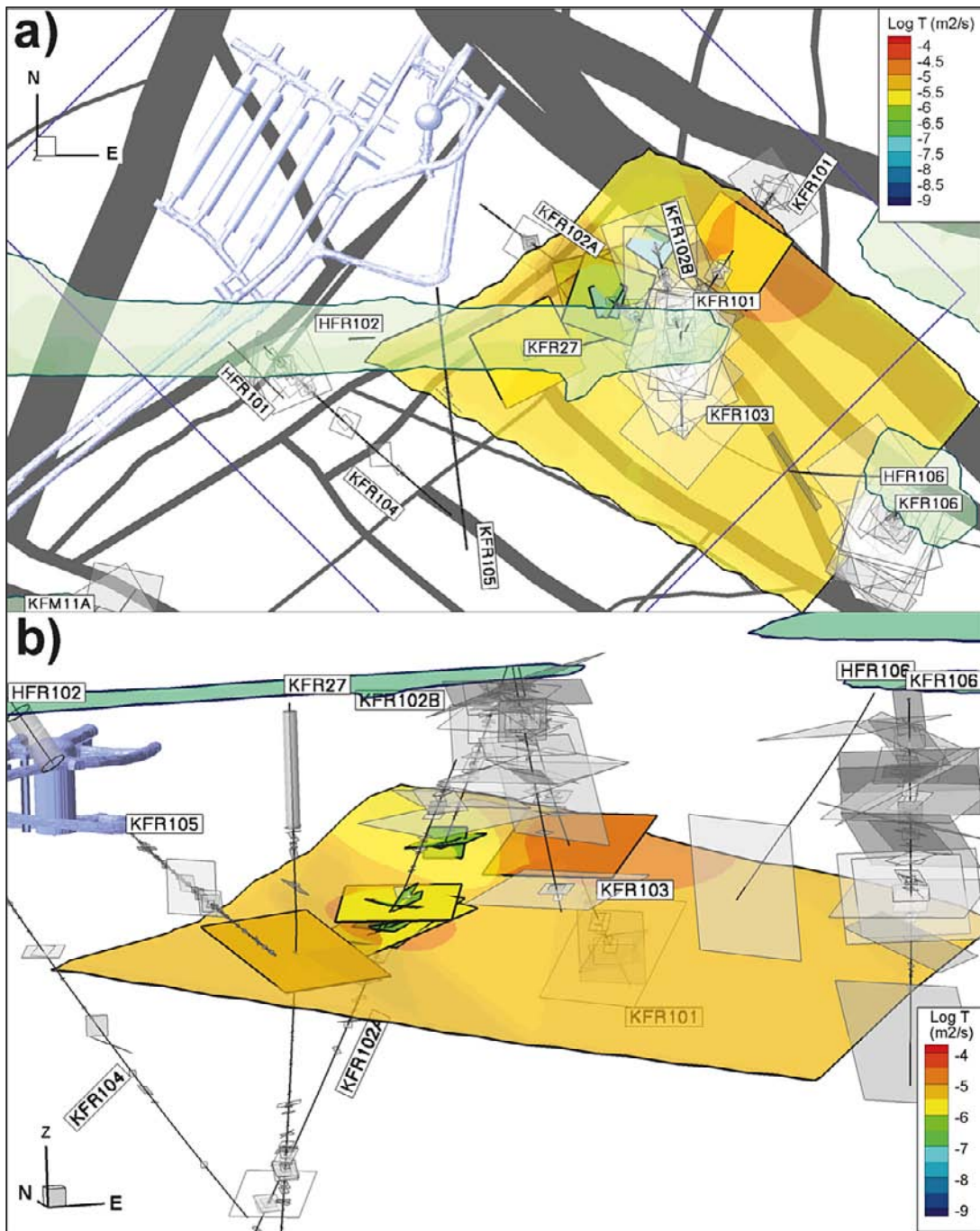


**Figure B-4.** Deterministically modelled Shallow Bedrock Aquifer (SBA) feature SBA6. The feature is coloured by transmissivity interpolated from the transmissivity of the borehole intercepts. The flow anomalies in the boreholes used for the parameterisation are also coloured by transmissivity; a) top view and b) perspective view from southwest.

### Hydraulic interferences

The hydraulic interferences (Section 4.4.2) that formed the basis of the modelled features were used to further evaluate their hydraulic properties (Table B-4). Diffusivities were observed in all features with the exception of feature SBA3 and SBA4 (cf. Figure 4-20), where no responses could be coupled to the individual features. A problem with the interference pumping test in KFR105 (opening of the borehole) is that the disturbance was not done directly in the interpreted features (SBA1 and SBA2), but assumed to be induced by a vertical fracture in connection with the features (at 133 m borehole length, see Appendix E). The evaluated hydraulic properties are thus thought to represent not only the features themselves but also the connection to borehole KFR105.

**Table B-4. Hydraulic properties of modelled deterministic Shallow Bedrock Aquifer (SBA) features evaluated from cross-hole data (interference tests and drilling responses). Transmissivity and storativity could be estimated only from interference tests with high apparent diffusivity (not from drilling responses).**

Feature	Disturb. borehole	Obs. b.h. section	Index 1 (m <sup>2</sup> /s)	T (m <sup>2</sup> /s)	S (-)	Index 1 class <sup>1)</sup>	Type <sup>2)</sup>
SBA1	KFR105	KFR27:2	1.22	1.3×10 <sup>-5</sup>	4.5×10 <sup>-5</sup>	M	I
SBA1	KFR105	KFR27:2	1.26			M	D
SBA1	KFR105	HFR102:1	0.36	4.6×10 <sup>-5</sup>	3.2×10 <sup>-4</sup>	L	I
SBA1	KFR105	HFR102:1	0.45			L	D
SBA2	KFR105	KFR102A:8	0.40	1.7×10 <sup>-5</sup>	1.7×10 <sup>-4</sup>	L	I
SBA2	KFR105	KFR102A:8	0.84			L	D
SBA2	KFR105	KFR103:2	1.14	4.9×10 <sup>-5</sup>	9.4×10 <sup>-5</sup>	M	I
SBA2	KFR105	KFR103:2	1.19			M	D
SBA2	KFR102A	KFR103:2	3.24			M	D
SBA3	HFR106	KFR103:2	1.56			M	D
SBA4 <sup>3)</sup>	KFR106	KFR103:1	25.6			H	D
SBA5 <sup>3)</sup>	KFR106	KFR103:1	33.5			H	D
SBA6	KFR27	KFR101:2	33.1			H	D
SBA6	KFR102A	KFR101:2	36.3			H	D
SBA6	KFR102A	KFR102B:1	18.2			H	D

<sup>1)</sup> Response Index 1 (normalised radial distance with regards to response time) classes according to Walger et al. (2010): L = Low; M = Medium; H = High.

<sup>2)</sup> I = Interference test; D = Drilling.

<sup>3)</sup> Evaluated from nitrogen flushing of KFR106. It cannot be deduced if the response relates to SBA4 (or ZFMWNNW3262) or SBA5.

An alternative way to describe the interference between borehole HFR106 and KFR103:2 is as an indirect response via deformation zone ZFMWNNW3262 (see Section 4.4.2). The observed drilling response between borehole KFR106 and observation section KFR103:1 was at c. 155 m borehole length in KFR106, corresponding to feature SBA5. An alternative way to describe the connection between borehole KFR106 and borehole section KFR103:1 may thus be with feature SBA5 only.

One of the interferences in one the modelled SBA-structures, SBA1, was assessed to be strong enough to allow an estimation of the transmissivity of the hydraulic connection (see Section 4.4.2) from the transient test evaluation (Table B-4).

A comparison of the transmissivities with the apparent hydraulic diffusivities for the borehole intercepts reveals that there is no correlation between transmissivity and apparent hydraulic diffusivity (Figure B-5). This probably reflects the heterogeneity of the features, but the statement also further support the conceptual model presented in Section 4.4.2 that the apparent hydraulic diffusivity of the sub-horizontal fracture system is highly influenced of crossing structures with high transmissivity. The estimated transmissivity of the hydraulic connection between boreholes KFR105 and KFR27, representing feature SBA1, from cross-hole evaluation at 1.3×10<sup>-5</sup> m<sup>2</sup>/s (Table B-4) can be compared to the single-hole transmissivity of the intercept in KFR27 which was estimated to 3.5×10<sup>-6</sup> m<sup>2</sup>/s (Table B-2).

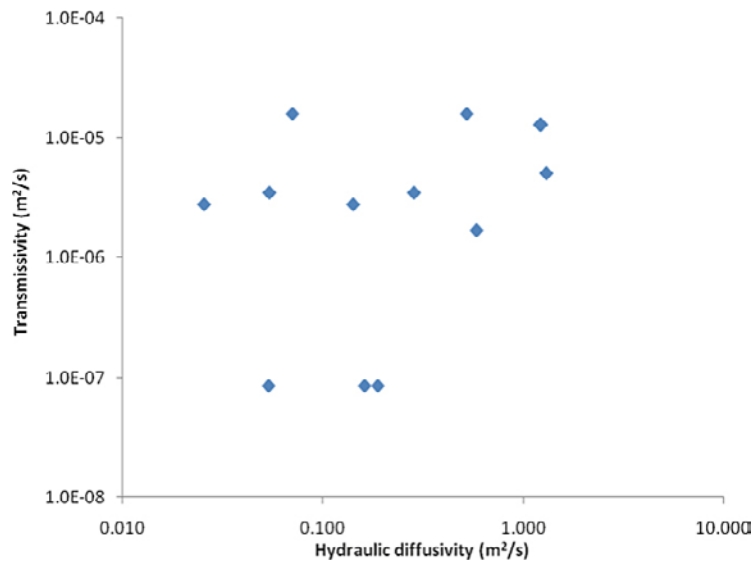


**Figure B-5.** Transmissivity for borehole intercepts of the deterministically modelled Shallow Bedrock Aquifer (SBA) features from single-hole tests versus apparent hydraulic diffusivity from cross-hole tests for the same borehole intercepts.

## Character of deformation zone sets

The earlier work associated with the Forsmark site investigation lead to the development of a conceptual model (Figure 3-4) and the identification of four orientation sets of deformation zones based on their geological character (Stephens et al. 2007). This subdivision has been confirmed and has been maintained in the current study. The different sets of zones at SFR are described below.

### Vertical to steeply dipping WNW to NW set

Members of this set of zones fall within the local minor to regional deformation zone size ranges, according to the terminology of Andersson et al. (2000). The set includes the dominant regional deformation zones ZFMWNW0001 (Singö) and ZFMNW0805A (formerly referred to as Zone 8) that can be said to define the Northern and Southern boundaries of the SFR Central block (Figure 3-5). It also includes the largest and oldest zones in the region c. 1.85 Ga (Stephens et al. 2007). It is this set that has been subject to most reactivation cycles.

The zones in the vertical to steeply dipping WNW to NW set are generally composite features, characterized by an initial development in the ductile regime followed by brittle reactivation. It is the only set that exhibits ductile deformation. The majority of the fractures are sealed and mylonites, cataclasites and cohesive breccias occur locally, especially in the most prominent zones in the set, i.e. ZFMWNW0001 and ZFMNW0805A. The bedrock within these zones is typically affected by a varying degree of oxidation. Two of the five deformation zones with occurrences of quartz dissolution (vuggy granite) belong to the WNW to NW set: ZFMNW0805A and ZFMWNW0835.

In the southern part of the SFR regional model area, in the vicinity of the SFR tunnels, ZFMWNW0001 along with ZFMWNW0813, ZFMWNW3259, ZFMNW0002 and, to a lesser extent, ZFMWNW1035, merge to comprise a complex broad deformation 'belt' (Figure 3-5). This can be seen in the detailed tunnel excavation mapping (Christiansson and Bolvede 1987) and the SHI results of KFM11A (Stephens et al. 2008). ZFMWNW0001 forms the core of the deformation belt while the other zones have lateral positions to the north and south. The dominant zone, ZFMWNW0001, referred to as the Singö deformation zone in earlier SFR models, is a major regional deformation zone with a total length of c. 30 km.

In the north, the Central block is bounded by a secondary deformation belt with similar orientation and character as the Singö belt, but is much smaller (Figure 3-5). On a larger regional scale, the magnetic data suggest that it is probably a splay from the main Singö deformation zone or, at least, is a member of the same WNW to NW system of deformation zones. This Northern boundary belt comprises ZFMNW0805A and a smaller splay ZFMNW0805B. ZFMNW0805A with a length between 3 and 4 km and a thickness of 60 m, has the same sequence of ductile deformation followed by brittle reactivation that is seen in the Southern boundary belt. ZFMNW0805B has the same character as the main zone, and merges with ZFMNW0805A at both its north-western and south-eastern ends

Inside the Central block there are six zones belonging to the WNW to NW set, four with high confidence and two with medium confidence in existence. They are modelled as being relatively short although the estimated lengths are uncertain with their traceability being restricted to lengths ranging from 524 to 1,044 m (Figure C-1). There also exists uncertainty to the continuity of these zones.

None of these zones have been modelled to intersect the existing SFR facility. They occur in the south-eastern part of the model volume but are modelled to terminate against various ENE to NE trending structures. Above the existing SFR facility, there are virtually no WNW to NW trending lineaments inside the Central block. A series of minor structures with similar orientation to those south-east of the pier may well be present in the existing facility and are possibly indicated in the tunnel mapping; however, they are most likely predominantly ductile and of reasonable rock engineering quality, and therefore not judged, at the time, to be very significant for the excavation. It has not been possible, nor is it considered realistic, to correlate the minor SHI based structures with the tunnel mapping for these structures. All four zones in the Central block, for which borehole information is available, have inferred dips that exceed 85° and are relatively thin in terms of current SHI methodology.



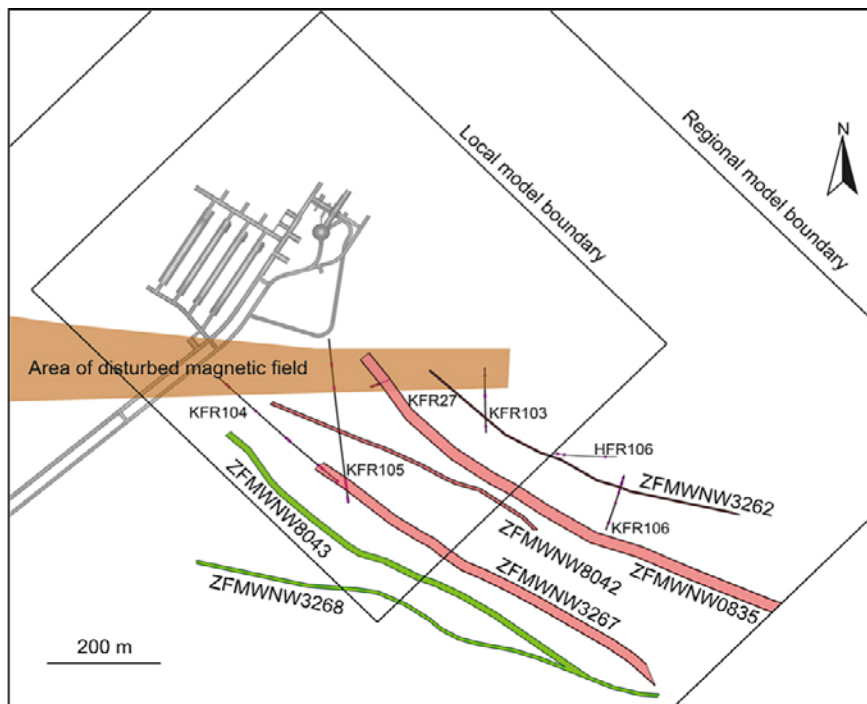


**Figure C-1.** Modelled deformation zones of the WNW to NW group lying inside the Central block (all zone dips are greater than 85°). The confidence in existence indicated by colours: high=red, medium=green.

#### **Vertical to steeply dipping NNE to ENE set**

The zones of the steep NNE to ENE set inside the SFR Central block (Figure C-2) have the same characteristics as described by Stephens et al. (2007). Compared with the WNW to NW set, the steep NNE to ENE zones inside the regional model area are shorter, falling within the size range of local minor- to local major deformation zones, according to the terminology of Andersson et al. (2000). However, their lengths are strongly controlled by existing tectonic structures, i.e. generally terminating against WNW to NW zones, which has strong truncation effects. The ENE sub-set also terminates against the structures in the NNE sub-set and the N-S to NNW set. The steep NNE to ENE zones are generally narrow, with thicknesses of around 5 m to 15 m. There are two clear exceptions of zones with much thicker modelled thicknesses: ZFMNNE0869 with 60 m and ZFMENE3115 with 28 m but, in both cases, the modelled thickness represents a packet of parallel lying smaller structures.

The steep NNE to ENE zones are formed in the brittle regime and are dominated by Sealed fractures. Three of the five deformation zones have occurrences of quartz dissolution (vuggy granite): ZFMENE3115, ZFMNE3118 and ZFMNNE0725.

#### **Vertical to steeply dipping N-S to NNW set**

There are five zones in this group, ZFMNNW0999, ZFMNNW1034, ZFMNNW1209, ZFMNNW3113 and ZFMNS3154. Only two of them, ZFMNNW1209 and ZFMNNW1034, lie within the Central block and have been identified with high confidence, based on tunnel and borehole data (Figure C-3). The other three zones lie to the north of zone ZFMNW0805A, i.e. the Northern boundary Belt, and are of medium confidence, being based solely on magnetic lineament interpretation. The members of this group have terminations against all three of the other steeply dipping deformation zone sets.

All the zones in this group that intersect the regional model volume are local minor in size according to the terminology of Andersson et al. (2000). The two high confidence zones have similar modelled thicknesses of 17 m and 18 m. However, although the 18 m modelled thickness of ZFMNNW1209 is based on SHI data, evidence for the zone seen in the rock caverns indicates the zone is comprised of a parallel group of thin discontinuous structures rather than a single thick discrete zone with a central core.

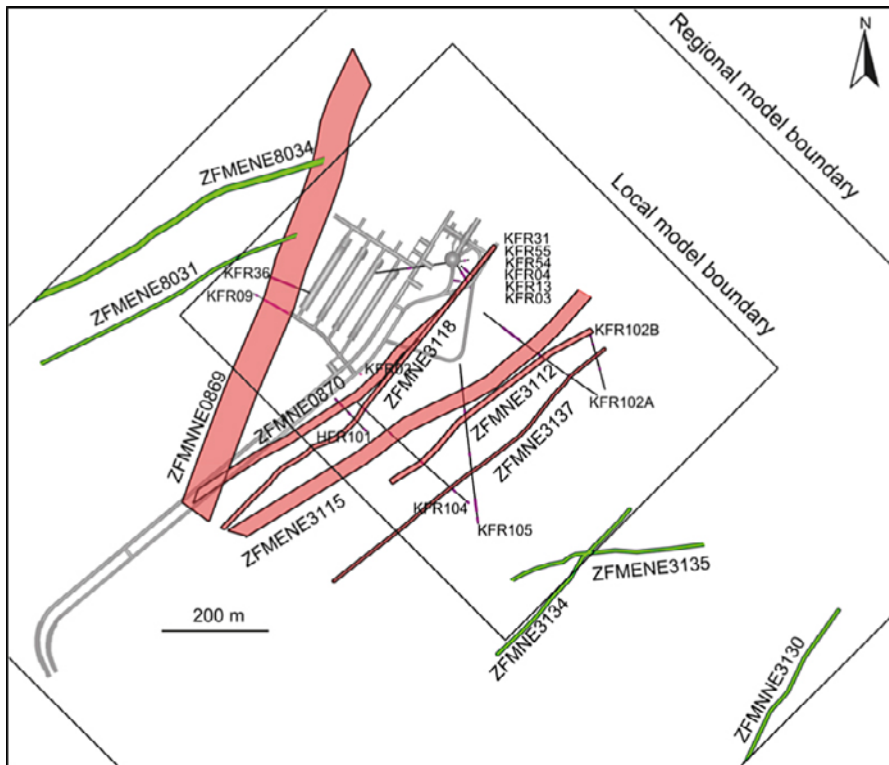


**Figure C-2.** NNE to ENE deformation zones penetrating the Central block between ZFMWNW0001 and ZFMNW0805A. The different colours refer to confidence in existence: high=red, medium=green.

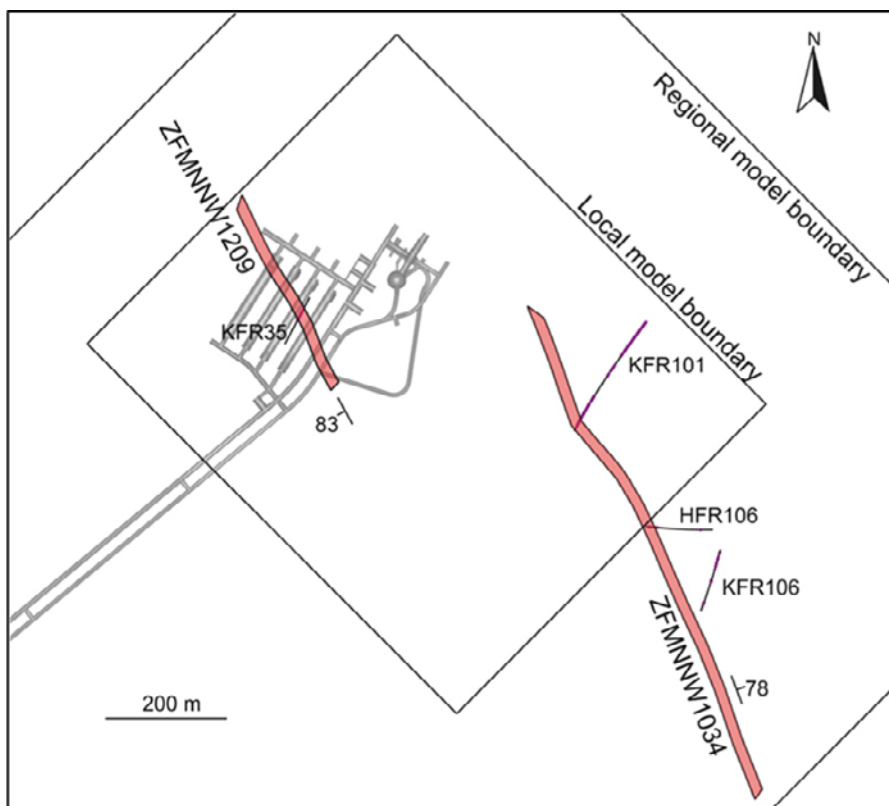


**Figure C-3.** N-S to NNW deformation zones penetrating the Central block between ZFMWNW0001 and ZFMNW0805A.

These zones are dominated by Sealed fractures. A subordinate brittle-ductile component is also locally present. As concluded in Stephens et al. (2007) on the basis of their low frequency of occurrence, this orientation set is judged to be of lower significance generally at Forsmark, relative to the other sets.

### Gently dipping zones

There are three gently dipping zones within the regional model area (Figure C-4). ZFMA1 has medium confidence and lies outside of the Central block on the southern side of ZFMWNW0001. ZFMB10 has low confidence and is located at significant depth beneath the local model volume. ZFM871 (zone H2) is located below SFR; it has high confidence as there exist several borehole intercepts (12 *target* intercepts and 7 *geometric* intercepts; Figure 2-6) as well as the tunnel penetration (Figure 4-3). No gently dipping deformation zones are interpreted to intercept the ground surface. The current modelled extension of ZFM871 (Curtis et al. 2011) is notably less than applied in previous models (Axelsson and Mærsk Hansen 1997), which may have notable effects on hydraulic flow simulations – particularly with consideration to land rise in future scenarios (e.g. in comparison to Holmén and Stigsson 2001). Measured drawdown suggests that the hydraulic connection of ZFM871 extends southeast of ZFMENE3115 (Section 4.5.4).

ZFMA1 corresponds to the A1 seismic reflector with an orientation of  $082^{\circ}/45^{\circ}$ . However, as earlier reported an alternative interpretation of the seismic reflector is that it is related, wholly or partly, to compositional variations in the bedrock (Stephens et al. 2007). ZFMB10 also corresponds to a seismic reflector, B10, which was identified during re-processing and reinterpretation of existing seismic data in connection with the current project (Juhlin and Zhang 2010). The inferred low confidence zone has an orientation of  $025^{\circ}/35^{\circ}$ , occurs at significant depth beneath the local model volume and there is no control on its character. In a similar fashion to A1, reflector B10 may be related wholly or partly to compositional variations in the bedrock.

ZFM871, formerly called Zone H2 during the SFR construction phase (Christiansson and Bolvede 1987), has an orientation of  $074^{\circ}/19^{\circ}$ . Its general character corresponds to the description of the other gently dipping fracture zones identified during the Forsmark site investigation as reported in Stephens et al. (2007). These zones are interpreted as having formed in the brittle regime and, relative to all the other sets, contain a higher frequency of Open fractures and incoherent crush material. Chlorite, calcite and clay minerals are conspicuous along the fractures in these zones. However, epidote, quartz, adularia, hematite, prehnite, laumontite, pyrite and asphaltite are also locally present. The zone is interpreted as consisting of a group of parallel oriented, smaller hydraulically conductive structures separated by ordinarily fractured rock. The spread of indications suggest that the structure is complex and has a stepped geometry.

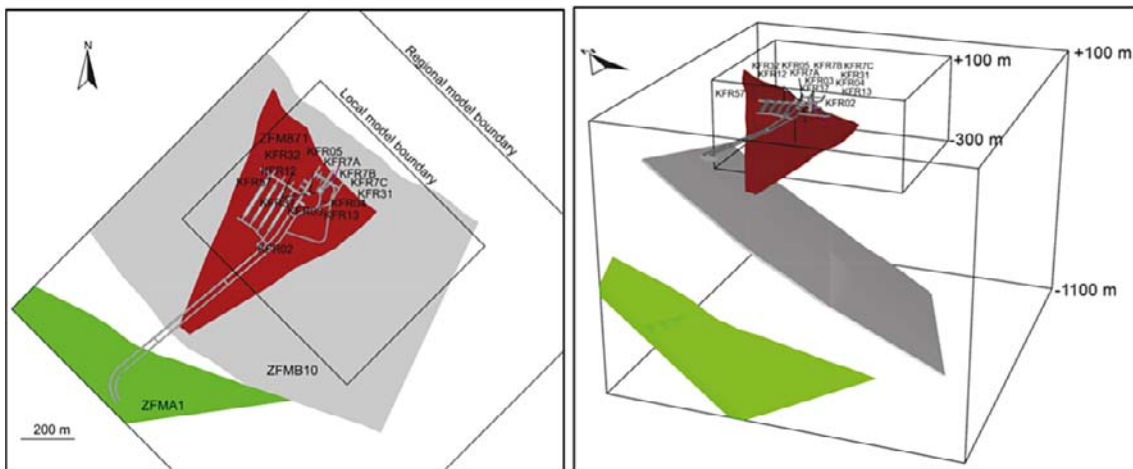


**Figure C-4.** Gently dipping zones penetrating the SFR regional model volume. ZFM871 (red, high confidence), ZFMA1 (green, medium confidence), ZFMB10 (grey, low confidence).

Due to the open and water-bearing character of ZFM871, identified during the earlier excavation phase and the number of gently dipping zones identified during the Forsmark site investigation, efforts have been made to identify the existence of similar gently dipping structures in the SFR regional model volume.

### **Confidence assessment and key uncertainties for the DZ modelling**

The overall confidence in the position, character and extent of the so called Southern and Northern bounding tectonic belts is high. Similarly, confidence is high in the steep to sub-vertical nature of the vast majority of the deformation zones in the SFR area as well as the surrounding Forsmark area, inferred from the underlying conceptual model presented by Stephens et al. (2007).

There is a high confidence that no, previously unknown, local major or larger gently dipping zone exists in the local model volume. When smaller gently dipping structures are considered, the confidence level is only medium and is tempered by experience from the existing SFR excavations, where zone ZFM871 is significant from an engineering viewpoint but has an undulating or stepped geometry and very heterogeneous character. Christiansson (1986) reports the zone's character as being very variable but generally having two to three gently dipping fracture sets, individually recorded zone thicknesses of up to 10 m and a hydraulic thickness varying from 2 to 20 m; the zone is associated with lenses of weathered and highly fractured rock, along with frequent clay-filled joints. The gently dipping fractures, in combination with an increased frequency of steeply dipping fractures, gives rise to the lenses being hydraulically interconnected. All of these conclusions, with minor adjustments, are supported by the current modelling work and the correlation of smaller zones between boreholes with similar heterogeneous geological characteristics is not straightforward. The uncertainty to the terminations of ZFM871 are discussed in Curtis et al. (2011, Appendix 11).

The importance of stress-release structures (i.e. not zones formed in response to tectonic shear stresses) has been advocated, similar to that proposed in the Forsmark site investigation (Stephens et al. 2007). There is high confidence that minor sub-horizontal structures do exist but with size of a couple of hundred metres or less, down to the single fracture scale (See Appendix B). These features are interpreted to occur in, at least, the upper 200 m of the rock mass. At very shallow depths, <15 m, these features are clearly related to stress release, with wide apertures filled with sediment and rock fragments (Carlsson 1979, Carlsson and Christiansson 2007).

The overall confidence level in the deterministic modelling is scale-related. The confidence is high for local major zones (ZFMWNW0001 and ZFMNW0805A), but the confidence level drops with the inclusion of increasingly smaller structures. The confidence levels in the SFR Central block, away from the existing tunnels, are generally lower than within the Forsmark local model area. The reason for this is that the modelling of steeply dipping deformation zones relies – to some extent – on the identification and interpretation of lineaments; lineaments are interpreted from magnetic minima which in turn are subject to several disturbances. In comparison to the Forsmark model area, the natural magnetic field at SFR (particularly the local model area) is strongly disrupted by the man-made pier, marine electric cable, tunnels, stored waste, and its containers in the caverns and Silo (e.g. Figure C-1). In addition, the identification of deformation zones associated with lineaments is complicated by magnetic disturbances along linear anomalies related to lithology, Quaternary marine sediments, and the Sea. These effects, as well as the focus on the detection of small-scale structures, inevitably imply lower confidence levels.

## Analysis of hydraulic data from the construction of SFR

This appendix presents the hydraulic data available prior to the Site Investigation for the SFR extension program; also referred to as the “old data set”. A three-dimensional over-view of the double-packer data are shown in Figure D-1. This old hydraulic data set was obtained during the investigation and construction phases for the existing SFR. It is composed of different data types: short-term “Steady-state” injection tests and Falling head tests, as well as Pressure build-up tests and Transient tests. This data set is judged to have an overall lower quality and confidence, and furthermore the detection limits are highly variable among the different test methods and test scales. It should also be noted that hydraulic tests performed over packed-off test sections include compartmentalized fracture transmissivity and may overestimate transmissivity owing to short-circuiting and more spherical flow dimensions (as compared to PFL-f data, described in Section 4.3.2). Furthermore there are no orientation data available in these older boreholes. There also exist uncertainties in the geological modelling of the old data set, which propagate into uncertainty in their hydraulic parameterisation. Not all the required geologic data are available for the interpretation of deformation zone intercepts according to the established Single Hole Interpretation methodology, leading to the concepts *target intercept* and *geometric intercept* (Section 2.3.4). Prior to analysis, a screening process was therefore undertaken with respect to confidence, overlapping data, and borehole coverage, as explained in Öhman and Follin (2010a).

### SBA7 and SBA8

A possible sub-horizontal stress-relief structure was defined by Curtis et al. (2011), based on the original interpretation of Zones H1 and H3, by Carlsson et al. (1985). This structure is referred to as SBA7, and parameterised by hydraulic data (Figure D-2; Table D-2). Among mapped sub-horizontal structures in the SFR facility (Figure 4-1), several are possible to extrapolate across tunnel sections (brown planes in Figure D-3), but can generally neither be linked to ambient hydraulic borehole data (Figure 4-3), nor to grouting requirements. However, two mapped sub-horizontal structures associated to grouting with 5 tonnes of cement (at chainage 5+780 and 5+805, respectively, in tunnel BT; red planes in Figure D-3) correlate geometrically to a hydraulic anomaly in KFR69 (PDZ2;  $T > 10^{-5}$  m<sup>2</sup>/s; Figure D-57), as well as, mapped inflow from a crush structure at the bottom of Ventilation Building VB2 (Christiansson and Bolvede 1987). Therefore, a possible SBA8 is defined (strike 182°, dip 12°) by matching the intercepts at: 1) 5+780 m in tunnel BT, 2) 127 m borehole length in KFR69 and 3) the lower part of the shaft VB2. These intercepts are indicated by blue arrows in Figure D-3. The modelled plane is terminated against the nearest deformation zones, ZFMNE0870 and ZFMNE0869. After a few meters, the mapped crush in VB2 vanishes to the north (terminates or possibly leaps below the tunnel mapping). Tunnel DT also provides evidence of discontinuation to the north (indicated by pink arrow in Figure D-3). Based on this, SBA8 is terminated to the north along a strike of 117°. It is noteworthy that HFR101 and KFR104 are subject to particularly large drawdown (Figure 4-30, Section 4.5.3, main report), suggesting horizontal hydraulic connection to the east of ZFMNE0870. The most transmissive PFL-f in KFR104 (No. 27, with interpreted strike 157°, dip 22°, and transmissivity of  $2.3 \cdot 10^{-6}$  m<sup>2</sup>/s; Figure D-3) is located approximately 80 m away from the tunnel intercept of SBA8. However, this PFL-f is not included in SBA8, as it is offset c. 15 m above the modelled SBA8 plane.

The purpose of modelling SBA8 is primarily to emphasize that hydraulically significant sub-horizontal structures do not only exist in the vicinity of the Northern boundary belt and ZFMNNW1034, but also close to the Southern boundary belt. In comparison to the sub-horizontal transmissive structures modelled in the new data set, SBA1-6 (see Appendix B), SBA8 the modelling of has a very *low confidence*. The reason for this is that SBA8 is primarily a geometrical extrapolation, based on tunnel grouting, mapped tunnel traces, and borehole transmissivity. The geological interpretations at the three intercepts involve uncertainties and inconsistencies. Moreover, important hydraulic data support is unavailable (e.g. hydraulic responses, oriented PFL-f data, EC, FWH, radar reflectors).

### Cross-hole interference tests

Interference tests are useful to gain insight into the connectivity between zones. The interference tests performed during 1985 to 1987 were re-assessed by Axelsson and Mærsk Hansen (1997). Their re-interpretation is shown with respect to the final geologic SFR model v. 1.0 in Figure D-4 to Figure D-13. Note that the tested borehole section is referred to as “pumped” in the figures; in reality

the disturbance was caused by releasing the shut-in pressure inside a borehole section. There are also two unintentional disturbances that have been evaluated as interference tests: a leaking packer in KFR7C and the penetration of ZFM871 with a grouting borehole (KFR80). There exists some reported data on drawdown and also evaluated effective conductivity of flow paths. However, responses have only been used qualitatively; classed as *direct response*, *indirect response* and *no response*. The largest spherical distance for monitored responses is referred to as  $r_{max}$ . The interferences within and between deformation zones are summarised in Table D-1. The general impression is that ZFM871 has a central role in the hydraulic connectivity around SFR; disturbances in ZFM871 are monitored in all steeply dipping deformation zones, and vice-versa, disturbances inside steeply dipping deformation zones are generally monitored in ZFM871. It can be noted that there are relatively fewer direct responses in ZFMNNE0869 from the disturbances in ZFM871; this mainly relates to the fact that most tests were performed in the vicinity of the Silo (i.e. close to the conjunction of ZFMNE0870, ZFMNW0805A,B, and ZFM871). There is less data available on the connectivity between ZFM871 and ZFMNNE0869.

Three tests were performed in (or immediately adjacent to) ZFMNE0870 (Figure D-4, Figure D-5, and Figure D-6). Results are scattered and relatively few monitoring sections were in use and functioning. The furthest direct response is 259 m between KFR04 and KFR02 (Figure D-6), providing evidence that ZFMNE0870 is a large-scale internally connected deformation zone. It is not possible to clearly state if the pressure pulse travels through ZFMNE0870 or ZFM871, or perhaps along their junction.

ZFM871 is interpreted as conductive and heterogeneous. There exists several evidence of internal connectivity as well as connectivity between ZFM871 and its surrounding steeply dipping deformation zones: ZFMNE0870, ZFMNW0805A,B, and ZFMNNE0869 (Figure D-7 to Figure D-12). There also exists evidence of lacking connectivity (i.e. monitored sections in ZFM871 not responding to an interference in ZFM871). Most striking is the unintentional interference test in KFR80 (penetration of ZFM871 during grouting; Figure D-8), which resulted in drawdown in KFR01, at 870 m distance. ZFM871 is better connected to ZFMNW0805A than it is to ZFMNW0805B (Figure D-7, Figure D-9, and Figure D-11), which is quite surprising with respect to the location of these two zones. In the single-hole transmissivity data there is a difference between the two zones ZFMNW0805A,B – consequent in both the new and old data – where ZFMNW0805A is more than twice as transmissive as ZFMNW0805B.

The deeper sections of KFR09 and KFR10 are better connected to ZFM871 than their upper sections are (Figure D-12). The upper sections are inside ZFMNNE0869, while the deeper sections are inside KFR09\_DZ2 and KFR10\_DZ2, respectively. This suggests that KFR09\_DZ2 is a splay of ZFMNNE0869, while KFR10\_DZ2 is an extension of ZFM871. This suspicion is also supported by single-hole transmissivity data (Figure D-24 and Figure D-25). The upper and deeper parts of the two boreholes are also well-connected (Figure D-13).

**Table D-1. Overview of cross-hole tests performed 1985 to 1987.**

Interference	Monitored sections					HRD
	NE0870	NNE0869 <sup>2)</sup>	NW0805A,B	ZFM871 <sup>3)</sup>	PDZ <sup>4)</sup>	
<b>NE0870<sup>1)</sup> (3 tests)</b>						
Direct response	9			5		12
No response	5			2		8
<b>NNE0869 (1 test)</b>						
Direct response		4		1		2
<b>NW0805A (1 test)</b>						
Direct response			2	1		
Indirect response	1		6	2		8
No response	4	6		5	1	21
<b>ZFM871 (5 tests)</b>						
Direct response	11	3	6	11	1	28
Indirect response	5	1	14	4		23
No response	6	10	7	8	2	51

<sup>1)</sup> Including one test below the Silo, at the rim of ZFMNE0870 (Zon 9). <sup>2)</sup> KFR09\_DZ2 interpreted as part of ZFMNNE0869 (Zon 3). <sup>3)</sup> KFR10\_DZ2 interpreted as extension of ZFM871 (Zon H2). <sup>4)</sup> KFR20\_DZ1.

## Hydraulic parameterisation of deformation zones

This appendix also describes the hydraulic parameterisation of deformation zones in the old data set. In this compilation, there are also some hydraulic data used from Site Investigation Forsmark, HFM34, HFM35 and KFM11A. There are HTHB and injection test data available from percussion boreholes HFM34 and HFM35, while sequential PFL data measured at the 5 m scale are available in the upper part of KFM11A (64 to 490 m borehole length), and transient injection test data at the 20 m scale in the lower part of KFM11A (470 to 840 m borehole length). Note an *important difference* between old (1982 to 1987) and new data (2000 to 2009; KFM11A, HFM34, HFM35 and Appendix E); the absence of transmissivity values in the old data (1982 to 1987; Figure D-17 to Figure D-55) implies that the borehole section *has not been tested*, or the available data are judged *invalid*, while in the newer data (2000 to 2009; Figure D-14 to Figure D-16 and Appendix E) the absence of transmissivity values means that the transmissivity is below detection limit.

A few complications can be identified in the process of assessing deformation zone transmissivity owing to data gaps and data uncertainty:

- 1) Some deformation zone intercepts (particularly ZFMWNW0001, Singö) are incomplete (i.e. a very short intercept relative to the modelled true thickness of the zone). In these cases it is difficult to conclude if the available hydraulic data are sufficient to parameterise the full extent of the deformation zone.
- 2) For a number of deformation zone intercepts there are no hydraulic data available, or the hydraulic data coverage is judged to be insufficient. In these cases no realistic analysis can be made and the particular intercept is rejected from the parameterisation.
- 3) Several deformation zone intercepts have been interpreted to reflect a junction or overlap of several deformation zones (e.g. KFM11A). It is often difficult to infer if the measured transmissivity inside these intercepts reflects combined hydraulic properties (additatively), if the junction enhances transmissivity, or if subordinates deformation zones are masked by the dominating zone.
- 4) Hydraulic data are measured over some borehole section length; it is not known exactly where inside this section the measured inflow occurs. Therefore, this causes uncertainty to whether the measured flow is located inside or outside a deformation zone intercept. If the deformation zones are assumed to be more transmissive than the surrounding rock mass, it may be reasonable to include all data sections that are partly inside the deformation zone intercept (Öhman and Follin 2010a). In this appendix it was decided to treat each deformation zone independently, with respect to the local pattern in hydraulic data.
- 5) Some deformation zone intercepts are not based on SHI interpretation (i.e. referred to as *target intercepts*; Section 2.3.4), but only on RVS geometric modelling (i.e. referred to as *geometrical intercepts* (Curtis et al. 2011)). The confidence on this latter type of intercepts is considerably lower. Geometrical intercepts were therefore treated cautiously with respect to the local pattern in hydraulic data: if a local anomalous pattern is observed, the geometrical intercept is adjusted to the hydraulic data test sections, if no such pattern can be observed and it is overlapped by target intercepts, it is considered for rejection.

There also exist Unresolved PDZs (possible deformation zones as identified from the simplified Single Hole Interpretation, but not deterministically defined in the geologic model). These are only considered to be of relevance if they correspond to large transmissivity values (see discussion in Appendix A).

Based on a preliminary version of the SFR geologic model v. 0.1, a sensitivity analysis was undertaken to evaluate the uncertainty arising from these type of complications (Öhman and Follin 2010a). In the light of all combined uncertainties, it was decided to perform the HRD/HCD classification based on visual inspection and judgment. The deformation zone intercept transmissivity are reported as depth-adjusted  $T_0$  in Table D-2. Deformation zone intercepts and the associated hydraulic transmissivities are shown on borehole basis (Figure D-14 to Figure D-62).

**Table D-2. Summary of HCD intercept transmissivity.**

ZFM	Borehole	Borehole length (m)		Elevation (m RHB 70)		$\Sigma T_i$ (m <sup>2</sup> /s)	Depth-adjusted $T_0$ (m <sup>2</sup> /s)	Logarithmic depth-adj. log $T_0$ (m <sup>2</sup> /s)		
		From	To	From	To			From data	Forsmark <sup>1)</sup>	SFR <sup>2)</sup>
								$\Sigma T_i$	SDM	2001
<b>Southern boundary belt</b>										
WNW0001	HFM34	37	192	-7.8	-154.9	1.1E-3	2.5E-3	-2.6	-4.6	-3.3
WNW0001	KFM11A	498	824	-429.1	-691.9	3.4E-6	8.8E-4	-3.1	-4.6	-3.3
WNW0001	KFR61	1.4	70.9	0	-47.9	4.3E-4	5.5E-4	-3.3	-4.6	-3.3
WNW0001	KFR62	45.64	82.8	-31.7	-58	2.3E-4	3.7E-4	-3.4	-4.6	-3.3
WNW0001	KFR64	0	41.38	0.3	-35.5	3.6E-5	4.3E-5	-4.4	-4.6	-3.3
WNW0001	KFR65	6.9	28.95	-6.9	-29	1.4E-5	1.7E-5	-4.8	-4.6	-3.3
WNW0001	KFR67	0	35.21	0	-31.9	1.2E-5	1.4E-5	-4.9	-4.6	-3.3
WNW0001	KFR71	65.7	120.9	-29.1	-31	7.8E-4	1.1E-3	-3.0	-4.6	-3.3
NW0002	KFM11A	652.5	735.42	-555.7	-622	8.7E-7	3.0E-4	-3.5	-4.6	-
WNW0813	KFM11A	245	400	-213	-346.1	1.4E-7	2.2E-6	-5.7	-7.1	-
WNW1035	HFM35	104	200	-81	-150.4	1.2E-4	3.8E-4	-3.4	-	-
WNW1035	KFM11A	714.9	736.4	-605.6	-622.8	8.9E-9	3.9E-6	-5.4	-	-
WNW1035	KFR68	0	10.2	0	-7.2	1.4E-3	1.4E-3	-2.8	-	-
WNW3259	KFM11A	400	498	-346.1	-429.1	1.4E-6	6.7E-5	-4.2	-	-
<b>Northern boundary belt</b>										
NW0805a	KFR08	41	104.4	-89.6	-95.1	1.9E-5	4.8E-5	-4.3	-4.6	-5.5
NW0805a	KFR11	41.45	95.65	-93.7	-103.1	5.8E-5	1.5E-4	-3.8	-4.6	-5.5
NW0805a	KFR24	60	159	-50.3	-133.4	2.0E-5	5.0E-5	-4.3	-4.6	-5.5
NW0805a	KFR25	60	195.09	-43.9	-140.3	4.3E-5	1.1E-4	-4.0	-4.6	-5.5
NW0805a	KFR56	57.18	eoh)	-59.5	-48.7	5.5E-7	9.4E-7	-6.0	-4.6	-5.5
NW0805a	KFR7A	43	74.45	-133.8	-134.9	9.1E-5	3.4E-4	-3.5	-4.6	-5.5
NW0805b	KFR08	3	19	-86.3	-87.7	6.1E-7	1.4E-6	-5.8	-4.6	-
NW0805b	KFR11	7	24	-87.7	-90.7	9.2E-6	2.2E-5	-4.7	-4.6	-
NW0805b	KFR24	0	46	0	-38.6	1.0E-5	1.2E-5	-4.9	-4.6	-
NW0805b	KFR25	0	60	0	-43.9	2.7E-5	3.3E-5	-4.5	-4.6	-
NW0805b	KFR38	153.6	181.7	-125.2	-148.9	4.3E-5	1.7E-4	-3.8	-4.6	-
NW0805b	KFR7A	3.5	43	-132.4	-133.8	1.4E-5	5.3E-5	-4.3	-4.6	-
<b>Steep N-S to NNW set</b>										
NNW1209	KFR33	46.2	114.6	-26.9	-74.2	6.0E-8	9.9E-8	-7.0	-7.8	-5.7
NNW1209	KFR35	32.7	70	-34	-49.7	1.1E-5	1.6E-5	-4.8	-7.8	-5.7
<b>Gently dipping</b>										
ZFM871	KFR02	114.8	124.45	-200.2	-209.9	2.0E-7	1.5E-6	-5.8	-3.6	-5.8
ZFM871	KFR03	81.86	95.95	-164.2	-178.3	2.2E-8	1.2E-7	-6.9	-3.6	-5.8
ZFM871	KFR04	91	100	-165.1	-173.8	5.0E-7	2.7E-6	-5.6	-3.6	-5.8
ZFM871	KFR12	21.25	31.5	-108.4	-118.6	2.6E-6	8.0E-6	-5.1	-3.6	-5.8
ZFM871	KFR13	61	68	-184.3	-191.3	3.0E-6	1.9E-5	-4.7	-3.6	-5.8
ZFM871	KFR21	108.6	129.3	-108.6	-129.3	1.2E-5	3.9E-5	-4.4	-3.6	-5.8
ZFM871	KFR22	139.98	160.1	-121.2	-138.7	3.3E-6	1.2E-5	-4.9	-3.6	-5.8
ZFM871	KFR23	71	107	-61.5	-92.7	6.3E-5	1.4E-4	-3.9	-3.6	-5.8
ZFM871	KFR31	228.76	232	-151.1	-153.8	1.8E-6	8.2E-6	-5.1	-3.6	-5.8
ZFM871	KFR32	163.1	186.1	-113.2	-130	1.2E-4	4.0E-4	-3.4	-3.6	-5.8
ZFM871	KFR33	158.04	167	-104.3	-110.5	3.9E-6	1.1E-5	-4.9	-3.6	-5.8
ZFM871	KFR37	183.43	193.6	-158.3	-167.3	5.4E-5	2.7E-4	-3.6	-3.6	-5.8
ZFM871	KFR7B	0	17	-133.3	-149.7	2.6E-5	1.1E-4	-4.0	-3.6	-5.8
ZFM871	KFR7C	6	32	-139	-163.5	6.7E-7	3.0E-6	-5.5	-3.6	-5.8
<b>Steep NNE to ENE set</b>										
NE0870	KFR02	32.5	37.5	-117.9	-122.9	1.1E-6	3.6E-6	-5.4	-7.4	-7.7
NE0870	KFR03	48	95.95	-130.4	-164.2	3.6E-7	1.5E-6	-5.8	-7.4	-7.7
NE0870	KFR04	14	63	-90.7	-138	1.4E-7	4.3E-7	-6.4	-7.4	-7.7
NE0870	KFR53	18.72	37.01	-89.9	-98.3	2.3E-8	6.0E-8	-7.2	-7.4	-7.7
NE0870	KFR55	17	38	-128.8	-132.8	1.7E-7	6.2E-7	-6.2	-7.4	-7.7
NE0870	KFR70	34.91	92.8	-24.7	-69.9	2.5E-6	4.0E-6	-5.4	-7.4	-7.7
NNE0869	KFR09	0	58.7	-77.4	-82.6	4.3E-5	9.4E-5	-4.0	-6.1	-4.7
NNE0869	KFR10	66	107.28	-125	-154.2	3.0E-6	1.2E-5	-4.9	-6.1	-4.7
NNE0869	KFR36	45	115.5	-27.4	-78.1	4.1E-5	6.9E-5	-4.2	-6.1	-4.7
NNE0869	KFR68	60.28	93.82	-42.6	-66.3	4.1E-6	7.0E-6	-5.2	-6.1	-4.7
<b>Possible stress-relief structure</b>										
SBA7	KFR21	26	33	-26	-33	7.7E-6	1.0E-5	-5.0	-	-
SBA7	KFR22	38	39	-32.9	-33.8	9.9E-7	1.4E-6	-5.9	-	-
SBA7	KFR23	23	25	-19.9	-22.5	3.9E-5	4.8E-5	-4.3	-	-
SBA7	KFR31	56	64	-34	-36.1	1.4E-6	2.0E-6	-5.7	-	-
SBA7	KFR33	55	60	-33	-37.1	7.8E-7	1.1E-6	-6.0	-	-
SBA7	KFR35	39	41	-25.4	-27	1.5E-6	1.9E-6	-5.7	-	-
SBA7	KFR37	31	35	-23.1	-26.6	2.1E-6	2.7E-6	-5.6	-	-
SBA7	KFR38	39	41	-28.4	-30.1	6.9E-6	9.2E-6	-5.0	-	-

<sup>1)</sup> Model values for the depth interval (0 to -100 m RHB 70), in the Forsmark SDM.

<sup>2)</sup> Model values from Holmén and Stigsson (2001).



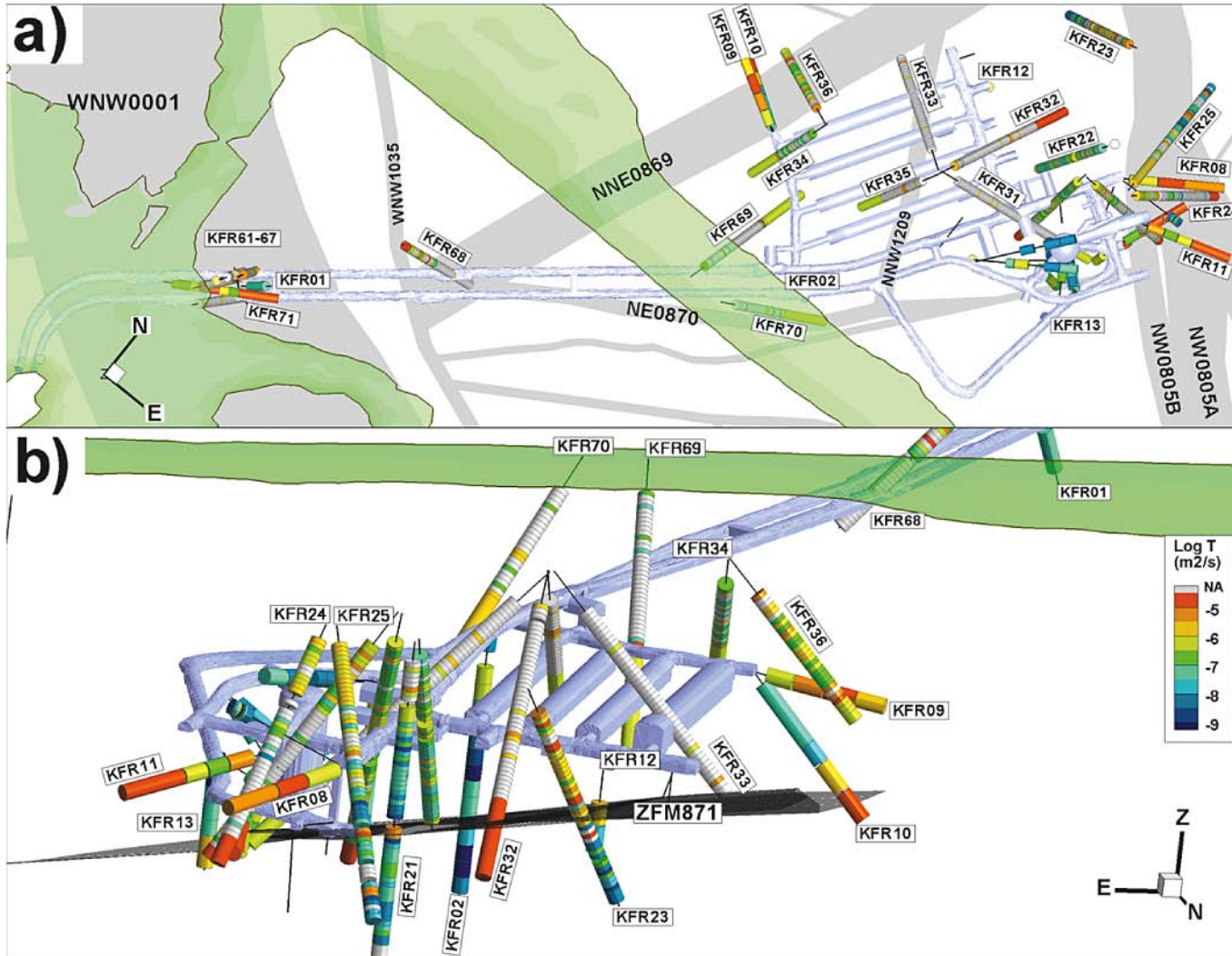


**Figure D-1.** Three-dimensional view of screened single-hole hydraulic data from the existing SFR; a) top view with traces of modelled deformation zones and b) side view towards south, along the dip of ZFM871.

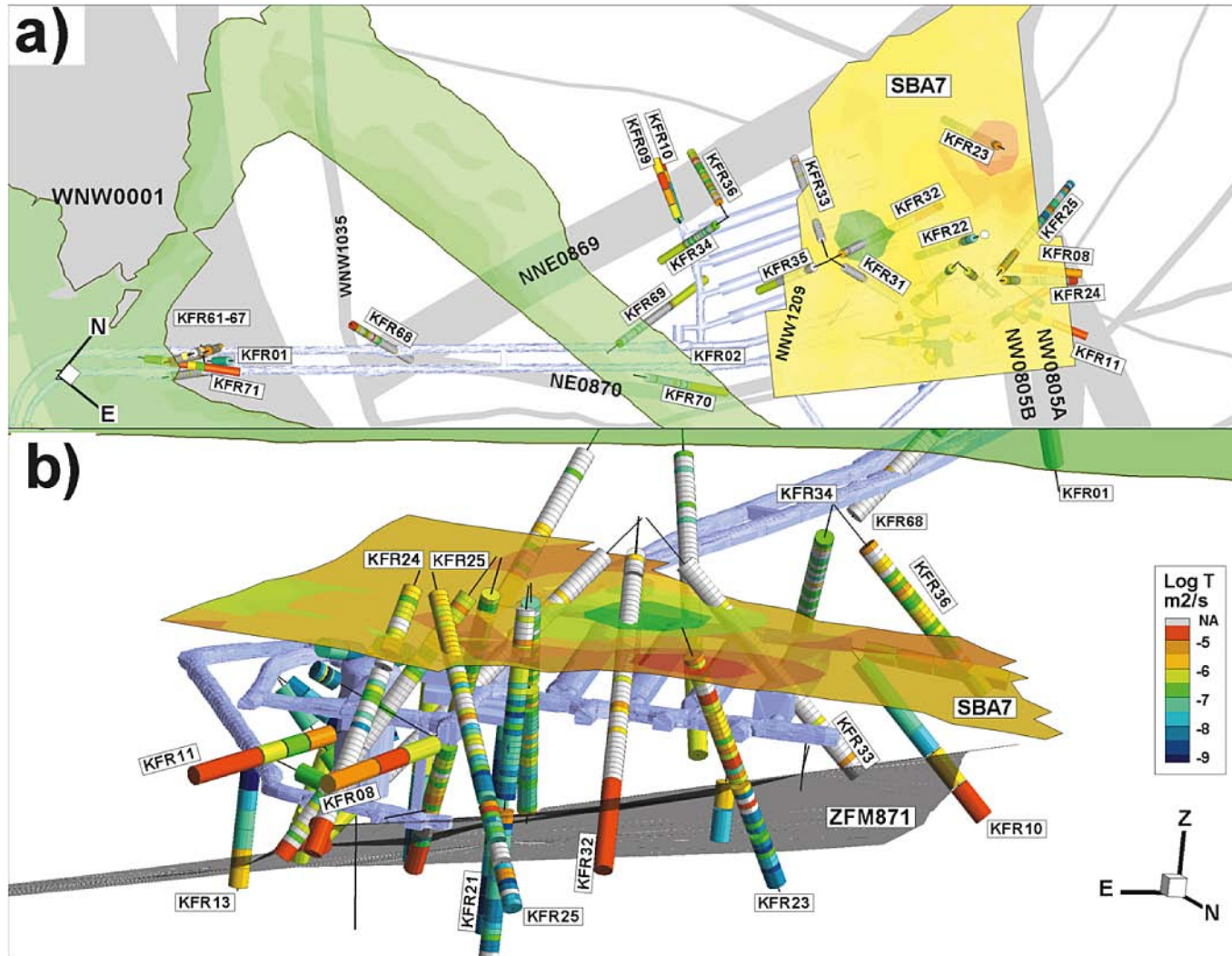


**Figure D-2.** Possible stress-relief structure SBA7 with double-packer hydraulic data from the existing SFR; a) top view with traces of modelled deformation zones and b) side view towards south.

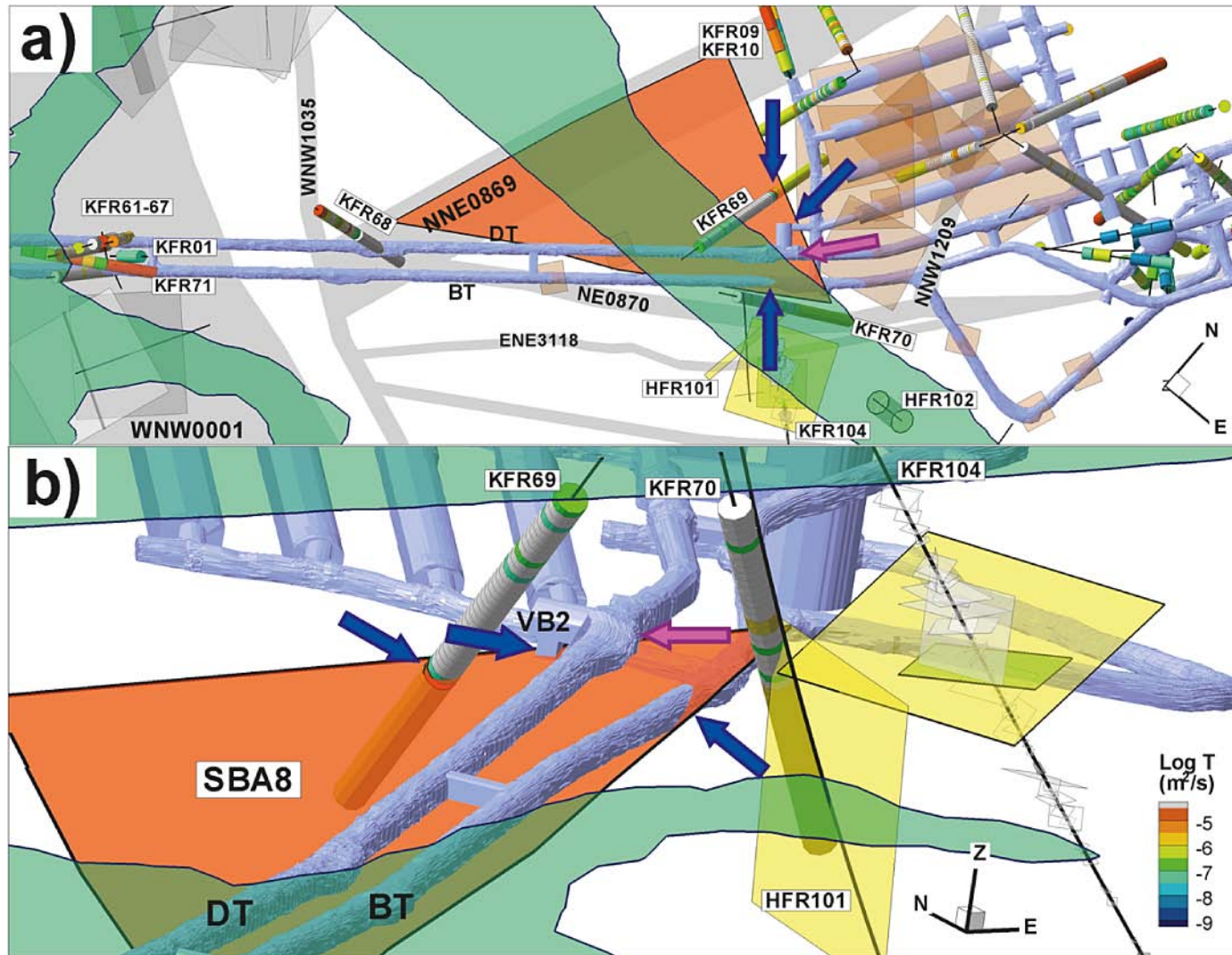


**Figure D-3.** Mapped sub-horizontal structures (brown planes; see Figure 4-1); a) top view, and b) side-view. The structure at 5–780 m associated to 5 tonnes grouting is extrapolated to nearest zone (referred to as SBA8; see Figure 4-3). Blue arrows indicate support and pink arrow indicate lacking support.

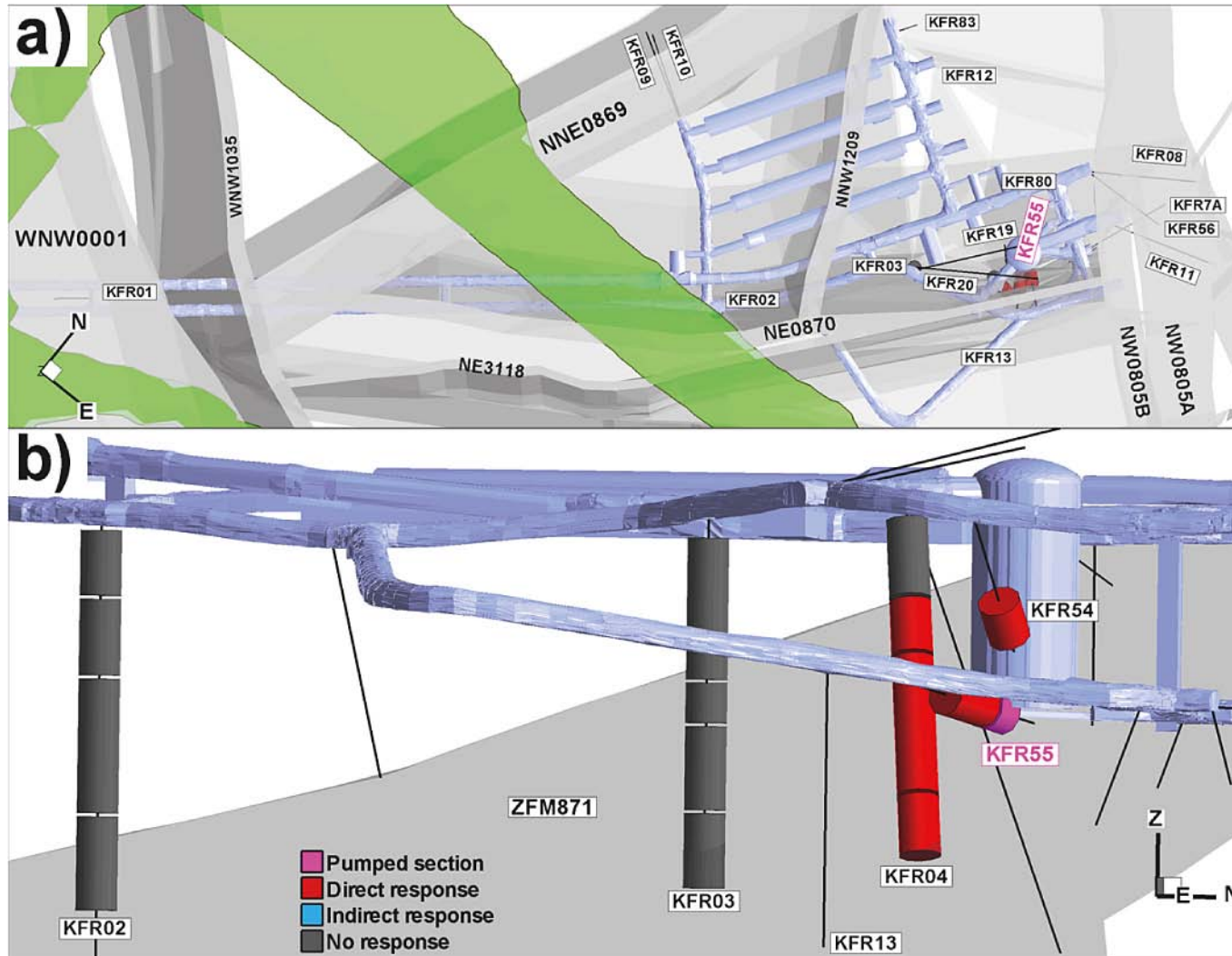


**Figure D-4.** Interference test below the Silo (1985-05-18), just west of ZFMNE0870 (Zon 9) conducted in KFR55 (40–48 m). Responses only found in the immediate vicinity;  $r_{max} = 41$  m. The transmissivity of the tested Section is quite low ( $T < 10^{-7}$  m<sup>2</sup>/s; Figure D-46).

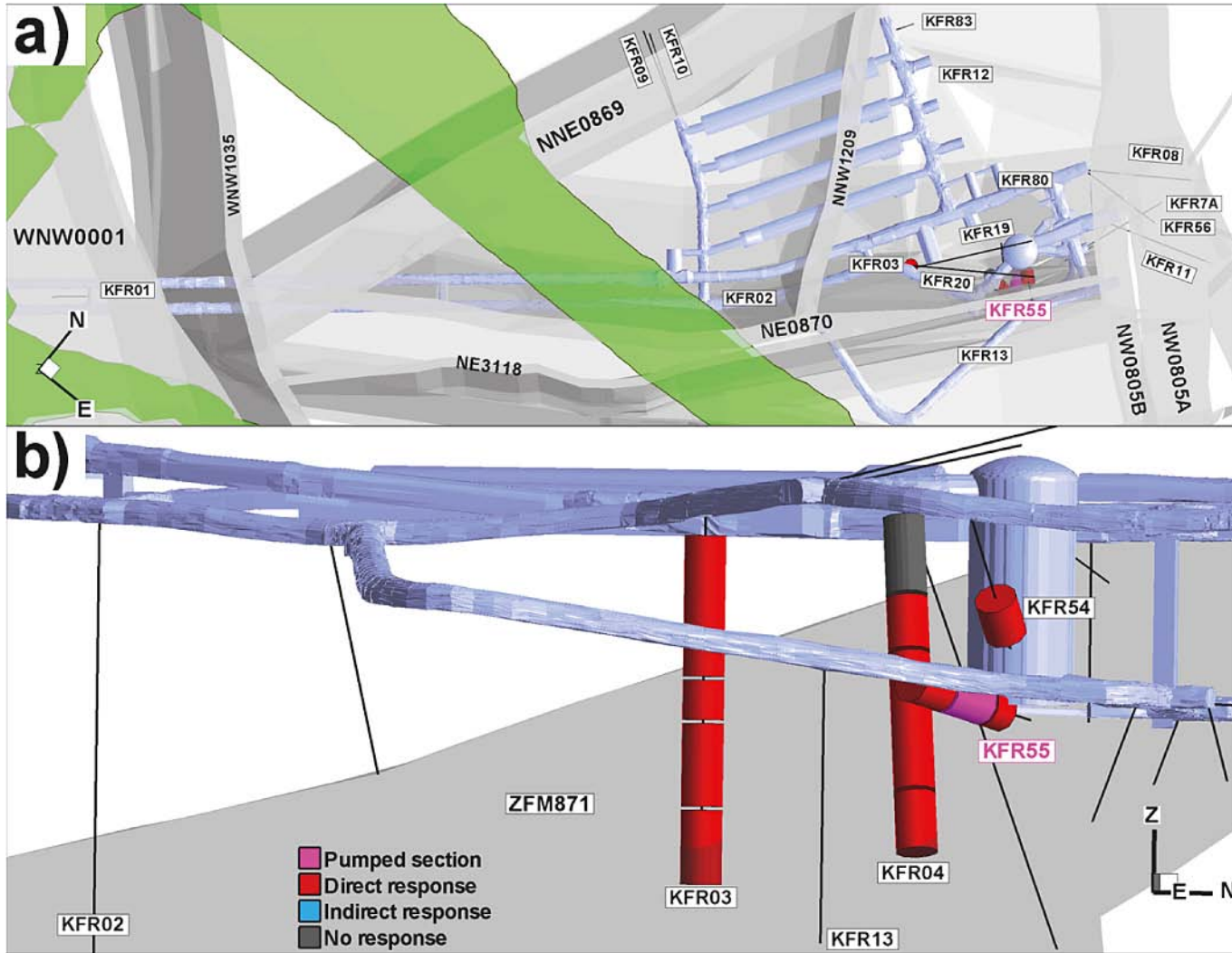


**Figure D-5.** Interference test below the Silo in ZFMNE0870 (Zon 9) conducted in KFR55 (22–39 m). Few monitored sections; responses in ZFMNE0870/ZFM871;  $r_{max} = 103$  m.

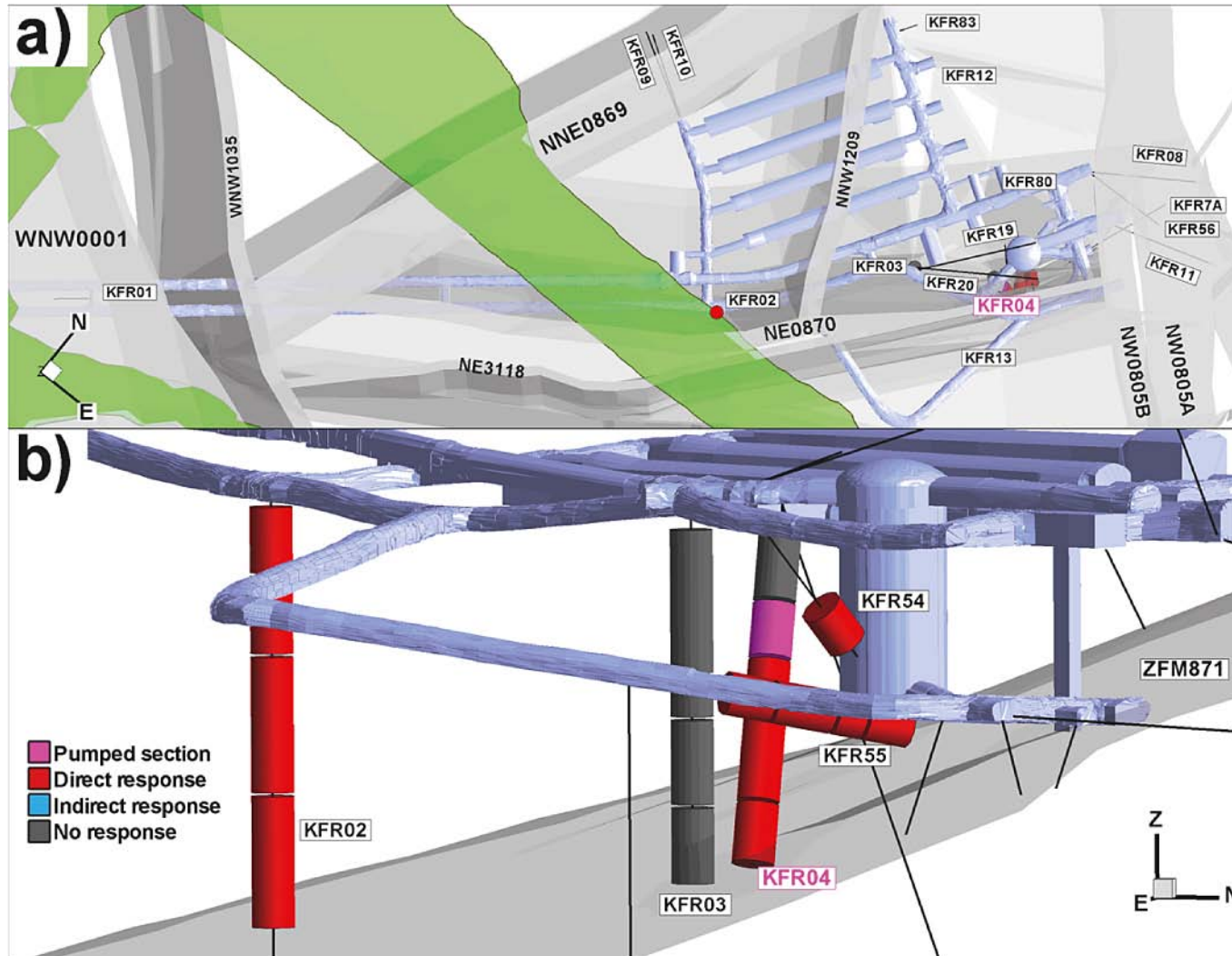


**Figure D-6.** Interference test in ZFMNE0870 (Zon 9) conducted in KFR04 (28–43 m). Few monitored sections; responses in ZFMNE0870/ZFM871;  $r_{max} = 259$  m (KFR02).

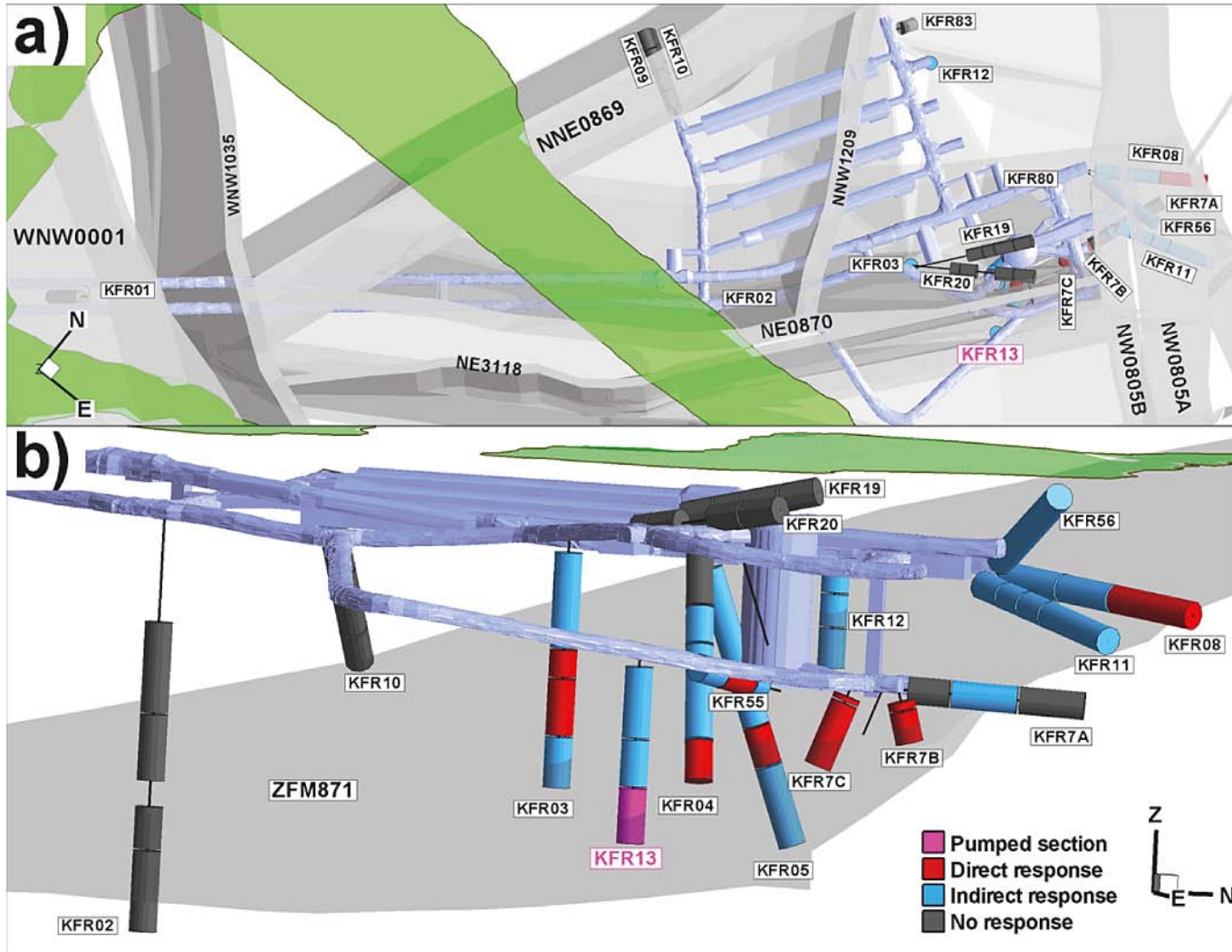


**Figure D-7.** Interference test in ZFM871 (1986-04-04), west of ZFMNE0870 (Zon 9), in KFR13 (54–76.6 m). Responses in ZFMNE0870, ZFM871, and ZFMNW0805A;  $r_{max} = 232$  m (KFR08).

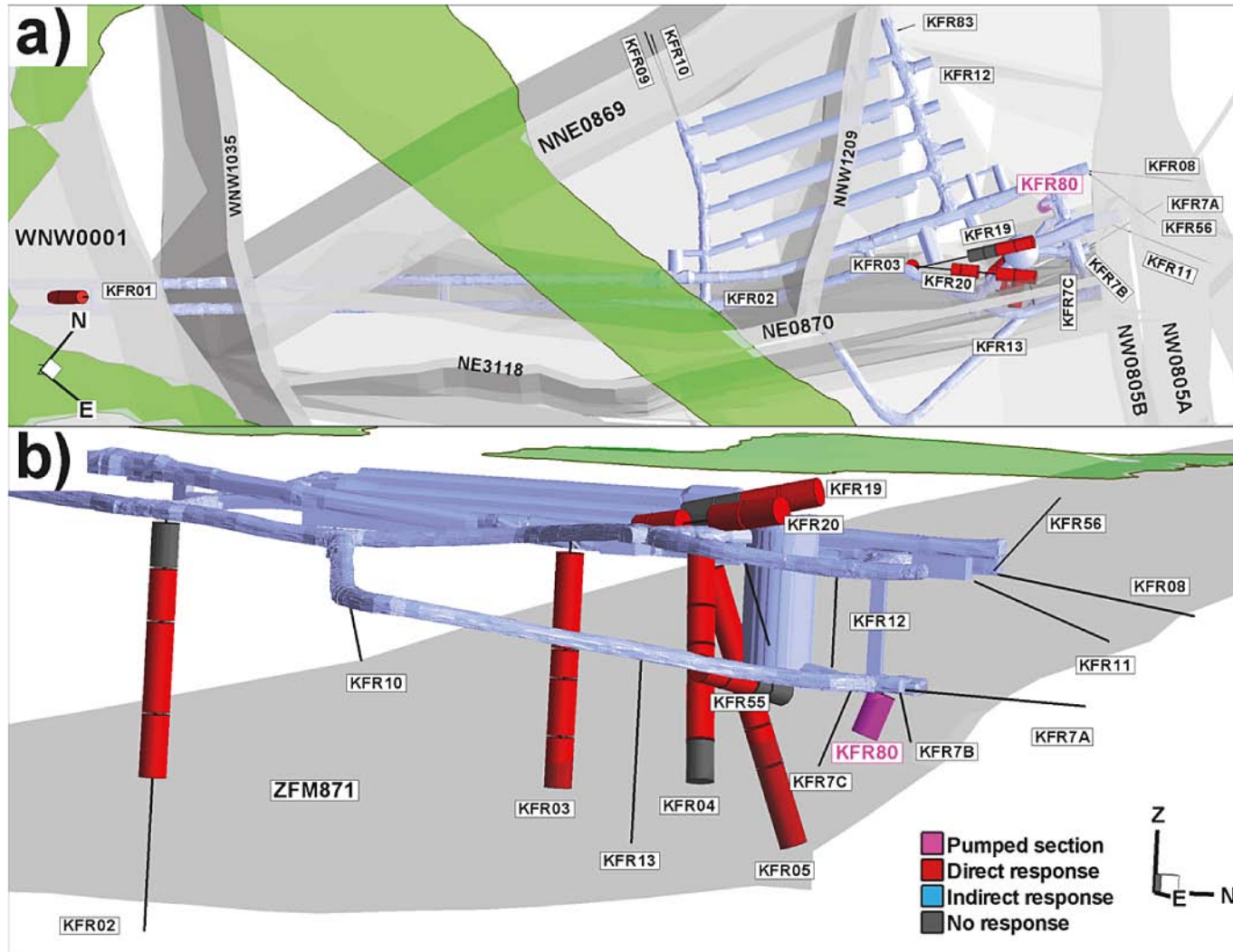


**Figure D-8.** "Unintentional interference test" (1986-01-02) in KFR80 (1.5–20 m) in ZFM871. Wide-spread responses in ZFMNE0870 and ZFM871, but also vertically;  $r_{max} = 871$  m (KFR01).







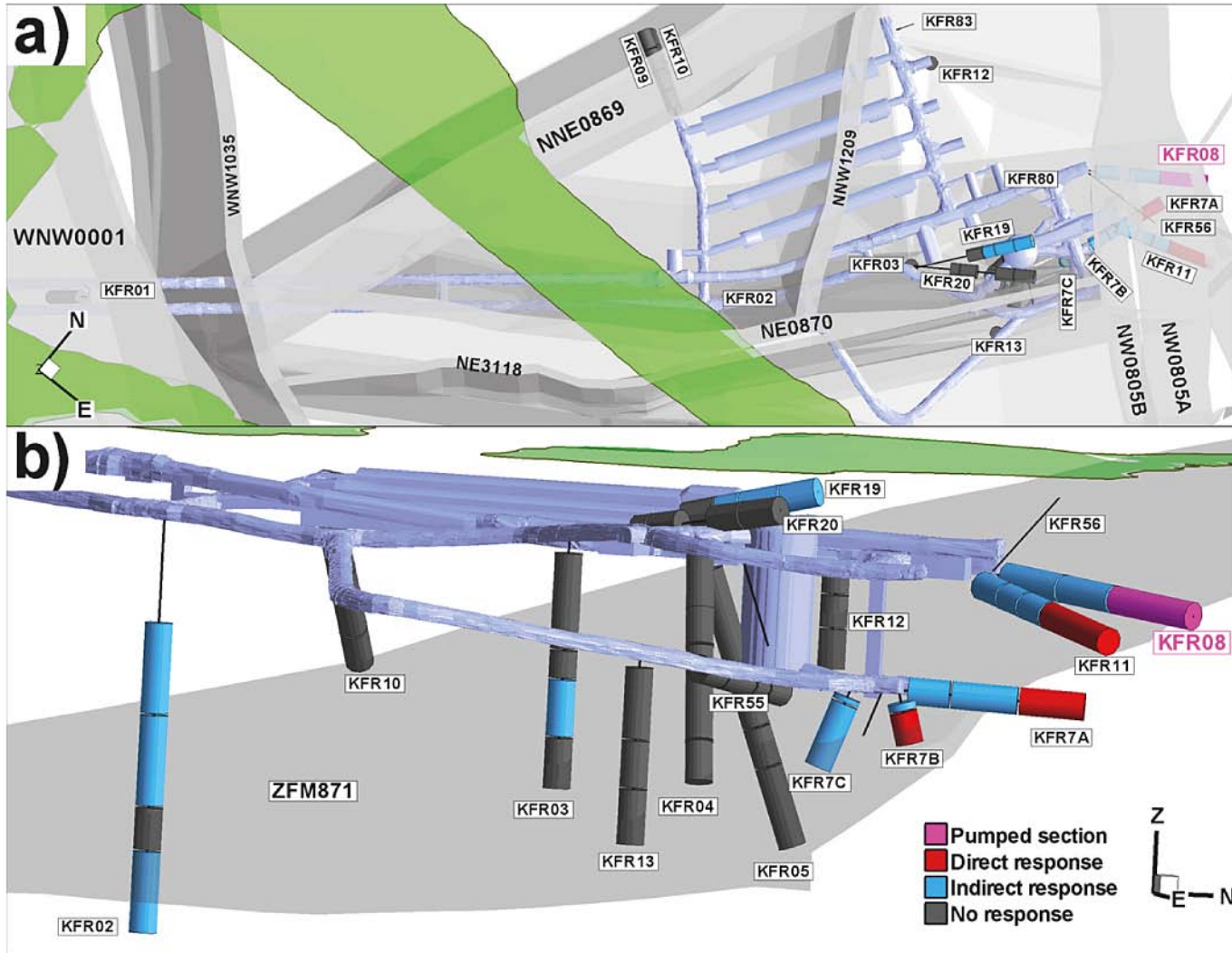


**Figure D-II.** Interference test in KFR08 (63–104 m) in ZFMNW0805A (1986-04-12). Three direct responses in ZFMNW0805A,B and ZFM871 and 17 indirect responses ( $r_{max} = 450$  m in KFR02).

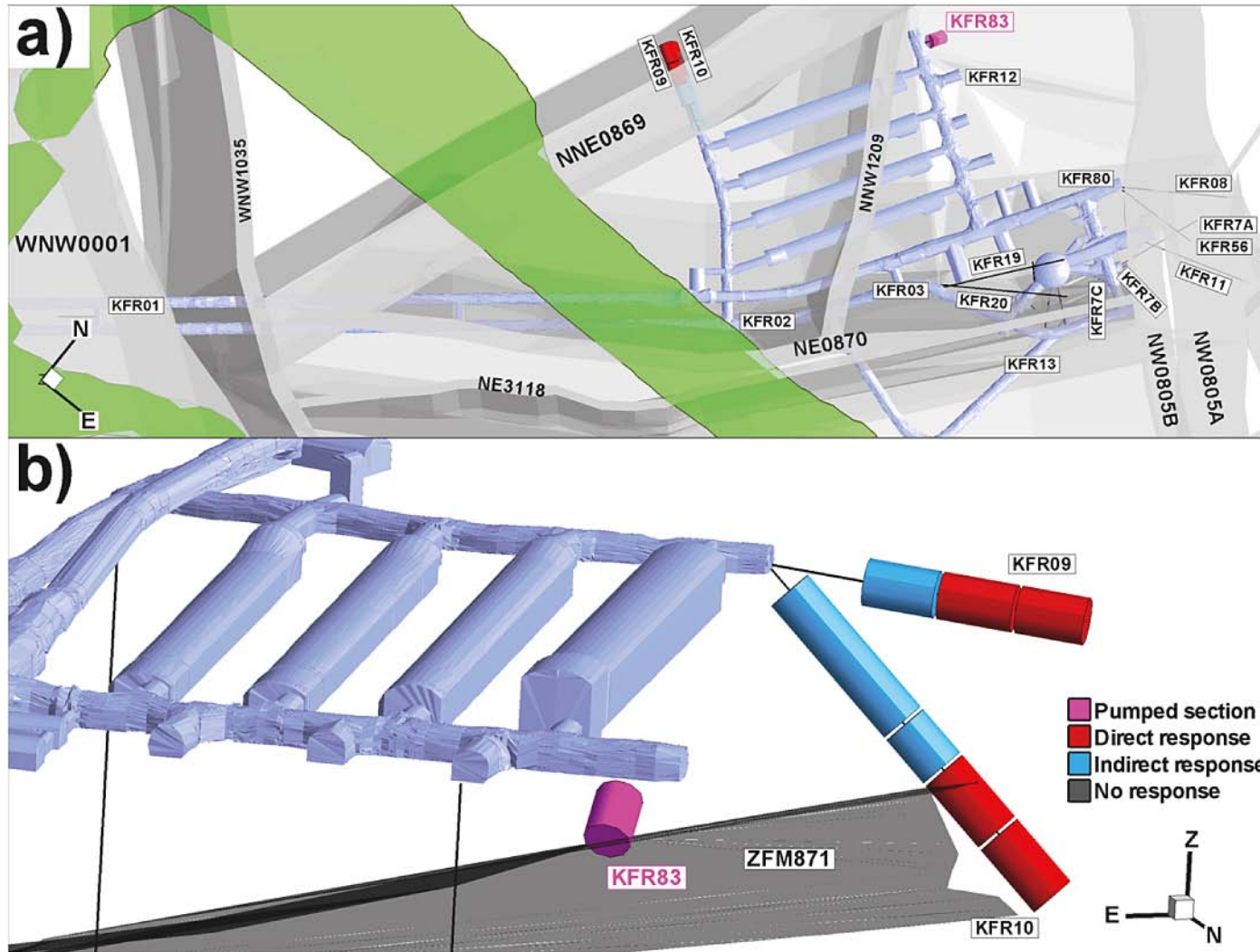


**Figure D-12.** Interference test in KFR83 (5–20 m) in ZFM871. Responses in ZFMNNE0869 (Zon 3); KFR10\_DZ2 interpreted as an extension of ZFM871, and KFR09\_DZ2 as a splay of ZFMNNE0869;  $r_{max} = 230$  m.

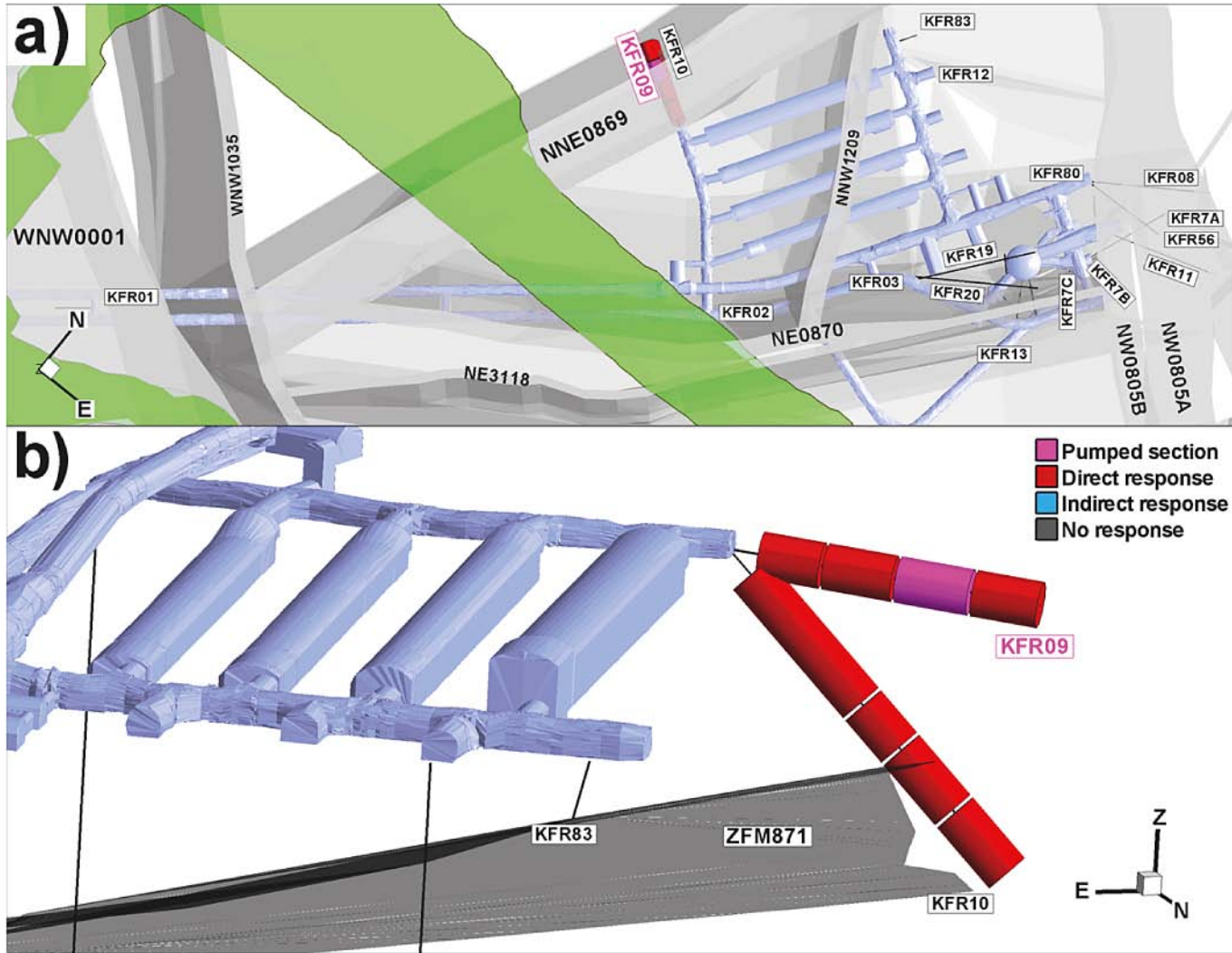


Figure D-13. Interference test in KFR09 (43–62 m) in ZFMNNE0869. Responses within the zone; KFR10\_DZ2 interpreted as an extension of ZFM871, and KFR09\_DZ2 as a splay of ZFMNNE0869;  $r_{max} = 67$  m.

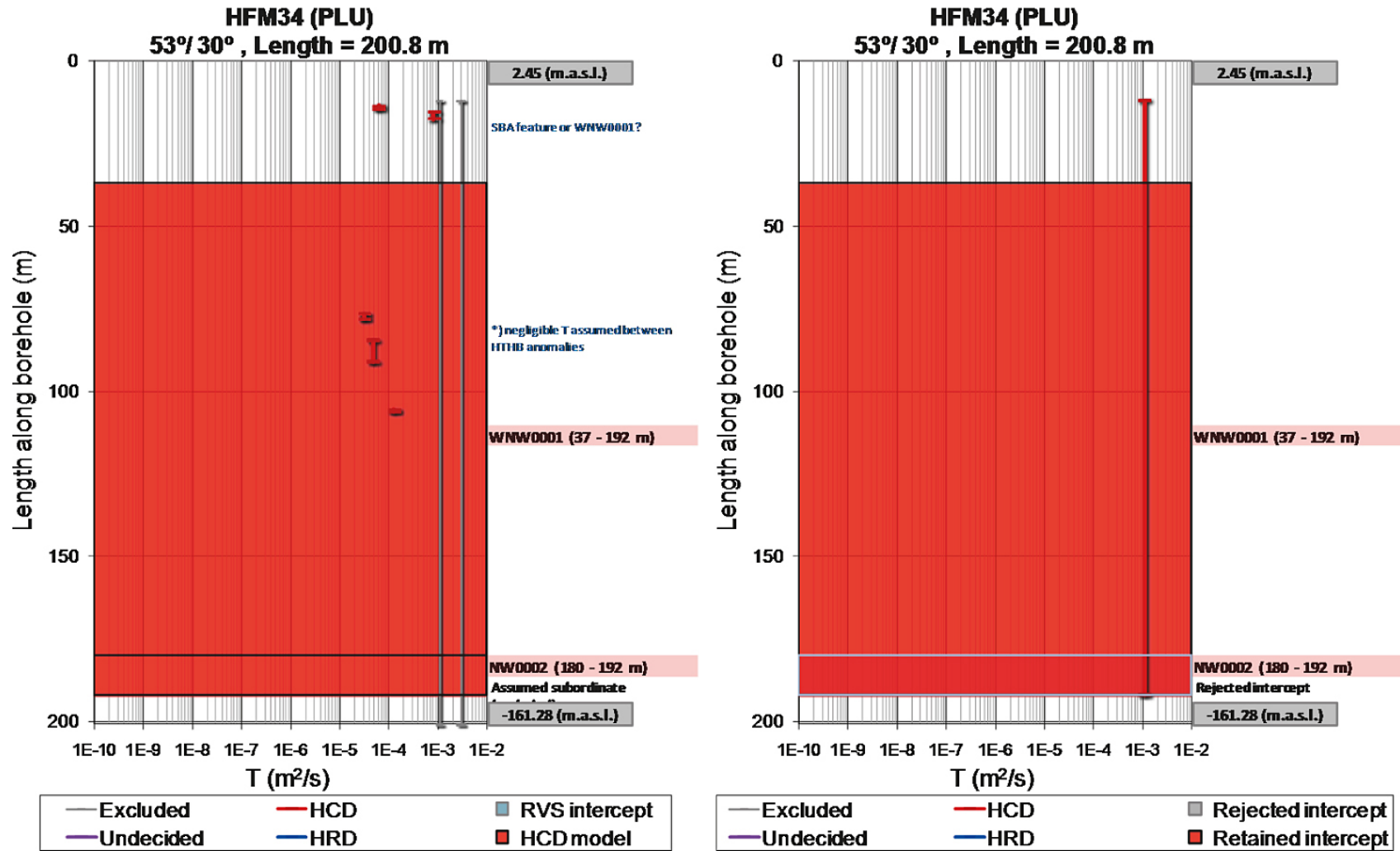


Figure D-14. HFM34: available data after screening process and modelled deformation zone intercepts (left) and interpreted total transmissivities and retained intercepts (right).

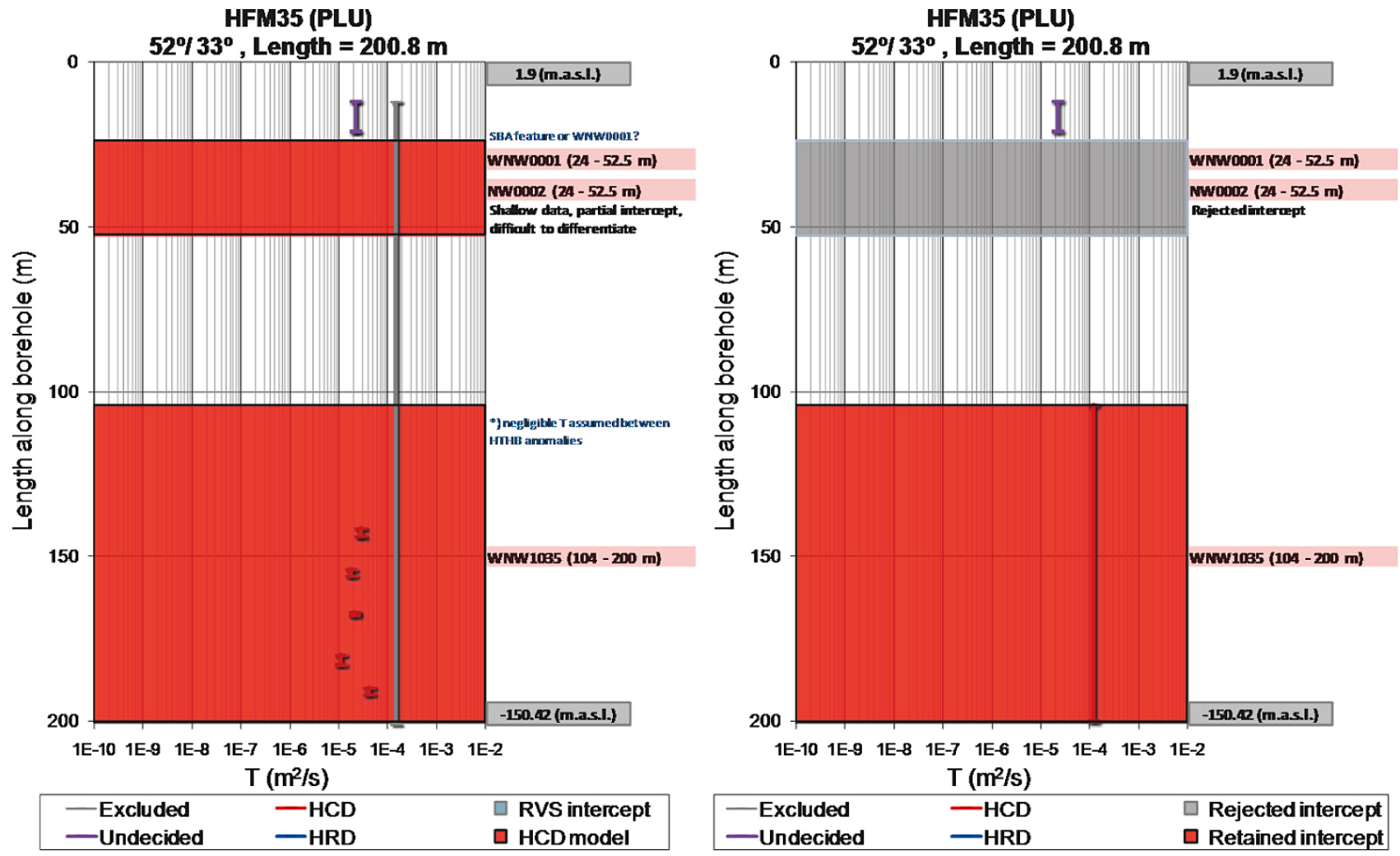


Figure D-15. HFM35: available data after screening process and modelled deformation zone intercepts (left) and interpreted total transmissivities and retained intercepts (right). The WNW0001/NW0002 intercept is rejected, as there exists intercepts with better coverage.

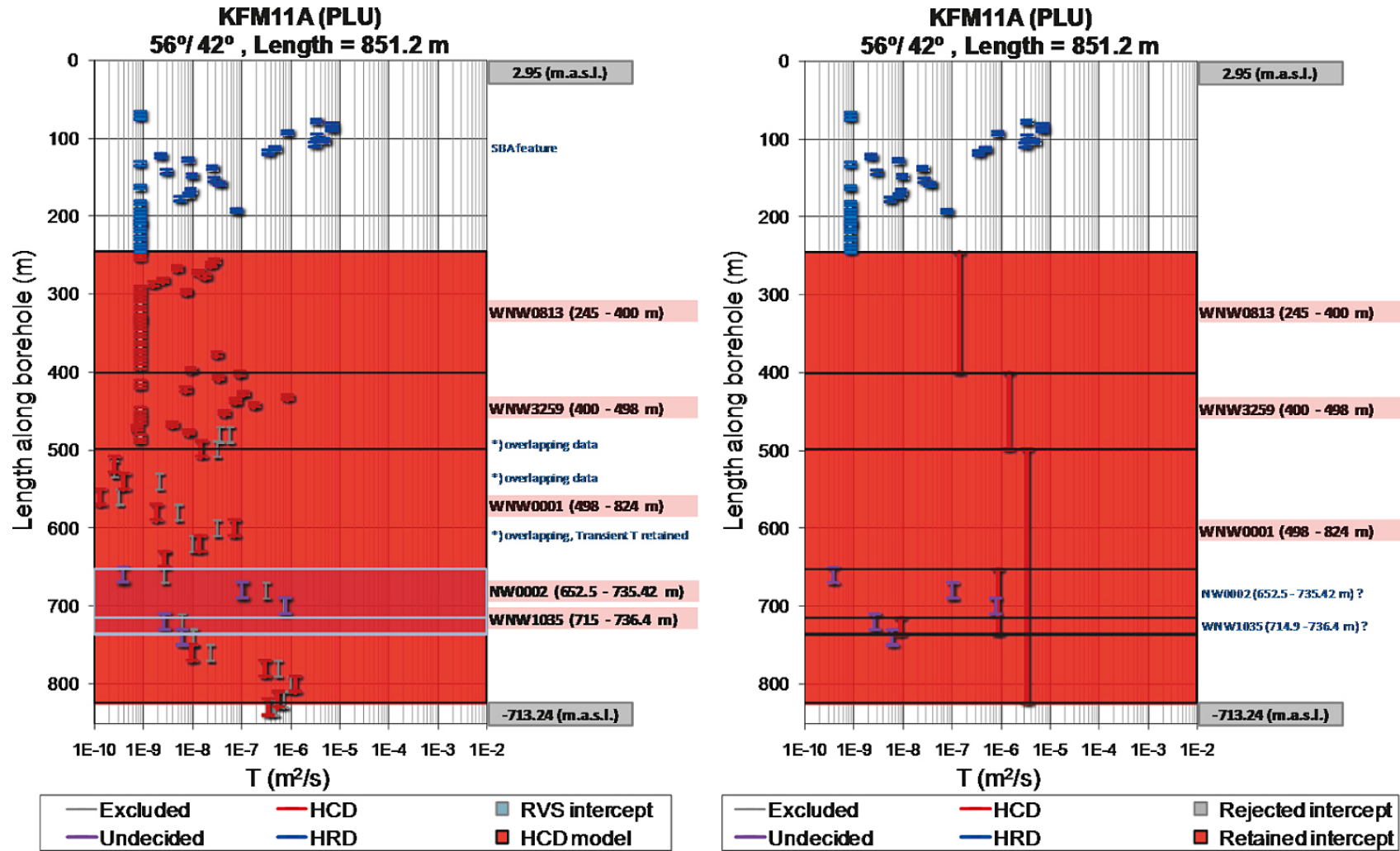


Figure D-16. KFM11A: available data after screening process and modelled deformation zone intercepts (left) and interpreted total transmissivities and retained intercepts (right). ZFMWNW0001 is overlapped by two RVS intercepts: ZFMNW0002 and ZFMWNW1035.



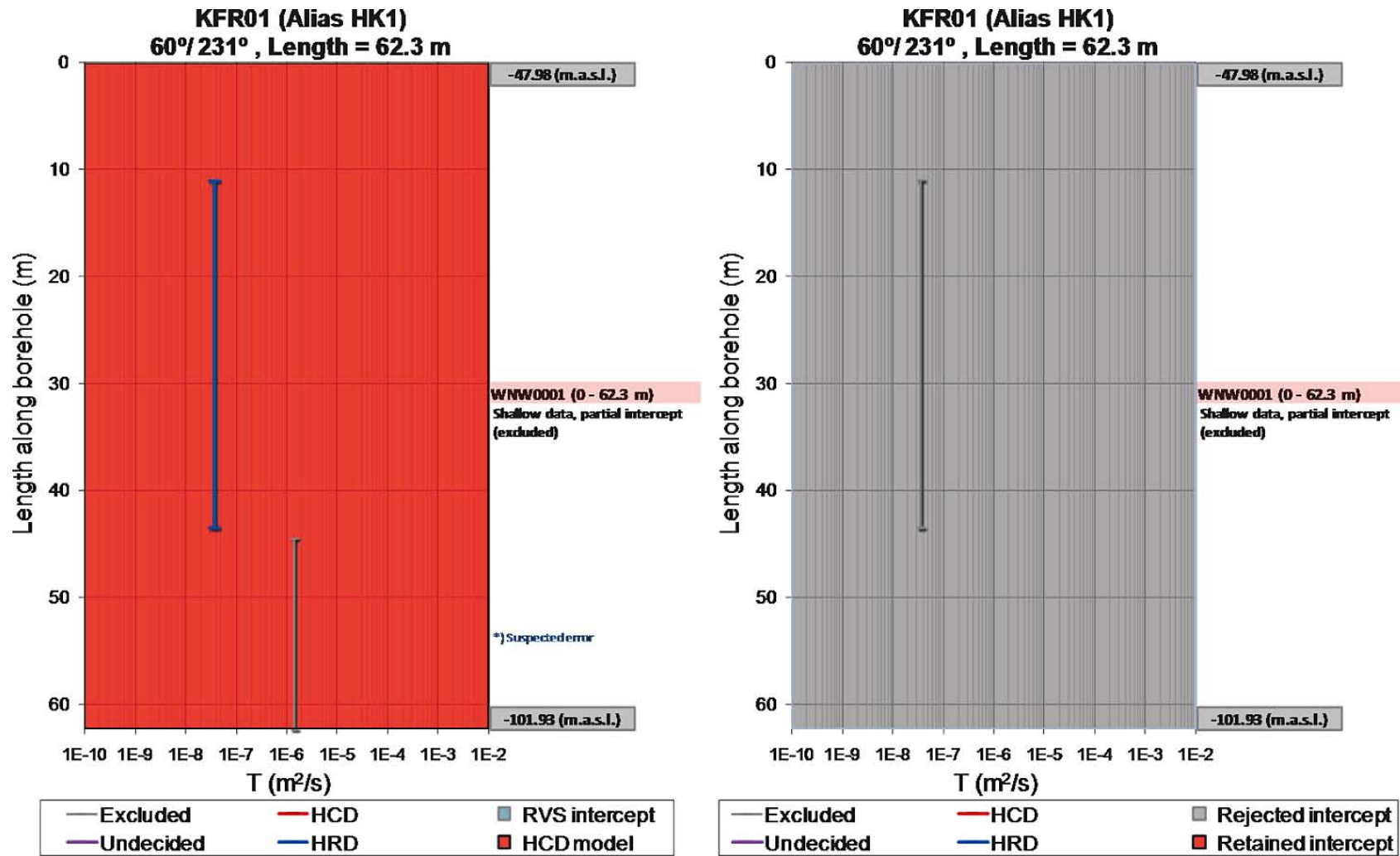


Figure D-17. KFR01: available data after screening process and modelled deformation zone intercepts (left) and interpreted total transmissivities and retained intercepts (right). The borehole reflects an incomplete, low-transmissive section of WNW0001, which is judged unrepresentative.

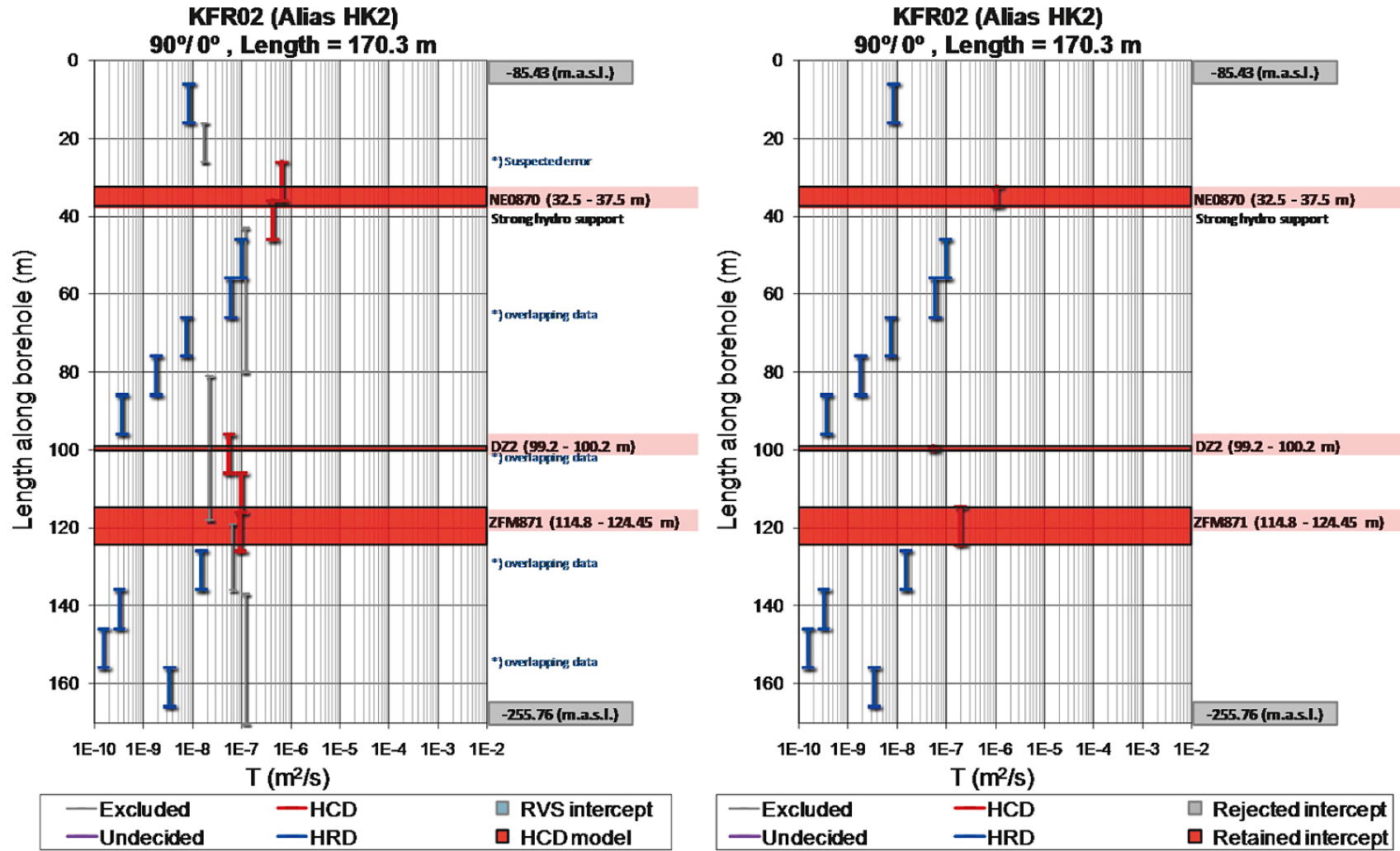


Figure D-18. KFR02: available data after screening process and modelled deformation zone intercepts (left) and interpreted total transmissivities and retained intercepts (right). This ZFM871-intercept suggests lower transmissivity in the south-western part of ZFM871.

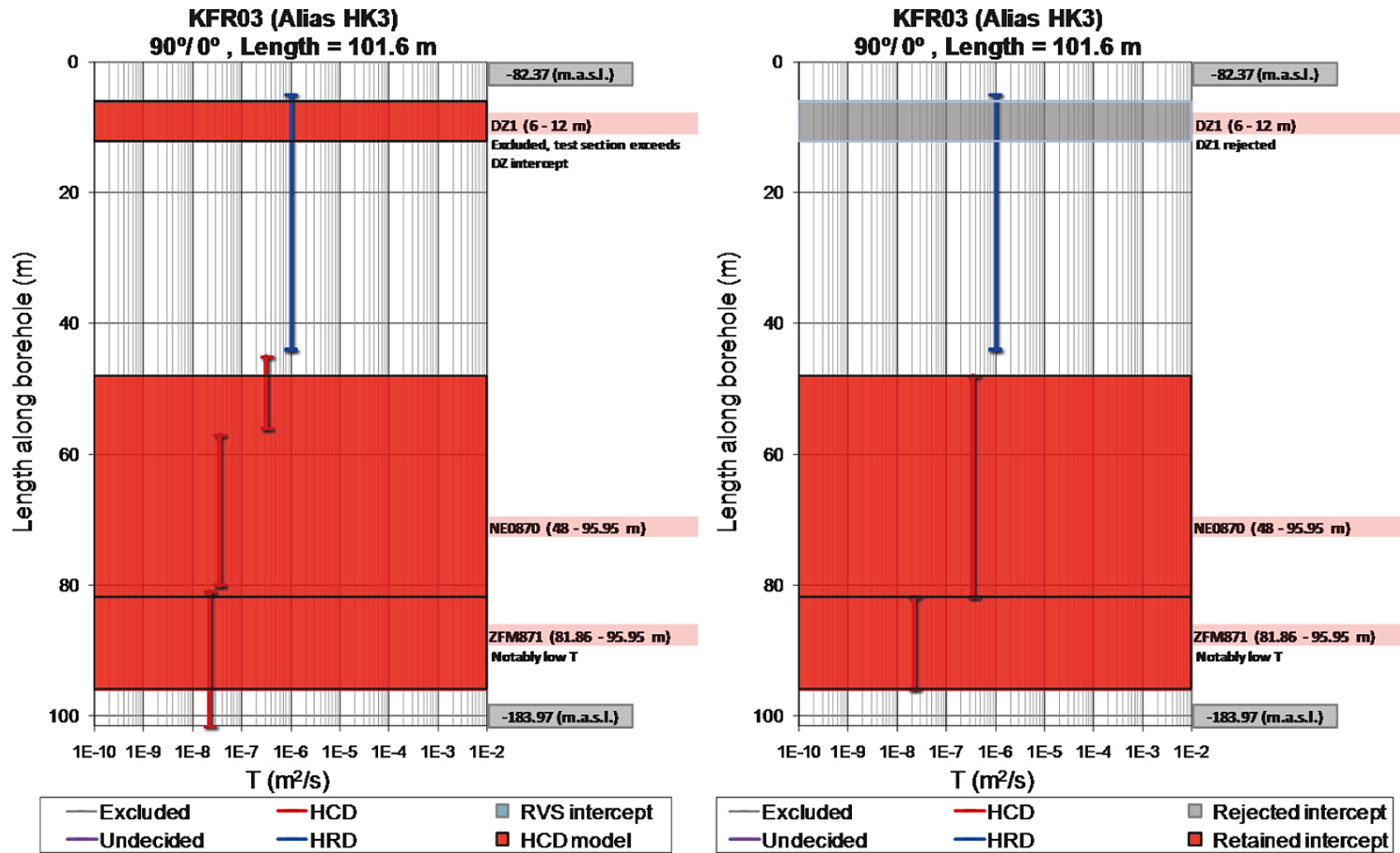


Figure D-19. KFR03: available data after screening process and modelled deformation zone intercepts (left) and interpreted total transmissivities and retained intercepts (right). The ZFM871 intercept has notably low transmissivity.

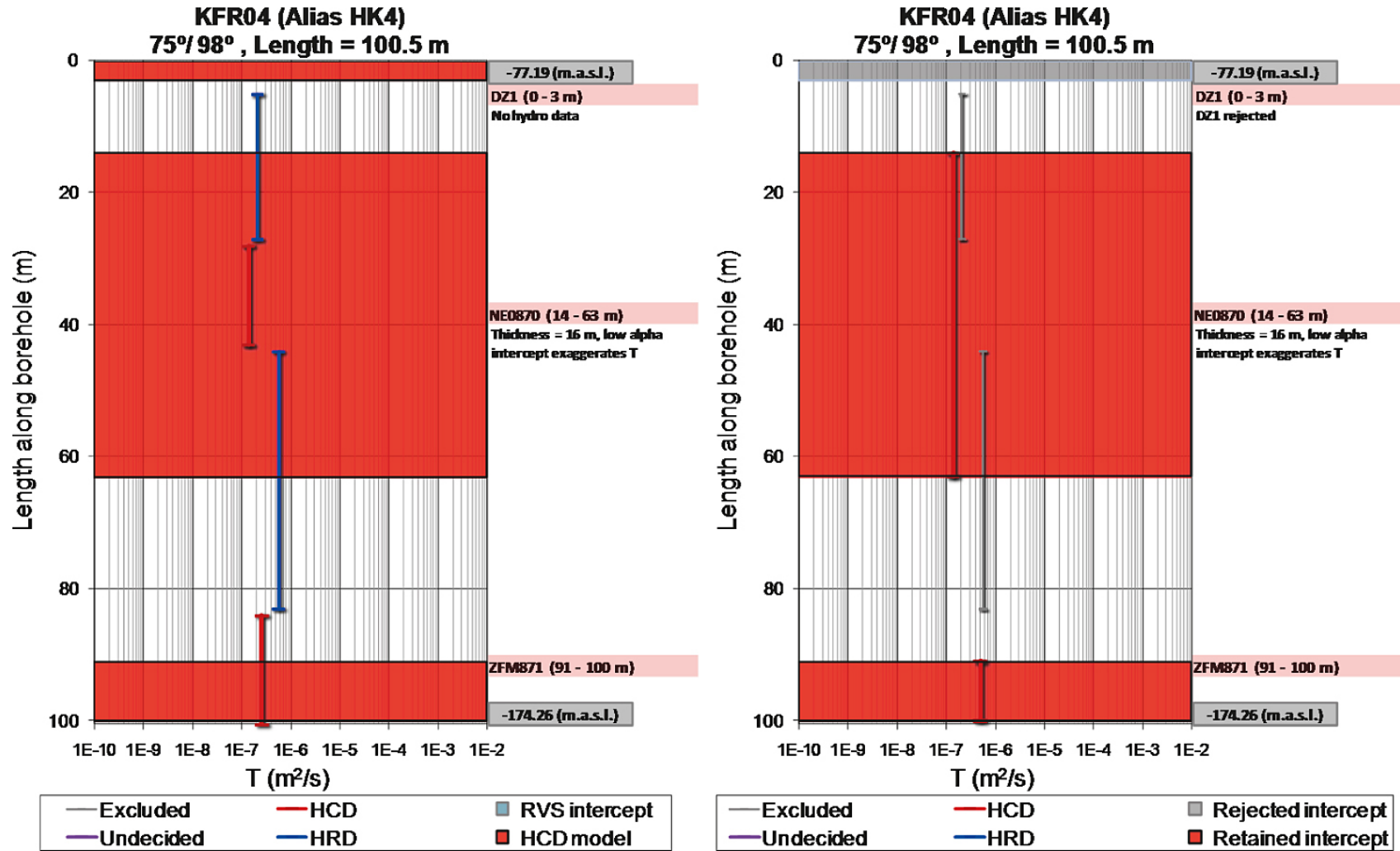


Figure D-20. KFR04: available data after screening process and modelled deformation zone intercepts (left) and interpreted total transmissivities and retained intercepts (right). NE0870 is characterised as a thin zone (<16 m); thus a somewhat lower transmissivity is judged representative.

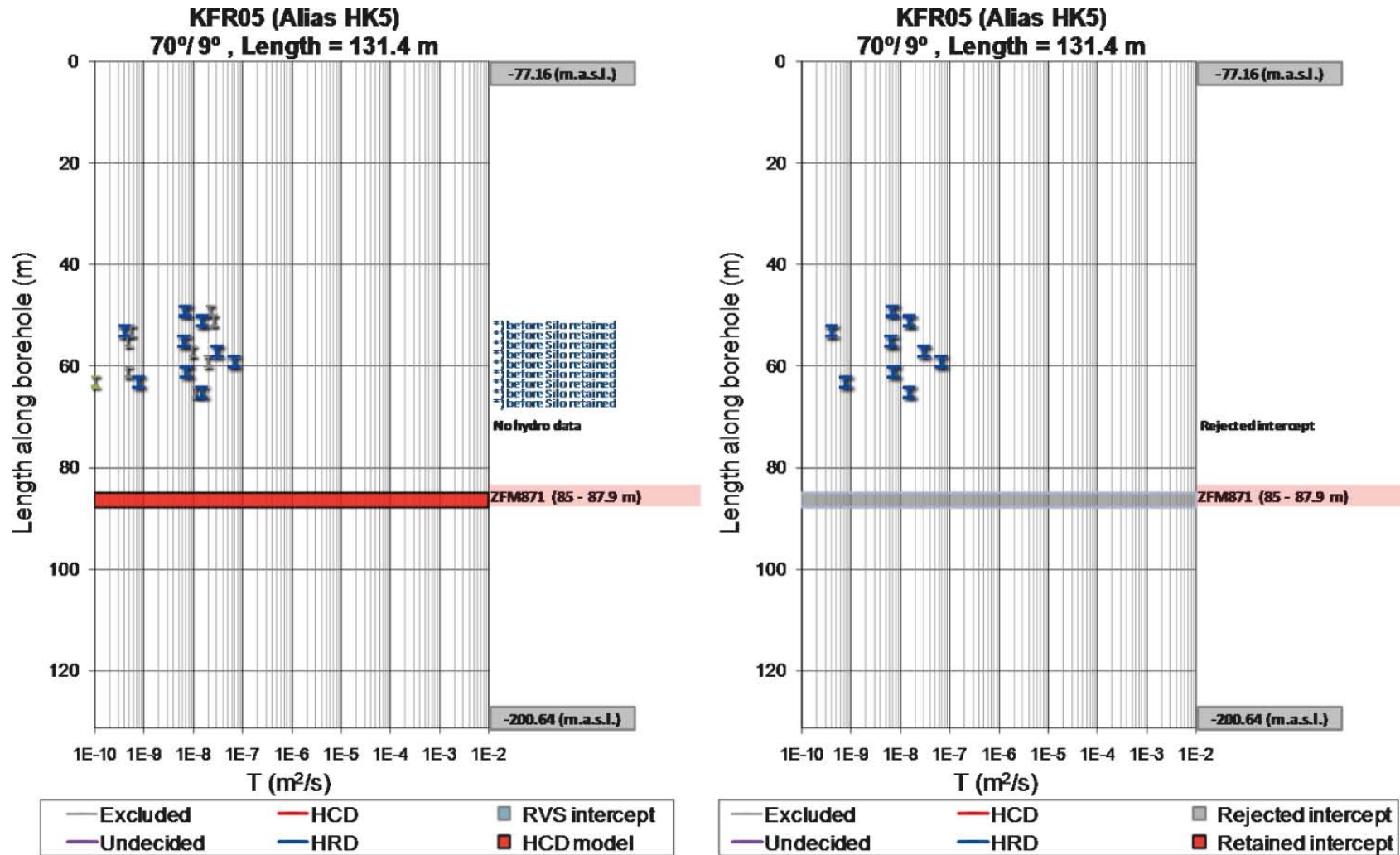
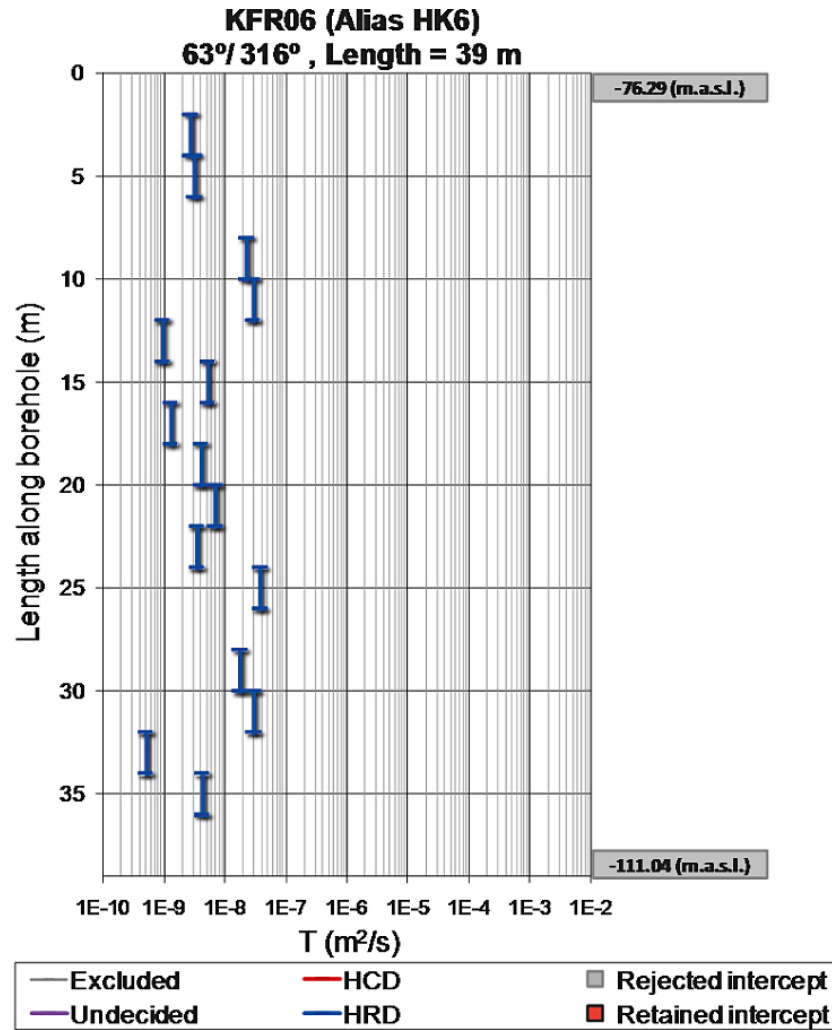
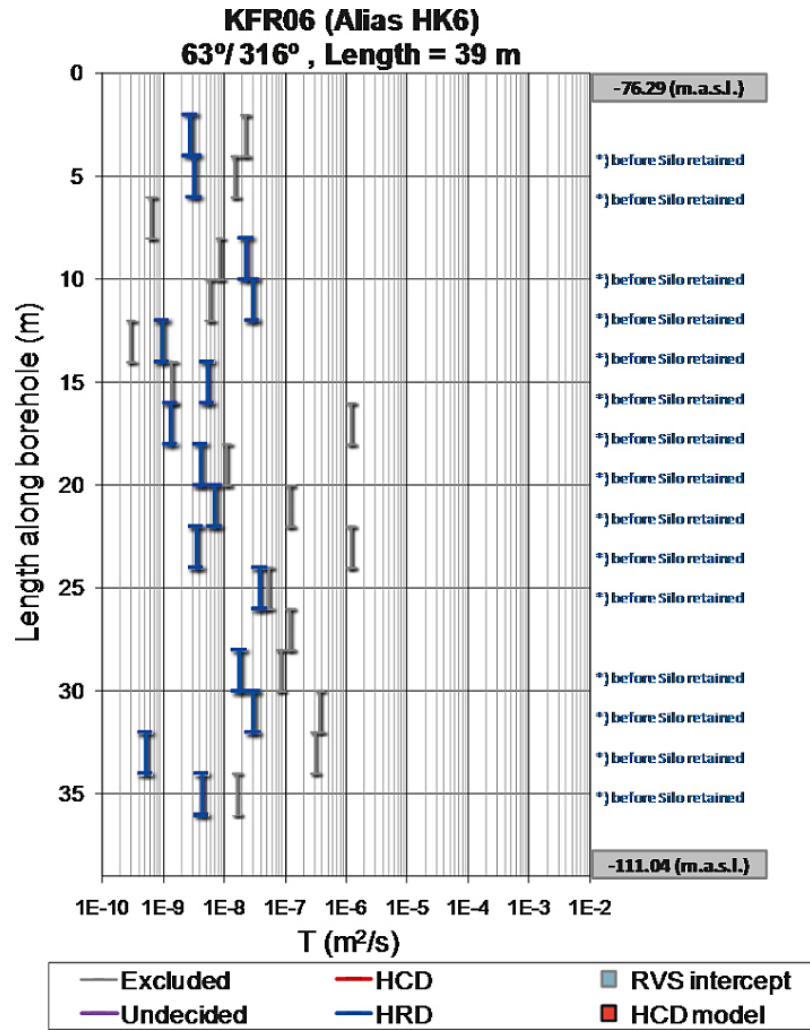


Figure D-21. KFR05: available data after screening process and modelled deformation zone intercepts (left) and interpreted total transmissivities and retained intercepts (right). No hydraulic data available inside the ZFM871 intercept.



**Figure D-22.** KFR06: available data after screening process and modelled deformation zone intercepts (left) and interpreted total transmissivities and retained intercepts (right). Measurements before and after construction of the Silo.

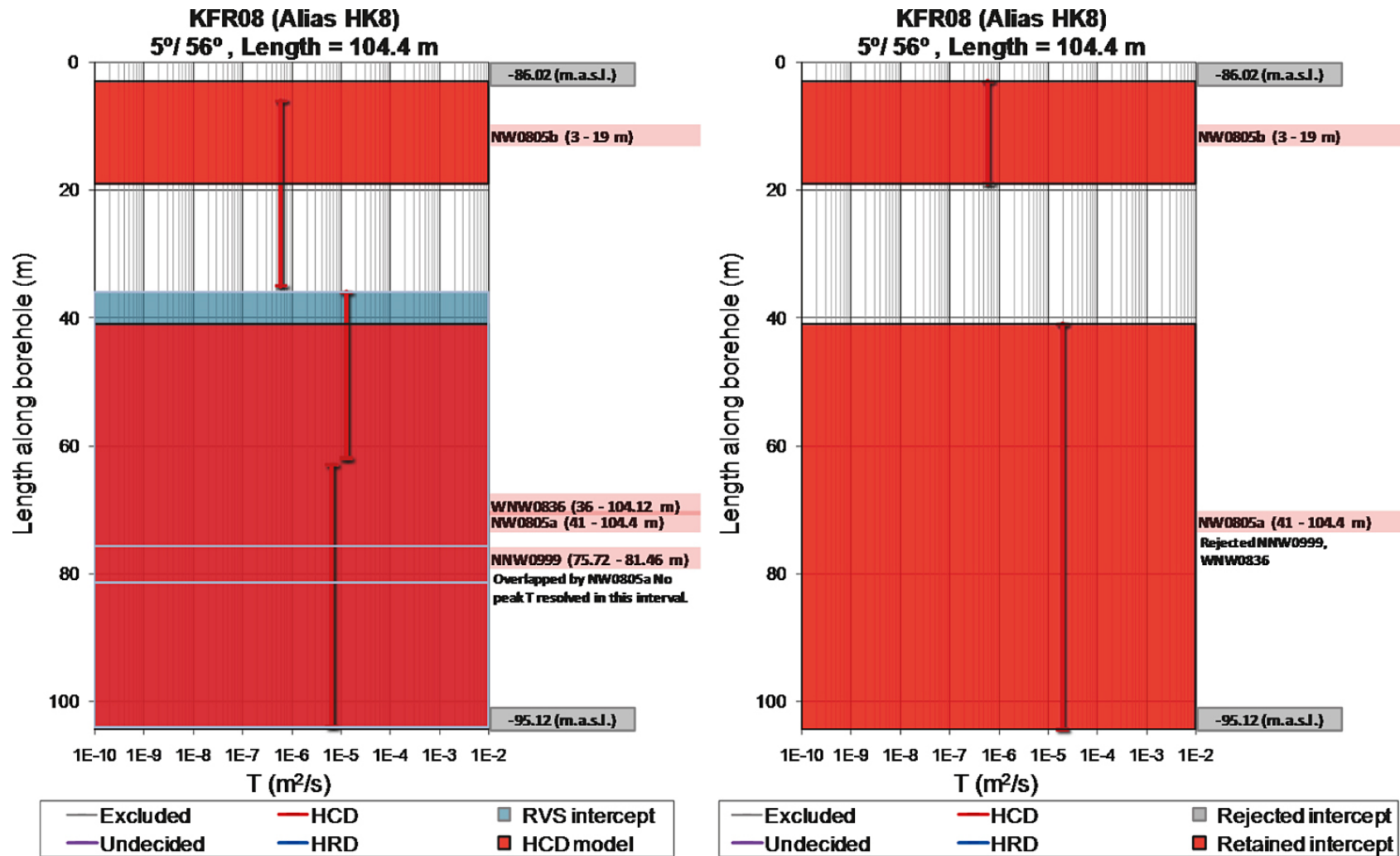


Figure D-23. KFR08: available data after screening process and modelled deformation zone intercepts (left) and interpreted total transmissivities and retained intercepts (right). Baltic watertype in both NW0805A,B intercepts.

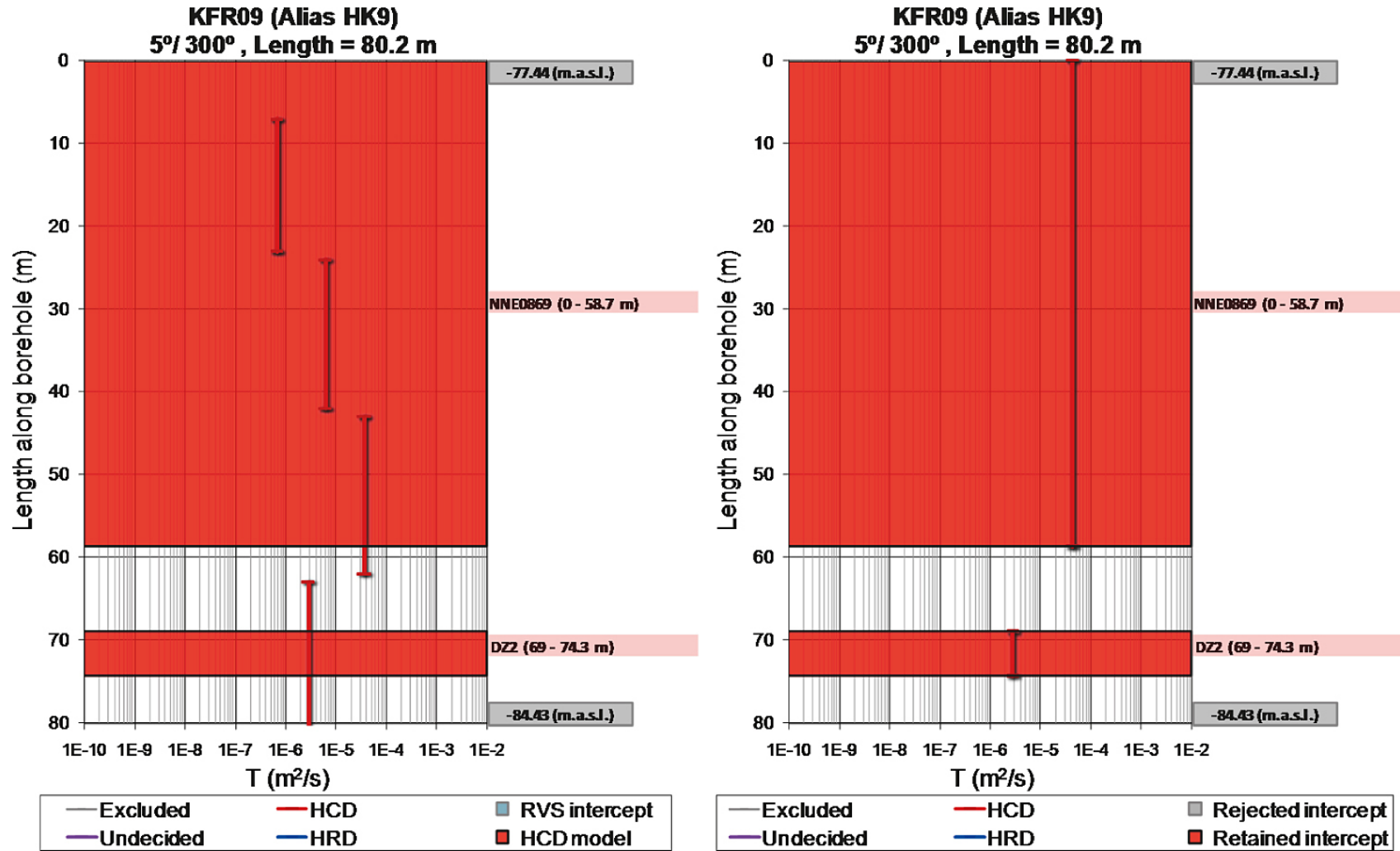


Figure D-24. KFR09: available data after screening process and modelled deformation zone intercepts (left) and interpreted total transmissivities and retained intercepts (right). KFR09\_DZ02 possibly being a splay of ZFMNNE0869.



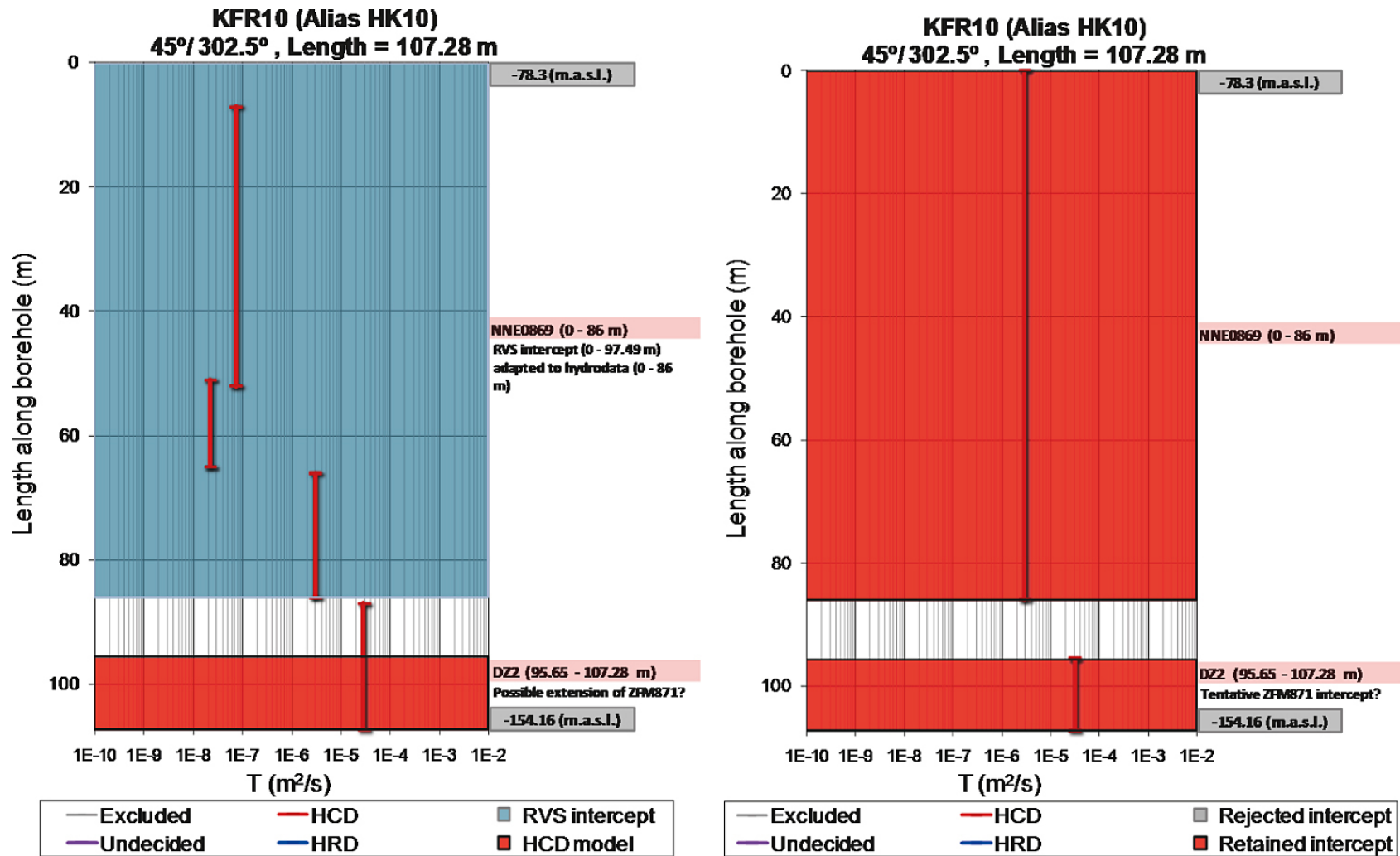


Figure D-25. KFR10: available data after screening process and modelled deformation zone intercepts (left) and interpreted total transmissivities and retained intercepts (right). KFR10\_DZ2 is assumed to be an extension of ZFM871 through NNE0869.

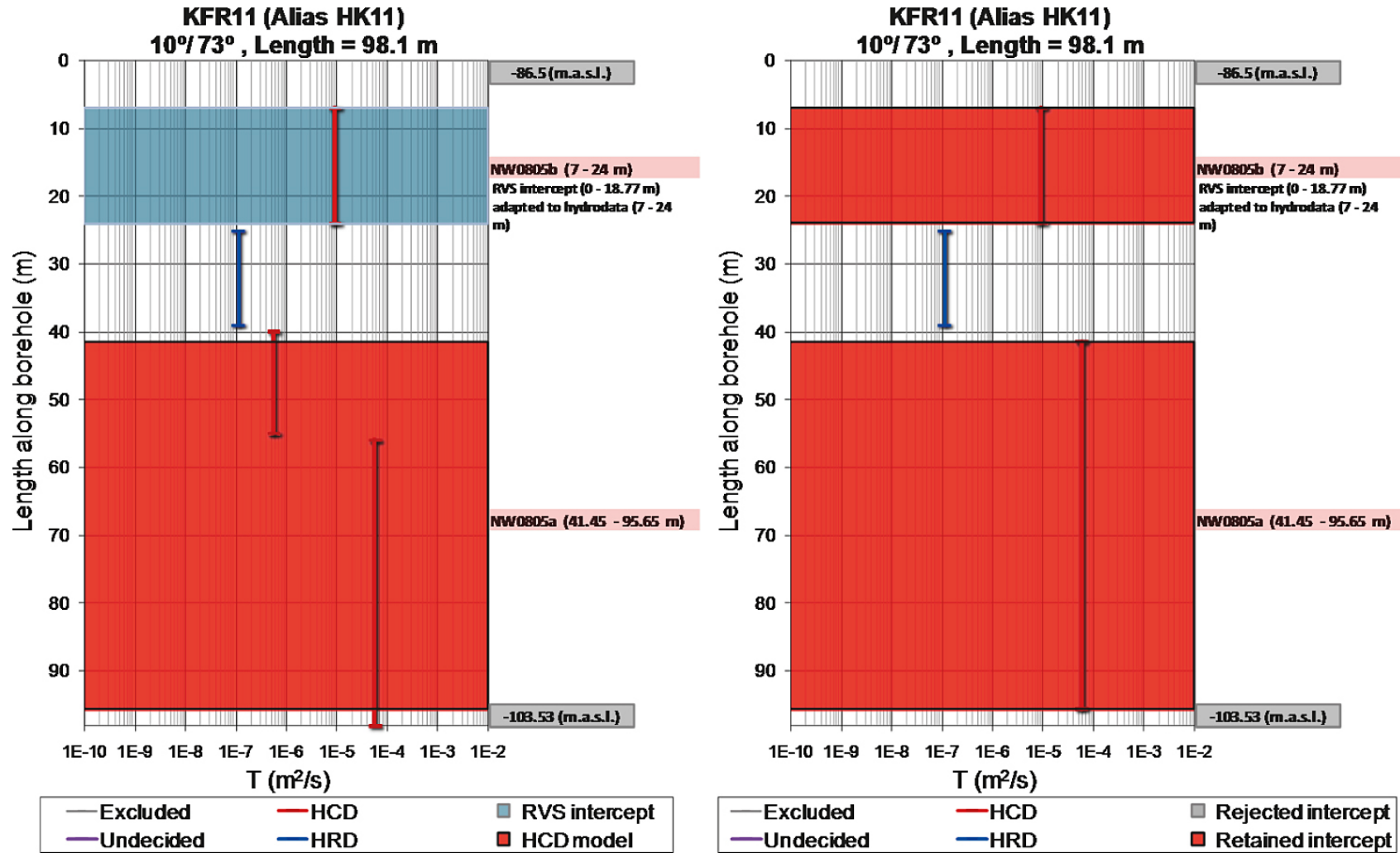


Figure D-26. KFR11: available data after screening process and modelled deformation zone intercepts (left) and interpreted total transmissivities and retained intercepts (right).

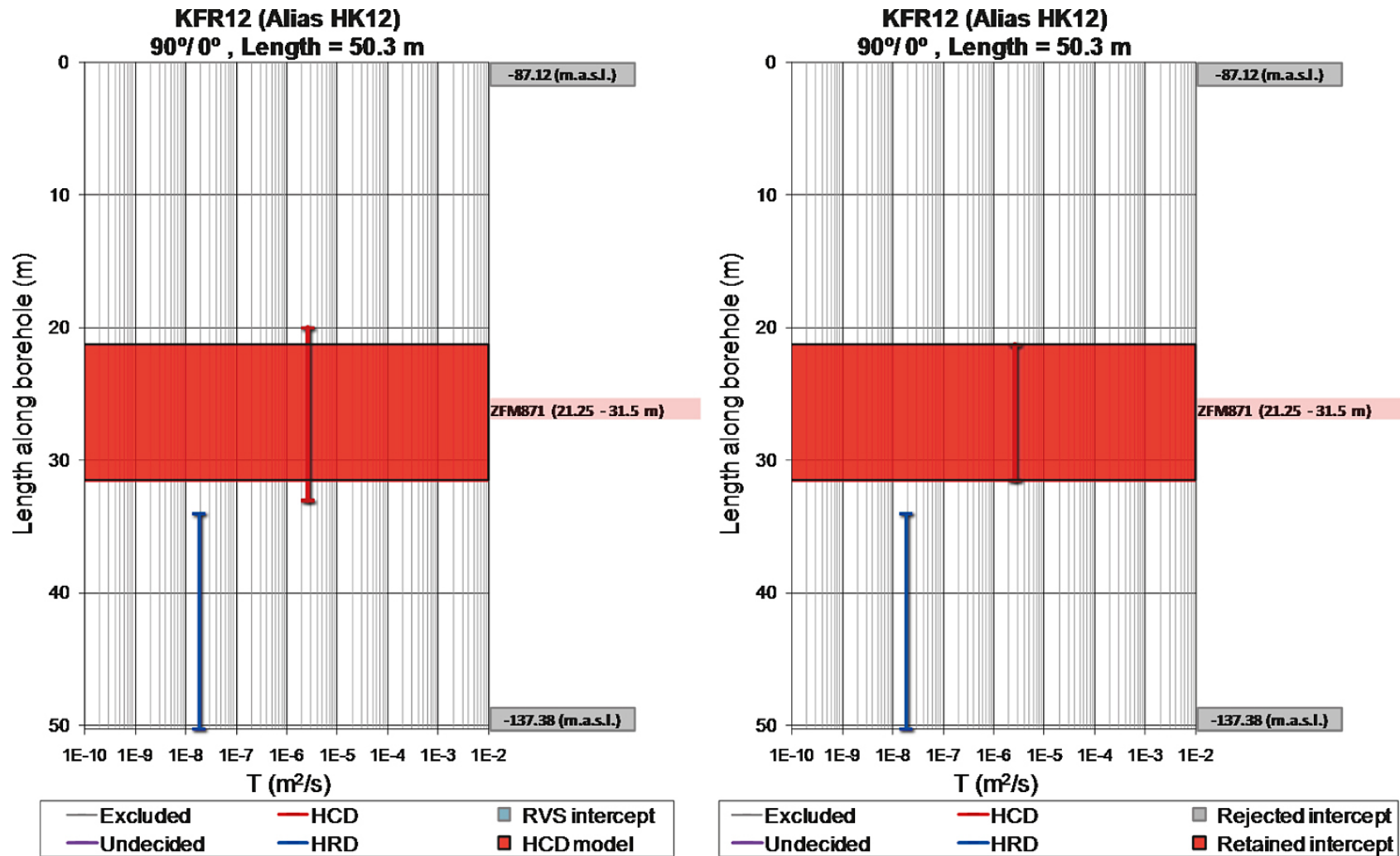


Figure D-27. KFR12: available data after screening process and modelled deformation zone intercepts (left) and interpreted total transmissivities and retained intercepts (right).

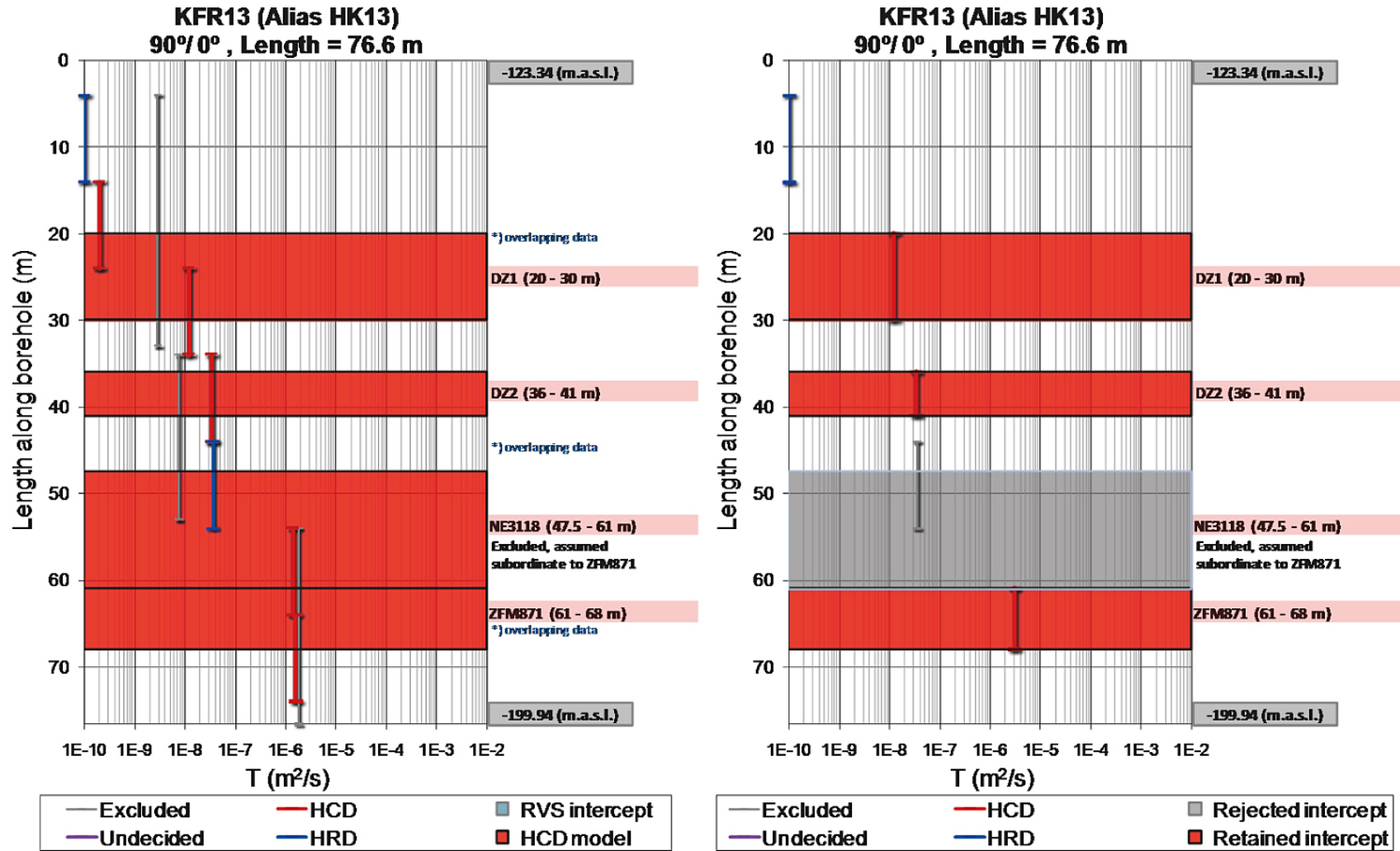


Figure D-28. KFR13: available data after screening process and modelled deformation zone intercepts (left) and interpreted total transmissivities and retained intercepts (right).

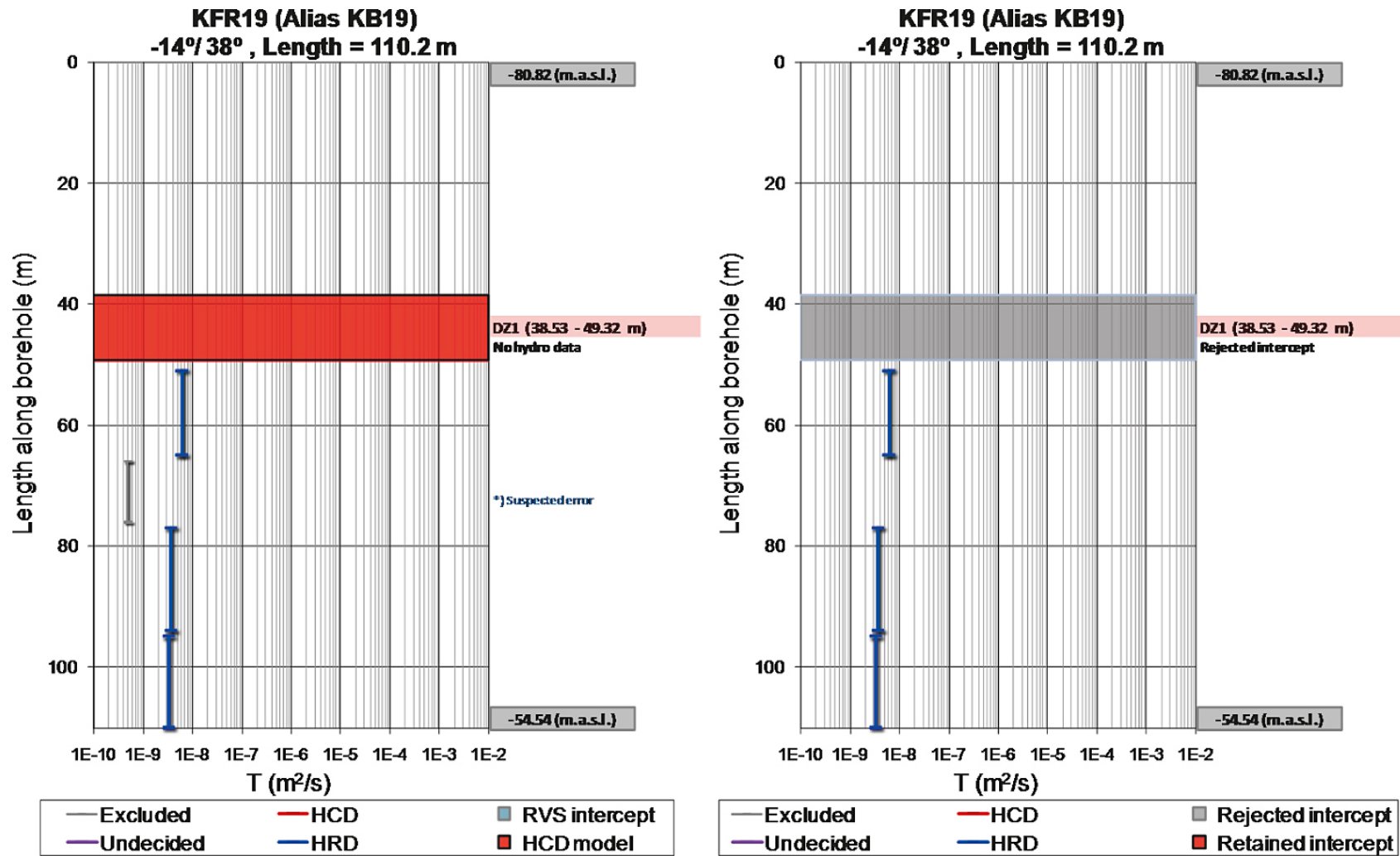


Figure D-29. KFR19: available data after screening process and modelled deformation zone intercepts (left) and interpreted total transmissivities and retained intercepts (right). Borehole length 77 to 85.5 m has Baltic water type.

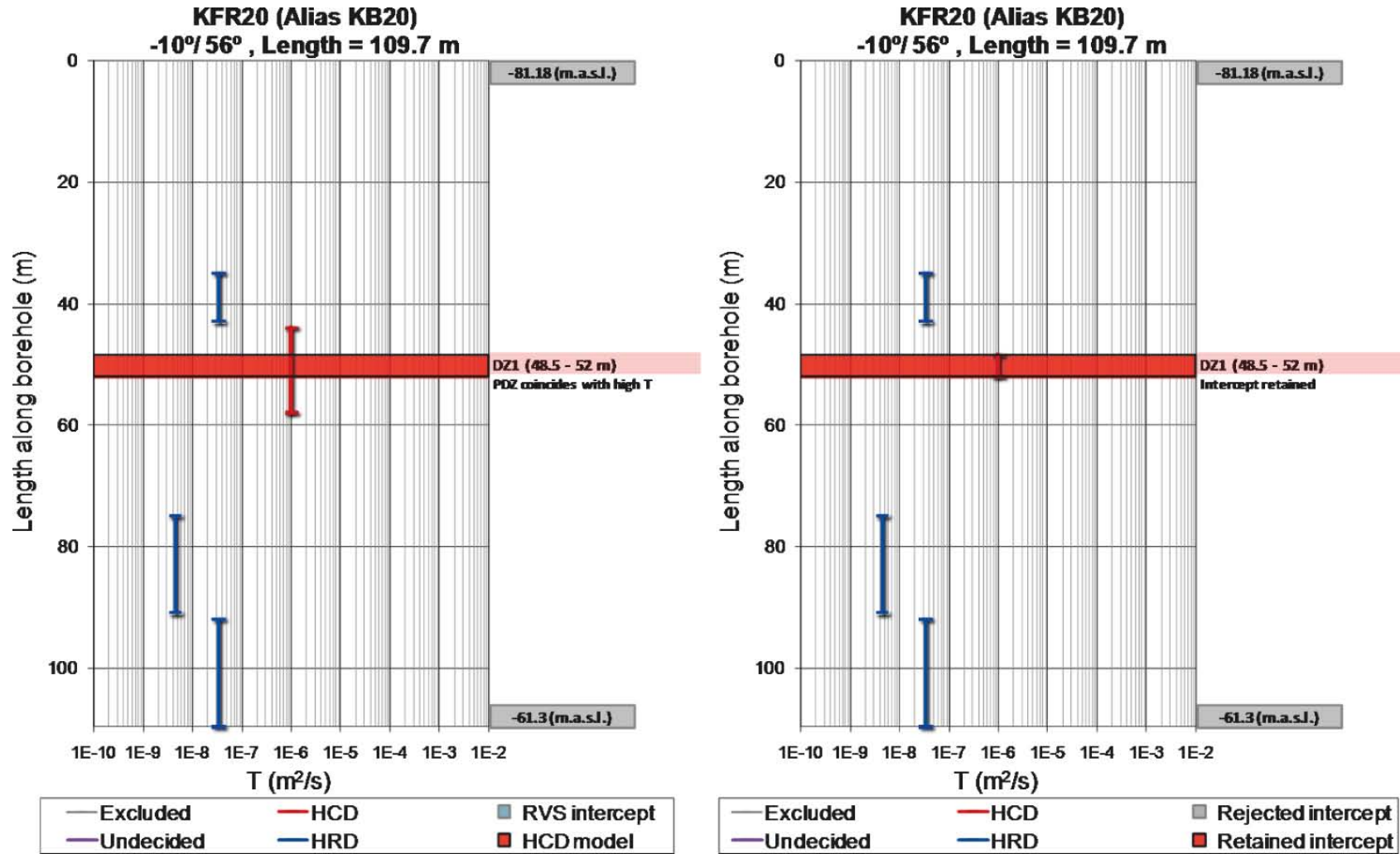


Figure D-30. KFR20: available data after screening process and modelled deformation zone intercepts (left) and interpreted total transmissivities and retained intercepts (right). KFR20\_DZ1 located 9 m west of ZFMNE0870.

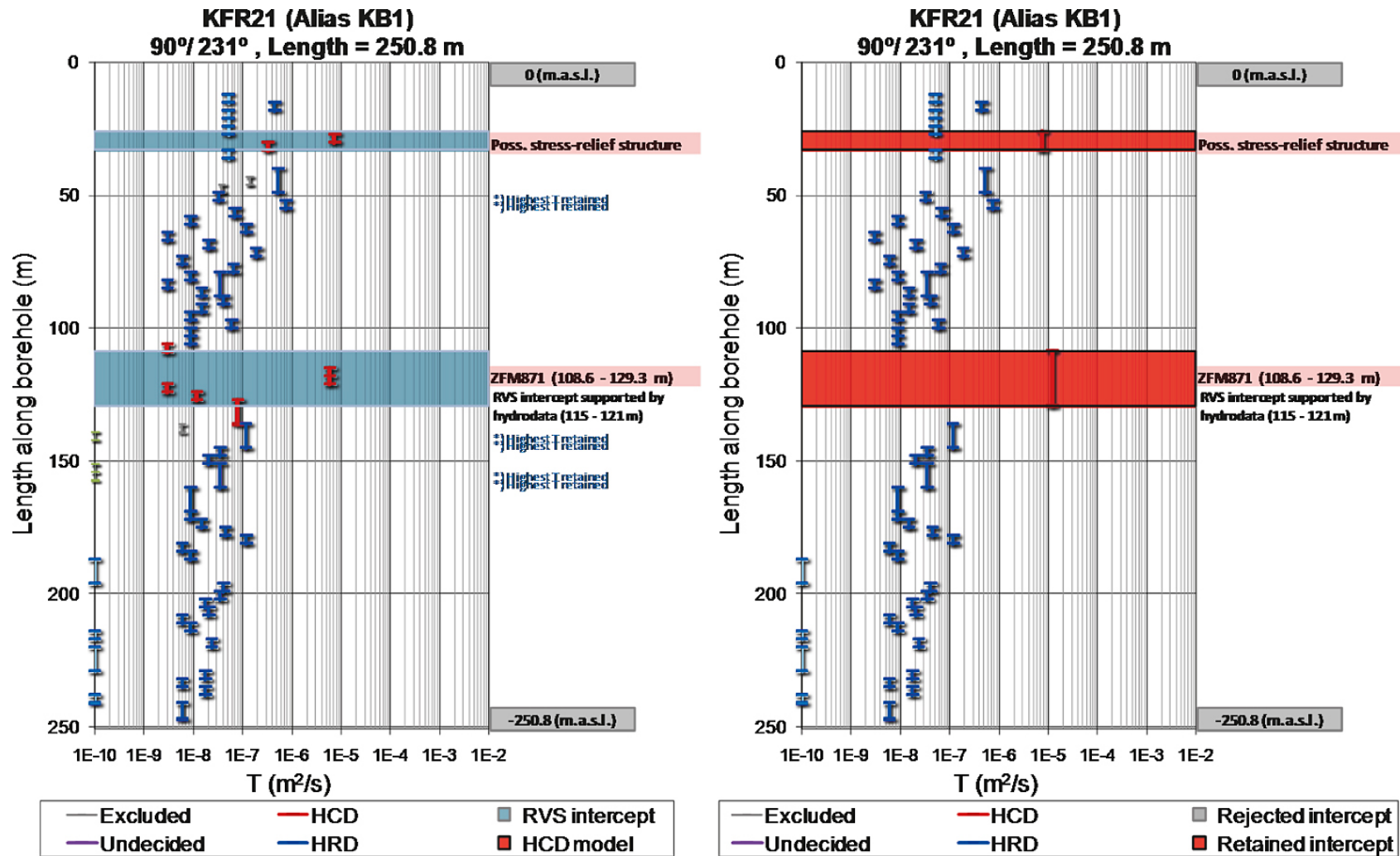


Figure D-31. KFR21: available data after screening process and modelled deformation zone intercepts (left) and interpreted total transmissivities and retained intercepts (right). Support for stress-relief structure (SBA7) found at c. 30 m borehole length.

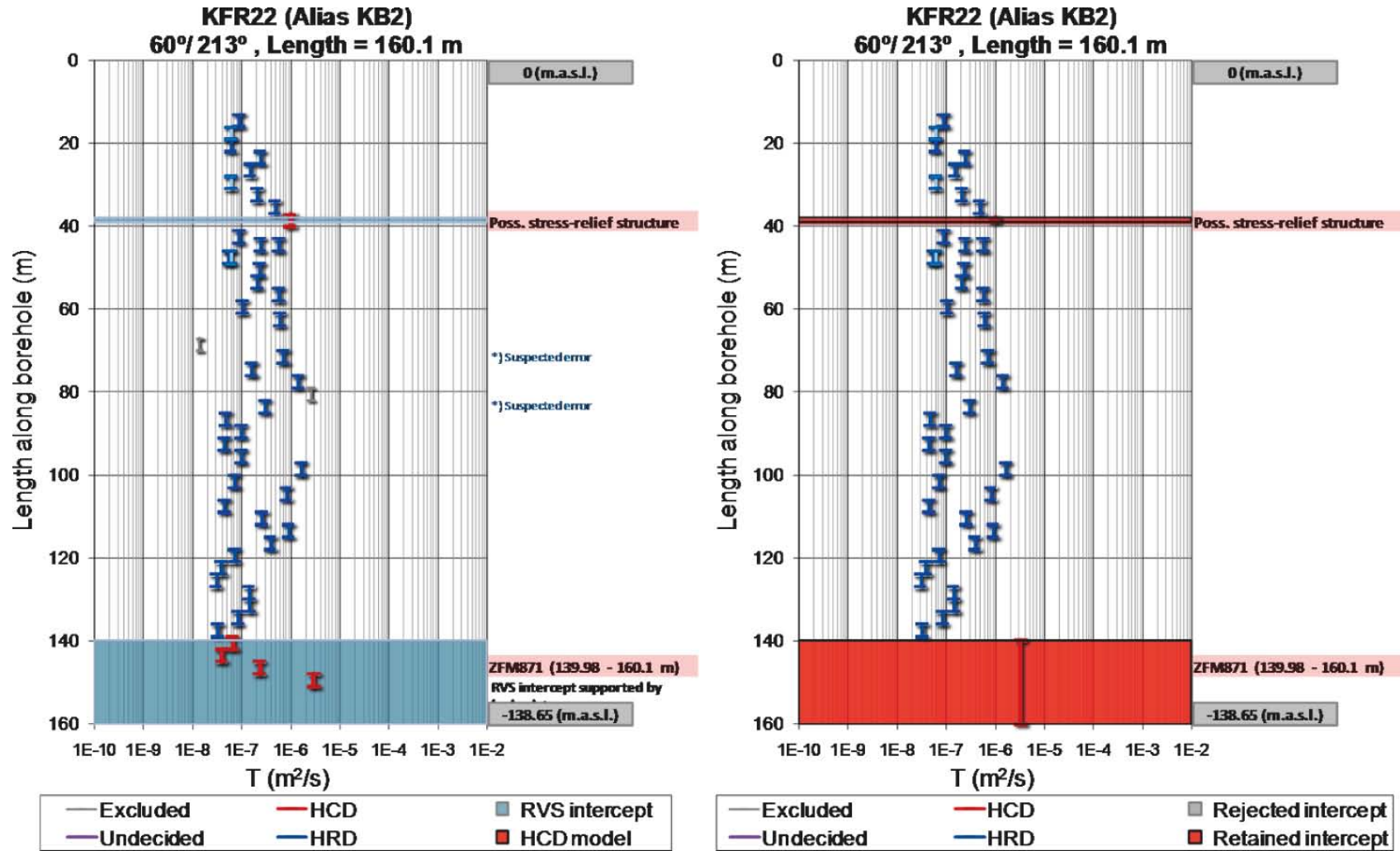


Figure D-32. KFR22: available data after screening process and modelled deformation zone intercepts (left) and interpreted total transmissivities and retained intercepts (right). Weak support for stress-relief structure (SBA7) found at c. 38 m borehole length.



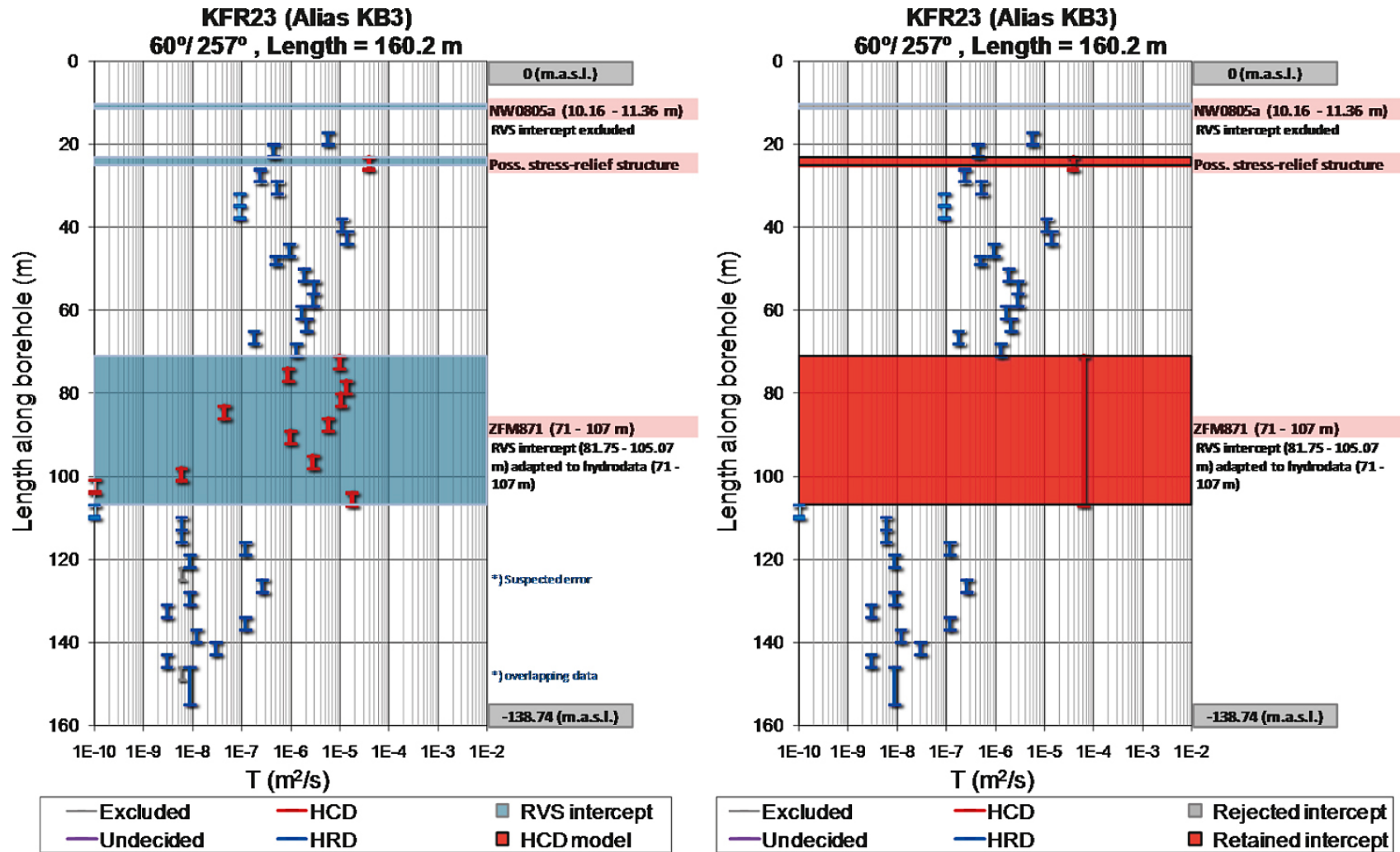
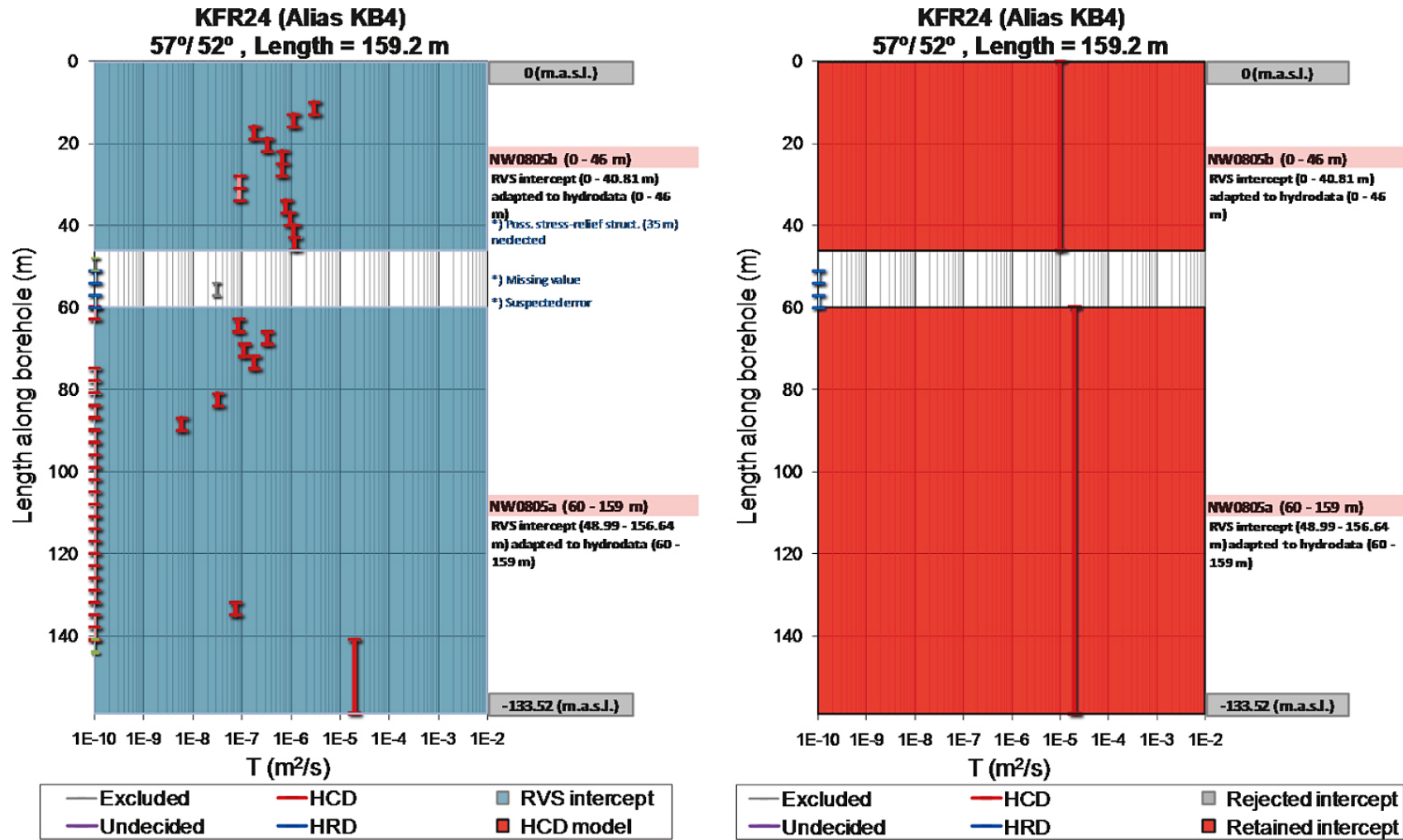


Figure D-33. KFR23: available data after screening process and modelled deformation zone intercepts (left) and interpreted total transmissivities and retained intercepts (right). Strong support for stress-relief structure (SBA7) found at 25 m borehole length.



**Figure D-34.** KFR24: available data after screening process and modelled deformation zone intercepts (left) and interpreted total transmissivities and retained intercepts (right). Stress-relief structure (SBA7) at 35 m borehole length cannot be resolved inside ZFMNW0805B. The peak transmissivity at 140 to 160 m borehole length corresponds to the elevation of ZFM871, if ZFM871 extends across NW0805A.

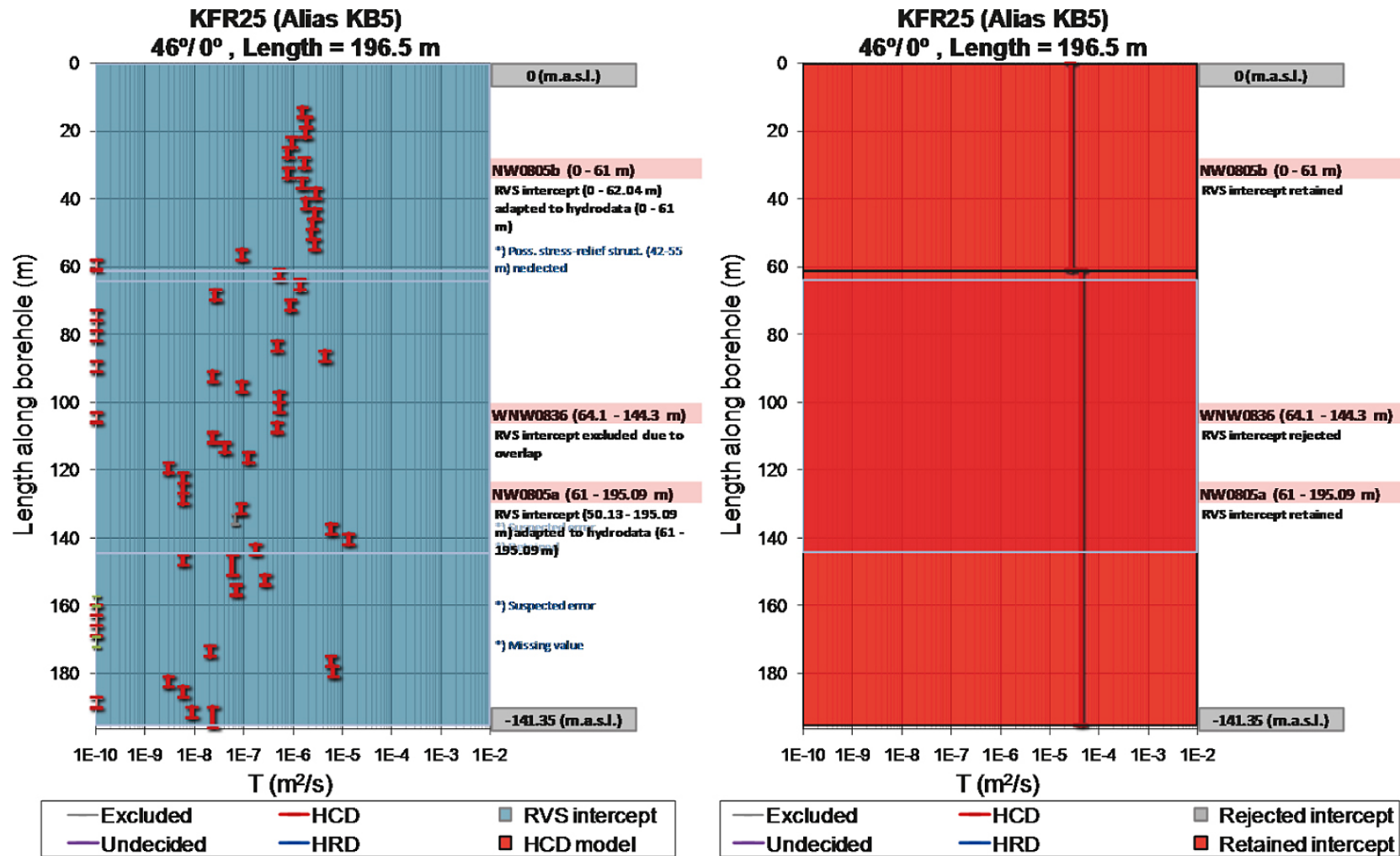


Figure D-35. KFR25: available data after screening process and modelled deformation zone intercepts (left) and interpreted total transmissivities and retained intercepts (right). Stress-relief structure (SBA7) at 42 to 55 m borehole length cannot be resolved inside ZFMNW0805B. The peak transmissivity at c. 140 m borehole length corresponds to the elevation of ZFM871, if ZFM871 extends across NW0805A (see Section 4.5.1).

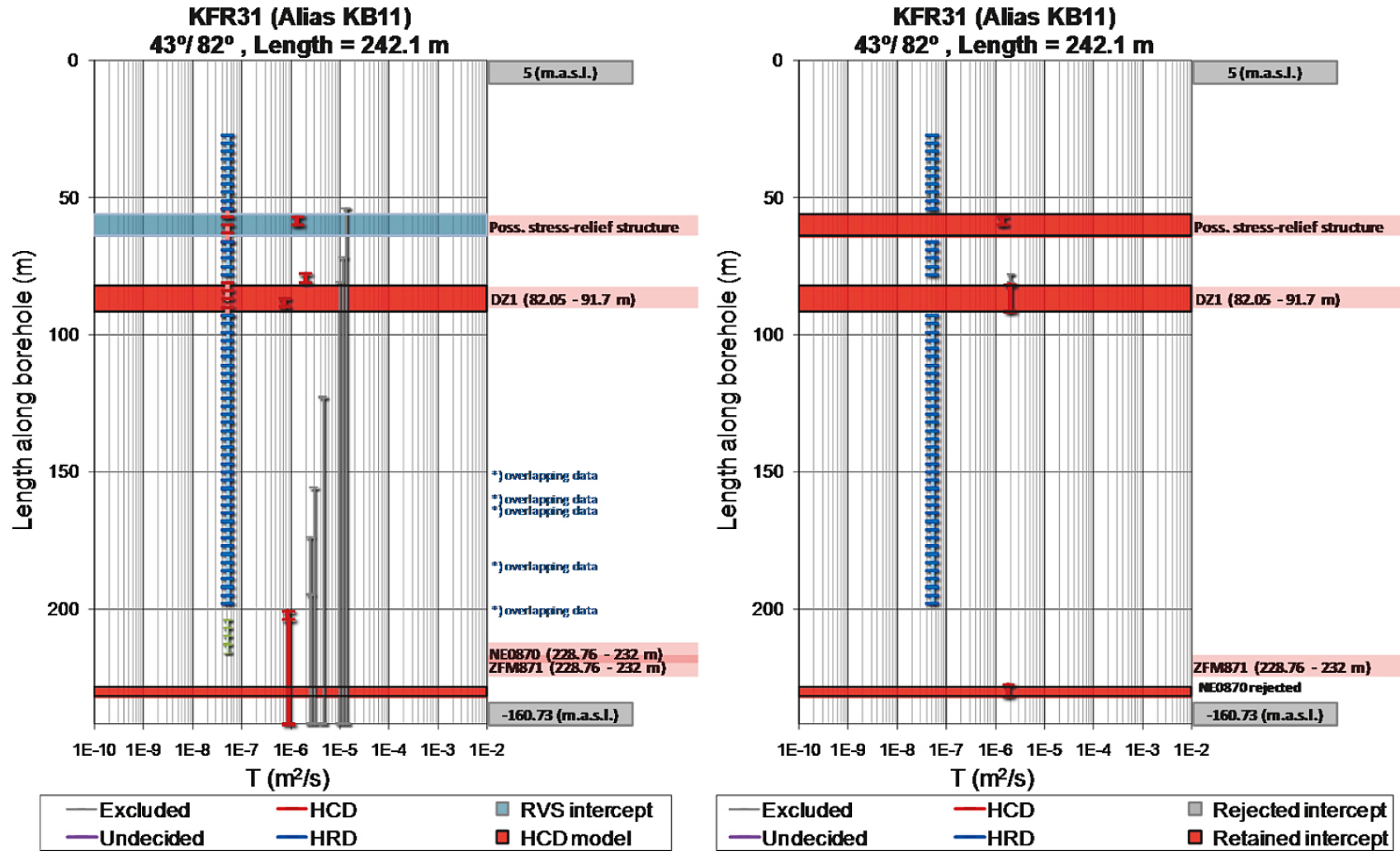


Figure D-36. KFR31: available data after screening process and modelled deformation zone intercepts (left) and interpreted total transmissivities and retained intercepts (right). Support for stress-relief structure (SBA7) found at c. 60 m borehole length.

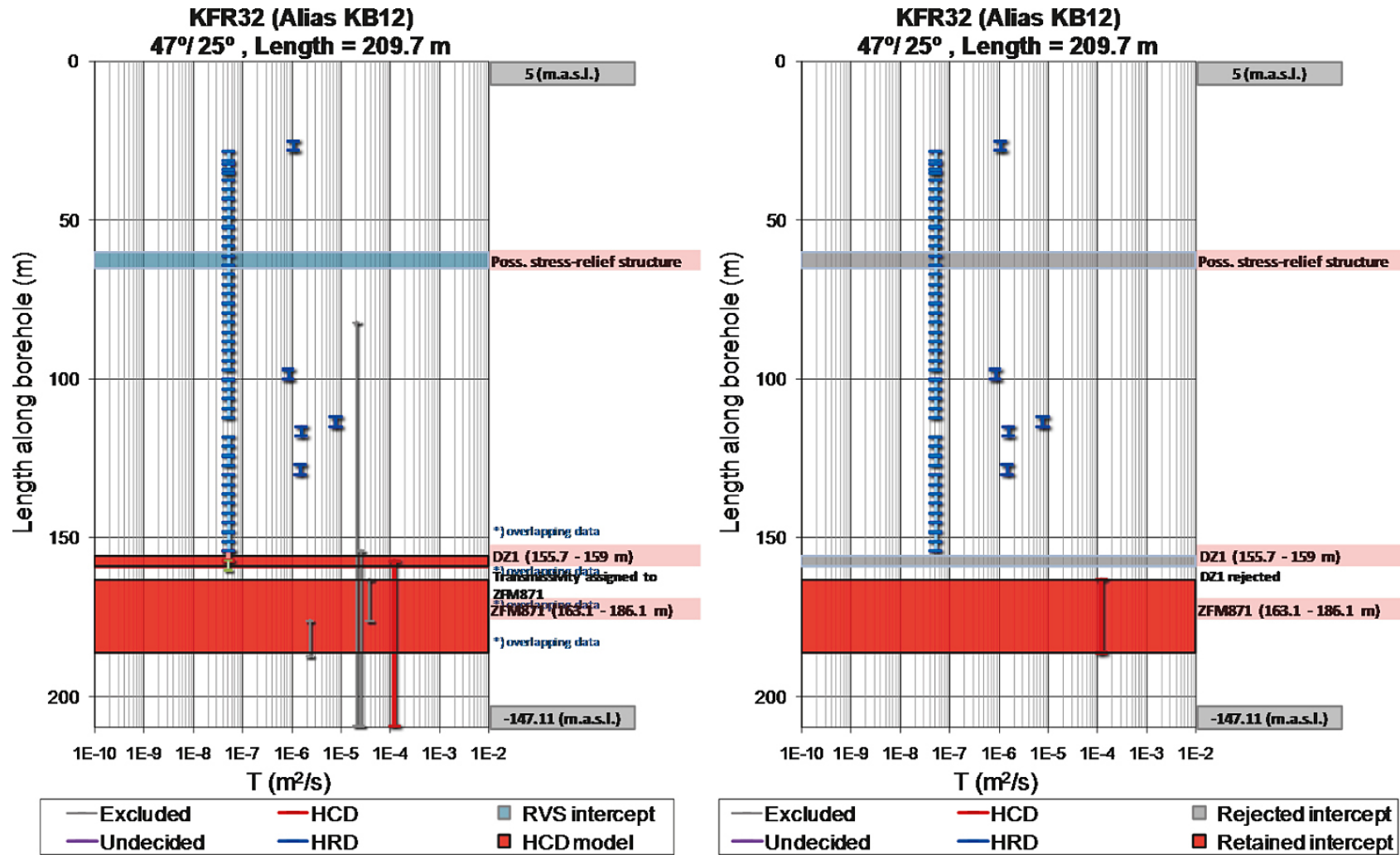


Figure D-37. KFR32: available data after screening process and modelled deformation zone intercepts (left) and interpreted total transmissivities and retained intercepts (right). No support for stress-relief structure (SBA7) found at c. 60 to 65 m borehole length.

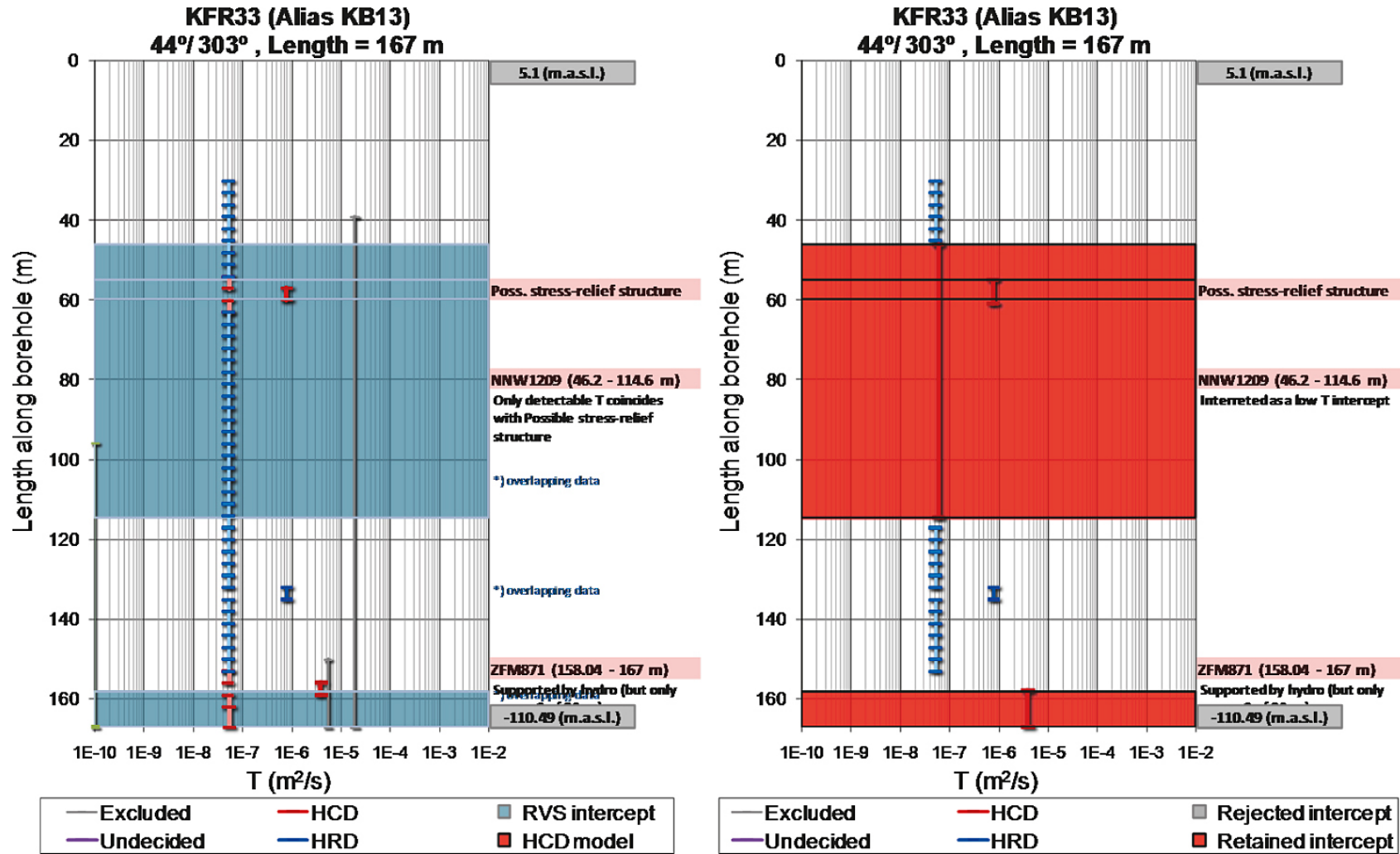
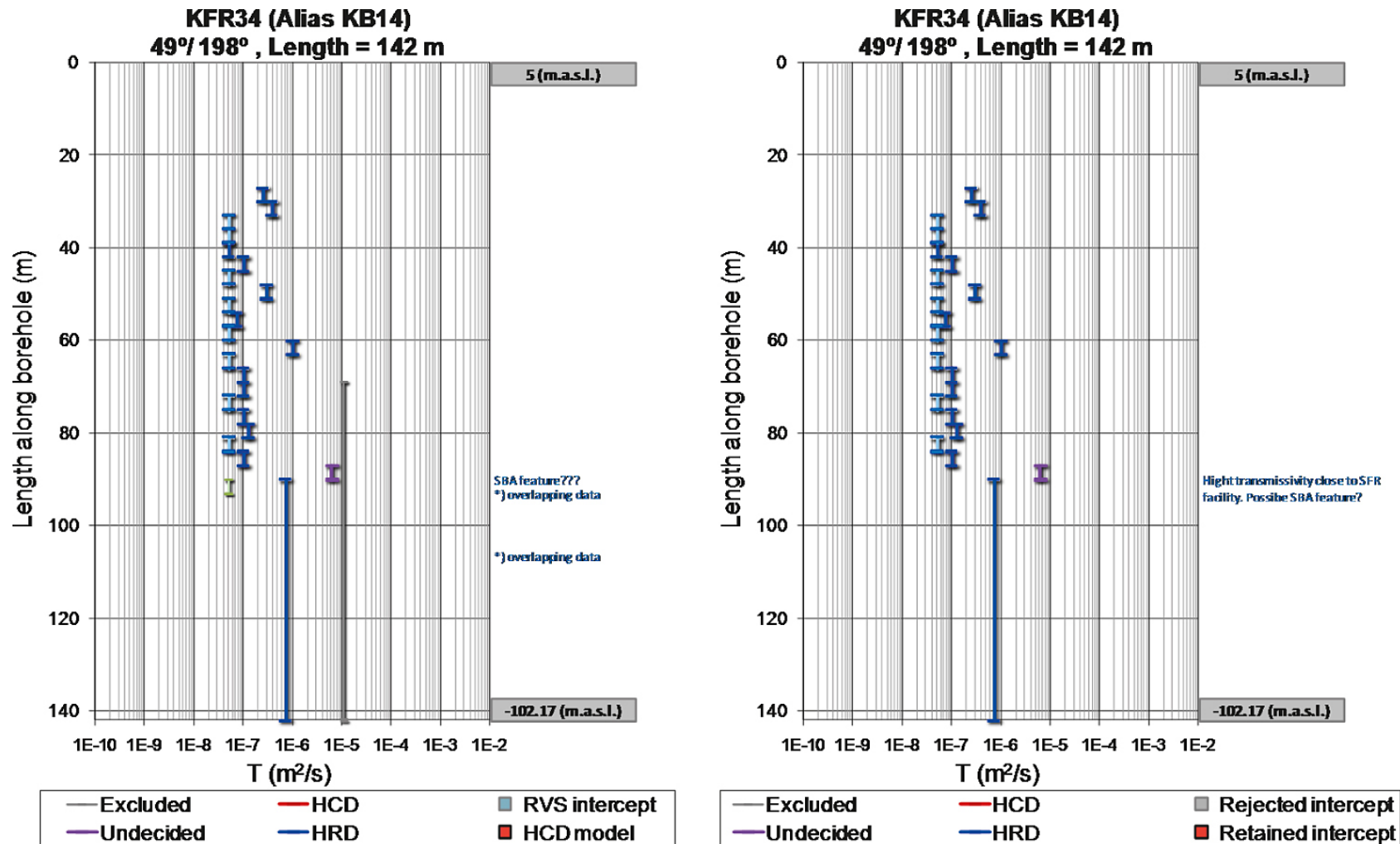
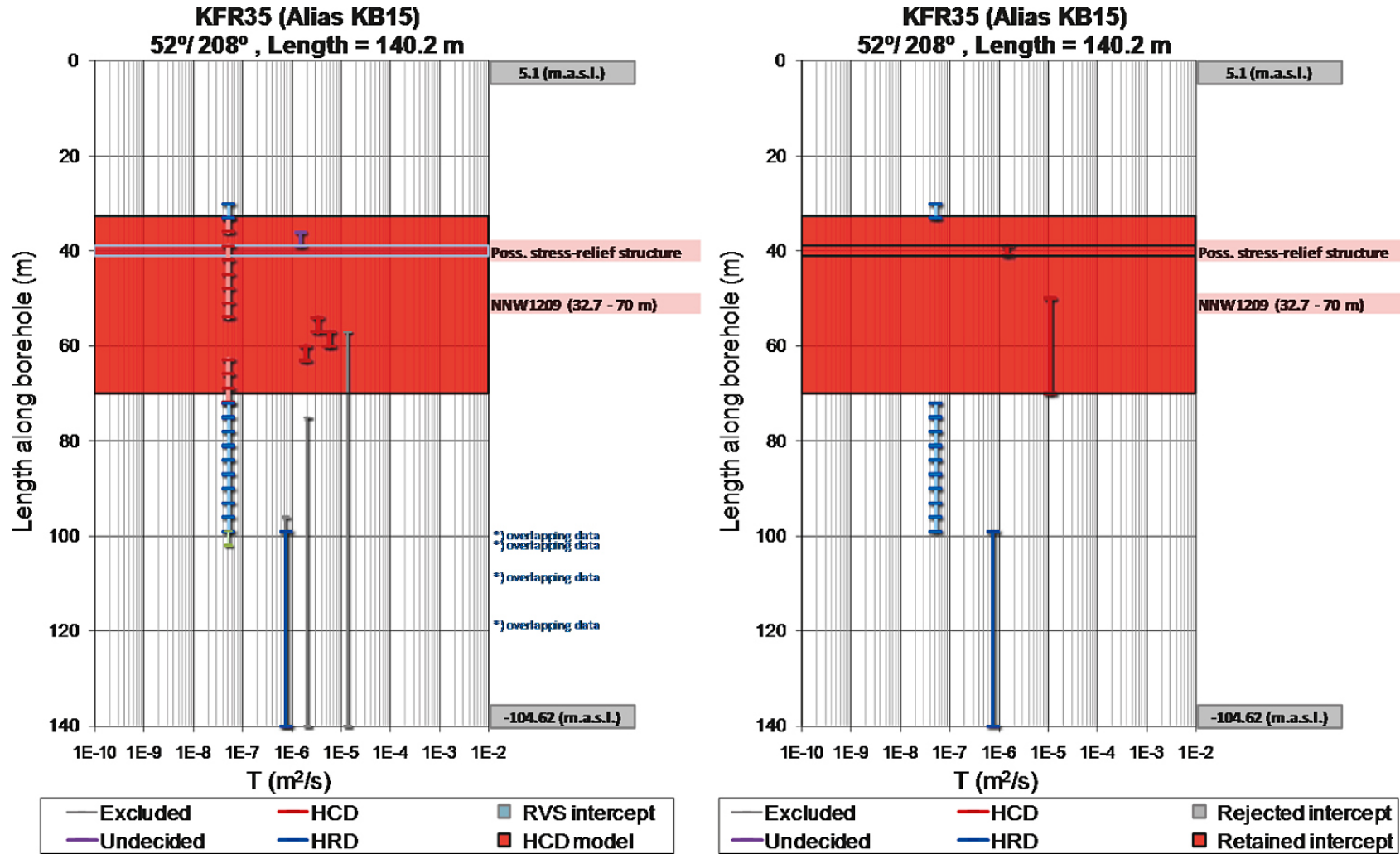


Figure D-38. KFR33: screened data and deformation zone intercepts (left) and interpreted total transmissivities and retained intercepts (right). The data at c. 55 to 60 m borehole length is taken as support for stress-relief structure (SBA7), instead of ZFMNNW1209.



**Figure D-39.** KFR34: available data after screening process and modelled deformation zone intercepts (left) and interpreted total transmissivities and retained intercepts (right). High transmissivity at c. 88 m borehole length ( $T \approx 10^{-5} \text{ m}^2/\text{s}$ ; c. -62 m.a.s.l.; just south-west of SFR storage facilities). Possibly related to KFR69\_DZ2?



**Figure D-40.** KFR35: available data after screening process and modelled deformation zone intercepts (left) and interpreted total transmissivities and retained intercepts (right). Support for stress-relief structure (SBA7) found at c. 40 m borehole length. High transmissivity below SFR ( $T \approx 10^{-6} \text{ m}^2/\text{s}$ ).



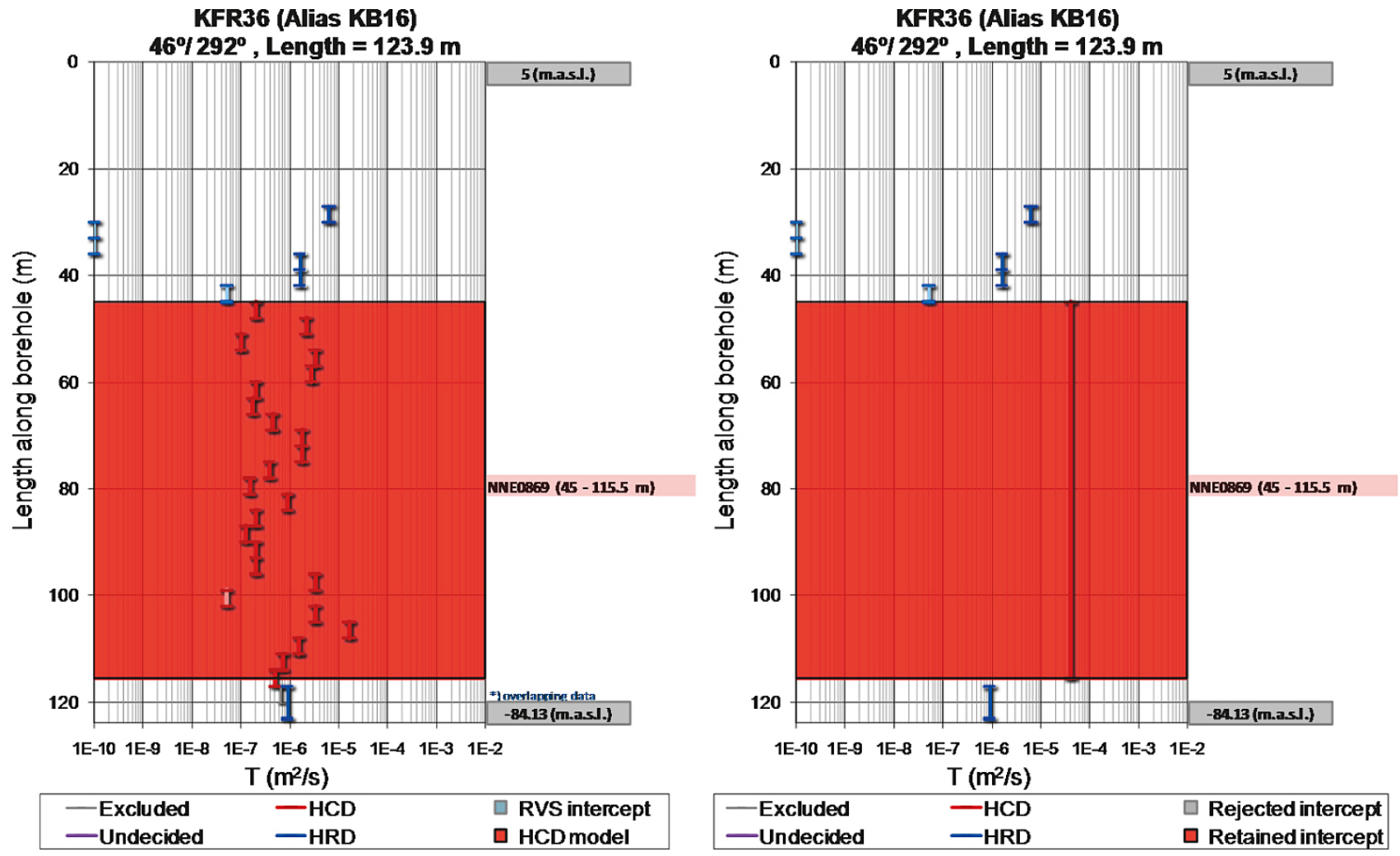


Figure D-41. KFR36: available data after screening process and modelled deformation zone intercepts (left) and interpreted total transmissivities and retained intercepts (right). High transmissivity also in the shallow rock above NNE0869.

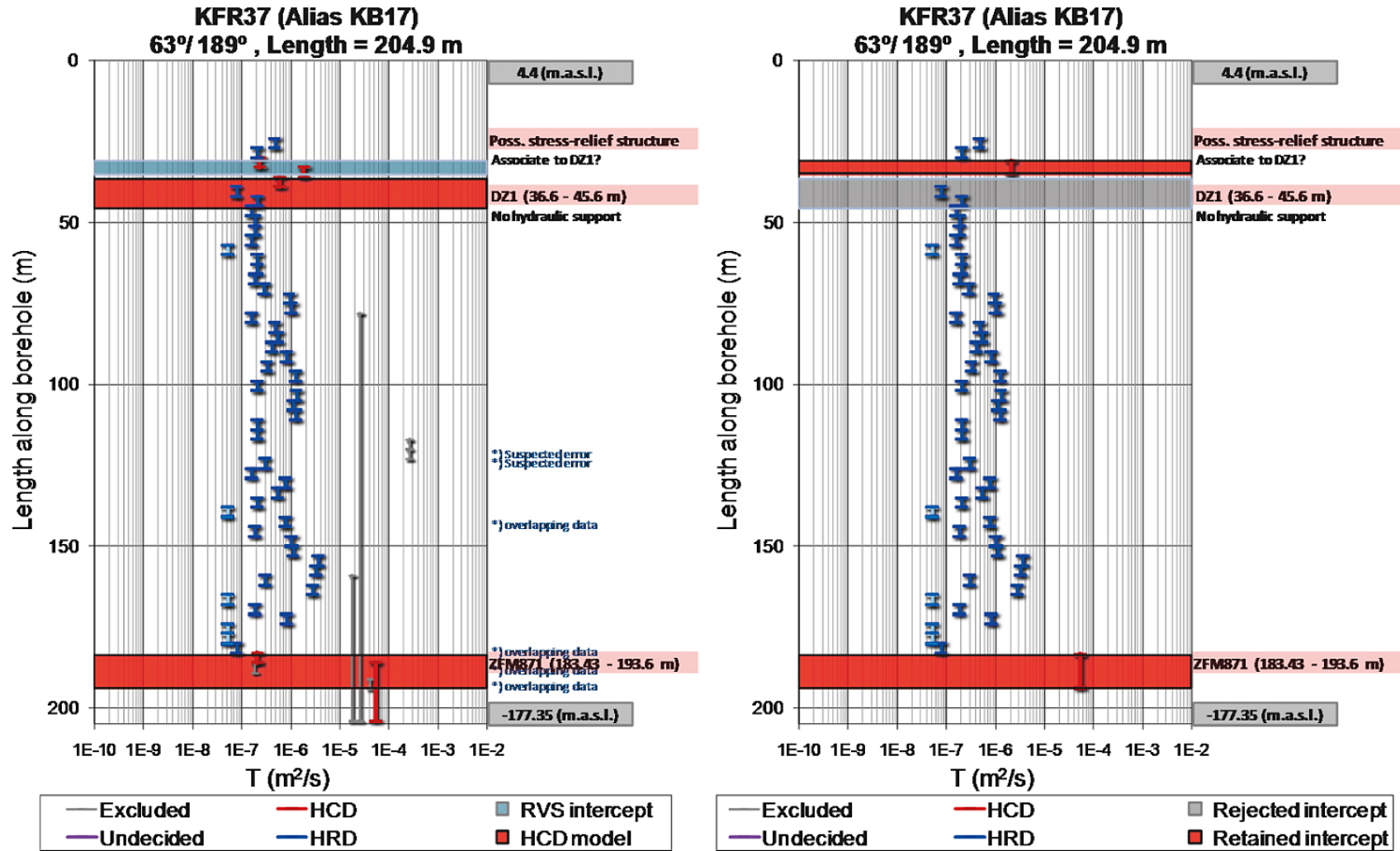


Figure D-42. KFR37: available data after screening process and modelled deformation zone intercepts (left) and interpreted total transmissivities and retained intercepts (right). Moderate support for stress-relief structure (SBA7) found at c. 33 m borehole length.

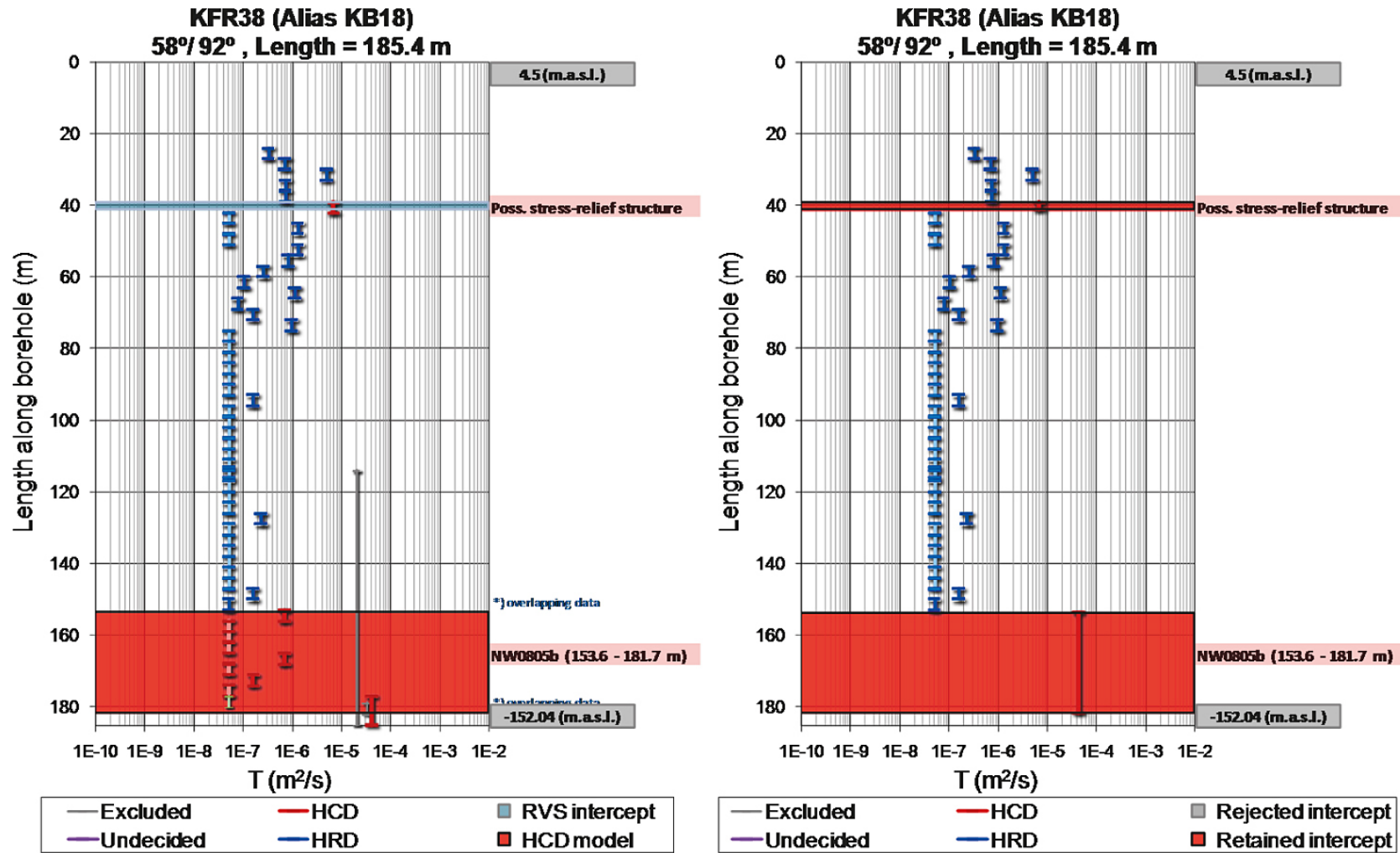


Figure D-43. KFR38: available data after screening process and modelled deformation zone intercepts (left) and interpreted total transmissivities and retained intercepts (right). Possible support for stress-relief structure (SBA7) found at c. 40 m borehole length. The peak transmissivity at c. 180 m borehole length corresponds to the elevation of ZFM871, if ZFM871 extends across NW0805B.

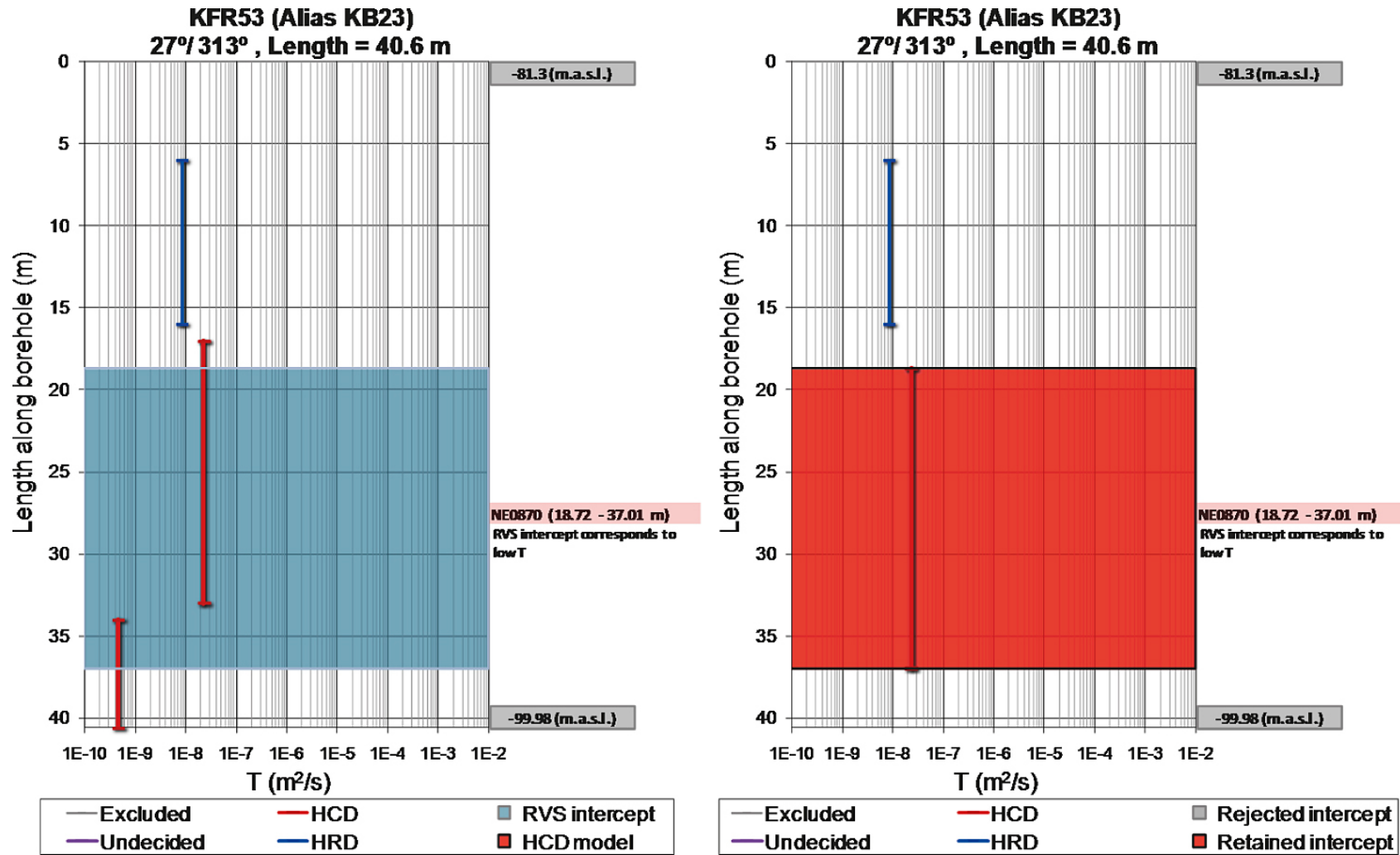


Figure D-44. KFR53: available data after screening process and modelled deformation zone intercepts (left) and interpreted total transmissivities and retained intercepts (right).

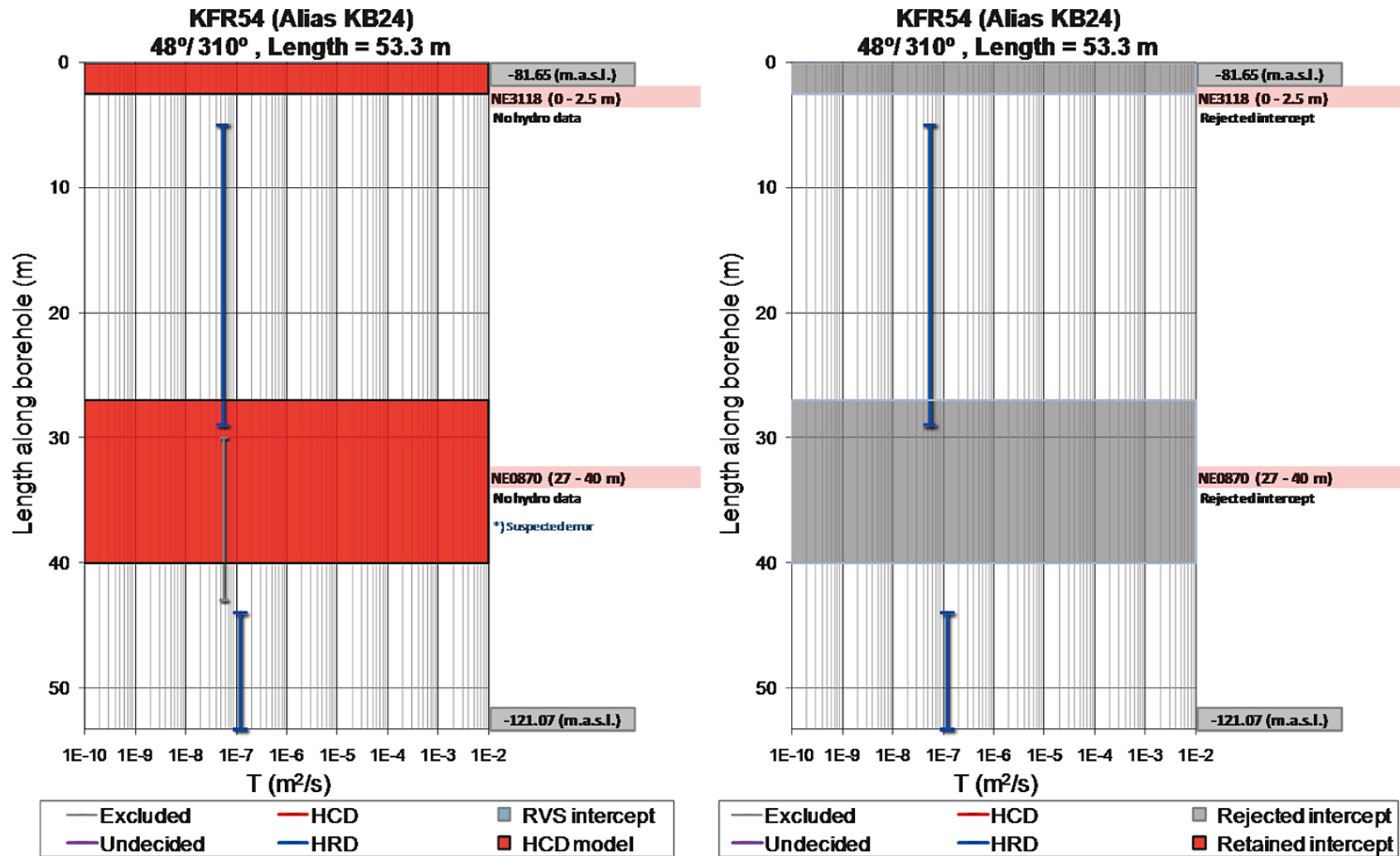


Figure D-45. KFR54: available data after screening process and modelled deformation zone intercepts (left) and interpreted total transmissivities and retained intercepts (right). KFR54 indicates low-transmissive rock in the vicinity of NE0870 and NE3118. Due to poor coverage, both intercepts are rejected.

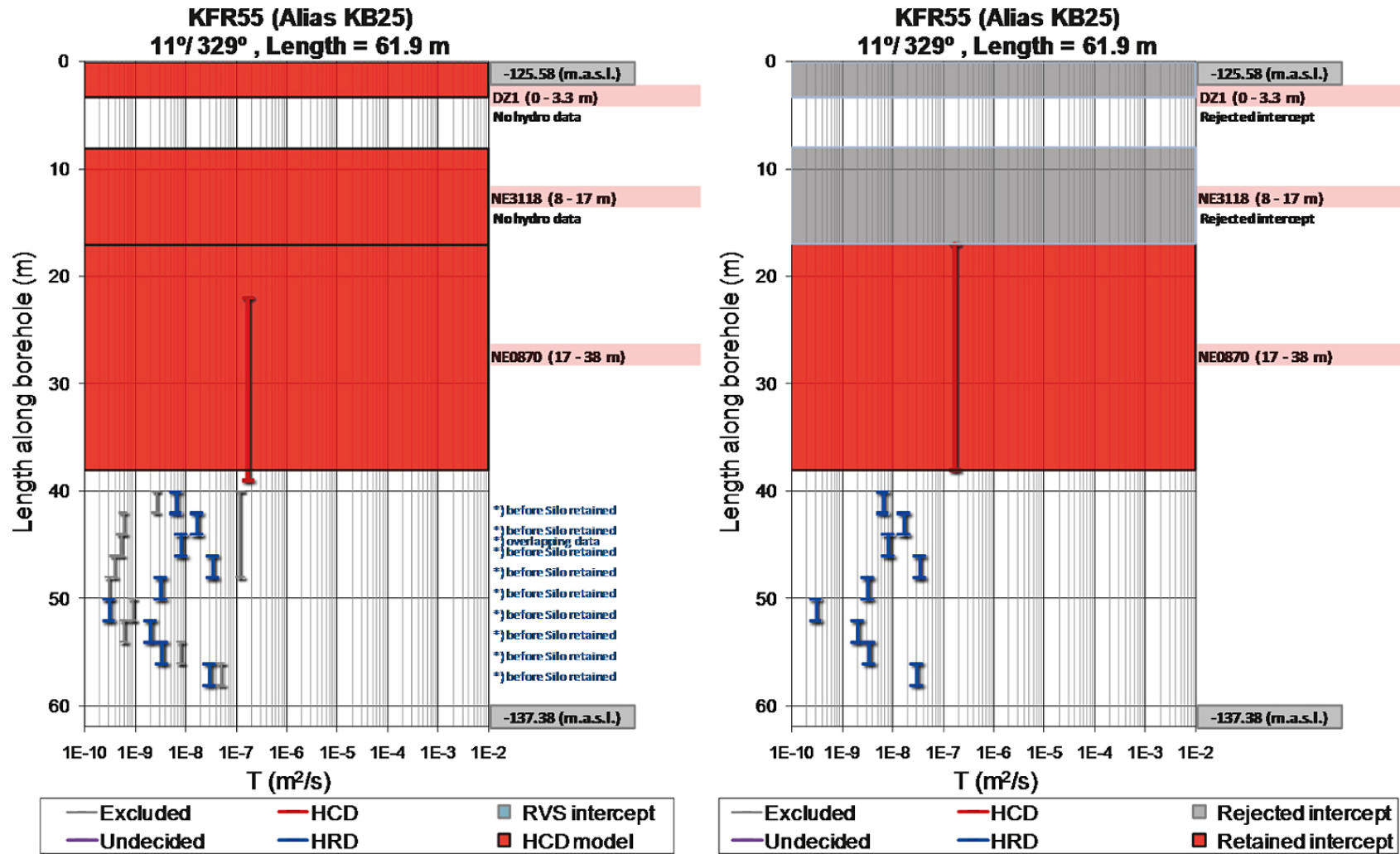


Figure D-46. KFR55: available data after screening process and modelled deformation zone intercepts (left) and interpreted total transmissivities and retained intercepts (right). Measurements before (blue) and after (grey) the construction of the Silo.

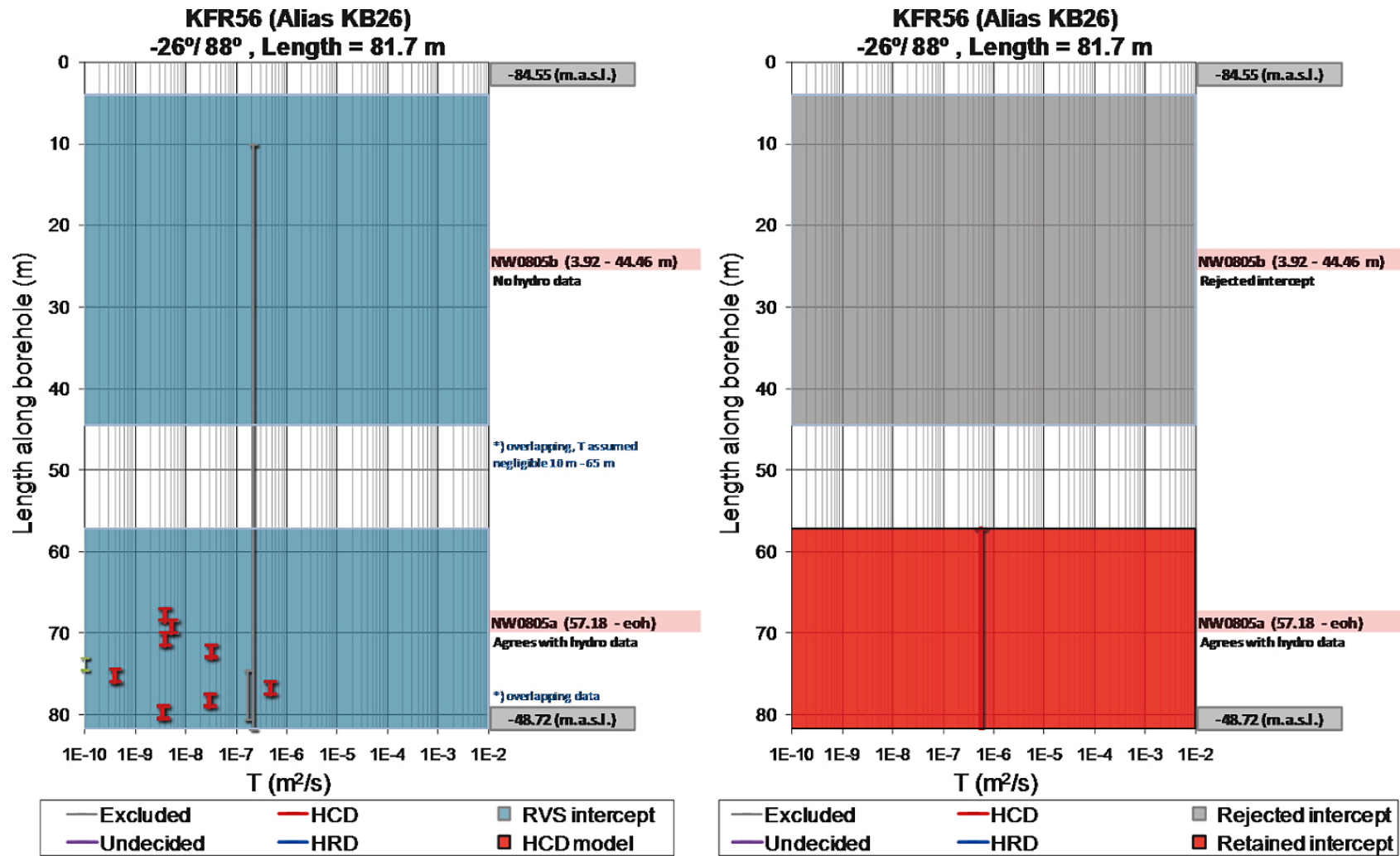
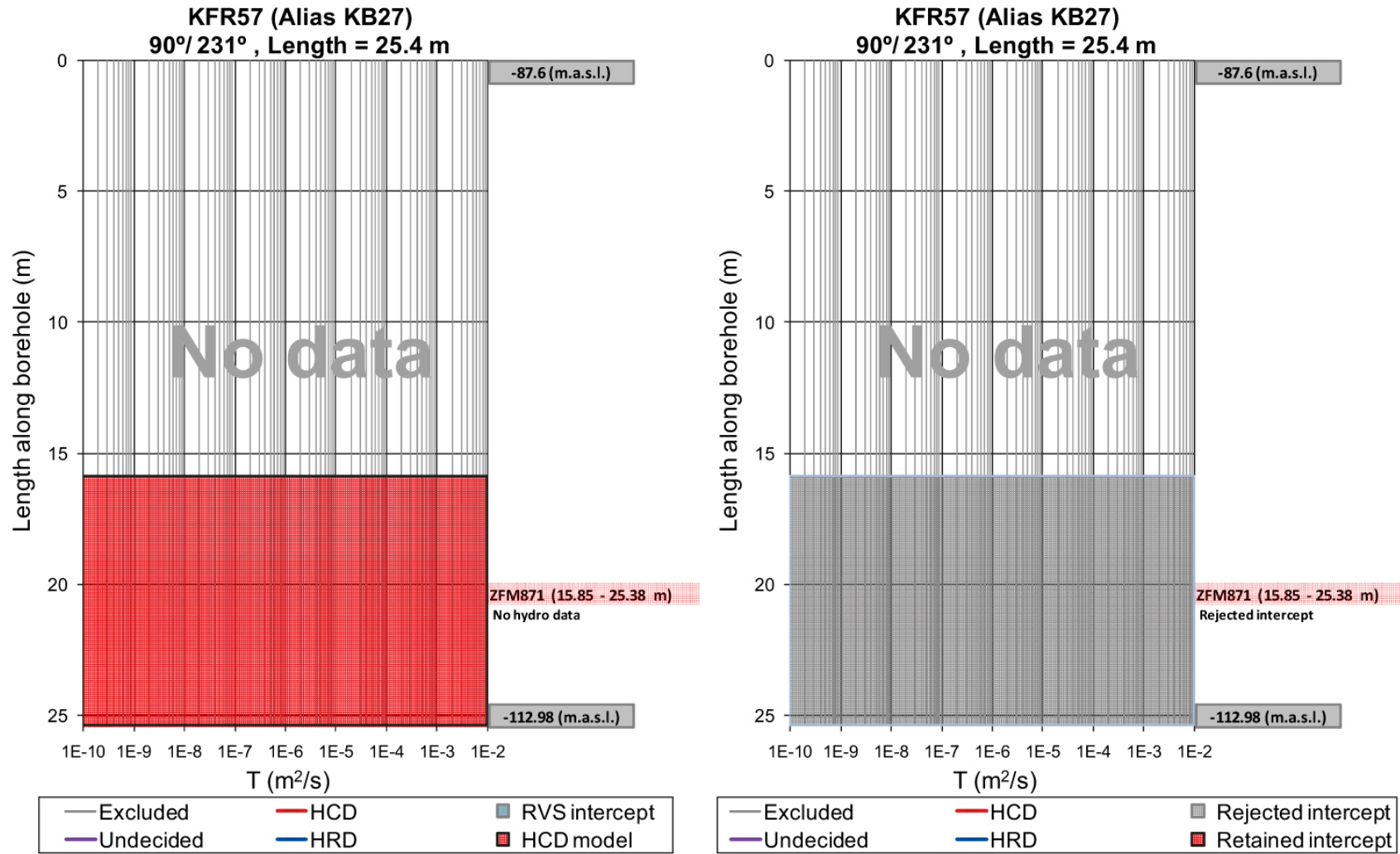


Figure D-47. KFR56: available data after screening process and modelled deformation zone intercepts (left) and interpreted total transmissivities and retained intercepts (right). Baltic water type in this borehole. Indication of low transmissivity in NW0805B ( $T \leq 2 \times 10^{-7} \text{ m}^2/\text{s}$ ), but rejected due to coverage.



**Figure D-48.** KFR57: available data after screening process and modelled deformation zone intercepts (left) and interpreted total transmissivities and retained intercepts (right).



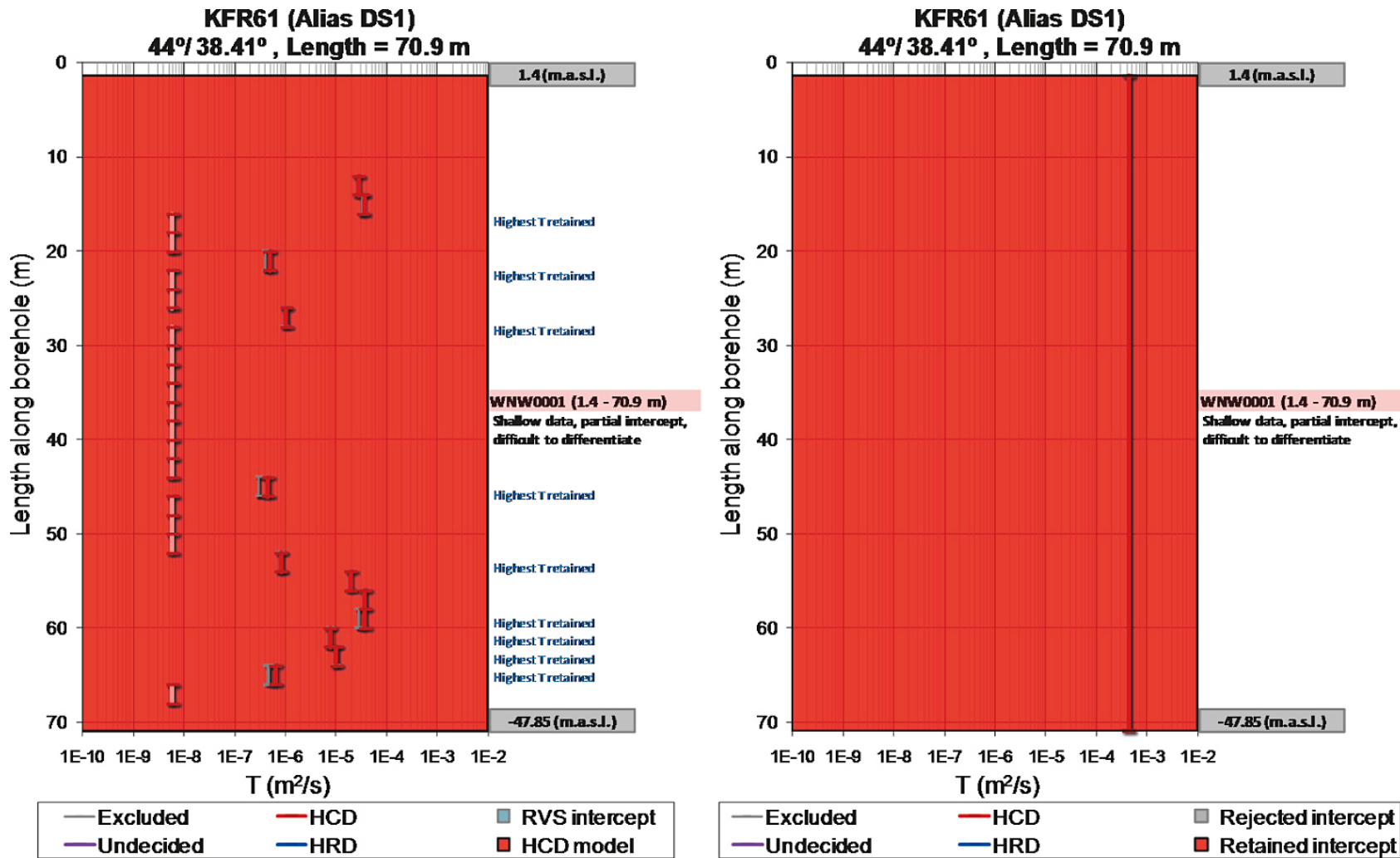


Figure D-49. KFR61: available data after screening process and modelled deformation zone intercepts (left) and interpreted total transmissivities and retained intercepts (right). An early borehole, drilled from the ice, targeting the predicted core of Singö deformation zone (incomplete intercept).

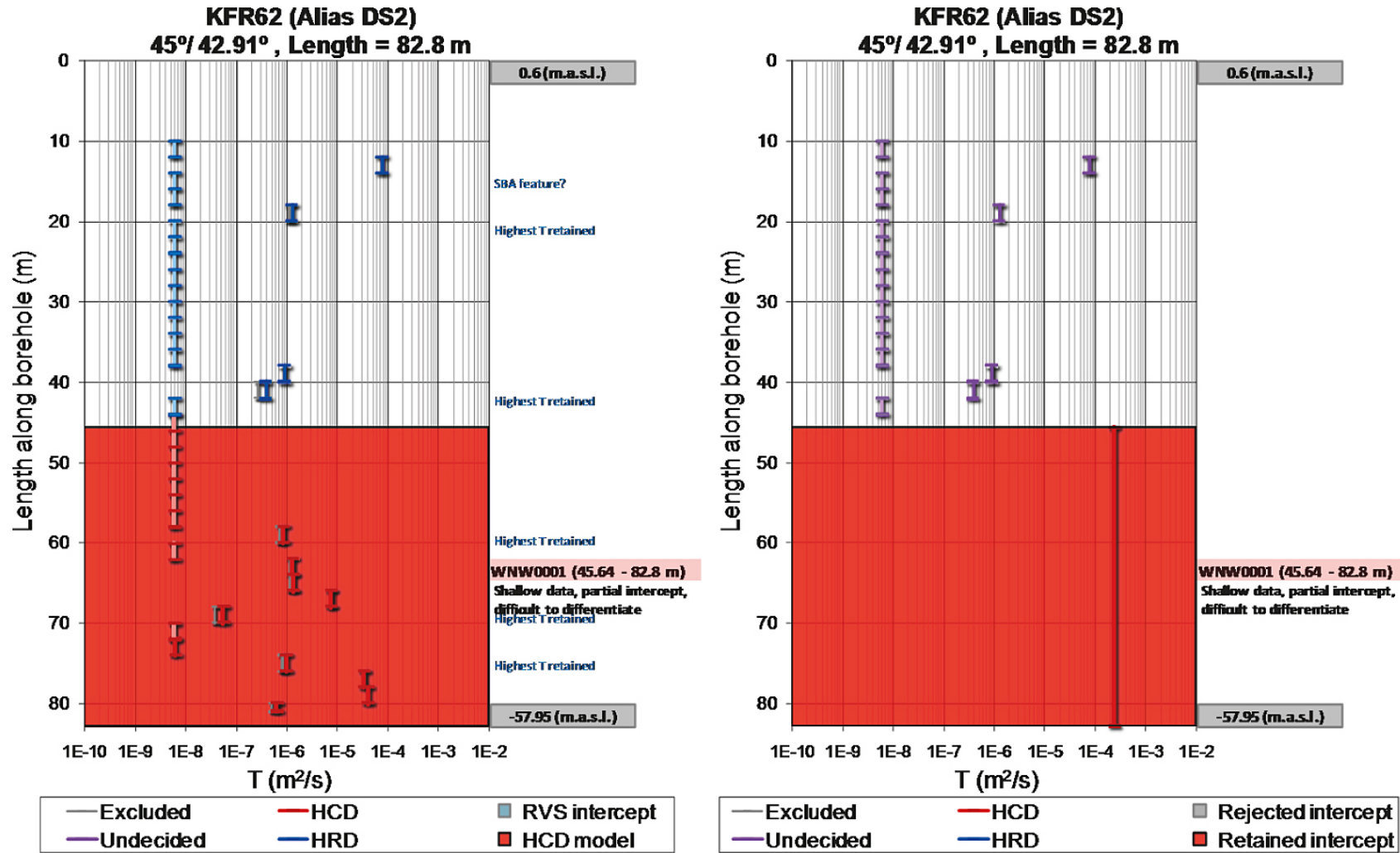
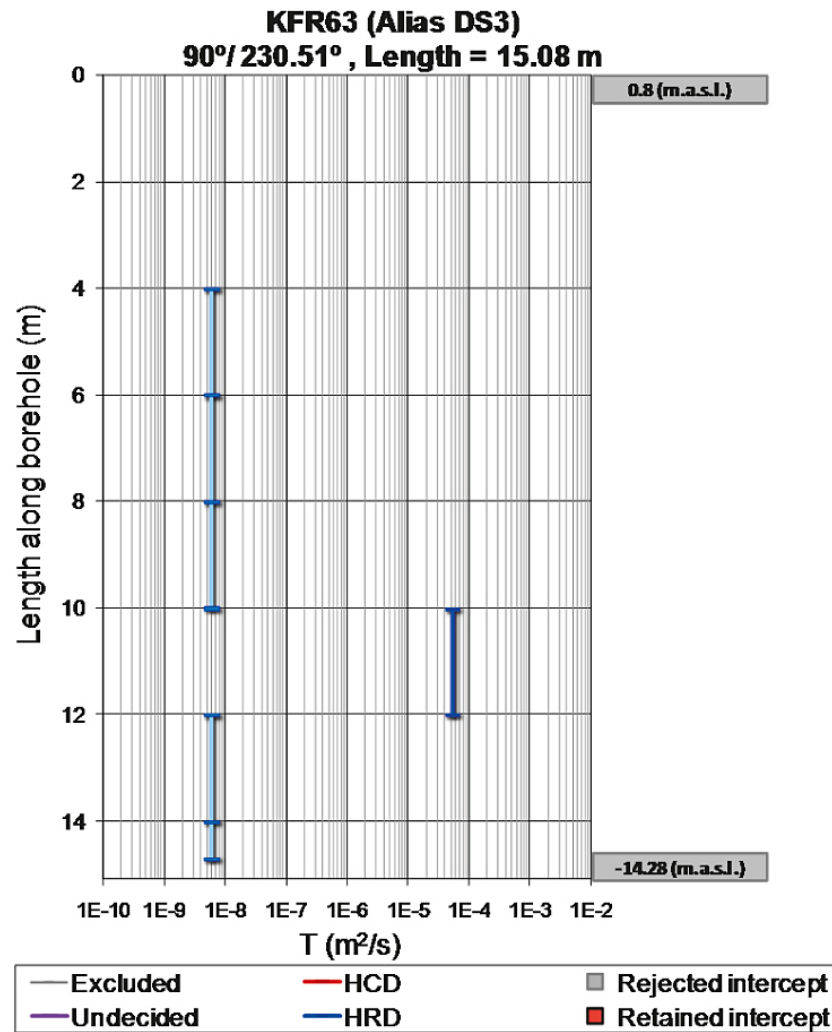
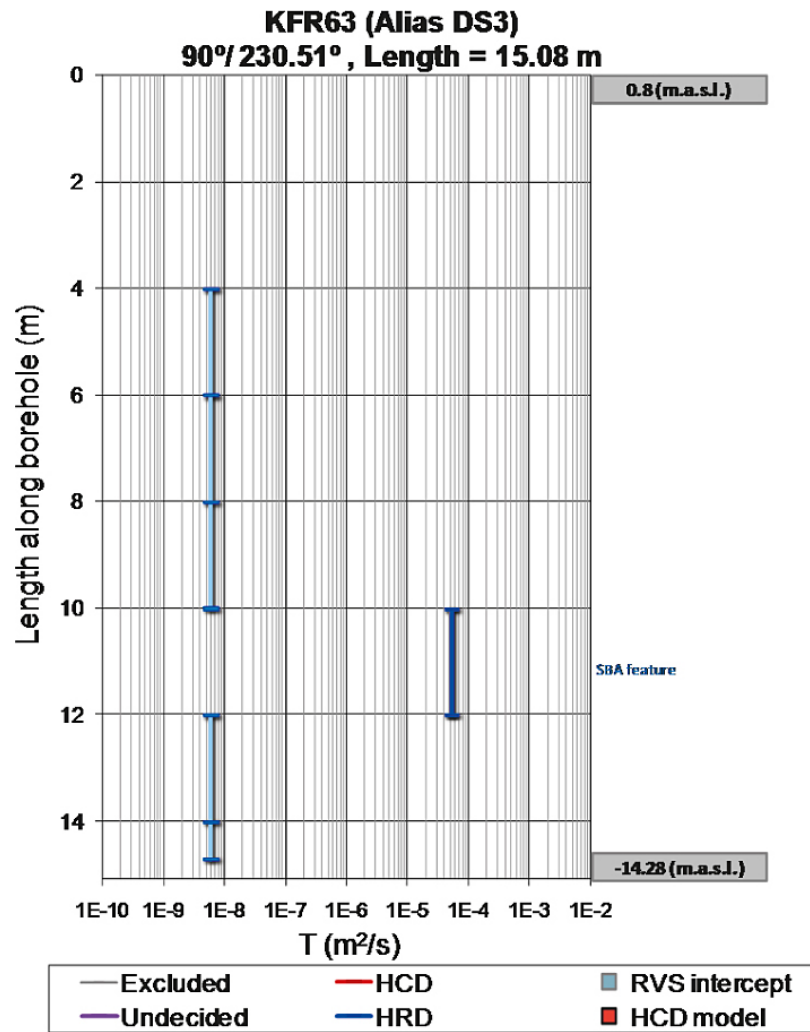
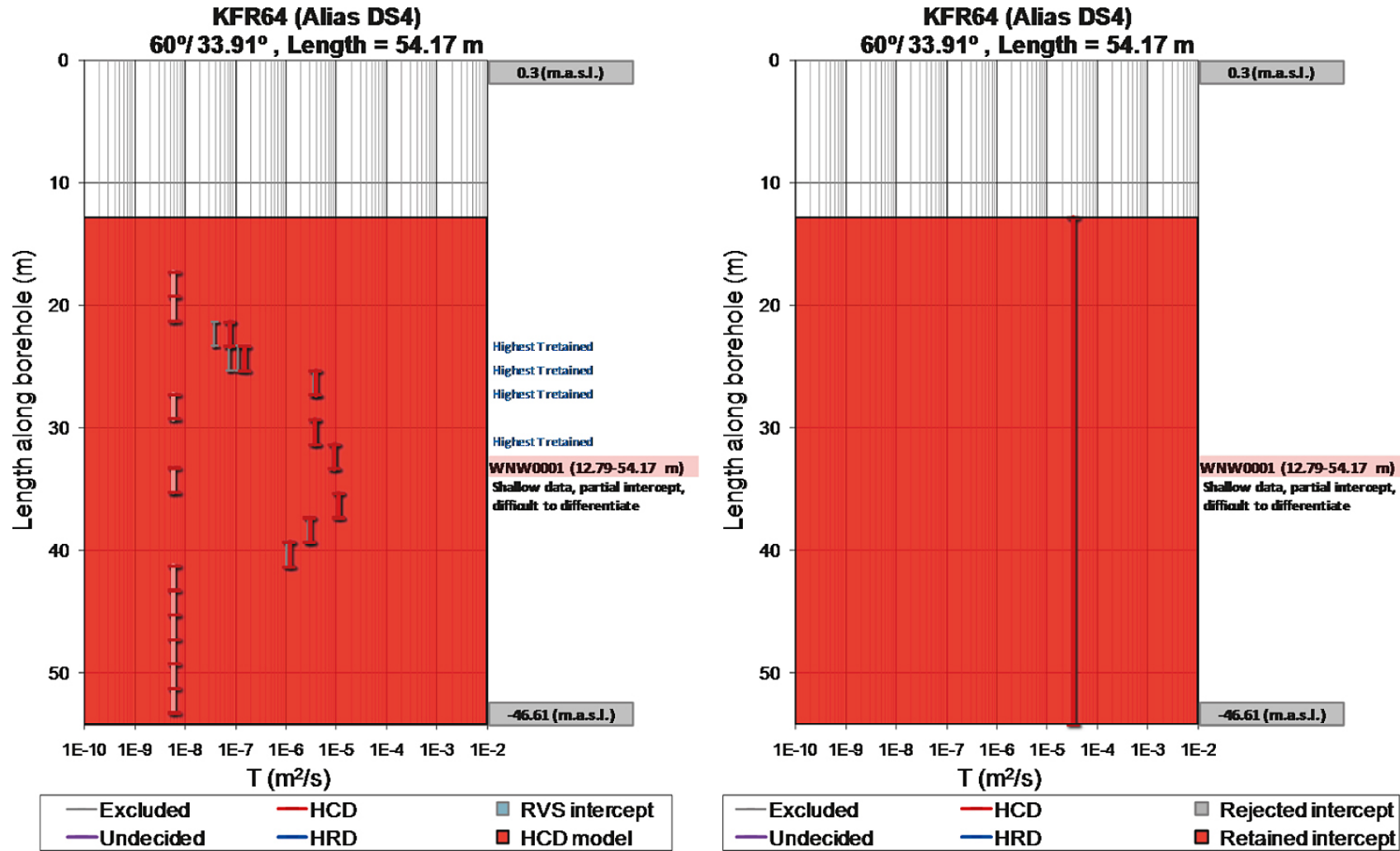


Figure D-50. KFR62: available data after screening process and modelled deformation zone intercepts (left) and interpreted total transmissivities and retained intercepts (right). An early borehole, drilled from the ice, targeting the predicted core of Singö deformation zone (incomplete intercept).



*Figure D-51. KFR63: available data after screening process and modelled deformation zone intercepts (left) and interpreted total transmissivities and retained intercepts (right). An early borehole drilled at the entry of the SFR access tunnels.*



**Figure D-52.** KFR64: available data after screening process and modelled deformation zone intercepts (left) and interpreted total transmissivities and retained intercepts (right). An early borehole, drilled from the ice, targeting the predicted core of Singö deformation zone (incomplete intercept).

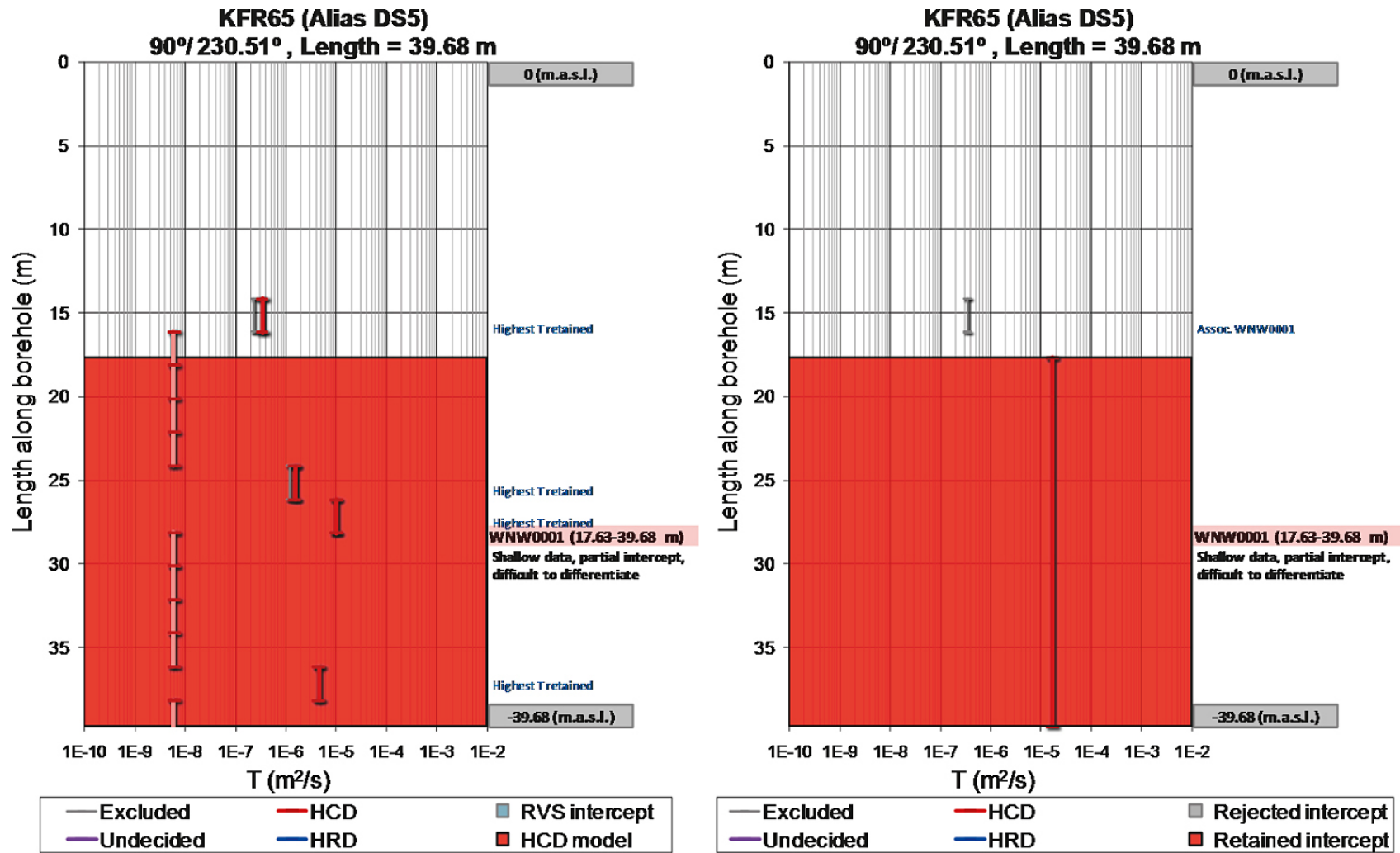
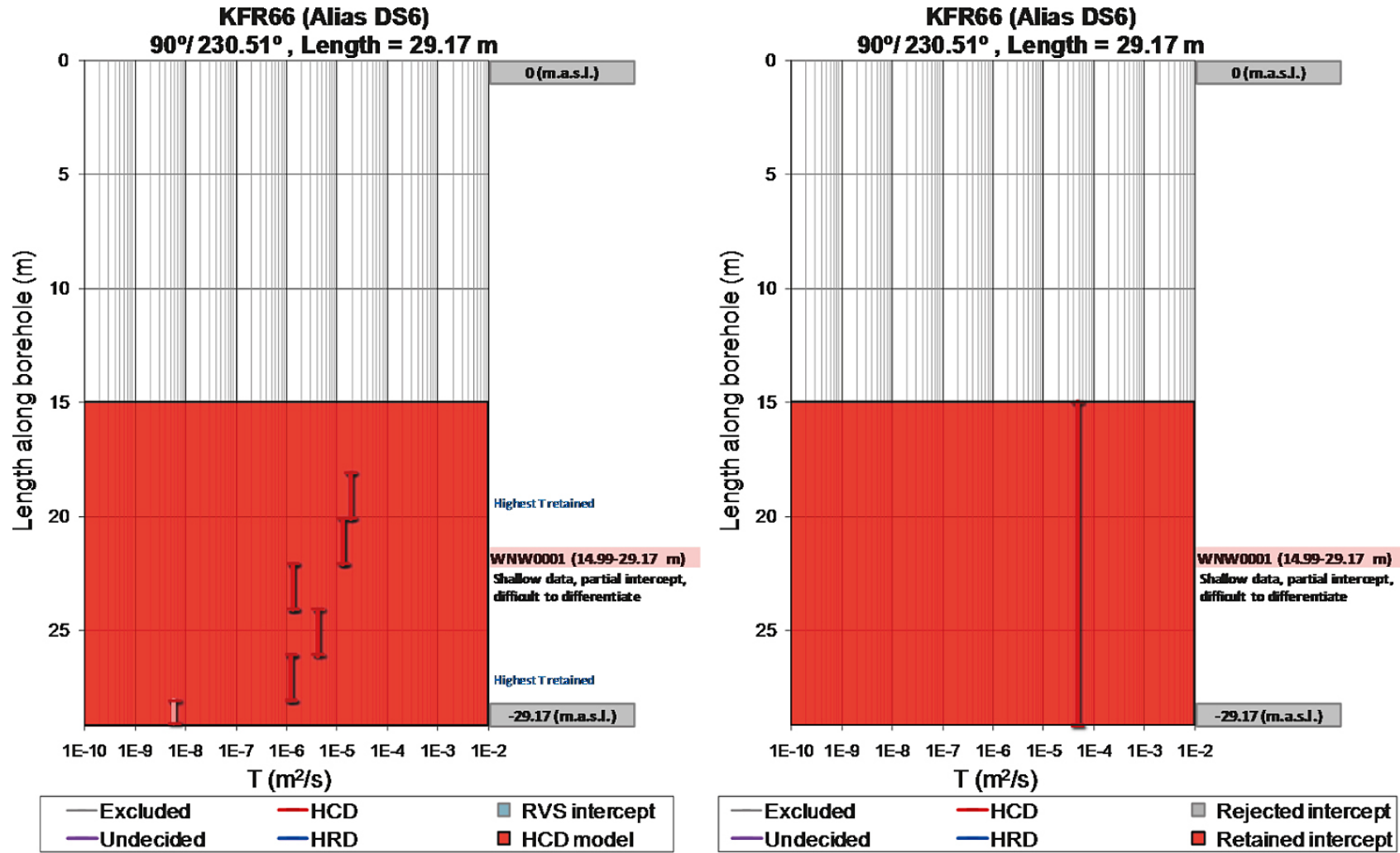


Figure D-53. KFR65: available data after screening process and modelled deformation zone intercepts (left) and interpreted total transmissivities and retained intercepts (right). An early borehole, drilled from the ice, targeting the predicted core of Singö deformation zone (incomplete intercept).



**Figure D-54.** KFR66: available data after screening process and modelled deformation zone intercepts (left) and interpreted total transmissivities and retained intercepts (right). An early borehole, drilled from the ice, targeting the predicted core of Singö deformation zone (incomplete intercept).

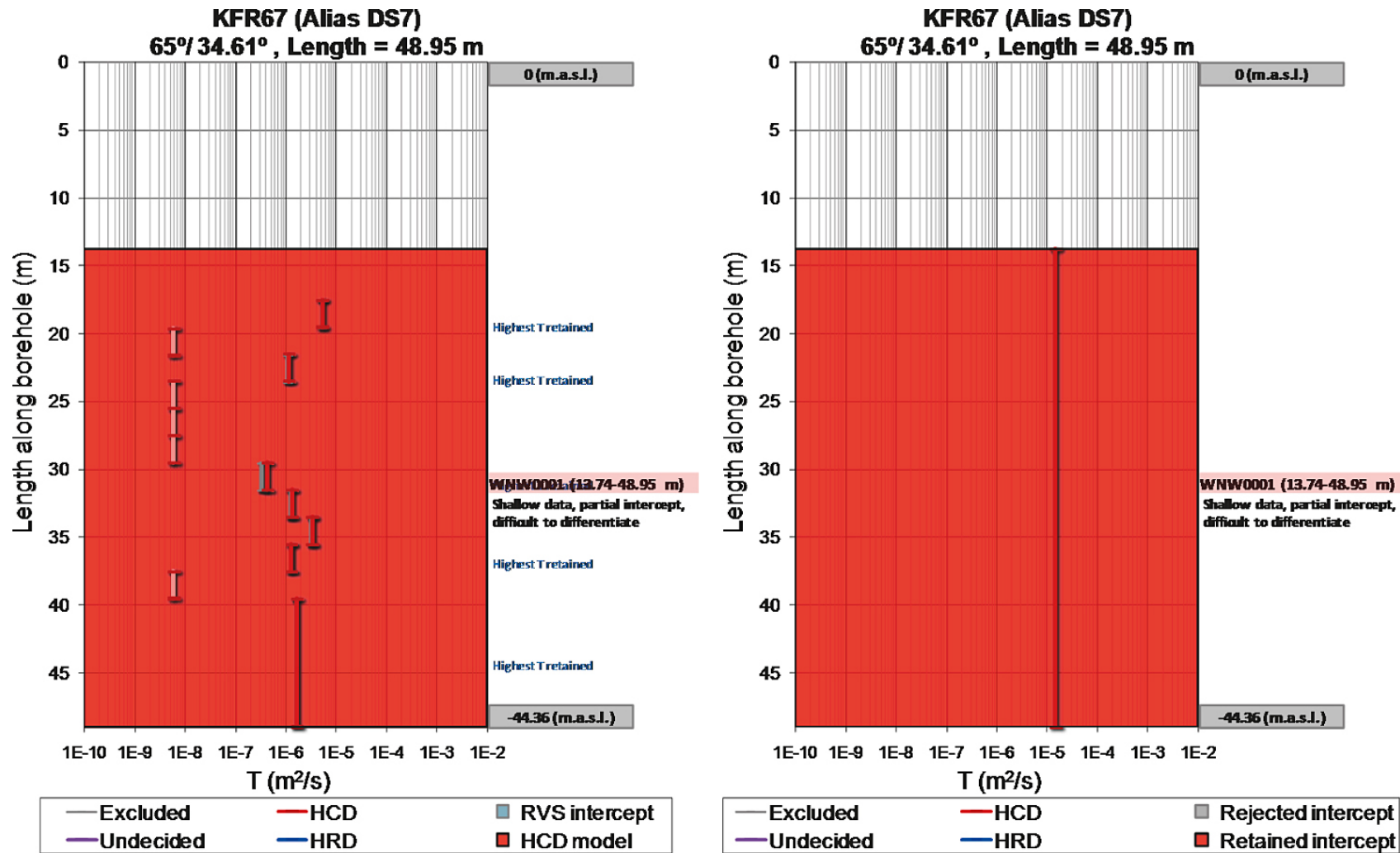
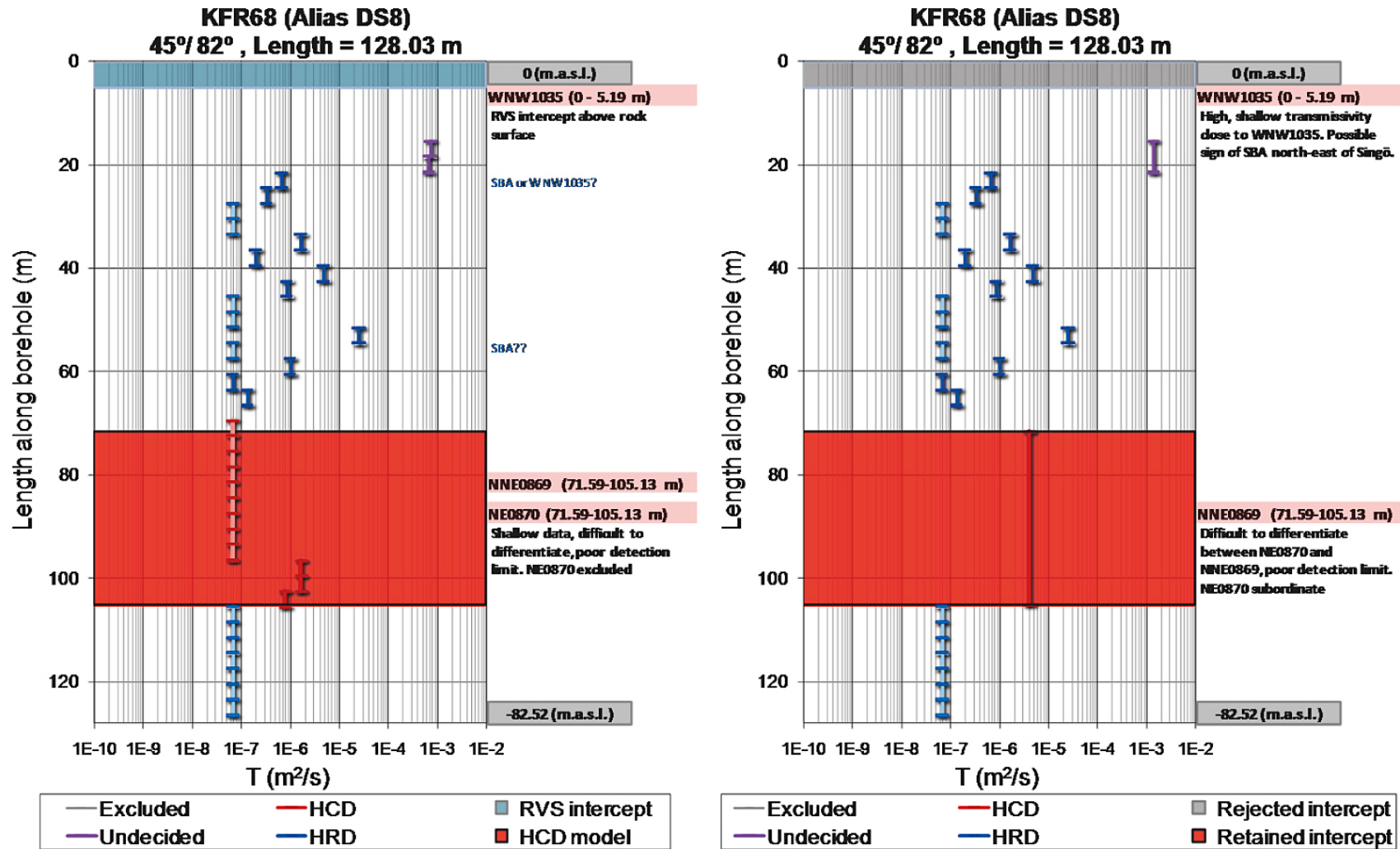
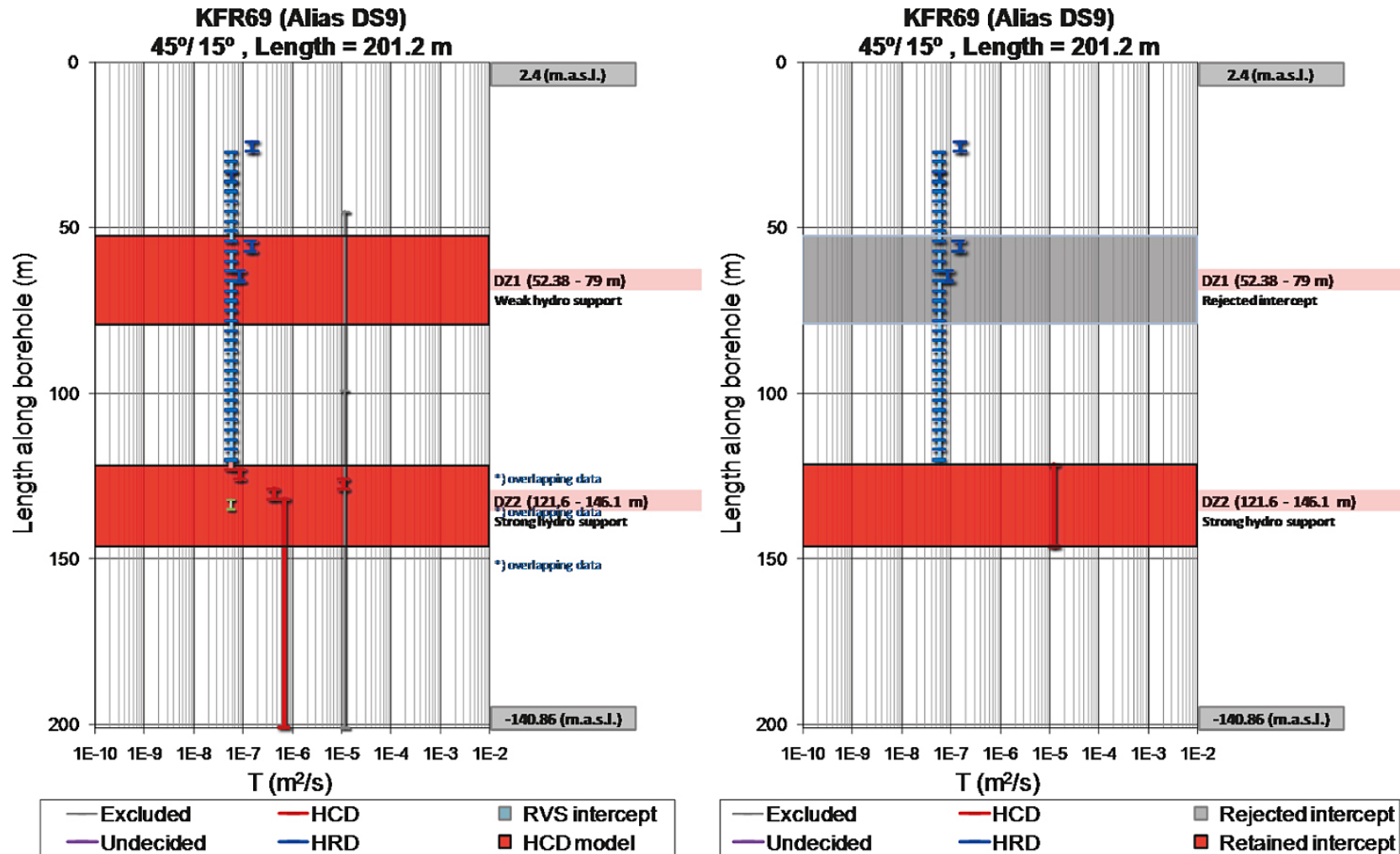


Figure D-55. KFR67: available data after screening process and modelled deformation zone intercepts (left) and interpreted total transmissivities and retained intercepts (right). An early borehole, drilled from the ice, targeting the predicted core of Singö deformation zone (incomplete intercept).



**Figure D-56.** KFR68: available data after screening process and modelled deformation zone intercepts (left) and interpreted total transmissivities and retained intercepts (right). Shallow, high-transmissive data close to RVS-intersection of WNW1035, possibly indicating presence of SBA north-east of Singö.





**Figure D-57.** KFR69: available data after screening process and modelled deformation zone intercepts (left) and interpreted total transmissivities and retained intercepts (right). The highly transmissive Possible Deformation Zone (PDZ) identified at c. 127 m borehole length (-88 m.a.s.l.), below SFR (see Table A-1) is most likely correlated to one of the grouted horizontal structures mapped in the SFR access tunnels (Figure 4-1 and Figure D-3).

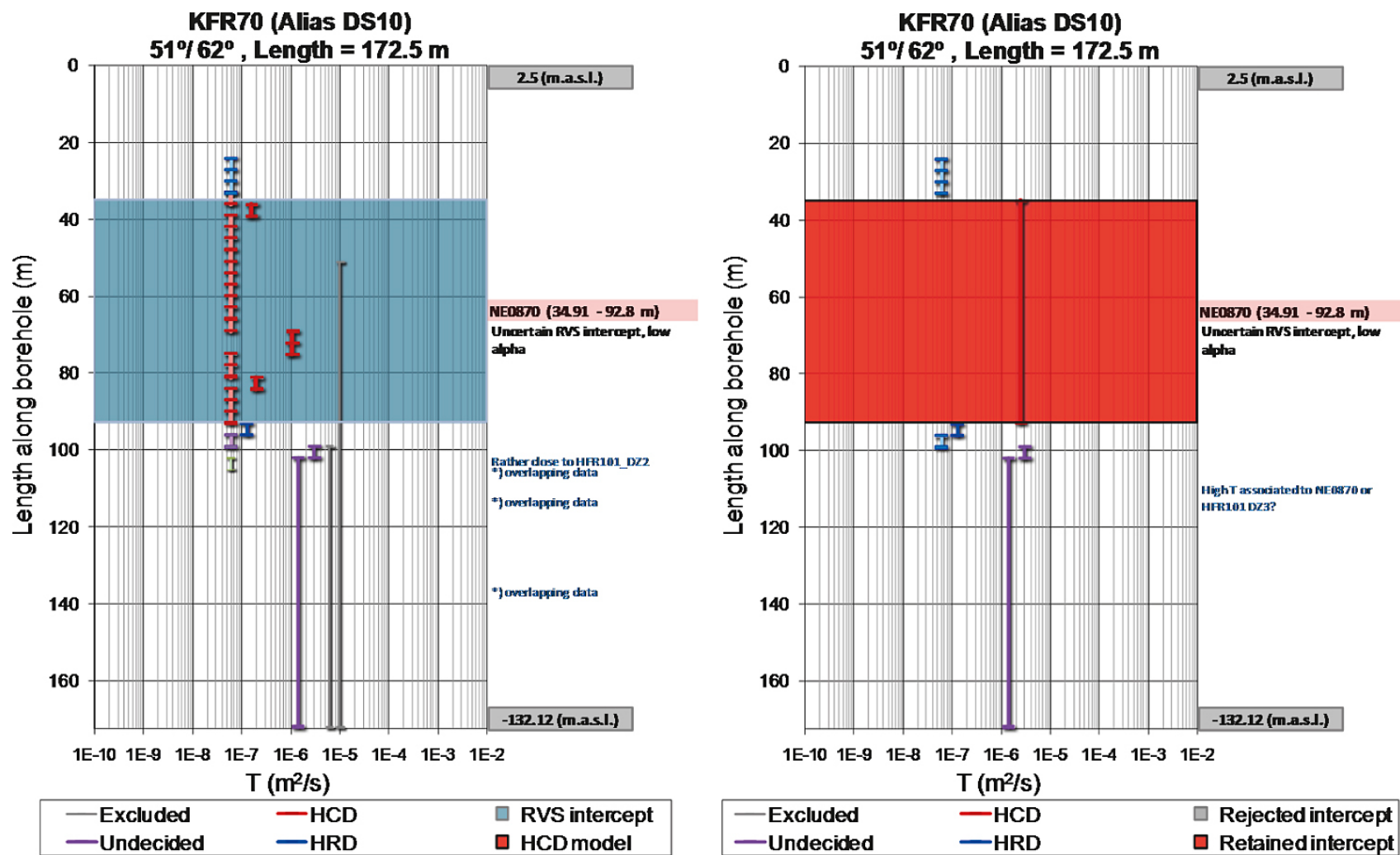


**Figure D-58.** KFR70: available data after screening process and deformation zone intercepts (left) and interpreted total transmissivities and retained intercepts (right). The RVS intercept of ZFMNE0870 is highly uncertain. Possibly, the high transmissivity below ZFMNE0870 relates to HFR101\_DZ2.

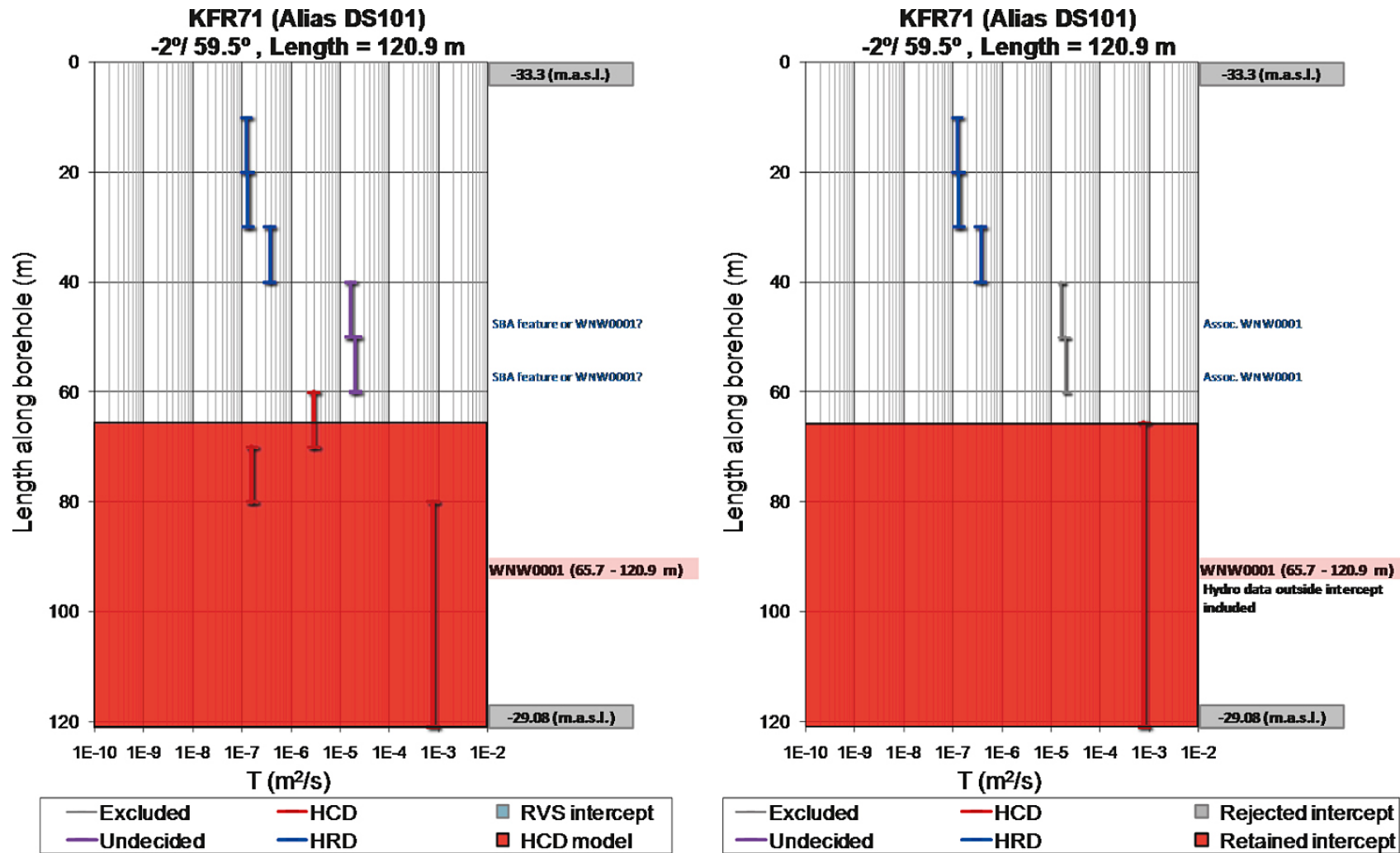


**Figure D-59.** KFR71 (pilot hole for tunnel construction through the core of WNW0001): available data after screening process and modelled deformation zone intercepts (left) and interpreted total transmissivities and retained intercepts (right). This borehole provides the best shallow intercept of WNW0001.

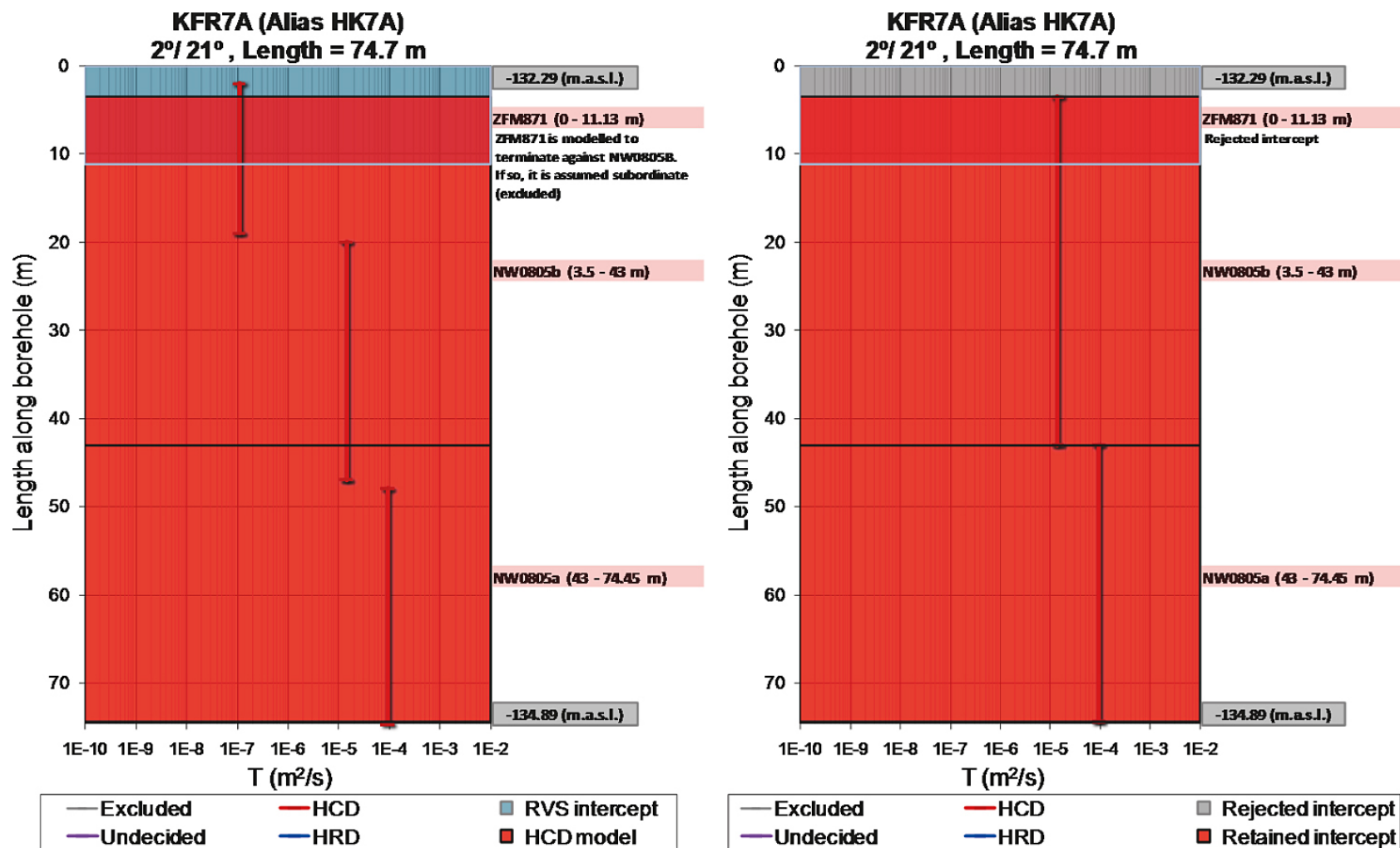


**Figure D-60.** KFR7A: available data after screening process and modelled deformation zone intercepts (left) and interpreted total transmissivities and retained intercepts (right). KFR7A is located at the junction of ZFM871 and NW0805A,B. In the geological model, ZFM871 is terminated against NW0805B. Hydrochemistry and drawdown data of the entire KFR7A has ZFM871 characteristics, suggesting extension of ZFM871 beyond its modelled termination.

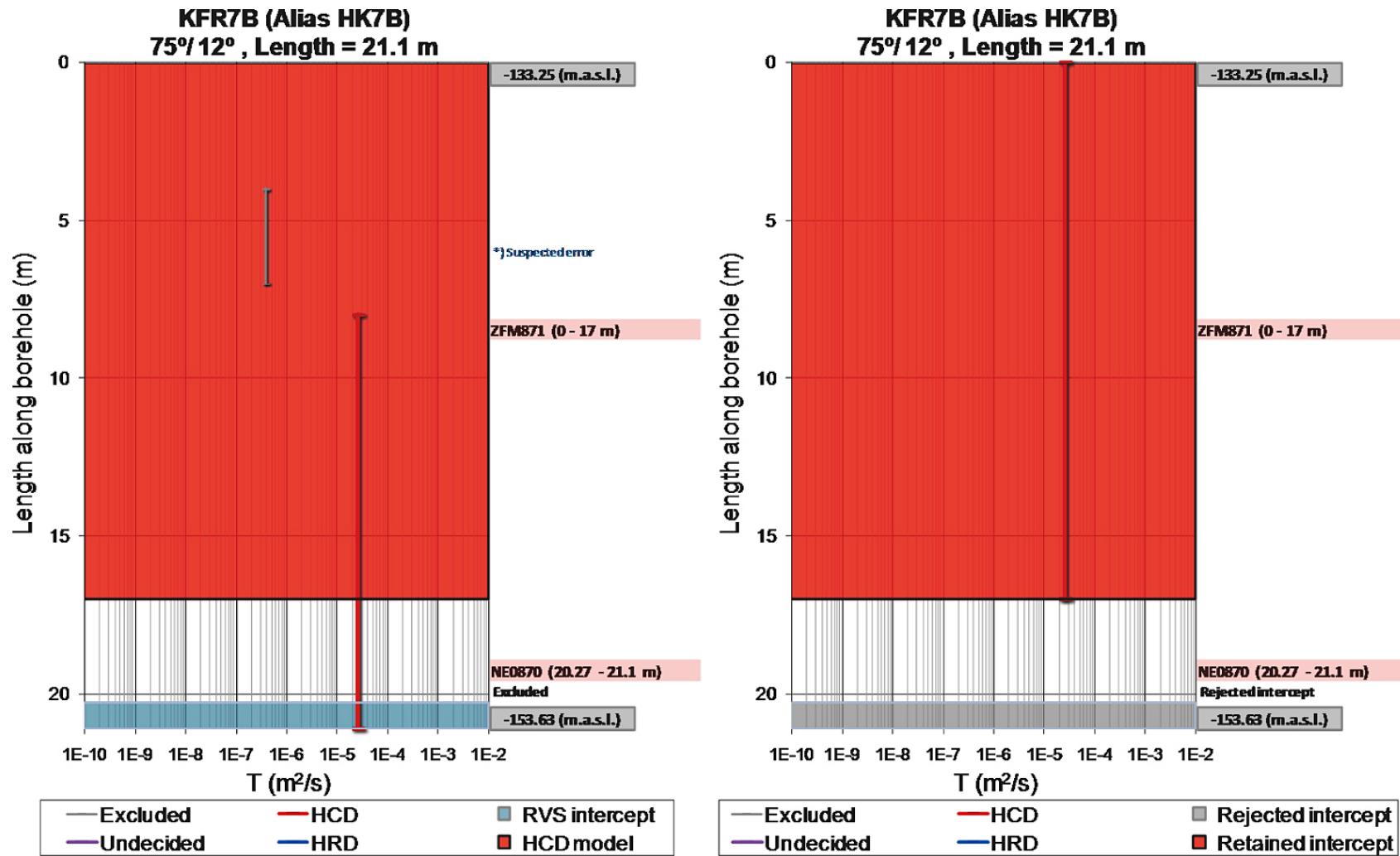


Figure D-61. KFR7B: available data after screening process and modelled deformation zone intercepts (left) and interpreted total transmissivities and retained intercepts (right). NE0870 assumed subordinate.

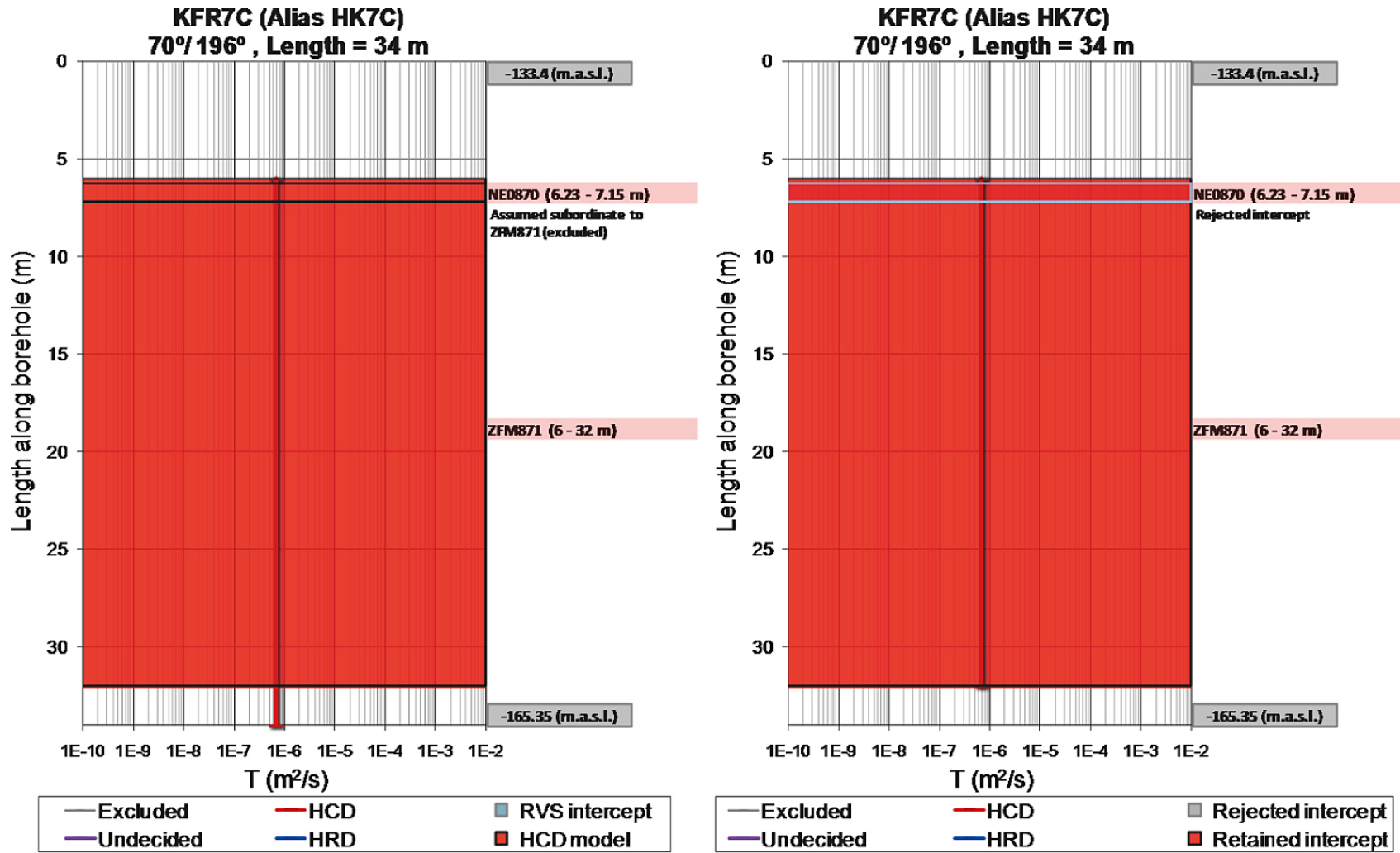
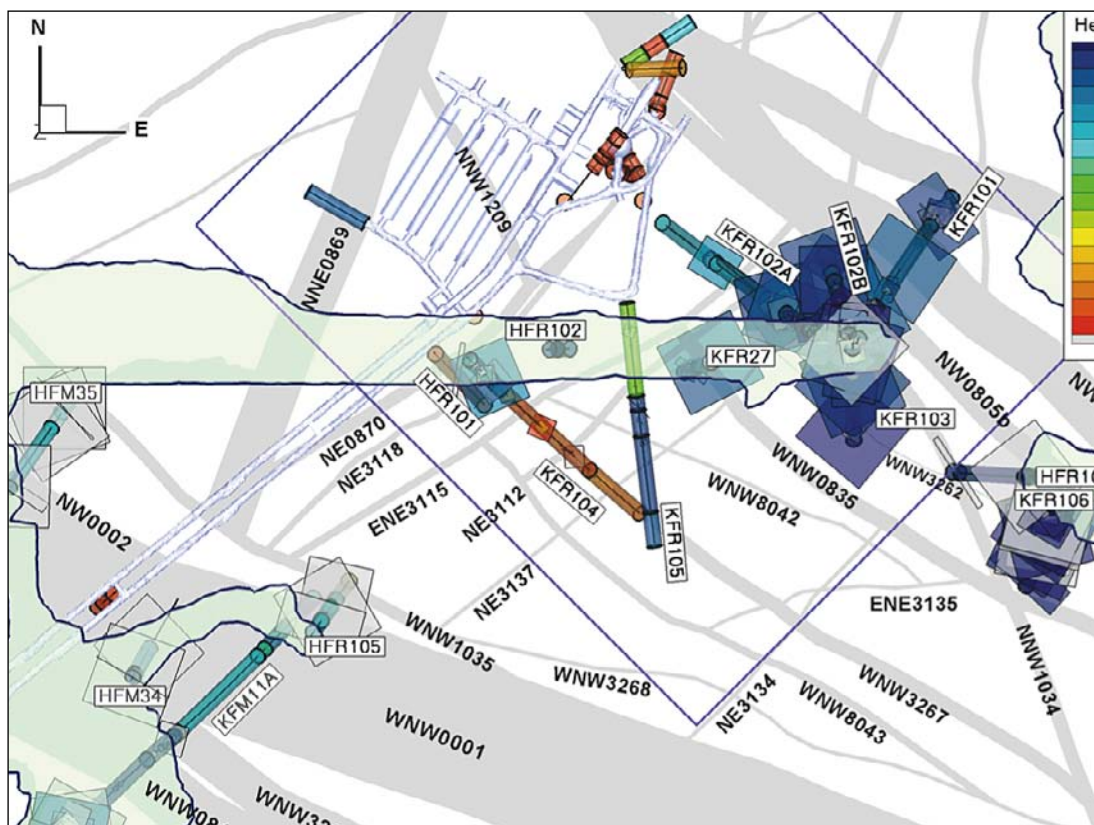


Figure D-62. KFR7C: available data after screening process and modelled deformation zone intercepts (left) and interpreted total transmissivities and retained intercepts (right). NE0870 assumed subordinate.

## Analysis of hydraulic data from the SFR extension investigation

This appendix describes the hydraulic parameterisation of deformation zones in the new data set: core boreholes KFR101, KFR102A, KFR102B, KFR103, KFR104, KFR105, and KFR106, as well as percussion boreholes HFR101, HFR102, HFR105, and HFR106. HFR106 and KFR106 are located outside the Local model domain (purple line; Figure E-1). Boreholes from Site Investigation Forsmark, KFM11A, HFM34, and HFM35, as well as the old data set obtained from the construction of SFR are presented in Appendix D. The final location and layout of the planned SFR extension has not yet been decided. It is currently assumed that it will be located within a similar depth interval as the existing SFR, i.e. approximately within an interval of  $-60$  to  $-140$  m RHB 70. It is also likely that the SFR extension will be located with certain respect distance to the Southern boundary belt (WNW001 with splays) and the Northern boundary belt (NW0805A and B), i.e. a fairly central location within the Local model domain (Figure E-1).

In terms of Open fracture, all boreholes inside the Local SFR domain have a relatively homogeneous character within the depth interval referred to as the Repository level (Figure 4-10 and Öhman and Follin 2010b). Open fractures are divided into five sets; EW, NE, NW, Gd, and Hz, which have fairly similar intensities ( $P_{32, \text{Open}} \approx 1 \text{ m}^2/\text{m}^3$ ). The borehole sampling bias artefacts is judged to be small for the combined data set; the Site Investigation program employed borehole orientations with gentle inclination ( $50$ – $60^\circ$ ) and various bearings.



**Figure E-1.** Top view of the new borehole data set; borehole location, point-water head in monitored sections, fresh-water head in PFL-f-features in context of the traces of the Geological model v. 1.0. PFL-f-features are shown as oriented planes with size related to transmissivity according to the v. 0.2 DFN parameterisation. The SFR Local model domain is shown by purple lines.

In terms of fracture hydraulic characteristics, the spatial patterns are more complex. Hydraulic data are more subject to depth trends, clustering, and lateral variation in comparison to fracture data. Moreover, the hydraulic data set is considerably smaller (less than 5% of the Open fractures are water bearing) and the censoring practical detection limit varies between boreholes, as well as, along the borehole length. Three depth intervals were defined for HRD transmissivity in Öhman and Follin (2010b). There is no new information that contradicts these depth intervals, and therefore the focus in this study is directed towards the relation to deformation zones as well as lateral variation.

The three boreholes with the lowest total transmissivity, HFR101, KFR104, and KFR105, are located in the Central block. The boreholes with largest total transmissivity are located close to either the Southern boundary belt or the Northern boundary belt (Figure E-1). The largest PFL-f transmissivities in HRD are horizontal or gently dipping and predominantly found close to the Northern boundary belt. However, KFR105 is sub-horizontal and has a limited vertical coverage, between c. -105 to -156 m RHB 70. If the hydraulic backbone indeed consists of horizontal sheets of interconnected fracture clusters, its potential existence in the Central block cannot be judged with confidence from KFR105. If boreholes are sorted by the maximum transmissivity found within the limited interval -105 to -156 m RHB 70 (HCD excluded), KFR105 has a median value (although still, KFR104 has the smallest value).

Possible hypotheses for the lateral trend in transmissivity are relations to:

- 1) The rock domain model, or
- 2) the deformation zone model, or
- 3) the hydraulic soil domain (HSD) model.

The transmissivity patterns fit the rock domain model quite well: low transmissivities are found in RFR01, and high transmissivities are found in RFR02. A model volume division based on the rock domain would be practical and convenient. However, there is a conceptual unease about using distinct boundaries, such as the interface between RFR01 and RFR02, to characterise large rock volumes that have gaps in data coverage. For example, KFR105 is intersected twice by the RFR01/RFR02 boundary, but these intercepts do not coincide with distinct differences in transmissivity. RFR01 forms a large volume between the Central block and the Southern boundary belt and is covered only by HFR101, KFR104 and parts of KFR105. It would seem unlikely, and conceptually uncertain, that RFR01 would represent a homogeneous rock unit with properties that are also similar in the vicinity of the Southern boundary belt. Moreover, the existing underground SFR storage facilities provide contradictory evidence; the facilities are located in RFR02 but have little inflow. A rock domain-based model is judged to imply too large conceptual uncertainty arising from gaps in borehole coverage.

It is conceptually more appealing to base the conceptual model on the deformation zone model. It would seem reasonable the Northern and Southern boundary belt have not only local effect on the fracture system, but also play an essential role in the large-scale connectivity of the flowing fracture system. The HRD transmissivity appears to be dominated by horizontal features; thus, it seems likely that high-transmissive HCDs that are well-connected have a key role in the connectivity between the deep fracture system and the Seafloor. There are distinct differences between HCDs in their potential to act as vertical conductors, i.e. apparent PFL transmissivity inside HCDs (Table 4-1). The role of HCDs as vertical conductors may be subject to spatially variable sediment properties, i.e. local thickness and vertical conductivity, which may severely constrain the contact between the Sea and the deep fracture system.

### **Characterization of deformation zones**

The transmissivity inside deformation intercepts have been summarised in Table 4-1. The parameter  $T_0$  reflects transmissivity that has been depth adjusted to the reference level 0 m RHB 70, Eq. (5-2). The HRD transmissivity is dominated by sub-horizontal PFL-f data, also referred to as SBA-structures. In the calculation of intercept transmissivity of steeply dipping deformation zones an additional parameter has been included,  $T_{0\text{NoSBA}}$ , in which PFL-f data dipping less than 35°, excluded from calculation of intercept transmissivity.



**Table E-1. Summary of HCD intercept transmissivity.**

ZFM	Borehole	Borehole length (m)		Elevation (m RHB 70)		Interval transmissivity <sup>3)</sup> (m <sup>2</sup> /s)			
		From	To	From	To	$\Sigma T_i$	$T_0$	$\lg T_0$	$\lg T_0^{(1)}_{No\ SBA}$
<b>Southern boundary belt</b>									
WNW0001	HFR105	21.12	92	-15.5	-79.2	1.25E-5	2.3E-5	-4.6	-5
WNW1035	HFR105	119	147	-103.8	-129.4	1.1E-5	3.1E-5	-4.5	-4.5
<b>Northern boundary belt</b>									
NW0805a	KFR101	242	341.76	-190.1	-262.0	6.1E-6	6.0E-5	-4.2	-4.3
NW0805b	KFR101	97	116	-76.9	-92.2	8.3E-6	1.9E-5	-4.7	-4.7
<b>Steep N-S to NNW set</b>									
NNW1034	HFR106	158	182	-127.1	-146.3	2.1E-5	8.7E-5	-4.1	-4.1
NNW1034	KFR101	13.72	88	-8.9	-69.5	5.0E-6	7.0E-6	-5.2	-6.5
NNW1034	KFR106	256	266	-238.6	-248.0	7.6E-6	8.6E-5	-4.1	-4.1
<b>Steep WNW to NW set</b>									
WNW0835_1	KFR27	108	120	-105.1	-117.1	8.1E-8	2.4E-7	-6.6	-6.9
WNW0835_2	KFR27	323	469	-319.5	-464.5	3.2E-6	1.7E-4	-3.8	-3.9
WNW3262	KFR103	180	182.5	-142.5	-144.5	5.1E-6	2.1E-5	-4.7	
WNW3262	KFR106	67	73	-61.9	-67.5	2.0E-5	3.7E-5	-4.4	-6.7
WNW3267	KFR104	396	454.57	-308.1	-351.7	1.1E-8	2.5E-7	-6.6	-6.6
WNW3267	KFR105	258	283	-149.4	-153.2	4.1E-8	1.8E-7	-6.7	-6.7
WNW8042	KFR105	170.8	176	-135.5	-136.4	2.7E-7	1.1E-6	-6.0	-6
<b>Steep NNE to ENE set</b>									
ENE3115	KFR105	45	52	-114.6	-115.8	6.1E-9	1.9E-8	-7.7	-7.7
ENE3115	KFR104	149	154	-117.7	-121.6	8.6E-9	2.8E-8	-7.6	-7.6
ENE3115*	KFR102A	422	503	-379.2	-451.0	1.7E-6	8.1E-5	-4.1	-5.2
NE0870	HFR101	28	41	-23.7	-35.8	1.0E-7 <sup>2)</sup>	1.3E-7	-6.9	
NE3112	KFR102A	302	325	-271.9	-292.6	1.9E-8	3.0E-7	-6.5	-6.5
NE3112	KFR102B	173	180	-137.2	-142.8	5.9E-7	2.3E-6	-5.6	-5.9
NE3112	KFR104	268	283	-210.8	-222.3	1.1E-7	9.8E-7	-6.0	-6
NE3112	KFR105	88.5	96.5	-122.0	-123.3	2.3E-9	7.6E-9	-8.1	-8.1
NE3118	HFR101	190	202	-170.1	-180.5	2.5E-7	1.4E-6	-5.8	-5.8
NE3118	KFR104	30	45.5	-21.7	-34.4	1.8E-7	2.4E-7	-6.6	-7.1
NE3137	KFR102A	149	161	-133.3	-144.2	9.5E-9	3.9E-8	-7.4	
NE3137	KFR102B	109	114	-85.8	-89.8	1.4E-7	3.3E-7	-6.5	
NE3137	KFR104	382	387	-297.6	-301.4	1.7E-9 <sup>2)</sup>	3.3E-8	-7.5	
NE3137	KFR105	191	205	-138.8	-141.0	5.4E-9	2.1E-8	-7.7	-7.8
<b>Possible deformation zones not included in the deterministic model</b>									
HFR101_DZ2	HFR101	101	115	-90.9	-103.6	2.6E-6	6.8E-6	-5.2	
HFR106_DZ1	HFR106	38	40	-30.9	-32.6	3.1E-5	4.3E-5	-4.4	
KFR101_DZ3	KFR101	179	186	-142.0	-147.5	1.3E-5	5.4E-5	-4.3	
KFR101_DZ4	KFR101	197	213	-156.0	-168.2	2.0E-8 <sup>2)</sup>	1.0E-7	-7.0	
KFR102B_DZ1	KFR102B	67	70	-51.9	-54.3	8.8E-7	1.5E-6	-5.8	
KFR102B_DZ3	KFR102B	149.5	150.5	-118.4	-119.2	5.0E-6	1.6E-5	-4.8	
KFR103_DZ1	KFR103	24.5	26.5	-17.5	-19.1	2.5E-7	3.0E-7	-6.5	
KFR103_DZ2	KFR103	84	91	-65.6	-71.2	1.6E-5	3.1E-5	-4.5	
KFR105_DZ5	KFR105	293.6	304	-154.7	-156.2	1.4E-8	6.4E-8	-7.2	
KFR106_DZ1	KFR106	15	20	-13.1	-17.8	4.9E-7	5.7E-7	-6.2	
KFR106_DZ2	KFR106	36.5	52	-33.2	-47.8	2.9E-6	4.2E-6	-5.4	
KFR106_DZ4	KFR106	84.5	86	-78.3	-79.7	1.5E-5	3.3E-5	-4.5	
KFR106_DZ5	KFR106	100.5	101	-93.3	-93.7	1.5E-5	3.8E-5	-4.4	
KFR106_DZ6	KFR106	153	157	-142.4	-146.1	2.4E-5	1.0E-4	-4.0	

<sup>1)</sup> SBA-structures, defined as PFL-f data dipping less than 35°, excluded from calculation of intercept transmissivity for steeply dipping zones.  $\lg T_{0, No\ SBA}$  is only reported for steeply dipping deformation zones; it is less relevant for PDZs not included in the deterministic model, as they tend to be sub-horizontal.

<sup>2)</sup> No PFL-f found inside deformation zone intercept. The maximum interval transmissivity has been assumed equal to the practical detection limit for 5 m section PFL data.

<sup>3)</sup> Depth-adjusted transmissivity coloured by logarithmic values (red = maximum, green = median, blue = minimum).

## KFR101

KFR101 was drilled northeast from the tip of the Pier through the Northern boundary belt (Figure E-1). It intersects ZFMNNW1034, ZFMNW0805A and B (Figure E-2). In the wedge between ZFMNW0805A and B, two possible deformation zones are intercepted, which are not included in the deterministic model. The largest PFL-f transmissivities are found in ZFMNW0805A and B and KFR101\_DZ3. The PFL-f record inside KFR101\_DZ3 is sub-horizontal (Figure E-3) and it is included in the deterministic sub-horizontal Shallow Bedrock Aquifer feature SBA6. The dominating PFL-f records inside ZFMNW0805A and B are sub-parallel to the deformation zone (Figure E-3). ZFMNNW1034 and the HRD are dominated by gently dipping and horizontal PFL-f data. The deterministic deformation zones have an enhanced intensity of steep EW- and NW-striking Open fractures (Figure E-4). However, there is little evidence of the steep EW set in PFL-f data.

## KFR102A

KFR102A is the deepest borehole drilled during the SFR extension investigation. It was drilled northwest from the tip of the Pier (Figure E-1). KFR102A is percussion-drilled down to c. 70.4 m borehole length (telescopic drilling); a steel pipe (Figure E-6f) is mounted in the interval 67 to 72 m borehole length for the diameter-transition to the subsequent core borehole drilling. The shallowest PFL-f, located at 72 m borehole length, is assumed to reflect an inflow in the interval 70.4 to 72 m bore length that is hidden behind the steel pipe; hence it cannot be assigned an orientation (Figure E-5). This upper PFL-f is possibly related to the horizontal structure SBA2.

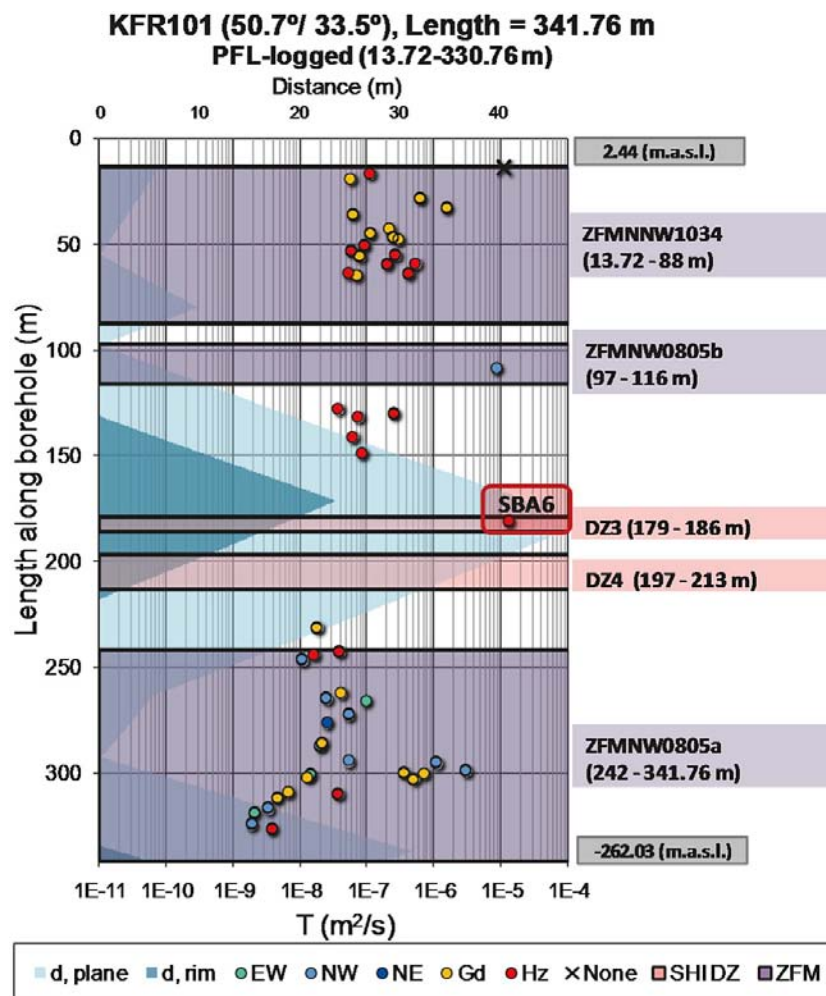


**Figure E-2.** Hydraulic data of KFR101 classified into HRD/HCD. Blue shades show distance to the central plane and the rim of nearest deformation zone, respectively. The PFL-f at 13.7 m borehole length is assumed to reflect leaking casing. High transmissive NW-striking steep PFL-f occur inside WNW0805A and B. The PFL-f data outside zones are few and low-transmissive. As an alternative, the horizontal PFL-f inside KFR101\_DZ3 has been modelled as part of the hydraulic feature SBA6.

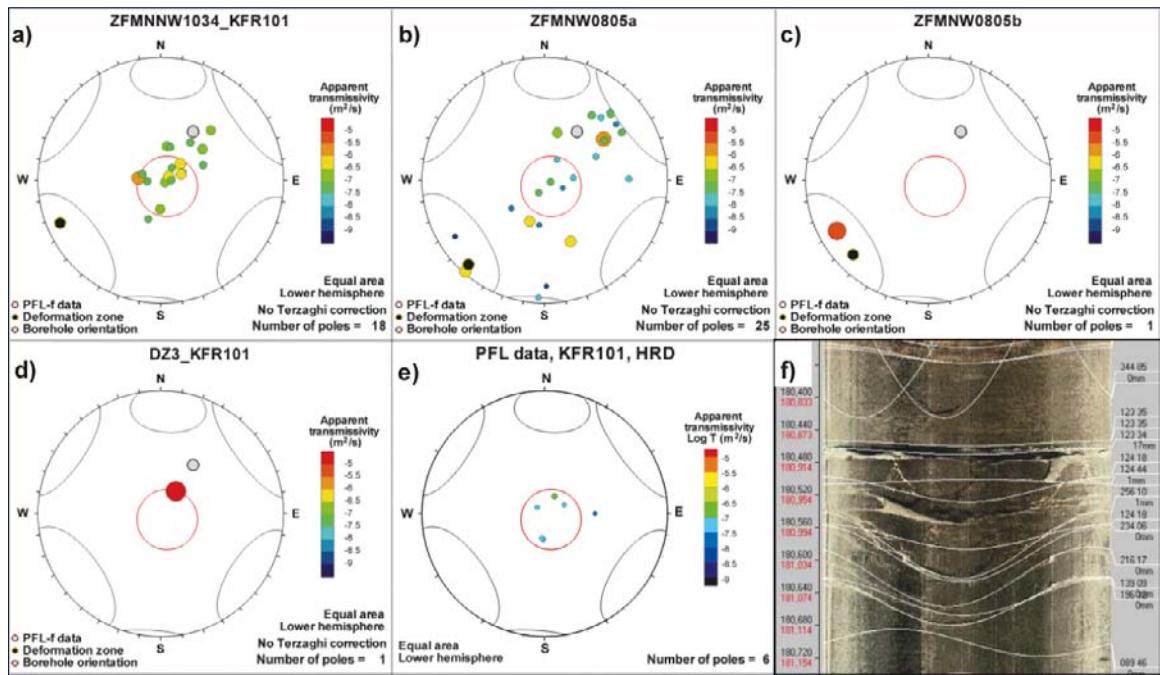


**Figure E-3.** PFL-f data orientation inside zones and inside HRD (a–e) and f) BIPS image of the most transmissive feature in KFR101\_DZ3, alternatively associated with the hydraulic feature SBA6.

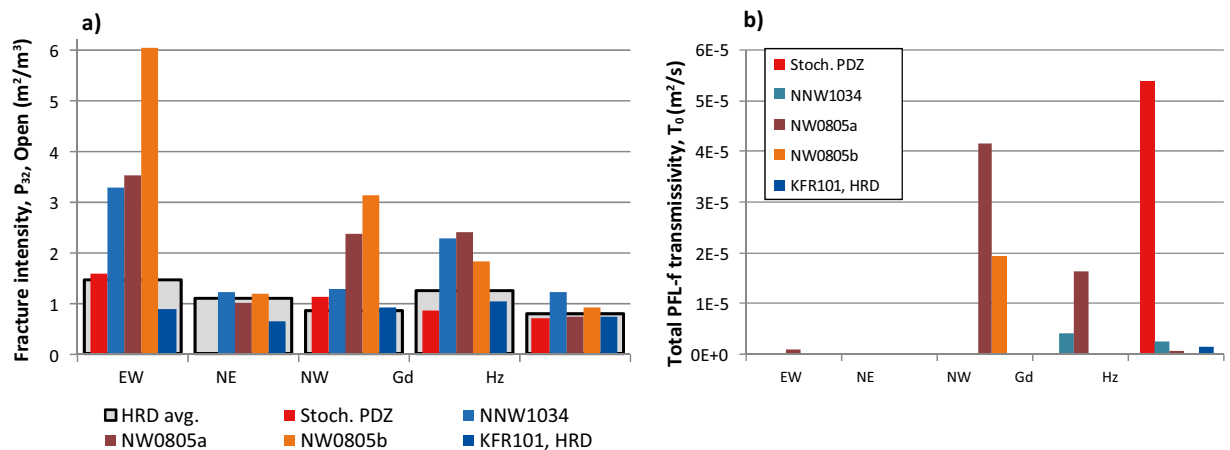


**Figure E-4.** Set-wise characteristics of KFR101 inside intercepted zones compared to the rock mass outside zones; a) intensity of Open fractures and b) sum of depth-adjusted PFL-f transmissivity.

Only NE to ENE striking deformation zones are intersected: ZFMNE3137, ZFMNE3112, and ZFMENE3115 (Figure E-5). Highly transmissive horizontal PFL-f are detected at approximately 190–205 m borehole length. These have been alternatively modelled as a shallow hydrogeological structure SBA6, based on high response index 1 with KFR102B and KFR101. There is also a horizontal radar reflector just below this interval (71°/12°) at 215 m borehole length. The HRD between ZFMNE3112 and ZFMENE3115 has a remarkable absence of detected PFL-f inflows. Gently dipping PFL-f with high transmissivity and porous granite is found inside the intercept of ZFMENE3115. These characteristics are anomalous; in the shallower intercepts of ZFMENE3115 (found in KFR104 and KFR105) are considerably shorter in terms of interval lengths, and show no evidence of enhanced transmissivity. Note also that ZFMENE3115 is the steeply dipping deformation zone that terminates ZFM871 to the southeast. The deepest part of KFR102A, below its intersection of ZFMENE3115, is located underneath ZFM871 (Zone H2).

The orientation of PFL-f data of KFR102A inside deformation zone intercepts are compared to the pattern outside intercepts (Figure E-6). BIPS images of the most transmissive features are also shown in Figure E-6. The intensity of Open fractures and depth-adjusted PFL-f transmissivity are shown for fracture sets inside intercepted zones and the rock mass outside in Figure E-7.

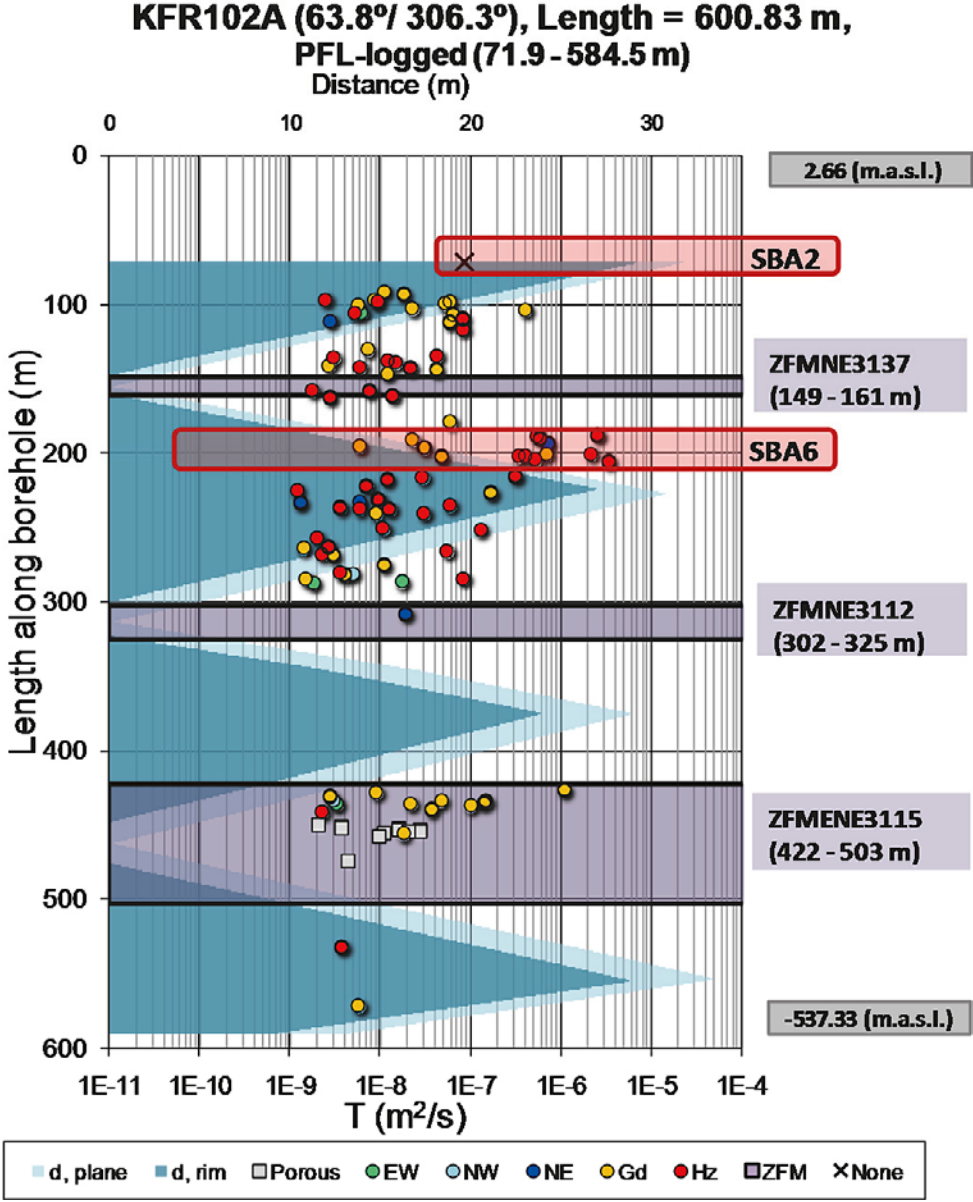


**Figure E-5.** Hydraulic data of KFR102A classified into HRD/HCD. Blue shades show distance to the central plane and the rim of nearest deformation zone, respectively. The high frequency of high-transmissive horizontal PFL-f at c. 200 m borehole length has been modelled as part of the hydraulic feature SBA6. The PFL-f at 72 m borehole length is assumed to reflect an inflow above casing, possibly associated to the hydraulic feature SBA2. ENE3115 has extraordinary high frequency of gently dipping high-transmissive PFL-f, while the HRD between ENE3112 and ENE3115 has a remarkable lack of PFL-f inflow.

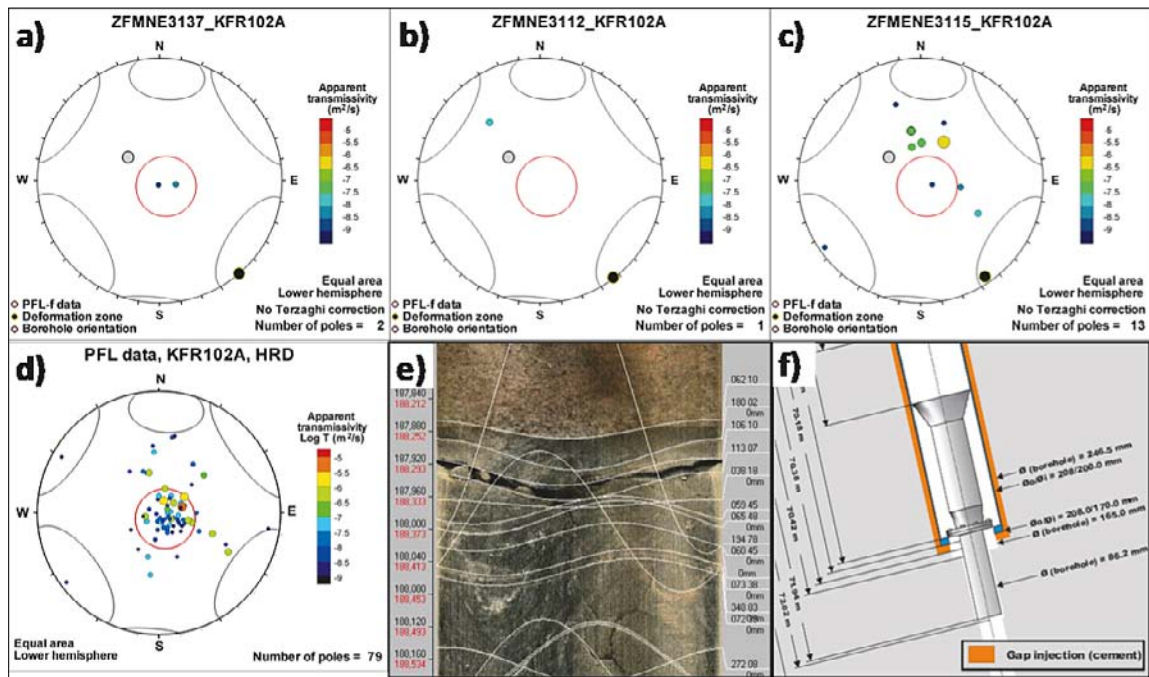


**Figure E-6.** PFL-f data orientation (a–c) inside zones and d) inside HRD, as well as, e) BIPS image of the most transmissive feature in KFR102A, alternatively associated with the hydraulic feature SBA6. The mounted steel pipe at c. 72 m borehole length shown in f) is modified from Nilsson and Ullberg (2009b).

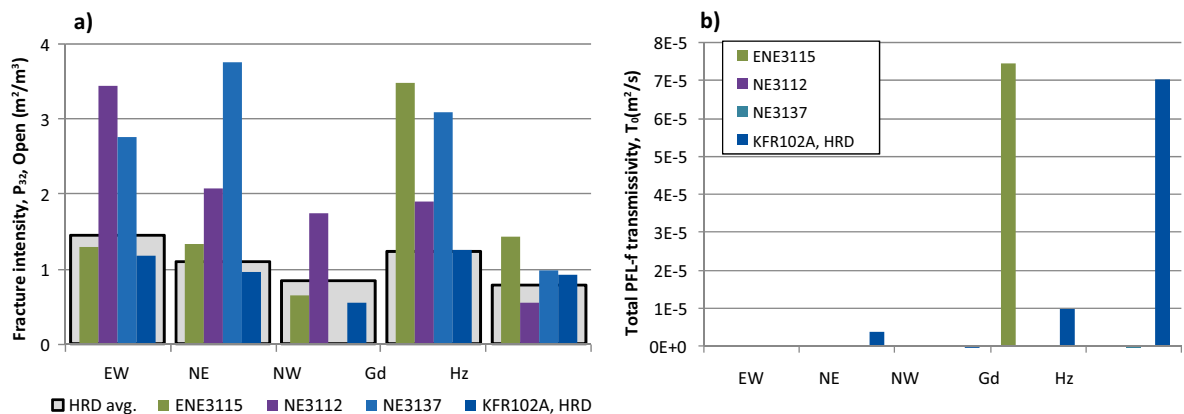


**Figure E-7.** Set-wise characteristics of KFR102A inside intercepted zones compared to the rock mass outside zones; a) intensity of Open fractures and b) sum of depth-adjusted PFL-f transmissivity.

### KFR102B

KFR102B is a complementary borehole to KFR102A. It was drilled as a in the vicinity of the Northern boundary belt, northwest from the tip of the Pier (Figure E-1). Apart from the dominance of horizontal PFL-f that are characteristic of the data close to the Northern boundary belt, there also exist steep EW-striking PFL-f in the upper c. 100 m. Shallow EW-striking PFL-f are also found in the nearby located borehole KFR103.

KFR102B intersects two NE-striking deterministic structures, ZFMNE3137 and ZFMNE3112, and two Unresolved PDZs (Figure E-8). Note that the deepest intercept, ZFMNE3112, is located very close to ZFMWNW0805B and ZFMNNW1034, and is alternatively modelled as an intercept of SBA6.

The orientation of PFL-f data of KFR102B inside deformation zone intercepts are compared to the pattern outside intercepts (Figure E-9). BIPS images of the most transmissive features are also shown in Figure E-9. The intensity of Open fractures and depth-adjusted PFL-f transmissivity are shown for fracture sets inside intercepted zones and the rock mass outside in Figure E-10.

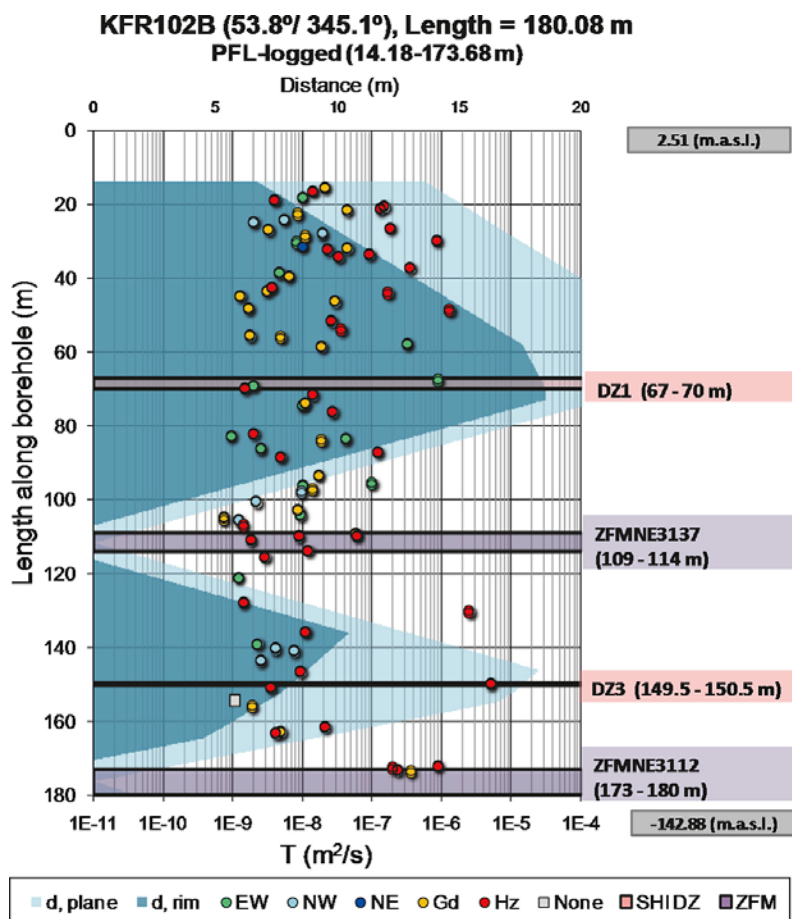


**Figure E-8.** Hydraulic data of KFR102B classified into HRD/HCD. Blue shades show distance to the central plane and the rim of nearest deformation zone, respectively. The high frequency of high-transmissive horizontal PFL-f at c. 170 m borehole length is alternatively modelled as part of the hydraulic feature SBA6.

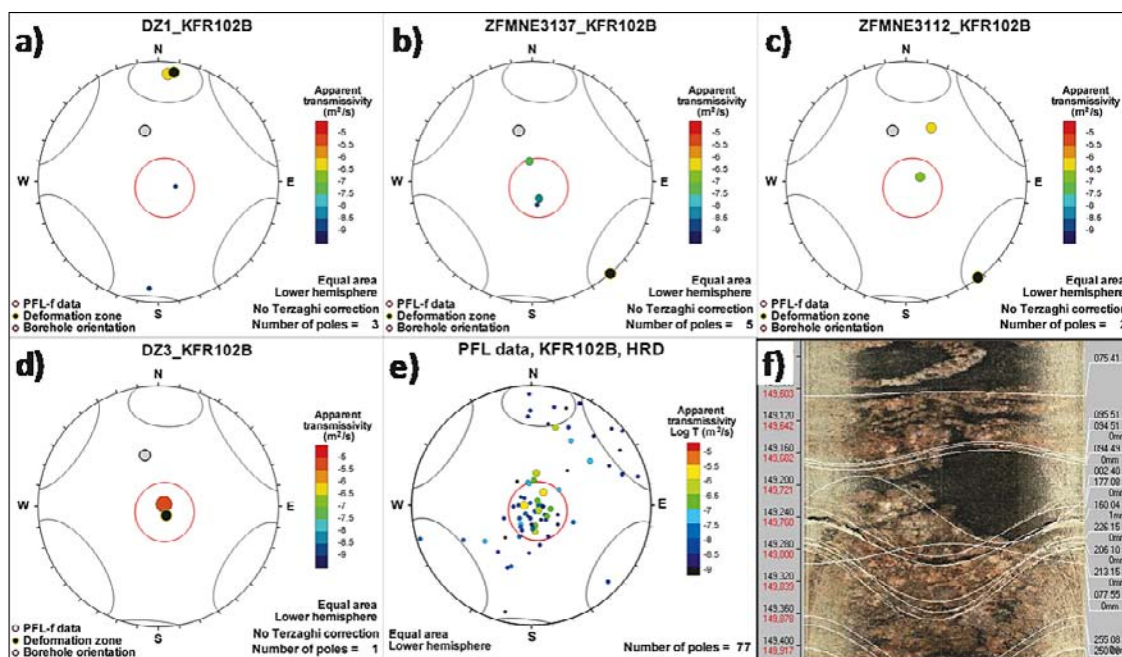


**Figure E-9.** PFL-f data orientation (a-d) inside zones and e) inside HRD, as well as f) BIPS image of the most transmissive feature, found in KFR102B\_DZ3.

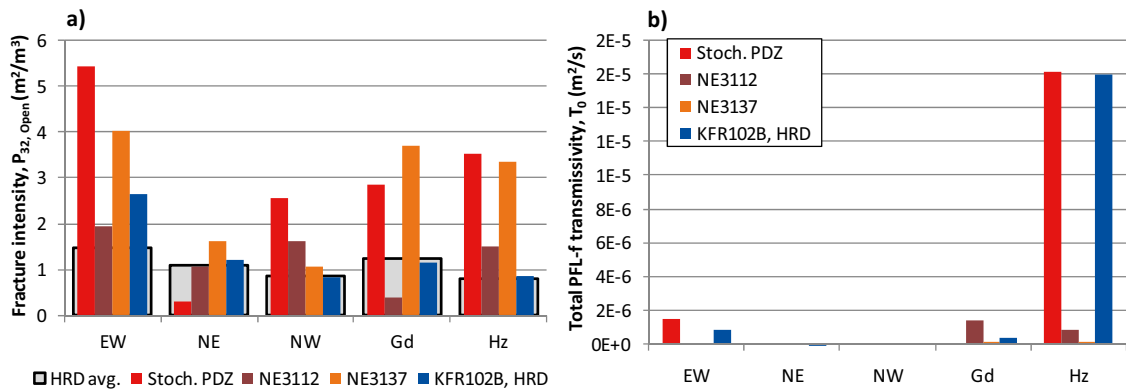


**Figure E-10.** Set-wise characteristics of KFR102B inside intercepted zones compared to the rock mass outside zones; a) intensity of Open fractures and b) sum of depth-adjusted PFL-f transmissivity.

### KFR103

KFR103 was drilled south from the tip of the Pier (Figure E-1). Similar to other boreholes drilled in the vicinity of the Northern boundary belt, it is dominated by horizontal PFL-f, but there also exist steep EW-striking PFL-f in the upper c. 50 m (Figure E-11). The frequency and transmissivity of PFL-f drops drastically with depth in KFR103. The uppermost PFL-f in KFR103 ( $T \approx 7 \times 10^{-5} \text{ m}^2/\text{s}$ ; the highest recorded transmissivity within the SFR extension investigation) is associated to leaking casing and hence excluded from the data set.

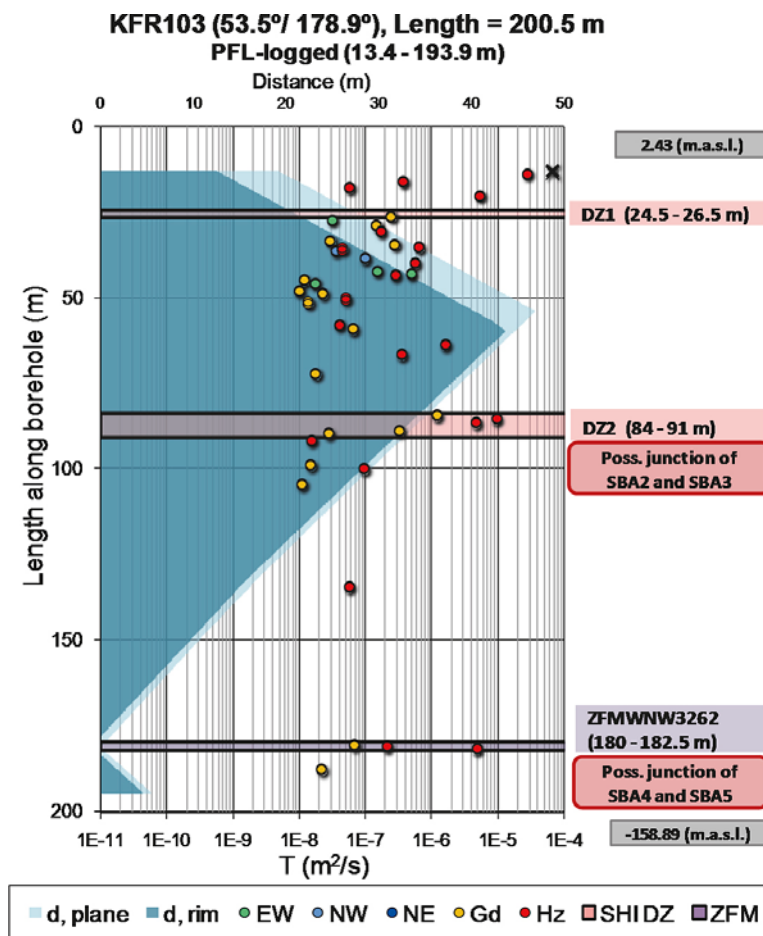


**Figure E-11.** Hydraulic data of KFR103 classified into HRD/HCD. Blue shades show distance to the central plane and the rim of nearest deformation zone, respectively. There are high-transmissive PFL-f in the vicinity of KFR103\_DZ1, but that may reflect shallow bedrock. In the alternative modelling of hydraulic SBA-structures, KFR103\_DZ3 is a junction of SBA2 and SBA3, and possibly, the WNW3262 intercept is a junction between SBA4 and SBA5. The PFL-f at 13.3 m borehole length (marked X) is assumed to reflect leaking casing.

KFR103 only intersects one WNW-striking deterministic structure, ZFMWNW3262, and two Unresolved PDZs. The ZFMWNW3262-intercept has similarities to the Unresolved PDZs found in boreholes close to the Northern boundary belt: narrow intercept containing horizontal highly transmissive PFL-f (Figure 5-8). Therefore the intercept is alternatively modelled as a junction between horizontal structures SBA4 and SBA5 (Figure 6-3). The lower Unresolved PDZ intercept (82 to 91 m; Figure E-11) is also alternatively modelled as a junction between horizontal structures SBA2 and SBA3 (Figure 6-3).

The orientation of PFL-f data of KFR103 inside deformation zone intercepts and outside intercepts, as well as BIPS images of the most transmissive features are shown in Figure E-12. The intensity of Open fractures and depth-adjusted PFL-f transmissivity are shown for fracture sets inside intercepted zones and the rock mass outside in Figure E-13.

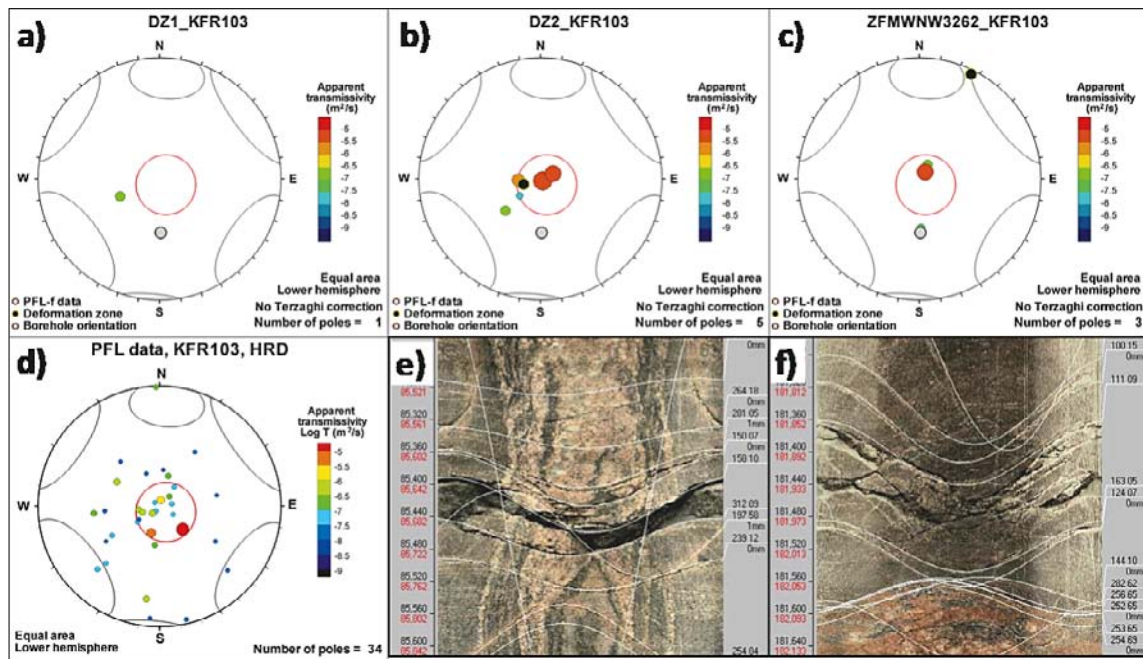


**Figure E-12.** PFL-f data orientation in KFR103; (a–c) inside zones and d) inside HRD, as well as BIPS images of the most transmissive features, found in e) KFR103\_DZ2 and f) ZFMWNW2362.

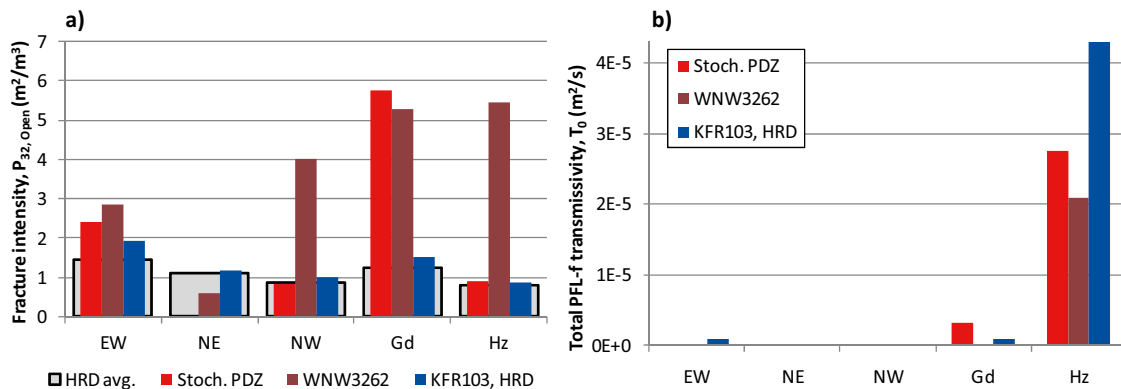


**Figure E-13.** Set-wise characteristics of KFR103 inside intercepted zones compared to the rock mass outside zones; a) intensity of Open fractures and b) sum of depth-adjusted PFL-f transmissivity.



## KFR104

KFR104 is located inside the Central block, drilled southeast from the middle of the Pier (Figure E-1). In comparison to boreholes drilled in the vicinity of the Northern boundary belt, it is less dominated by horizontal PFL-f (Figure E-14). The frequency and transmissivity of PFL-f drops notably with depth in KFR104.

KFR104 intersects four NE to ENE-striking deformation structures, ZFMNE3118, ZFMENE3115, ZFMNE3112, and ZFMNE3137, as well as one WNW-striking, ZFMWNW3267 (Figure E-14). There are no signs of increased transmissivity in the two upper intercepts, ZFMNE3118, ZFMENE3115, or in the deep intercept ZFMNE3137 (Figure E-14). Isolated steep EW-striking PFL-f are found inside ZFMNE3112 and ZFMWNW3267 (Figure E-14; note that steep PFL-f are relatively uncommon at these depths). No Unresolved PDZs are intercepted and no horizontal SBA-structures are modelled from KFR104.

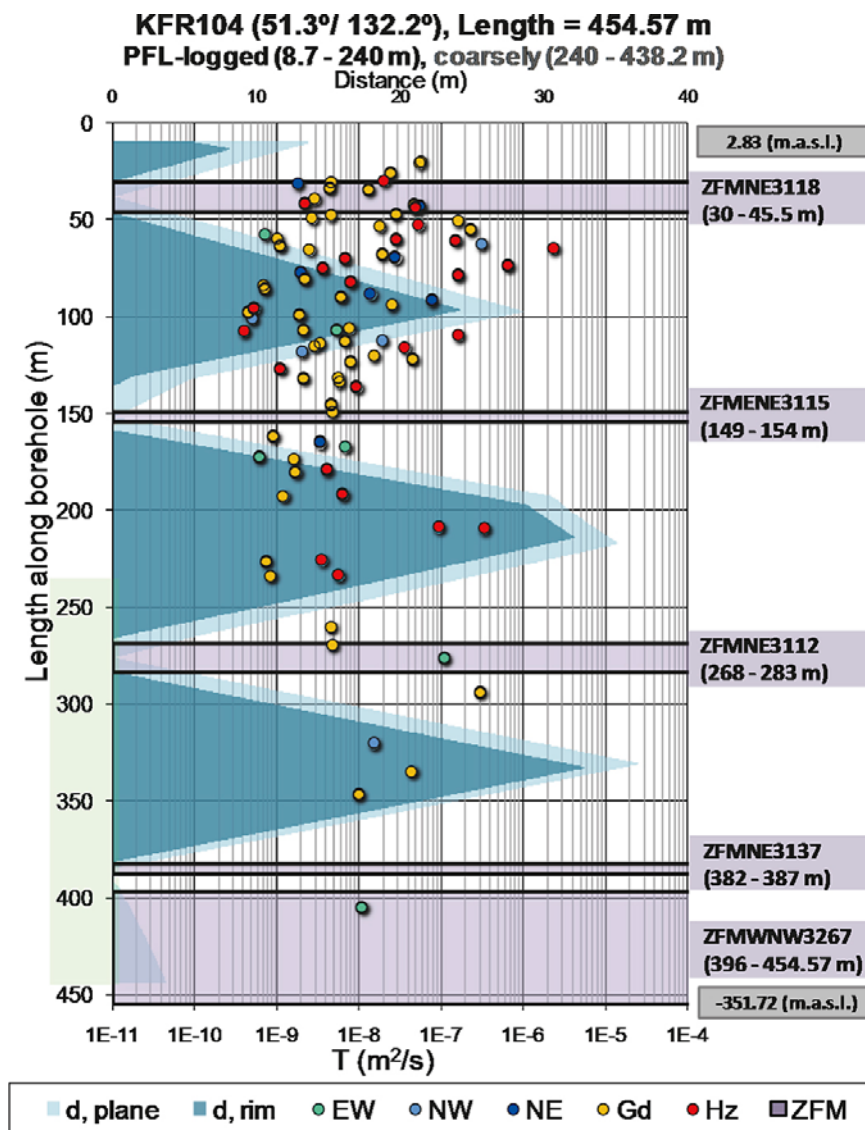


**Figure E-14.** Hydraulic data of KFR104 classified into HRD/HCD. Blue shades show distance to the central plane and the rim of nearest deformation zone, respectively. PFL-f transmissivity is notably lower inside shallow ENE intercepts (NE3118 and ENE3115) than the surrounding HRD transmissivity. Steep EW-striking PFL-f are found in ENE3112 and in WNW3267. The horizontal high-transmissive PFL-f at c. 210 m borehole length has the lowest fresh-water head (-15.9 m), suggesting hydraulic connection to SFR.

Exceptionally large in situ drawdown was estimated from PFL-f data in the interval 145 to 320 m borehole length (elevation range -115 to -250 m RHB 70; PFL fresh-water heads ranging from -15 to -6 m). This drawdown reflects indirect hydraulic connection to SFR or ZFM871 (Zone H2). ZFM871 terminates against ZFMENE3115 at an elevation interval -226 to -246 m RHB 70, approximately 80 to 100 m away (spherical distance) from this interval in KFR104.

The orientation of PFL-f data of KFR104 inside deformation zone intercepts are compared to the pattern outside intercepts (Figure E-15). BIPS images of the most transmissive features are also shown in Figure E-15. The intensity of Open fractures and depth-adjusted PFL-f transmissivity are shown for fracture sets inside intercepted zones and the rock mass outside in Figure E-16.

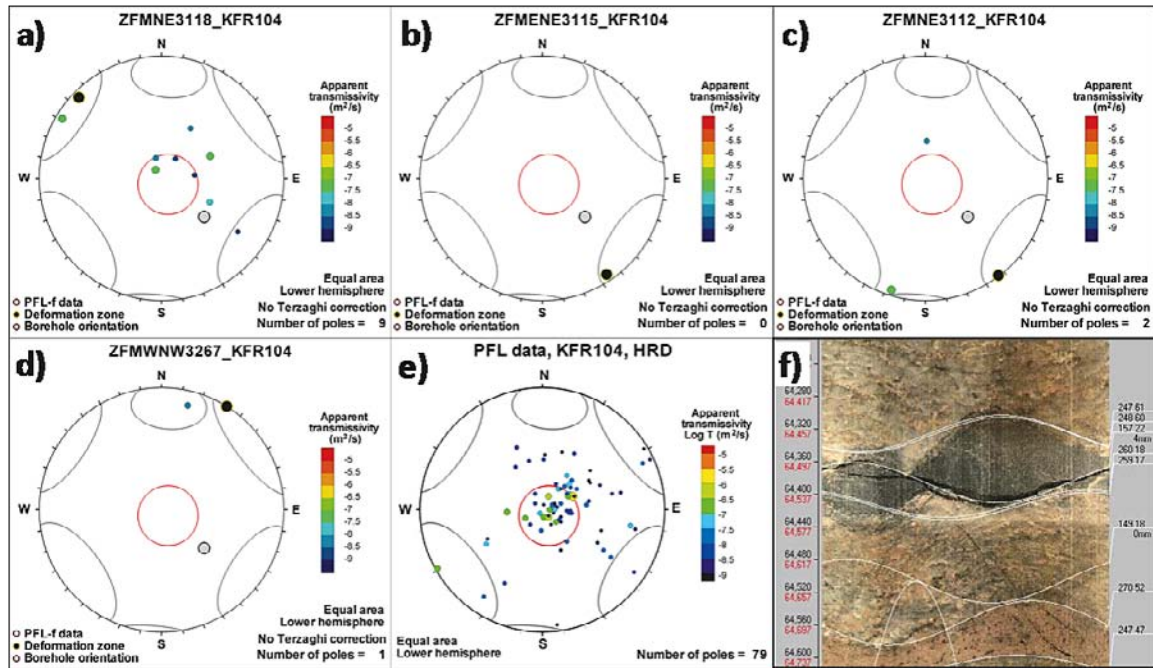


Figure E-15. PFL-f data orientation in KFR104; (a-d) inside zones and e) inside HRD, as well as f) BIPS image of the most transmissive feature found at c. 65 m borehole length.

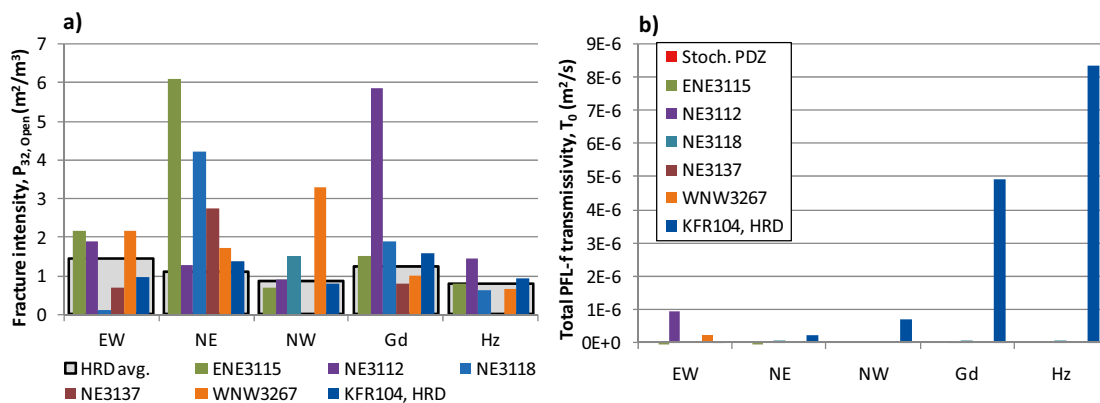
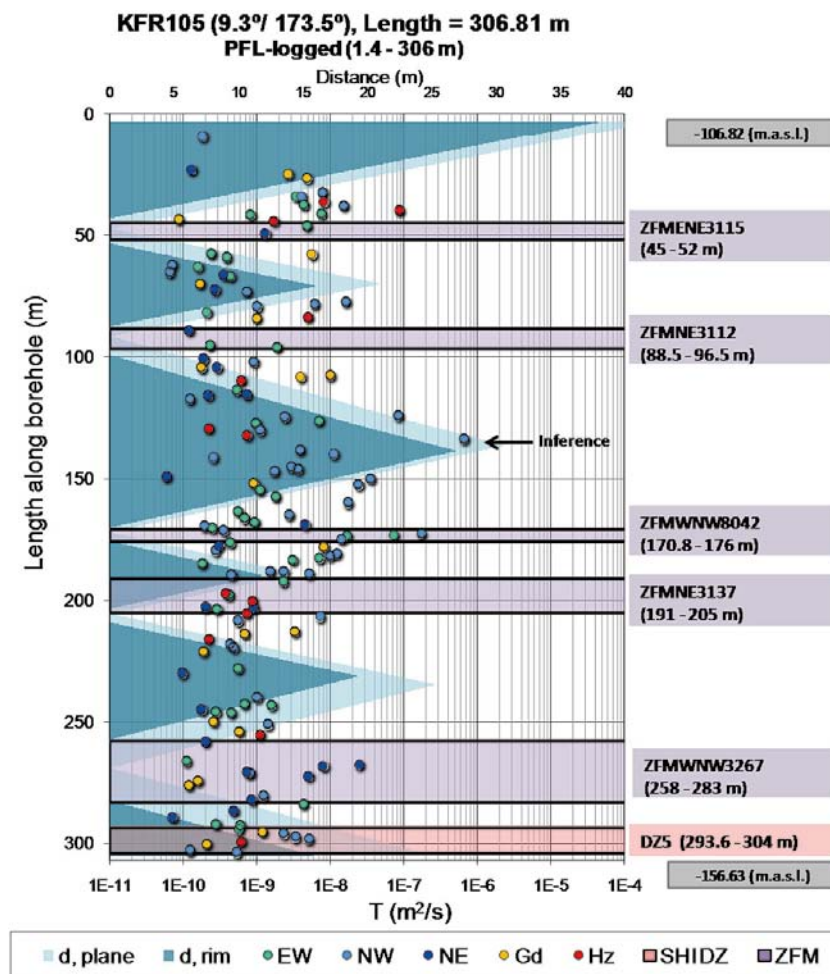


Figure E-16. Set-wise characteristics of KFR104 inside intercepted zones compared to the rock mass outside zones; a) intensity of Open fractures and b) sum of depth-adjusted PFL-f transmissivity.

## KFR105

KFR105 is located inside the Central block, an underground sub-horizontal borehole drilled south from the NBT (Nedre ByggTunnel) tunnel of SFR (Figure E-1). In comparison to other boreholes, it demonstrates a notable lack of horizontal PFL-f (Figure E-17). Instead, it is dominated by low-transmissive steep PFL-f that are predominantly NW-striking. A central question is to what extent this pattern is merely an *artefact of sampling bias*, contra demonstrating a *true difference in hydraulic characteristics of the Central block* (discussed in Section 5, main report). Note also that KFR105 has considerably low practical detection limits for PFL-f data, partly related to the absence of highly transmissive features, but also related to technical differences in set-up and evaluation, as it is an underground borehole (Väisäsvaara 2009). As KFR105 is an underground borehole, drilling resulted in a strong drawdown disturbance of atmospheric pressure (i.e. PWH  $\approx -107$  m). Inferences were registered in several surrounding boreholes when the drilling of KFR105 reached 133 m length (Figure 4-25; see arrow in Figure E-17).

KFR105 intersects three NE to ENE-striking deformation structures, ZFMENE3115, ZFMNE3112, and ZFMNE3137, as well as two WNW-striking, ZFMWNW8042 and ZFMWNW3267 (Figure E-17). With the exception of ZFMWNW8042, there are no general signs of increased transmissivity inside the deformation zone intercepts (Figure E-17). Note that the PFL-f inside ZFMWNW8042 are parallel to the deterministic structure (NW-striking). An unusual dominance of steep NE-striking PFL-f are found inside ZFMWNW3267. Similar to findings in KFR104 (cf. Figure E-14), structures ZFMENE3115 and ZFMNE3137 coincide with lower transmissivity.



**Figure E-17.** Hydraulic data of KFR105 classified into HRD/HCD. Blue shades show distance to the central plane and the rim of nearest deformation zone, respectively. PFL-f transmissivity is lower inside ENE intercepts (NE3118 and ENE3115) than the surrounding HRD transmissivity. Steep NW-striking PFL-f are found in WNW8042, while low-transmissive steep EW-striking PFL-f are found in WNW3267. Inferences were registered in surrounding boreholes when the drilling of KFR105 reached 133 m length (arrow).

One low-transmissive Unresolved PDZ is intercepted at the end of the borehole. It is clearly different to Unresolved PDZs found in the vicinity of the Northern boundary belt. It has minor significance in the hydrogeological model, as it is not more transmissive than the surrounding HRD. Possibly, it can be assumed to be a splay of ZFMWNW3267.

The disturbances observed from KFR105 (Figure 4-25 and Figure 4-22) were used in modelling the horizontal extension of SBA1 and SBA6 (located 50 m above, respectively 65 m below KFR105; Figure 6-3). No horizontal SBA-structures are modelled to intersect KFR105.

The orientation of PFL-f data of KFR105 inside deformation zone intercepts are compared to the pattern outside intercepts (Figure E-18). BIPS images of the most transmissive features are also shown in Figure E-18. The intensity of Open fractures and depth-adjusted PFL-f transmissivity are shown for fracture sets inside intercepted zones and the rock mass outside in Figure E-19.

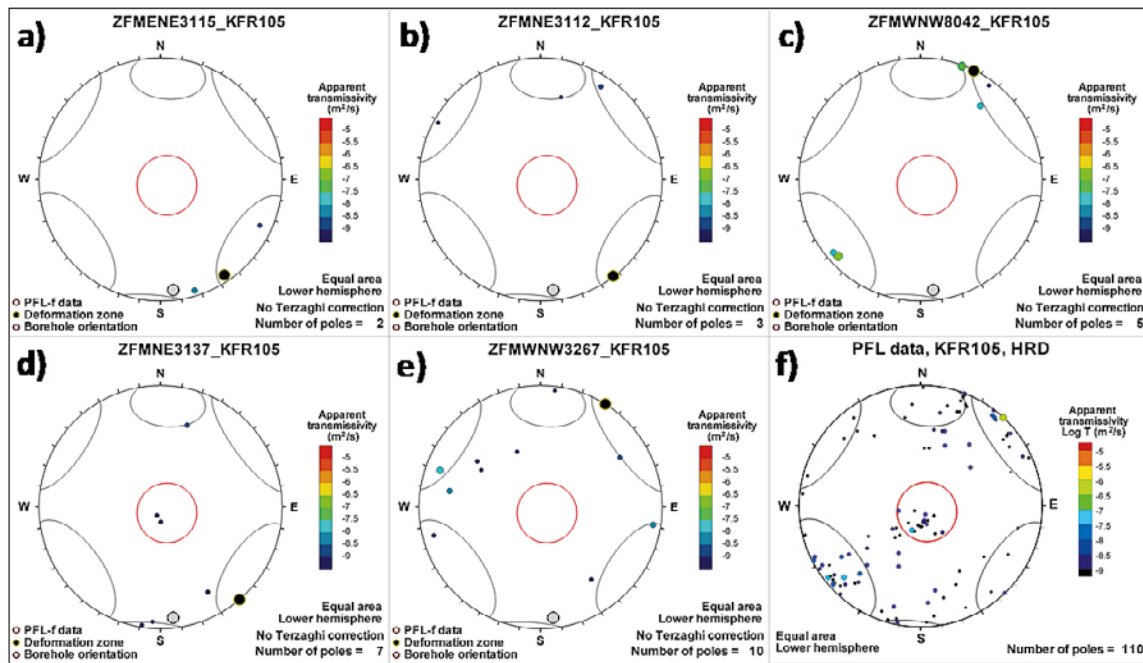


Figure E-18. PFL-f data orientation in KFR105; (a-e) inside zones and f) inside HRD.

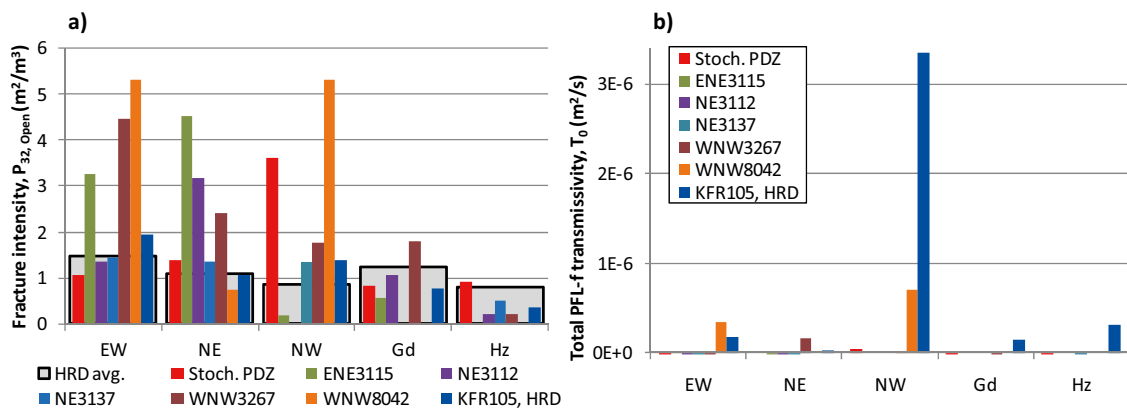
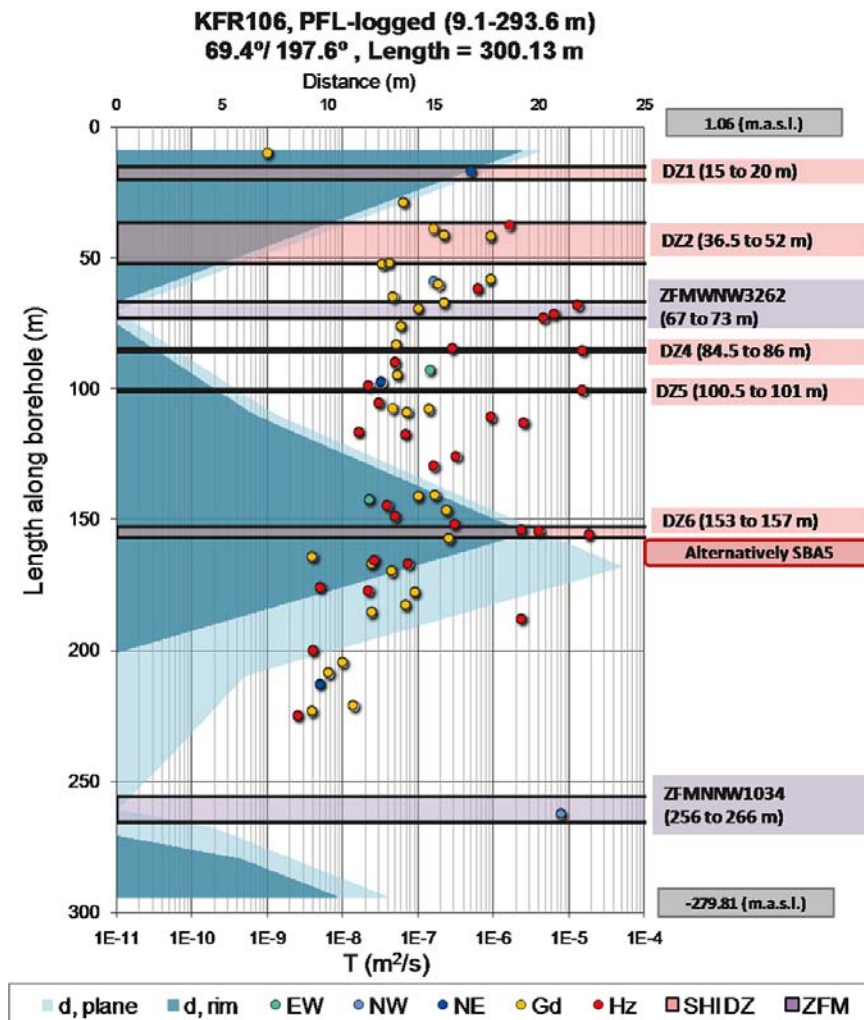


Figure E-19. Set-wise characteristics of KFR105 inside intercepted zones compared to the rock mass outside zones; a) intensity of Open fractures and b) sum of depth-adjusted PFL-f transmissivity.

## KFR106

KFR106 is located outside the Local SFR modelling domain. It was drilled southwest from an islet located just southeast of the tip of the pier (Figure E-1) and is judged to exhibit strong hydraulic characteristics of the Northern boundary belt. Note that KFR106 has rather similar characteristics to the other boreholes in terms of Open fractures (Figure 4-10). However, KFR106 has very particular patterns in hydraulic data, *which has played an essential role in interpreting the differences between the Northern boundary belt and the Central block* (cf. Figure E-20 and Figure E-17).

KFR106 is dominated by horizontal, high-transmissive PFL-f, both inside deformation zone intercepts, but also in the less fractured rock in between (Figure E-20). The deformation zone intercepts have relatively narrow intercepts and coincide rather distinctly with peaks PFL-f transmissivity. *This is quite different from the general notion of poor correlation between deterministic structures and anomalies in PFL-f data.* Two deterministic structures are intercepted, ZFMWNW3262 and ZFMNNW1034, as well as five Unresolved PDZs (Figure E-20). ZFMNNW1034 coincides well with a steep, high-transmissive, NW-striking PFL-f ( $T \approx 8 \times 10^{-6} \text{ m}^2/\text{s}$  at the depth of  $-245 \text{ m RHB } 70$ ). A very similar finding is made in the HFR106 intercept of ZFMNNW1034 ( $T \approx 2 \times 10^{-5} \text{ m}^2/\text{s}$ ; Figure E-33). This was taken as evidence for ZFMNNW1034 as being well-connected to the sea, and thus forming a large-scale positive flow boundary for the deep rock in the vicinity of the Northern boundary belt (Chapter 5; see also Figure 5-15).



**Figure E-20.** Hydraulic data of KFR106 classified into HRD/HCD. Blue shades show distance to the central plane and the rim of nearest deformation zone, respectively. High-transmissive horizontal PFL-f are found in ZFMWNW3262, KFR106\_DZ2, KFR106\_DZ4, KFR106\_DZ5, and KFR106\_DZ6. A single high-transmissive, steep NW-striking PFL-f is found in NNW1034. Under undisturbed conditions outward-directed flow is only measured in ZFMWNW3262, KFR106\_DZ4, KFR106\_DZ5, and NNW1034, suggesting distant connections to SFR. ZFMWNW3262 is alternatively modelled as SBA4 and KFR106\_DZ6 as SBA5.

Several of the Unresolved PDZs also have distinct intercepts, closely correlated to peaks in horizontal PFL-f transmissivity (Figure E-20; this applies also to ZFMWNW3262). ZFMWNW3262 and the Unresolved PDZs, KFR106\_DZ4, DZ5, and DZ6, all have transmissivities on the order  $10^{-5}$  m<sup>2</sup>/s, suggesting horizontal structures that are hydraulically supported by the vertical conductor ZFMNNW1034. A 3D-visualisation of the seemingly inconsistent PFL-f geometry and the modelled geometry of ZFMWNW3262 is shown in Figure 5-8. The ZFMWNW3262 intercept is alternatively modelled as SBA4, and KFR106\_DZ6 as SBA5.

The orientation of PFL-f data of KFR106 inside deformation zone intercepts are compared to the pattern outside intercepts (Figure E-21). BIPS images of the most transmissive features are also shown in Figure E-21. The intensity of Open fractures and depth-adjusted PFL-f transmissivity are shown for fracture sets inside intercepted zones and the rock mass outside in Figure E-22.

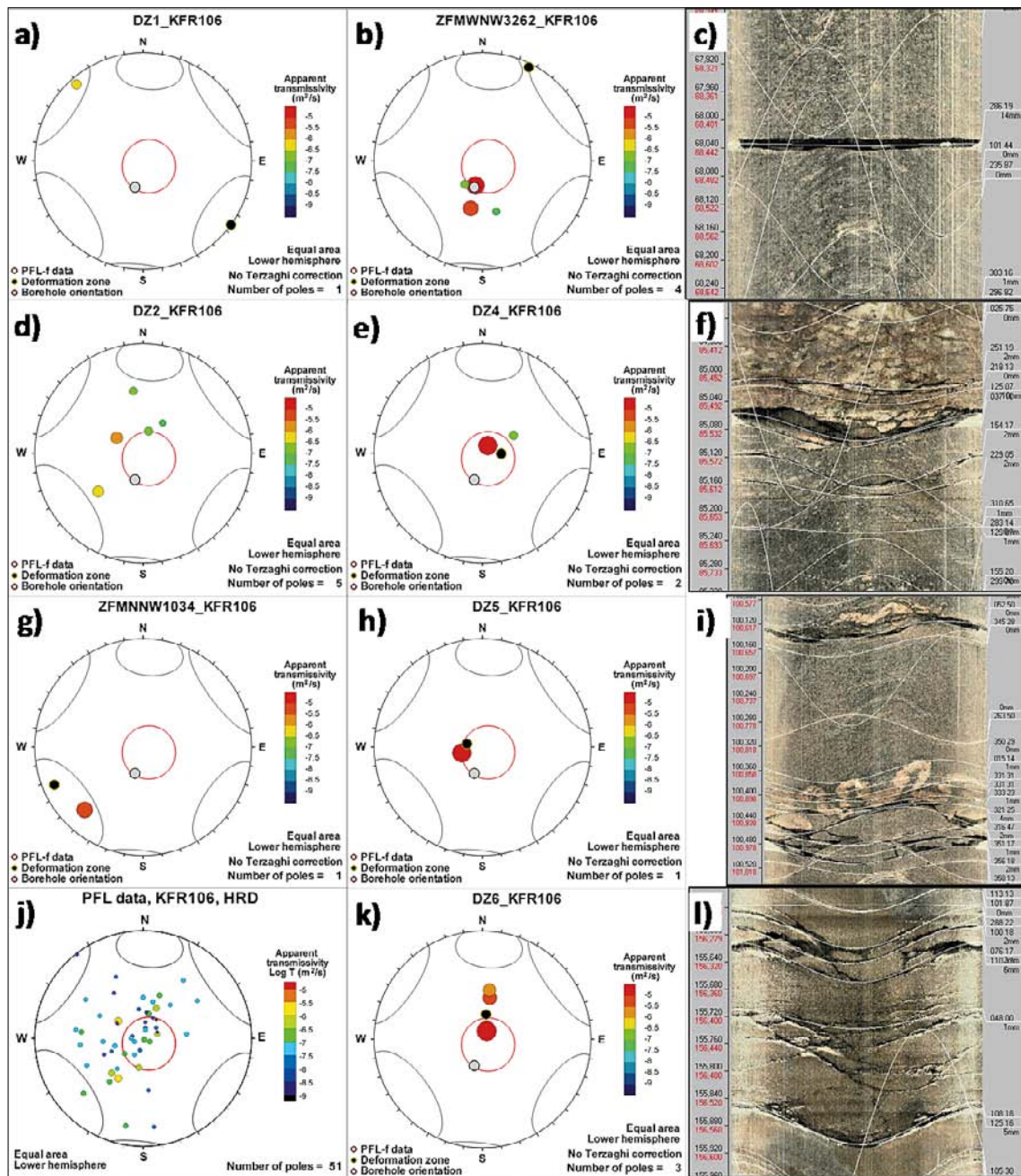


**Figure E-21.** PFL-f data orientation in KFR106; (a,b,d,e,g,h, and k) inside zones and j) inside HRD. The most transmissive feature in the zones of the middle column (b,e,h, and k) are shown as BIPS images to the right (c,f,i, and l). WNW3262 (b, c) is alternatively modelled as SBA4 and KFR106\_DZ6 (k, l) as SBA5.

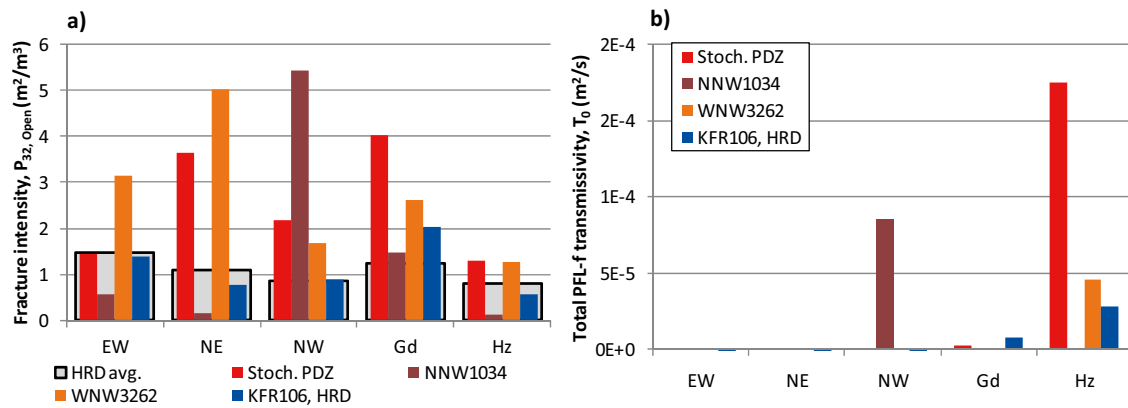


**Figure E-22.** Set-wise characteristics of KFR106 inside intercepted zones compared to the rock mass outside zones; a) intensity of Open fractures and b) sum of depth-adjusted PFL-f transmissivity.

### KFR27

KFR27 is a steep borehole (average inclination  $86^\circ$ ) drilled from the Pier (Figure E-1). During the construction phase of SFR (1984–1986) KFR27 was drilled down to a borehole length of 147.5 m for stress measurements. The core of this borehole section is unavailable. During the SFR extension investigation it was extended down to 501.6 m borehole length (Nilsson and Ullberg 2009a). The extended drilling of KFR27 caused not only interferences in several monitored sections in ZFM871, but also in the deepest section of KFR101, outside the Northern boundary belt. The upper 99.3 m borehole length of KFR27 is only covered by sequential PFL data measured over 5 m test sections (i.e. no PFL-f data). The PFL-f data in the range 99.3 to 130 m borehole length have a 0.5 m resolution (i.e. coarser than the standard 0.1 m resolution).

More or less along its entire trajectory, KFR27 is located along the boundary of the steeply dipping deformation zone ZFMWNW08035, with two defined target intercepts (Figure E-23). The transmissivity and PFL-f intensity inside the range 300 to 480 m borehole length is clearly above normal for the deep rock. However, in comparison to how data in KFR101, KFR102A, KFR102B, KFR103 and KFR106 are influenced by the Northern boundary belt deformation zones, the hydraulic data in KFR27 seems relatively unaffected by ZFMWNW08035. In the range 100 to 300 m borehole length there is no sign of influence from ZFMWNW08035, although the borehole is at most 1 m outside the rim of the modelled zone geometry.

Based in high heterogeneity in transmissivity and high fresh-water gradients, ZFMWNW08035 is interpreted as a highly channelized deformation zone. The only strong hydraulic evidence is found at c. 424 m borehole length, where 3 steep NW-striking PFL-f data comprise more than half of the total transmissivity found inside intercepts with a total length of 158 m (Figure E-24 and Figure E-25). In contrast, the PFL-f record at 192 m (associated to SBA6) borehole length has a measured electrical conductivity of 1,216 mS/m, which is considerably higher than the Baltic Sea (c. 890 mS/m). Inside the borehole interval 250 to 280 m ( $-246$  to  $-276$  m RHB 70), low-transmissive PFL-f features have been interpreted with low fresh-water head (ranging from  $-15$  to  $-7$  m). The closest monitored sections in ZFM871 (KFR02:2 and KFR13:1) have fresh-water heads of  $-25$  and  $-39$  m, respectively. ZFM871 is modelled to terminate against ZFMENE3115, only 60 m away from KFR27, at an elevation range  $-218$  to  $-238$  m RHB 70.

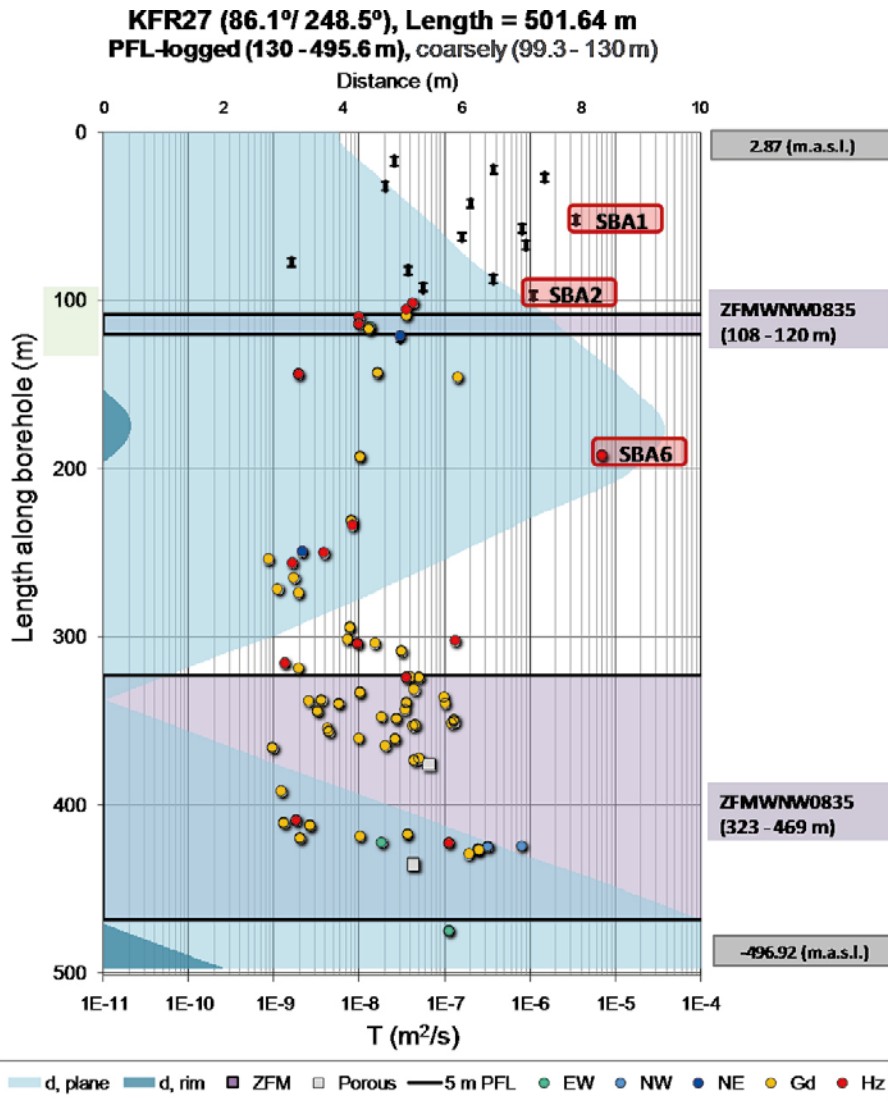


**Figure E-23.** Hydraulic data of KFR27 classified into HRD/HCD. Blue shades show distance to the central plane and the rim of nearest deformation zone (WNW0835), respectively. The core is unavailable for the upper 147 m borehole length, and Boremap-coupled PFL-f data is unavailable for the upper 99.3 m borehole length. The vertical borehole follows the modelled boundary of WNW0835, and less than 10 m away from its central plane. Three high-transmissive steep NW-striking PFL are found in WNW0835 at c. 424 m borehole length. The high-transmissive horizontal PFL-f at c. 192 m borehole length is alternatively modelled as SBA6. High-transmissive 5 m PFL sections (with horizontal Open fractures) have been modelled as SBA1 and SBA2.

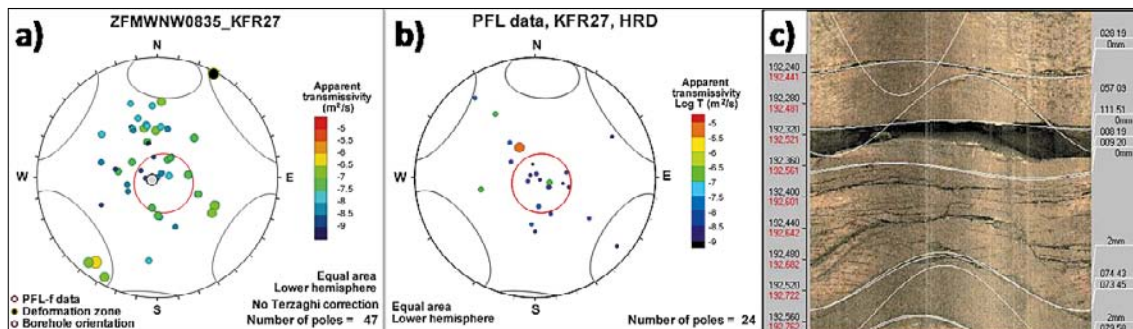


**Figure E-24.** PFL-f data orientation in KFR27; a) inside zones and b) inside HRD, as well as c) a BIPS image of the most transmissive feature at c. 192 m borehole length, with 4 cm aperture. This horizontal feature is alternatively modelled as SBA6.



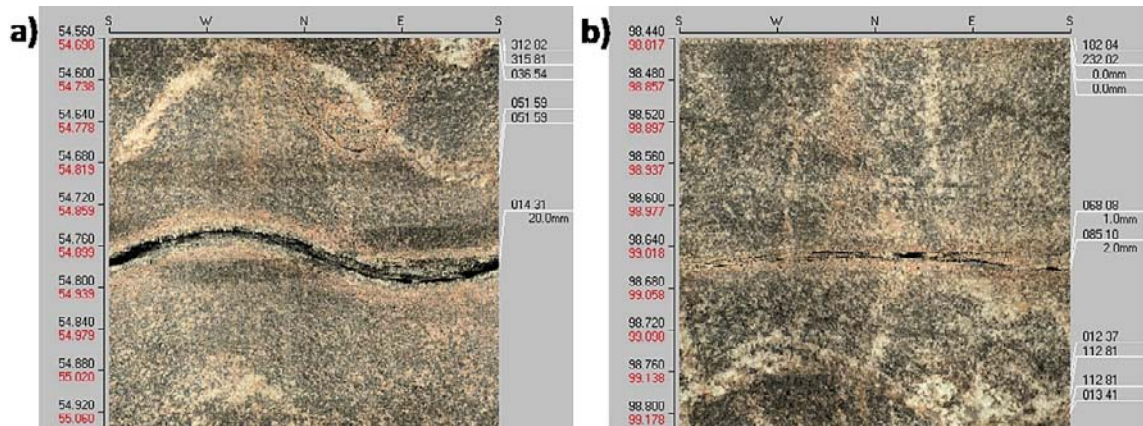


**Figure E-25.** BIPS images of two features in the upper part of KFR27 that have been modelled as hydraulic SBA-structures; a) an Open fracture oriented ( $014^{\circ}/31^{\circ}$ ) with 6 mm aperture as SBA1 and b) two Open fractures with mean orientation ( $084^{\circ}/09^{\circ}$ ) and 1 mm aperture as SBA2 (cf. Figure E-23). Boremap-coupled PFL-f data are unavailable in the upper 99.3 m borehole length in KFR27; the best data at hand is 5 m interval PFL data. A third transmissive PFL-f is identified at c. 52.7 m borehole length ( $T \approx 1.5 \times 10^{-6} \text{ m}^2/\text{s}$ ) which coincides with an Open fracture oriented ( $260^{\circ}/11^{\circ}$ ); however **no** aperture can be observed in BIPS.

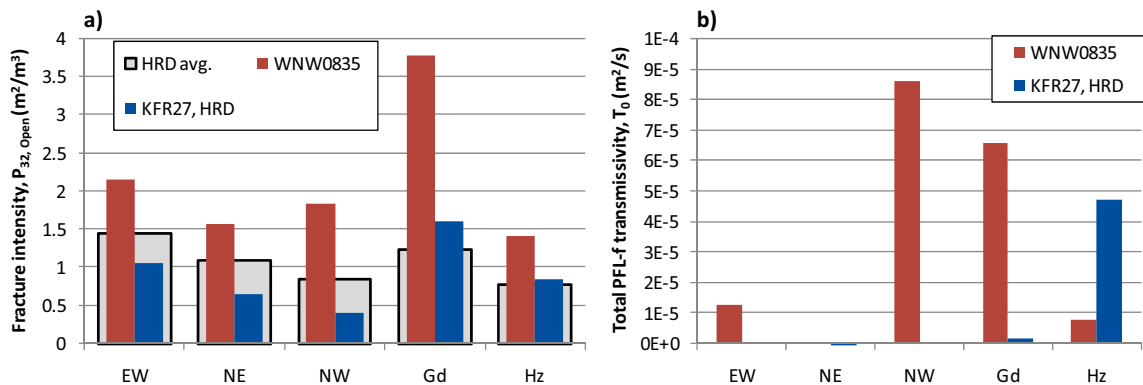


**Figure E-26.** Set-wise characteristics of KFR27 inside intercepted zones compared to the rock mass outside zones; a) intensity of Open fractures and b) sum of depth-adjusted PFL-f transmissivity.

During non-pumped conditions, an exceptionally low electrical conductivity was measured inside the borehole interval 310 to 440 m (a minimum value of 100 mS/m; Figure E-27). This interval of low EC values coincides – not only with the lower intercept of ZFMWNW0835 – but also with diffuse PFL inflow from porous granite (Figure E-23; the occurrence with porous granite is otherwise rare at SFR (Curtis et al. 2011)). This particular water seems to have a limited supply, as the low EC above c. 430 m is successively being depleted during pumped conditions (Figure E-27). The transmissive features inside the interval, 409.6 to 435.6 m borehole length (Figure 4-33), have an estimated EC value of 1,103 mS/m, Eq. (4-5).

In the hydrogeochemical modelling, this observation has been judged to be an artefact of drilling activities (Nilsson et al. 2010). An EC value of 100 mS/m corresponds to a glacial remnant, which must have been completely isolated from mixing with deep saline water or from marine water types. This is highly unexpected as the low EC measurements were made at large depth, below more saline, dense water. This decision was taken based on two facts: 1) *tap water* was used during early drilling activities and 2) some details of the drilling activities remain *unclear*.

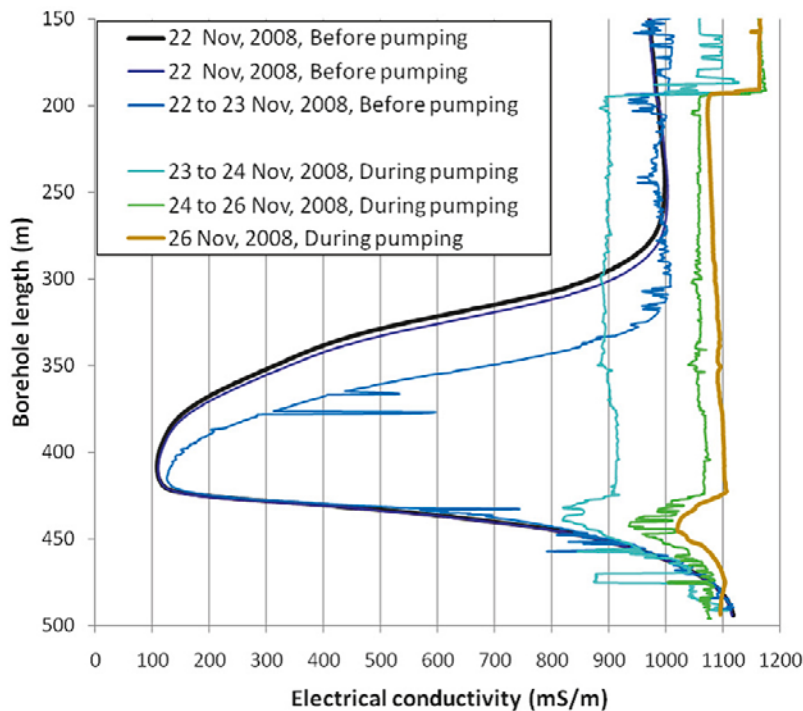


**Figure E-27.** Electric conductivity of borehole water in borehole KFR27 measured during PFL logging. The exceptionally low EC values below 300 m borehole length are likely to be an artefact of drilling activities.

A few particular conditions of the drilling activities in KFR27 are summarised here; further details are given in Nilsson and Ullberg (2009a).

- The existing KFR27 (drilled in 1981, down to 146.92 m borehole length) was reamed, rinsed, and extended down to 148.51 m. During these activities, 13 m<sup>3</sup> of tap water from Forsmarks Kraftgrupp AB was used as flushing water. The amount of return water could not be measured, but it was estimated that much or most of the flush water was retrieved (Nilsson G 2011, personal communication). Scope calculations render that 0.5 m<sup>3</sup> corresponds to the volume of 100 m borehole length. After these activities the borehole was nitrogen flushed 15 times (i.e. the borehole water was emptied using high gas pressure).
- During the extension of KFR27 (148.5 to 501 m borehole length), a total of 353 m<sup>3</sup> flushing water was pumped into the borehole. The flushing water was taken from HFR101 and had an EC value of c. 1,100 mS/m. Most of this flushing water, c. 290 m<sup>3</sup>, was lost into the formation at 192 m borehole length (i.e. SBA6; Figure E-23). After these activities the borehole was nitrogen flushed 11 times (i.e. the borehole water was emptied using high gas pressure).
- At the end of drilling the extension (i.e. close to 450 to 500 m borehole length), the logged EC value of the flushing water being pumped into the borehole is reported to be 100 mS/m (see Figure 5-12 in Nilsson and Ullberg 2009a). However, this anomalous EC value was logged during a Sunday/Monday and is therefore probably an artefact of stagnant water or air in the system (Nilsson G 2011, personal communication).
- PFL logging was executed one month after completion of the drilling. The largest calculated *drawdown* coincides with the depth interval of a hypothetical extrapolation of ZFM871 (Figure E-28). The largest *flow* during PFL-logging coincides with SBA6 at 192 m borehole length (in agreement with flush-water loss during drilling).
- In PFL logging under non-pumped conditions, only inward-directed flow has been registered above 192 m borehole length (i.e. flow into the borehole has only been detected above SBA6). Thus, if any contaminant tap water has flowed into KFR27 at depth, *it must have been into the empty borehole*, just after nitrogen flush out, or shortly thereafter (Figure E-29).

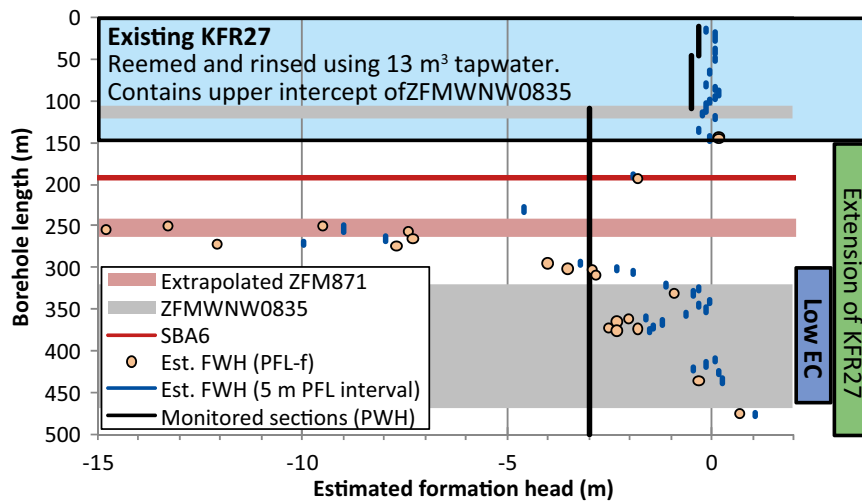


**Figure E-28.** Formation head around KFR27 in context with hydraulic structures (SBA6 at c. 192 m), the two intercepts of ZFMWNW0835, as well as, an extrapolated interval of ZFM871. The largest drawdown is clearly correlated to the depth interval of the ZFM871 extrapolation.

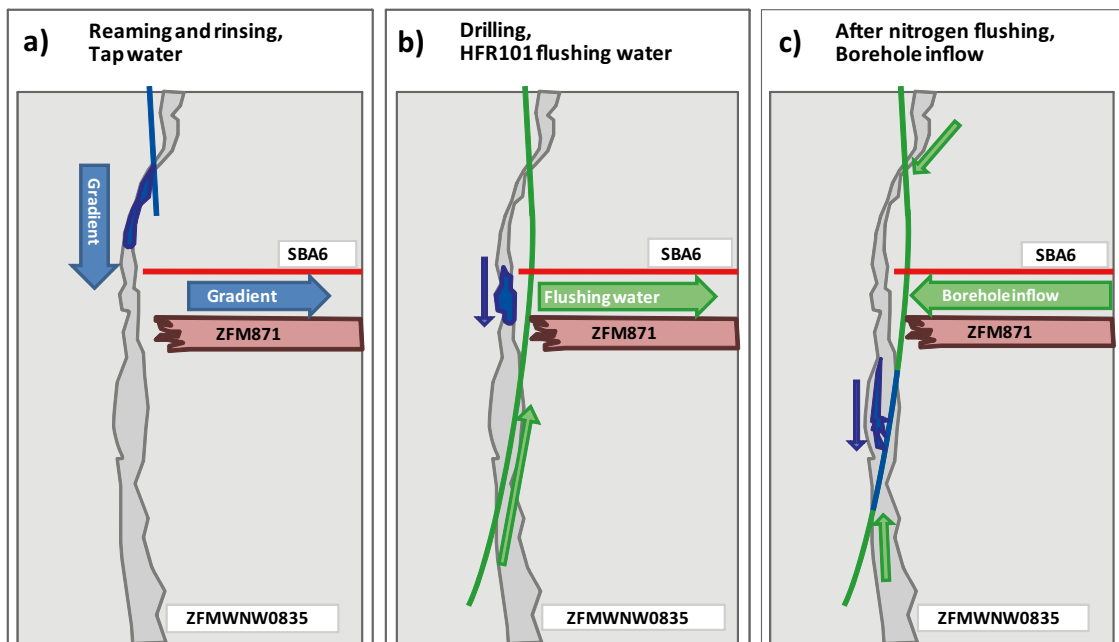


**Figure E-29.** Hypothesis on the low EC measured at the bottom of KFR27 relating to contamination of tap water; a) tap water enters ZFMWNW0835 during the early drilling phase, b) the contaminant tap water flows downwards in an isolated channel of ZFMWNW0835, if the downward hydraulic gradient exceeds the buoyancy effects, and c) the contaminant tap water flows into the empty borehole after nitrogen flushing, or shortly thereafter, due to an upward directed gradient along the borehole.

Based on the large amounts of more saline flush water used in the extension phase, as well as, to the gradients along the borehole (Figure E-28), any contaminant tap water of the early drilling phase reaching the bottom of KFR27 via the borehole can be ruled out.

Based on these facts only three possibilities remain:

- 1) The SFR data set does exhibit other evidence of isolated glacial remnants (however, the other evidence are of considerably less extreme characteristics; Section 4.6). Perhaps isolated glacial remnants do exist even at great depth (possibly related to the porous granite), in spite of buoyancy and mixing processes,

- 2) tap water *has* been involved during drilling and *some uncertainties* exist in details of the drilling activities (e.g. Figure 5-12 in Nilsson and Ullberg 2009a). Perhaps some unknown contamination occurred at the end of drilling activities, or at the onset of the PFL logging,
- 3) the two intercepts of ZFMWNW0835 (Figure E-23) provide an *alternative flow path* between the upper part (contaminated by tap water) and the lower part of the borehole. An isolated channel of ZFMWNW0835 may have offered refuge from mixing with the later, more saline flushing water of HFR101, as well as, depletion during nitrogen flushing (Figure E-29). The inflow into the deep section of KFR27 may even have been caused by the nitrogen flushing, or shortly thereafter as the outflow via SBA6 resumes.

This issue cannot be fully resolved. Although none of the listed speculations are considered to be very likely, the last alternative is seen as the better option. It is based on geological and hydrogeological reasoning and is in line with the interpreted characteristics of ZFMWNW0835.

### Percussion boreholes

There is considerably lower confidence in percussion borehole data, both in terms of fracture data and hydraulic data. As no core is available, the geologic mapping is based on BIPS analysis, which misses all fractures that are not visible in BIPS. Furthermore, it is often difficult to make the distinction between the aperture of Open fractures and dark mineral infilling of Sealed fractures. From a hydrogeological modelling point, usage of percussion borehole fracture data implies the risk of underestimating fracture intensity, as well as blending the characteristics of Open fractures with those of Sealed fractures. For example, Sealed fractures have different orientation characteristics (e.g. Öhman and Follin 2010b).

The hydraulic data in percussion boreholes are referred to as HTHB data, which is a combination of borehole-scale pumping tests and impeller flow-logging, which typically registers the largest 2–3 borehole inflows. The latter is reported to have a detection limit on the order  $10^{-7}$  to  $10^{-6}$  m<sup>2</sup>/s. It measures cumulative flow, and therefore it may be expected that the practical detection limit depends on the inflow at depth. Owing to its high detection limit, HTHB data do not provide detailed information on the flowing fracture network. However, it provides auxiliary information on identified large transmissivities.

Due to the reasons listed above, it is not possible to perform Boremap coupling for percussion hydraulic data with the same level of confidence as PFL-f coupling. Nevertheless, the orientation of HTHB data was estimated by inspection of BIPS and fracture data, following the same procedure as for PFL-f coupling (e.g. Öhman et al. 2010). If a single Open fracture with large aperture is found, the HTHB orientation is taken from that feature. If several Open fractures with similar orientations and apertures are found, the HTHB orientation is taken as their mean orientation. These estimated orientations are highly uncertain (Table E-2).

**Table E-2. Estimated orientation of HTHB data.**

IDCODE	Borehole length (m)	HTHB trans. (m <sup>2</sup> /s)	Log T	PWH (m)	Est. orientation			CLASS
					Strike	Dip	Set	
HFR101	107.7	2.6E-6	-5.6	-31	9	86	NE	HFR101_DZ2
HFR101	196.5	2.5E-7	-6.6	-31	222	89	NE	ZFMNE3118
HFR105	55.7	5.7E-6	-5.2	-5.9	106	58	EW-NW	ZFMWNW0001
HFR105	89.3	6.0E-6	-5.2	-6.3	330	22	Hz	ZFMWNW0001
HFR105	119.7	1.1E-5	-5	-6.3	12	38	Gd	ZFMWNW1035
HFR106	39	3.1E-5	-4.5	-0.2	233	7	Hz	HFR106_DZ1 (SBA3)
HFR106	177.9	2.1E-5	-4.7	-0.6	327	86	NW	ZFMNNW1034

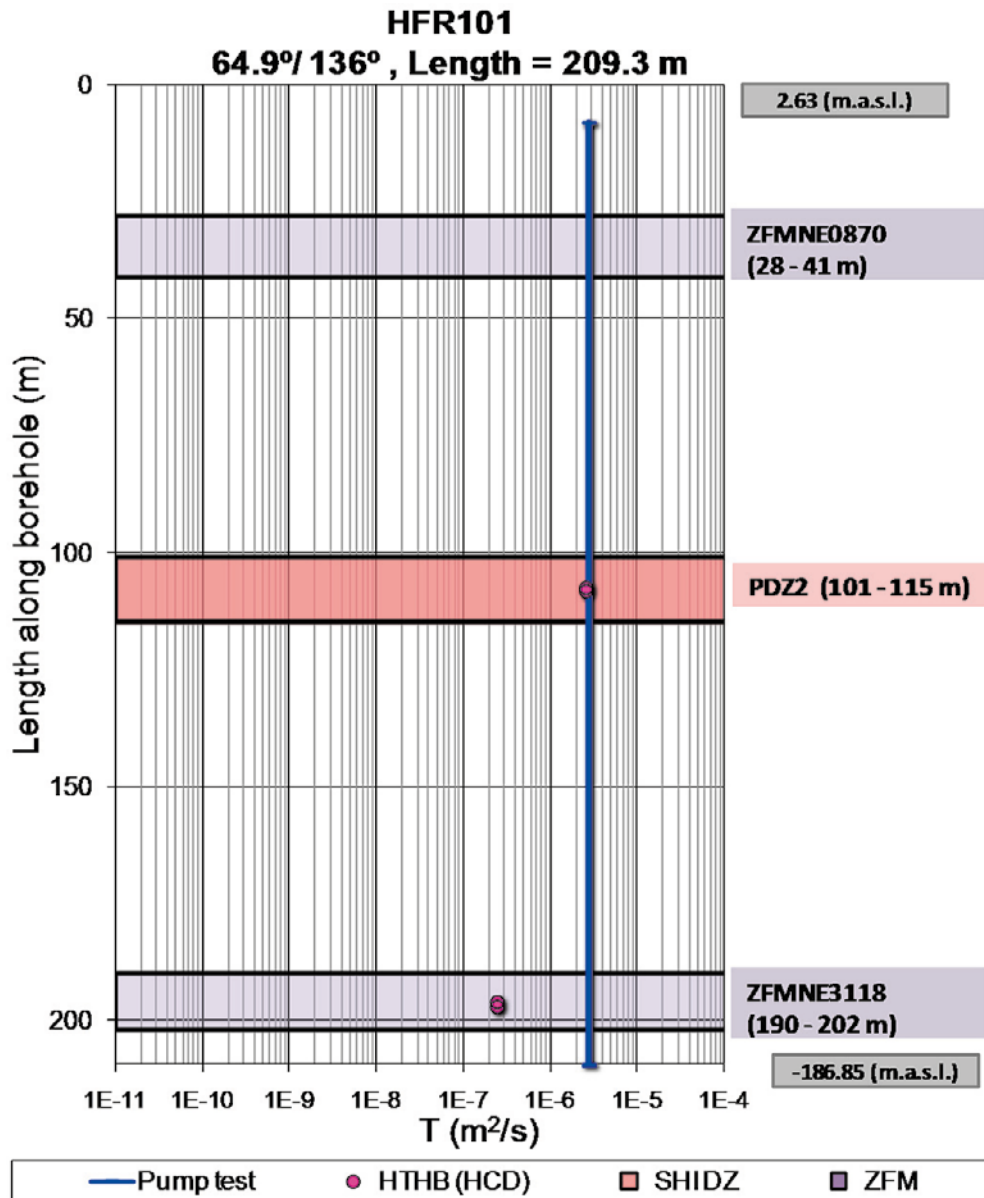


**Figure E-30.** Hydraulic data of HFR101 classified into HRD/HCD. Due to the low point-water head (-31 m) water was injected into the borehole during testing. No detectable transmissivity was found in NE0870 (estimated detection limit  $10^{-7}$  m<sup>2</sup>/s). Both HTHB data in HFR101\_DZ2 and NE3118 have been interpreted as steep NE-striking features.

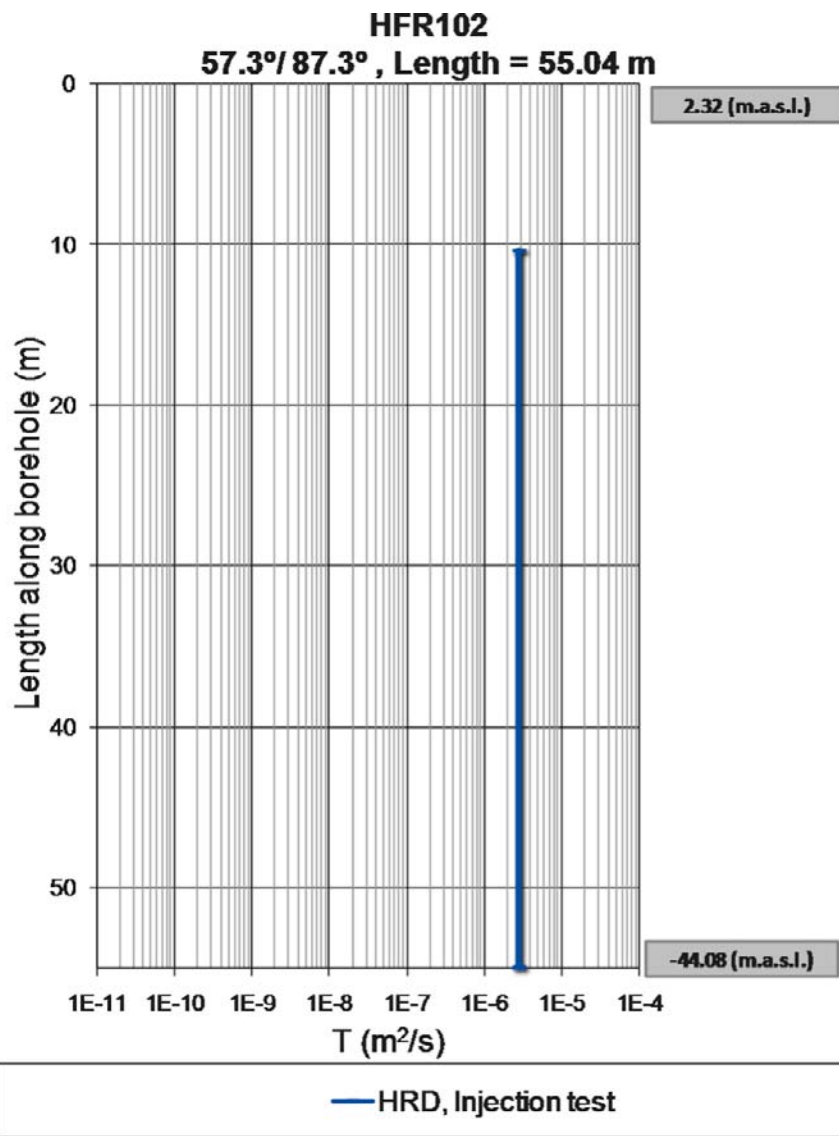


*Figure E-31. Hydraulic data of HFR102. No zones have been interpreted in this shallow borehole. Impeller flow logging was not performed. The transmissivity of this borehole has been alternatively interpreted as part of SBA1.*

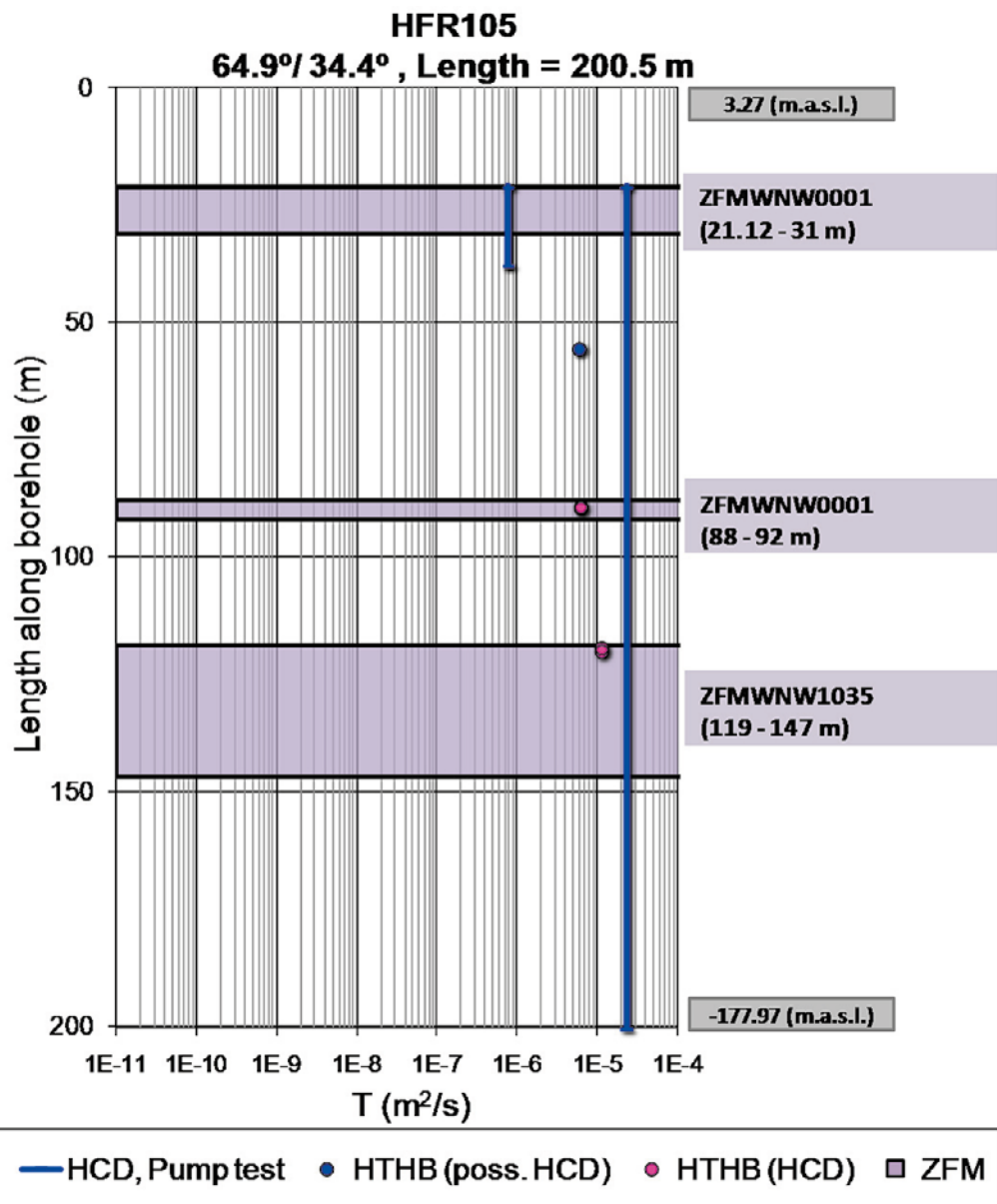


*Figure E-32. Hydraulic data of HFR105 classified into HRD/HCD. The HTHB data at c. 56 m borehole length (between the two intercepts of WNW0001) has been associated to WNW0001.*

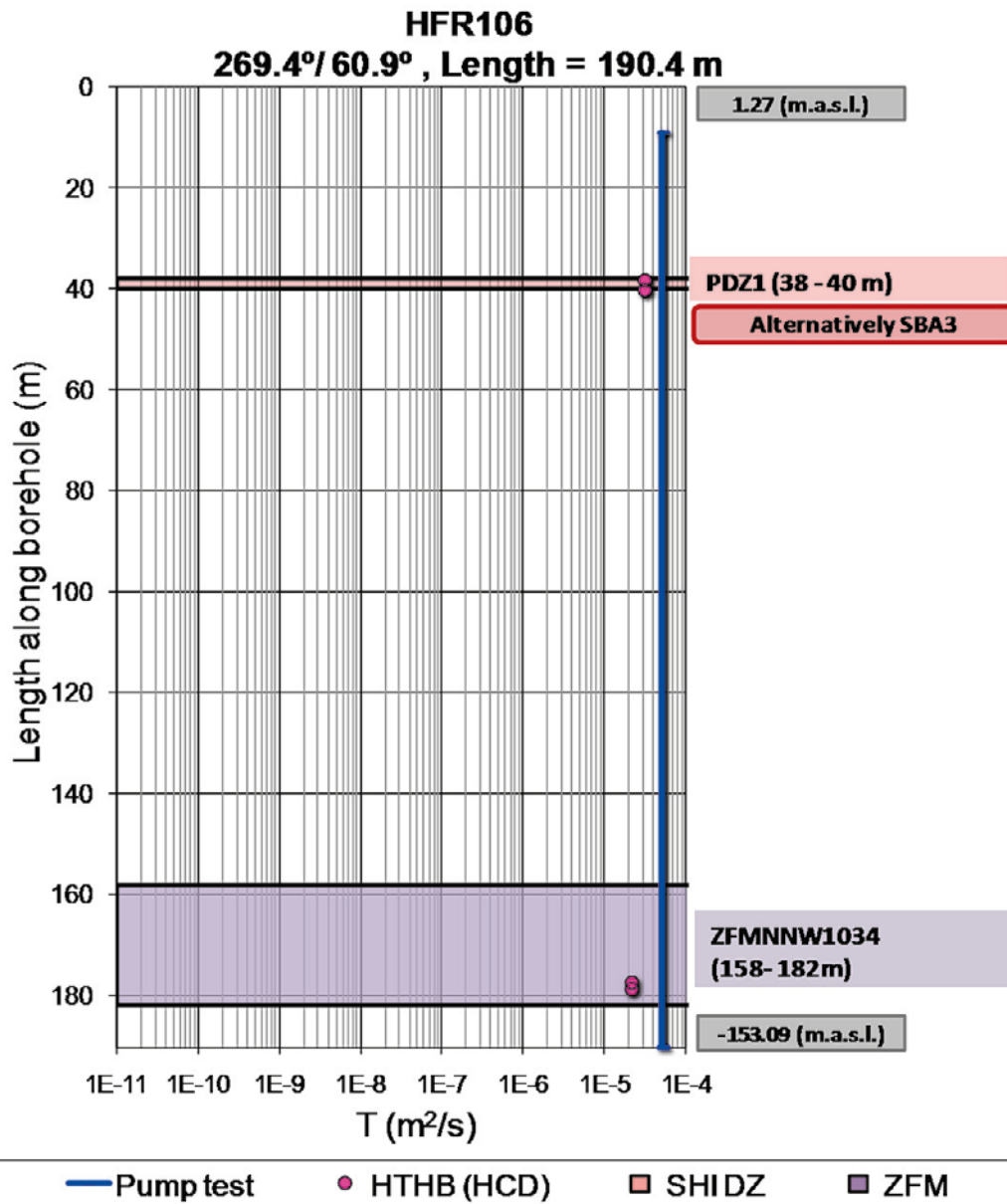


*Figure E-33. Hydraulic data of HFR106 classified into HRD/HCD. The HTHB data at c. 40 m borehole length (inside HFR106\_DZ1) is estimated to be horizontal and is alternatively modelled as SBA3.*



### Monitored head and sea level fluctuation in the new data set

The general pattern in head and drawdown around the SFR facility is presented in Section 4.5 (main report). This appendix presents the time series of monitored head from boreholes of the new data set. The purpose is to provide more detailed insight into the data that underlie the discussions in Section 4.5.3. The time series are presented as daily average values since the time of section installation. The time series are also plotted in context of the sea level fluctuations in order to differentiate between influence from fluctuations and ongoing trends over time.

Several disturbances from the drilling activities in the site investigation cause noise in monitored heads. Such disturbances are useful for evaluating hydraulic responses in the model domain (Sections 4.4.2 and 5.1, main report). However, for the purposes in this appendix, the inclusion of such disturbances is unfavourable for readability. Therefore, the most obvious disturbances have been removed from the time series data in the figures below. The geometrical data for the borehole sections shown in Figure F-1 to Figure F-12 are summarized in Table F-1.

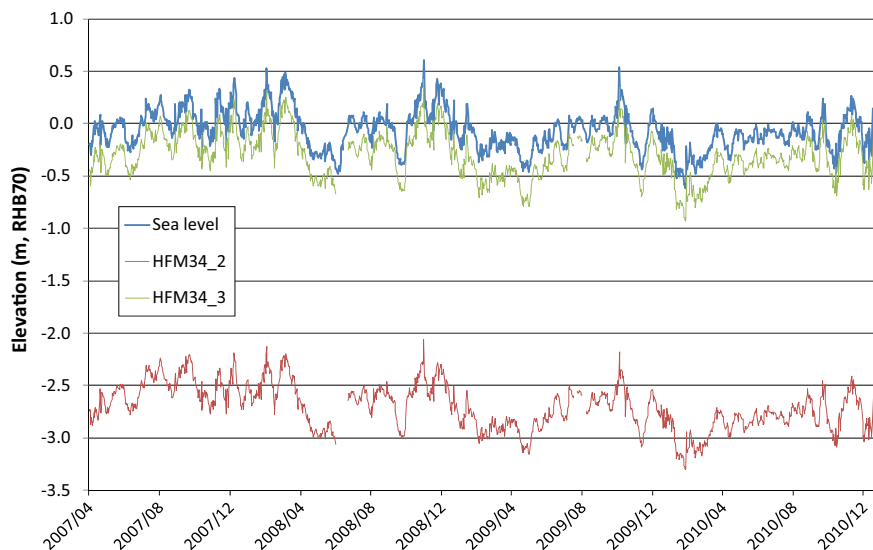


**Figure F-1.** Sea level fluctuation and monitored point-water head in HFM34. Unavailable data in the deepest section, HFM34\_1, as its point-water head is below the gauge at  $-14$  m RHB 70.

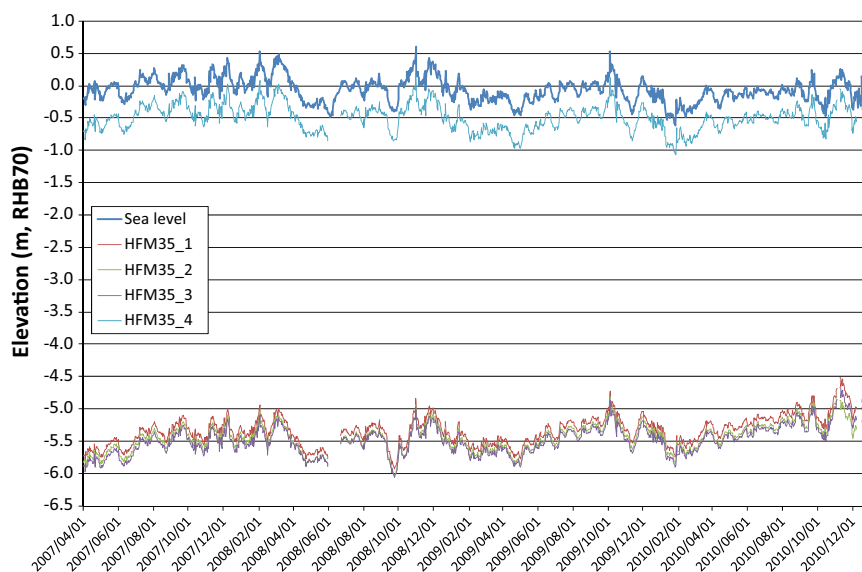


**Figure F-2.** Sea level fluctuation and monitored point-water head in HFM35.

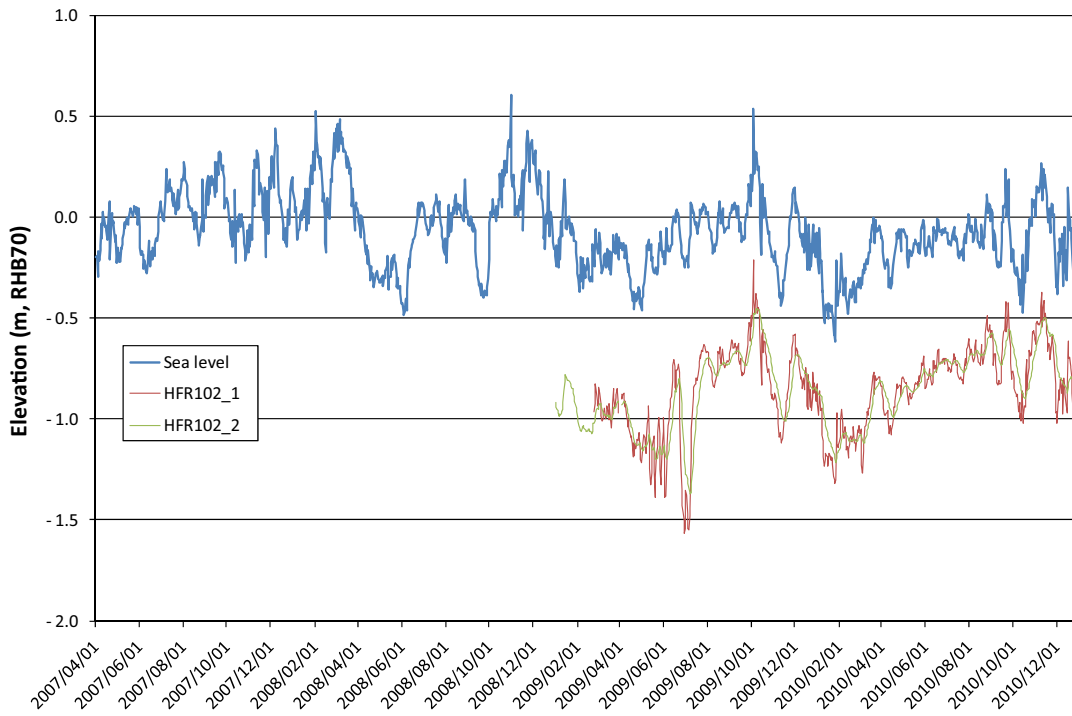


Figure F-3. Sea level fluctuation and monitored point-water head in HFR102.

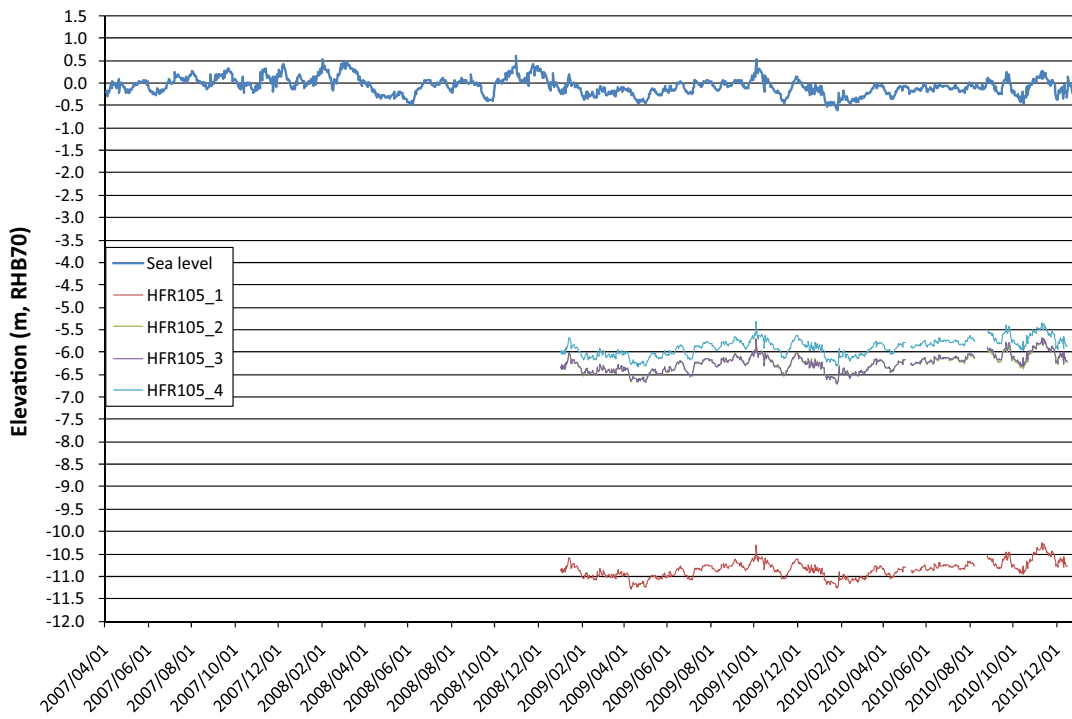
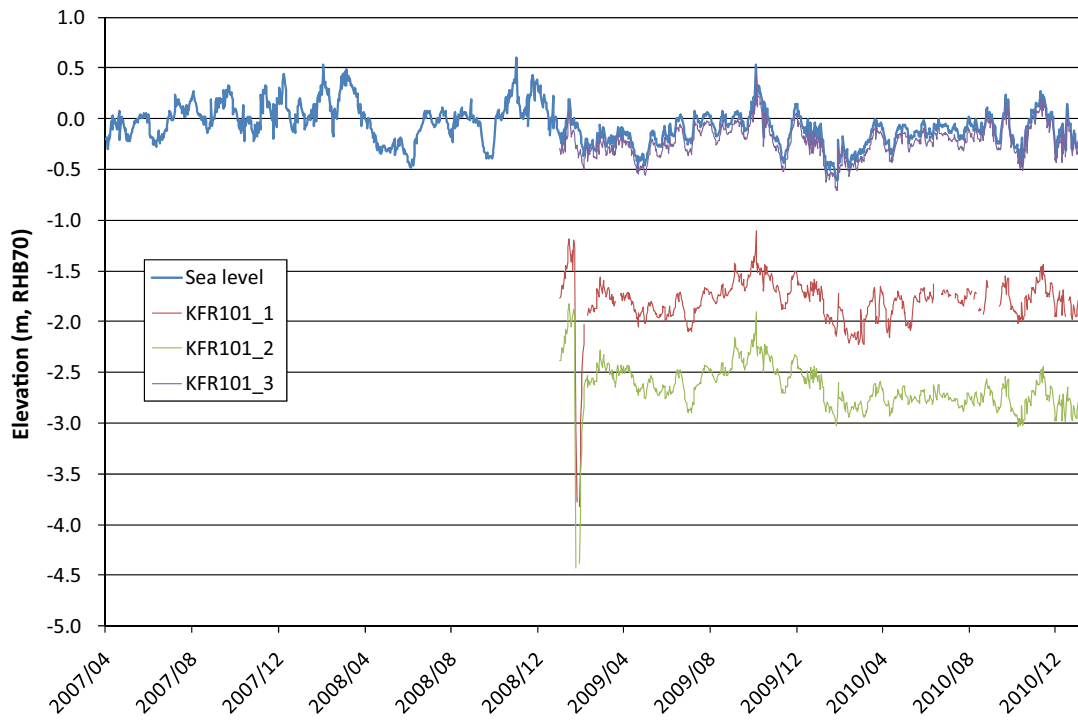
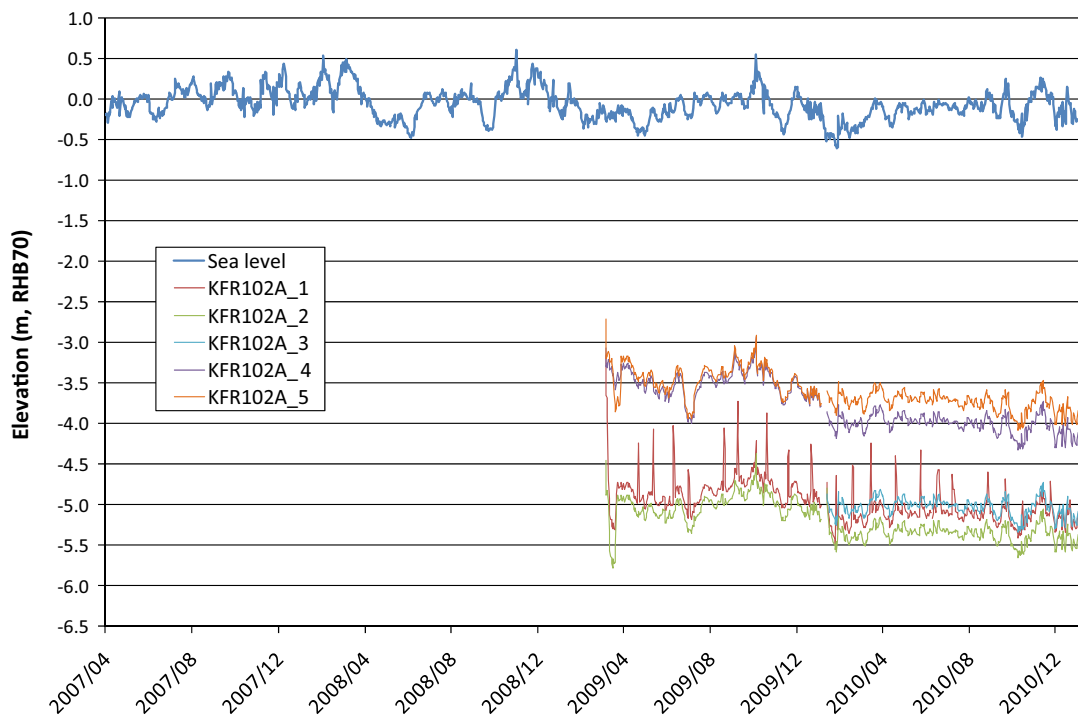


Figure F-4. Sea level fluctuation and monitored point-water head in HFR105.



**Figure F-5.** Sea level fluctuation and monitored point-water head in KFR101.



**Figure F-6.** Sea level fluctuation and monitored point-water head in KFR102A.

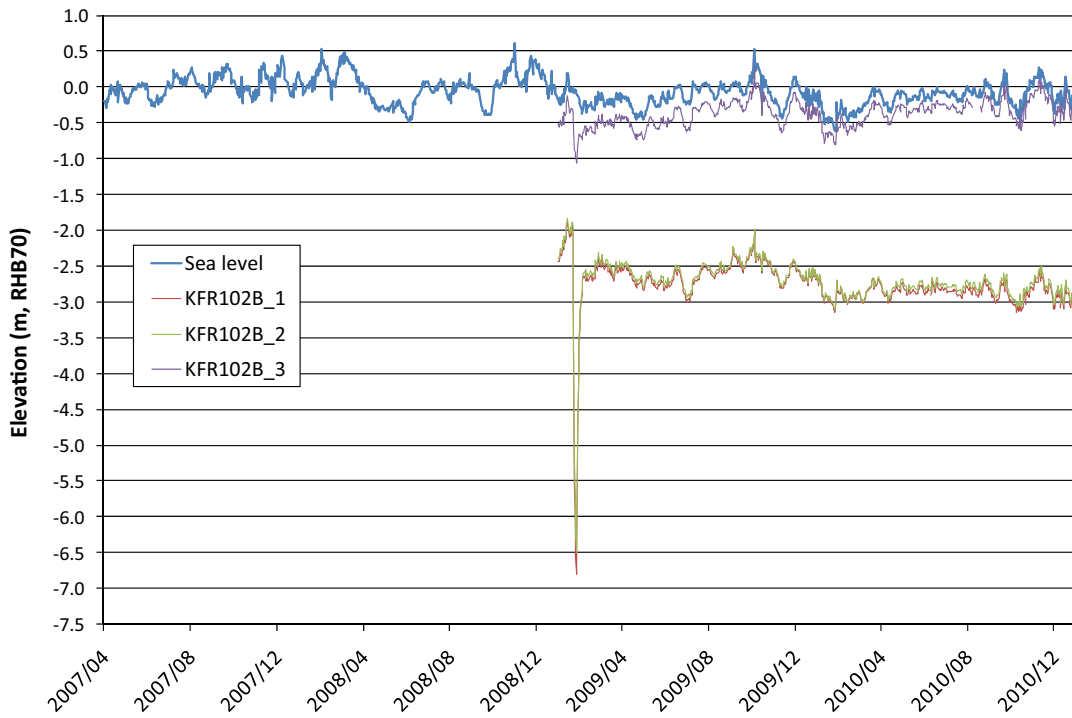


**Figure F-7.** Sea level fluctuation and monitored point-water head in KFR102B.

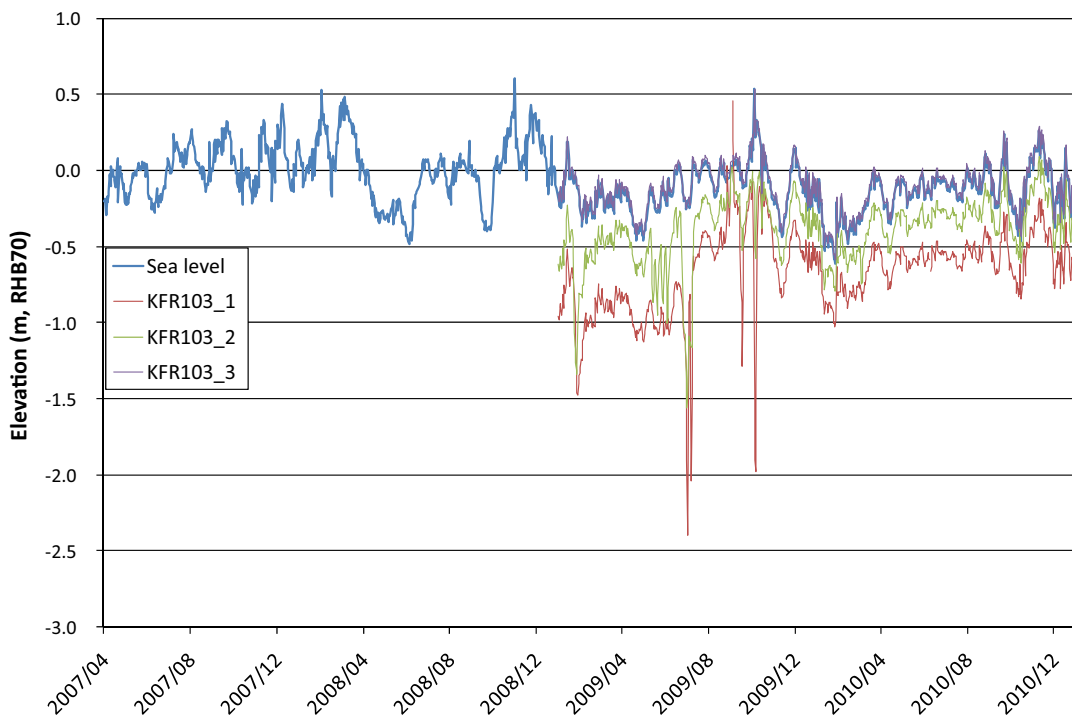


**Figure F-8.** Sea level fluctuation and monitored point-water head in KFR103.

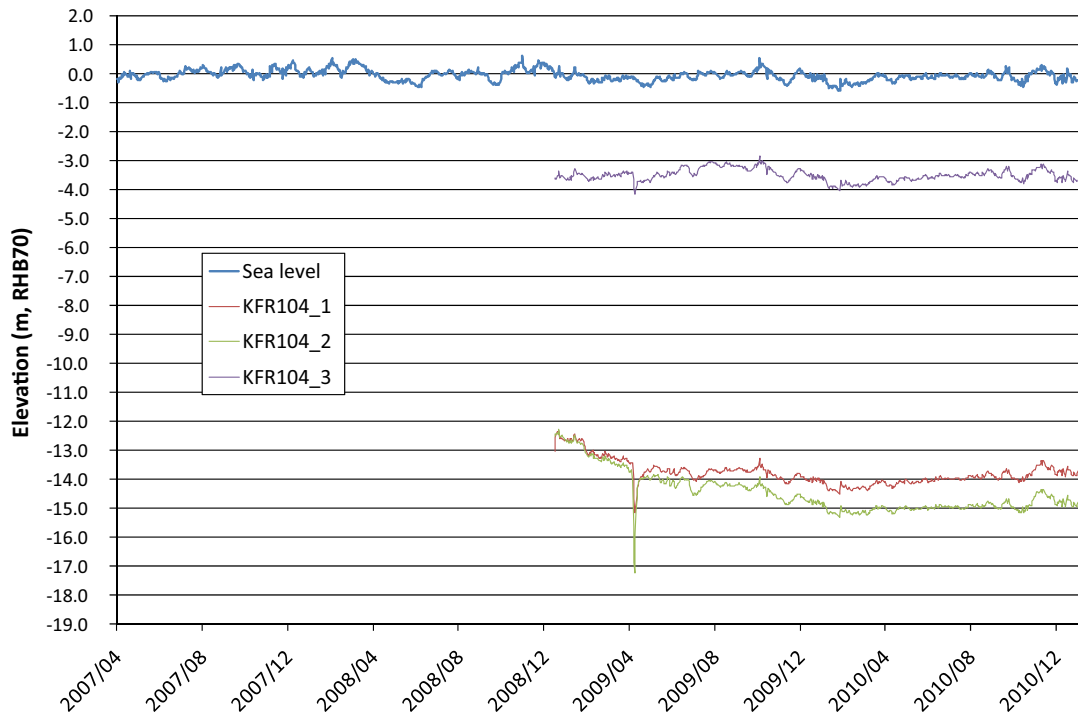


**Figure F-9.** Sea level fluctuation and monitored point-water head in KFR104.



**Figure F-10.** Sea level fluctuation and calculated fresh -water head\* for monitored sections in KFR105.

\*According to installation specifications in SKBdoc 1255740

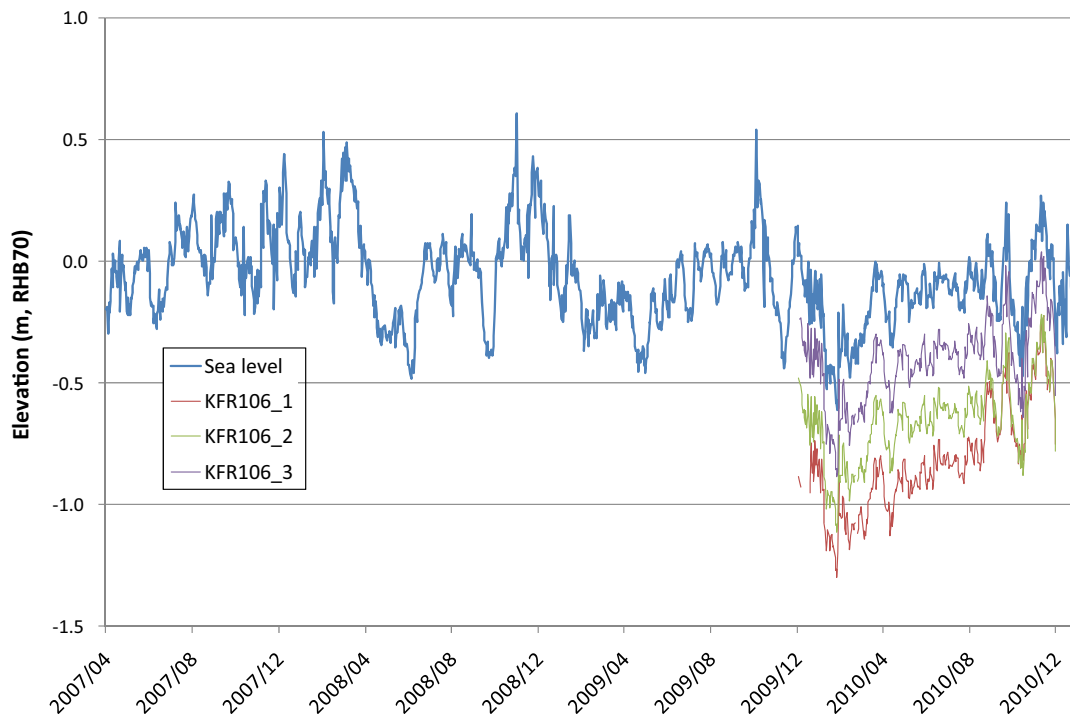


Figure F-11. Sea level fluctuation and monitored point-water head in KFR106.

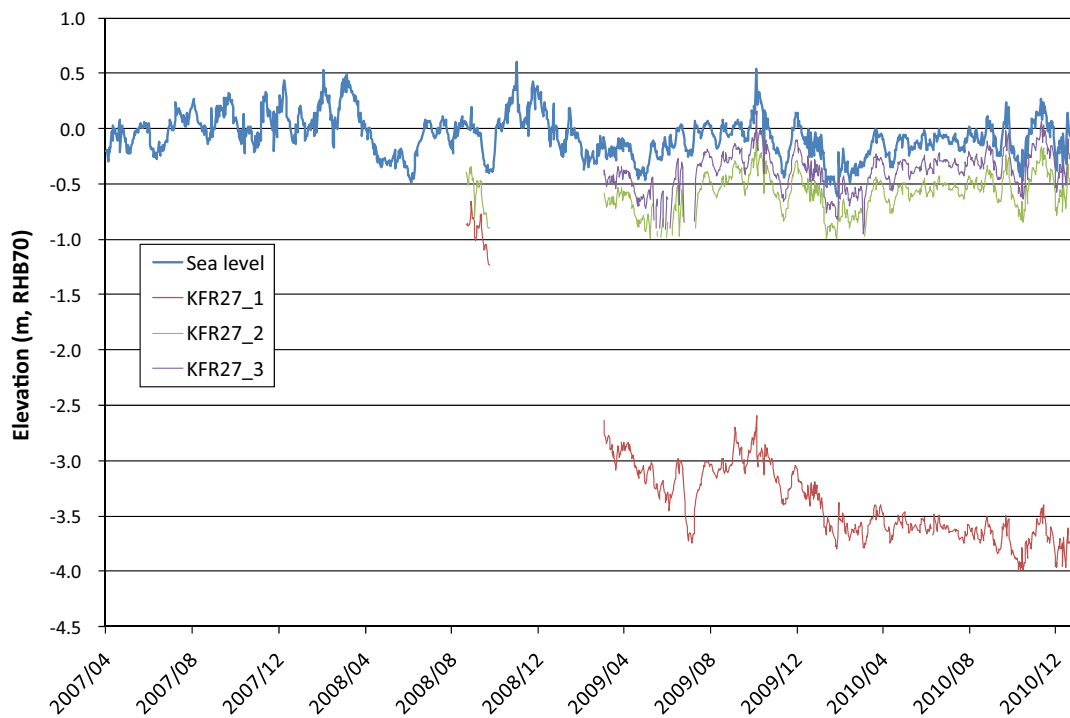


Figure F-12. Sea level fluctuation and monitored point-water head in KFR27.

**Table F-1. Geometry of monitored borehole sections.**

Borehole section	$r_{\text{SFR}}^1$ (m)	Borehole length (m)		Section length (m)	Elevation (m, RHB70)		Head (m)
		Upper	Lower		Upper	Lower	
HFM34_2	69.4	22	90	68.0	-16.4	-74.3	-2.9
HFM34_3	80.1	11.99 <sup>2)</sup>	21	9.0	-7.8 <sup>2)</sup>	-15.5	-0.5
HFM35_1	215.2	182	200.75	18.8	-137.3	-150.4	-5.3
HFM35_2	204.2	151	181	30.0	-115.4	-136.6	-5.4
HFM35_3	179.2	34	150	116.0	-26.6	-114.7	-5.4
HFM35_4	166.9	12.04 <sup>2)</sup>	33	21.0	-8.4	-25.8	-0.6
HFR102_1	96.4	28	55.04	27.0	-21.4	-44.1	-0.8
HFR102_2	112.2	9.04 <sup>2)</sup>	27	18.0	-5.4 <sup>2)</sup>	-20.6	-0.8
HFR105_1	176.9	134	200.5	66.5	-117.5	-178.0	-10.9
HFR105_2	165.8	107	133	26.0	-92.9	-116.6	-6.3
HFR105_3	164.4	61	106	45.0	-51.2	-92.0	-6.3
HFR105_4	170.3	21.04 <sup>2)</sup>	60	39.0	-15.4 <sup>2)</sup>	-50.3	-5.9
KFR101_1	361.1	279.5	341.76	62.3	-217.8	-262.0	-1.6
KFR101_2	317.0	91	278.5	187.5	-72.0	-217.0	-2.5
KFR101_3	287.5	13.72 <sup>2)</sup>	90	76.3	-8.9 <sup>2)</sup>	-71.2	-0.1
KFR102A_1	349.6	444	600.83	156.8	-398.7	-537.3	-5.1
KFR102A_2	284.2	423	443	20.0	-380.1	-397.9	-5.3
KFR102A_3	226.9	255	422	167.0	-229.5	-379.2	-5.0
KFR102A_4	192.8	220	254	34.0	-197.8	-228.6	-4.0
KFR102A_5	190.8	214	219	5.0	-192.4	-196.9	-1.0
KFR102A_6	190.4	185	213	28.0	-166.0	-191.5	-0.9
KFR102A_7	198.2	103	184	81.0	-91.4	-165.1	-1.2
KFR102A_8	220.5	70.38 <sup>2)</sup>	102	31.6	-61.6 <sup>2)</sup>	-90.5	-1.4
KFR102B_1	226.5	146	180.08	34.1	-115.6	-142.9	-2.5
KFR102B_2	232.4	128	145	17.0	-101.1	-114.8	-2.4
KFR102B_3	251.0	13.95 <sup>2)</sup>	127	113.1	-8.9 <sup>2)</sup>	-100.3	-0.3
KFR103_1	317.9	178	200.5	22.5	-140.9	-158.9	-0.6
KFR103_2	294.9	79	177	98.0	-61.6	-140.1	-0.5
KFR103_3	283.2	13.33 <sup>2)</sup>	78	64.7	-8.5 <sup>2)</sup>	-60.8	0.0
KFR104_1	306.5	333	454.57	121.6	-260.6	-351.7	-13.8
KFR104_2	180.1	98	332	234.0	-76.9	-259.9	-14.2
KFR104_3	74.4	8.73 <sup>2)</sup>	97	88.3	-4.3 <sup>2)</sup>	-76.1	-3.4
KFR105_1	285.4	265	306.81	41.8	-150.0	-156.6	-1.3
KFR105_2	216.6	170	264	94.0	-135.0	-150.3	-0.8
KFR105_3	153.1	138	169	31.0	-130.2	-135.0	-0.7
KFR105_4	128.3	120	137	17.0	-127.2	-130.0	-0.1
KFR105_5	61.0	4	119	115.0	-107.0	-127.0	-8.2
KFR106_1	611.0	260	300.13	40.1	-242.4	-279.8	-0.8
KFR106_2	589.3	143	259	116.0	-133.0	-241.4	-0.6
KFR106_3	573.6	8.86 <sup>2)</sup>	142	133.1	-7.3 <sup>2)</sup>	-132.1	-0.3
KFR27_1	225.0	110	501.64	391.6	-107.1	-496.9	-3.0
KFR27_2	126.2	47	109	62.0	-44.1	-106.1	-0.5
KFR27_3	145.0	11.91 <sup>2)</sup>	46	34.1	-9.0 <sup>2)</sup>	-43.1	-0.3

<sup>1)</sup> Radial distance to the nearest wall of the SFR facility.

<sup>2)</sup> In the uppermost borehole sections, the upper end of sections are taken as equal to the lower end of the casing.

## Updating the Hydro-DFN

The system of Open fractures at SFR has previously been described by means of a preliminary Hydro-DFN, referred to as model version 0.2 (Öhman and Follin 2010b). The preliminary Hydro-DFN was defined by a global orientation model, for which the fracture set-specific properties intensity, size, and transmissivity were parameterised. A DFN model can be sub-divided into different fracture domains in order to resolve spatial variability in fracture-set specific properties. In the preliminary Hydro-DFN, three depth domains were defined:

1. Shallow domain (0 to –60 m RHB70).
2. Repository domain (–60 to –245 m RHB70).
3. Deep domain (–245 to –1,100 m RHB70).

The depth domain concept was introduced to reflect depth trends in the flowing fracture network observed in data. The boundary between the Repository and Deep domains was based on the modelled depth of the gently dipping zone ZFM871 in the preliminary geological model v. 0.1 (Curtis et al. 2009). The model for ZFM871 was changed in the final geological model v. 1.0, hence the boundary between the Repository and Deep domains is also changed in the final Hydro-DFN model v. 1.0. The change is explained below.

Fracture size cannot be directly inferred from borehole data and is therefore the most uncertain geometrical parameter in the Hydro-DFN model. Open fracture sizes  $s$  are here assumed to be power-law distributed, defined by a shape parameter (size scaling exponent),  $k_r$ , and the bounds for modelled fractures,  $r_0$  to  $r_{max}$ . In the preliminary Hydro-DFN v. 0.2, two alternative methods were considered to define  $k_r$ . Both methods were explored in the Hydro-DFN v. 1.0 (referred to as Connectivity analysis and Tectonic continuum (Öhman and Follin 2010b); see Section G.4.1).

The geologic model v. 1.0 was unavailable during the v.0.2 modelling stage, which necessitated a number of assumptions and simplifications in the model setup. The interpretation of the hydro-geological system at SFR has progressed since the v. 0.2 modelling stage (Chapters 4 and 5, main report), primarily due to data analysis in context of the final geological model, as well as, the inclusion of additional data (KFR106 and HFR106). Furthermore, nine methodological aspects in Hydro-DFN parameterisation were raised in Table 5-1 in Öhman and Follin (2010b). This appendix addresses these aspects, as well as, demonstrates their implementation in order to update the Hydro-DFN parameterisation. These updates are summarized in Table G-1.

**Table G-1. Updates of the Hydro-DFN (relative to preliminary v.0.2).**

<b>Orientation model :</b>	Global orientation model used (defined by set mean poles and Fisher $k$ ). The uncertainty in fracture orientation measurements can be estimated (dihedral angle, $\Omega$ [°]; see Stigsson 2007). This uncertainty parameter can be used to reduce artefacts of measurement errors in the determination of dispersion in fracture orientation (section G.2). These data were unavailable during the v. 0.2 stage.
<b>Underlying data: Open fracture intensity, <math>P_{32\text{Open}}</math> (<math>m^2/m^3</math>), and PFL-f</b>	
Final HRD definitions	During the v. 0.2 stage the HRD was preliminary taken from SHI definitions. The definitions in the geological model v. 1.0 imply minor changes to data classification (Table G-3).
SBA-structures	Deterministic SBA-structures deplete high-transmissive sub-horizontal PFL-f from the HRD population (i.e. underlying data for the Hydro-DFN; section G.1.7).
Depth-domains	Boundary between Repository and Deep changed from $z = -245$ m to $-200$ m (section G.3).
Additional data	Additional boreholes KFR106 and HFR106 (outside the Local SFR model domain; section G.1.1).
Data judgment	Data judged as biased, unrepresentative, uncertain, or poorly resolved are excluded (sections G.1.6 and G.3.1).
Max. Terzaghi weight	Set to 7.0 in both data and simulations (section G.3.1). This is similar to SDM-Site Forsmark and corresponds to a minimum bias angle of $8.2^\circ$ (during the v. 0.2 stage this angle was set to $1^\circ$ , owing to the simplified model setup).



---

**Depth domains:** The depth domains in the v. 0.2 model were defined based on a preliminary modelled geometry of ZFM871. The final termination of ZFM871 (geological model v. 1.0) necessitates reconsidering of depth domain boundaries.

**Final definitions: (m elevation)**

Shallow	$z > -60$
Repository	$-60 \geq z > -200$
Deep	$-200 \geq z > -1,100$

---

**Fracture generation:** Fractures are generated over the entire Regional SFR model domain to provide realistic geometry of boreholes and deformation zones (section G.4). To reduce the computational demand, the following sequence was used:

- 1) Unresolved DZs (i.e. borehole intervals with deformation characteristics, as defined in the SHI, that could not deterministically modelled in the geological model v.1.0) were generated by a special conditional routine. These structures are linked to a structural wedge (Northern boundary belt and ZFMNNW1034), as well as, Southern boundary belt.
- 2) Large fractures, side length 300 to 10 m (generated in a large volume enclosing SFR Regional domain; Figure G-14).
- 3) Medium-sized fractures ( $10 \geq L > 0.5$  m; generated in cylinders around each of the 7 core boreholes; Figure G-15).
- 4) Small fractures ( $0.5 \geq L > 0.067$  m; generated in thin cylinders around each of the 7 core boreholes (Figure G-15).

---

**Connectivity analysis:** The flowing fracture system is defined as the subset of open fractures in contact (directly or indirectly) with positive hydraulic boundaries (Figure G-16). The following geological structures are taken as such boundaries:

- 1) Deterministic deformation zones (ZFM structures).
- 2) Unresolved PDZs (identified in the SHI but not included in the geological model).
- 3) SBA-structures (SBA1–SBA7).

---

**Simulated borehole exploration:**

- 1) Generated fracture networks are explored geometrically/statistically. No borehole flow simulations are performed (cf. Follin et al. 2007c and Öhman and Follin 2010b).
- 2) The borehole exploration is simulated by scan-line sampling (i.e. zero radius borehole). The scan lines are approximated as the upper and lower points of the true borehole extension.
- 3) To reduce geometrical sampling bias the intersected fractures are Terzaghi-compensated (Maximum Terzaghi weight = 7.0, or minimum bias angle = 8.2°).

---

**Relating simulations to PFL-f data:**

The PFL-f data are subject to several practical shortcomings and limitations that must be accounted for in the Hydro-DFN calibration (section G.1.8). For consistency to PFL-f data, the simulated borehole exploration of flowing fracture networks exclude the following features:

- 1) Fractures in borehole intervals outside PFL-f logging (percussion boreholes, casing, uppermost 130 m of KFR27, etc.)
- 2) Fractures inside deterministic structure intercepts (ZFM structures, Unresolved PDZs, and SBA-structures; see item on hydraulic boundaries for connectivity analysis). The reason is that PFL-f data inside such intercepts are deterministically modelled and hence excluded from the HRD data set.
- 3) Fractures with transmissivity below the practical detection limit. The practical detection limit varies from borehole to borehole, but also along borehole length (ranging from c.  $8 \times 10^{-11}$  to  $6 \times 10^{-8}$  m<sup>2</sup>/s).
- 4) Fracture spacing below the practical resolution of the PFL device. PFL-f data are decimetre-scale intervals with detected flow. A single feature is associated to each recorded flow (so-called “Best Choice”, while other potential candidates in its vicinity ( $L_A \pm 0.2$  m) are referred to as “Alternative Best Choices”. Hence, the simulated borehole exploration must be discretised by the same resolution as the PFL device to obtain a consistent comparison to data. All fractures inside a “PFL resolution interval” contribute to its detectable transmissivity, but the interpreted orientation is taken from the most transmissive fracture (i.e. analogous to so-called “Best Choice PFL-f”). PFL resolutions 0.1 m and 0.3 m are compared.

---

**Calibration** (sections G.4 and G.5):

- 1) Simulated borehole exploration of the flowing fracture network (i.e. network of connected Open fractures) is compared to PFL-f data. The measured specific capacity of PFL-f data is assumed equivalent to fracture transmissivity (i.e. the hydraulic choking phenomenon discussed in Öhman and Follin (2010b) is neglected).
  - 2) All boreholes are pooled and transmissivity distributions of intersected fractures are compared per set and per depth domain.
  - 3) The primary aim is to match data by adjusting the size-transmissivity relationships.
  - 4) If necessary, the size-scaling parameter,  $k_r$ , is adjusted.
-

## Underlying data

The main components of the Hydro-DFN are open fractures and PFL-f data in cored boreholes (see detailed descriptions in Öhman and Follin (2010b)). Only the recent data set is used, as the quality of historic data set is inadequate for DFN modelling (Section 2.3.3, main report). For the same reason percussion data (HTHB data) are also excluded, as lack of core support risks underestimating intensity and mistaking sealed fractures with dark mineral infill as open apertures, as well as, poor resolution in hydraulic HTHB data. The deep borehole KFM11A is located inside the SFR Regional domain, but outside the SFR Local model domain. It was decided not to include KFM11A in the parameterisation. The reason for exclusion is that its HRD coverage (borehole length outside deformation zones) is located south of the Singö deformation zone, and therefore it is less representative of the target volume for the SFR extension. However, it should be pointed out that KFM11A does not drastically deviate from the borehole data inside the SFR Local model domain (Section G.3.1).

Thus, in essence the underlying data of the v. 1.0 Hydro-DFN model are the same as for the preliminary Hydro-DFN, v. 0.2. With minor modifications, the underlying data are the cored boreholes inside the SFR Local model domain: KFR101, KFR102A, KFR102B, KFR103, KFR104, KFR105, and KFR27. As discussed in Section G.1.6, PFL-f data above 130 m borehole length in KFR27 are excluded. Furthermore, to reduce artefacts of sampling bias, the steeply dipping sets of KFR27 and sets Gd and Hz in KFR105 are excluded from the calculation of open fracture intensity (Figure G-12). The reason for this is that fracture sets that are almost parallel to the borehole are statistically underrepresented and difficult to detect in geologic mapping (referred to as “blind zone”), and cannot be sufficiently compensated by Terzaghi weighting. KFR106 was not included in the preliminary Hydro-DFN, as it was unavailable during the v.0.2 stage (Section G.1.1); in the Hydro-DFN v. 1.0 it is only included to provide an alternative transmissivity parameterisation (Section G.1.9).

## G.1 Premises of the Hydro-DFN model v. 1.0

### G.1.1 Additional borehole data

Two additional boreholes have become available since the v.0.2 stage, KFR106 and HFR106. Strictly speaking, these boreholes are located inside the SFR Regional domain, but outside the SFR Local SFR model domain, and should therefore not be included in the Local model (cf. KFM11A). In comparison to boreholes in the SFR Local domain, the open fractures in KFR106 have similar orientation characteristics (Figure G-6a and b), as well as, set-wise intensity (Figure G-8). On the other hand, its hydraulic data are clearly affected by its proximity to the Northern boundary belt (or alternatively, a structural wedge between the Northern boundary belt and ZFMNNW1034; see Section 5.3, main report, and Appendix A). Thus, it is not evident how or if KFR106 should be implemented to improve the representation of the target domain for the SFR extension (i.e. how or if its data should be included in the Hydro-DFN model parameterisation). In other words, if its hydraulic characteristics truly reflect the proximity to the structural wedge, it is not even representative for the general bedrock outside the SFR Local domain. On the other hand, KFR106 has contributed significantly to improve the hydraulic understanding of the site (Chapter 5, main report), particularly in terms of cross-hole hydraulic interferences and the large-scale trend in PFL-f transmissivity and the geological structures (Section G.1.2).

It was decided *not to include* KFR106 in the DFN model Base case. One reason for this is that it is located outside the strict definitions of the SFR Local domain, but more importantly it is judged to represent the hydraulic characteristics of a location that is not considered likely for the SFR extension. However, KFR106 is included for an alternative transmissivity parameterisation (Section G.1.9; although based on the same orientation, intensity, and size distribution setup as in the base case).

### G.1.2 Spatial inference to geological structures

The geological model v. 1.0 does not only provide a context for the spatial inference of observed trends in data (Chapters 4 and 5, main report), but also a framework for improving the realism in generating the flowing fracture network. The hydraulic data analysis has led to a conceptual model with a low-transmissive Central block and gradually increasing transmissivity towards the Northern

boundary belt and ZFMNNW1034 (Chapter 5, main report). This trend was reinforced by the additional high-transmissive data in KFR106 and HFR106 that were unavailable during the v. 0.2 stage. It is still unclear to what extent this observation reflects an actual lateral trend (i.e. properties at the individual fracture scale), relative to, an *apparent scaling effect* (i.e. reflecting effective properties related to flow path length; see discussions on the role of PFL data subject to hydraulic chokes in Öhman and Follin (2010b)). In other words, measurements inside the Central block reflect longer flow paths to the positive hydraulic boundaries and are therefore more subject to bottlenecks in upstream connectivity of the flowing fracture network.

### **G.1.3 Final distinction between deterministic and stochastic features**

In the classic model methodology (Rhén et al. 2003), the bedrock is divided between Hydraulic Conductor Domains (HCD; with a deterministic modelled geometry) and Hydraulic Rock mass Domains (HRD; with a stochastic representation of features). The role of the Hydro-DFN model is to describe the HRD (i.e. cover the subset of the flowing fracture network that is below the deterministic resolution of the geological model). Hence, an important role of the geological model is to divide the borehole data into: 1) deterministic structures (such data are used to parameterise the HCD of the hydro geological model) and 2) stochastic features (these data are used to parameterise the Hydro-DFN). It should be noted that in addition to the deterministically modelled geological structures (ZFM), so-called deterministically modelled SBA-structures and Unresolved PDZs are modelled separately, which also imply excluding data from the HRD (see Figure G-1).

### **G.1.4 Unresolved PDZs**

The starting point of the three-dimensional geological modelling is a geological interpretation in order to define borehole intervals with deformation zones characteristics. This interpretation is performed on individual boreholes basis according to an established modelling methodology referred to as Single Hole Interpretation. Hence, pending on the final classification between HRD and HCD of the geologic model v. 1.0, the preliminary DFN parameterisation (v. 0.2) was made for fracture data outside Possible Deformation Zones, as defined by the Single Hole Interpretation. In total, 31 of these PDZs (of which, 14 belong to the new data set) could not be included as deterministic structures in the final geologic model v. 1.0. These are therefore referred to as “Unresolved PDZs” and modelled separately (Case 1; see Appendix A). Most of these Unresolved PDZs have been interpreted as uncertain or less hydraulically significant (low transmissivity, low confidence in existence, and/or interpreted as minor structures due to their location close to the existing SFR). However, some of these are highly transmissive ( $T > 10^{-5} \text{ m}^2/\text{s}$ ), which implies that they constitute a significant uncertainty in the hydrogeological model (Table G-2). The uncertainty related to these structures can potentially be reduced, depending on the degree to which they can be geometrically constrained (see methodology described in Appendix A). The modelling of Unresolved PDZs is expected to have an important role in the connectivity analysis, as it enhances the connectivity between the flowing fracture network in the Central block to the tectonic boundary belts (Figure G-16).

### **G.1.5 Borehole sections outside PDZs included in deterministic structures**

On the other hand, four borehole sections *outside PDZs* (as defined during the SHI) were included in deterministic structures of the geological model v. 1.0 (Curtis et al. 2011) (Table G-3). In other words, these borehole intervals were assumed to belong to HRD in the preliminary Hydro-DFN v. 0.2. Overall, the differences between the SHI PDZ definitions and the final distinction between HRD and HCD in the geological model v. 1.0 are minor. Most noteworthy is that the Deep HRD domain borehole coverage is poorer than what was expected during the v. 0.2 stage. The updated information on sample size motivates re-assessing the boundary between the Repository and Deep domains. However, the main reason for adjusting the depth domains is that the boundary in the Hydro-DFN v. 0.2 was based on a preliminary modelled geometry of ZFM871 (geologic model v. 0.1 (Curtis et al. 2009)) that was rejected in the final geological model. Without the conceptual support from ZFM871, the boundary between the Repository and Deep domains is re-assessed in context of data depth trends (see Section G.3).

**Table G-2. Unresolved PDZs of the recent site SFR investigation (SHI PDZs that were NOT included in ZFMs in the Geological model SFR v. 1.0).**

PDZ	Borehole length (m)			Elevation (z, m)		Domain	PFL-f data		
	From	To	$\Delta L$ <sup>1)</sup>	From	To		No.	$\Sigma Tw$	$\Sigma T$ (m <sup>2</sup> /s)
KFR102B_DZ1 <sup>3)</sup>	67	70	3	-51.91	-54.34	Shallow	3	5.5	8.8E-7
KFR102B_DZ3 <sup>3)</sup>	149.5	150.5	1	-118.4	-119.19	Repository	1	1.2	5.0E-6
KFR103_DZ1 <sup>3)</sup>	24.5	26.5	2	-17.50	-19.12	Shallow	1	1.2	2.5E-7
KFR106_DZ1 <sup>3)</sup>	15	20	5	-13.05	-17.75	Shallow	1	3.9	4.9E-7
KFR106_DZ2 <sup>3)</sup>	36.5	52	15.5	-33.24	-47.78	Shallow	5	7.6	2.9E-6
KFR106_DZ4 <sup>3)</sup>	84.5	86	1.5	-78.28	-79.68	Repository	2	2.5	1.5E-5
KFR106_DZ5 <sup>3)</sup>	100.5	101	0.5	-93.28	-93.74	Repository	1	1.0	1.5E-5
KFR101_DZ3 <sup>4)</sup>	179	186	7	-142.0	-147.47	Repository	1	1.1	1.3E-5
KFR103_DZ2 <sup>4)</sup>	84	91	7	-65.61	-71.24	Repository	5	6.1	1.6E-5
KFR106_DZ6 <sup>4)</sup>	153	157	4	-142.4	-146.14	Repository	3	4.7	2.4E-5
HFR106_DZ1 <sup>4)</sup>	38	40	2	-30.9	-32.6	Shallow	NA <sup>2)</sup>	NA <sup>2)</sup>	3.1E-5
KFR101_DZ4 <sup>5)</sup>	197	213	16	-156.0	-168.22	Repository	0	-	-
KFR105_DZ5 <sup>5)</sup>	293.6	304	10.4	-154.7	-156.23	Repository	9	16.7	1.4E-8
HFR101_DZ2 <sup>5)</sup>	101	115	14	-90.9	-103.6	Repository	NA <sup>2)</sup>	NA <sup>2)</sup>	2.6E-6
			<b>Total</b>						
			<b>88.9</b>						

<sup>1)</sup> The borehole interval length is different from the true thickness (true thickness is geometrically estimated from intersection angle between borehole and structure).

<sup>2)</sup> Unresolved PDZs in percussion boreholes HFR101 and KFR106 have low confidence in existence and lack PFL-f data. Transmissivity taken from HTHB data, although orientation estimates are highly uncertain.

<sup>3)</sup> Stochastically modelled according to conditional method described in Appendix A.

<sup>4)</sup> Included in SBA-structures (not modelled).

<sup>5)</sup> Low confidence/low significance (not modelled).

**Table G-3. Borehole sections outside SHI PDZs included in deterministic structures of the Geological model v. 1.0 (Curtis et al. 2011). Data inside these intervals were assumed to belong to the HRD during the preliminary Hydro-DFN.**

IDCODE	Borehole length (m)			Elevation (z, m)		Domain	PFL-f data		
	From	To	Length	From	To		No.	$\Sigma Tw$	$\Sigma T$ (m <sup>2</sup> /s)
KFR104	405	447 <sup>1)</sup>	42	-314.86	-346.11	Deep	0	-	( $\leq 1.7E-9$ ) <sup>2)</sup>
KFR105	191	205	14	-138.77	-141.02	Repository	7	12.6	5.36E-9
KFR27	379.5	389	9.5	-375.63	-385.07	Deep	0	-	( $\leq 1.7E-9$ ) <sup>2)</sup>
KFR27	401	421	20	-396.99	-416.85	Deep	6	7.23	5.37E-8
			<b>Total</b>						
			<b>85.5</b>						

<sup>1)</sup> Only PFL-f logged down to 438 m.

<sup>2)</sup> No transmissivity could be detected. Instead, the practical detection limit is specified.

### G.1.6 KFR27 representativeness

KFR27 has a central position inside the Central block, a region with little data coverage that is considered likely to host the SFR extension. The borehole also covers depths where data are scarce. However, there exist limitations in data quality of KFR27, as well as, concerns to its representativeness of HRD (rock mass outside deformation zones). On the other hand, exclusion of borehole data reduces the data set and a smaller sample size increases exposure to the local heterogeneity of retained boreholes. The decision on how to treat the KFR27 data is delicate with implications in both hydrogeological interpretation and DFN parameterisation. The concerns with KFR27 can be summarised as:

- 3) Sampling bias: the borehole is almost vertical (an average inclination of  $-86^\circ$ ), which effectively censors the sampling of vertical fractures to such an extent that they cannot be sufficiently compensated by Terzaghi-weighting.

- 4) Data quality and data gaps: its upper part (0 to 147.5 m) was drilled during the construction of the existing SFR. The core in this upper part is unavailable today. PFL-f data are only available below 99.3 m borehole length (i.e. coarsely resolved above 130 m and lacking core support). The upper 99.3 m borehole length is only covered by sequential PFL data measured over 5 m sections, which cannot be coupled to Boremap fractures.
- 6) Deformation zone influence: in principle, the entire borehole KFR27 lies inside the modelled geometric bounds of a steeply dipping deformation zone (ZFMWNW0835), yet, only two distinct *target intercepts* have been defined (notation by Curtis et al. 2011). Inside and in the vicinity of its lower intercept (–320 to –464 m RHB 70) a strong hydraulic signature of the zone can be observed in PFL-f data, while above c. 300 m borehole length (c. –297 m RHB 70) the hydraulic pattern does not differ notably from other borehole data, not even inside the upper intercept of ZFMWNW0835 (–105 to –117 m RHB 70). It is therefore unclear to which extent the borehole interval between the *target intercepts* is representative of rock mass outside deformation zones.

The decision on how to treat KFR27 is delicate. It was decided to include data from KFR27 as far as possible. However, it is judged that KFR27 cannot be used to calculate intensity of steeply dipping fracture sets and that hydraulic data above 130 m borehole length are not used in calibration (although verified in a consistency check, Figure G-19). It should be noted that the decision to include its PFL-f data below 130 m depth, *may* underestimate the intensity of steeply dipping fractures in the Deep domain. Therefore the simulated steeply dipping sets were allowed to exceed PFL-f intensity.

### G.1.7 Deterministic modelling of high-transmissive data

A modelling alternative has been suggested, in which high-transmissive sub-horizontal PFL-f is deterministically modelled as so-called SBA-structures (see Appendix B). SBA-structures are primarily defined on hydrogeological merits and are not part of the geological model. In terms of Hydro-DFN modelling, the main consequence of introducing the SBA concept is that the most transmissive fraction of sub-horizontal PFL-f data is depleted from the HRD data set, and instead used to parameterise the SBA-structures (Figure G-1; details provided in Table B-3, Appendix B). The SBA concept had not been introduced during the v. 0.2 stage, and therefore the preliminary Hydro-DFN included this fraction of high-transmissive PFL-f in the stochastic DFN representation. Thus, the decision to provide a deterministic inference for these data is probably the single most significant adjustment for the updated the Hydro-DFN.

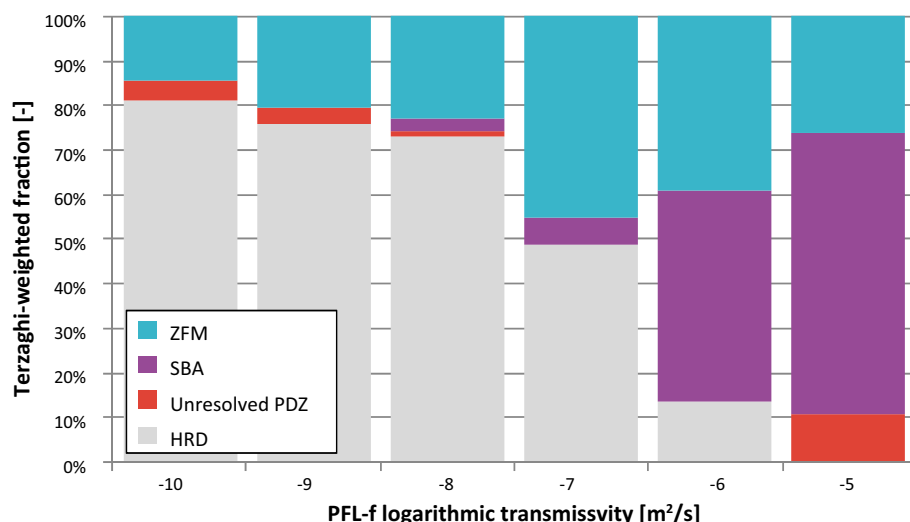


**Figure G-1.** Classification of PFL-f data\* into deterministic deformation zones (ZFM), deterministic SBA-structures, Unresolved PDZs, and the remaining HRD. Only the most relevant data included (only the Repository and Deep domains, and only from cored boreholes inside the SFR Local model domain).

\*The y-axis is Terzaghi weighted to reflect intensity of transmissivity distribution. However, to improve the readability, the classification is shown as relative fractions (%), as the intensity is very low for highly transmissive features.

### G.1.8 Role of PFL-f data as calibration target

The PFL-f data from the SFR extension investigations are presented and discussed in Chapter 4, main report. A PFL-f record reflects the *specific capacity*,  $Q/\Delta h$  ( $\text{m}^2/\text{s}$ ), or also referred to as *apparent transmissivity*, of a detected flow anomaly. Due to the hydraulic choking phenomenon at fracture intersections (Öhman and Follin 2010b), it is unlikely that this measured apparent transmissivity is equivalent with the actual transmissivity of intersected fractures. However, the purpose of the Hydro-DFN is to provide input to regional-scale modelling with DarcyTools, which does not explicitly account for hydraulic choking in downstream flow simulations. Therefore, *for the purpose of providing compatible input for downstream modelling*, it was considered more reasonable to assume the equivalence between PFL-f data and explicit fracture transmissivity (see discussions in Öhman and Follin 2010b).

The PFL logging is subject to a practical detection limit, expressed as a transmissivity threshold, which varies from borehole to borehole, but also along the borehole length. This threshold depends on drawdown applied, as well as, data noisiness. Consequently, it is particularly high in the vicinity of highly transmissive structures (e.g. deformation zones, SBA-structures, and abundance of stochastic features). For example, the detection limit may be lower further away from deformation zones and at depth, where the abundance of flowing features is lower. The subsurface borehole KFR105 is one such example,

The position of a PFL-f record is determined with decimetre-scale precision ( $L_A \pm 0.2$  m). Although several potential flowing fractures can often be found within this geometrical uncertainty interval,  $L_A \pm 0.2$  m, only one feature is selected as the “Best Choice”, according to the methodology (Öhman et al. 2010). The other potential features inside the geometrical uncertainty interval are referred to as “Alternative Best Choices”, and excluded from further analysis. It can be noted that c. 80% of the PFL-f spacing ranges from 0.6 to 7 m (Figure G-2), but very few detected PFL-f data have a spacing shorter than c. 0.3 m. This suggests that: either flowing features are rarely spaced closer than 0.3 m, or the practical spatial resolution of the PFL-f device is on the order 0.1 to 0.3 m. In simulated borehole exploration, on the other hand, fracture intersection can be determined with a virtually unlimited precision. The number of possible intercepts is intimately related to the detection resolution (particularly so for clustered fracture networks), and hence the practical resolution of the PFL-f device must be mimicked in simulated borehole exploration for a consistent comparison to data. Two resolutions are therefore applied in the simulated borehole exploration: 0.1 m and 0.3 m. All fractures intercepted inside a “PFL-f resolution interval” add up to its total transmissivity, but only its most transmissive fracture (i.e. a synthetic analogy to “Best Choice”) is sampled and compared to the PFL-f data set.

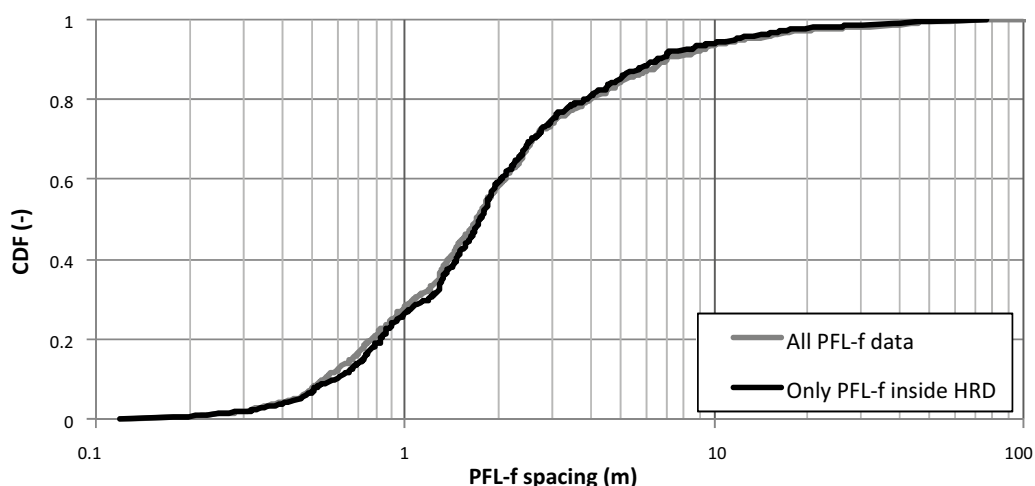


Figure G-2. Cumulative distribution of PFL-f spacing.

The Hydro-DFN is calibrated by matching the transmissivity-intensity distributions of connected network of open fractures, as seen by simulated exploration boreholes, to the HRD PFL-f data set (Figure G-3). Note that the HRD data set is defined as the remnant data set after the exclusion of all records located inside any type of deterministic structure: 1) deterministic deformation zones (ZFM; see Appendix C), 2) Unresolved PDZs (borehole sections with deformation zone characteristics that could not be deterministically modelled in the geologic model SFR v. 1.0; see Appendix A), and 3) SBA-structures (See Appendix B). The comparison between PFL-f data and simulations is made per set and depth domain (i.e.  $5 \times 3 = 15$  data subsets), but these data subsets are pooled from all boreholes.

Fracture transmissivity,  $T$ , is parameterised as a direct function of fracture radius,  $r$ :

$$T(r) = a r^b \quad (\text{G-1})$$

where the factor,  $a$ , is the transmissivity of a fracture with one-meter radius and an exponent,  $b$ , determines the transmissivity scaling with size. For the Connectivity analysis, the typical values for  $a$  are on the order  $10^{-9}$  to  $10^{-8}$  m<sup>2</sup>/s, while the exponent  $b$  is typically close to 1 (Table G-5). The fitted values for the Tectonic continuum approach have a comparatively larger spread (Table G-6). As an alternative parameterisation, the KFR106 PFL-f data are included in the pooled calibration target (Section G.1.9), and the necessary adjustments to the transmissivity-size relation for including KFR106 are reported in (Table G-7).

The gently dipping to sub-horizontal sets (i.e. Gd and Hz) dominate over steeply dipping sets both in terms of frequency and transmissivity (Figure G-3). Moreover, set Hz dominates over set Gd in the Shallow domain, particularly in the upper transmissivity tail, although this domination seems to vanish at depth. Sets Gd and Hz also have larger sample sizes (i.e. total sum of Terzaghi weights in Figure G-3), which is probably related to censoring effects of the practical detection limit in PFL logging (i.e. although low-transmissive steeply dipping features may very well exist, they cannot be detected). As sets Gd and Hz dominate in both transmissivity and sample size, they are the primary focus in the calibration procedure.

### G.1.9 Model alternative including KFR106 PFL-f data

KFR106 provides additional data that were unavailable during the v. 0.2 Hydro-DFN. In comparison to boreholes inside the SFR Local model domain (i.e. the underlying data set of v. 0.2 Hydro-DFN), considerably higher PFL-f transmissivities are found in KFR106 at Repository level (see depth domain discussions in Section G.3). This was interpreted as part of a lateral trend associated to a structural wedge between the Northern boundary belt and ZFMNNW1034. On the other hand, in the Shallow and Deep domains, the PFL-f data of KFR106 are not very different from KFR104 (KFR104 is located in the Central block, which is interpreted as low-transmissive). However, the total borehole coverage of the Shallow and Deep domains is considerably less than in the Repository domain (Figure G-7), which makes it difficult to differentiate between trends and local heterogeneity. Strictly speaking, KFR106 is located outside the Local SFR model domain, which motivates excluding it from the Hydro-DFN parameterisation and particularly so if it exhibits characteristics that are unrepresentative for the target area for the SFR extension.

On the other hand, it is unclear if the observed lateral trend in PFL-f data reflects *actual fracture-scale properties*, or an *apparent scaling effect* in effective properties related to flow path length. Moreover, the PFL-f data set is relatively small (compared to the data set for Open fractures). Adding KFR106 to the calibration data set increases the data set for calibrating the three depth domains. Furthermore, after associating the most anomalous hydraulic data of KFR106 deterministic structures (ZFMs, Unresolved DZs, and SBAs), the remaining HRD data is considerably less anomalous. The effect of including KFR106 data to the pooled data of the SFR Local domain is demonstrated in terms of complementary-cumulative PFL-f intensity (i.e. sum of Terzaghi weights per borehole length; Figure G-4). The largest effects are found for sets Gd and Hz in the Repository domain (Figure G-4). In the Shallow and Deep domains, the effects are negligible, as well as, for set NW in the Repository domain (not shown).

Hence, the effect of including KFR106 data on the parameterised transmissivity-size relations is judged to be of interest. This alternative parameterisation is presented in (Table G-7). It should be pointed out that the inclusion of KFR106 data concerns only PFL-f data (i.e. the orientation model and open fracture intensity are not updated with respect to KFR106 data).

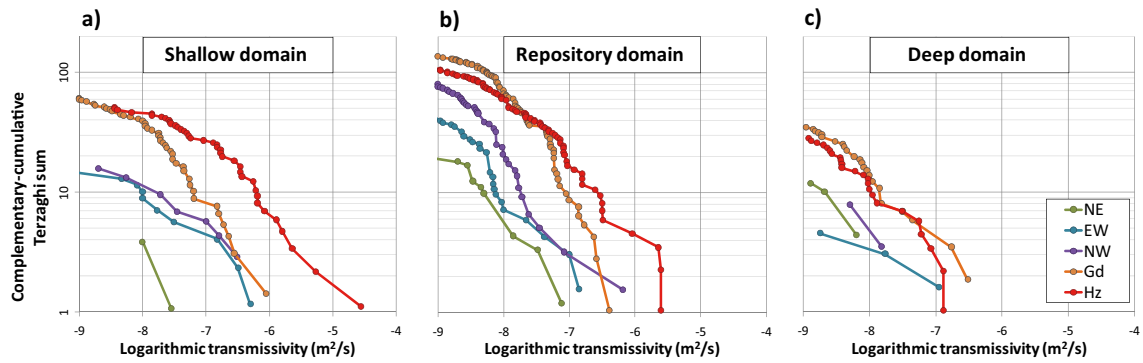


**Figure G-3.** Set-wise PFL-f transmissivity distributions per depth domain used as calibration target for simulated borehole exploration of the connected network of open fractures.

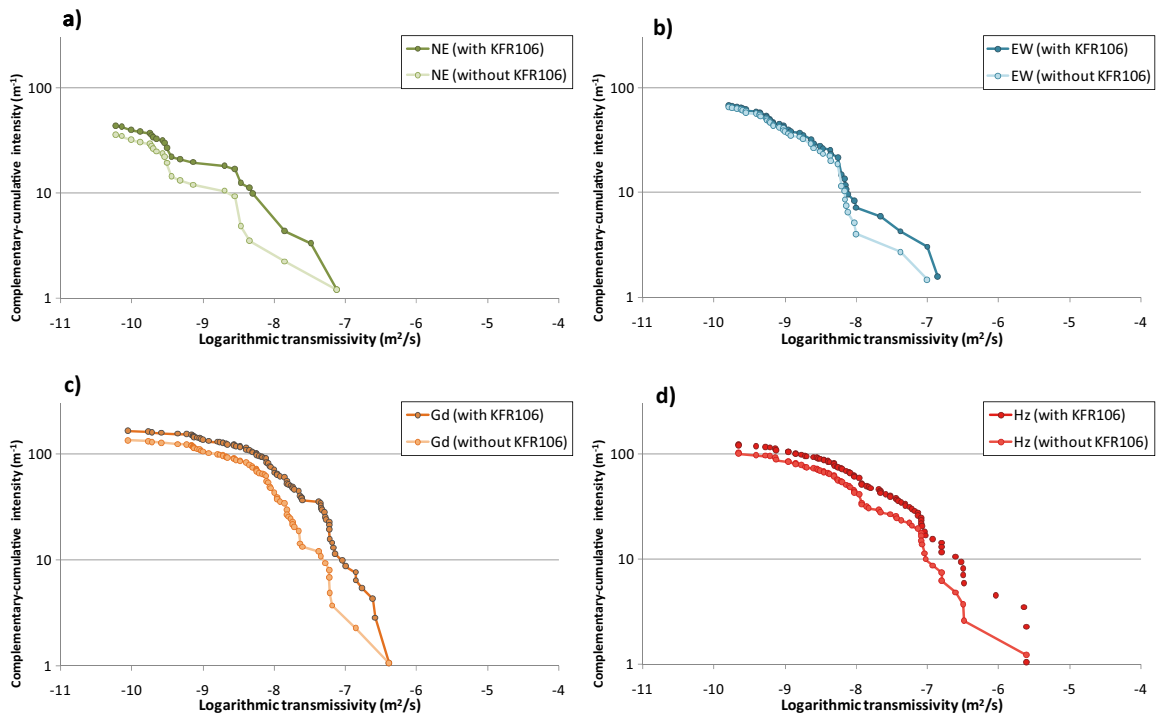


**Figure G-4.** Repository domain. The effect on PFL-f transmissivity distributions with the inclusion of KFR106. The NW set is not shown, as KFR106 provides no additional such data in this depth domain.

## G.2 Updating the orientation model

Fracture orientation is parameterised by a global orientation model, defined by fracture set mean poles (defined by its trend and plunge) and the spread around the mean pole. The dispersion around the mean pole is assumed to be radial-symmetric and following the unimodal Fisher distribution (defined by the Fisher concentration parameter,  $\kappa$ ). Geological fracture mapping of core data entails uncertainty in measurement of fracture orientation. This measurement error is estimated as a maximum dihedral angle,  $\Omega$  [°]. Large uncertainties or errors in orientation data tend to exaggerate the parameterised dispersion of fracture sets (i.e. underestimate the Fisher concentration parameter,  $\kappa$ ). Therefore, in order to reduce the risk of overestimating fracture set dispersion induced by measurement errors, the orientation parameterisation is updated for a delimited subset of orientation data with lower  $\Omega$  (i.e. excluding fracture data with orientation uncertainty exceeding a certain threshold).

The uncertainty parameter,  $\Omega$ , was unavailable during the v.0.2 stage. Therefore artificial inclusion of measurement errors was reduced by excluding fractures mapped as *not visible in BIPS*. The reason for this is that fracture orientations measured in the core are subject to the additional uncertainty in the core orientation, and generally have a considerably lower confidence in fracture orientation. However, a fracture that is not visible in BIPS does not necessarily imply a large orientation uncer-



tainty; this depends on its solid angle versus the borehole (i.e. its alpha-angle,  $\alpha$ ). Fracture orientations with high  $\alpha$  are less subject to the uncertainty in the core orientation, e.g. horizontal fractures in KFR27 or steep EW-striking in KFR105. Consequently, some fractures not visible in BIPS have low  $\Omega$ , and can be included in the orientation analysis (Figure G-5a). On the other hand, fractures that *are* visible in BIPS may have a high  $\Omega$ , due to uncertainty in borehole geometry, and should be excluded from the orientation analysis. In this study, it was tested if the fracture set parameterisation can be improved by using the parameter  $\Omega$  to reduce the measurement error component.

More precisely, all data were randomly assigned to fracture sets, according to the methodology described in Öhman and Follin (2010b). Fracture set mean poles, Fisher concentrations, and relative intensities were re-calculated for varying  $\Omega$  thresholds. It was decided to use a  $\Omega$ -threshold of  $10^\circ$  for steeply dipping sets and  $15^\circ$  for sets Gd and Hz (Table G-4). Inclusion of KFR106 data has no dramatic effect on the orientation pattern (Figure G-6a and b). Nevertheless, it was decided not to include KFR106 in the determination of the orientation model, as it is considered to be less representative of the target volume.

In a second step, fracture data with higher orientation uncertainty (i.e. large  $\Omega$  and fractures without mapped orientation) must be accounted for in calculations of set-specific intensity. Assumptions must be made to formulate a realistic strategy to associate uncertain data subset (high  $\Omega$ ), to the pre-defined sets based on the high-accuracy data (low  $\Omega$ ). Alternative strategies can be considered for this, for example by means of:

- 1) Set inference based on mineral infill characteristics. Set-specific “mineral signatures” could be learnt from the high-confidence orientation data. These signatures could then be used to estimate the set-specific intensities of low-confidence orientation data. The “final” set-specific intensity is then the sum of the high-confidence and low-confidence intensities. Scope calculations suggest that it is difficult to establish confident “mineral signatures” (this conclusion was also drawn during SDM-Site Forsmark (Fox et al. 2007)), and hence this method was abandoned.
- 2) Assuming intensity proportionality between high-confidence orientation data and low-confidence orientation data. In this method, *relative* set-specific intensities could first be estimated from the fracture data with low  $\Omega$ . These relative intensities could then be re-scaled by the total fracture intensity (including all fractures), in order to obtain the “final” set-specific intensities. This approach relies on the assumption that there is no systematic discrepancy in orientation uncertainty between fracture sets. Fractures sub-parallel to the borehole axis can be expected to have a higher orientation uncertainty (i.e. steeply dipping fractures); however, in the SFR data set it would appear that particularly many sub-horizontal fractures have a  $\Omega > 10^\circ$  (Figure G-5; primarily in KFR102A and KFR27).
- 3) Set inference based on measured orientation without consideration to confidence. In this method, the low-confidence data are only excluded during the derivation of the orientation model. In the subsequent intensity calculations, fracture data are assigned to fracture sets according to their measured (yet uncertain) orientation. The motivation for this approach is that: 1) the measurement error is generally relatively small in the SFR data set (Figure G-5a), and 2) the low-confidence data does not exhibit a uniform random-type distribution (Figure G-6c and d). Only about 15% of the total population exceed  $\Omega = 15^\circ$  (most of these are not visible in BIPS).

It was decided to apply strategy 3. Most of the low-confidence data seems to belong to sets Hz and Gd (Figure G-5b and Figure G-6c and d); it would be inappropriate to assign these data proportionally to all sets (i.e. including steeply dipping sets), without using guidance from “approximate orientation”.

It is non-trivial to determine the optimum  $\Omega$  threshold for the distinction between “low-confidence” and “high-confidence” data, as the exclusion of less accurate data implies reducing the sample size. A too strict criterion introduces data gaps in spatial coverage of the model domain (i.e. as  $\Omega$  is spatially dependent), which introduces an uncertainty to the representativeness of the remaining, more accurate data, as it is more subject to local heterogeneity. In the end, an inappropriate  $\Omega$ -threshold may therefore provide fracture set parameterisation that is unrepresentative of the entire model domain.

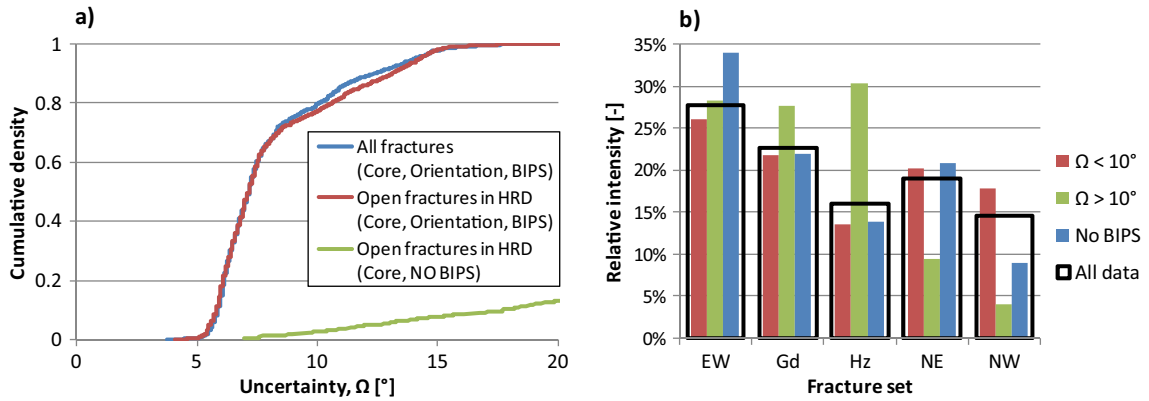


**Figure G-5.** Fracture orientation uncertainty,  $\Omega$ , distribution in cored boreholes inside the SFR Local model domain; a) cumulative distributions and b) histogram of relative set intensity in Open and Partly open fractures within the repository depth interval  $-60$  to  $-245$  m RHB70.

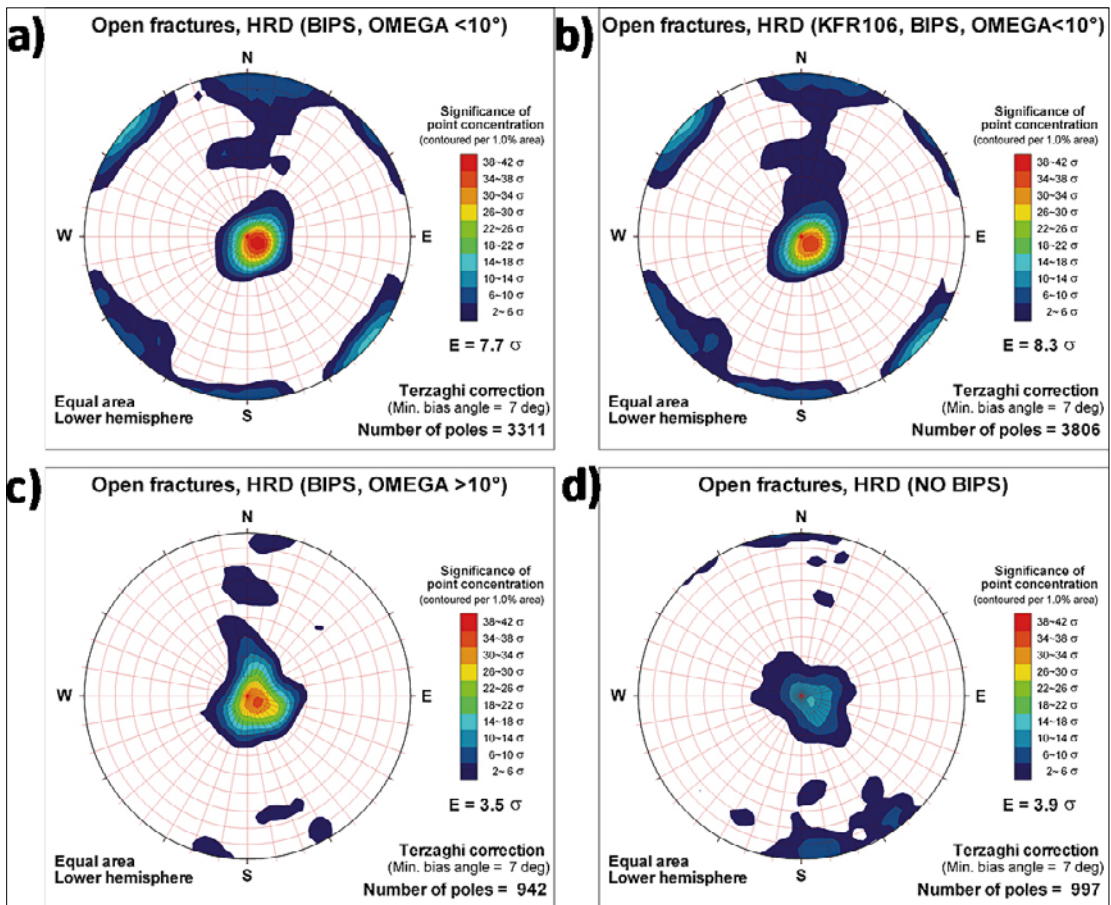


**Figure G-6.** Orientation of Open fractures in HRD in cored boreholes; a) inside the Local domain visible in BIPS and with  $\Omega < 10^\circ$ , b) inclusion of KFR106, c) inside the Local domain visible in BIPS and with  $\Omega \geq 10^\circ$ , and d) not visible in BIPS. Upper part of KFR27 with unavailable core excluded.

Therefore, various  $\Omega$  thresholds were tested, compared in terms of  $\kappa$ , and evaluated visually in terms of Kamb-contoured stereograms. It was decided to use a  $\Omega$ -threshold of  $10^\circ$  for the steep sets and  $15^\circ$  for sets Gd and Hz (Table G-4). The updated orientation model is presented in (Table G-4); the details on the numerical procedure used in are described in Öhman and Follin (2010b). This orientation model is applied globally to all three depth domains, and is independent of subsequent parameterisation steps (intensity, size, and transmissivity; see Table G-5 and Table G-6).

**Table G-4. Global orientation model with 5 sets; soft sector parameterisation by iteration.**

Set	Acronym	Trend	Plunge	Fisher $\kappa$	No. fractures
EW-striking <sup>1)</sup>	EW	4.8	13.9	10.1	844
NW-striking <sup>1)</sup>	NW	233.8	7.2	13.7	410
NE-striking <sup>1)</sup>	NE	125.4	1.8	13.7	615
Horizontal <sup>2)</sup>	Hz	127.5	83.7	41.9	866
Gently dipping <sup>2)</sup>	Gd	339.1	87	7.2	1,198

<sup>1)</sup> Based on fractures with  $\Omega \leq 10^\circ$ .

<sup>2)</sup> Based on fractures with  $\Omega \leq 15^\circ$ .

### G.3 Depth domains

The depth domain concept is a modelling technique designed to reproduce data depth trends in a simplified way. Model depth domains can be described as a coarse vertical discretisation of the observed, gradual depth trends in hydrogeological properties. Thus, the modelled depth domain boundaries *do not relate to actual* distinct, abrupt hydrogeological alteration occurring in reality. In order to reduce numerical artificial effects, the depth domain boundaries should be defined to represent depth intervals, or horizontal units, with relatively homogeneous hydrogeological properties. For the same reason, the depth domain boundaries should preferably avoid intersecting the storage facilities of the existing SFR, as well as its planned extension. Moreover, these boundaries should be defined to enclose well-balanced data coverage that is representative of the depth domain (i.e. sufficient borehole coverage, preferably from multiple boreholes with mixed orientation bias).

In the preliminary Hydro-DFN, v. 0.2, the boundary between the Repository and the Deep domains was drawn along the preliminary geologic modelled ZFM871 (i.e. an approximate elevation of –245 m). However, in the final geologic model, ZFM871 is terminated at ZFMENE3115 and thus, does not constitute the assumed geologic boundary for separating the two depth domains. Furthermore, a steep deformation zone, ZFMWNW0835, is modelled in the very vicinity KFR27, suggesting that its hydraulic data are potentially affected by proximity the zone – more or less over its entire extent (G.1.6). In effect, this reduces the sample size of HRD data at depth (Table G-3) and motivates adjusting the definition of the Deep depth domain.

Lacking conceptual support from structural geology, it was decided to define depth domains based on analysis of hydrogeological characteristics with consideration to their role in the numerical model. The bedrock above the storage facilities of the existing SFR (i.e. uppermost 60 m) is characterised by a high intensity of open fractures and high-transmissive PFL-f data. Hence, it is sensible to define a Shallow domain, extending down to –60 m elevation, to confine typical superficial characteristics to the bedrock above storage facility depths. The boundary between the Repository and Deep domains is comparatively less clear-cut to define. The primary objective is to define a well-represented Repository domain for typical storage facility depths (both with consideration to balanced borehole coverage and homogeneous hydraulic properties). On the other hand, all data below the Repository domain will be pooled into a Deep domain that represents the remaining model domain depths, down to 1,100 m elevation. The parameterisation of Deep domain may therefore have an important role in simulated regional-scale flow under saturated conditions in the Safety Assessments. In other words, any type of data excluded from the Repository domain (say, a PFL-f record at –245 m elevation) will be attributed to the Deep domain in the Hydro-DFN, and can be generated down to –1,100 m elevation. However, raising the boundary between Repository and Deep domains from –245 m to –200 m elevation improves the balance in borehole coverage between the two domains (Figure G-7). Based on data analysis (Section G.3.1), it was finally decided to set the boundary between Repository and Deep domains to –200 m elevation.

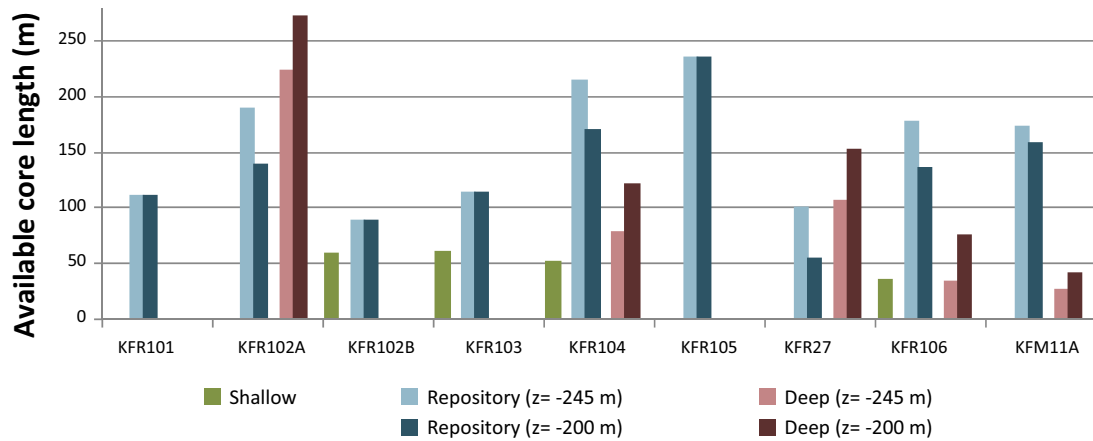


**Figure G-7.** Available HRD core length in boreholes per depth domain, depending on boundary between the Repository and Deep domains. Raising the boundary to  $-200$  m elevation improves the coverage of the Deep domain.

### G.3.1 Intensity of open fractures and PFL-f data

Fracture intensity,  $P_{32}$  [ $\text{m}^2/\text{m}^3$ ], is a three-dimensional entity that can be estimated from one-dimensional borehole fracture frequency  $P_{10}$  [ $1/\text{m}$ ]. It is well-known that borehole data are geometrically biased for fractures sub-parallel to the borehole. Several methods have been suggested in literature to compensate this geometrical sampling bias. In this analysis, it was decided to estimate  $P_{32}$  by scaling  $P_{10}$  (measured fracture frequency in boreholes) with Terzaghi-weights,  $w$ ,

$$w = \frac{1}{\sin(\max(\alpha, \alpha_{\min}))} \quad (\text{G-2})$$

where  $\alpha$  is the solid angle between the borehole and the fracture plane. The Terzaghi method does not take the relation between fracture size and borehole radius into account. Therefore, a minimum bias angle,  $\alpha_{\min}$ , is used to avoid unrealistically high weights for very small  $\alpha$  (i.e. infinity for  $\alpha = 0^\circ$ ). It was decided to set the maximum Terzaghi weight equal to 7, corresponding to a minimum bias angle  $\alpha_{\min} = 8.2^\circ$ , which is equivalent to that used in SDM-Site Forsmark. Fracture intensity,  $P_{32}$  [ $\text{m}^2/\text{m}^3$ ], can then be calculated as the sum of Terzaghi-weights divided by borehole length. It should be noted that this is different from the preliminary Hydro-DFN, where the simplified model setup necessitated a very low minimum bias angle,  $1^\circ$ .

The intensity of open fractures and PFL-f data is calculated for all cored boreholes, and divided into different depth intervals (Figure G-8 and Figure G-9, respectively). Note that KFM11A and KFR106 are included, but borehole sections inside deterministic geological structures (HCD) are excluded. The two alternative boundaries between the Repository and Deep domains,  $-245$  m and  $-200$  m elevation, are compared (Figure G-8c,d and d,f, respectively). The average intensity of depth domains can be calculated on borehole basis, or on borehole-length basis (referred to as ‘‘Borehole avg.’’ and ‘‘BHL avg.’’ in Figure G-8).

The overall impression is that the open fracture intensity is relatively evenly distributed among sets, depth domains, and boreholes. Set intensities are about  $1 \text{ m}^2/\text{m}^3$ , but higher in the Shallow domain, and particularly for sets EW and Gd. The lower intensity of steeply dipping sets in KFR27, as well as, for sets Gd and Hz in KFR105 is partly related to sampling bias of unfavourable borehole orientations that cannot be fully compensated by Terzaghi weighting. Discrepancies can be identified for the boreholes located outside the SFR Local model domain, KFM11A and KFR106, although these are not dramatic in relation to the variability between boreholes inside the Local domain.

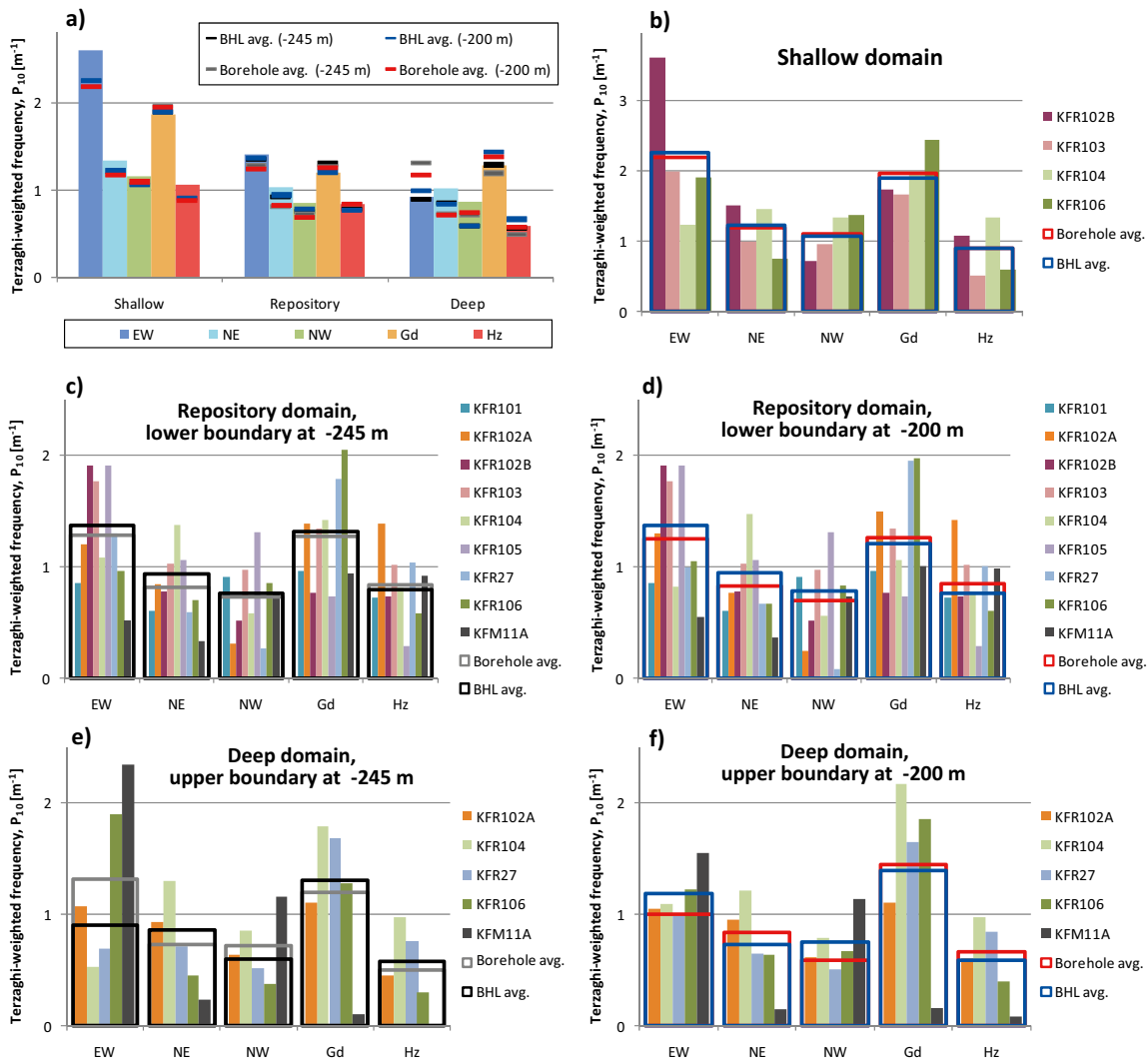


**Figure G-8.** Open fracture HRD intensity based on all borehole data, depending on averaging method (per borehole or weighted by borehole length), as well as, on the boundary between the Repository and Deep domains ( $-245$  m or  $-200$  m elevation); a) compares the intensity of the v. 0.2 Hydro-DFN model against the different alternatives.

The differences between depth domains, fracture sets, and boreholes outside the SFR Local domain are clearly more evident in overall pattern of PFL-f data (Figure G-9). Please note that Figure G-9 includes PFL-f data inside Unresolved PDZs and SBA-structures, although they are not part of the HRD (i.e. data sample used as calibration target for the Hydro-DFN). The purpose of including these data in Figure G-9 is to provide an overall overview of the hydraulic data pattern. It should also be noted that PFL-f below  $10^{-8}$  m<sup>2</sup>/s are partly censored by the practical detection limit.

Most notably, transmissivities exceeding  $10^{-6}$  m<sup>2</sup>/s occur only above  $-200$  m elevation. The “Undefined interval”,  $-200$  m to  $-245$  m elevation, clearly has an intermediate transmissivity pattern, lying somewhere between the Repository and the Deep intervals.

Excluding PFL-f data inside SBA-structures and Unresolved PDZs, as well as, boreholes outside the SFR Local domain, dramatically reduces the intensity of high-transmissive PFL-f in the depth interval  $-60$  m to  $-200$  m elevation (Figure G-10). This signifies the importance of introducing this type of deterministic structures for modelling the Repository domain.

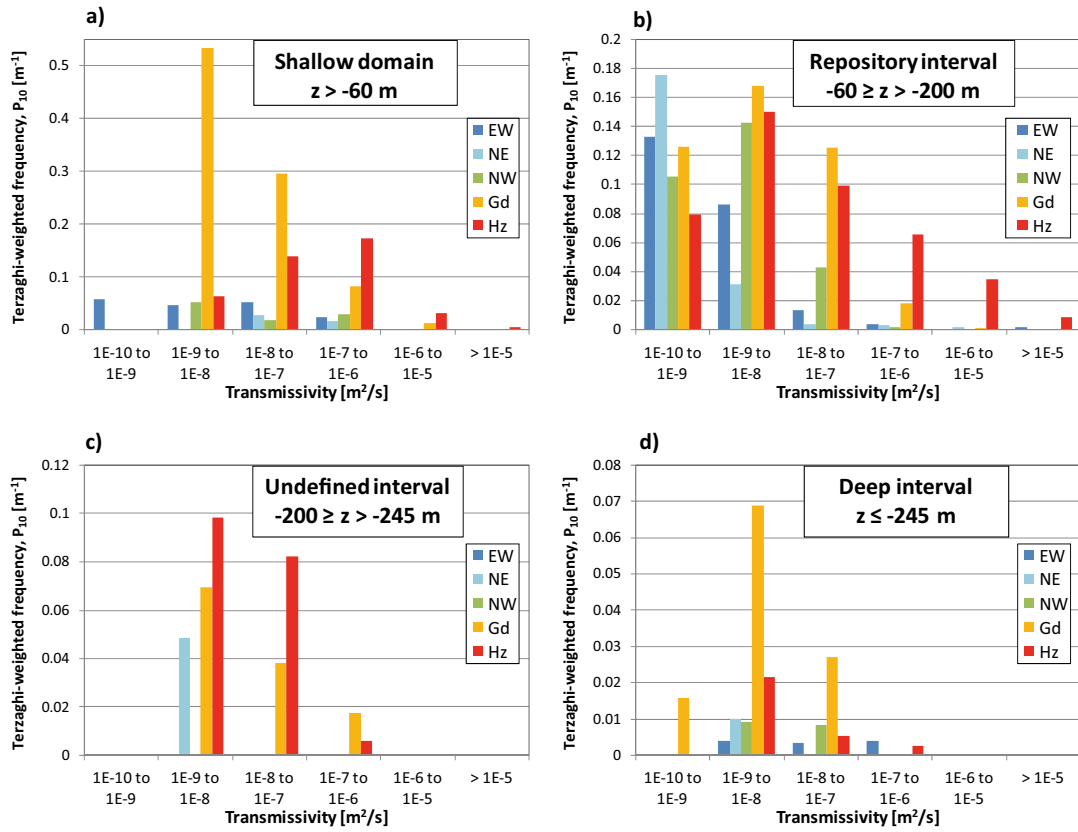


**Figure G-9.** Overall PFL- $f$  intensity outside deterministic structures (HCD) in 4 depth intervals. All boreholes included (e.g. KFM11A and KFR106), as well as, data inside Unresolved PDZs and deterministic SBA-structures.

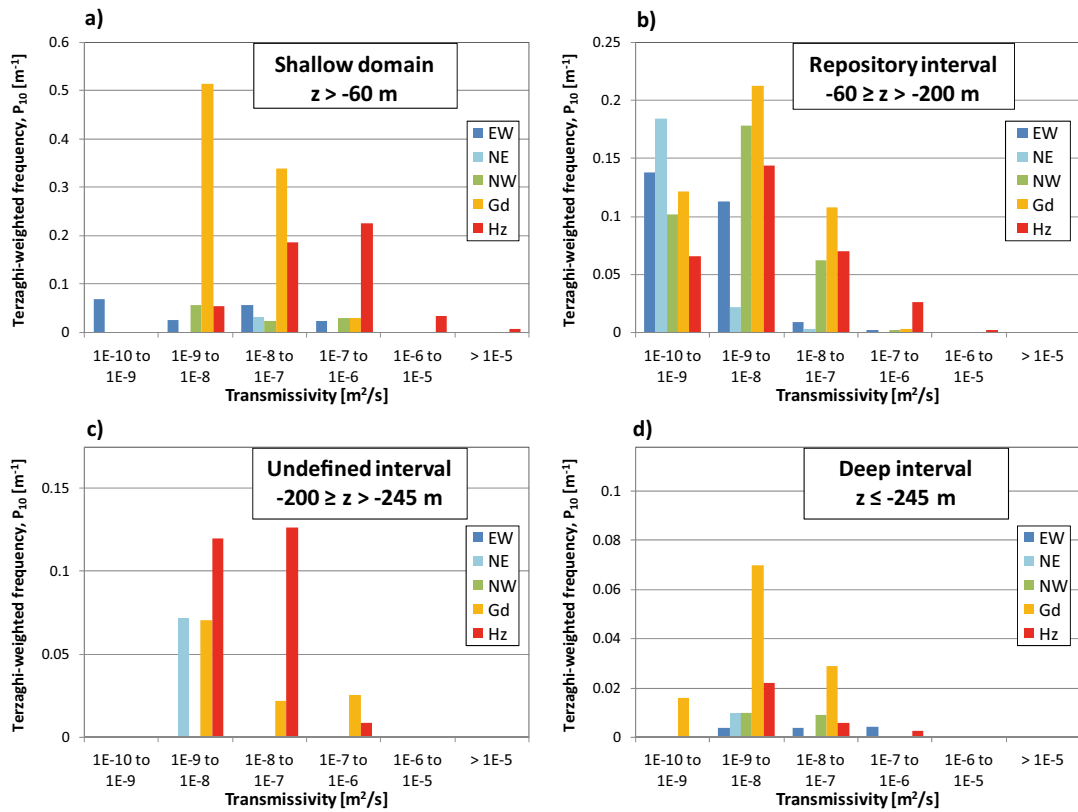


**Figure G-10.** HRD PFL- $f$  intensity in 4 depth intervals (excluding HCD, Unresolved PDZs, and deterministic SBA-structures). Only boreholes inside the SFR Local domain are included (i.e. KFM11A and KFR106 are excluded; inclusion of KFR106 is compared in Figure G-11).

The exclusion of SBA-structures and Unresolved PDZs also reveals a gradual decline with depth in the upper tail of distributions. The maximum transmissivity exceeds  $10^{-5}$  m<sup>2</sup>/s in the Shallow domain,  $10^{-6}$  m<sup>2</sup>/s in the “Repository interval”, and  $10^{-7}$  m<sup>2</sup>/s in the “Undefined interval”. Based on these findings, it is judged more reasonable to pool the “Undefined interval” with the Deep interval. The purpose of doing so is to “concentrate” the hydraulic characteristics of likely target depths for the extension of SFR into homogeneous domain, as well as, improving the underlying sample size for calibrating the deeper part of the model volume. On the other hand, this may exaggerate transmissivity of the Deep domain, as this “Undefined interval” is perhaps not very representative for depths down to -1,100 m elevation.

As KFR106 data is considered for inclusion in an alternative transmissivity parameterisation (Section G.1.9), an equivalent figure is also presented (Figure G-11). Only minor differences can be identified between Figure G-10 and Figure G-11; for example: set Gd in the Repository interval.

In spite of relatively minor discrepancies in boreholes located outside the Local domain, it was decided to exclude both KFM11A and KFR106 from the parameterised open fracture intensity. Furthermore, sets particularly exposed to sampling bias were also excluded (steeply dipping sets in KFR27 and sets Gd and Hz in KFR105; indicated by dashed lines in Figure G-12). It was also decided to use borehole-length weighted average for calculating intensity of depth domains (indicated by blue lines in Figure G-12). As stated earlier, the effect of these decisions have a relatively minor impact on the calculated intensity of depth domains (cf. Figure G-8). Thus, the determined intensities of the Hydro-DFN model v. 1.0 are not very different from the intensities of the preliminary Hydro-DFN model v. 0.2 (compare blue lines and coloured bars in Figure G-12a). The most evident change is an increased intensity of sets Gd and Hz in the Deep domain, a domain that is now defined as the interval -200 m to -1,100 m elevation.

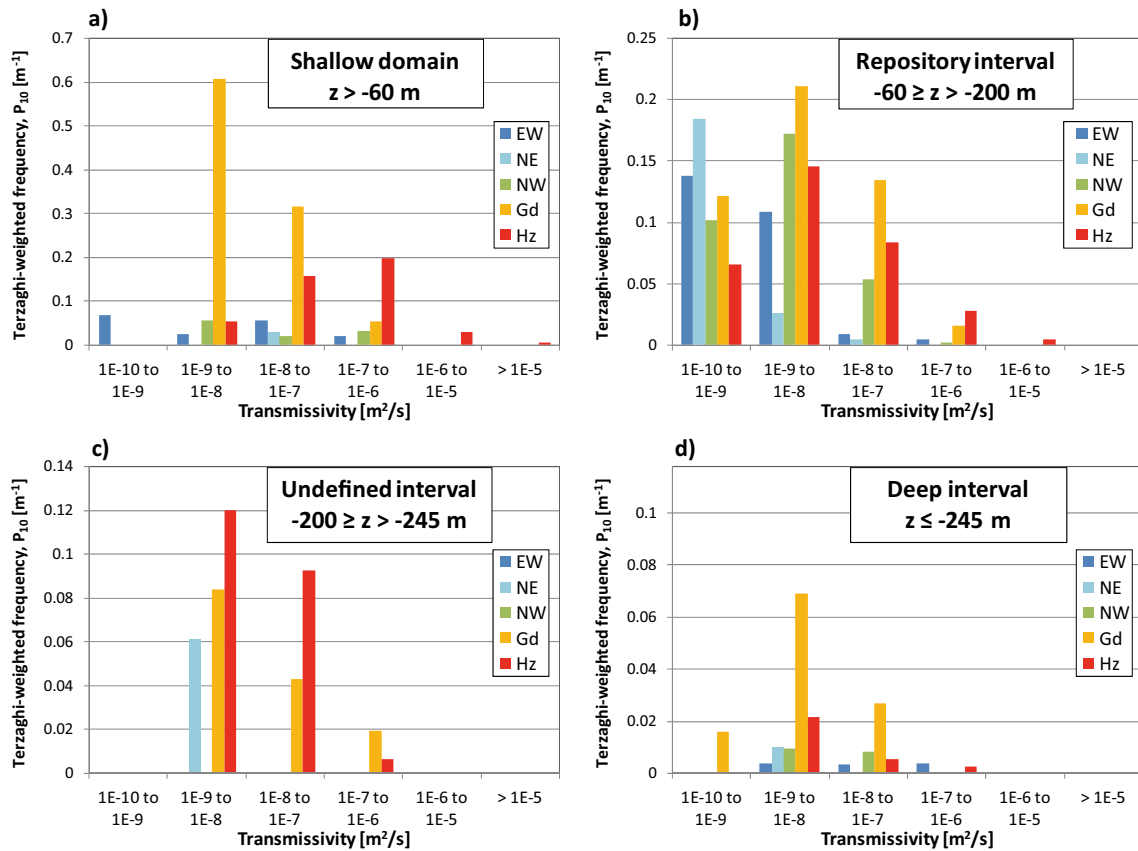


**Figure G-11.** HRD PFL-f intensity in 4 depth intervals of boreholes in the SFR Local domain, as well as, KFR106 (excluding HCD, Unresolved PDZs, SBA-structures, and KFM11A).

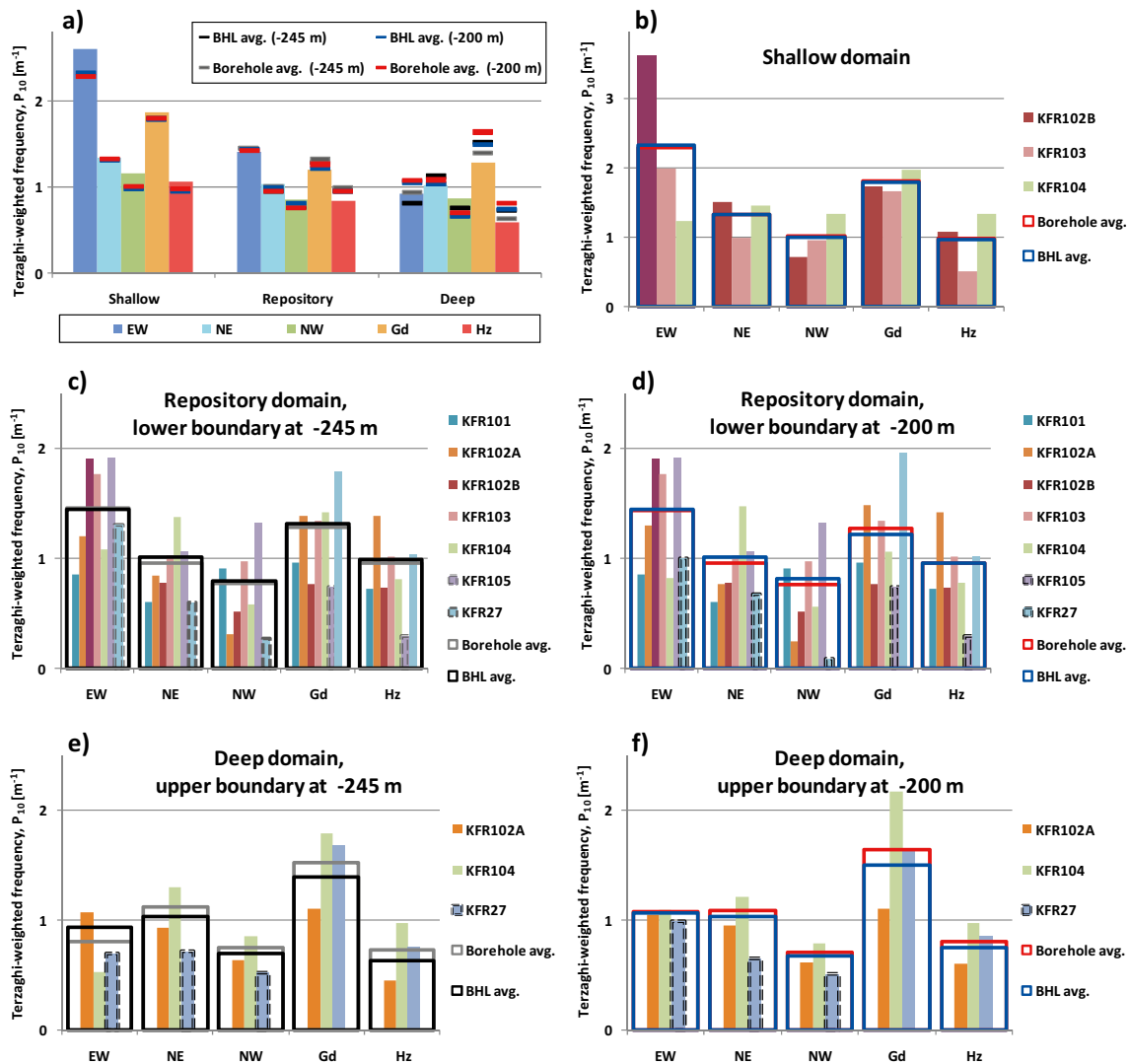


**Figure G-12.** Open fracture HRD intensity based on selected borehole data, depending on averaging method (per borehole or weighted by borehole length), as well as, on the boundary between the Repository and Deep domains (-245 m or -200 m elevation); a) compares the intensity of the v. 0.2 Hydro-DFN against the different alternatives. Dashed lines indicate data exclusion from calculated averages.

### G.3.2 Fracture domains based on rock domain model

A central question is if the rock domain model motivates dividing the rock mass into separate fracture domains. RFR01 covers the central to South-Western part of the SFR Local model domain, which is associated with lower PFL-f transmissivity. RFR02 covers the Eastern part (assumed to be influenced by ZFMNNW1034), but also the Northern part with the existing SFR disposal facilities. The most striking differences are that horizontal set is more clustered in RFR02 and that set EW is virtually absent in RFR01. The contrasts are smaller than found in the preliminary comparison made between South-western and North-eastern boreholes (Öhman and Follin 2010b). It is important to interpret these contrasts cautiously, with respect to local heterogeneity, data gaps, sampling bias, and borehole emplacement. There is a clear risk of overestimating these contrasts.

The EW set is not associated to large transmissivity values, and thus may be expected to have a minor role in the hydrological model. The EW-striking fractures are found at shallow depth in three boreholes originating from the tip of the pier: KFR102B, KFR103, and KFR101 (note that KFR101 is excluded as it is intercepted by ZFMNNW1034). These three boreholes basically origin from the same point, and therefore it may reflect local dominance of set EW. Local EW dominance is also found in KFR102A at larger depth (-125 m RHB70).



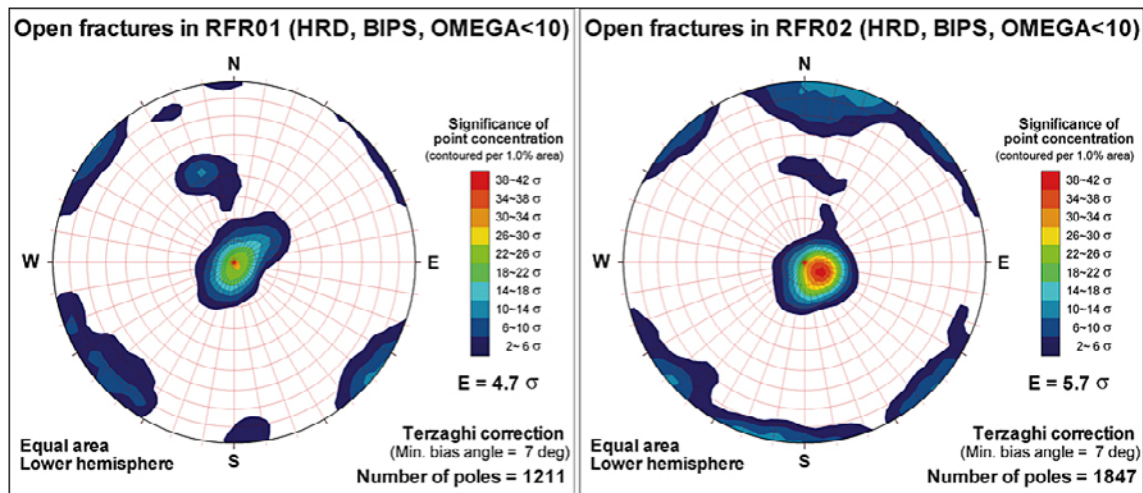


**Figure G-13.** Orientation of Open fractures in HRD per Rock Domain; a) RFR01 and b) RFR02. Only cored boreholes inside the Local domain, visible in BIPS, and with  $\Omega < 10^\circ$ ; upper part of KFR27 with unavailable core excluded.

The horizontal set, on the other hand, is conceptualized as the hydraulic backbone. One reason for the less dominance of set Hz in RFR01 could be that the sub-horizontal borehole KFR105 has a larger contribution of data. Another reason could be that boreholes are located further away from dominant zones. It may be suspected that NW could be influenced by Singö. Set NW is found in the entire extent of KFR105, in the upper and lower parts of KFR104, but is largely absent in KFR27.

As there is a difficulty with interpreting contrasts with respect to borehole locations, heterogeneity, the boreholes that are intersected by the Rock Domain boundary could shed some light. Rock Domain model intersections occur in KFR27 and KFR105; no correlations are evident, neither in terms of Open fracture intensity, nor in PFL-f transmissivity. In fact a change in transmissivity can be observed in KFR27: high transmissivity in the upper part (11.82 to 207.84 m borehole length; RFR01), followed by low transmissivity as it enters RFR02. However, this is a contradiction to expectations, and would seem more likely to reflect the depth trend in transmissivity. This notion should be judged in the light of KFR27 data deficiencies (e.g. its proximity to ZFMWNW0835; Section G.1.6).

In the light of heterogeneity, data gaps, and sampling bias, the differences between RFR01 and RFR02 are considered to be negligible. In summary, it is reassuring that the Rock domain model is partly in agreement with observed trends hydraulic properties, although it is not judged sufficient to merit separation into lateral fracture domains. In the end, the suggested conceptual model (Chapter 5, main report) is considered to provide a more realistic inference for the large-scale transmissivity trend.

#### G.4 Fracture generation

Open fractures are generated over the entire SFR Regional domain. The three depth domains (Shallow, Repository, and Deep) are generated simultaneously, according to their different parameter specifications. The following sequence is used to reduce computational demand. Large fractures ( $300 \geq L > 10$  m) are first generated within a large volume that encloses the SFR Regional domain. In a second step, all fractures strictly outside the SFR Regional domain are removed (Figure G-14). Medium-size fractures ( $10 \geq L > 0.5$  m) are considered to be less important for the large-scale connectivity, and are therefore only generated inside cylinder volumes that enclose the simulated boreholes (Figure G-15). Similarly, the smallest fraction of fractures ( $0.5 \geq L > 0.067$  m) is only generated inside a second order of cylinder shells. To avoid numerical artefacts, the cylinder radii were somewhat larger than half the diagonal of the largest generated fractures. In total 36 cylinder volumes were used to represent the three depth domains and the two fracture-size classes for all simulated boreholes.

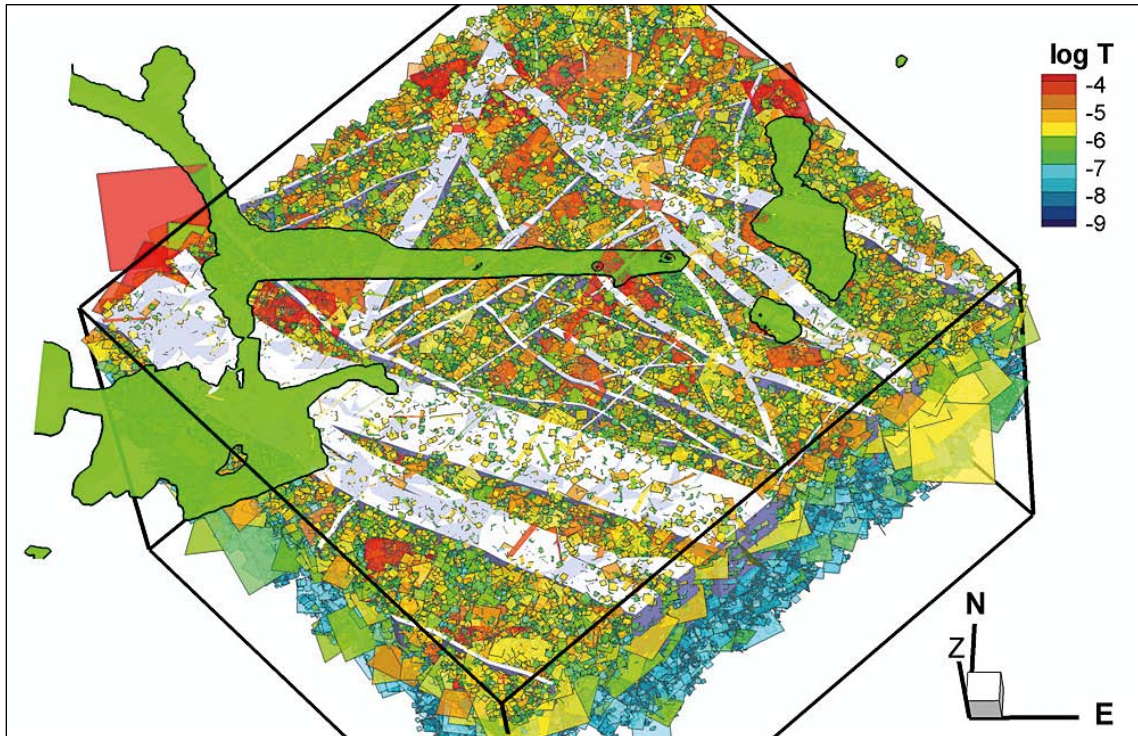


**Figure G-14.** Large fractures ( $300 \geq L > 10$  m) are generated inside a large volume enclosing the SFR Regional domain. Different characteristics are assigned in the three depth domains (Shallow, Repository, and Deep). All fractures strictly outside the SFR Regional domain are removed.

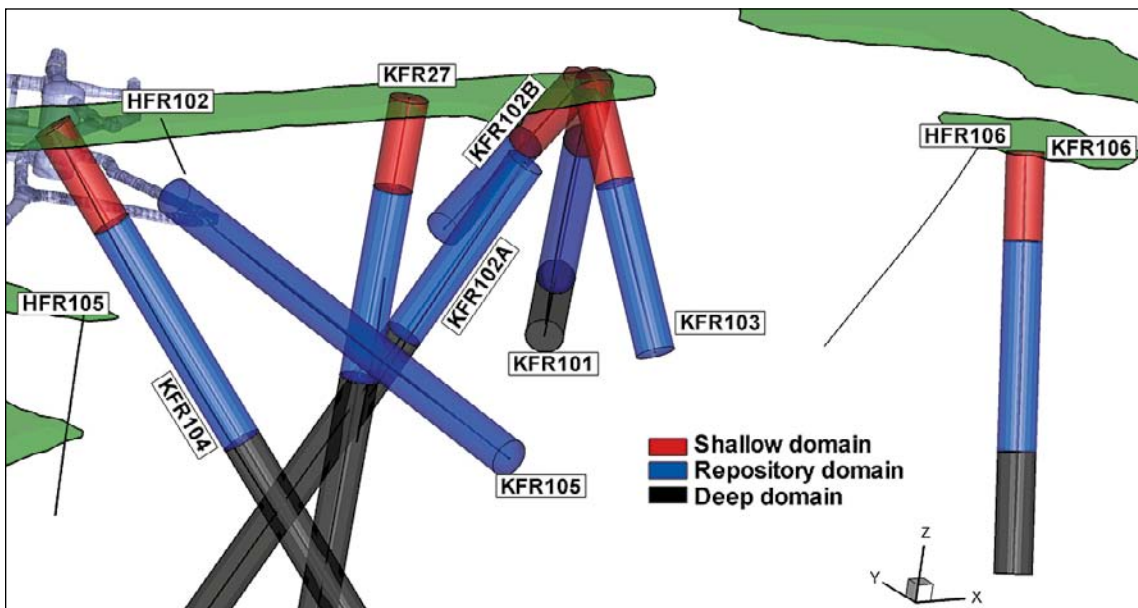


**Figure G-15.** Generation cylinders for medium fractures ( $10 \geq L > 0.5$  m). Similar cylinders are used for small fractures ( $0.5 \geq L > 0.067$  m), but are too thin for visibility.

After the complete fracture generation in the three depth domains, the fractures that are not part of the globally connected flowing fracture network are removed. The connected fracture system is defined as the subset of open fractures in contact (directly or indirectly) with structures regarded as positive hydraulic boundaries (Figure G-16). These structures are:

- 1) Deterministic deformation zones of the geological model (ZFM structures).
- 2) Unresolved PDZs (identified in the SHI but not included in the geological model; stochastically represented according to methodology described in Appendix A).
- 3) SBA-structures (SBA1-SBA7).

Next, borehole exploration is simulated for connected fracture networks and compared against PFL-f data, according to methodology described in Section G.1.8. The transmissivity parameterisation is fitted by trial and error for 50 realisations, until the PFL-f data are reasonably well matched (Section G.5). Simulated borehole exploration is also evaluated in terms of simulated orientation patterns (Figure G-23) and PFL-f intensity on borehole basis (Figure G-24 to Figure G-29). Finally, a consistency check was also performed for the uppermost 130 m of KFR27 (Figure G-19); a borehole section with a central location for the SFR extension, but excluded from the calibration, as it has coarsely and poorly resolved PFL data without core support.

#### G.4.1 Size-parameterisation alternatives

Fracture size is the most uncertain geometrical parameter of the Hydro-DFN model. The reason for this is that the parameter cannot be directly inferred from borehole data. The size of open fractures is assumed to be power-law distributed, as defined by a size scaling exponent,  $k_s$ , and the bounds for modelled fractures,  $r_0$  to  $r_{max}$  (see Figure 2-3, main report). The minimum fractures radius is set equal to borehole radius,  $r_0 = 0.038$  m, and the largest fracture radius is set to  $r_{max} = 169$  m (equivalent to a side length of 300 m, which is the resolution level for the deterministic structures in the geological model).

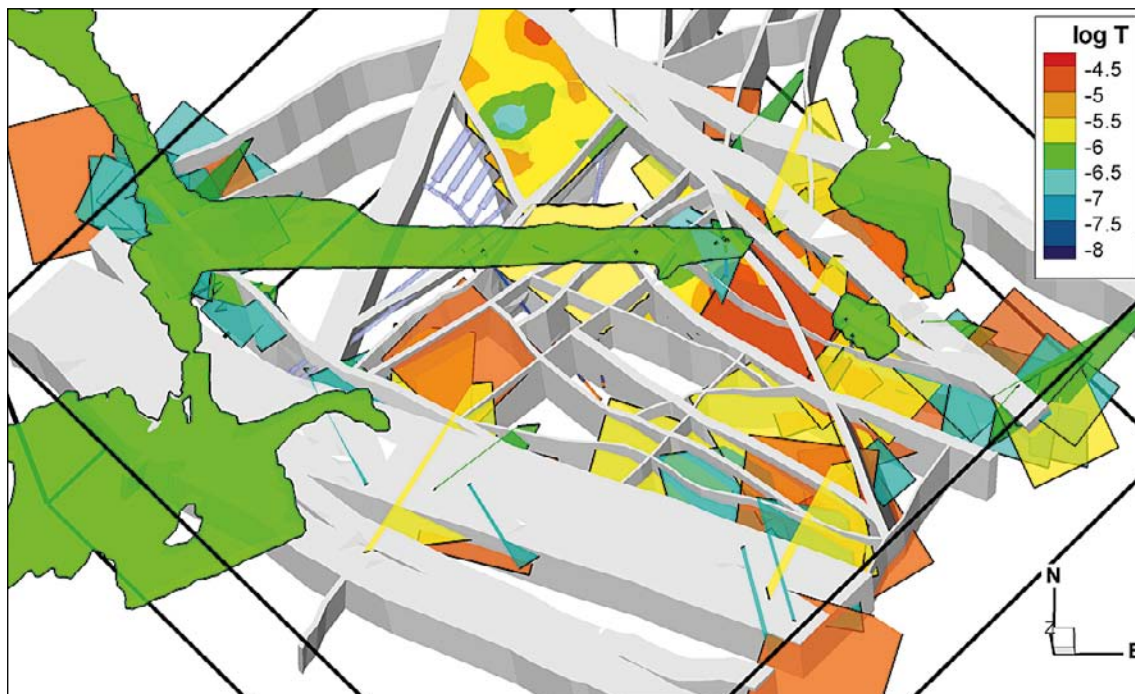


**Figure G-16.** Structures used as boundaries in the connectivity analysis; deterministic geological structures (ZFM; grey-shaded), deterministic SBA-structures (interpolated irregular planes), and Unresolved PDZs (quadratic planes coloured by transmissivity). Green areas represent ground surface.

Two alternative methods to define the size scaling exponent for steeply dipping sets,  $k_r$ , were considered in the preliminary Hydro-DFN model v. 0.2. These alternative methods are referred to as Connectivity analysis and Tectonic continuum, and the details of these concepts are described in Öhman and Follin (2010b). The fundamentals of the Connectivity analysis are two assumptions: 1) the observed intensity differences between open fractures and PFL-f data reflects the connectivity of the flowing fracture network, and 2) this connectivity can be reproduced by finding the underlying size distribution of the parent population (i.e. open fractures). In the alternative method, Tectonic continuum,  $k_r$  is solved from two defined points in the cumulative power-law intensity scaling. The two fixed points are: 1) the total open fracture intensity,  $P_{32, \text{Open}}$  at  $r_0 = 0.038$  m, and the intensity of steeply dipping deformation zones,  $P_{32, \text{HCD}}$  at  $r_{\text{max}} = 169$  m. The Tectonic continuum is difficult to apply for sets Gd and Hz; their  $k_r$  are therefore taken directly from the Connectivity analysis approach.

In essence, low-transmissive steeply dipping fractures are modelled as *small* in the Connectivity analysis ( $k_r \geq 3.0$ ), while in the Tectonic continuum approach they are modelled with *similar size* as sets Gd and Hz ( $k_r < 3.0$ ; cf. Figure G-17 and Figure G-18, respectively). Hence, the two approaches are considered to provide realistic bounds for the size uncertainty.

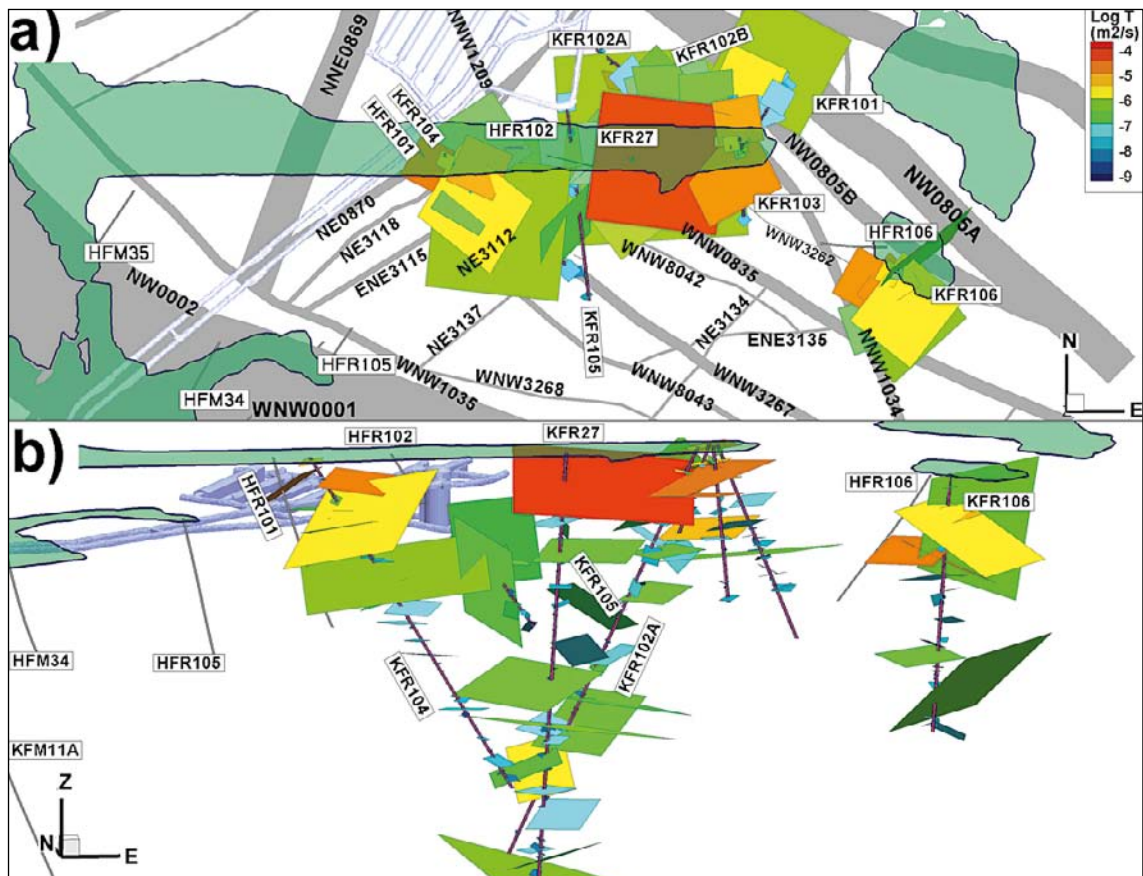


**Figure G-17.** Simulated exploration of connected open fractures with size distribution determined by Connectivity analysis. Steeply dipping fractures are modelled as short and low-transmissive ( $k_r \geq 3.0$ ; see Table G-5).

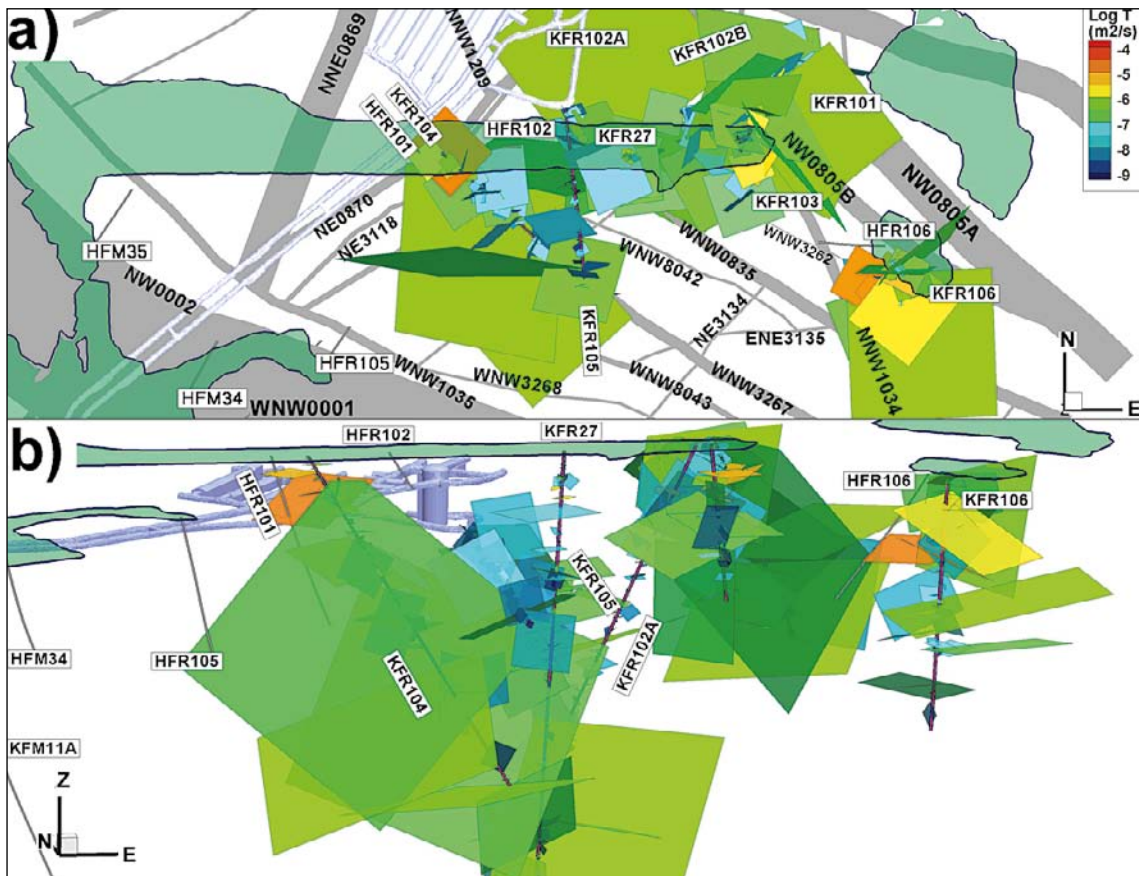


**Figure G-18.** Simulated exploration of connected open fractures with size distribution determined by Tectonic continuum. Steeply dipping fractures are modelled as short and low-transmissive ( $k_r < 3.0$ ; see Table G-6).

## G.5 Results

The orientation model (Table G-4) is assumed to be global to the SFR domain, and is assigned alike to all three depth domains. The remaining parameters of the Hydro-DFN, intensity, size scaling, and transmissivity relations, are both set- and depth domain-specific (i.e. fitted for 5 sets in 3 depth domains, with a total of 15 parameter sets; Table G-5 and Table G-6). Intensity is taken as the borehole length-weighted average of selected data (i.e. blue lines in Figure G-12). The size-scaling exponent,  $k_r$ , is highly uncertain as its determination suffers from non-uniqueness (Connectivity analysis) and concerns to validity of underlying assumptions (Tectonic continuum). Hence,  $k_r$  was taken directly from the preliminary Hydro-DFN (both Connectivity analysis and Tectonic continuum approaches). However, for the connectivity analysis approach, it was found necessary to reduce  $k_r$  of steeply dipping sets, as indicated by footnote 4) in Table G-5.

The size-transmissivity relations, as determined by coefficients  $a$  and  $b$  in Eq. (G-1), are fitted by trial and error with the target to reproduce the PFL-f data set. The calibration is made on pooled borehole basis for simulated borehole exploration in 50 realisations of connected open fractures. Simulations are compared against data in terms of complementary-cumulative distributions (Terzaghi sum versus transmissivity; Figure G-20, Figure G-21, and Figure G-22). Some calibration targets suffer from small sample size (e.g. set NE), which is supposedly due to effects of low transmissivity censored by the practical detection limit. This causes uncertainty in the determination of size-transmissivity relations. Furthermore, it is also not always possible to properly reproduce the shape of the data distributions. In such cases it was decided to fit size-transmissivity relations that cover the general pattern of data (i.e. the major part of data should be enclosed by the stochastic variability between realizations). The calibration is presented in sections G.5.1 to G.5.3.

**Table G-5. Hydro-DFN model parameterisation, based on Connectivity Analysis.**

Domain		Intensity <sup>2)</sup>		Size		Orientation <sup>3)</sup>			Transmissivity (T = a r <sup>b</sup> )	
Shallow	Set	P <sub>32</sub> (r <sub>0</sub> , 169 m)	P <sub>32</sub> Tot	r <sub>0</sub>	k <sub>r</sub>	Tr	PI	Fisher κ	a	b
m (RHB70)	EW	2.32	2.33	0.038	3.2 <sup>4)</sup>	4.8	13.9	10.1	2.1E-8	1.3
z > -60	NW	0.99	1.00	0.038	3.2 <sup>4)</sup>	233.8	7.2	13.7	5.3E-8	1.3
	NE	1.31	1.32	0.038	3.45	125.4	1.8	13.7	1.8E-8	1.0
	Gd	1.79	1.79	0.038	2.79	339.1	87	7.2	2.1E-8	1.09
	Hz	0.96	0.97	0.038	2.6	127.5	83.7	41.9	9.8E-8	1.32
Repository <sup>1)</sup>	Set	P <sub>32</sub> (r <sub>0</sub> , 169 m)	P <sub>32</sub> Tot	r <sub>0</sub>	k <sub>r</sub>	Tr	PI	Fisher κ	a	b
m (RHB70)	EW	1.44	1.45	0.038	3.1 <sup>4)</sup>	4.8	13.9	10.1	2.1E-9	1.1
-60 ≥ z	NW	0.81	0.82	0.038	3.0 <sup>4)</sup>	233.8	7.2	13.7	1.1E-8	1.1
z > -200	NE	1.00	1.00	0.038	3.3 <sup>4)</sup>	125.4	1.8	13.7	2.2E-9	1.3
	Gd	1.21	1.22	0.038	2.72	339.1	87	7.2	4.0E-9	0.8
	Hz	0.95	0.96	0.038	2.55	127.5	83.7	41.9	8.5E-10	1.35
Deep <sup>1)</sup>	Set	P <sub>32</sub> (r <sub>0</sub> , 169 m)	P <sub>32</sub> Tot	r <sub>0</sub>	k <sub>r</sub>	Tr	PI	Fisher κ	a	b
m (RHB70)	EW	1.06	1.07	0.038	3.2 <sup>4)</sup>	4.8	13.9	10.1	3.6E-9	1.6
-200 ≥ z	NW	0.67	0.67	0.038	3.15 <sup>4)</sup>	233.8	7.2	13.7	4.7E-9	1.13
z > -1,100	NE	1.03	1.03	0.038	3.2 <sup>4)</sup>	125.4	1.8	13.7	1.9E-9	1.0
	Gd	1.49	1.49	0.038	2.7	339.1	87	7.2	2.7E-10	1.6
	Hz	0.75	0.75	0.038	2.75	127.5	83.7	41.9	1.9E-9	1.15

<sup>1)</sup> Based on data characteristics and borehole coverage the boundary between the Repository and Deep domains is changed to -200 m elevation. In the v. 0.2 model the boundary was set to -245 m elevation, based on the preliminary geometrical modelling of ZFM871 (SFR geologic model v.0.1).

<sup>2)</sup> The smallest modelled deterministic zones are on the order 300 m (SFR geologic model v.1.0), corresponding to a radius of 169 m. Stochastic fractures are therefore assumed to have a maximum radius of 169 m.

<sup>3)</sup> Global orientation model used for all three depth domains.

<sup>4)</sup> Adjusted k<sub>r</sub>, relative to the preliminary Hydro-DFN v. 0.2 (Öhman and Follin 2010b).

**Table G-6. Hydro-DFN model parameterisation, assuming Tectonic Continuum.**

Domain		Intensity <sup>2)</sup>		Size <sup>3)</sup>		Orientation <sup>4)</sup>			Transmissivity (T = a r <sup>b</sup> )	
Shallow	Set	P <sub>32</sub> (r <sub>0</sub> , 169 m)	P <sub>32</sub> Tot	r <sub>0</sub>	k <sub>r</sub>	Tr	PI	Fisher κ	a	b
m (RHB70)	EW	2.32	2.33	0.038	2.694	4.8	13.9	10.1	1.6E-9	1.25
z > -60	NW	0.99	1.00	0.038	2.626	233.8	7.2	13.7	3.3E-9	1.2
	NE	1.31	1.32	0.038	2.778	125.4	1.8	13.7	1.2E-9	1.0
	Gd	1.79	1.79	0.038	2.79	339.1	87	7.2	2.1E-8	1.09
	Hz	0.96	0.97	0.038	2.60	127.5	83.7	41.9	9.8E-8	1.32
Repository <sup>1)</sup>	Set	P <sub>32</sub> (r <sub>0</sub> , 169 m)	P <sub>32</sub> Tot	r <sub>0</sub>	k <sub>r</sub>	Tr	PI	Fisher κ	a	b
m (RHB70)	EW	1.44	1.45	0.038	2.63	4.8	13.9	10.1	7.9E-11	1.4
-60 ≥ z	NW	0.81	0.82	0.038	2.596	233.8	7.2	13.7	1.3E-9	1.1
z > -200	NE	1.00	1.00	0.038	2.752	125.4	1.8	13.7	8.6E-11	1.35
	Gd	1.21	1.22	0.038	2.72	339.1	87	7.2	4.0E-9	0.8
	Hz	0.95	0.96	0.038	2.55	127.5	83.7	41.9	8.5E-10	1.35
Deep <sup>1)</sup>	Set	P <sub>32</sub> (r <sub>0</sub> , 169 m)	P <sub>32</sub> Tot	r <sub>0</sub>	k <sub>r</sub>	Tr	PI	Fisher κ	a	b
m (RHB70)	EW	1.06	1.07	0.038	2.585	4.8	13.9	10.1	7.1E-13	2.5
-200 ≥ z	NW	0.67	0.67	0.038	2.597	233.8	7.2	13.7	1.5E-10	1.31
z > -1,100	NE	1.03	1.03	0.038	2.75	125.4	1.8	13.7	1.6E-10	1.25
	Gd	1.49	1.49	0.038	2.7	339.1	87	7.2	1.4E-10	1.7
	Hz	0.75	0.75	0.038	2.75	127.5	83.7	41.9	1.3E-9	1.25

<sup>1)</sup> Based on data characteristics and borehole coverage the boundary between the Repository and Deep domains is changed to -200 m elevation. In the v. 0.2 model the boundary was set to -245 m elevation, based on the preliminary geometrical modelling of ZFM871 (SFR geologic model v.0.1).

<sup>2)</sup> The smallest modelled deterministic zones are on the order 300 m (SFR geologic model v.1.0), corresponding to a radius of 169 m. Stochastic fractures are therefore assumed to have a maximum radius of 169 m.

<sup>3)</sup> Taken from the preliminary Hydro-DFN v. 0.2.

<sup>4)</sup> Global orientation model used for all three depth domains.

As a final consistency check, the simulated borehole exploration is compared to the available data in the uppermost 130 m of KFR27. For several reasons, these data (5 m sequential PFL data; blue dots in Figure G-19) were excluded from the DFN calibration (see section G.1.6). On the other hand, the borehole has a central location with respect to the planned SFR extension, which motivates a particular evaluation of DFN realizations against available data. The transmissivity of intersected connected open fractures in simulated borehole exploration was summed over 5 m intervals and compared against the available 5 m sequential PFL data (Figure G-19). Note that only 19 such 5 m intervals remain after excluding intervals intersected by SBA1, SBA2 and ZFMWNW0835. Overall, the agreement is reasonable for both the Connectivity analysis and Tectonic continuum cases. However, it can be noted that a number of realisations have a very high upper tail transmissivity (half the realisations have a record exceeding  $T = 10^{-5} \text{ m}^2/\text{s}$ ), and that the number of intervals below detection limit tends to underestimated (5 records in data, versus typically 2 in simulations). Thus, the impression is that the parameterised Hydro-DFN is somewhat pessimistic (conservative).

An alternative transmissivity parameterisation is provided based on the inclusion of KFR106 PFL-f data (Section G.1.9). The adjusted parameters are provided in Table G-7 and the corresponding calibration to PFL-f data are presented in section G.5.4. It should be noted that only the transmissivity-size relationship is adjusted (orientation, intensity, and size models are identical to Table G-5 and Table G-6, respectively). The primary focus is the transmissivity of sets Hz and Gd, which have been identified as the most significant components of the Hydro-DFN model.

In comparison to boreholes inside the Local SFR model domain, the PFL-f transmissivity of KFR106 is *high* in the Repository Domain, but *low* in the Shallow and Deep domains. Consequently, inclusion of KFR106 in the DFN parameterisation causes an *increase* in modelled intensity/transmissivity of connected Open fractures in the Repository domain, but a slight *reduction* in the Shallow domain (Table G-7). In terms of relative borehole coverage (Figure G-7), the contribution from KFR106 is the highest in the Shallow domain (17%), and lowest in the Deep domain (12%). The Deep domain is dominated by PFL-f data in KFR27 and KFR102A. The inclusion of KFR106 data did not require an updated parameterisation for the Deep domain (Table G-7; Figure G-32).

**Table G-7. Hydro-DFN model adjustments to include KFR106 ( $T = a \text{ rb}$ ).**

	Set	Connectivity analysis		Tectonic continuum	
		a	b	a	b
Shallow domain	Gd	–	–	1.6E–8	1.3
	Hz	8.1E–8	1.25	8.6E–8	1.35
Repository domain	EW	3.2E–9	1.1	1.2E–10	1.4
	NE	3.2E–9	1.3	1.5E–10	1.35
	Gd	5.9E–9	0.95	5.5E–9	0.95
	Hz	1.5E–9	1.35	1.2E–9	1.5

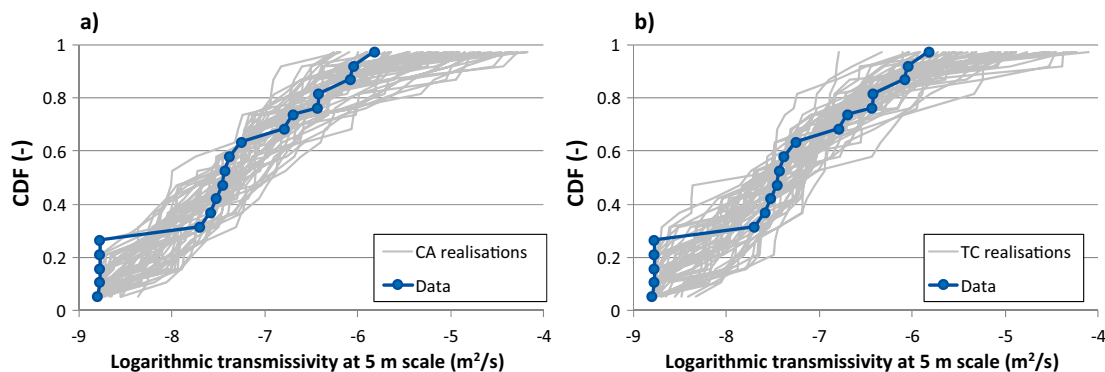


**Figure G-19.** Simulated transmissivity in the upper 130 m of KFR27. PFL data measured over 5 m borehole intervals versus simulated borehole exploration in 50 realisations. Two methods to fit the size-scaling exponent,  $k_r$ , are compared: Connectivity Analysis (CA) and Tectonic Continuum (TC). Intervals intersected by SBA1, SBA2 and ZFMWNW0835 are excluded.

### G.5.1 Pooled borehole calibration (base case)

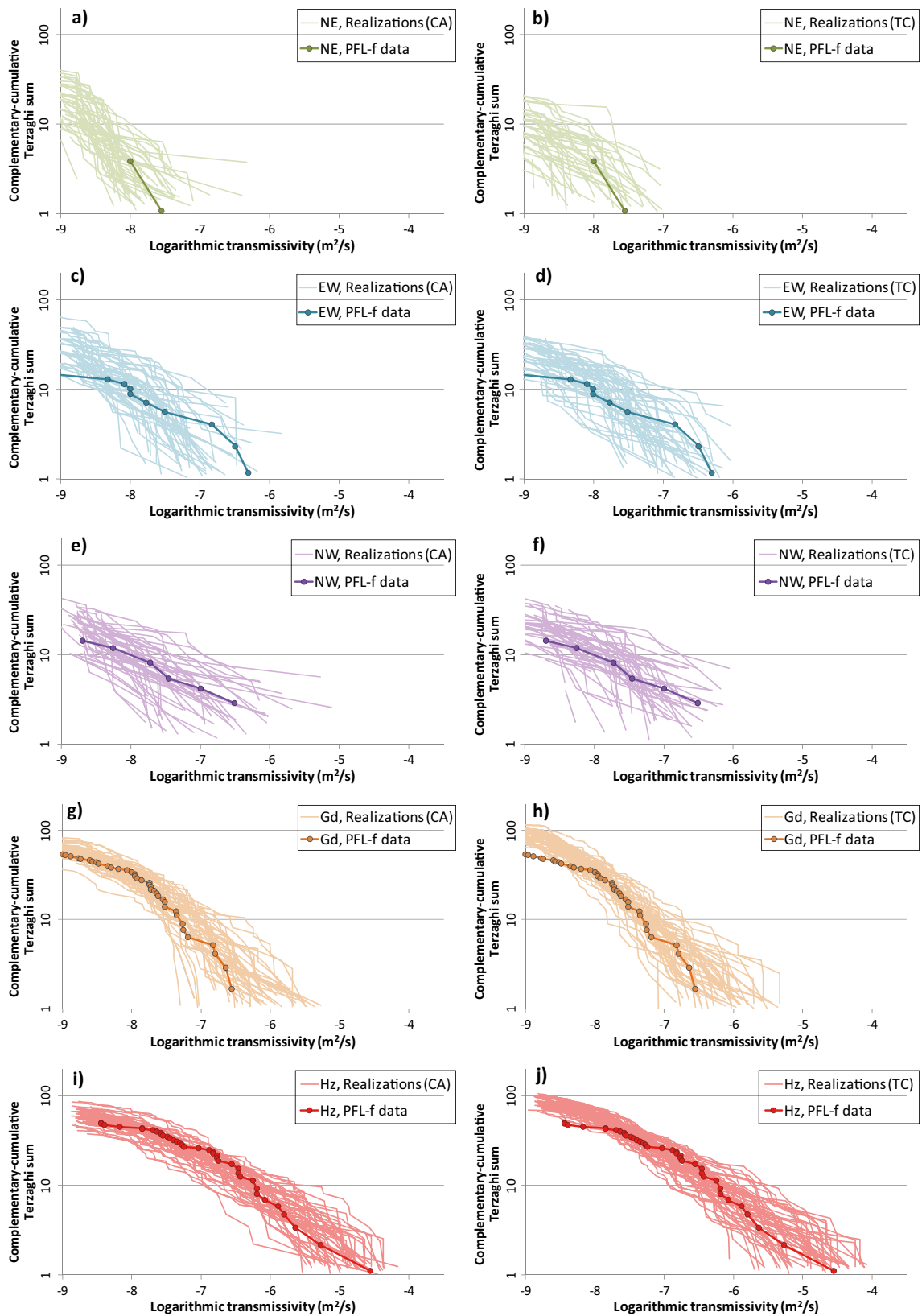


**Figure G-20.** Shallow domain, excluding KFR106 and assuming 0.3 m PFL resolution. Set-wise PFL-f transmissivity distributions versus simulated borehole exploration of connected open fractures in 50 realisations. Two methods to fit the size-scaling exponent,  $k$ , are compared: Connectivity Analysis (CA) and Tectonic Continuum (TC).



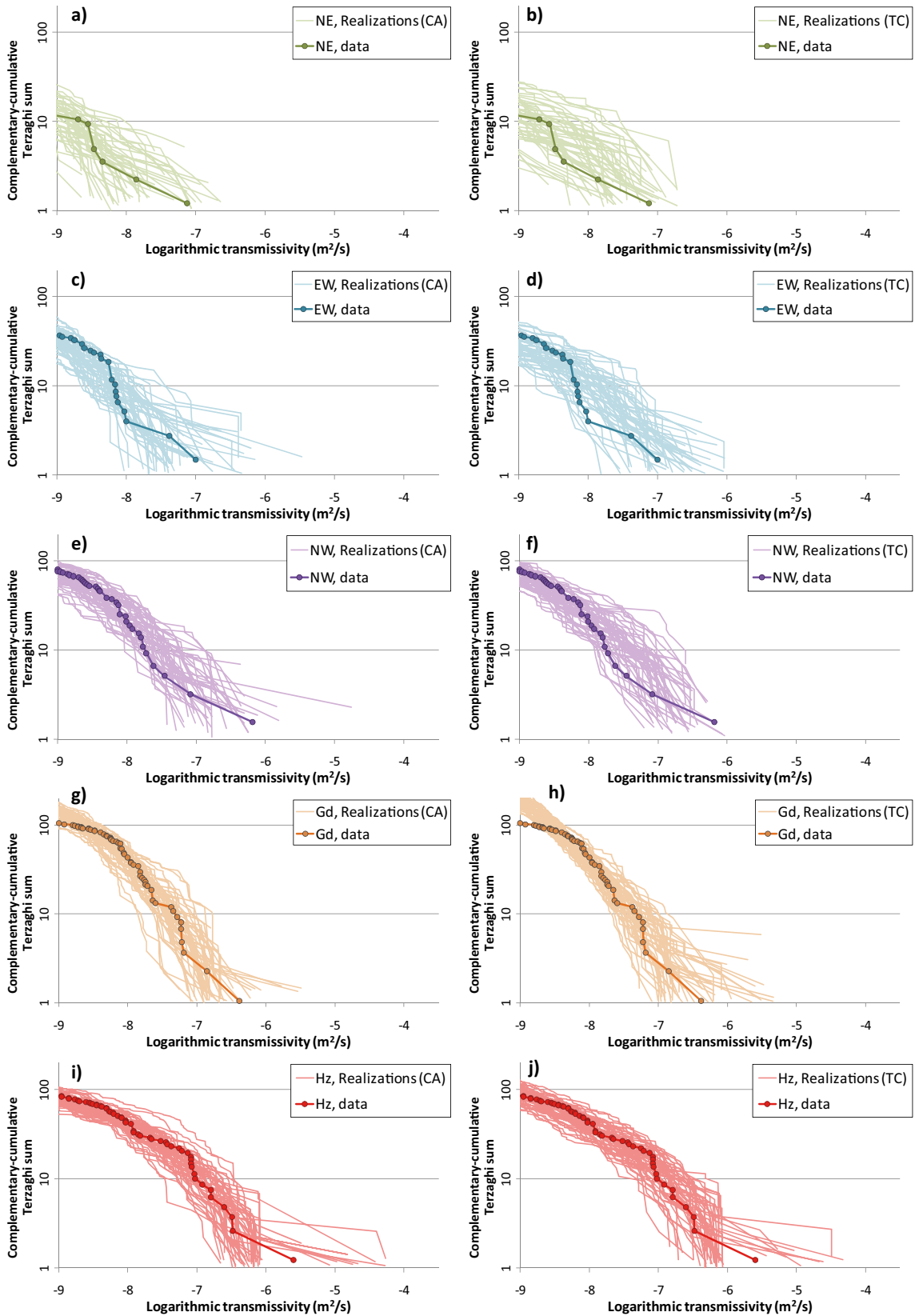


**Figure G-21.** Repository domain, excluding KFR106 and assuming 0.3 m PFL resolution. Set-wise PFL- $f$  transmissivity distributions versus simulated borehole exploration of connected open fractures in 50 realisations. Two methods to fit the size-scaling exponent,  $k_p$ , are compared: Connectivity Analysis (CA) and Tectonic Continuum (TC).

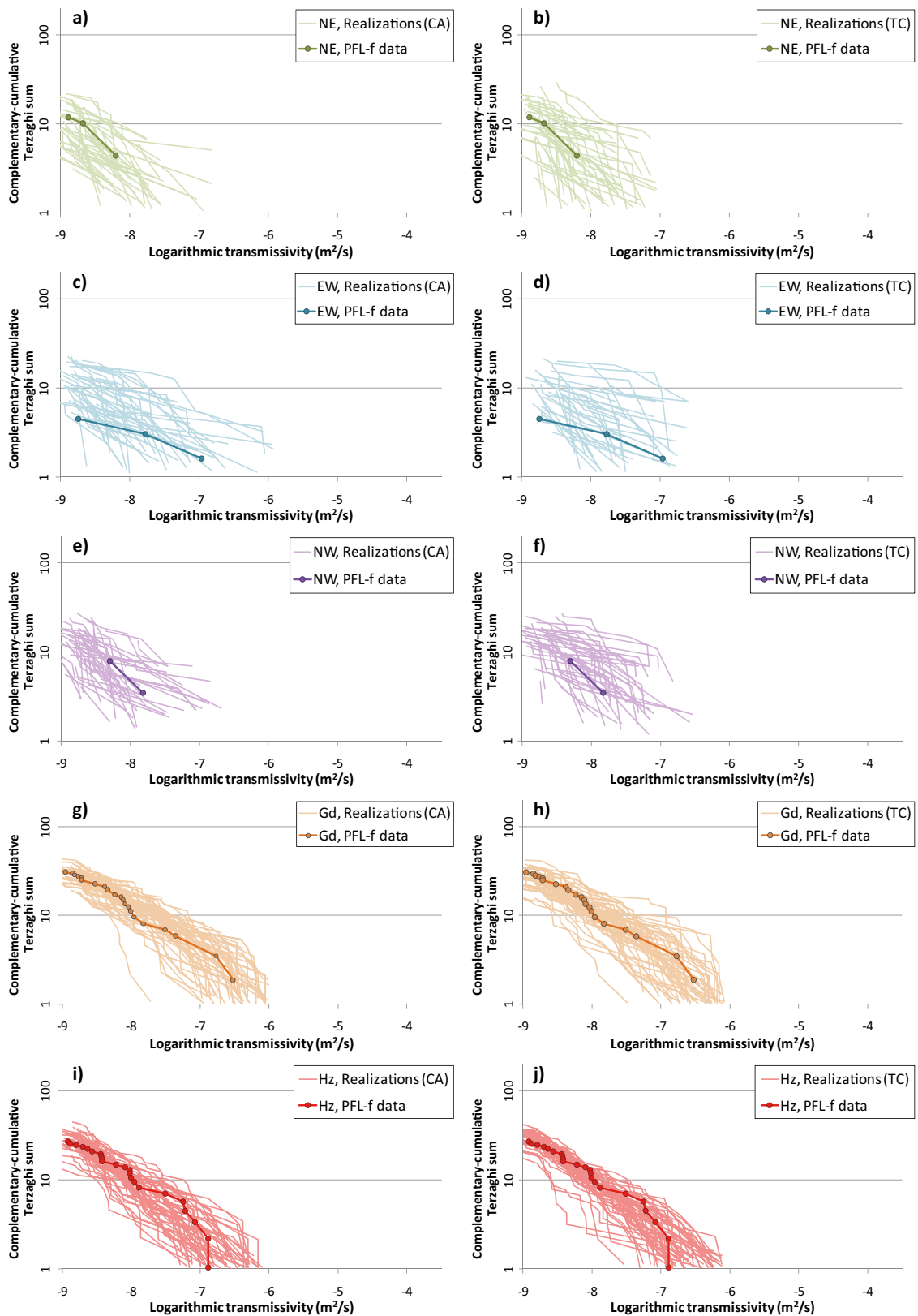


**Figure G-22.** Deep domain, excluding KFR106 and assuming 0.3 m PFL resolution. Set-wise PFL-f transmissivity distributions versus simulated borehole exploration of connected open fractures in 50 realisations. Two methods to fit the size-scaling exponent,  $k_r$ , are compared: Connectivity Analysis (CA) and Tectonic Continuum (TC).

### G.5.2 Evaluation on orientation basis (base case)

The orientation pattern of simulated borehole exploration is evaluated on pooled borehole basis. No systematic discrepancy can be identified between simulations and PFL-f data, neither for the Connectivity analysis, nor for the Tectonic continuum approach (Figure G-23).

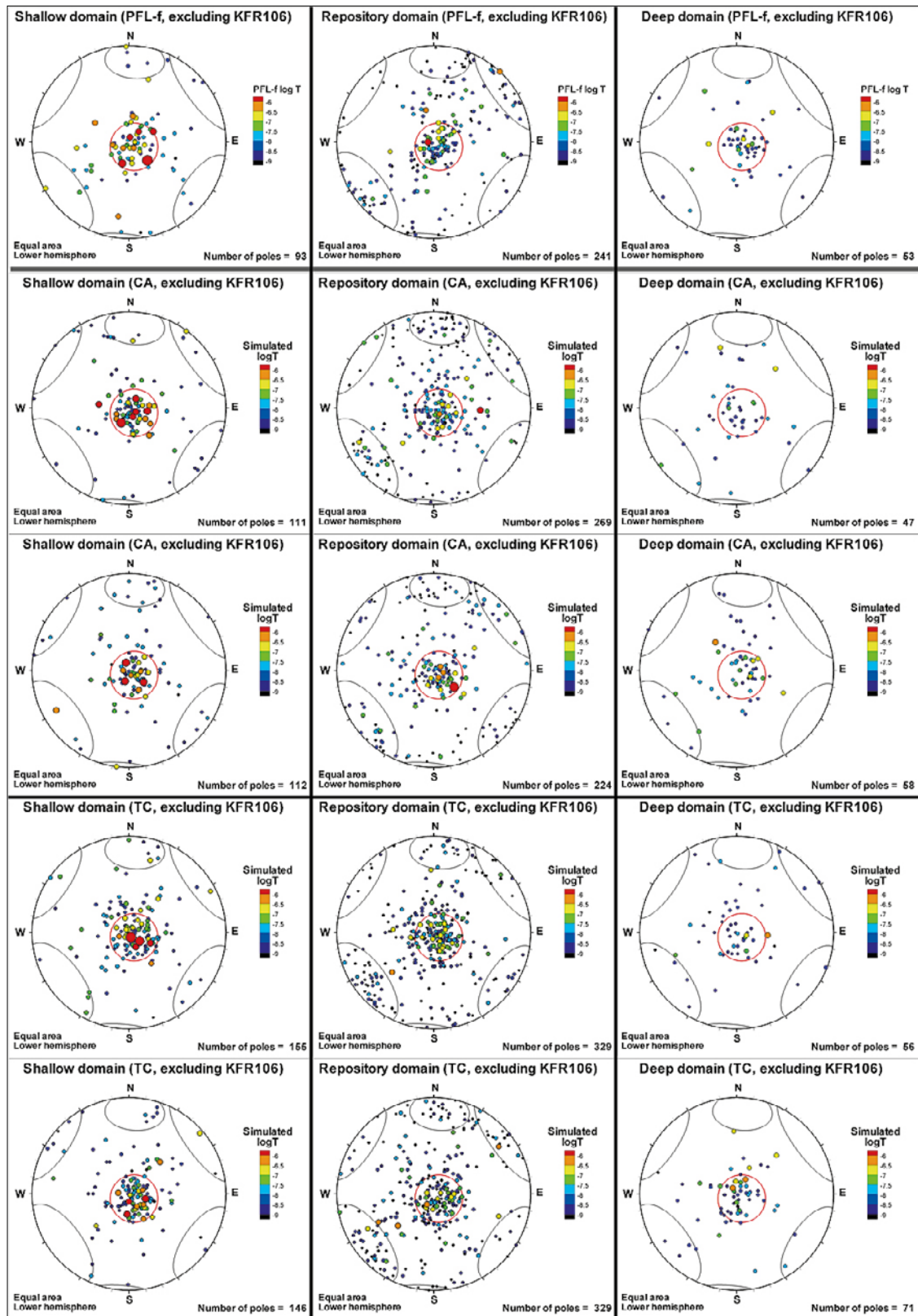


Figure G-23. Stereograms of PFL-f data (top row) in depth domains versus simulated borehole exploration realisations based on Connectivity Analysis (CA) and Tectonic Continuum (TC).

### G.5.3 Evaluation on borehole basis (base case)

The DFN parameterisation is calibrated on pooled borehole basis, and thus does not address variability between boreholes within a depth domain. In other words, the DFN model is not designed to reproduce deviant hydraulic characteristics observed at individual borehole scale. Thus, the cross-borehole variability observed in data may relate factors not addressed in the DFN model, such as the hypothesised large-scale transmissivity trend (Chapter 5, main report) or simply local heterogeneities in the bedrock. However, to some extent the variability between boreholes may be geometrically related, such as geometrical sampling bias and the borehole orientation versus the surrounding deformation zones (i.e. which control the connected flowing fracture network). Therefore, comparisons are made between the expectation value in the simulated borehole exploration (average of 50 realisations) and PFL-f data on individual borehole scale.

The evaluations on borehole basis are made in terms of transmissivity distributions, divided into sets, depth domains, and boreholes. The primary focus is on the upper tail of transmissivity distributions as these have the most significant impact in the hydrogeological model (i.e. primarily sets Gd and Hz, with transmissivities exceeding  $10^{-6}$  m<sup>2</sup>/s). The x-axis of the histograms reflect logarithmic transmissivity bins, which are labelled by their mid-values (e.g. “-6” refers to values in the range  $-6.5 < \log T \leq -5.5$ ). The y-axis of the histograms show Terzaghi sum of bins, Eq. (G-2); these do not require borehole-length normalisation as the simulated borehole length is equivalent to the underlying data (i.e. PFL-logged length outside deterministic deformation zones, Unresolved PDZs, and deterministic SBA-structures).

The evaluation of the Shallow, Repository, and Deep domains is demonstrated for the Connectivity analysis (Figure G-24, Figure G-25, and Figure G-26, respectively), as well as, for the Tectonic continuum approach (Figure G-27, Figure G-28, and Figure G-29, respectively). The Repository domain is covered by several closely located boreholes with similar characteristics. To condense the comparisons somewhat, the boreholes located close to the tip of the Pier, KFR101, KFR102A, KFR102B, and KFR103, are pooled into a group referred to as “KFR101 to KFR103” and compared to boreholes of the Central block (KFR104 and KFR105; Figure G-25 and Figure G-28). The PFL-f data are fairly well reproduced by simulated borehole exploration when *all boreholes are pooled* (i.e. the underlying calibration criterion; see Figure G-25d and Figure G-28d). On borehole basis, some deviating patterns observed in PFL-f data are reproduced in simulated borehole exploration (inferred as geometrical artefacts), whereas other patterns are not (inferred as local heterogeneity, or possibly lateral trend). For example, the relative dominance of steeply dipping sets over set Hz in KFR105 is partly reproduced in the model (cf. Figure G-25a and c), and thus partly relate to sampling bias (in spite of Terzaghi weighing). On the other hand, set Hz is underestimated in “KFR101 to KFR103” and overestimated in KFR105 (cf. Figure G-25a and c), which suggests that the observed patterns in data are not only an effect of geometrical sampling bias.

In fact, the systematic overestimation of set Hz in the Central block (KFR104 and KFR105) and its underestimation at the tip of the Pier (KFR101 to KFR103) is common to all depth domains. The reason for this is that the interpreted large-scale trend with increasing transmissivity towards the Northern boundary belt (or potentially the structural wedge) is not implemented in the DFN model. However, it should be pointed out that, as stated in sections G.1.2 and G.1.8, it is unclear if the observed trend in PFL-f data reflects an *actual lateral trend* (i.e. properties at the individual fracture scale), or an *apparent transmissivity trend* (i.e. scale-dependent effective properties of flow paths; see discussions on the role of PFL data subject to hydraulic chokes in Öhman and Follin (2010b)).

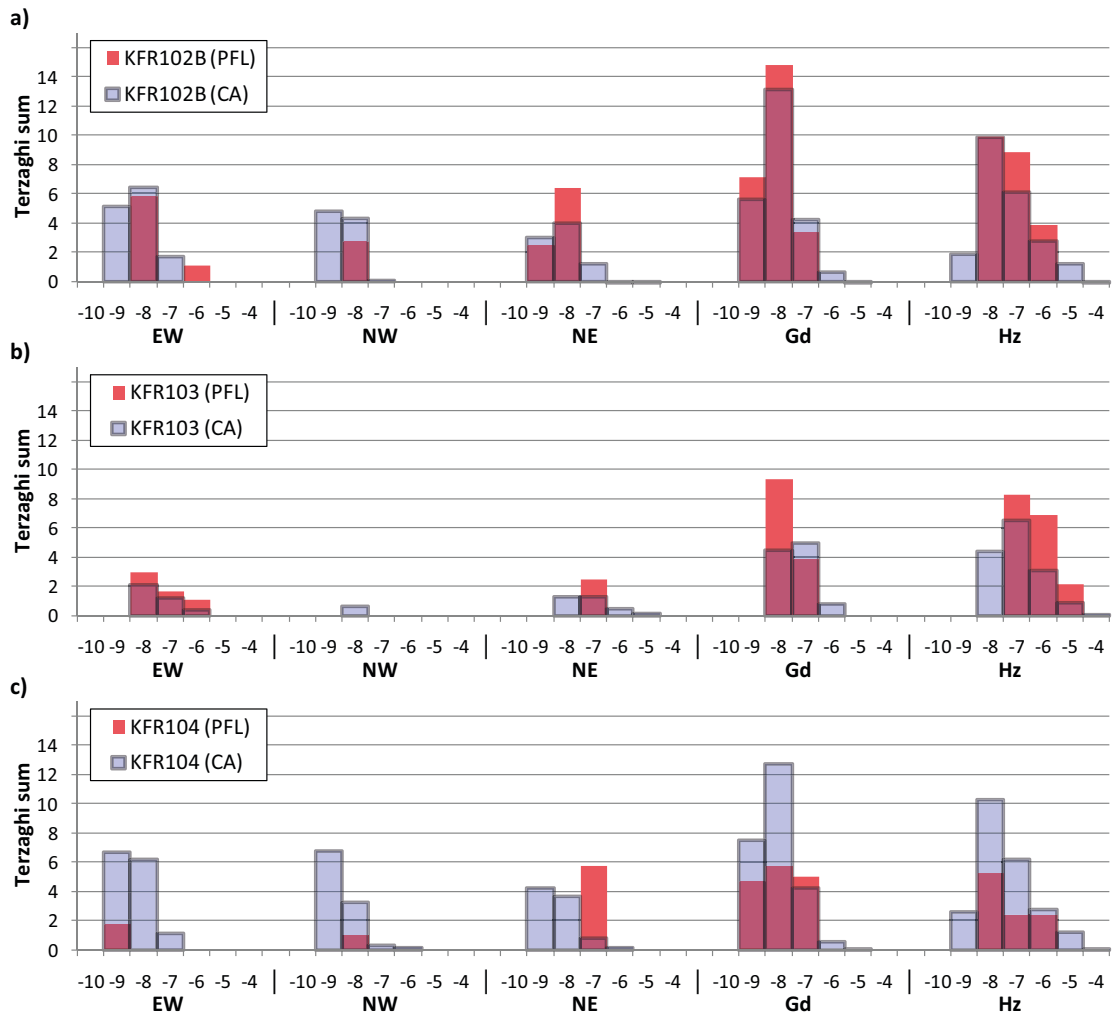


**Figure G-24.** Borehole-wise evaluation for Shallow domain for size-scaling exponent,  $k$ , determined by Connectivity Analysis (CA). Transmissivity distributions of PFL-f data and mean of 50 simulated borehole explorations of connected open fracture realisations.

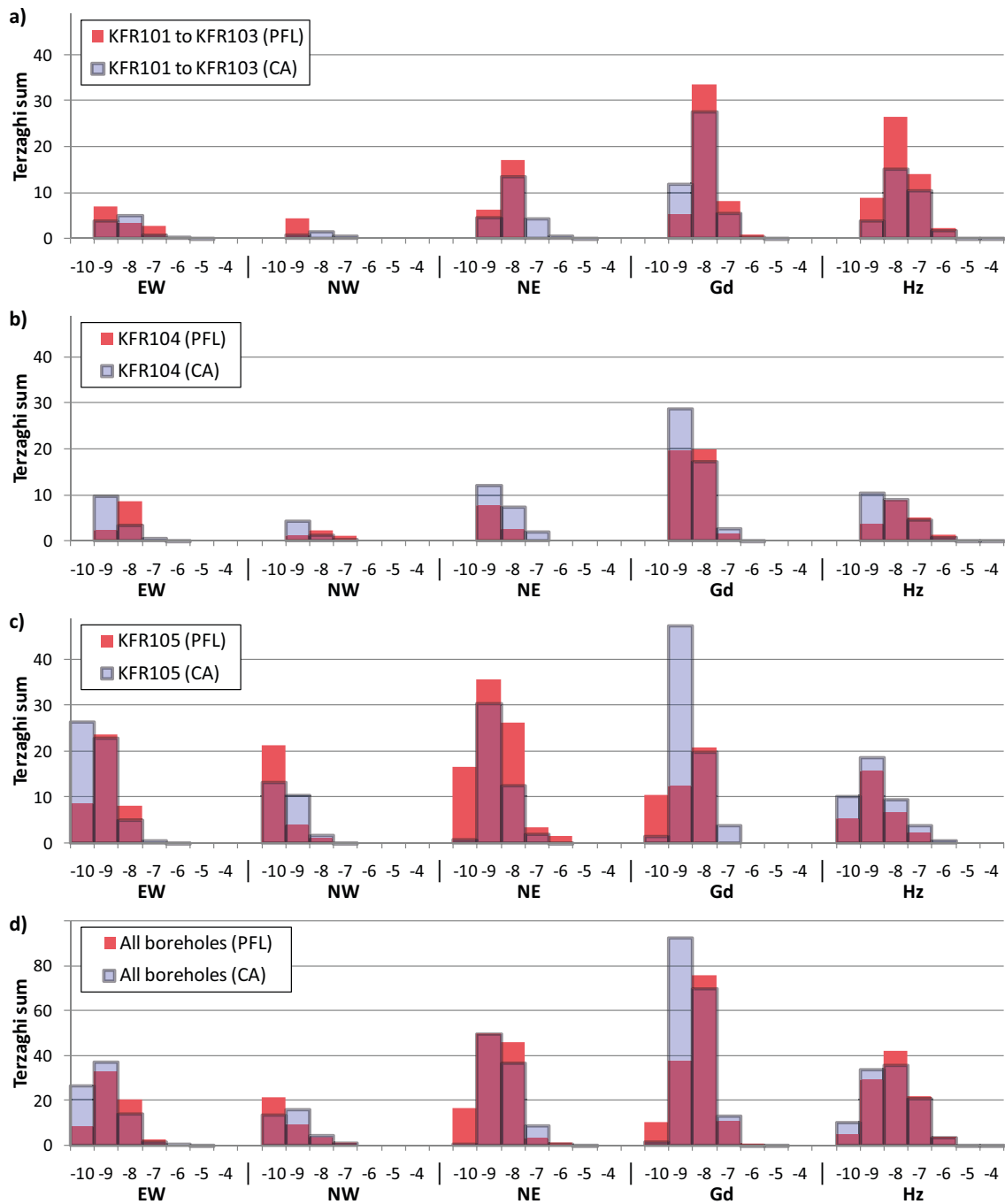


**Figure G-25.** Borehole-wise evaluation for Repository domain for size-scaling exponent,  $k_r$ , determined by Connectivity Analysis (CA). Transmissivity distributions of PFL-f data and mean of 50 simulated borehole explorations of connected open fracture realisations.

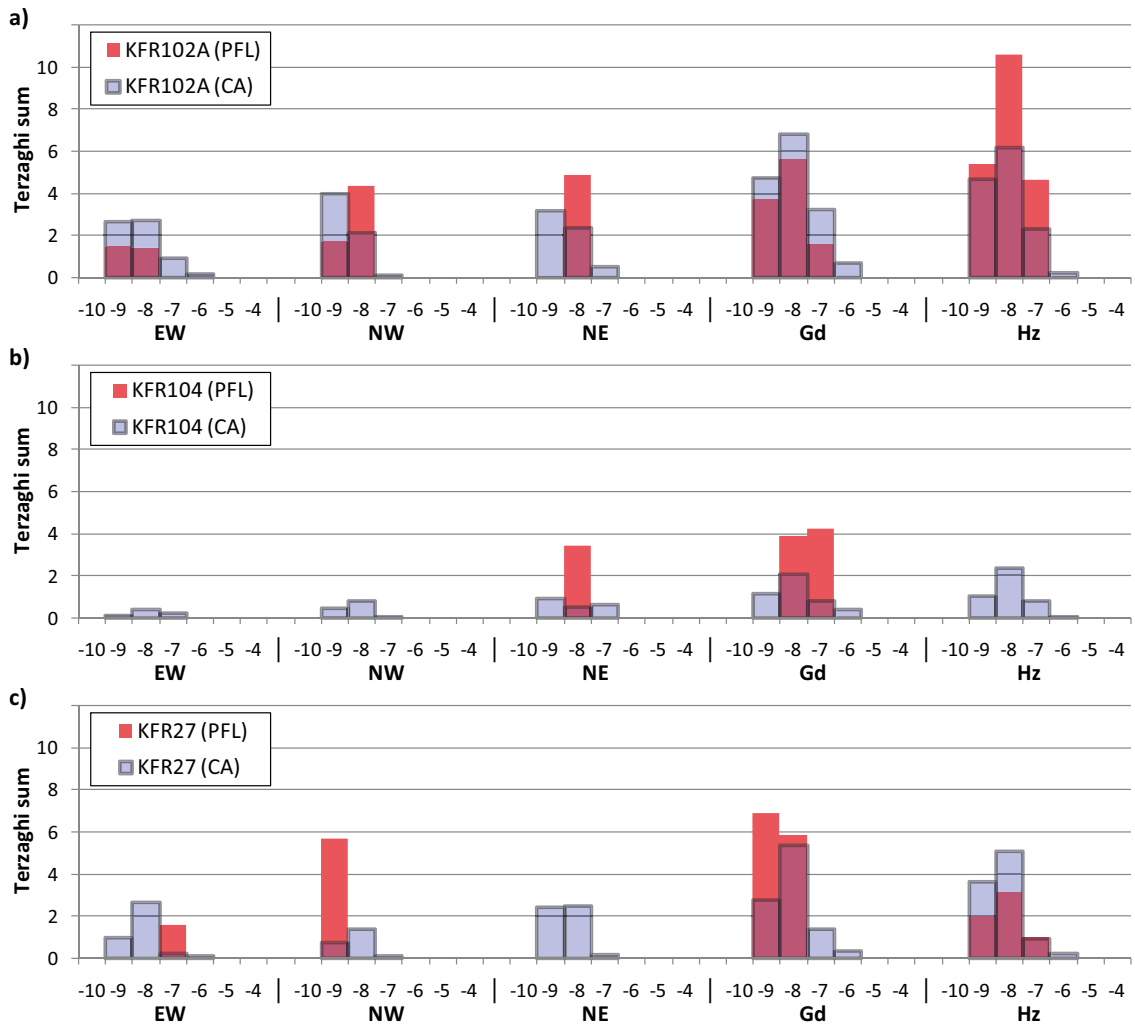


**Figure G-26.** Borehole-wise evaluation for Deep domain for size-scaling exponent,  $k_n$ , determined by Connectivity Analysis (CA). Transmissivity distributions of PFL-f data and mean of 50 simulated borehole explorations of connected open fracture realisations.

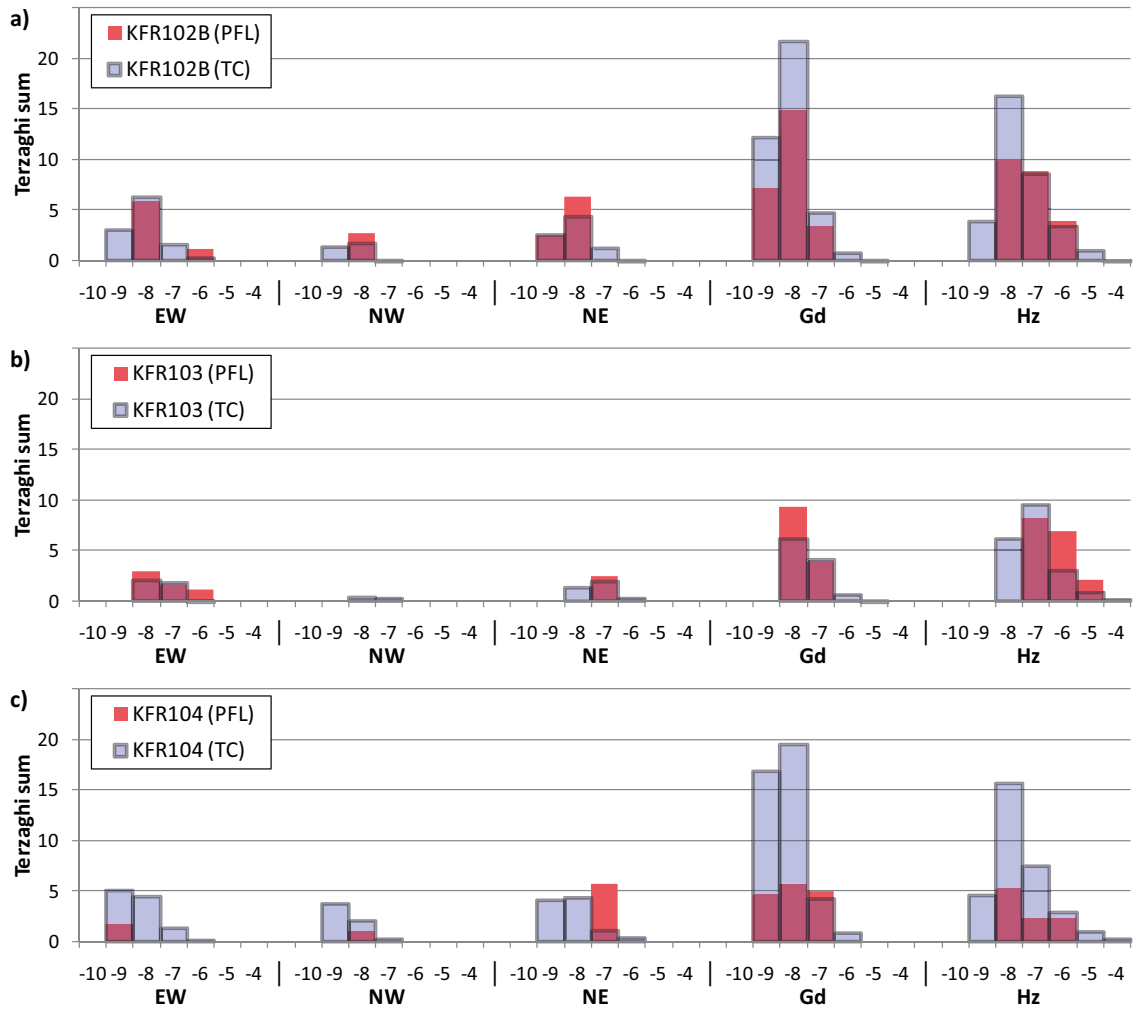


**Figure G-27.** Borehole-wise evaluation for Shallow domain for size-scaling exponent,  $k$ , determined by Tectonic Continuum (TC). Transmissivity distributions of PFL-f data and mean of 50 simulated borehole explorations of connected open fracture realisations.



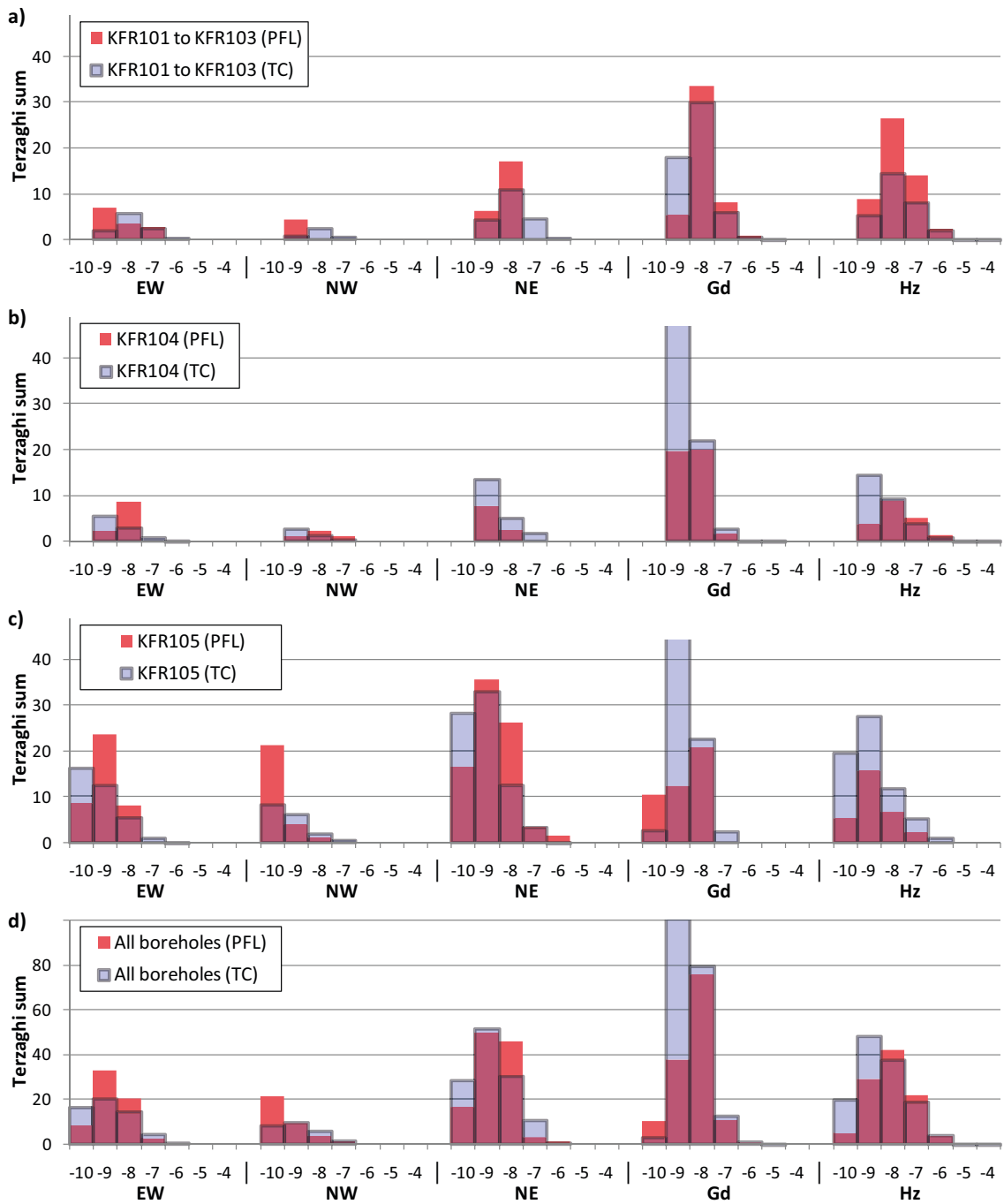


**Figure G-28.** Borehole-wise evaluation for Repository domain for size-scaling exponent,  $k$ , determined by Tectonic Continuum (TC). Transmissivity distributions of PFL-f data and mean of 50 simulated borehole explorations of connected open fracture realisations.

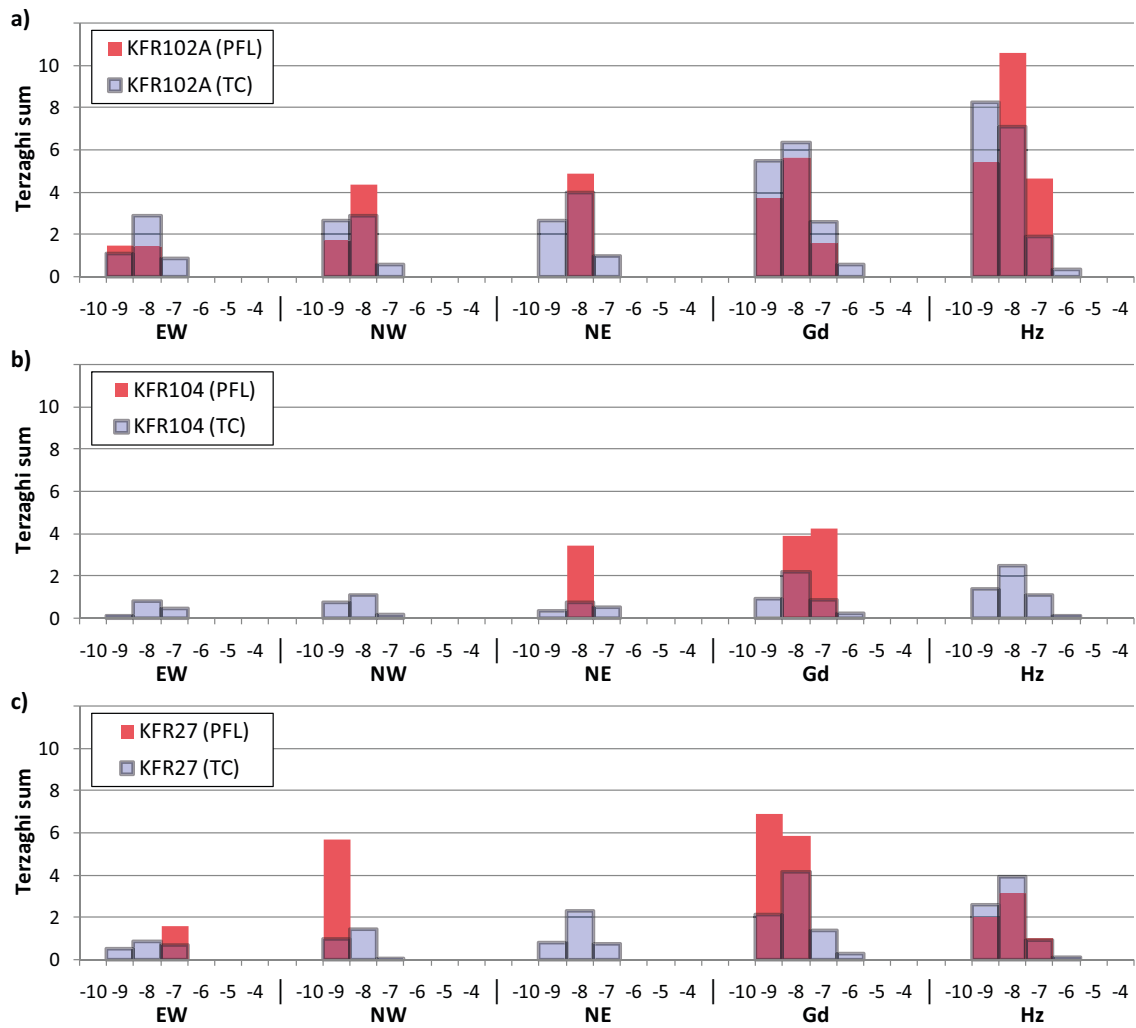


**Figure G-29.** Borehole-wise evaluation for Deep domain for size-scaling exponent,  $k$ , determined by Tectonic Continuum (TC). Transmissivity distributions of PFL-f data and mean of 50 simulated borehole explorations of connected open fracture realisations.

### G.5.4 Pooled borehole calibration, including KFR106

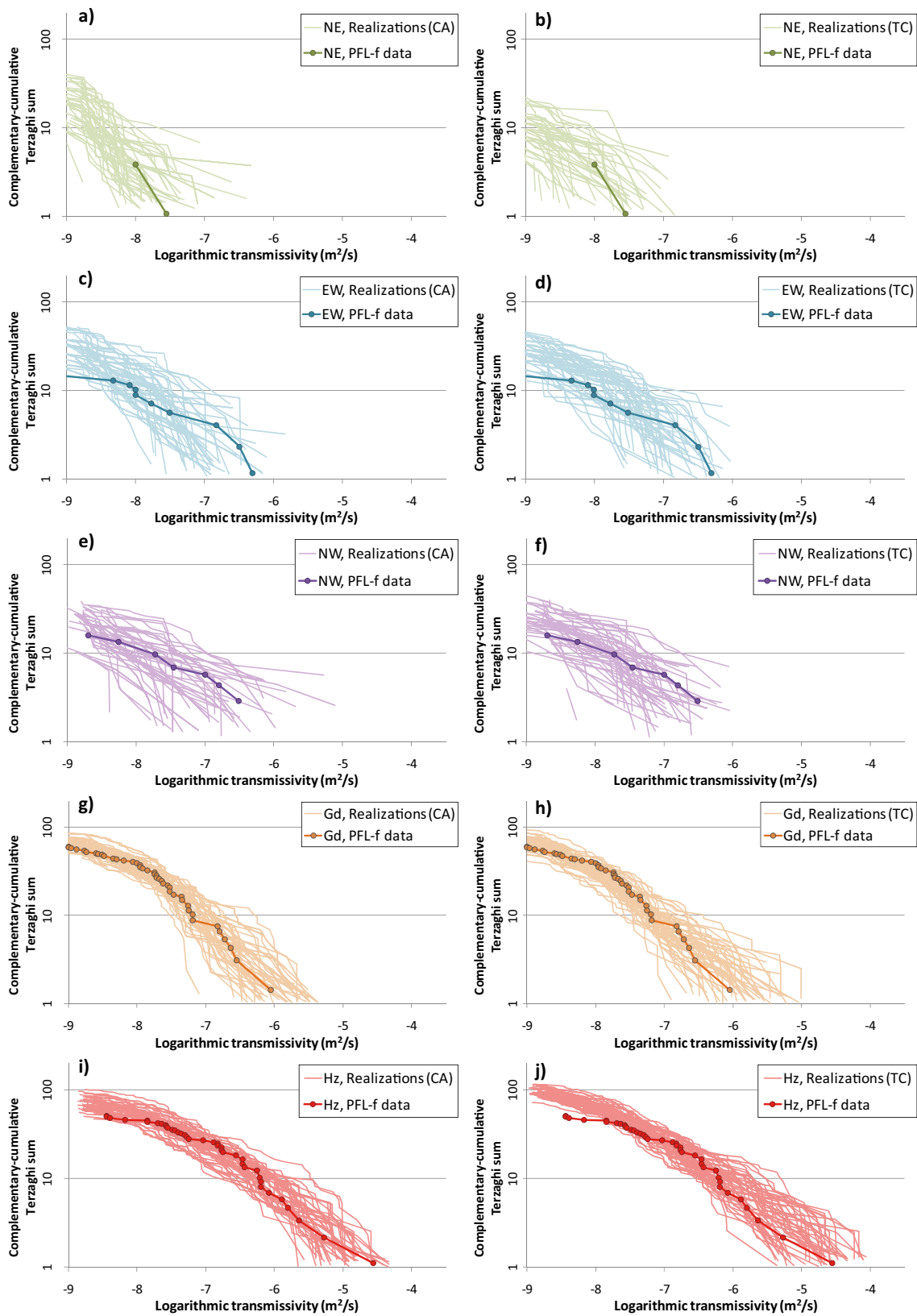


**Figure G-30.** Shallow domain, including KFR106 and assuming 0.3 m PFL resolution. Set-wise PFL-f transmissivity distributions versus simulated borehole exploration of connected open fractures in 50 realisations. Two methods to fit the size-scaling exponent,  $k_p$ , are compared: Connectivity Analysis (CA) and Tectonic Continuum (TC).

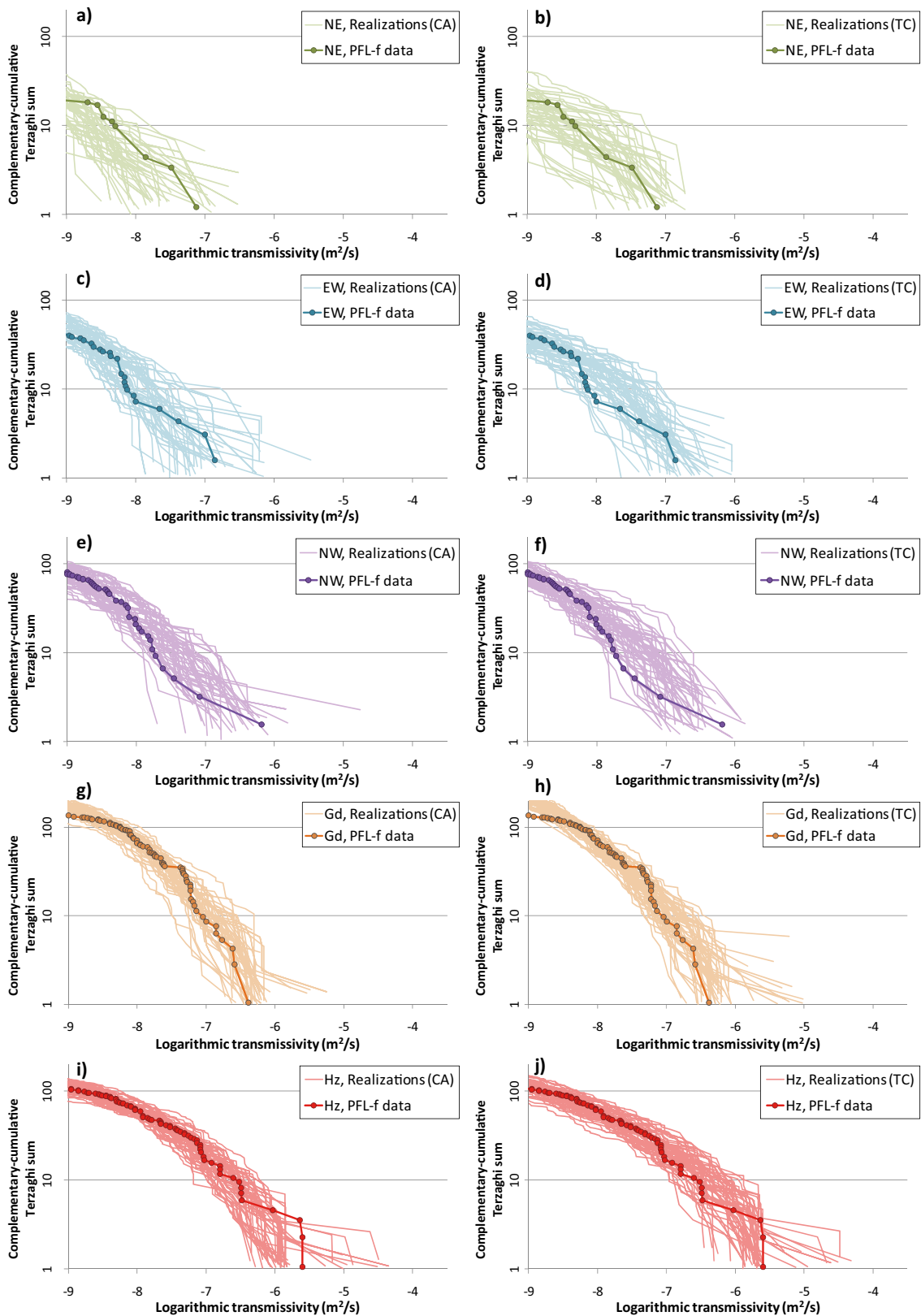


**Figure G-31.** Repository domain, including KFR106 and assuming 0.3 m PFL resolution. Set-wise PFL-f transmissivity distributions versus simulated borehole exploration of connected open fractures in 50 realisations. Two methods to fit the size-scaling exponent,  $k_r$ , are compared: Connectivity Analysis (CA) and Tectonic Continuum (TC).

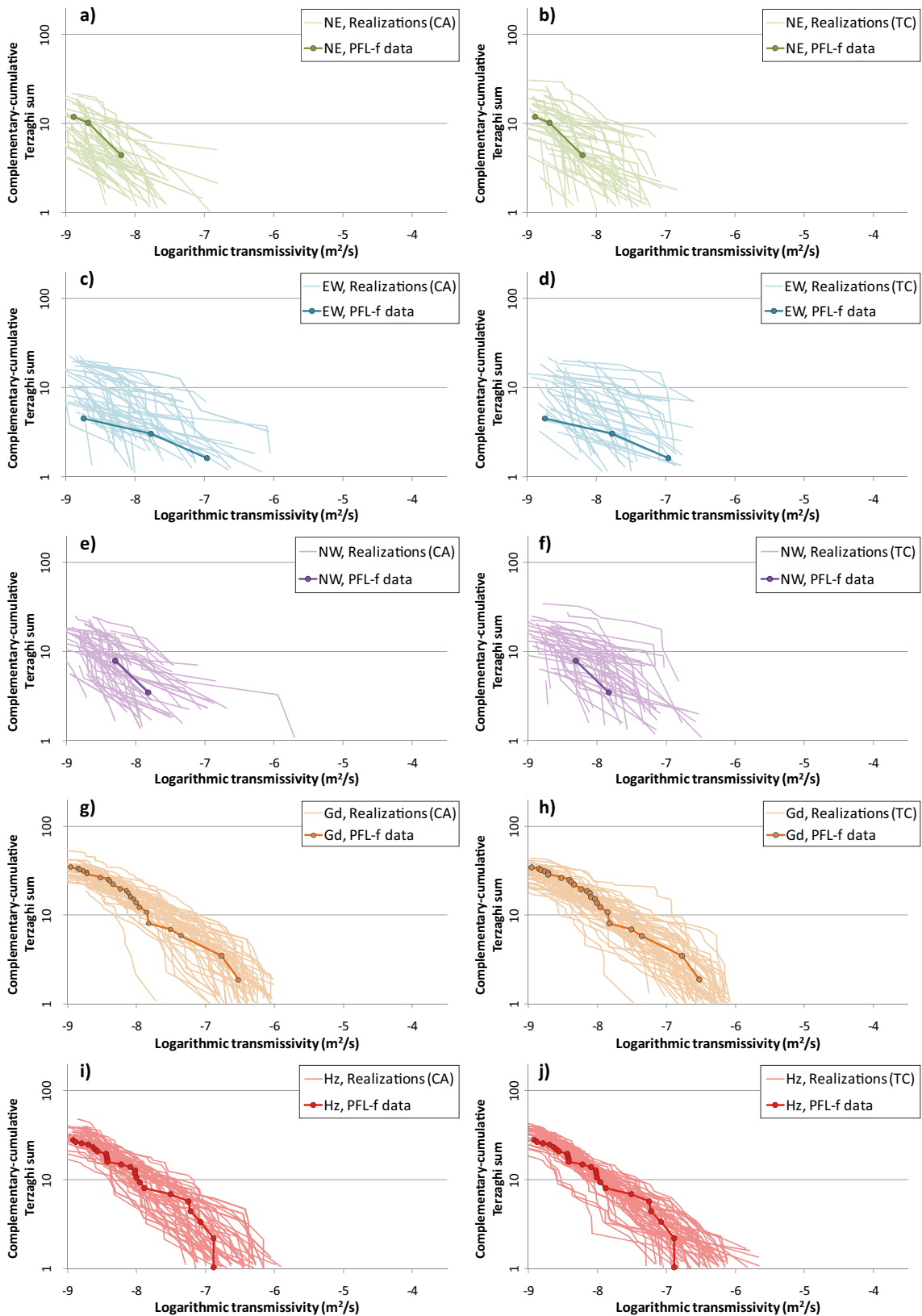


**Figure G-32.** Deep domain, including KFR106 and assuming 0.3 m PFL resolution. Set-wise PFL-f transmissivity distributions versus simulated borehole exploration of connected open fractures in 50 realisations. Two methods to fit the size-scaling exponent,  $k_n$ , are compared: Connectivity Analysis (CA) and Tectonic Continuum (TC).

The simulated orientation pattern is evaluated also for the case including KFR106 PFL-f data (Figure G-33). The discrepancy between simulations and data is judged to be within stochastic variability, i.e. similar to the simulations excluding KFR106 (Figure G-23).

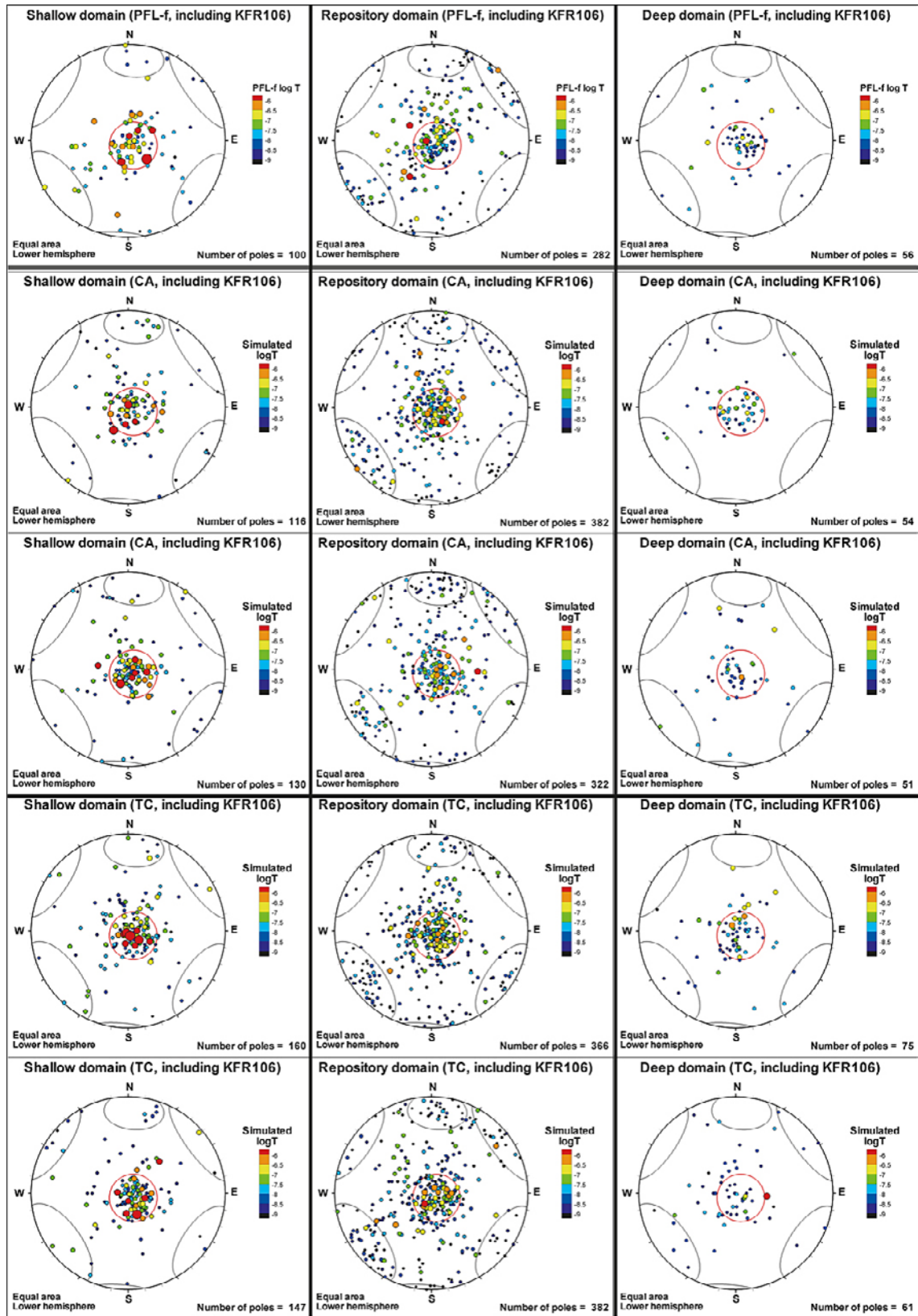


**Figure G-33.** Stereograms of PFL-f data (top row) in depth domains versus simulated borehole exploration realisations based on Connectivity Analysis (CA) and Tectonic Continuum (TC).

### G.5.5 Evaluation on borehole basis, including KFR106

The alternative parameterisation including KFR106 (i.e. Table G-7) is evaluated on individual borehole basis, similar the procedure in Section G.5.3. The PFL-f transmissivity distributions are compared to simulated borehole exploration (average of 50 realisations). The comparisons are made per set, depth domain, and borehole. To clarify some of the comparisons, closely located boreholes with similar characteristics are pooled: e.g. “KFR104 and KFR105”, or “KFR101 to KFR103”. The difference to the earlier evaluation (Section G.5.3) is that KFR106 is now included, both in the underlying PFL-f data, as well as, in the simulated borehole exploration. All three depth domains are represented in KFR106 (Figure G-7), although its coverage of the Shallow and Deep domains is relatively small (35.6 and 75.5 m, respectively). It should be noted that although KFR106 is the borehole with highest transmissivities at Repository depth (e.g. Figure G-35), its transmissivity data are low in the Shallow and Deep domains, and in fact very similar to KFR104 (Figure G-34 and Figure G-36).

The evaluation of the Shallow, Repository, and Deep domains is demonstrated for the Connectivity analysis (Figure G-34, Figure G-35, and Figure G-36, respectively), as well as, for the Tectonic continuum approach (Figure G-37, Figure G-38, and Figure G-39, respectively). The Repository domain is covered by many boreholes, therefore all boreholes located close to the tip of the Pier KFR101, KFR102A, KFR102B, and KFR103 are pooled. This pooled sample is referred to as “KFR101 to KFR103” and compared to boreholes of the Central block (KFR104 and KFR105; see Figure G-25 and Figure G-28).

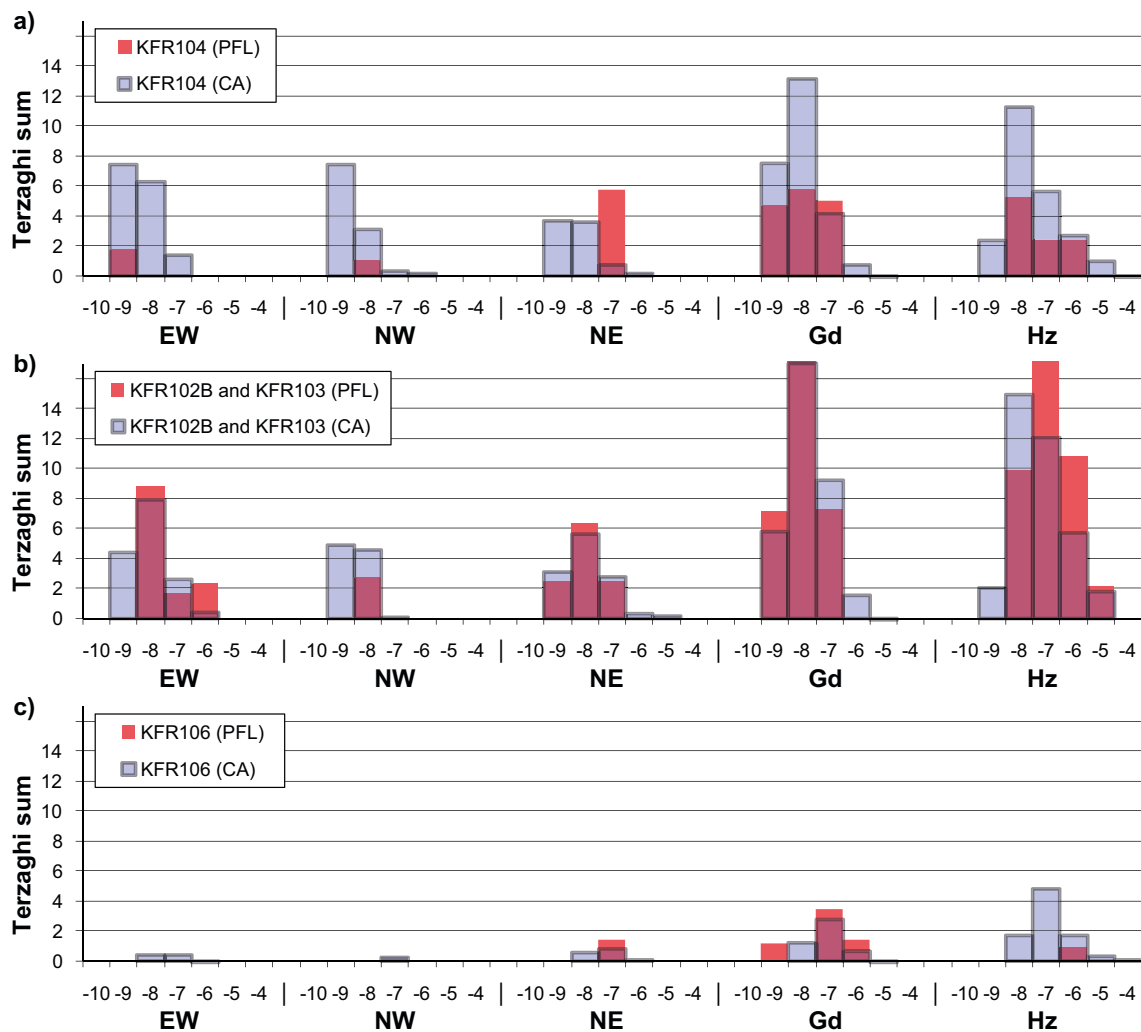


**Figure G-34.** Borehole-wise evaluation for Shallow domain for size-scaling exponent,  $k_s$ , determined by Connectivity Analysis (CA). Transmissivity distributions of PFL-f data and mean of 50 simulated borehole explorations of connected open fracture realisations.

Common for all depth domains is that set Hz is systematically overestimated in the Central block (KFR104 and KFR105), and underestimated at the tip of the Pier (KFR101 to KFR103). The reason for this is that the interpreted large-scale trend with increasing transmissivity towards the Northern boundary belt (or potentially the structural wedge) is not implemented in the DFN model. However, it should be pointed out that, as stated in sections G.1.2 and G.1.8, it is unclear if the observed trend in PFL-f data reflects an *actual lateral trend* (i.e. properties at the individual fracture scale), or an *apparent transmissivity trend* (i.e. scale-dependent effective properties of flow paths; see discussions on the role of PFL data subject to hydraulic chokes in Öhman and Follin (2010b)).

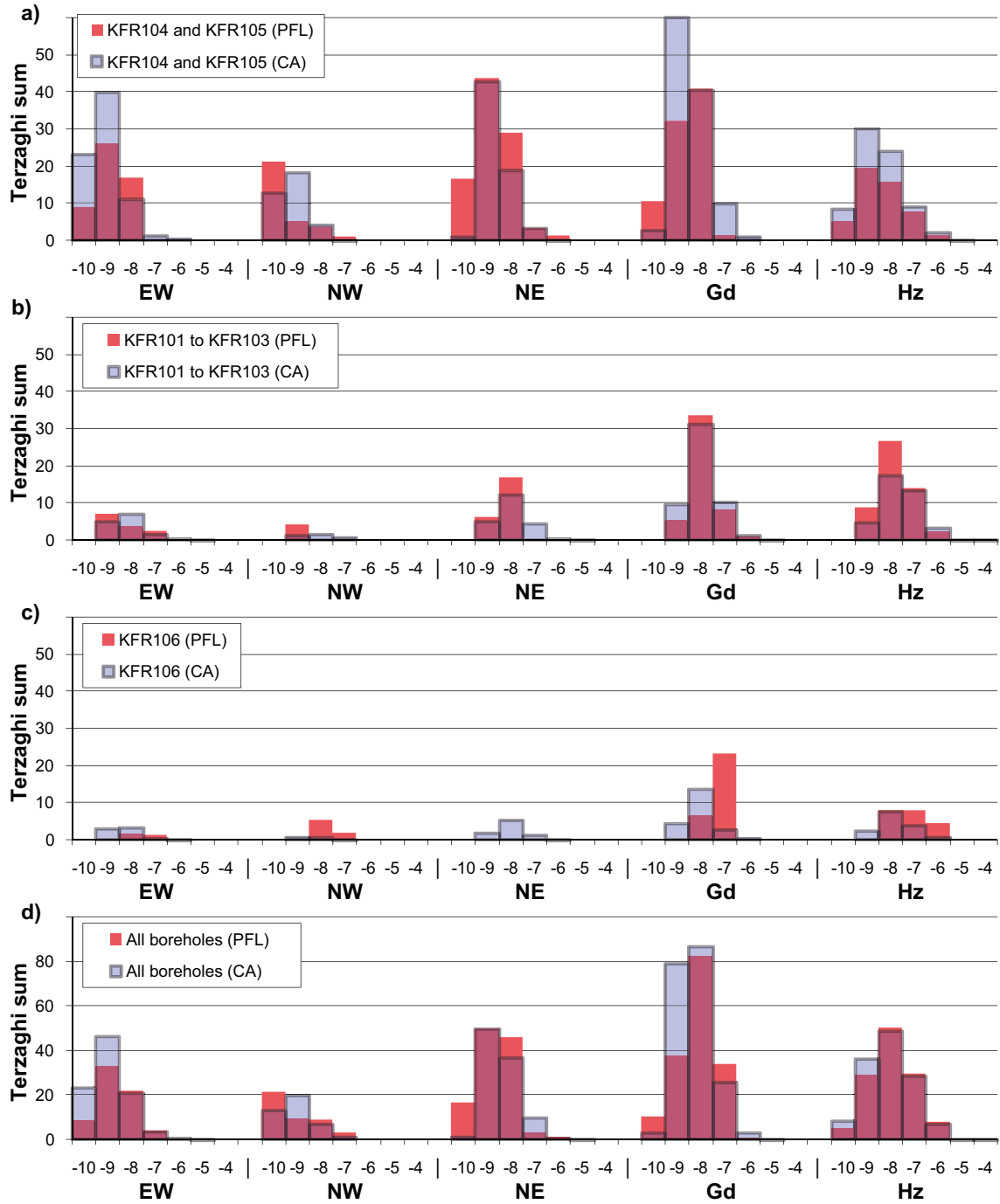


**Figure G-35.** Borehole-wise evaluation for Repository domain for size-scaling exponent,  $k_s$ , determined by Connectivity Analysis (CA). Transmissivity distributions of PFL-f data and mean of 50 simulated borehole explorations of connected open fracture realisations.



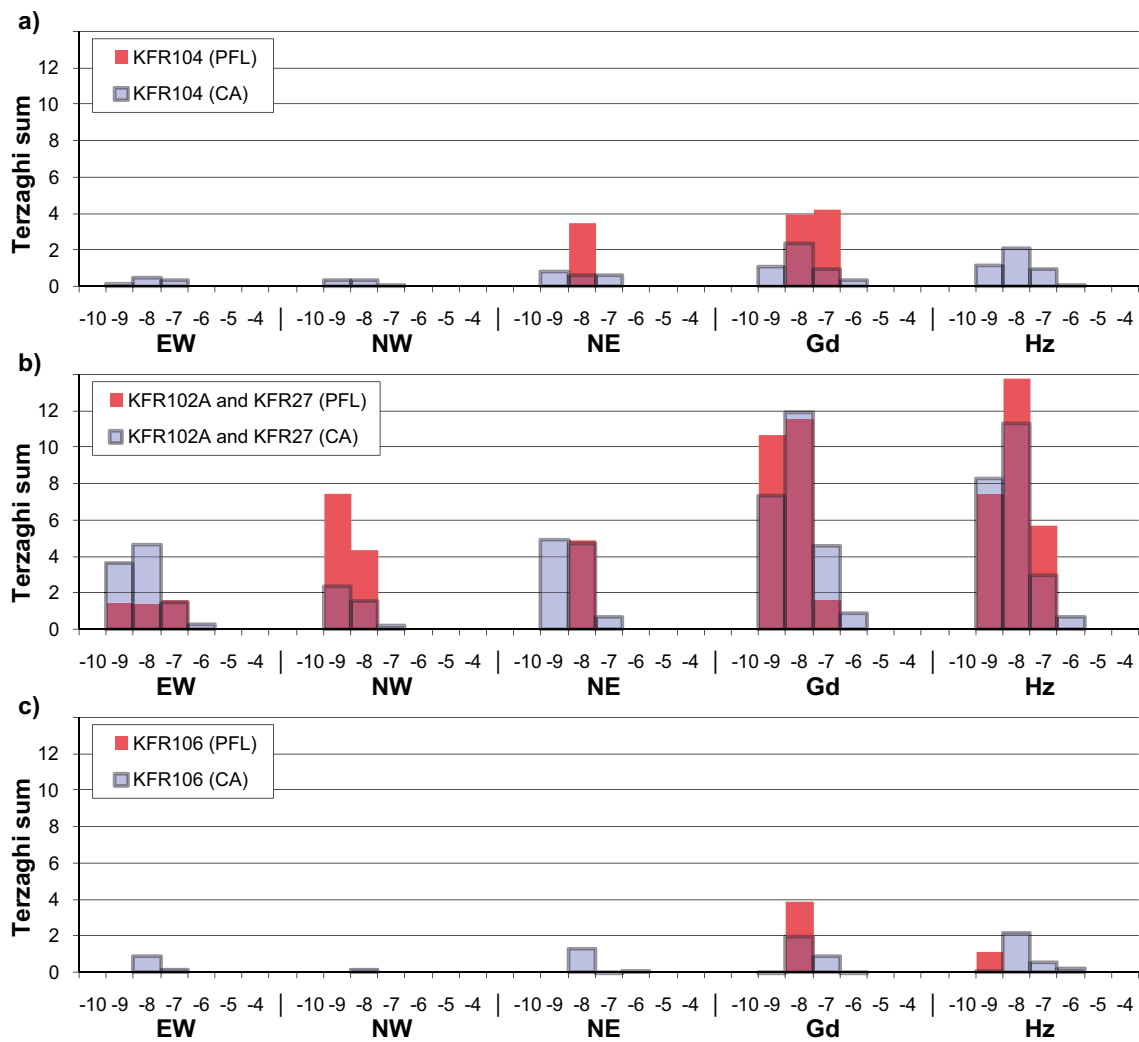


**Figure G-36.** Borehole-wise evaluation for Deep domain for size-scaling exponent,  $k_n$ , determined by Connectivity Analysis (CA). Transmissivity distributions of PFL-f data and mean of 50 simulated borehole explorations of connected open fracture realisations.

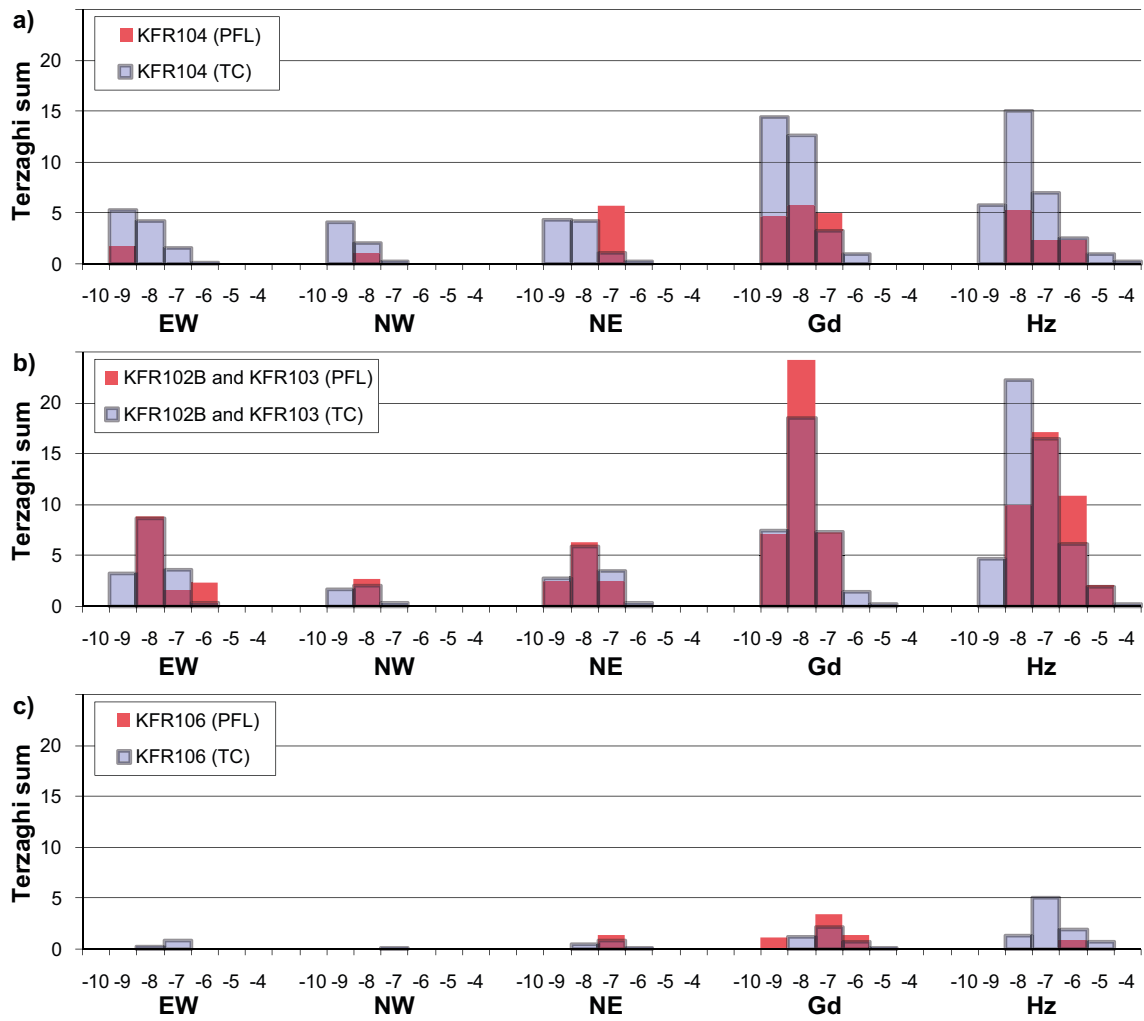


**Figure G-37.** Borehole-wise evaluation for Shallow domain for size-scaling exponent,  $k$ , determined by Tectonic Continuum (TC). Transmissivity distributions of PFL-f data and mean of 50 simulated borehole explorations of connected open fracture realisations.

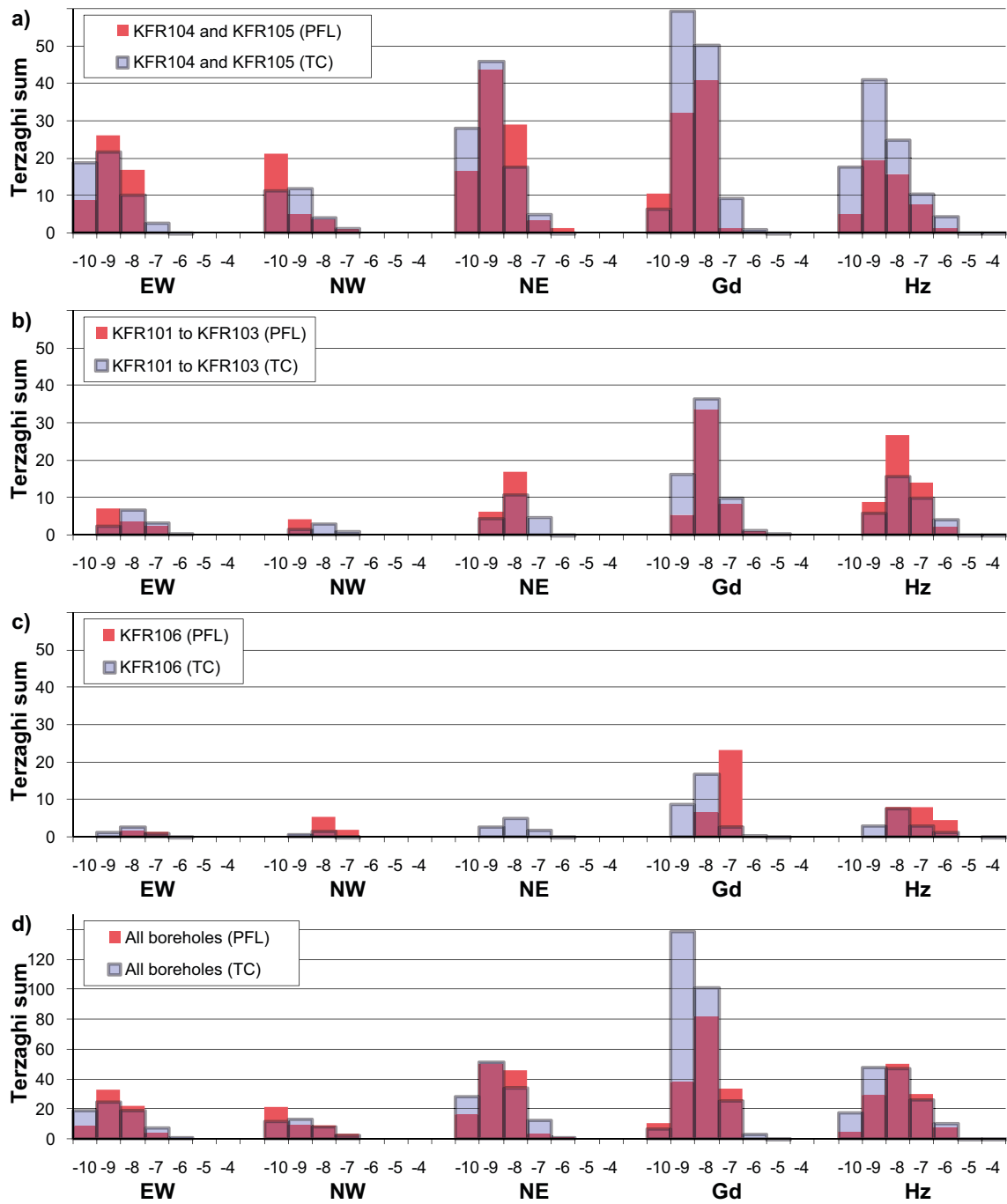


**Figure G-38.** Borehole-wise evaluation for Repository domain for size-scaling exponent,  $k$ , determined by Tectonic Continuum (TC). Transmissivity distributions of PFL-f data and mean of 50 simulated borehole explorations of connected open fracture realisations.

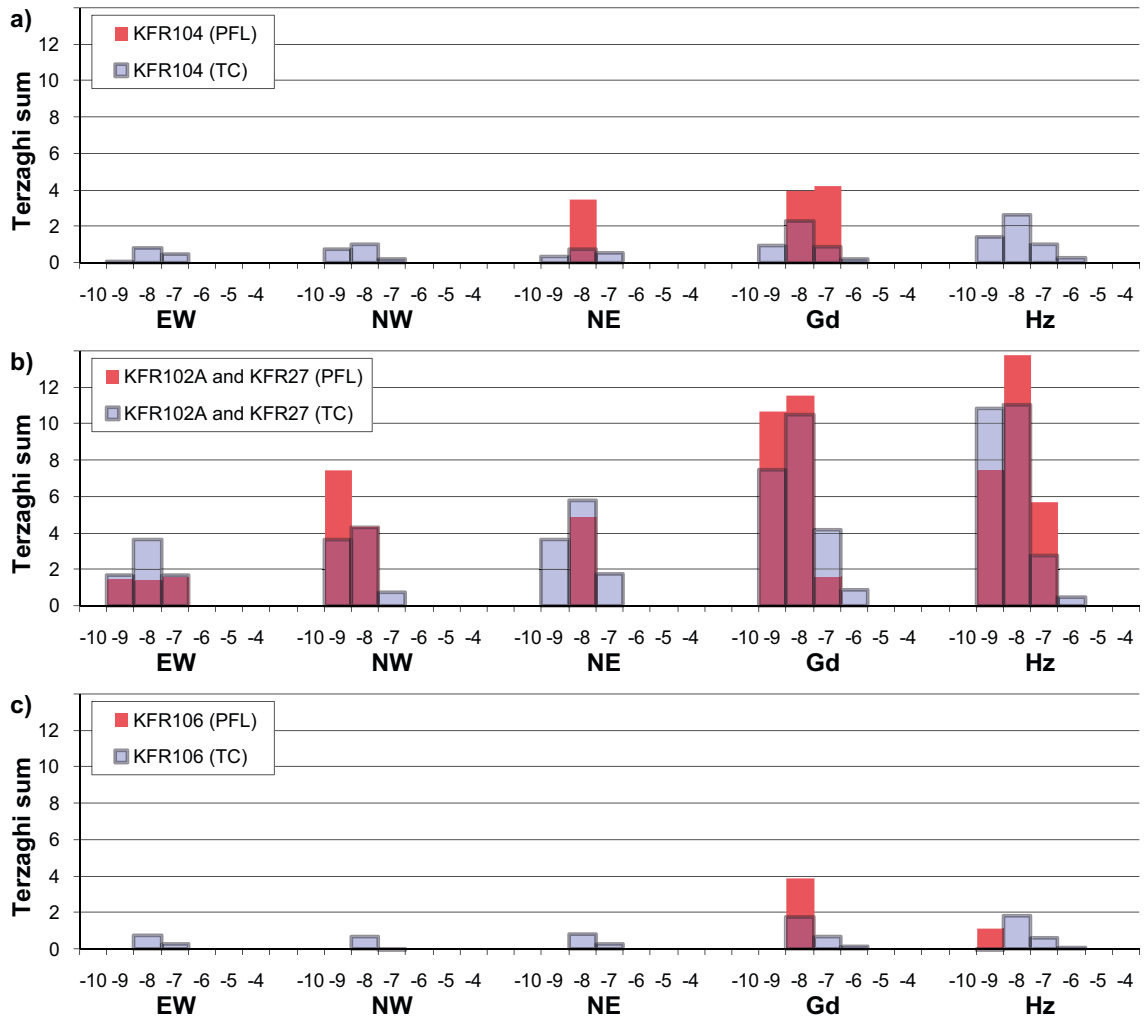


**Figure G-39.** Borehole-wise evaluation for Deep domain for size-scaling exponent,  $k$ , determined by Tectonic Continuum (TC). Transmissivity distributions of PFL- $f$  data and mean of 50 simulated borehole explorations of connected open fracture realisations.

### Underlying data for Shallow Bedrock Aquifer structures


The deterministic modelling of Shallow Bedrock Aquifer (SBA) structures is briefly described in Appendix B. This appendix presents a compilation of available hydrogeological data at SBA-structure intercepts, as well as, details of the modelled geometry. The underlying data are presented in so-called “property tables”, following the structure used in the deterministic modelling of deformation zones (Curtis et al. 2011). It should be noted that SBA-structures are not primarily defined based on geological merits, but are instead the result of hydrogeological interpretations (mainly observed hydraulic interferences and hydraulic data support). The SBA-structures are not perceived as uniform, planar geological structures, but instead as networks of connected horizontal to gently dipping fractures, with uncertain extension outside borehole coverage. Therefore, local data in borehole intercepts is expected to be comparatively less representative of the general SBA-structure characteristics, and hence, the term “property table” may be somewhat misleading.

The compiled data tables for SBA1 to SBA8 are presented in Sections H.1 to H.8, respectively. For a given SBA-structure, the data-table organisation can be described as follows:

- 1) A list of borehole/tunnel intercepts for the SBA-structure.
- 2) Presentation of relevant data for each listed intercepts; geometrical, geological, and hydraulic data.
- 3) Modelled SBA-structure properties; supporting hydrogeology, modelling geometry, and modelled terminations.
- 4) Hydraulic interpretation of the SBA-structure.

The SBA-structure geometry is modelled in RVS, following similar principles as used in the geological modelling; borehole intercepts are used as conditional points, and the geometrical extension is estimated by guidance from hydraulic responses, versus lack of responses. Unlike steeply dipping deformation zones, there are no known ground-surface trace data available for delimiting the extension of SBA-structures. Based on judgment of data, the SBA-structures are truncated against the central planes of surrounding steeply dipping deformation zones. The primary output from the RVS modelling is unfavourable for implementation in hydrogeological modelling (triangular mesh of long, thin, disconnected elements). Therefore, the geometries are post-processed into regularly triangulated meshes. Consequently, terminations against ambient steeply dipping deformation zones are limited by the resolution of triangles, and therefore inexact. Given the uncertainty in SBA-structure extensions combined with deformation-zone widths, these mismatches are considered irrelevant compared to the benefits of contiguous regular meshes.

## H.1 Property tables for SBA1

Shallow Bedrock Aquifer Feature SBA1																																																																					
<b>Borehole intersections (metres along borehole)</b>																																																																					
HFR102: 53.0–55.04 m (eoh)																																																																					
KFR27: 50–56 m																																																																					
<b>Borehole intercept details</b>																																																																					
<b>Borehole intersections for SBA1</b>																																																																					
BH	Target intercept																																																																				
	Sec_up BH length (m) [z (m RHB 70)]	Sec_low BH length (m) [z (m RHB 70)]																																																																			
HFR102	53.0 [−42.4]	55.04 [−44.1]																																																																			
<b>Comment:</b> Modelled geometric intercept at 55.04 m.																																																																					
<b>Fracture characterization:</b> A frequency of 0.5 open fractures/m and 3.0 sealed fractures/m. No core available. No BIPS image below 54.75 m.																																																																					
<table border="1"> <thead> <tr> <th colspan="14">Borehole HFR102</th> </tr> <tr> <th>Length</th> <th>Elevation</th> <th>Open</th> <th>Sealed</th> <th>Open Total</th> <th>Sealed Total</th> <th>Total</th> <th>Crush</th> <th>Sealed</th> <th>ROD Reversed</th> <th>Fracture</th> <th>Fracture</th> <th>Open</th> <th>Core Loss</th> </tr> <tr> <th>1m:200m</th> <th>M.A.S.L.</th> <th>Fractures</th> <th>Fractures</th> <th>Fractures</th> <th>Fractures</th> <th>Fractures</th> <th>Zone</th> <th>Network</th> <th>100 = 0, Low value = High staple</th> <th>Open Frac Orientation</th> <th>Sealed Frac Orientation</th> <th>Aperture (mm)</th> <th></th> </tr> </thead> <tbody> <tr> <td>54</td> <td>44</td> <td>0</td> <td>0</td> <td>0</td> <td>0</td> <td>0</td> <td></td> <td></td> <td></td> <td>0</td> <td>90</td> <td>0</td> <td>10</td> </tr> </tbody> </table>														Borehole HFR102														Length	Elevation	Open	Sealed	Open Total	Sealed Total	Total	Crush	Sealed	ROD Reversed	Fracture	Fracture	Open	Core Loss	1m:200m	M.A.S.L.	Fractures	Fractures	Fractures	Fractures	Fractures	Zone	Network	100 = 0, Low value = High staple	Open Frac Orientation	Sealed Frac Orientation	Aperture (mm)		54	44	0	0	0	0	0				0	90	0	10
Borehole HFR102																																																																					
Length	Elevation	Open	Sealed	Open Total	Sealed Total	Total	Crush	Sealed	ROD Reversed	Fracture	Fracture	Open	Core Loss																																																								
1m:200m	M.A.S.L.	Fractures	Fractures	Fractures	Fractures	Fractures	Zone	Network	100 = 0, Low value = High staple	Open Frac Orientation	Sealed Frac Orientation	Aperture (mm)																																																									
54	44	0	0	0	0	0				0	90	0	10																																																								
																																																																					
<table border="1"> <tbody> <tr> <td>53.000</td> <td>53.100</td> <td>53.200</td> <td>53.300</td> <td>53.400</td> <td>53.500</td> <td>53.600</td> <td>53.700</td> <td>53.800</td> <td>53.900</td> <td>54.000</td> <td>54.100</td> <td>54.200</td> <td>54.300</td> <td>54.400</td> <td>54.500</td> <td>54.600</td> <td>54.700</td> <td>54.750</td> </tr> <tr> <td>53.048</td> <td>53.148</td> <td>53.248</td> <td>53.348</td> <td>53.448</td> <td>53.549</td> <td>53.649</td> <td>53.749</td> <td>53.849</td> <td>53.949</td> <td>54.049</td> <td>54.149</td> <td>54.249</td> <td>54.350</td> <td>54.450</td> <td>54.550</td> <td>54.650</td> <td>54.700</td> <td>54.750</td> </tr> </tbody> </table>														53.000	53.100	53.200	53.300	53.400	53.500	53.600	53.700	53.800	53.900	54.000	54.100	54.200	54.300	54.400	54.500	54.600	54.700	54.750	53.048	53.148	53.248	53.348	53.448	53.549	53.649	53.749	53.849	53.949	54.049	54.149	54.249	54.350	54.450	54.550	54.650	54.700	54.750																		
53.000	53.100	53.200	53.300	53.400	53.500	53.600	53.700	53.800	53.900	54.000	54.100	54.200	54.300	54.400	54.500	54.600	54.700	54.750																																																			
53.048	53.148	53.248	53.348	53.448	53.549	53.649	53.749	53.849	53.949	54.049	54.149	54.249	54.350	54.450	54.550	54.650	54.700	54.750																																																			
<b>Hydraulic data (HFR102)</b>																																																																					
T = 2.8·10 <sup>−6</sup> m <sup>2</sup> /s																																																																					
<p>The transmissivity is the total borehole transmissivity measured by an injection test (between a packer c. 1.4 m below the end of the casing and the borehole bottom). There is no information on the transmissivity distribution along the borehole, but the total transmissivity was assumed to be concentrated at the end of the borehole (BIPS imaging and flow logging not possible at the very end of the borehole). The transient evaluation of the injection test shows no indication of a positive hydraulic boundary (sea), which in combination with the shallow depth of the borehole below the SFR pier (−6 to −44 m) suggests sub-horizontal flow.</p>																																																																					

## Shallow Bedrock Aquifer Feature SBA1

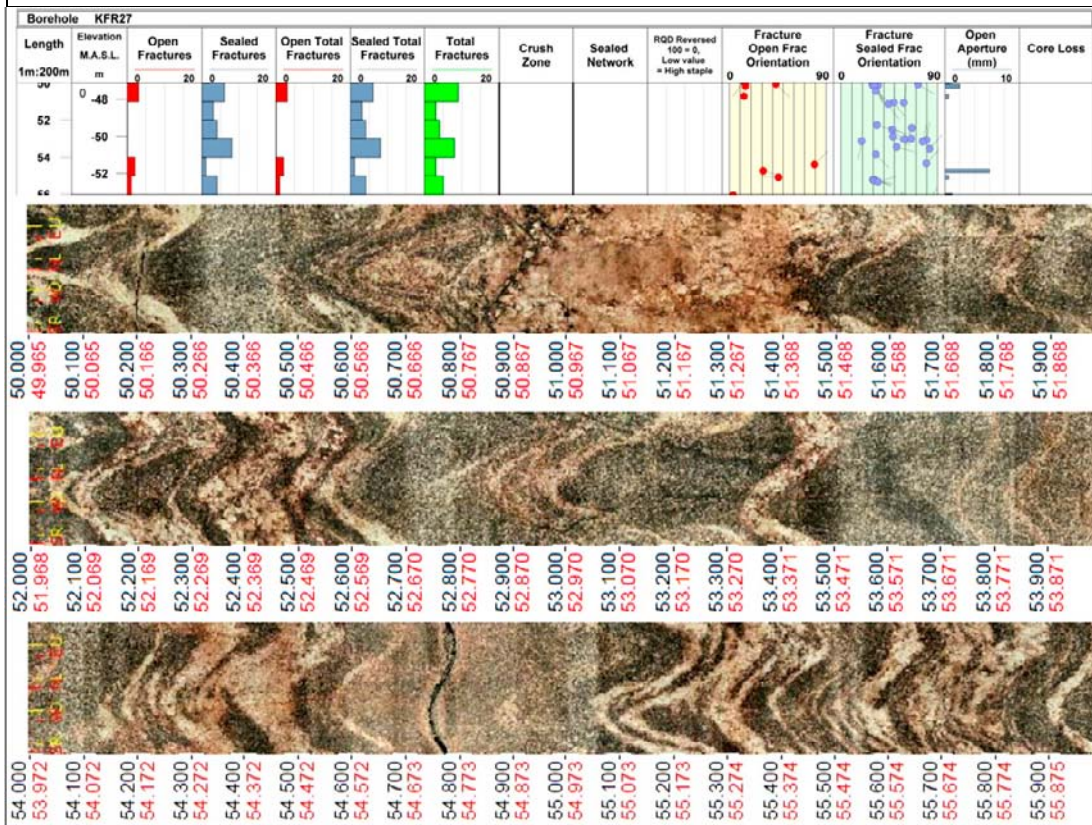
### Borehole intersections for SBA1

BH	Target intercept	
	Sec_up BH length (m) [z (m RHB 70)]	Sec_low BH length (m) [z (m RHB 70)]
KFR27	50.0 [-47.1]	56.0 [-53.1]

**Comment:** Modelled geometric intercept at 55.0 m.

**Fracture characterization:** A frequency of 1.0 open fractures/m and 4.3 sealed fractures/m. No core available. One oriented radar reflector at 55.3 m (018/09).

Notable is the open fracture (orientation 014/31) with 6 mm aperture at 55.74 m.



#### Hydraulic data (KFR27)

Two flow anomalies:

50.17 m,  $T = 1.8 \cdot 10^{-6} \text{ m}^2/\text{s}$ , orientation 322/13

54.74 m,  $T = 1.8 \cdot 10^{-6} \text{ m}^2/\text{s}$ , orientation 014/31

(The total transmissivity of the measurement section was assumed equally distributed on the two anomalies)

$$\Sigma T = 3.5 \cdot 10^{-6} \text{ m}^2/\text{s}.$$

Flow anomalies were interpreted from difference flow logging (PFL) with a 5 m test section and 0.5 m steps, making the exact location of the anomalies uncertain. The exact location of the anomalies and the orientation was interpreted through correlation with core logging data (Boremap).

## Shallow Bedrock Aquifer Feature SBA1

### Modelled properties

#### Modelled geometry

**Strike/dip (right-hand-rule):** 090/27

**Trace length at ground surface:** 193 m

**Model thickness / model thickness span :** No thickness was applied

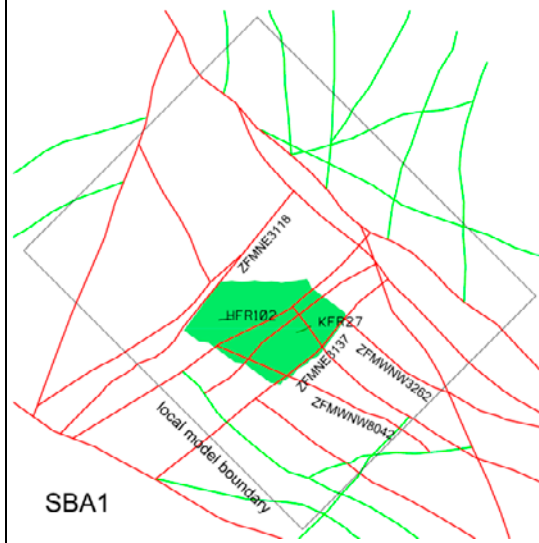
**Confidence in existence:** Medium

The degree of confidence describes the overall confidence in conceptual existence of sub-horizontal transmissive features with good hydraulic connection in the involved boreholes.

**Confidence in modelled geometry:** Low

Geometric intercept	Elevation (m RHB 70)	Orientation (°)
HFR102	-44.08	n/a
KFR27	-52.13	359/20

Orientation calculated from mean pole orientation of oriented flow anomalies.



*The northern edge intersects ground surface*

**Modelling procedure:** The basis for the modelling of feature SBA1 was the observed hydraulic interferences in the lower section of borehole HFR102 during drilling of KFR105 and at an interference test in the same borehole. The hydraulic interferences was hypothesized to be transmitted from KFR105 via other structures to borehole KFR27 and then through feature SBA1 to borehole HFR102. The response was classified as low and medium based on "Index 1" (propagation speed) and "Index 2 new" (response strength), respectively. The estimated hydraulic diffusivity (from transient evaluation of the interference test) of the hydraulic connection was  $1.4 \cdot 10^{-1} \text{ m}^2/\text{s}$  (Walger et al. 2010).

The feature has been modelled as a surface passing through two borehole control points in HFR102 and KFR27. Feature SBA1 is modelled to terminate at zones ZFMNE3118, extension of ZFMWNNW3262, ZFMNE3137 and ZFMWNNW8042. The northern edge of the structure intersects with the ground surface (sea bottom). The modelled dip and strike of the feature was a judgement based on observed fracture orientations at the borehole intercepts. The modelled feature is not considered to be a continuous single fracture but part of a sub-horizontal fracture system related to stress relief. The range in elevation (of the control points) indicates this system may have a thickness of about 10 m.

The sub-horizontal orientation of the fracture system is further supported by the lack of signs of a positive hydraulic boundary (the sea) at the injection test in HFR102. The modelled contact with the sea (intersection with the sea bottom) at the northern edge does not seem to influence the hydraulic responses in the feature. Other support for the feature is an apparent positive hydraulic boundary at an interpreted distance of c. 30 m from the sub-horizontal borehole KFR105 (SBA1 modelled to be located at a distance of 50 m above KFR105). There is also a radar reflector located at a distance of about 20 m from the borehole which is sub-parallel to the borehole.

#### Hydraulic interpretation

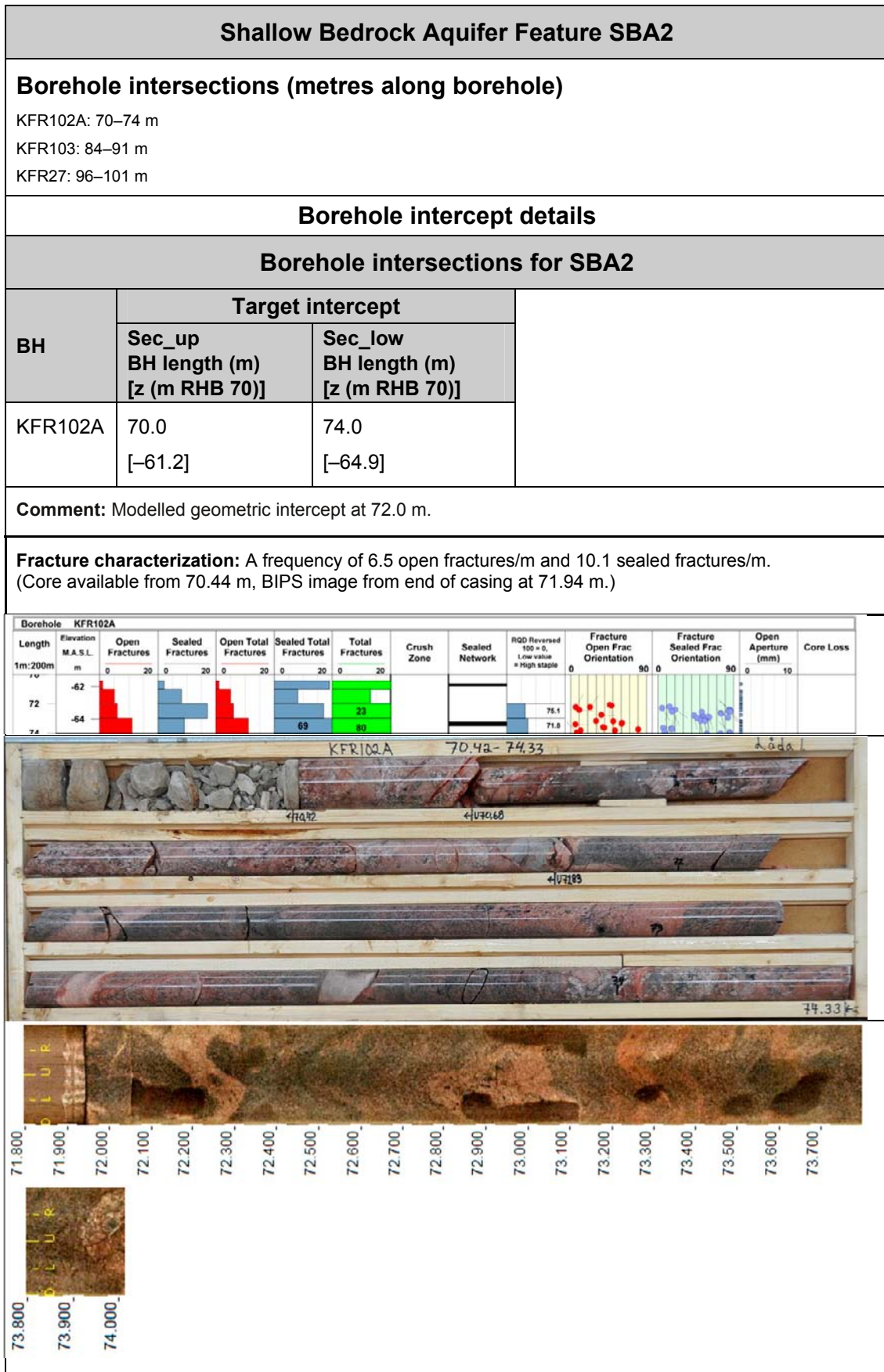
**T:**  $3.1 \cdot 10^{-6} \text{ m}^2/\text{s}$

**Log T:** -5.5,  $\sigma = 0.07$

T was calculated as the geometric mean value of the estimated transmissivity of the individual intercepts. In the hydrogeological modelling, the transmissivity of the feature was conditioned to the observations at the borehole intercepts. The two intercepts have similar transmissivities.



## H.2 Property tables for SBA2



## Shallow Bedrock Aquifer Feature SBA2

### Hydraulic data (KFR102A)

One flow anomaly:  
72.00 m,  $T = 8.6 \cdot 10^{-8} \text{ m}^2/\text{s}$

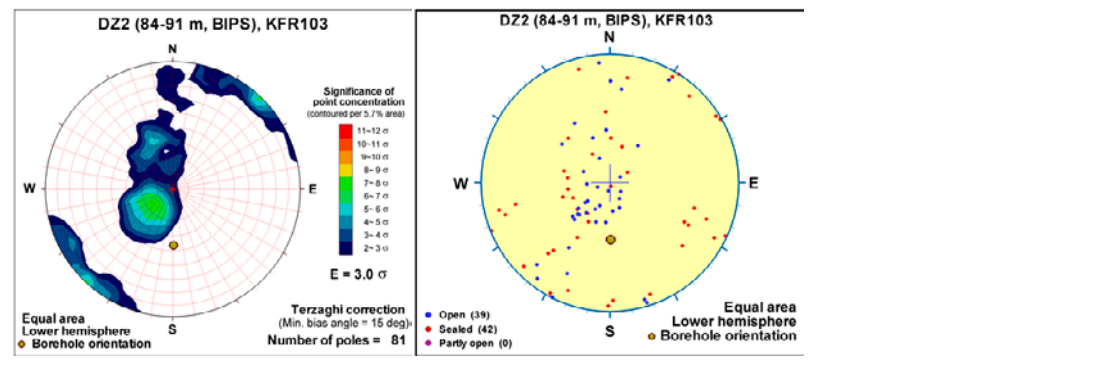
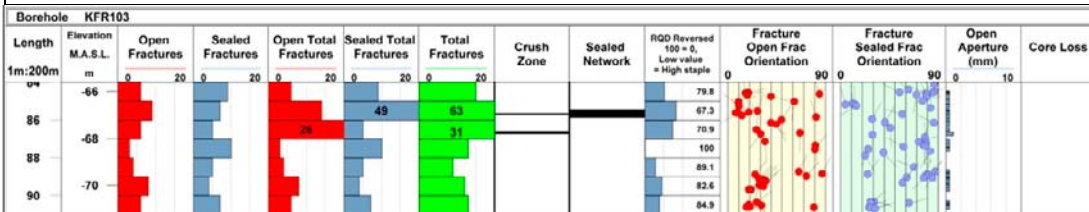
The observed flow anomaly was located at the end of the borehole casing. The associated flowing feature is assumed to be located behind the casing pipe, and the exact location and the orientation could thus not be determined.

### Borehole intersections for SBA2

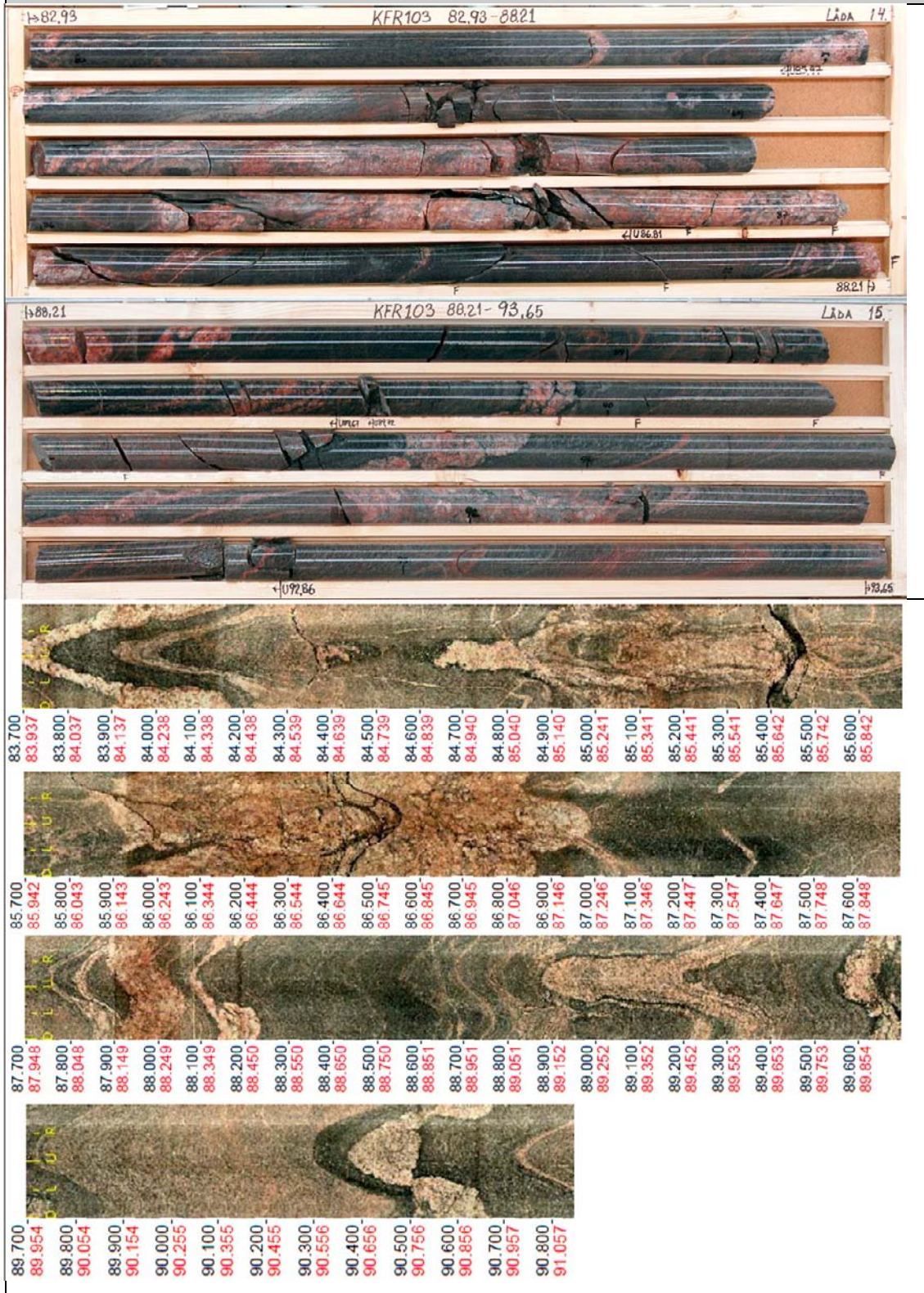
BH	Target intercept	
	Sec_up BH length (m) [z (m RHB 70)]	Sec_low BH length (m) [z (m RHB 70)]
KFR103	84.0 [-65.6]	91.0 [-71.2]

**Comment:** Modelled geometric intercept at 86.0 m. Same intercept as SBA3.

**Fracture characterization:** Increased frequency of open fractures and two crushed intervals at 85.67–85.71 and 86.61–86.74 m. A frequency of 6.0 open fractures/m and 6.7 sealed fractures/m. Fracture apertures up to 1 mm. Locally significantly decreased resistivity and magnetic susceptibility. There are also two caliper anomalies at c. 85.9 m and 86.8 m. (SHI DZ2 84.0–91.0 m, confidence level = 3.)



## Shallow Bedrock Aquifer Feature SBA2



## Shallow Bedrock Aquifer Feature SBA2

### Hydraulic data (KFR103)

Six flow anomalies:

- 84.58 m,  $T = 1.2 \cdot 10^{-6} \text{ m}^2/\text{s}$ , orientation 357/15
- 85.67 m,  $T = 9.5 \cdot 10^{-6} \text{ m}^2/\text{s}$ , orientation 223/02
- 86.61 m,  $T = 4.7 \cdot 10^{-6} \text{ m}^2/\text{s}$ , orientation 157/09
- 89.15 m,  $T = 3.3 \cdot 10^{-7} \text{ m}^2/\text{s}$ , orientation 318/32
- 89.69 m,  $T = 2.8 \cdot 10^{-8} \text{ m}^2/\text{s}$ , orientation 321/18
- 91.83 m,  $T = 1.5 \cdot 10^{-8} \text{ m}^2/\text{s}$ , orientation 327/16

$$\Sigma T = 1.6 \cdot 10^{-5} \text{ m}^2/\text{s}.$$

The cluster of high-transmissive flow anomalies at 84.6–86.6 m corresponds to a large open fracture and the two crushed intervals.

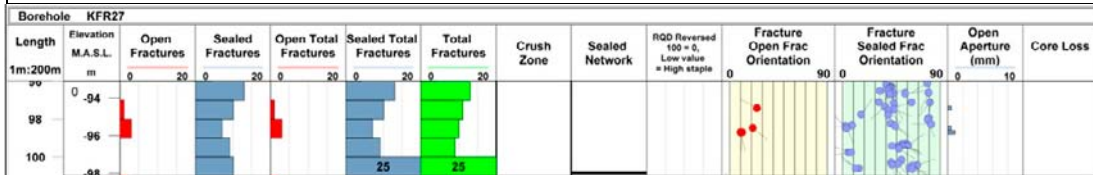
Flow anomalies were interpreted from difference flow logging (PFL). The exact location of the anomalies and the orientation was interpreted through correlation with core logging data (Boremap).

### Borehole intersections for SBA2

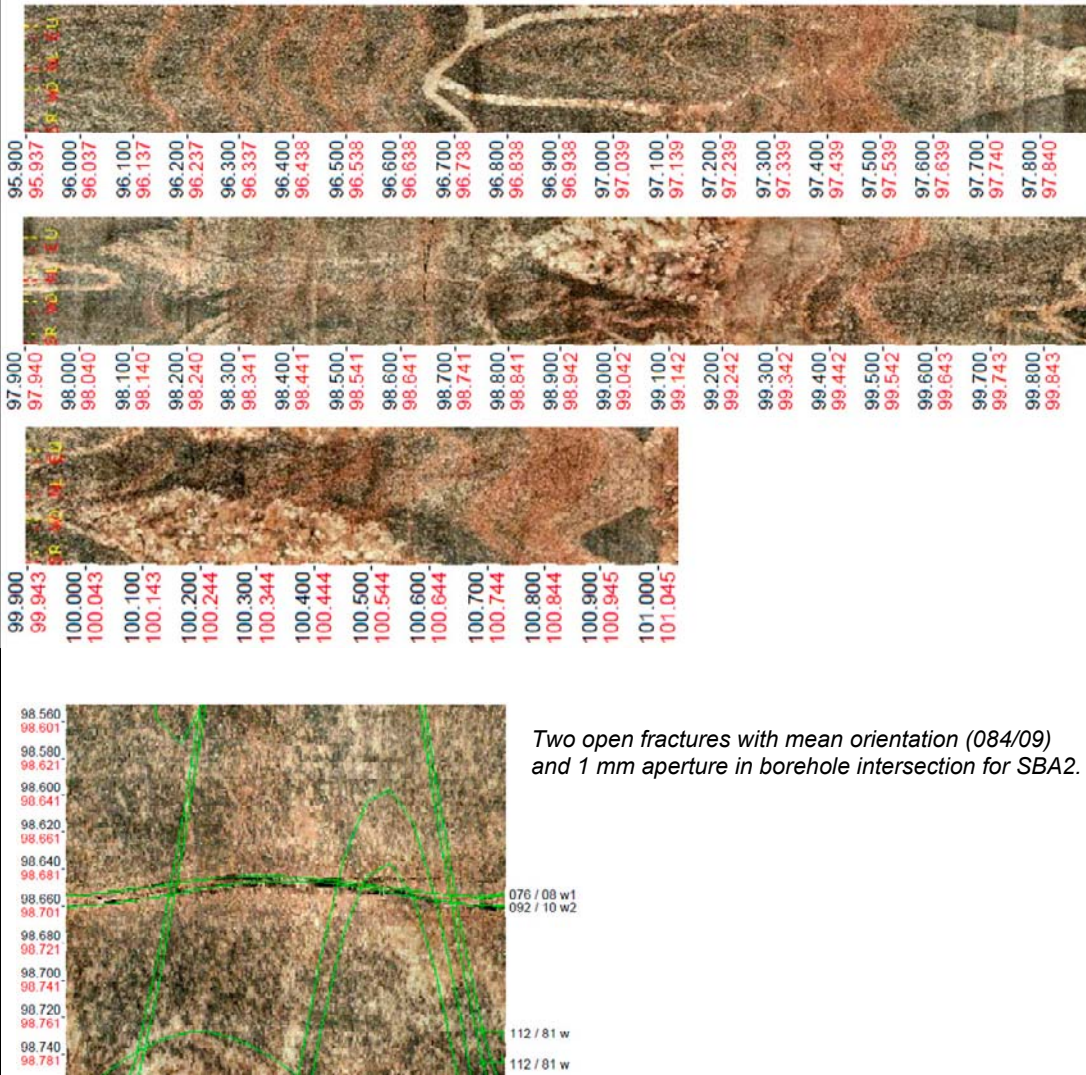
BH	Target intercept	
	Sec_up BH length (m) [z (m RHB 70)]	Sec_low BH length (m) [z (m RHB 70)]
KFR27	96.0 [-93.1]	101.0 [-98.1]

**Comment:** Modelled geometric intercept at 96.6 m.

**Fracture characterization:** A frequency of 0.8 open fractures/m and 9.8 sealed fractures/m. No core available.



## Shallow Bedrock Aquifer Feature SBA2



### Hydraulic data (KFR27)

One flow anomaly:  
 98.7 m,  $T = 1.1 \cdot 10^{-6} \text{ m}^2/\text{s}$ , orientation 084/09

Flow anomalies were interpreted from difference flow logging (PFL) with a 5 m test section and 0.5 m steps, making the exact location of the anomalies uncertain. The exact location of the anomalies and the orientation was interpreted through correlation with core logging data (Boremap).

## Shallow Bedrock Aquifer Feature SBA2

### Modelled properties

#### Modelled geometry

**Strike/dip (right-hand-rule):** 134/15

**Trace length at ground surface:** No intercept with the ground surface

**Model thickness / model thickness span :** No thickness was applied

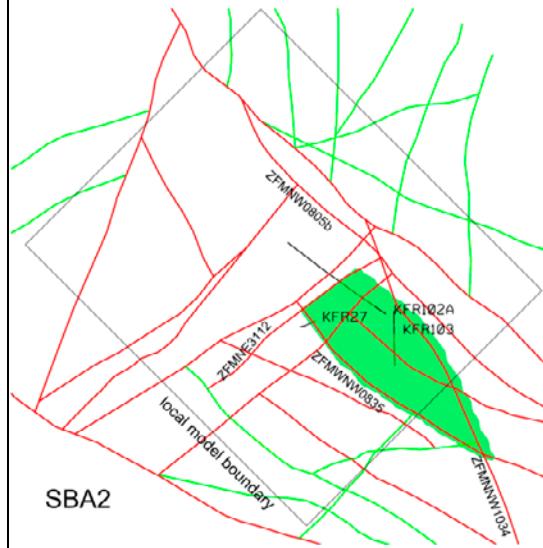
**Confidence in existence:** Medium

The degree of confidence describes the overall confidence in conceptual existence of subhorizontal transmissive features with good hydraulic connection in the involved boreholes.

**Confidence in modelled geometry:** Low

Geometric intercept	Elevation (m RHB 70)	Orientation (°)
KFR102A	-63.06	n/a
KFR103	-67.22	325/12
KFR27	-93.75	084/09

Orientation calculated from mean pole orientation of oriented flow anomalies.



*No intersection with the ground surface*

**Modelling procedure:** The basis for the modelling of feature SBA2 was the observed hydraulic interferences in the boreholes KFR102A and KFR103 during drilling of KFR105 and during an interference test in the same borehole. The hydraulic interferences was hypothesized to be transmitted from KFR105 via other structures to borehole KFR27 (the same as for SAB1) and then through feature SBA2 to borehole KFR102A and KFR103. The response was classified as low/medium and medium based on "Index 1" (propagation speed) and "Index 2 new" (response strength), respectively. The estimated hydraulic diffusivity (from transient evaluation of the interference test) of the hydraulic connection was  $2.2 \cdot 10^{-1} \text{ m}^2/\text{s}$  (geometric mean).

The feature has been modelled as a subhorizontal surface passing through three borehole control points in KFR102A, KFR103 and KFR27. Feature SBA2 is modelled to terminate at zones ZFMNE3112, ZFMNNW1034 and ZFMWNW0835. The modelled feature is not considered to be a continuous single fracture but part of a subhorizontal fracture system related to stress relief. The range in elevation (of the control points) indicates this system may have a thickness of about 30 m.


#### Hydraulic interpretation

**T:**  $1.1 \cdot 10^{-6} \text{ m}^2/\text{s}$

**Log T:** -5.9,  $\sigma = 1.1$

T was calculated as the geometric mean value of the estimated transmissivity of the individual intercepts. In the hydrogeological modelling, the transmissivity of the feature was conditioned to the observations at the borehole intercepts. The relatively high standard deviation of the transmissivity indicates a heterogeneous feature.

### H.3 Property tables for SBA3

Shallow Bedrock Aquifer Feature SBA3																																																																																			
<b>Borehole intersections (metres along borehole)</b>																																																																																			
HFR106: 38–40 m KFR103: 84–91 m																																																																																			
<b>Borehole intercept details</b>																																																																																			
<b>Borehole intersections for SBA3</b>																																																																																			
BH	Target intercept																																																																																		
	Sec_up BH length (m) [z (m RHB 70)]	Sec_low BH length (m) [z (m RHB 70)]																																																																																	
HFR106	38.0 [-30.9]	40.0 [-32.6]																																																																																	
<b>Comment:</b> Modelled geometric intercept at 39.45 m.																																																																																			
<b>Fracture characterization:</b> A frequency of 2.5 open fractures/m and 4.5 sealed fractures/m. Notable open fractures with apertures up to 6 mm. No alteration. One non-oriented radar reflector at 38 m. Distinct decrease in the bulk resistivity and significant caliper anomalies. (SHI DZ1 38.0–40.0 m, confidence level = 1.)																																																																																			
<table border="1"> <thead> <tr> <th colspan="14">Borehole HFR106</th> </tr> <tr> <th>Length</th> <th>Elevation M.A.S.L.</th> <th>Open Fractures</th> <th>Sealed Fractures</th> <th>Open Total Fractures</th> <th>Sealed Total Fractures</th> <th>Total Fractures</th> <th>Crush Zone</th> <th>Sealed Network</th> <th>R20 Reversed 100 m/s Low value = High step</th> <th>Fracture Open Frac Orientation</th> <th>Fracture Sealed Frac Orientation</th> <th>Open Aperture (mm)</th> <th>Core Loss</th> </tr> </thead> <tbody> <tr> <td>1m:200m</td> <td>m</td> <td>0</td> <td>0</td> <td>0</td> <td>0</td> <td>0</td> <td></td> <td></td> <td></td> <td>0</td> <td>90</td> <td>0</td> <td>0</td> </tr> <tr> <td>-30</td> <td>-32</td> <td></td> <td></td> <td></td> <td></td> <td></td> <td></td> <td></td> <td></td> <td></td> <td></td> <td></td> <td></td> </tr> <tr> <td>40</td> <td></td> <td></td> <td></td> <td></td> <td></td> <td></td> <td></td> <td></td> <td></td> <td></td> <td></td> <td></td> <td></td> </tr> </tbody> </table>														Borehole HFR106														Length	Elevation M.A.S.L.	Open Fractures	Sealed Fractures	Open Total Fractures	Sealed Total Fractures	Total Fractures	Crush Zone	Sealed Network	R20 Reversed 100 m/s Low value = High step	Fracture Open Frac Orientation	Fracture Sealed Frac Orientation	Open Aperture (mm)	Core Loss	1m:200m	m	0	0	0	0	0				0	90	0	0	-30	-32													40													
Borehole HFR106																																																																																			
Length	Elevation M.A.S.L.	Open Fractures	Sealed Fractures	Open Total Fractures	Sealed Total Fractures	Total Fractures	Crush Zone	Sealed Network	R20 Reversed 100 m/s Low value = High step	Fracture Open Frac Orientation	Fracture Sealed Frac Orientation	Open Aperture (mm)	Core Loss																																																																						
1m:200m	m	0	0	0	0	0				0	90	0	0																																																																						
-30	-32																																																																																		
40																																																																																			
																																																																																			
<table border="1"> <tbody> <tr><td>37.900</td></tr> <tr><td>37.925</td></tr> <tr><td>37.950</td></tr> <tr><td>38.026</td></tr> <tr><td>38.000</td></tr> <tr><td>38.126</td></tr> <tr><td>38.100</td></tr> <tr><td>38.226</td></tr> <tr><td>38.200</td></tr> <tr><td>38.327</td></tr> <tr><td>38.300</td></tr> <tr><td>38.427</td></tr> <tr><td>38.400</td></tr> <tr><td>38.528</td></tr> <tr><td>38.500</td></tr> <tr><td>38.626</td></tr> <tr><td>38.600</td></tr> <tr><td>38.729</td></tr> <tr><td>38.700</td></tr> <tr><td>38.829</td></tr> <tr><td>38.800</td></tr> <tr><td>38.929</td></tr> <tr><td>38.900</td></tr> <tr><td>39.030</td></tr> <tr><td>39.000</td></tr> <tr><td>39.130</td></tr> <tr><td>39.100</td></tr> <tr><td>39.231</td></tr> <tr><td>39.200</td></tr> <tr><td>39.331</td></tr> <tr><td>39.300</td></tr> <tr><td>39.432</td></tr> <tr><td>39.400</td></tr> <tr><td>39.532</td></tr> <tr><td>39.500</td></tr> <tr><td>39.632</td></tr> <tr><td>39.600</td></tr> <tr><td>39.733</td></tr> <tr><td>39.700</td></tr> <tr><td>39.833</td></tr> <tr><td>39.800</td></tr> <tr><td>39.934</td></tr> <tr><td>39.900</td></tr> <tr><td>40.034</td></tr> </tbody> </table>														37.900	37.925	37.950	38.026	38.000	38.126	38.100	38.226	38.200	38.327	38.300	38.427	38.400	38.528	38.500	38.626	38.600	38.729	38.700	38.829	38.800	38.929	38.900	39.030	39.000	39.130	39.100	39.231	39.200	39.331	39.300	39.432	39.400	39.532	39.500	39.632	39.600	39.733	39.700	39.833	39.800	39.934	39.900	40.034																										
37.900																																																																																			
37.925																																																																																			
37.950																																																																																			
38.026																																																																																			
38.000																																																																																			
38.126																																																																																			
38.100																																																																																			
38.226																																																																																			
38.200																																																																																			
38.327																																																																																			
38.300																																																																																			
38.427																																																																																			
38.400																																																																																			
38.528																																																																																			
38.500																																																																																			
38.626																																																																																			
38.600																																																																																			
38.729																																																																																			
38.700																																																																																			
38.829																																																																																			
38.800																																																																																			
38.929																																																																																			
38.900																																																																																			
39.030																																																																																			
39.000																																																																																			
39.130																																																																																			
39.100																																																																																			
39.231																																																																																			
39.200																																																																																			
39.331																																																																																			
39.300																																																																																			
39.432																																																																																			
39.400																																																																																			
39.532																																																																																			
39.500																																																																																			
39.632																																																																																			
39.600																																																																																			
39.733																																																																																			
39.700																																																																																			
39.833																																																																																			
39.800																																																																																			
39.934																																																																																			
39.900																																																																																			
40.034																																																																																			
<b>Hydraulic data (HFR106)</b>																																																																																			
One flow anomaly:																																																																																			
39.14 m, $T = 3.1 \cdot 10^{-5} \text{ m}^2/\text{s}$ , orientation 233/07																																																																																			
The flow anomaly was interpreted from spinner flow logging (HTHB) at 38.0–40.0 m. The exact location of the anomaly and the orientation was interpreted through correlation with fracture data (Boremap). However, it is not possible to perform the coupling with the same level of confidence as for difference flow logging and core logging data.																																																																																			

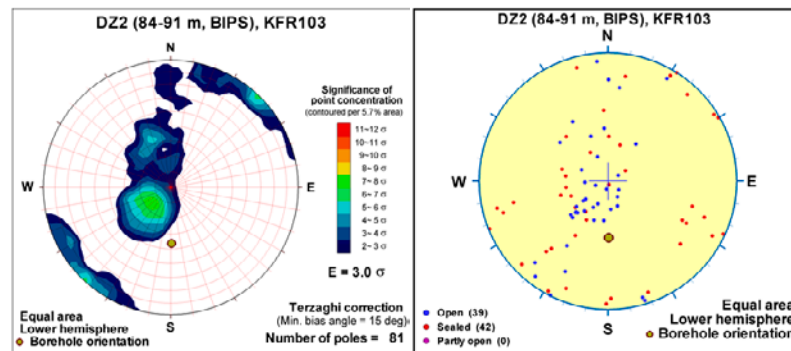
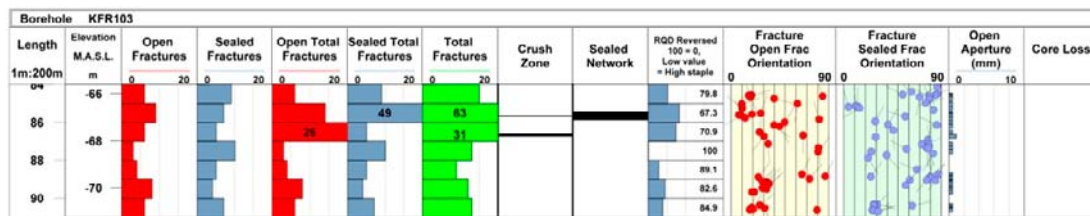
## Shallow Bedrock Aquifer Feature SBA3

### Borehole intersections for SBA3

BH	Target intercept	
	Sec_up BH length (m) [z (m RHB 70)]	Sec_low BH length (m) [z (m RHB 70)]
KFR103	84.0 [-65.6]	91.0 [-71.2]

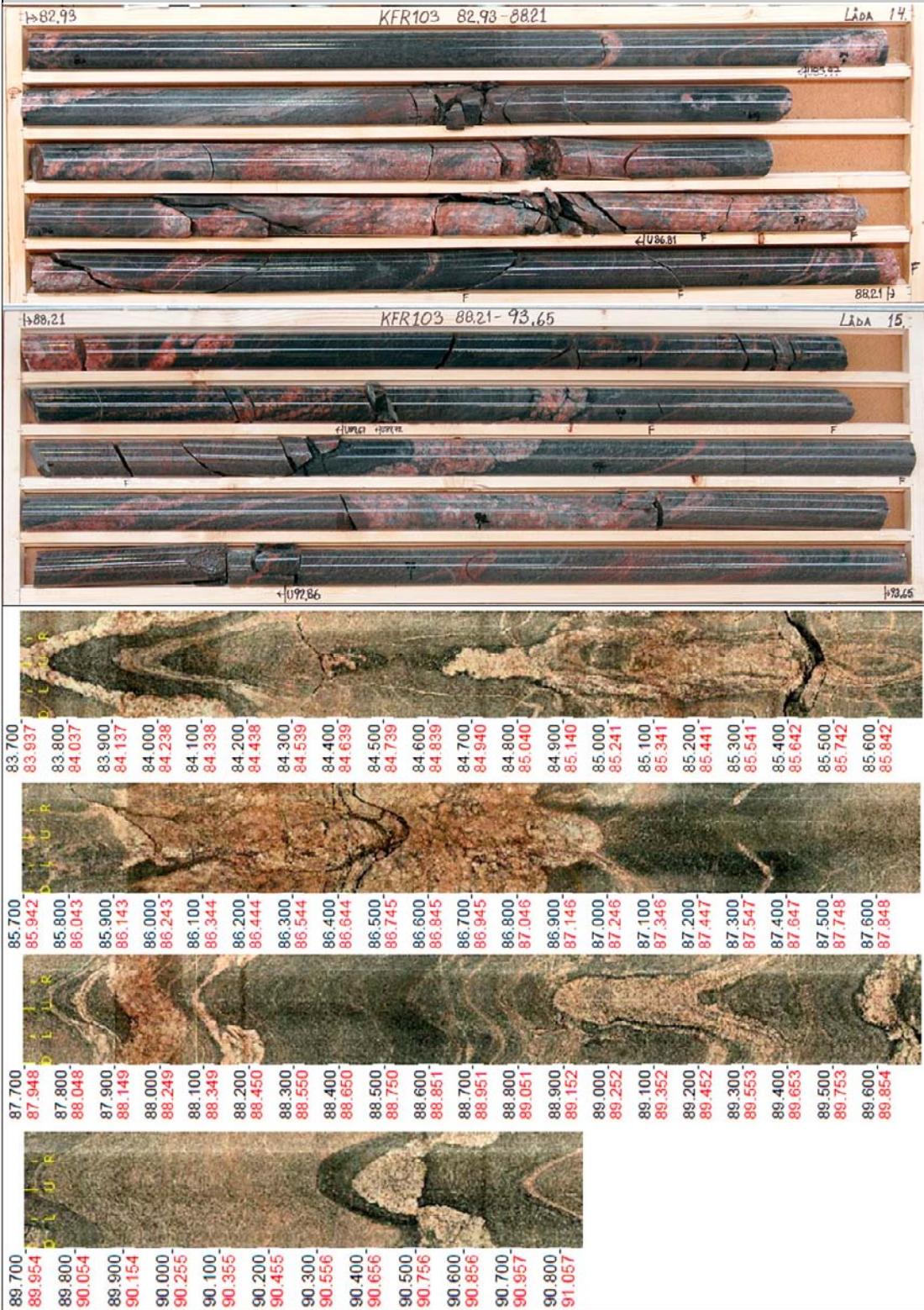
**Comment:** Modelled geometric intercept at 86.0 m. Same intercept as SBA2.

**Fracture characterization:** Increased frequency of open fractures and two crushed intervals at 85.67–85.71 and 86.61–86.74 m. A frequency of 6.0 open fractures/m and 6.7 sealed fractures/m. Fracture apertures up to 1 mm. Locally significantly decreased resistivity and magnetic susceptibility. There are also two caliper anomalies at c. 85.9 m and 86.8 m. (SHI DZ2 84.0–91.0 m, confidence level = 3.)





### Shallow Bedrock Aquifer Feature SBA3



## Shallow Bedrock Aquifer Feature SBA3

### Hydraulic data (KFR103)

Six flow anomalies:

84.58 m,  $T = 1.2 \cdot 10^{-6} \text{ m}^2/\text{s}$ , orientation 357/15  
 85.67 m,  $T = 9.5 \cdot 10^{-6} \text{ m}^2/\text{s}$ , orientation 223/02  
 86.61 m,  $T = 4.7 \cdot 10^{-6} \text{ m}^2/\text{s}$ , orientation 157/09  
 89.15 m,  $T = 3.3 \cdot 10^{-7} \text{ m}^2/\text{s}$ , orientation 318/32  
 89.69 m,  $T = 2.8 \cdot 10^{-8} \text{ m}^2/\text{s}$ , orientation 321/18  
 91.83 m,  $T = 1.5 \cdot 10^{-8} \text{ m}^2/\text{s}$ , orientation 327/16

$\Sigma T = 1.6 \cdot 10^{-5} \text{ m}^2/\text{s}$ .

The cluster of high-transmissive flow anomalies at 84.6–86.6 m corresponds to a large open fracture and the two crushed intervals.

Flow anomalies were interpreted from difference flow logging (PFL). The exact location of the anomalies and the orientation was interpreted through correlation with core logging data (Boremap).

### Modelled properties

#### Modelled geometry

**Strike/dip (right-hand-rule):** 239/10

**Trace length at ground surface:** No intercept with the ground surface

**Model thickness / model thickness span :** No thickness was applied

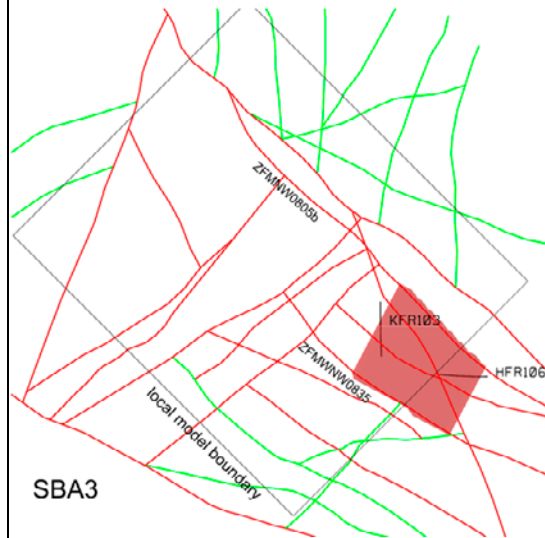
**Confidence in existence:** Medium

The degree of confidence describes the overall confidence in conceptual existence of subhorizontal transmissive features with good hydraulic connection in the involved boreholes.

**Confidence in modelled geometry:** Low

Geometric intercept	Elevation (m RHB 70)	Orientation (°)
HFR106	-32.15	233/07
KFR103	-66.88	325/12

Orientation calculated from mean pole orientation of oriented flow anomalies.



*No intersection with the ground surface*

**Modelling procedure:** The basis for the modelling of feature SBA3 was the observed hydraulic interferences between the boreholes HFR106 and KFR103. The response in KFR103:2 to drilling in HFR106 was classified as medium based on “Index 1” (propagation speed). The estimated hydraulic diffusivity (evaluated from response time) of the hydraulic connection was  $1.0 \cdot 10^{-1} \text{ m}^2/\text{s}$ .

The feature has been modelled as a subhorizontal surface passing through two borehole control points in HFR106 and KFR103. Feature SBA3 is modelled to terminate at zones ZFMNW0805b and ZFMWNW0835. It is further terminated in NW to not intersect with boreholes KFR101, KFR102A and KFR102B, and in SE to not intersect with borehole KFR106. The modelled dip and strike of the feature was a judgement based on observed fracture orientations at the borehole intercepts. The modelled feature is not considered to be a continuous single fracture but part of a subhorizontal fracture system related to stress relief. The range in elevation (of the control points) indicates this system may have a thickness of about 30 m.

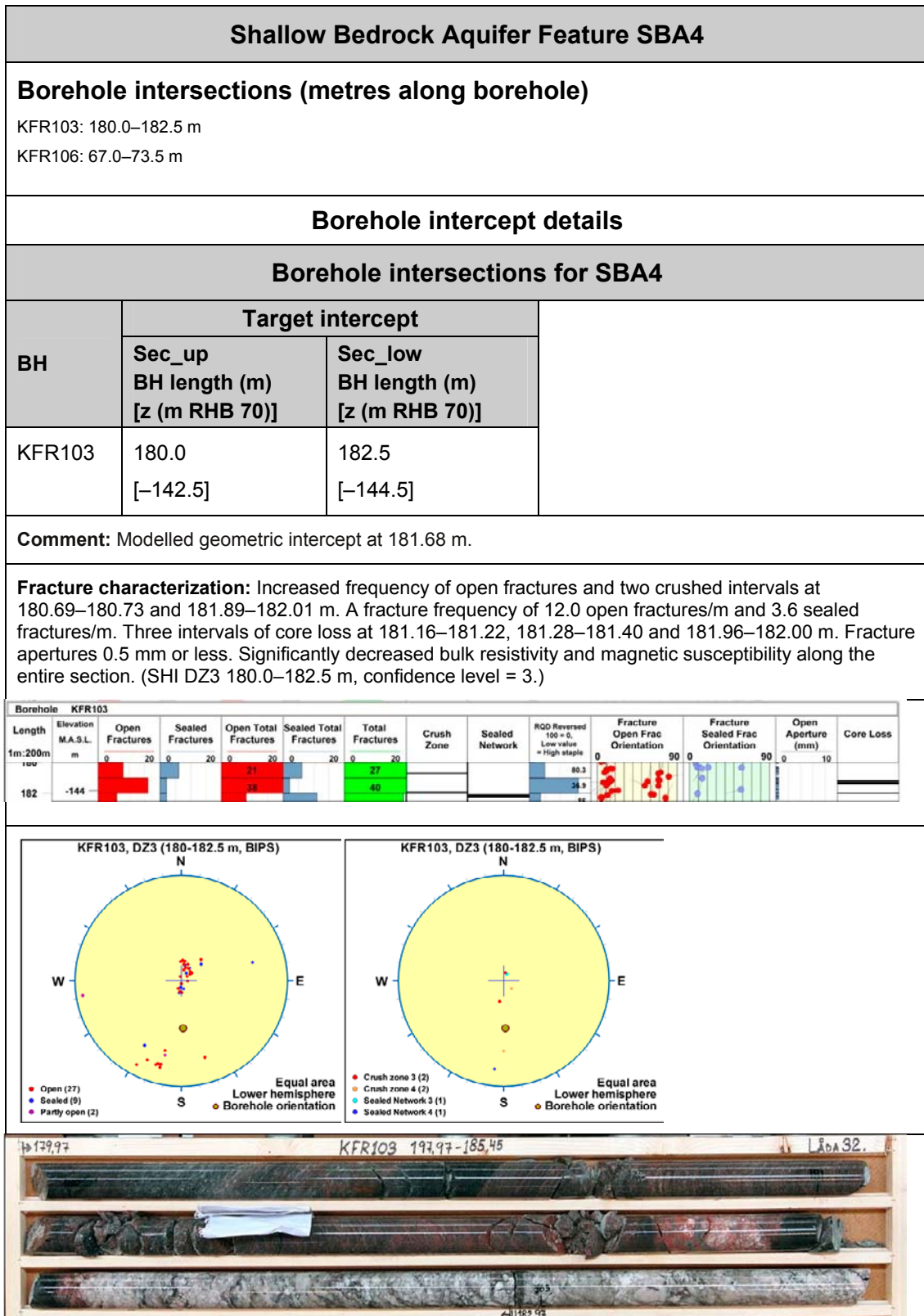
### Hydraulic interpretation

**T:**  $2.2 \cdot 10^{-5} \text{ m}^2/\text{s}$

**Log T:** -4.7,  $\sigma = 0.21$

T was calculated as the geometric mean value of the estimated transmissivity of the individual intercepts. In the hydrogeological modelling, the transmissivity of the feature was conditioned to the observations at the borehole intercepts.

#### H.4 Property tables for SBA4



## Shallow Bedrock Aquifer Feature SBA4



179.500  
179.986  
179.600  
180.086  
179.700  
180.187  
179.800  
180.287  
179.900  
180.387  
180.000  
180.488  
180.100  
180.588  
180.200  
180.688  
180.300  
180.789  
180.400  
180.889  
180.500  
180.989  
180.600  
181.090  
180.700  
181.190  
180.800  
181.290  
180.900  
181.391  
181.000  
181.491  
181.100  
181.591  
181.200  
181.692  
181.300  
181.792  
181.400  
181.892



181.500  
181.993  
181.600  
182.093  
181.700  
182.193  
181.800  
182.294  
181.900  
182.394  
182.000  
182.494  
182.100  
182.595

### Hydraulic data (KFR103)

Three flow anomalies:

180.69 m,  $T = 6.8 \cdot 10^{-8} \text{ m}^2/\text{s}$ , orientation 268/33

181.23 m,  $T = 2.1 \cdot 10^{-7} \text{ m}^2/\text{s}$ , orientation 120/11

181.89 m,  $T = 4.8 \cdot 10^{-6} \text{ m}^2/\text{s}$ , orientation 130/06

$\Sigma T = 5.1 \cdot 10^{-6} \text{ m}^2/\text{s}$ .

The flow anomalies correspond to crushes and core losses. These three anomalies together with a fourth at 187.9 m form an isolated cluster of flow anomalies in the lower part of the borehole.

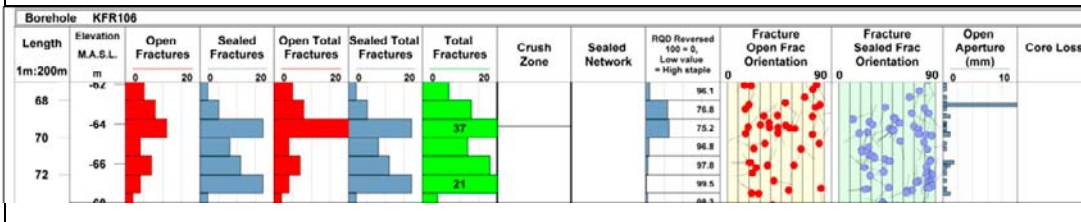
Flow anomalies were interpreted from difference flow logging (PFL). The exact location of the anomalies and the orientation was interpreted through correlation with core logging data (Boremap).

### Borehole intersections for SBA4

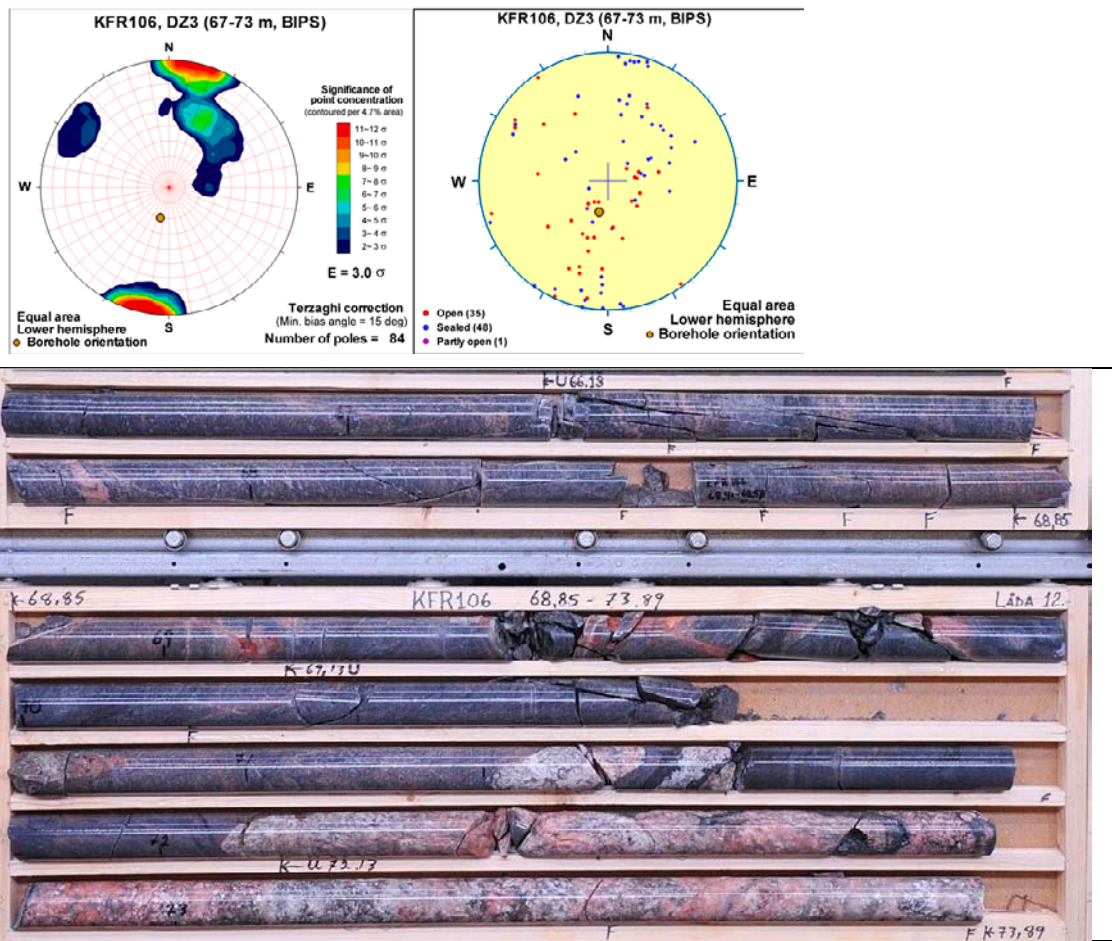
BH	Target intercept	
	Sec_up BH length (m) [z (m RHB 70)]	Sec_low BH length (m) [z (m RHB 70)]
KFR106	67.0 [-61.9]	73.5 [-68.0]

**Comment:** Modelled geometric intercept at 70.87 m.

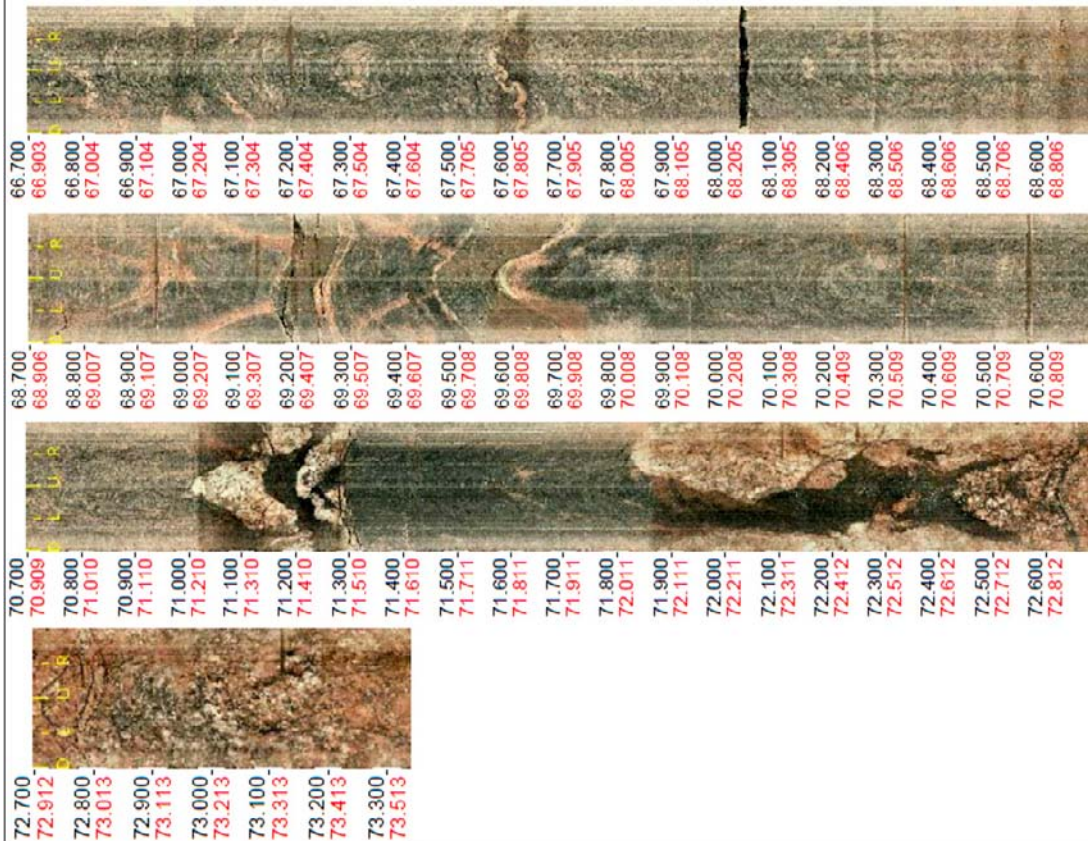
**Fracture characterization:** Locally increased frequency of open and sealed fractures. A frequency of 6.2 open fractures/m and 9.2 sealed fractures/m (calculated over the interval. One minor crush at 69.38–69.42 m and one ductile shear zone at 69.25–69.99 m (256/44). Fracture apertures generally between 0.5 and 1.5 mm with one example up to 12 mm. One radar reflector interpreted without orientation at 72 m. A few narrow low resistivity anomalies and one distinct fluid temperature anomaly, which in combination indicate the occurrence of water bearing fractures. (SHI DZ3 67.0–73.0 m, confidence level = 3.)



## Shallow Bedrock Aquifer Feature SBA4



## Shallow Bedrock Aquifer Feature SBA4



### Hydraulic data (KFR106)

Five flow anomalies:

67.22 m,  $T = 2.2 \cdot 10^{-7} \text{ m}^2/\text{s}$ , orientation 307/22

68.24 m,  $T = 1.3 \cdot 10^{-5} \text{ m}^2/\text{s}$ , orientation 286/19

69.38 m,  $T = 1.0 \cdot 10^{-7} \text{ m}^2/\text{s}$ , orientation 255/40

71.50 m,  $T = 6.3 \cdot 10^{-6} \text{ m}^2/\text{s}$ , orientation 284/37

73.02 m,  $T = 4.6 \cdot 10^{-6} \text{ m}^2/\text{s}$ , orientation 206/26

$$\Sigma T = 2.4 \cdot 10^{-5} \text{ m}^2/\text{s}.$$

Flow anomalies were interpreted from difference flow logging (PFL). The exact location of the anomalies and the orientation was interpreted through correlation with core logging data (Boremap).

## Shallow Bedrock Aquifer Feature SBA4

### Modelled properties

#### Modelled geometry

**Strike/dip (right-hand-rule):** 235/19

**Trace length at ground surface:** No intercept with the ground surface

**Model thickness / model thickness span :** No thickness was applied

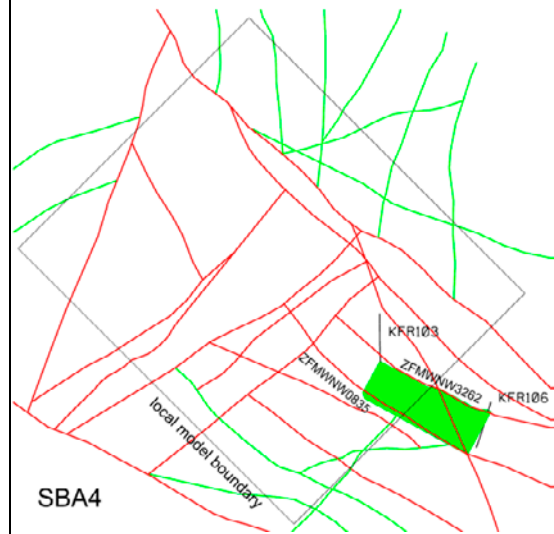
**Confidence in existence:** Medium

The degree of confidence describes the overall confidence in conceptual existence of subhorizontal transmissive features with good hydraulic connection in the involved boreholes.

**Confidence in modelled geometry:** Low

Geometric intercept	Elevation (m RHB 70)	Orientation (°)
KFR103	-143.87	239/07
KFR106	-65.49	267/25

Orientation calculated from mean pole orientation of oriented flow anomalies.



*No intersection with the ground surface*

**Modelling procedure:** The basis for the modelling of feature SBA4 was the observed hydraulic interferences between the boreholes KFR106 and KFR103. The response in KFR103:1 to nitrogen flushing in KFR106 was classified as high based on “Index 1” (propagation speed). However, It cannot be deduced if this response relates to SBA4 or SBA5 (or ZFMWNNW3262).

The feature has been modelled as a surface passing through two borehole control points in KFR103 and KFR106. These intercepts are also modelled as the intercept with deformation zone ZFMWNNW3262, but since the intercepts have similarities to other SBA features (narrow intercept with horizontal highly transmissive fractures), feature SBA4 is modelled as an additional hydraulic connection between these boreholes. Feature SBA4 is modelled to terminate at zones ZFMWNNW3262 and ZFMWNNW0835. It is further terminated at boreholes KFR103 in NW and KFR106 in SE. The modelled dip and strike of the feature was a judgement based on observed fracture orientations at the borehole intercepts. The modelled feature is not considered to be a continuous single fracture but part of a subhorizontal fracture system related to stress relief.

#### Hydraulic interpretation

**T :**  $1.1 \cdot 10^{-5} \text{ m}^2/\text{s}$

**Log T:** -5.0,  $\sigma = 0.48$

T was calculated as the geometric mean value of the estimated transmissivity of the individual intercepts. In the hydrogeological modelling, the transmissivity of the feature was conditioned to the observations at the borehole intercepts.

## H.5 Property tables for SBA5

Shallow Bedrock Aquifer Feature SBA5																																																																					
<b>Borehole intersections (metres along borehole)</b>																																																																					
KFR103: 180.0–182.5 m																																																																					
KFR106: 153.0–157.0 m																																																																					
<b>Borehole intercept details</b>																																																																					
<b>Borehole intersections for SBA5</b>																																																																					
BH	Target intercept																																																																				
	Sec_up BH length (m) [z (m RHB 70)]	Sec_low BH length (m) [z (m RHB 70)]																																																																			
KFR103	180.0 [-142.5]	182.5 [-144.5]																																																																			
<b>Comment:</b> Modelled geometric intercept at 182.31 m. Same control point as SBA4 (within 0.6 m).																																																																					
<b>Fracture characterization:</b> Increased frequency of open fractures and two crushed intervals at 180.69–180.73 and 181.89–182.01 m. A fracture frequency of 12.0 open fractures/m and 3.6 sealed fractures/m. Three intervals of core loss at 181.16–181.22, 181.28–181.40 and 181.96–182.00 m. Fracture apertures 0.5 mm or less. Significantly decreased bulk resistivity and magnetic susceptibility along the entire section. (SHI DZ3 180.0–182.5 m, confidence level = 3.)																																																																					
<table border="1"> <thead> <tr> <th colspan="14">Borehole KFR103</th> </tr> <tr> <th>Length</th> <th>Elevation M.A.S.L.</th> <th>Open Fractures</th> <th>Sealed Fractures</th> <th>Open Total Fractures</th> <th>Sealed Total Fractures</th> <th>Total Fractures</th> <th>Crush Zone</th> <th>Sealed Network</th> <th>ROD Reversed 100 = 0, Low value = High staple</th> <th>Fracture Open Frac Orientation</th> <th>Fracture Sealed Frac Orientation</th> <th>Open Aperture (mm)</th> <th>Core Loss</th> </tr> </thead> <tbody> <tr> <td>1m:200m</td> <td>m</td> <td>0 20</td> <td>0 20</td> <td>0 20</td> <td>0 20</td> <td>0 20</td> <td></td> <td></td> <td>80.3 36.9</td> <td>0 90</td> <td>0 90</td> <td>0 10</td> <td></td> </tr> <tr> <td>182</td> <td>-144</td> <td>[Red bar]</td> <td>[Blue bar]</td> <td>[Red bar]</td> <td>[Blue bar]</td> <td>[Green bar]</td> <td></td> <td></td> <td></td> <td>[Red dots]</td> <td>[Blue dots]</td> <td></td> <td></td> </tr> </tbody> </table>														Borehole KFR103														Length	Elevation M.A.S.L.	Open Fractures	Sealed Fractures	Open Total Fractures	Sealed Total Fractures	Total Fractures	Crush Zone	Sealed Network	ROD Reversed 100 = 0, Low value = High staple	Fracture Open Frac Orientation	Fracture Sealed Frac Orientation	Open Aperture (mm)	Core Loss	1m:200m	m	0 20	0 20	0 20	0 20	0 20			80.3 36.9	0 90	0 90	0 10		182	-144	[Red bar]	[Blue bar]	[Red bar]	[Blue bar]	[Green bar]				[Red dots]	[Blue dots]		
Borehole KFR103																																																																					
Length	Elevation M.A.S.L.	Open Fractures	Sealed Fractures	Open Total Fractures	Sealed Total Fractures	Total Fractures	Crush Zone	Sealed Network	ROD Reversed 100 = 0, Low value = High staple	Fracture Open Frac Orientation	Fracture Sealed Frac Orientation	Open Aperture (mm)	Core Loss																																																								
1m:200m	m	0 20	0 20	0 20	0 20	0 20			80.3 36.9	0 90	0 90	0 10																																																									
182	-144	[Red bar]	[Blue bar]	[Red bar]	[Blue bar]	[Green bar]				[Red dots]	[Blue dots]																																																										
<table border="1"> <thead> <tr> <th colspan="7">KFR103, DZ3 (180-182.5 m, BIPS)</th> <th colspan="7">KFR103, DZ3 (180-182.5 m, BIPS)</th> </tr> </thead> <tbody> <tr> <td colspan="7"> </td> <td colspan="7"> </td> </tr> </tbody> </table>														KFR103, DZ3 (180-182.5 m, BIPS)							KFR103, DZ3 (180-182.5 m, BIPS)																																																
KFR103, DZ3 (180-182.5 m, BIPS)							KFR103, DZ3 (180-182.5 m, BIPS)																																																														



## Shallow Bedrock Aquifer Feature SBA5



179.500  
179.986  
179.600  
180.086  
179.700  
180.187  
179.800  
180.287  
179.900  
180.387  
180.000  
180.488  
180.100  
180.588  
180.200  
180.688  
180.300  
180.789  
180.400  
180.889  
180.500  
180.989  
180.600  
181.090  
180.700  
181.190  
180.800  
181.290  
180.900  
181.391  
181.000  
181.491  
181.100  
181.591  
181.200  
181.692  
181.300  
181.792  
181.400  
181.892



181.500  
181.993  
181.600  
182.093  
181.700  
182.193  
181.800  
182.294  
181.900  
182.394  
182.000  
182.494  
182.100  
182.595

### Hydraulic data (KFR103)

Three flow anomalies:  
 180.69 m,  $T = 6.8 \cdot 10^{-8} \text{ m}^2/\text{s}$ , orientation 268/33  
 181.23 m,  $T = 2.1 \cdot 10^{-7} \text{ m}^2/\text{s}$ , orientation 120/11  
 181.89 m,  $T = 4.8 \cdot 10^{-6} \text{ m}^2/\text{s}$ , orientation 130/06  
 $\Sigma T = 5.1 \cdot 10^{-6} \text{ m}^2/\text{s}$ .

The flow anomalies correspond to crushes and core losses. These three anomalies together with a fourth at 187.9 m form an isolated cluster of flow anomalies in the lower part of the borehole.

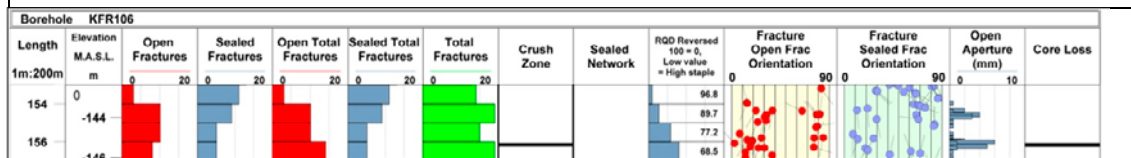
Flow anomalies were interpreted from difference flow logging (PFL). The exact location of the anomalies and the orientation was interpreted through correlation with core logging data (Boremap).

### Borehole intersections for SBA5

BH	Target intercept	
	Sec_up BH length (m) [z (m RHB 70)]	Sec_low BH length (m) [z (m RHB 70)]
KFR106	153.0 [-142.4]	157.0 [-146.1]

**Comment:** Modelled geometric intercept at 155.00 m.

**Fracture characterization:** Local increased frequency of open fractures. A fracture frequency of 7.8 open fracture/m and 7.5 sealed fractures/m. Crushed interval at 156.08–156.24 m. Fracture apertures between 0.5 and 6 mm. One oriented radar reflector at 157 m (292/61 or 122/20). Two narrow low resistivity anomalies, two caliper anomalies and a distinct fluid temperature anomaly, which in combination indicate the occurrence of water bearing fractures. (SHI DZ6 153.0–157.0 m, confidence level = 3.)





## Shallow Bedrock Aquifer Feature SBA5

### Hydraulic data (KFR106)

Three flow anomalies:  
 154.36 m,  $T = 2.3 \cdot 10^{-6} \text{ m}^2/\text{s}$ , orientation 098/38  
 154.58 m,  $T = 4.0 \cdot 10^{-6} \text{ m}^2/\text{s}$ , orientation 100/32  
 156.08 m,  $T = 1.8 \cdot 10^{-5} \text{ m}^2/\text{s}$ , orientation 116/07  
 $\Sigma T = 2.4 \cdot 10^{-5} \text{ m}^2/\text{s}$ .

The most transmissive flow anomaly corresponds to the crushed interval at 156.08 m.

Flow anomalies were interpreted from difference flow logging (PFL). The exact location of the anomalies and the orientation was interpreted through correlation with core logging data (Boremap).

### Modelled properties

#### Modelled geometry

**Strike/dip (right-hand-rule):** 121/06

**Trace length at ground surface:** No intercept with the ground surface

**Model thickness / model thickness span :** No thickness was applied

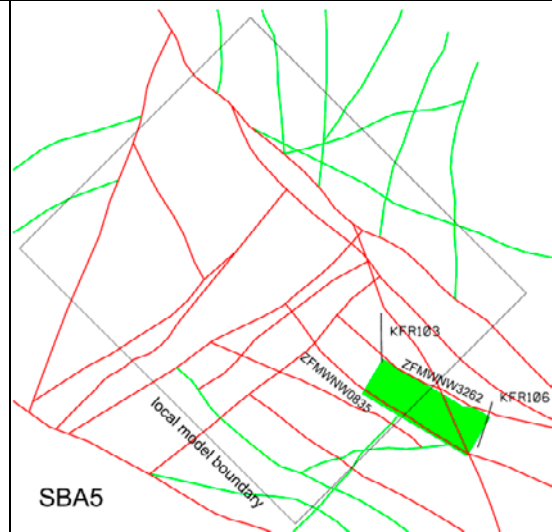
**Confidence in existence:** Medium

The degree of confidence describes the overall confidence in conceptual existence of subhorizontal transmissive features with good hydraulic connection in the involved boreholes.

**Confidence in modelled geometry:** Low

Geometric intercept	Elevation (m RHB 70)	Orientation (°)
KFR103	-144.37	239/07
KFR106	-144.27	101/26

Orientation calculated from mean pole orientation of oriented flow anomalies.



*No intersection with the ground surface*

**Modelling procedure:** The basis for the modelling of feature SBA5 was the observed hydraulic interferences between the boreholes KFR106 and KFR103. The response in KFR103:1 to nitrogen flushing in KFR106 was classified as high based on "Index 1" (propagation speed). However, It cannot be deduced if this response relates to SBA4 or SBA5 (or ZFMWNNW3262).

The feature has been modelled as a subhorizontal surface passing through two borehole control points in KFR103 and KFR106. The intercept in KFR103 is also modelled as the intercept with deformation zone ZFMWNNW3262, but since the intercept have similarities to other SBA features (narrow intercept with horizontal highly transmissive fractures), feature SBA5 is modelled as an additional hydraulic connection between these boreholes. Feature SBA5 is modelled to terminate at zones ZFMWNNW3262 and ZFMWNNW0835. It is further terminated at boreholes KFR103 in NW and KFR106 in SE. The modelled dip and strike of the feature was a judgement based on observed fracture orientations at the borehole intercepts. The modelled feature is not considered to be a continuous single fracture but part of a subhorizontal fracture system related to stress relief.

### Hydraulic interpretation

**T:**  $1.1 \cdot 10^{-5} \text{ m}^2/\text{s}$

**Log T:** -5.0,  $\sigma = 0.48$

T was calculated as the geometric mean value of the estimated transmissivity of the individual intercepts. In the hydrogeological modelling, the transmissivity of the feature was conditioned to the observations at the borehole intercepts.

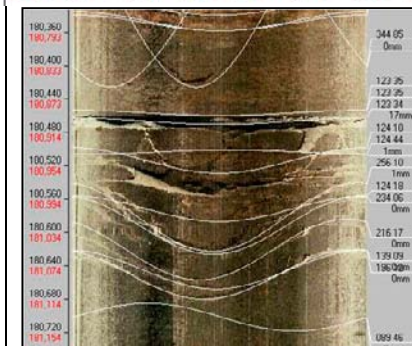
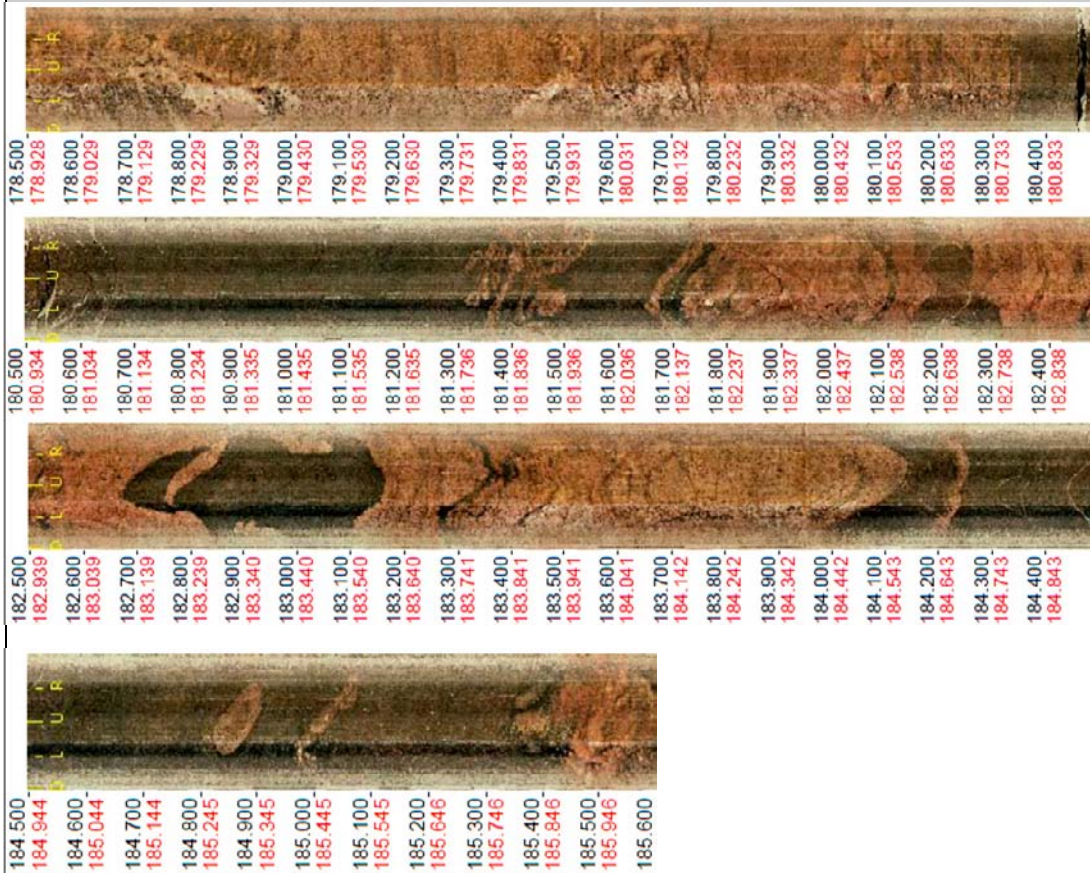
## H.6 Property tables for SBA6

Shallow Bedrock Aquifer Feature SBA6																																																																																																													
<b>Borehole intersections (metres along borehole)</b>																																																																																																													
KFR101: 179.0–186.0 m																																																																																																													
KFR102A: 187.0–207.0 m																																																																																																													
KFR102B: 171.0–175.0 m																																																																																																													
KFR27: 191.5–195.0 m																																																																																																													
<b>Borehole intercept details</b>																																																																																																													
<b>Borehole intersections for SBA6</b>																																																																																																													
BH	Target intercept																																																																																																												
	Sec_up BH length (m) [z (m RHB 70)]	Sec_low BH length (m) [z (m RHB 70)]																																																																																																											
KFR101	179.0 [−142.0]	186.0 [−147.5]																																																																																																											
<b>Comment:</b> Modelled geometric intercept at 181.09 m.																																																																																																													
<b>Fracture characterization:</b> Increased frequency of open fractures. A fracture frequency of 5.0 open fractures/m and 7.3 sealed fractures/m. Occasional slickensides. One crushed interval at 180.95–181.01 m. Fractures aperture 0.5 mm or less with one fracture at 17 mm. One distinct low resistivity anomaly at c. 181 m. One radar reflector at 181 m oriented 076/21. (DZ3 179.0–186.0 m, confidence level = 3.)																																																																																																													
<table border="1"> <thead> <tr> <th colspan="13">Borehole KFR101</th> </tr> <tr> <th>Length</th> <th>Elevation</th> <th>Open</th> <th>Sealed</th> <th>Open Total</th> <th>Sealed Total</th> <th>Total</th> <th>Crush</th> <th>Sealed</th> <th>RGD Reversed</th> <th>Fracture</th> <th>Fracture</th> <th>Open</th> <th>Core</th> </tr> <tr> <th>m:200m</th> <th>M.A.S.L.</th> <th>Fractures</th> <th>Fractures</th> <th>Fractures</th> <th>Fractures</th> <th>Fractures</th> <th>Zone</th> <th>Network</th> <th>100 = 0,</th> <th>Open Frac</th> <th>Sealed Frac</th> <th>Aperture</th> <th>Loss</th> </tr> <tr> <th></th> <th>m</th> <th>0 20</th> <th>0 20</th> <th>0 20</th> <th>0 20</th> <th>0 20</th> <th></th> <th></th> <th>Low value = High staple</th> <th>Orientation</th> <th>Orientation</th> <th>(mm)</th> <th></th> </tr> </thead> <tbody> <tr> <td>180</td> <td>-144</td> <td>[Bar chart]</td> <td>[Bar chart]</td> <td>[Bar chart]</td> <td>[Bar chart]</td> <td>22</td> <td></td> <td></td> <td>[Bar chart]</td> <td>[Scatter plot]</td> <td>[Scatter plot]</td> <td>[Bar chart]</td> <td></td> </tr> <tr> <td>182</td> <td>-144</td> <td>[Bar chart]</td> <td>[Bar chart]</td> <td>[Bar chart]</td> <td>[Bar chart]</td> <td>22</td> <td></td> <td></td> <td>[Bar chart]</td> <td>[Scatter plot]</td> <td>[Scatter plot]</td> <td>[Bar chart]</td> <td></td> </tr> <tr> <td>184</td> <td>-146</td> <td>[Bar chart]</td> <td>[Bar chart]</td> <td>[Bar chart]</td> <td>[Bar chart]</td> <td></td> <td></td> <td></td> <td>[Bar chart]</td> <td>[Scatter plot]</td> <td>[Scatter plot]</td> <td>[Bar chart]</td> <td></td> </tr> </tbody> </table>													Borehole KFR101													Length	Elevation	Open	Sealed	Open Total	Sealed Total	Total	Crush	Sealed	RGD Reversed	Fracture	Fracture	Open	Core	m:200m	M.A.S.L.	Fractures	Fractures	Fractures	Fractures	Fractures	Zone	Network	100 = 0,	Open Frac	Sealed Frac	Aperture	Loss		m	0 20	0 20	0 20	0 20	0 20			Low value = High staple	Orientation	Orientation	(mm)		180	-144	[Bar chart]	[Bar chart]	[Bar chart]	[Bar chart]	22			[Bar chart]	[Scatter plot]	[Scatter plot]	[Bar chart]		182	-144	[Bar chart]	[Bar chart]	[Bar chart]	[Bar chart]	22			[Bar chart]	[Scatter plot]	[Scatter plot]	[Bar chart]		184	-146	[Bar chart]	[Bar chart]	[Bar chart]	[Bar chart]				[Bar chart]	[Scatter plot]	[Scatter plot]	[Bar chart]	
Borehole KFR101																																																																																																													
Length	Elevation	Open	Sealed	Open Total	Sealed Total	Total	Crush	Sealed	RGD Reversed	Fracture	Fracture	Open	Core																																																																																																
m:200m	M.A.S.L.	Fractures	Fractures	Fractures	Fractures	Fractures	Zone	Network	100 = 0,	Open Frac	Sealed Frac	Aperture	Loss																																																																																																
	m	0 20	0 20	0 20	0 20	0 20			Low value = High staple	Orientation	Orientation	(mm)																																																																																																	
180	-144	[Bar chart]	[Bar chart]	[Bar chart]	[Bar chart]	22			[Bar chart]	[Scatter plot]	[Scatter plot]	[Bar chart]																																																																																																	
182	-144	[Bar chart]	[Bar chart]	[Bar chart]	[Bar chart]	22			[Bar chart]	[Scatter plot]	[Scatter plot]	[Bar chart]																																																																																																	
184	-146	[Bar chart]	[Bar chart]	[Bar chart]	[Bar chart]				[Bar chart]	[Scatter plot]	[Scatter plot]	[Bar chart]																																																																																																	
<table border="1"> <thead> <tr> <th colspan="6">DZ3 (179-186 m, BIPS), KFR101</th> <th colspan="6">DZ3 (179-186 m, BIPS), KFR101</th> </tr> </thead> <tbody> <tr> <td colspan="6"> </td> <td colspan="6"> </td> </tr> </tbody> </table>													DZ3 (179-186 m, BIPS), KFR101						DZ3 (179-186 m, BIPS), KFR101																																																																																										
DZ3 (179-186 m, BIPS), KFR101						DZ3 (179-186 m, BIPS), KFR101																																																																																																							

### Shallow Bedrock Aquifer Feature SBA6



## Shallow Bedrock Aquifer Feature SBA6



*Detail of the most transmissive feature in the section 179.0–186.0 m.*

### Hydraulic data (KFR101)

One single flow anomaly:  
180.95 m,  $T = 1.3 \cdot 10^{-5} \text{ m}^2/\text{s}$ , orientation 124/18

The single high-transmissive flow anomaly corresponds to the crushed interval.

Flow anomalies were interpreted from difference flow logging (PFL). The exact location of the anomalies and the orientation was interpreted through correlation with core logging data (Boremap).

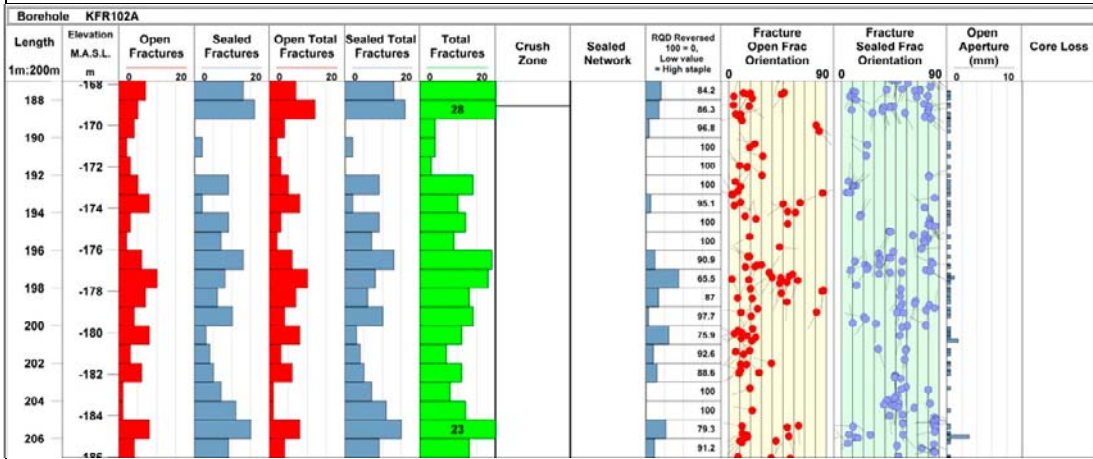
## Shallow Bedrock Aquifer Feature SBA6

### Borehole intersections for SBA6

BH	Target intercept	
	Sec_up BH length (m) [z (m RHB 70)]	Sec_low BH length (m) [z (m RHB 70)]
KFR102A	187.0 [-167.9]	207.0 [-186.0]

**Comment:** Modelled geometric intercept at 205.11 m.

**Fracture characterization:** A fracture frequency of 4.9 open fractures/m and 7.5 sealed fractures/m. One crushed interval at 188.30–188.32 m. One radar reflector at 207 m oriented 012/45 and one, more significant, just below the section at 215 m oriented 071/12 or 020/39.

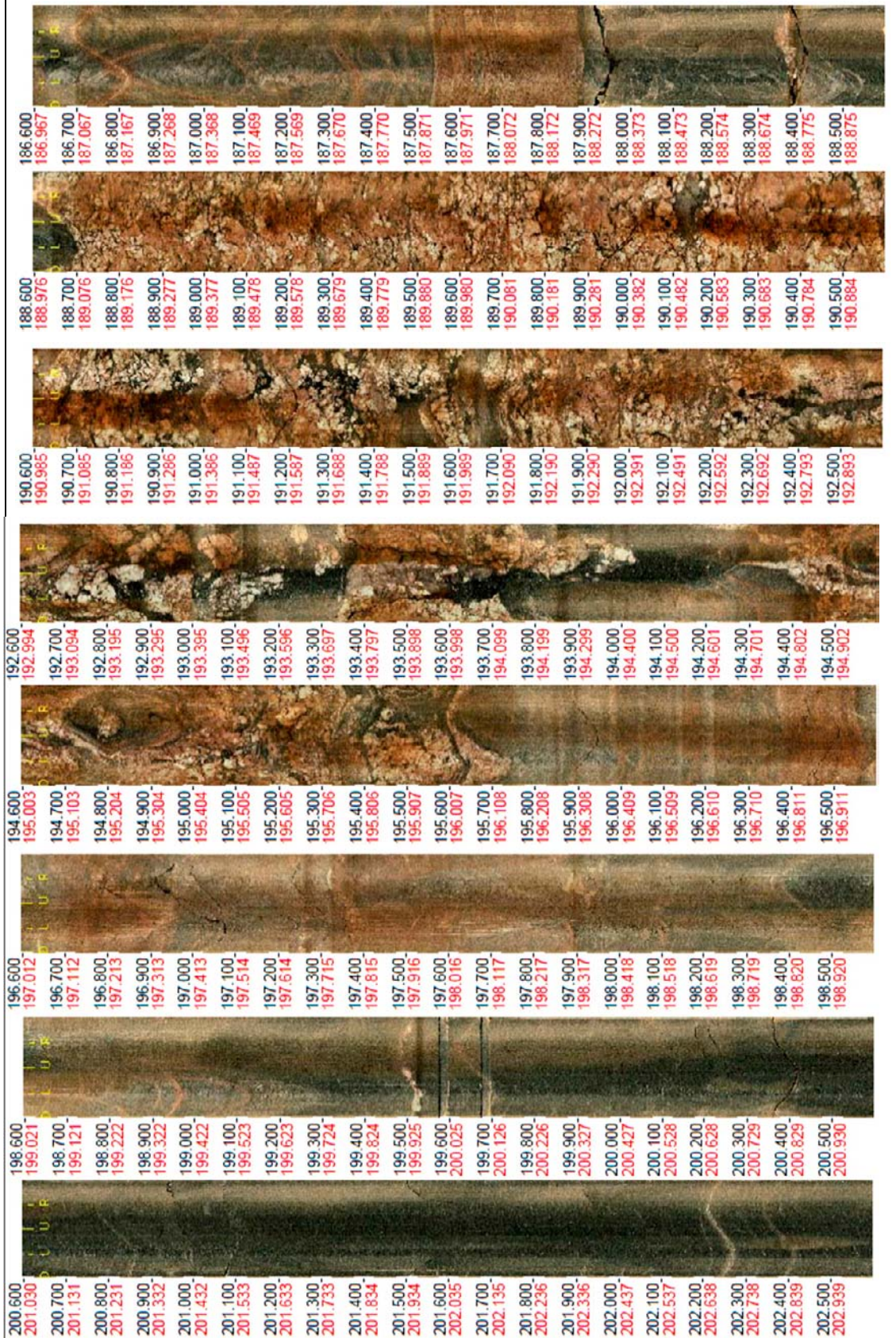


# Shallow Bedrock Aquifer Feature SBA6

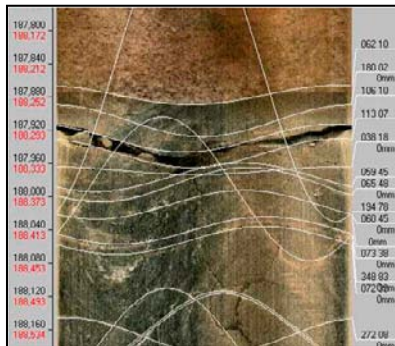




## Shallow Bedrock Aquifer Feature SBA6



## Shallow Bedrock Aquifer Feature SBA6



Detail of the transmissive crushed interval at 188.3 m.

### Hydraulic data (KFR102A)

14 flow anomalies:

188.30 m,  $T = 2.6 \cdot 10^{-6} \text{ m}^2/\text{s}$ , orientation 109/09  
 188.77 m,  $T = 5.4 \cdot 10^{-7} \text{ m}^2/\text{s}$ , orientation 345/09  
 190.35 m,  $T = 6.0 \cdot 10^{-7} \text{ m}^2/\text{s}$ , orientation 196/23  
 192.01 m,  $T = 2.3 \cdot 10^{-8} \text{ m}^2/\text{s}$ , orientation 205/30  
 196.32 m,  $T = 5.9 \cdot 10^{-9} \text{ m}^2/\text{s}$ , orientation 208/16  
 196.89 m,  $T = 3.0 \cdot 10^{-8} \text{ m}^2/\text{s}$ , orientation 246/14  
 197.45 m,  $T = 3.1 \cdot 10^{-8} \text{ m}^2/\text{s}$ , orientation 125/40  
 200.81 m,  $T = 2.2 \cdot 10^{-6} \text{ m}^2/\text{s}$ , orientation 147/20  
 201.52 m,  $T = 7.0 \cdot 10^{-7} \text{ m}^2/\text{s}$ , orientation 146/12  
 202.01 m,  $T = 4.1 \cdot 10^{-7} \text{ m}^2/\text{s}$ , orientation 201/39  
 202.38 m,  $T = 3.5 \cdot 10^{-7} \text{ m}^2/\text{s}$ , orientation 205/09  
 203.32 m,  $T = 4.8 \cdot 10^{-8} \text{ m}^2/\text{s}$ , orientation 163/18  
 204.50 m,  $T = 5.3 \cdot 10^{-7} \text{ m}^2/\text{s}$ , orientation 195/20  
 205.89 m,  $T = 3.4 \cdot 10^{-6} \text{ m}^2/\text{s}$ , orientation 166/16

$\Sigma T = 1.1 \cdot 10^{-5} \text{ m}^2/\text{s}$ .

Flow anomalies were interpreted from difference flow logging (PFL). The exact location of the anomalies and the orientation was interpreted through correlation with core logging data (Boremap).

## Shallow Bedrock Aquifer Feature SBA6

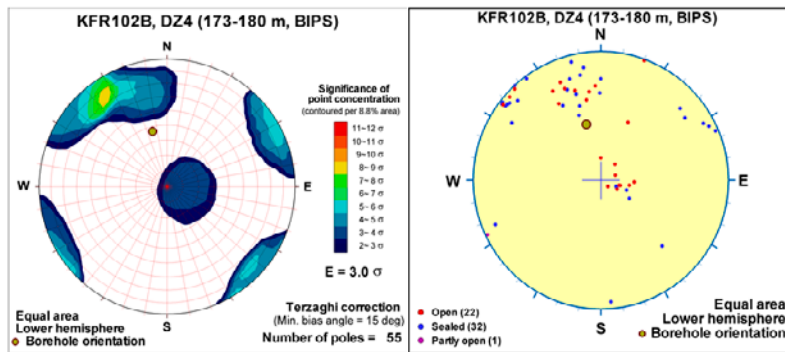
### Borehole intersections for SBA6

BH	Target intercept	
	Sec_up BH length (m) [z (m RHB 70)]	Sec_low BH length (m) [z (m RHB 70)]
KFR102B	171.0 [-135.6]	175.0 [-138.8]

**Comment:** Modelled geometric intercept at 173.33 m.

**Fracture characterization:** The intersection is located at the rim of the zone ZFMENE3112 (173.0–175.0 m). Increased frequency of sealed fractures and sealed fracture networks. A fracture frequency of 3.8 open fractures/m and 12.0 sealed fractures/m (calculated for the section 171–175 m). Significantly decreased resistivity and magnetic susceptibility in the interval 172.0–173.5 m. (SHI DZ4 173.0–180.0 m, confidence level = 3.)

Length 1m:200m	Elevation M.A.S.L. m	Open Fractures	Sealed Fractures	Open Total Fractures	Sealed Total Fractures	Total Fractures	Crush Zone	Sealed Network	RQD Reversed 100 = 0, Low value = High staple	Fracture Open Frac Orientation	Fracture Sealed Frac Orientation	Open Aperture (mm)	Core Loss
172	0-135								96.3				
174	-138								87.2				



## Shallow Bedrock Aquifer Feature SBA6



### Hydraulic data (KFR102B)

Four flow anomalies:

171.95 m,  $T = 8.7 \cdot 10^{-7} \text{ m}^2/\text{s}$ , orientation 214/06

172.60 m,  $T = 2.0 \cdot 10^{-7} \text{ m}^2/\text{s}$ , orientation 216/13

173.15 m,  $T = 2.3 \cdot 10^{-7} \text{ m}^2/\text{s}$ , orientation 161/10

173.57 m,  $T = 3.6 \cdot 10^{-7} \text{ m}^2/\text{s}$ , orientation 115/41

$\Sigma T = 1.7 \cdot 10^{-6} \text{ m}^2/\text{s}$ .

The four flow anomalies form an isolated cluster of anomalies.

Flow anomalies were interpreted from difference flow logging (PFL). No flow logging data was done below approximately 173.8 m. The exact location of the anomalies and the orientation was interpreted through correlation with core logging data (Boremap).

## Borehole intersections for SBA6

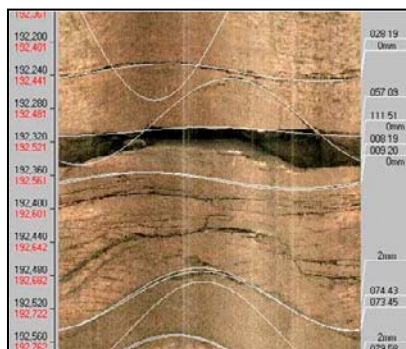
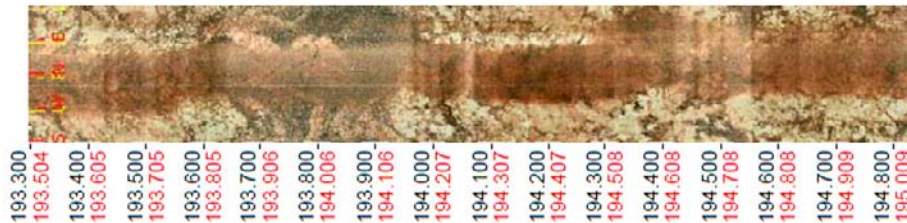
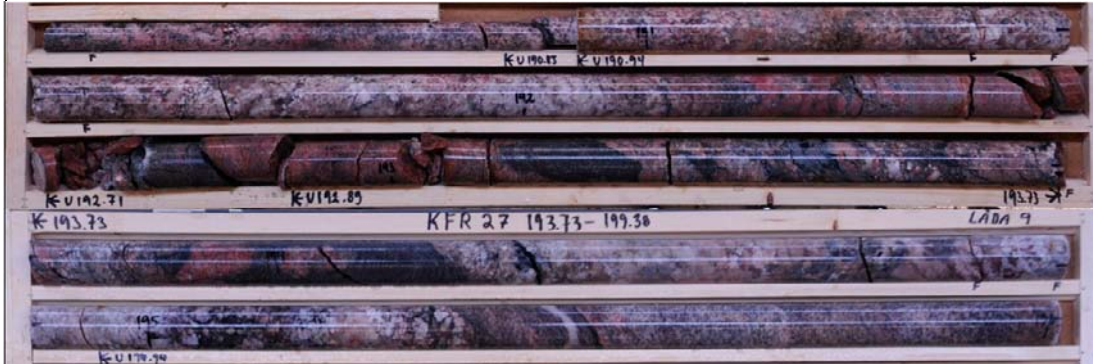
BH	Target intercept	
	Sec_up BH length (m) [z (m RHB 70)]	Sec_low BH length (m) [z (m RHB 70)]
KFR27	191.5 [-188.6]	195.0 [-192.1]

**Comment:** Modelled geometric intercept at 192.75 m.

**Fracture characterization (191.5–195.0):** A fracture frequency of 7.4 open fractures/m and 1.4 sealed fractures/m. One crushed interval at 192.51–192.71 m. Predominant minerals in open fractures are chlorite, calcite, muscovite and hematite. One radar reflector at 195 m oriented 090/15.

## Shallow Bedrock Aquifer Feature SBA6

Borehole KFR27													
Length	Elevation M.A.S.L. m	Open Fractures	Sealed Fractures	Open Total Fractures	Sealed Total Fractures	Total Fractures	Crush Zone	Sealed Network	RQD Reversed 100 = 0, Low value = High staple	Fracture Open Frac Orientation	Fracture Sealed Frac Orientation	Open Aperture (mm)	Core Loss
192	0	10	0	10	0	10			43.7	0	0	0	
	-190	10	0	10	0	10			85.4	0	0	0	
194	-192	10	0	10	0	10			100	0	0	0	



*BIPS image of the most transmissive feature at 192.5 m borehole length, with 4 cm aperture.*

### Hydraulic data (KFR27)

Two flow anomalies:

192.51 m,  $T = 6.8 \cdot 10^{-6} \text{ m}^2/\text{s}$ , orientation 063/23

193.01 m,  $T = 1.0 \cdot 10^{-8} \text{ m}^2/\text{s}$ , orientation 033/19

$\Sigma T = 6.8 \cdot 10^{-6} \text{ m}^2/\text{s}$ .

The high-transmissive flow anomaly corresponds to the crushed interval.

Flow anomalies were interpreted from difference flow logging (PFL). The exact location of the anomalies and the orientation was interpreted through correlation with core logging data (Boremap).

## Shallow Bedrock Aquifer Feature SBA6

### Modelled properties

#### Modelled geometry

**Strike/dip (right-hand-rule):** Subhorizontal undulating (097/17)

**Trace length at ground surface:** No intercept with the ground surface

**Model thickness / model thickness span :** No thickness was applied

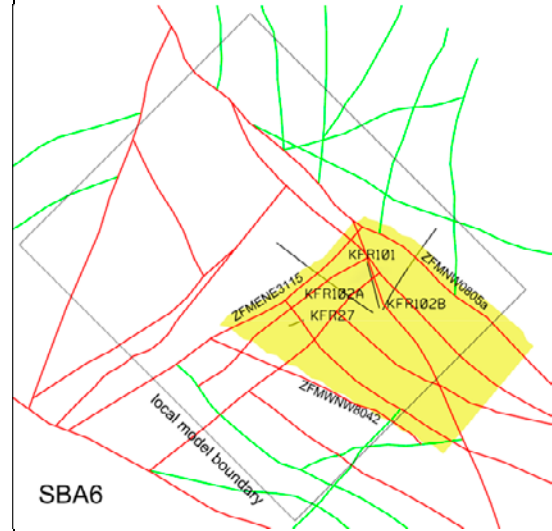
**Confidence in existence:** High

The degree of confidence describes the overall confidence in conceptual existence of subhorizontal transmissive features with good hydraulic connection in the involved boreholes.

**Confidence in modelled geometry:** Medium

Geometric intercept	Elevation (m RHB 70)	Orientation (°)
KFR101	-143.66	124/18
KFR102A	-184.31	179/15
KFR102B	-137.48	147/13
KFR27	-189.84	49/20

Orientation calculated from mean pole orientation of oriented flow anomalies.



*No intersection with the ground surface*

**Modelling procedure:** The basis for the modelling of feature SBA6 was the observed hydraulic interferences between the boreholes KFR101, KFR102A, KFR102B and KFR27. The response in section KFR101:2 to nitrogen flushing in KFR27 and KFR102A, and in KFR102B:1 due to nitrogen flushing in KFR102A, was classified as high based on "Index 1" (propagation speed). The estimated hydraulic diffusivity (evaluated from response time) of the hydraulic connection was  $9.6 \cdot 10^{-1} \text{ m}^2/\text{s}$  (geometric mean). A common denominator for these interferences was that at the same time responses were also observed in boreholes intersecting zone ZFM871 (zone H2).

The feature has been modelled as a subhorizontal surface passing through four borehole control points in KFR101, KFR102A, KFR102B and KFR27. Feature SBA6 is modelled to terminate at zones ZFMNW0805a, ZFMWNW0842 and ZFMENE3115. It is further terminated before borehole KFR106 in SE. The modelled feature is not considered to be a continuous single fracture but part of a subhorizontal fracture system related to stress relief. The range in elevation (of the control points) indicates this system may have a thickness of about 50 m. A subhorizontal structure is however supported by the subhorizontal radar reflectors in KFR101, KFR102A and KFR102B. Further support of an extensive transmissive feature with subhorizontal orientation is the large radius of influence estimated during pumping tests in KFR102A and KFR27, showing no signs of hydraulic boundaries.

#### Hydraulic interpretation

**T:**  $6.4 \cdot 10^{-6} \text{ m}^2/\text{s}$

**Log T:** -5.2,  $\sigma = 0.41$

T was calculated as the geometric mean value of the estimated transmissivity of the individual intercepts. In the hydrogeological modelling, the transmissivity of the feature was conditioned to the observations at the borehole intercepts.

The feature has high support from high hydraulic interferences as well as radar reflectors at a number of boreholes in NW. However, the extension towards SE is unknown.

## H.7 Property tables for SBA7

Shallow Bedrock Aquifer Feature SBA7																																																																																																															
<b>Borehole intersections (metres along borehole)</b>																																																																																																															
KFR21: 26.0–33.0 m																																																																																																															
KFR22: 38.0–39.0 m																																																																																																															
KFR23: 23.0–25.0 m																																																																																																															
KFR24: 34.0–37.0 m																																																																																																															
KFR25: 42.0–55.0 m																																																																																																															
KFR31: 56.0–64.0 m																																																																																																															
KFR32: 60.0–65.0 m																																																																																																															
KFR33: 55.0–60.0 m																																																																																																															
KFR35: 39.0–41.0 m																																																																																																															
KFR37: 31.0–35.0 m																																																																																																															
KFR38: 39.0–41.0 m																																																																																																															
<b>Borehole intercept details</b>																																																																																																															
<b>Borehole intersections for SBA7</b>																																																																																																															
BH	Target intercept																																																																																																														
	Sec_up BH length (m) [z (m RHB 70)]	Sec_low BH length (m) [z (m RHB 70)]																																																																																																													
KFR21	26.0 [–26.0]	33.0 [–33.0]																																																																																																													
<b>Comment:</b> Modelled geometric intercept at 30.99 m.																																																																																																															
<b>Fracture characterization:</b> The original interpretation of the feature was based on the identification of drill core sections with a slightly raised frequency of open fractures with occasional clay infilling. No core or BIPS image are available.																																																																																																															
<table border="1"> <thead> <tr> <th colspan="14">Borehole KFR21</th> </tr> <tr> <th>Length</th> <th>Elevation</th> <th>Fracture</th> <th>Sealed</th> <th>Open Total</th> <th>Sealed Total</th> <th>Total</th> <th>Crush</th> <th>Sealed</th> <th>RQD Reversed</th> <th>Fracture</th> <th>Fracture</th> <th>Open</th> <th>Core Loss</th> </tr> <tr> <th>1m:200m</th> <th>M.A.S.L.</th> <th>Frequency</th> <th>Fractures</th> <th>Fractures</th> <th>Fractures</th> <th>Fractures</th> <th>Zone</th> <th>Network</th> <th>100 = 0, Low value = High staple</th> <th>Open Frac Orientation</th> <th>Sealed Frac Orientation</th> <th>Aperture (mm)</th> <th></th> </tr> <tr> <th>z</th> <th>m</th> <th>0 20</th> <th>0 20</th> <th>0 20</th> <th>0 20</th> <th>0 20</th> <th></th> <th></th> <th></th> <th>0 90 0</th> <th>0 90 0</th> <th>0 10</th> <th></th> </tr> </thead> <tbody> <tr> <td>28</td> <td>-28</td> <td style="background-color: red;">█</td> <td></td> <td></td> <td></td> <td></td> <td></td> <td></td> <td></td> <td style="background-color: yellow;">█</td> <td style="background-color: green;">█</td> <td></td> <td></td> </tr> <tr> <td>30</td> <td>-30</td> <td style="background-color: red;">█</td> <td></td> <td></td> <td></td> <td></td> <td></td> <td></td> <td></td> <td style="background-color: yellow;">█</td> <td style="background-color: green;">█</td> <td></td> <td></td> </tr> <tr> <td>32</td> <td>-32</td> <td style="background-color: red;">█</td> <td></td> <td></td> <td></td> <td></td> <td></td> <td></td> <td></td> <td style="background-color: yellow;">█</td> <td style="background-color: green;">█</td> <td></td> <td></td> </tr> </tbody> </table>														Borehole KFR21														Length	Elevation	Fracture	Sealed	Open Total	Sealed Total	Total	Crush	Sealed	RQD Reversed	Fracture	Fracture	Open	Core Loss	1m:200m	M.A.S.L.	Frequency	Fractures	Fractures	Fractures	Fractures	Zone	Network	100 = 0, Low value = High staple	Open Frac Orientation	Sealed Frac Orientation	Aperture (mm)		z	m	0 20	0 20	0 20	0 20	0 20				0 90 0	0 90 0	0 10		28	-28	█								█	█			30	-30	█								█	█			32	-32	█								█	█		
Borehole KFR21																																																																																																															
Length	Elevation	Fracture	Sealed	Open Total	Sealed Total	Total	Crush	Sealed	RQD Reversed	Fracture	Fracture	Open	Core Loss																																																																																																		
1m:200m	M.A.S.L.	Frequency	Fractures	Fractures	Fractures	Fractures	Zone	Network	100 = 0, Low value = High staple	Open Frac Orientation	Sealed Frac Orientation	Aperture (mm)																																																																																																			
z	m	0 20	0 20	0 20	0 20	0 20				0 90 0	0 90 0	0 10																																																																																																			
28	-28	█								█	█																																																																																																				
30	-30	█								█	█																																																																																																				
32	-32	█								█	█																																																																																																				
<b>Hydraulic data (KFR21)</b>																																																																																																															
$\Sigma T = 7.7 \cdot 10^{-6} \text{ m}^2/\text{s}$ .																																																																																																															
The transmissivity was interpreted from injection tests in 3 m sections. There is no data on fracture orientation from the borehole and the transmissivity data could thus not be linked to oriented fractures.																																																																																																															

## Shallow Bedrock Aquifer Feature SBA7

### Borehole intersections for SBA7

BH	Target intercept	
	Sec_up BH length (m) [z (m RHB 70)]	Sec_low BH length (m) [z (m RHB 70)]
KFR22	38.0 [-32.9]	39.0 [-33.8]

**Comment:** Modelled geometric intercept at 37.22 m.

**Fracture characterization:** The original interpretation of the feature was based on the identification of drill core sections with a slightly raised frequency of open fractures with occasional clay infilling. No core or BIPS image are available.

Borehole KFR22													
Length	Elevation M.A.S.L.	Fracture Frequency	Sealed Fractures	Open Total Fractures	Sealed Total Fractures	Total Fractures	Crush Zone	Sealed Network	RQD Reversed 100 = 0, Low value = High staple	Fracture Open Frac Orientation	Fracture Sealed Frac Orientation	Open Aperture (mm)	Core Loss
1m:200m	m	0 20	0 20	0 20	0 20	0 20				0 90 0	0 90 0	0 10	

#### Hydraulic data (KFR22)

$$\Sigma T = 9.9 \cdot 10^{-7} \text{ m}^2/\text{s}.$$

The transmissivity was interpreted from injection tests in 3 m sections. There is no data on fracture orientation from the borehole and the transmissivity data could thus not be linked to oriented fractures.

### Borehole intersections for SBA7

BH	Target intercept	
	Sec_up BH length (m) [z (m RHB 70)]	Sec_low BH length (m) [z (m RHB 70)]
KFR23	23.0 [-20.0]	25.0 [-21.7]

**Comment:** Modelled geometric intercept at 22.97 m.

**Fracture characterization:** The original interpretation of the feature was based on the identification of drill core sections with a slightly raised frequency of open fractures with occasional clay infilling. No core or BIPS image are available.

Borehole KFR23													
Length	Elevation M.A.S.L.	Fracture Frequency	Sealed Fractures	Open Total Fractures	Sealed Total Fractures	Total Fractures	Crush Zone	Sealed Network	RQD Reversed 100 = 0, Low value = High staple	Fracture Open Frac Orientation	Fracture Sealed Frac Orientation	Open Aperture (mm)	Core Loss
1m:200m	m	0 20	0 20	0 20	0 20	0 20				0 90 0	0 90 0	0 10	
24													

#### Hydraulic data (KFR23)

$$\Sigma T = 3.9 \cdot 10^{-5} \text{ m}^2/\text{s}.$$

The transmissivity was interpreted from injection tests in 3 m sections. There is no data on fracture orientation from the borehole and the transmissivity data could thus not be linked to oriented fractures.



## Shallow Bedrock Aquifer Feature SBA7

### Borehole intersections for SBA7

BH	Target intercept	
	Sec_up BH length (m) [z (m RHB 70)]	Sec_low BH length (m) [z (m RHB 70)]
KFR24	34.0 [-28.5]	37.0 [-31.0]

**Comment:** Modelled geometric intercept at 35.57 m.

**Fracture characterization:** The original interpretation of the feature was based on the identification of drill core sections with a slightly raised frequency of open fractures with occasional clay infilling. The intercept is located within the intercept of the zone ZFMNW0805b (0–46 m). No core or BIPS image available.

Borehole KFR24													
Length	Elevation M.A.S.L.	Fracture Frequency	Sealed Fractures	Open Total Fractures	Sealed Total Fractures	Total Fractures	Crush Zone	Sealed Network	RQD Reversed 100 = 0, Low value = High stage	Fracture Open Frac Orientation	Fracture Sealed Frac Orientation	Open Aperture (mm)	Core Loss
1m:200m	m	0 20	0 20	0 20	0 20	0 20				0 90 0	0 90 0	0 10	
36	-30												

#### Hydraulic data (KFR24)

No interpretation has been done of the transmissivity of the intercept specifically.

$T = 8.1 \cdot 10^{-7} \text{ m}^2/\text{s}$  for the section 34.0–37.0 m.

The transmissivity was interpreted from injection tests in 3 m sections. There is no data on fracture orientation from the borehole and the transmissivity data could thus not be linked to oriented fractures.

### Borehole intersections for SBA7

BH	Target intercept	
	Sec_up BH length (m) [z (m RHB 70)]	Sec_low BH length (m) [z (m RHB 70)]
KFR25	42.0 [-30.2]	55.0 [-39.6]

**Comment:** Modelled geometric intercept at 45.86 m.

**Fracture characterization:** The original interpretation of the feature was based on the identification of drill core sections with a slightly raised frequency of open fractures with occasional clay infilling. The intercept is located within the intercept of the zone ZFMNW0805b (0–61 m). No core or BIPS image available.

## Shallow Bedrock Aquifer Feature SBA7

Borehole KFR25													
Length	Elevation	Fracture	Sealed	Open Total	Sealed Total	Total	Crush	Sealed	RQD Reversed	Fracture	Fracture	Open	Core Loss
1m:200m	M.A.S.L.	Frequency	Fractures	Fractures	Fractures	Fractures	Zone	Network	100 = 0, Low value = High staple	Open Frac Orientation	Sealed Frac Orientation	Aperture (mm)	
m	m	0 20	0 20	0 20	0 20	0 20			0	90 0	90 0	0 10	
42		█											
44	-32	█											
46	-34	█											
48		█											
50	-36	█											
52	-38	█											
54		█											

### Hydraulic data (KFR25)

No interpretation has been done of the transmissivity of the intercept specifically.

$T = 1.9 \cdot 10^{-6} \text{ m}^2/\text{s}$  for the section 40.0–43.0 m

$T = 2.9 \cdot 10^{-6} \text{ m}^2/\text{s}$  for the section 43.0–46.0 m

$T = 2.6 \cdot 10^{-6} \text{ m}^2/\text{s}$  for the section 46.0–49.0 m

$T = 2.4 \cdot 10^{-6} \text{ m}^2/\text{s}$  for the section 49.0–52.0 m

$T = 2.8 \cdot 10^{-6} \text{ m}^2/\text{s}$  for the section 52.0–55.0 m

The transmissivity was interpreted from injection tests in 3 m sections. There is no data on fracture orientation from the borehole and the transmissivity data could thus not be linked to oriented fractures.

## Borehole intersections for SBA7

BH	Target intercept	
	Sec_up BH length (m) [z (m RHB 70)]	Sec_low BH length (m) [z (m RHB 70)]
KFR31	56.0 [-33.3]	64.0 [-38.8]

**Comment:** Modelled geometric intercept at 59.92 m.

**Fracture characterization:** The original interpretation of the feature was based on the identification of drill core sections with a slightly raised frequency of open fractures with occasional clay infilling.

Borehole KFR31													
Length	Elevation	Fracture	Sealed	Open Total	Sealed Total	Total	Crush	Sealed	RQD Reversed	Fracture	Fracture	Open	Core Loss
1m:200m	M.A.S.L.	Frequency	Fractures	Fractures	Fractures	Fractures	Zone	Network	100 = 0, Low value = High staple	Open Frac Orientation	Sealed Frac Orientation	Aperture (mm)	
m	m	0 20	0 20	0 20	0 20	0 20			0	90 0	90 0	0 10	
50	-34	█											
58		█											
60	-36	█											
62	-38	█											
64		█											

### Shallow Bedrock Aquifer Feature SBA7



No BIPS image.

#### Hydraulic data (KFR31)

$T = 1.4 \cdot 10^{-6} \text{ m}^2/\text{s}$  for the section 57.0–60.0 m

Transmissivity below the measurement limit for the rest of the interval.

The transmissivity was interpreted from injection tests in 3 m sections. There is no data on fracture orientation from the borehole and the transmissivity data could thus not be linked to oriented fractures.

#### Borehole intersections for SBA7

BH	Target intercept	
	Sec_up BH length (m) [z (m RHB 70)]	Sec_low BH length (m) [z (m RHB 70)]
KFR32	60.0 [-38.5]	65.0 [-42.1]

**Comment:** Modelled geometric intercept at 59.93 m.

**Fracture characterization:** The original interpretation of the feature was based on the identification of drill core sections with a slightly raised frequency of open fractures with occasional clay infilling.

## Shallow Bedrock Aquifer Feature SBA7

Borehole KFR32													
Length	Elevation	Fracture	Sealed	Open Total	Sealed Total	Total	Crush	Sealed	RQD Reversed	Fracture	Fracture	Open	Core Loss
1m:200m	M.A.S.L.	Frequency	Fractures	Fractures	Fractures	Fractures	Zone	Network	100 = 0, Low value = High staple	Open Frac Orientation	Sealed Frac Orientation	Aperture (mm)	
m		0 20	0 20	0 20	0 20	0 20			0	90 0	90 0	0 10	
60	-38	█											



No BIPS image.

### Hydraulic data (KFR32)

Transmissivity below the measurement limit (about  $5 \cdot 10^{-8} \text{ m}^2/\text{s}$ ) in the interval. The transmissivity was interpreted from injection tests in 3 m sections.

### Borehole intersections for SBA7

BH	Target intercept	
	Sec_up BH length (m) [z (m RHB 70)]	Sec_low BH length (m) [z (m RHB 70)]
KFR33	55.0 [-33.0]	60.0 [-36.4]

**Comment:** Modelled geometric intercept at 56.42 m.

**Fracture characterization:** The original interpretation of the feature was based on the identification of drill core sections with a slightly raised frequency of open fractures with occasional clay infilling. The intercept is located within the intercept of the zone ZFMNNW1209 (46.2–114.6 m). No core or BIPS image available.

## Shallow Bedrock Aquifer Feature SBA7

Borehole KFR33													
Length	Elevation	Open	Sealed	Open Total	Sealed Total	Total	Crush	Sealed	RQD Reversed	Fracture	Fracture	Open	Core Loss
1m:200m	M.A.S.L.	Fractures	Fractures	Fractures	Fractures	Fractures	Zone	Network	100 = 5, Low value = High staple	Open Frac Orientation	Sealed Frac Orientation	Aperture (mm)	
m		0 20	0 20	0 20	0 20	0 20				0 90 0	0 90 0	0 10	
56	-34												
58													
60	-36												

### Hydraulic data (KFR33)

$$\Sigma T = 7.8 \cdot 10^{-7} \text{ m}^2/\text{s}.$$

The transmissivity was interpreted from injection tests in 3 m sections. There is no data on fracture orientation from the borehole and the transmissivity data could thus not be linked to oriented fractures.

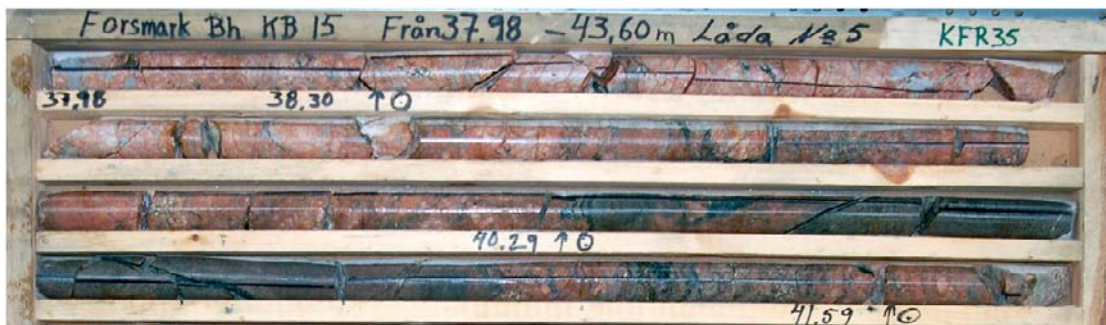
### Borehole intersections for SBA7

BH	Target intercept	
	Sec_up BH length (m) [z (m RHB 70)]	Sec_low BH length (m) [z (m RHB 70)]
KFR35	39.0 [-25.4]	41.0 [-27.0]

**Comment:** Modelled geometric intercept at 40.91 m.

**Fracture characterization:** The intercept is located within the intercept of the zone ZFMNNW1209 (32.7–70.0 m). The total fracture frequency in the drill core is generally high with a conspicuous fracture concentration in the interval between about 31 and 82 m length, where the fracture frequency locally exceeds 20 fractures/metre outside sealed networks and crush zones. (SHI DZ1 32.7–70.0 m.)

Borehole KFR35													
Length	Elevation	Open	Sealed	Open Total	Sealed Total	Total	Crush	Sealed	RQD Reversed	Fracture	Fracture	Open	Core Loss
1m:200m	M.A.S.L.	Fractures	Fractures	Fractures	Fractures	Fractures	Zone	Network	100 = 5, Low value = High staple	Open Frac Orientation	Sealed Frac Orientation	Aperture (mm)	
m		0 20	0 20	0 20	0 20	0 20				0 90 0	0 90 0	0 10	
40	-26								68 74				



No BIPS image.

### Hydraulic data (KFR35)

$$\Sigma T = 1.5 \cdot 10^{-6} \text{ m}^2/\text{s}.$$

The transmissivity was interpreted from injection tests in 3 m sections. There is no data on fracture orientation from the borehole and the transmissivity data could thus not be linked to oriented fractures.

## Shallow Bedrock Aquifer Feature SBA7

### Borehole intersections for SBA7

BH	Target intercept	
	Sec_up BH length (m) [z (m RHB 70)]	Sec_low BH length (m) [z (m RHB 70)]
KFR37	31.0 [-23.1]	35.0 [-26.6]

**Comment:** Modelled geometric intercept at 33.72 m.

**Fracture characterization:** The original interpretation of the feature was based on the identification of drill core sections with a slightly raised frequency of open fractures with occasional clay infilling. The intercept is located adjacent to the intercept of the possible deformation zone (DZ1 36.6–45.6 m).

Borehole KFR37													
Length	Elevation M.A.S.L.	Fracture Frequency	Sealed Fractures	Open Total Fractures	Sealed Total Fractures	Total Fractures	Crush Zone	Sealed Network	RQD Reversed 100 = 0, Low value = High staple	Fracture Open Frac Orientation	Fracture Sealed Frac Orientation	Open Aperture (mm)	Core Loss
1m:200m	m	0 20	0 20	0 20	0 20	0 20				0 90	0 90	0 10	
32	-24	█								█	█		
34	-26	█								█	█		



No BIPS image.

#### Hydraulic data (KFR37)

$$\Sigma T = 2.1 \cdot 10^{-6} \text{ m}^2/\text{s}.$$

The transmissivity was interpreted from injection tests in 3 m sections. There is no data on fracture orientation from the borehole and the transmissivity data could thus not be linked to oriented fractures.

## Shallow Bedrock Aquifer Feature SBA7

### Borehole intersections for SBA7

BH	Target intercept	
	Sec_up BH length (m) [z (m RHB 70)]	Sec_low BH length (m) [z (m RHB 70)]
KFR38	39.0 [-28.4]	41.0 [-30.1]

**Comment:** Modelled geometric intercept at 39.77 m.

**Fracture characterization:** The original interpretation of the feature was based on the identification of drill core sections with a slightly raised frequency of open fractures with occasional clay infilling.

Borehole KFR38													
Length	Elevation M.A.S.L.	Fracture Frequency	Sealed Fractures	Open Total Fractures	Sealed Total Fractures	Total Fractures	Crush Zone	Sealed Network	RQD Reversed 100 = 0, Low value = High staple	Fracture Open Frac Orientation	Fracture Sealed Frac Orientation	Open Aperture (mm)	Core Loss
1m:200m	m	0 20	0 20	0 20	0 20	0 20				0 90 0	0 90 0	0 10	
40	-30												



No BIPS image.

#### Hydraulic data (KFR)

$$\Sigma T = 6.9 \cdot 10^{-6} \text{ m}^2/\text{s}.$$

The transmissivity was interpreted from injection tests in 3 m sections. There is no data on fracture orientation from the borehole and the transmissivity data could thus not be linked to oriented fractures.

## Shallow Bedrock Aquifer Feature SBA7

### Modelled properties

#### Modelled geometry

**Strike/dip (right-hand-rule):** 070/03

**Trace length at ground surface:** No intercept with the ground surface

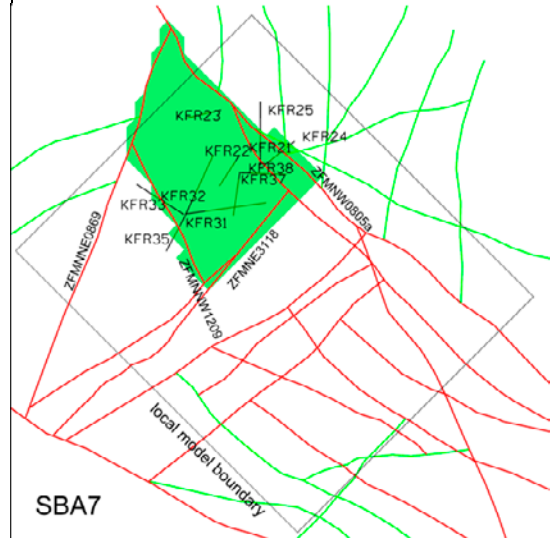
**Model thickness / model thickness span :** No thickness was applied

**Confidence in existence:** Low

The degree of confidence in existence describes the overall confidence in conceptual existence of subhorizontal transmissive features with good hydraulic connection in the involved boreholes.

**Confidence in modelled geometry:** Low

Geometric intercept	Elevation (m RHB 70)	Orientation (°)
KFR21	-30.99	n/a
KFR22	-32.23	n/a
KFR23	-19.89	n/a
KFR24	-29.83	n/a
KFR25	-32.98	n/a
KFR31	-36.02	n/a
KFR32	-38.46	n/a
KFR33	-33.95	n/a
KFR35	-26.92	n/a
KFR37	-25.51	n/a
KFR38	-29.08	n/a



*No intersection with the ground surface*

**Modelling procedure:** This possible sub-horizontal stress-relief structure was based on the original interpretation from mainly hydraulic data of zones H1 and H3 by Carlsson et al. (1985). The original interpretation was in turn based on the identification of drill core sections with a slightly raised frequency of open fractures with occasional clay infilling and, most importantly, in terms of the original interpretation, hydraulic connection between a number of the boreholes involved. The new evaluation resulted in a feature with essentially the same extent, position and thickness, although H1 and H3 have been modelled as a single feature rather than being split as in the original model. The feature is horizontal, lies at a depth of c. 25 m, has a hydraulic thickness of c. 10 m and is interpreted as a stress release feature rather than a deformation zone related to regional-scale tectonic activity.

The feature has been modelled as a subhorizontal surface passing through four borehole control points in KFR21, KFR22, KFR23, KFR24, KFR25, KFR31, KFR32, KFR33, KFR35, KFR37 and KFR38. Feature SBA7 is modelled to terminate at ZFMNNE0869, ZFMNW0805a, ZFMNE3118 and ZFMNNW1209. The modelled feature is not considered to be a continuous single fracture but part of a subhorizontal fracture system related to stress relief. The range in elevation (of the control points) indicates this system may have a thickness of about 20 m.

#### Hydraulic interpretation

**T:**  $3.0 \cdot 10^{-6} \text{ m}^2/\text{s}$

**Log T:** -5.5,  $\sigma = 0.58$

T was calculated as the geometric mean value of the estimated transmissivity of the individual intercepts. In the hydrogeological modelling, the transmissivity of the feature was conditioned to the observations at the borehole intercepts.

There is no hydraulic evidence for the feature in the boreholes KFR24, KFR25 (located within the zone ZFMNW0805b) and KFR32 in terms of transmissivity anomalies.



## H.8 Property tables for SBA8

Shallow Bedrock Aquifer Feature SBA8																																																																																																																																																																																																																																																																									
<b>Borehole and tunnel intersections (metres along borehole/tunnel)</b>																																																																																																																																																																																																																																																																									
KFR69: 121.6–146.1 m																																																																																																																																																																																																																																																																									
Tunnel BT: Chainage 5+780 m																																																																																																																																																																																																																																																																									
Shaft VB2: Lower end of shaft																																																																																																																																																																																																																																																																									
Borehole/tunnel intercept details																																																																																																																																																																																																																																																																									
Borehole intersections for SBA8																																																																																																																																																																																																																																																																									
BH	Target intercept																																																																																																																																																																																																																																																																								
	Sec_up BH length (m) [z (m RHB 70)]	Sec_low BH length (m) [z (m RHB 70)]																																																																																																																																																																																																																																																																							
KFR69	121.6 [-84.2]	146.1 [-101.6]																																																																																																																																																																																																																																																																							
<b>Comment:</b> Modelled geometric intercept at 126.92 m.																																																																																																																																																																																																																																																																									
<b>Fracture characterization:</b> Increased frequency of broken and unbroken fractures with sealed fracture networks in the upper 4 m of the interval. 10–20 broken fractures/m throughout the interval. Generally fracture orientations deviating from the orientation of the foliation with $\alpha$ -angles > 45°. (SHI DZ2 121.6–146.1 m, confidence level = 3.)																																																																																																																																																																																																																																																																									
<table border="1"> <thead> <tr> <th colspan="14">Borehole KFR69</th> </tr> <tr> <th>Length</th> <th>Elevation</th> <th>Fracture</th> <th>Sealed</th> <th>Open Total</th> <th>Sealed Total</th> <th>Total</th> <th>Crush</th> <th>Sealed</th> <th>RQD Reversed</th> <th>Fracture</th> <th>Fracture</th> <th>Open</th> <th>Core Loss</th> </tr> <tr> <th>1m:200m</th> <th>M.A.S.L.</th> <th>Frequency</th> <th>Fractures</th> <th>Fractures</th> <th>Fractures</th> <th>Fractures</th> <th>Zone</th> <th>Network</th> <th>100 = 0</th> <th>Open Frac</th> <th>Sealed Frac</th> <th>Aperture</th> <th></th> </tr> <tr> <th></th> <th>m</th> <th></th> <th></th> <th></th> <th></th> <th></th> <th></th> <th></th> <th>Low value = High staple</th> <th>Orientation</th> <th>Orientation</th> <th>(mm)</th> <th></th> </tr> <tr> <th></th> <th></th> <th>0 20</th> <th>0 20</th> <th>0 20</th> <th>0 20</th> <th>0 20</th> <th></th> <th></th> <th></th> <th>0 90</th> <th>0 90</th> <th>0 10</th> <th></th> </tr> </thead> <tbody> <tr> <td>122</td> <td></td> <td></td> <td></td> <td></td> <td></td> <td></td> <td></td> <td></td> <td></td> <td></td> <td></td> <td></td> <td></td> </tr> <tr> <td>124</td> <td>-86</td> <td></td> <td></td> <td></td> <td></td> <td></td> <td></td> <td></td> <td></td> <td></td> <td></td> <td></td> <td></td> </tr> <tr> <td>126</td> <td>-88</td> <td></td> <td></td> <td></td> <td></td> <td></td> <td></td> <td></td> <td></td> <td></td> <td></td> <td></td> <td></td> </tr> <tr> <td>128</td> <td>-90</td> <td></td> <td></td> <td></td> <td></td> <td></td> <td></td> <td></td> <td></td> <td></td> <td></td> <td></td> <td></td> </tr> <tr> <td>130</td> <td>-92</td> <td></td> <td></td> <td></td> <td></td> <td></td> <td></td> <td></td> <td></td> <td></td> <td></td> <td></td> <td></td> </tr> <tr> <td>132</td> <td>-94</td> <td></td> <td></td> <td></td> <td></td> <td></td> <td></td> <td></td> <td></td> <td></td> <td></td> <td></td> <td></td> </tr> <tr> <td>134</td> <td>-96</td> <td></td> <td></td> <td></td> <td></td> <td></td> <td></td> <td></td> <td></td> <td></td> <td></td> <td></td> <td></td> </tr> <tr> <td>136</td> <td>-98</td> <td></td> <td></td> <td></td> <td></td> <td></td> <td></td> <td></td> <td></td> <td></td> <td></td> <td></td> <td></td> </tr> <tr> <td>138</td> <td>-100</td> <td></td> <td></td> <td></td> <td></td> <td></td> <td></td> <td></td> <td></td> <td></td> <td></td> <td></td> <td></td> </tr> <tr> <td>140</td> <td></td> <td></td> <td></td> <td></td> <td></td> <td></td> <td></td> <td></td> <td></td> <td></td> <td></td> <td></td> <td></td> </tr> <tr> <td>142</td> <td></td> <td></td> <td></td> <td></td> <td></td> <td></td> <td></td> <td></td> <td></td> <td></td> <td></td> <td></td> <td></td> </tr> <tr> <td>144</td> <td></td> <td></td> <td></td> <td></td> <td></td> <td></td> <td></td> <td></td> <td></td> <td></td> <td></td> <td></td> <td></td> </tr> <tr> <td>146</td> <td></td> <td></td> <td></td> <td></td> <td></td> <td></td> <td></td> <td></td> <td></td> <td></td> <td></td> <td></td> <td></td> </tr> </tbody> </table>														Borehole KFR69														Length	Elevation	Fracture	Sealed	Open Total	Sealed Total	Total	Crush	Sealed	RQD Reversed	Fracture	Fracture	Open	Core Loss	1m:200m	M.A.S.L.	Frequency	Fractures	Fractures	Fractures	Fractures	Zone	Network	100 = 0	Open Frac	Sealed Frac	Aperture			m								Low value = High staple	Orientation	Orientation	(mm)				0 20	0 20	0 20	0 20	0 20				0 90	0 90	0 10		122														124	-86													126	-88													128	-90													130	-92													132	-94													134	-96													136	-98													138	-100													140														142														144														146													
Borehole KFR69																																																																																																																																																																																																																																																																									
Length	Elevation	Fracture	Sealed	Open Total	Sealed Total	Total	Crush	Sealed	RQD Reversed	Fracture	Fracture	Open	Core Loss																																																																																																																																																																																																																																																												
1m:200m	M.A.S.L.	Frequency	Fractures	Fractures	Fractures	Fractures	Zone	Network	100 = 0	Open Frac	Sealed Frac	Aperture																																																																																																																																																																																																																																																													
	m								Low value = High staple	Orientation	Orientation	(mm)																																																																																																																																																																																																																																																													
		0 20	0 20	0 20	0 20	0 20				0 90	0 90	0 10																																																																																																																																																																																																																																																													
122																																																																																																																																																																																																																																																																									
124	-86																																																																																																																																																																																																																																																																								
126	-88																																																																																																																																																																																																																																																																								
128	-90																																																																																																																																																																																																																																																																								
130	-92																																																																																																																																																																																																																																																																								
132	-94																																																																																																																																																																																																																																																																								
134	-96																																																																																																																																																																																																																																																																								
136	-98																																																																																																																																																																																																																																																																								
138	-100																																																																																																																																																																																																																																																																								
140																																																																																																																																																																																																																																																																									
142																																																																																																																																																																																																																																																																									
144																																																																																																																																																																																																																																																																									
146																																																																																																																																																																																																																																																																									

# Shallow Bedrock Aquifer Feature SBA8



### Shallow Bedrock Aquifer Feature SBA8



No BIPS image.

#### Hydraulic data (KFR69)

$$\Sigma T = 1.1 \cdot 10^{-5} \text{ m}^2/\text{s}$$

High transmissivity of the interval 123–132 m length ( $1.1 \cdot 10^{-5} \text{ m}^2/\text{s}$ ). The dominating transmissivity is contained in the in the section 126–129 m length. Moderate transmissivity in the interval 132–201 m length ( $6.9 \cdot 10^{-7} \text{ m}^2/\text{s}$ ).

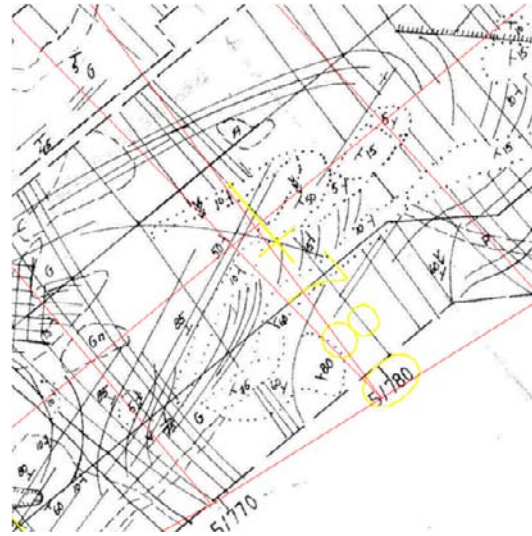
The transmissivity was interpreted from injection tests in 3 m sections and longer. There is no data on fracture orientation from the borehole and the transmissivity data could thus not be linked to oriented fractures.

#### Tunnel intersections for SBA8

Tunnel	Target intercept	
	Sec_up [z (m RHB 70)]	Sec_low [z (m RHB 70)]
Tunnel BT	Chainage 5+780 m [approx. – 77 m]	Chainage 5+780 m [approx. – 77 m]
Comment:		

### Shallow Bedrock Aquifer Feature SBA8

**Fracture characterization (Chainage 5+780 m):** Heavily grouted at this tunnel section. This inferred to be associated with gently dipping fractures some of which are mapped in the tunnel roof (see drawing below).



**Hydraulic data (tunnel BT)**

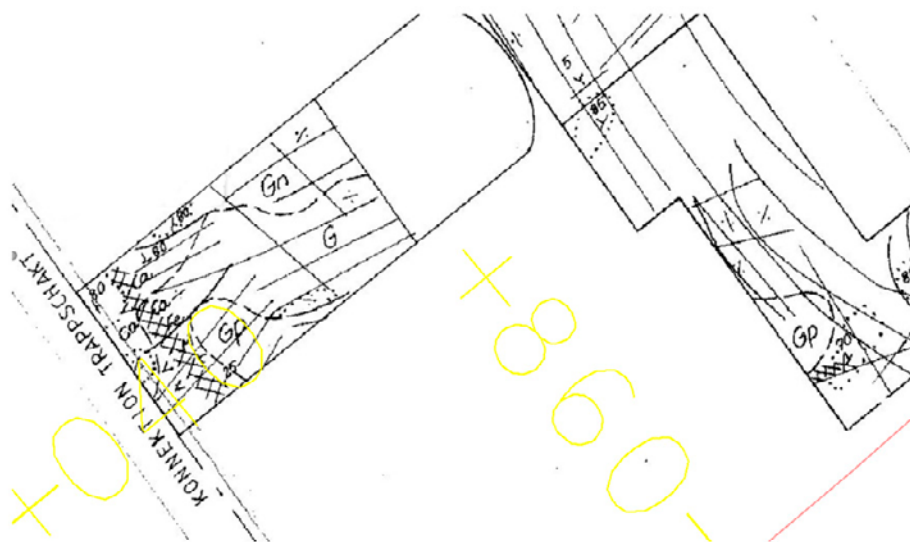
5 metric tonnes of cement grouting required at chainage 5+780 m and 5+805 m in tunnel BT.

### Tunnel intersections for SBA8

Tunnel	Target intercept	
	Sec_up [z (m RHB 70)]	Sec_low [z (m RHB 70)]
VB2	Bottom of shaft [approx. -82 m]	Bottom of shaft [approx. -82 m]

**Comment:**

**Fracture characterization:** Crushed section at the bottom of ventilation building, shaft VB2.



## Shallow Bedrock Aquifer Feature SBA8

### Hydraulic data (Shaft VB2)

Mapped inflow from a crushed section at the bottom of ventilation building, shaft VB2.

### Modelled properties

#### Modelled geometry

**Strike/dip (right-hand-rule):** 183/12

**Trace length at ground surface:** No intercept with the ground surface

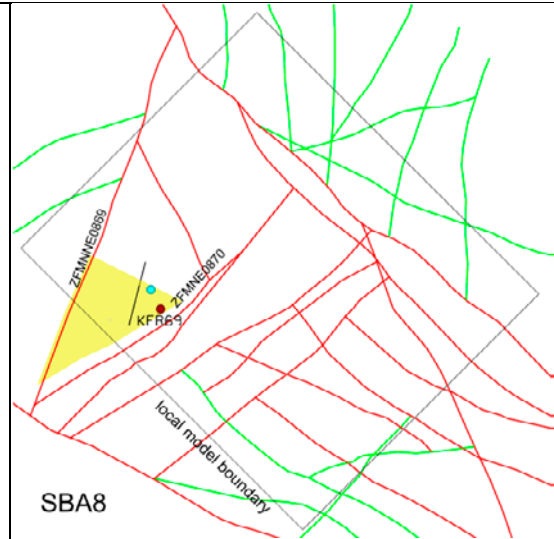
**Model thickness / model thickness span :** No thickness was applied

**Confidence in existence:** Low

The degree of confidence in existence describes the overall confidence in conceptual existence of subhorizontal transmissive features with good hydraulic connection in the involved boreholes.

**Confidence in modelled geometry:** Low

Geometric intercept	Elevation (m RHB 70)	Orientation (°)
KFR69	-87.96	n/a
Tunnel BT	c. -77	n/a
Shaft BV2	c. -82	n/a

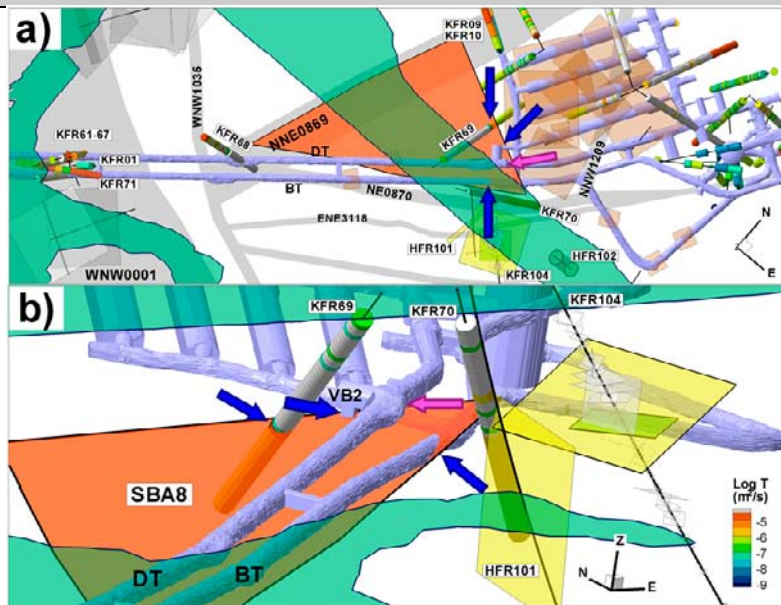


*Red sphere indicates intersection with tunnel BT, Blue sphere indicates intersection with shaft VB2. No ground surface intersection.*

**Modelling procedure:** The modelling of the feature was based on the geometrical correlation between the grouted subhorizontal structures in tunnel BT, the hydraulic anomaly in borehole KFR69 and the water-bearing structure in shaft VB2. There is no hydraulic interference data available.

The feature has been modelled as a subhorizontal surface passing through three control points in borehole, KFR69, tunnel BT and shaft VB2. Feature SBA8 is modelled to terminate at the nearest deformation zones ZFMNNE0870 and ZFMNNE0869. The feature is terminated to the north along a strike of 117° based on the vanishing of the mapped crush in the northern part of shaft and the lack of signs of it in tunnel DT. The modelled feature is not considered to be a continuous single fracture but part of a subhorizontal fracture system related to stress relief. The range in elevation (of the control points) indicates this system may have a thickness of about 10 m.

## Shallow Bedrock Aquifer Feature SBA8



Shallow Bedrock Aquifer Feature SBA8; a) top view, and b) side-view. The feature at 5-780 m associated to 5 metric tonnes grouting is extrapolated to nearest deformation zones. Blue arrows indicate support and pink arrow indicate lacking support.

### Hydraulic interpretation

T:  $1.1 \cdot 10^{-5} \text{ m}^2/\text{s}$

Log T:  $-5.0$ ,  $\sigma = \text{n/a}$

T was estimated from one borehole intercept only.